Study of the catalytic hydrogenation of triglycerides and their derivatives

Umberto Pasqual Laverdura

Université de Strasbourg

UNIVERSITÉ DE STRASBOURG

EDSC École Doctorale des Sciences Chimiques

ÉCOLE DOCTORALE des SCIENCES CHIMIQUES

ICPEES – Institut de Chimie et Procédés pour l'Énergie, l'Environnement et la Santé

THÈSE présentée par :

Umberto PASQUAL LAVERDURA

soutenue le : **09 décembre 2019**

pour obtenir le grade de : **Docteur de l'université de Strasbourg**

Discipline/ Spécialité : Catalyse hétérogène

Étude de l'hydrogénation catalytique sélective des triglycerides et de leurs dérivés

THÈSE dirigée par :

[Mme COURSON Claire]	Maître de conférences
[Mme GALLUCCI Katia]	Directeur de recherche, Università degli studi di L'Aquila

RAPPORTEURS :

[M PAUL Sébastien]	Professeur, Ecole Centrale de Lille UCCS (UMR CNRS 8181)
[Mme DI BENEDETTO Almerinda]	Professeur, Università degli studi di Napoli – Federico II

AUTRES MEMBRES DU JURY :

[M PFEIFER Cristoph]	Professeur, University of Natural Resources and Life Sciences Vienna

Umberto PASQUAL LAVERDURA

Étude de l'hydrogénation catalytique sélective des triglycerides et de leurs dérivés

Résumé

Ce projet industriel concerne l'étude de l'hydrogénation catalytique sélective des huiles végétales (huile de soja et huile de colza, et la validation de la technologie de production, afin de maximiser la teneur en acide oléique et d'élargir la gamme de ses utilisations non-comestibles comme lubrifiant ou molécule plateforme dans la production de polymères et de plastiques. Cette thèse a pour but le développement de catalyseurs bimétalliques à base de métaux de transition (Cu et Ni) et d'un métal noble (Pd) supportés sur silice. Les principaux objectifs de ce travail sont la synthèse (par deux méthodes comparées) et les caractérisations de ces catalyseurs afin d'identifier les interactions métal support, l'optimisation des conditions réactionnelles à l'échelle du laboratoire, la modélisation cinétique et la transposition des catalyseurs à l'échelle industrielle pour une utilisation en réacteur pilote (proposition d'un schéma industriel, étude de faisabilité, bilans matière et chaleur).

Résumé en anglais

This industrial project concerns the study of the selective catalytic hydrogenation of vegetable oils (soybean oil and rapeseed oil), and the validation of the production technology, in order to maximize the oleic acid content and widen the range of its inedible uses as biodegradable lubricant or platform molecule in the production of polymers and plastics. This PhD aims to develop bimetallic catalysts based on transition metals (copper and/or nickel) and a noble metal (Pd) supported on silica. The main objectives of this work are the synthesis (by two compared methods) and the characterizations of these catalysts in order to identify the best metal-support interactions, the optimization of reaction conditions on a laboratory scale, the kinetic modeling and the transposition of the catalysts on an industrial scale for use in pilot reactors (proposal of an industrial scheme, feasibility study, material and heat balances).

Résumé de la thèse de doctorat

I. Introduction au sujet et aux problèmes de la recherche

Dans le cadre d'un programme de doctorat industriel financé (PON FSE FSESR 2014_2020 PhD with Industrial characterization), les recherches proposées concernent les thèmes de la chimie verte, en particulier l'étude de l'hydrogénation catalytique sélective des huiles végétales (huile de soja et huile de colza), afin de maximiser la teneur en acide oléique et d'élargir la gamme des utilisations non comestibles.

Cette étude se base sur l'intérêt croissant des pays développés (Amérique du Nord et Europe) pour les réglementations gouvernementales sur les composés d'origine biologique plus intensifs [1]. Parmi les composants bifonctionnels commercialisés pour les plastiques d'origine biologique, il faut également inclure l'acide sébacique et l'acide 11-aminoundécanoïque, tous deux issus de l'huile de ricin, ainsi que les acides azélaïque et pélargonique dérivés de l'acide oléique, finalement abordés dans ces travaux.

L'acide oléique, également appelé acide cis-9-octadécénoïque, est un acide carboxylique monoinsaturé à dix-huit atomes de carbone, il appartient à la série des oméga-9. Il possède les caractéristiques requises pour être utilisé comme lubrifiant biodégradable et constitue un élément de base dans la production de polymères et de plastiques à partir de ressources renouvelables, en remplacement et/ou en complément de ceux obtenus à partir d'huiles minérales. Il est considéré comme un élément de base de la chimie verte des polymères et son

utilisation dans l'industrie devrait augmenter. Cela stimule la R & D en vue de l'optimisation des procédés de production. En Italie, il faut souligner l'engagement de la CNR sur le sujet [2].

L'intérêt spécifique pour l'acide oléique est justifié par sa stabilité en présence d'oxygène, ne se polymérisant pas spontanément, et le fait qu'il reste liquide même à basse température. Ces caractéristiques facilitent son utilisation industrielle dans des processus de transformation continue.

La production d'acide oléique est limitée et seules quelques huiles à forte teneur en acide oléique peuvent être utilisées (huile de tournesol ou huile de tournesol OGM), ce qui limite la disponibilité de l'acide oléique sur le marché. Une revue de la littérature a révélé comment appliquer l'hydrogénation sélective à toutes les huiles courantes sur le marché. Les triglycérides et les esters méthyliques peuvent également être hydrogénés.

Le principal défi de cette étude est représenté par l'application d'un catalyseur hétérogène qui permet de saturer les doubles liaisons disponibles dans les acides gras en C18, tels que C18:2 (acide linoléique) et C18:3 (acide linolénique), avec une faible formation de l'acide saturé correspondant (acide stéarique C18:0) et un rendement maximal de C18:1. Actuellement, les catalyseurs à base de Ni ne permettent pas un faible pourcentage de C18:0, ils sont couramment utilisés en hydrogénation complète dans l'industrie alimentaire.

Nos activités de recherche ont porté sur l'étude d'un procédé catalytique sélectif pour l'hydrogénation d'huiles végétales naturelles et la validation de la technologie de production, toujours à l'échelle du laboratoire, en étudiant les techniques les plus récentes tant pour la préparation que pour la caractérisation des catalyseurs, en particulier les catalyseurs non nobles (cuivre (Cu) et nickel (Ni)) et les catalyseurs nobles (Pd, Rh, Ru et Pt), cités dans la littérature sur l'hydrogénation sélective.

En outre, pendant la période industrielle du programme de doctorat, il était prévu de réaliser le développement et l'optimisation de l'ensemble du système de processus d'innovation à mettre en œuvre autour du réacteur, l'évolution des utilités et des coûts de production de l'huile enrichie en acide oléique.

Dans le cadre d'une large étude sur l'hydrogénation des huiles végétales, Zaccheria et al. ont montré comment l'hydrogénation des huiles de canola et de soja permettait d'obtenir de faibles niveaux d'acides saturés et d'isomères trans avec un catalyseur à base de cuivre préparé par imprégnation sur un support de silice amorphe [3]. D'autres auteurs ont utilisé différents types de catalyseurs, à base de palladium [4] et de nickel [5], en jouant sur les conditions opératoires pour obtenir une faible teneur en produits indésirables.

II. Matériels et méthodes

Dans cette thèse, un catalyseur commercial et 11 catalyseurs synthétisés ont été testés dans un réacteur d'hydrogénation à l'échelle du laboratoire pour hydrogéner sélectivement les huiles de tournesol et de canola:

- le catalyseur commercial est un catalyseur Lindlar de Sigma-Aldrich, 4-5% Pd supporté sur du carbonate de calcium, pour augmenter la sélectivité le catalyseur a été dopé avec de l'oxyde de plomb qui modifie les sites actifs du catalyseur Lindlar;
- un autre catalyseur à base de Pd, le Pd supporté sur hydrotalcite (1% Pd/HT), a été synthétisé avec une méthode proposée par Di Nicola et al. [6] ; dans cette méthode, la réduction du Pd est obtenue en réagissant avec du cyclohexène;
- deux catalyseurs à base de cuivre (5% et 10% en poids) sur oxyde de silicium ont été synthétisés par deux méthodes de synthèse proposées par Yujun et al. (Hydrolyse-Précipitation notée - HP) [7] et par Liang-Feng et al. (Ammoniac-Evaporation notée - AE) [8];
- afin d'améliorer l'activité des catalyseurs tout en maintenant la sélectivité à l'acide oléique, des catalyseurs bimétalliques cuivre-nickel ou cuivre-palladium ont été synthétisés. Le nickel et le palladium sont des phases plus actives dans l'hydrogénation des acides gras que le cuivre. Les échantillons bimétalliques de cuivre-palladium et de cuivre-nickel ont été préparés par les deux mêmes méthodes que celles utilisées pour les échantillons de cuivre : Hydrolyse-précipitation (HP) [7] et évaporation d'ammoniac (AE) [8]. Il a également été décidé de synthétiser des échantillons monométalliques de palladium et de nickel pour les comparer avec des échantillons bimétalliques.

Les catalyseurs ont été caractérisés par analyse élémentaire (ICP), diffraction des rayons X (DRX), adsorption de N_2 (BET), réduction programmée de la température (TPR), spectroscopie Raman, spectroscopie FTIR, spectrométrie photoélectronique à rayons X (XPS), microscopie électronique à balayage avec spectroscopie à rayons X à dispersion d'énergie (SEM-EDS) et microscopie électronique à transmission (TEM). Les catalyseurs réduits ont également été caractérisés.

Les essais d'hydrogénation sélective ont été effectués dans un réacteur de laboratoire, le cœur de ce système est un réacteur Parr Instrument 4560 (600 ml) fonctionnant en mode semi-batch, alimentant l'hydrogène en

continu. Afin d'analyser la composition à différents temps de réaction, des échantillons ont été prélevés dans le réacteur, transestérifiés par une méthode standardisée [9] et analysés par GC-FID. Le chromatographe en phase gazeuse utilisé était un GC VARIAN 3400 équipé d'un détecteur FID, d'un injecteur Split/Splitless et d'une colonne capillaire Supelco SP-2380 conçue pour l'analyse des esters méthyliques d'acides gras (FAME) ; l'analyse a été réalisée dans des conditions isothermes à 180 °C, avec un détecteur et un injecteur à 220 °C avec de l'azote comme gaz vecteur. Le débit de la colonne Split/Splitless était de 25 ml/min.

Afin de développer la procédure d'hydrogénation et la méthode d'analyse du produit, certains tests ont été effectués avec un catalyseur commercial, le catalyseur Lindlar (Pd réduit supporté par du carbonate de calcium empoisonné au plomb), normalement utilisé pour les réactions d'hydrogénation. Des échantillons d'huile de tournesol et d'huile de colza ont été utilisés comme réactifs (voir tableaux 1 pour les compositions avant réaction).

Tableau 1 Composition de l'huile de colza de canola et de l'huile de tournesol.

Huile végétale	C18:0%	C18:1*c*%	C18:1*t* %	C18:2%	C18:2 isom%	C18:3%	Indice d'iode
Canola	1.3	67.8	0.0	20.5	0.1	10.3	121
Tournesol	2.8	32.5	0.0	64.5	0.0	0.2	140

Les performances de réactivité ont été évaluées en termes de conversion de l'acide linolénique (le cas échéant), de conversion de l'acide linoléique et de variation de l'indice d'iode. Afin d'évaluer la sélectivité envers divers acides, un simple schéma de réactions en série du pseudo premier ordre, omettant l'isomérisation des doubles liaisons, a été pris en compte [10].

III. Caractérisation des catalyseurs

Pour le catalyseur Lindlar, l'analyse ICP-AES a déterminé que la teneur en palladium avant le test est conforme aux valeurs indiquées par le fournisseur (Pd = 4,5%). De même, les teneurs en plomb et en calcium sont conformes aux valeurs précédemment indiquées dans la littérature [11–14].

Les courbes d'adsorption de N_2 permettent d'identifier un matériau macroporeux (isotherme de type II). Les isothermes ont une petite hystérésis de type H3, cette forme isotherme est rapportée dans la littérature comme pseudo-type II. Il a été possible d'évaluer une faible surface (S_{BET} 4,12±0,09 m2/g, V_{BJH} 7,81±0,05 mm^3/g et taille moyenne des pores 7,21±0,87 nm) par les méthodes BET-BJH ; étant donné la macroporosité de ce

matériau, la faible surface mesurée et la particularité de l'application de la méthode BET pour les matériaux mésoporeux, cette détermination de la taille moyenne des pores peut être considérée comme une estimation indicative [15].

La principale phase cristalline identifiée par diffraction des rayons X est le carbonate de calcium, les autres phases contenant du palladium ou du plomb sont impossibles à identifier soit parce que les raies de carbonate de calcium les recouvrent soit parce que la teneur de ces éléments est trop faible.

Dans les mesures ICP-AES effectuées sur des matériaux synthètisés, la teneur nominale en Pd est désignée par la teneur en palladium métallique. En fait, la dernière étape de la préparation du Pd/HT est la réduction par le cyclohexène comme indiqué précédemment. Les valeurs nominales du rapport molaire Mg/Al et la teneur en Pd sont confirmées. La présence de la phase hydrotalcique a été confirmée par DRX.

Les courbes d'adsorption de N_2 permettent d'identifier un matériel mésoporeux (isotherme de type IV). A partir de la forme de la boucle d'hystérésis, il est possible d'établir une boucle d'hystérésis de type H3; ce type d'isothermes est généralement associé à des agrégats de particules en plaques, par exemple certaines argiles, mais aussi des réseau de pores qui consistent en quelques macropores, non remplis de condensat. Les courbes permettent d'évaluer une S_{BET} 50.7±0.5 m^2/g, un V_{BJH} 0.25±0.02 cm^3/g, et une taille moyenne de pore de 19.92±0.32 nm. En étudiant le diagramme BJH, le catalyseur montre des pores dans la zone mésoporeuse mais aussi quelques macro-pores (entre 50 nm et 100 nm). Bien que certaines micro-porosités soient présentes, elles ne sont pas significatives dans le volume des pores.

Dans le tableau 2, les mesures de la teneur en métaux par ICP-AES sont comparées aux charges théoriques introduites lors de la synthèse. Les teneurs nominales des métaux sont rapportées aux teneurs réelles en métaux des échantillons, les variations des teneurs métalliques peuvent être attribuées à l'erreur expérimentale.

Tableau 2 Compositions élémentaires de catalyseurs à base de silice.

Échantillon	**Charges nominales**			**Mesures ICP-AES**		
	Cu [%]	**Ni [%]**	**Pd [%]**	**Cu [%]**	**Ni [%]**	**Pd [%]**
$Cu5SiO_2HP$	5	0	0	5.8±0.2	0	0
$Cu10SiO_2HP$	10	0	0	10.8±0.3	0	0
$Cu5SiO_2AE$	5	0	0	6.5±0.1	0	0

$Cu10SiO_2AE$	10	0	0	11.7±0.2	0	0
$Cu10Ni5SiO_2HP$	10	5	0	8.3±0.2	4.4±0.1	0
$Cu10Pd1SiO_2HP$	10	0	1	8.5±0.2	0	0.79±0.05
$Cu10Ni5SiO_2AE$	10	5	0	8.9±0.2	4.6±0.1	0
$Cu10Pd1SiO_2AE$	10	0	1	8.7±0.2	0	0.59±0.04
$Ni5SiO_2HP$	0	5	0	0	3.9±0.1	0
$Pd1SiO_2HP$	0	0	1	0	0	0.66±0.04
$Ni5SiO_2AE$	0	5	0	0	4.7±0.1	0
$Pd1SiO_2AE$	0	0	1	0	0	0.58±0.02

Les courbes expérimentales d'adsorption et de désorption de N_2 ont la même forme pour tous les matériaux synthétisés (tableau 3) : entre le type II et le type IV(a) de la classification IUPAC des isothermes de physisorption [15].

Tous les matériaux synthétisés dans ce travail présentent une boucle d'hystérésis, corroborant l'hypothèse de la présence de mésoporosité. La boucle d'hystérésis, qui présente des caractéristiques à la fois du type H2(a) et du type H2(b) selon la classification de l'UICPA, est associée à des structures complexes dans lesquelles il existe un effet de réseau entre les pores. Ce type de boucle d'hystérésis H2(a) est par exemple observé pour de nombreux gels de silice, des verres poreux, ainsi que pour la silice SBA-16 et KIT-5, tandis que H2(b) est observé pour les mousses de silice mésocellulaire et certaines silices ordonnées après traitement hydrothermique [15].

La distribution des volumes de pores par rapport à la taille des pores (graphique BJH) montre que : pour les échantillons monométalliques, la majorité des pores se trouve dans la zone mésoporeuse, pour les bimétalliques, la majorité se trouve dans la zone mésoporeuse avec un croisement de queue de 50 nm, la valeur limite méso/macro.

Tableau 3 Mesure de la surface BET (S_{BET}), du volume cumulé de BJH ($V_{BJH,des}$) et du diamètre moyen des pores ($D_{av,BJH}$) pour les matériaux synthétisés.

Échantillon	S_{BET} **[m^2g^{-1}]**	$V_{BJH,des}$ **[cm^3g^{-1}]**	$D_{av,BJH}$ **[nm]**

Cu5SiO_2HP	342	1.58	18.7
Cu10SiO_2HP	359	1.71	20.3
Cu5SiO_2AE	208	0.55	10.6
Cu10SiO_2AE	256	0.69	10.8
Cu10Ni5SiO_2HP	277	0.59	10.0
Cu10Pd1SiO_2HP	225	0.81	14.9
Cu10Ni5SiO_2AE	263	0.53	6.41
Cu10Pd1SiO_2AE	194	0.61	12.3
Ni5SiO_2HP	332	0.69	14.2
Pd1SiO_2HP	321	0.95	10.8
Ni5SiO_2AE	311	0.69	8.9
Pd1SiO_2AE	274	0.55	8.0

La fraction nominale des métaux étant égale, les produits HP présentent une surface BET supérieure à celle des produits AE correspondants, ainsi que le volume des pores et le diamètre moyen. Les différentes tailles de pores peuvent jouer un rôle essentiel dans la diffusion intraparticulaire pendant la réaction. La surface inférieure dans le cas de l'AE peut s'expliquer par la température plus basse maintenue pendant la formation du SiO_2 et aussi par le pH différent pendant la formation de la structure cuivre-silice.

Les diffractogrammes de rayons X montrent les phases cristallines détectées dans les matériaux tels que synthétisés : tous les matériaux montrent la contribution d'une phase amorphe. Cela se produit parce que le support sur lequel les phases actives sont déposées est principalement composé de silice amorphe, SiO_2, les deux méthodes de synthèse donnent des diffractogrammes similaires (§3.3.3). La phase qui pourrait apparaître lors de la préparation des catalyseurs au cuivre, à partir de réactifs d'oxyde de silicium sous forme liquide ou colloïdale, peut être un phyllosilicate de cuivre, dans lequel le cuivre est très bien dispersé à l'intérieur de la matrice de silice, formant des liaisons chimiques entre Si et Cu. Les techniques FTIR et Raman sont utilisées pour confirmer la présence de phyllosilicates de cuivre et essayer de mieux caractériser la majeure partie de la phase amorphe.

La DRX (§3.3.3.1) détecte avec difficulté les phases qui sont formées par la combinaison de Cu et de Si, ce problème est finalement résolu par l'étude des spectres FTIR et Raman (§3.3.3.2) identifiant les chrysocolles (phyllosilicates de Cu). La même tendance est également observée pour les catalyseurs monométalliques de Ni : après le traitement thermique, on trouve une forme particulière de silicate de Ni (Pimelite) pour l'AE ; dans les catalyseurs monométalliques le Pd est sous forme d'oxyde. D'un point de vue morphologique, les deux méthodes de synthèse donnent deux structures externes différentes, en particulier AE semble être formée par des structures lamellaires lisses tandis que HP est beaucoup plus poreuse comme cela a également été observé le MEB (§3.3.7.1). Les images MEB montrent en revanche que dans la synthèse HP, certains cristaux de taille moyenne inférieure à 5 nm sont identifiables, les matériaux AE sont plus uniformes et on trouve moins de structure. Une information essentielle a été donnée sur la distribution des métaux qui semblent bien répartis sur le support.

Les échantillons de catalyseurs ont été analysés après réduction, les résultats de la TPR (§3.3.5.1) montrent que les matériaux présentent un seul pic de consommation de H_2 pour tous les échantillons, indépendamment de la méthode de synthèse. Ce pic se situe dans la zone indiquée dans la littérature pour la réduction des précurseurs d'oxydes métalliques. La surface de Cu a été étudiée par chimisorption de N_2O et a mis en évidence une surface plus élevée, et donc une dispersion plus importante, pour les échantillons HP que pour les échantillons AE.

La DRX après réduction des catalyseurs au cuivre montre la présence similtanée de cuivre métallique et de Cu_2O, avec des proportions respectives différentes selon la méthode de synthèse. En particulier, pour la méthode AE, les matériaux contiennent une quantité plus importante de Cu métallique. après réduction, les échantillons monométalliques au palladium et au nickel montrent respectivement du Pd et du Ni métalliques. Les mêmes conclusions obtenues par la méthode DRX se retrouvent également par la méthode XPS sur les matériaux réduits (§3.3.6) : différents rapports sont observés entre le Cu métallique et le Cu_2O à la surface des catalyseurs.

La morphologie après réduction met en évidence des petits cristaux de phase active bien répartis et de dimensions moyennes inférieures à 7 nm pour les deux synthèses.

Les catalyseurs bimétalliques sont également étudiés et présentent des caractéristiques intéressantes et uniques ; les DRX des matériaux tels que synthétisés sont similaires aux matériaux monométalliques, avec une

différence notable pour le Cu-Pd : les raies de diffraction X sont décalées sous l'effet de l'introduction de PdO dans la structure du CuO. Un effet similaire a été observé pour les échantillons réduits avec la formation de la structure CuPd, il faut préciser que pour la méthode HP, cette phase CuPd est plus facilement mise en évidence. Les températures de réduction des matériaux bimétalliques sont plus élevées que pour le catalyseur monométallique au Cu correspondant, ce qui indique une plus grande interaction avec le support. Cependant, les surfaces de cuivre sont conformes aux valeurs obtenues avec les catalyseurs monométalliques à base de Cu. Les catalyseurs bimétalliques partagent les mêmes caractéristiques XPS que les catalyseurs monométalliques Pd et Ni ; pour le Cu-Pd, la teneur en Cu^0 par rapport au Cu^+ est plus évidente, probablement en raison des structures CuPd.

Enfin, les caractéristiques morphologiques de ces matériaux ne s'écartent pas trop des caractéristiques des matériaux monométalliques ; il est important de dire qu'il est pratiquement impossible de différencier Cu et Ni ou Cu et Pd par une analyse EDS in situ ou par une caractéristique morphologique quelconque.

IV. Tests de réactivité

Les tests pour la procédure d'hydrogénation avec le catalyseur Lindlar ont été effectués en combinant deux niveaux de température de 60 °C et 180 °C sous deux niveaux différents de pression d'hydrogène de 4 ou 12 bars ; la quantité de catalyseur est de 4 mg de catalyseur/ml d'huile, de l'huile de canola a été utilisée. Un test dans des conditions moyennes, 120 °C à 8 bars, a également été effectué. Des échantillons d'huile ont été prélevés toutes les 30 minutes pendant 6 heures.

Lors de tests successifs, on a également testé différentes concentrations de catalyseur, à savoir 2 mg de catalyseur/ml et 1 mg de catalyseur/ml.

Ces essais préliminaires montrent que la meilleure conversion des composés polyinsaturés a été atteinte après 1 h à 180 °C et 4 bars : ces essais après 1 h ont permis d'atteindre un pourcentage relatif de C18:1 de 87 %, et des conversions de C18:3 et C18:2 respectivement de 42 % et 69 %. L'augmentation de la pression améliore légèrement ces conversions, mais davantage d'isomères trans ont été trouvés après la réaction.

Les effets du recyclage du catalyseur, de la concentration du catalyseur et du type d'huiles végétales ont été étudiés dans les mêmes conditions de fonctionnement (4 bars de H_2 et 180 °C) au cours de tests sur cinq cycles. Les tests cycliques montrent une perte d'activité du catalyseur au cours des cycles d'hydrogénation : un pourcentage relatif de C18:1 de 80%.

Les tests ont été effectués en utilisant une quantité moindre de catalyseur, 2 mg de catalyseur/ml et 1 mg de catalyseur/ml. Les résultats montrent qu'il est possible d'obtenir la même conversion des huiles végétales polyinsaturées avec un temps de réaction légèrement supérieur (de 1h avec 4 mg de catalyseur/ml à 2h avec 1 mg de catalyseur/ml).

Des essais ont été réalisés dans les mêmes conditions que pour le catalyseur Lindlar avec le catalyseur Pd/HT avec une quantité de catalyseur plus faible (de 2 mg de catalyseur/ml à 0,5 mg de catalyseur/ml), et en récupérant le catalyseur après le premier cycle. Les tests montrent que l'activité du catalyseur augmente après le premier cycle, ce qui suggère une activation ou une modification du catalyseur/support. Les résultats sont conformes aux tests avec le catalyseur Lindlar.

Les catalyseurs supportés sur silice, réduits à 450 °C, ont été testés à 180 °C et 200 °C sous une pression d'hydrogène de 4 bar ou 12 bar, la quantité de catalyseur était de 4 mg de catalyseur/mL d'huile, l'huile utilisée était de l'huile de canola. La même analyse GC des échantillons d'huile a été effectuée. Il apparaît que l'augmentation de la teneur en cuivre est favorable (180 °C/4 bar), puisque les teneurs en acides linoléique et linoléique passent respectivement de 53 % à 3 % et de 75 % à moins de 10 % et de 60 % à 48 %, pour l'acide linoléique (Figure 1).

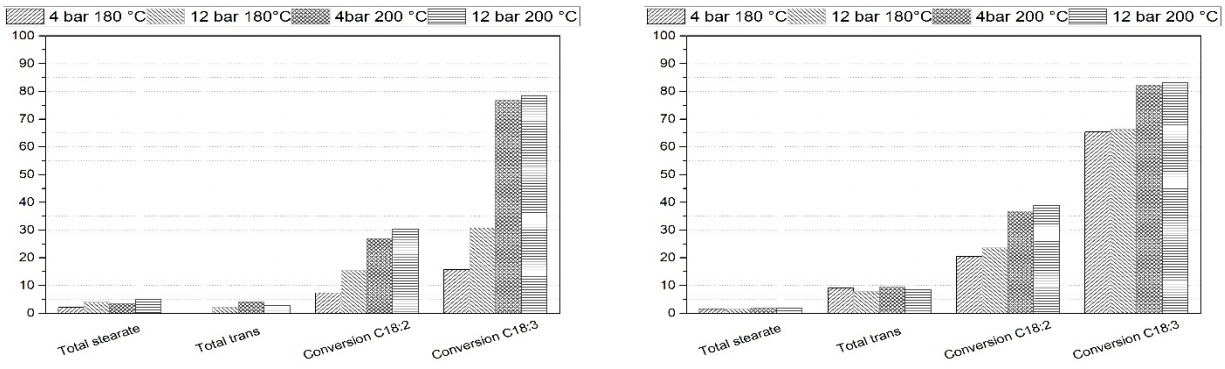

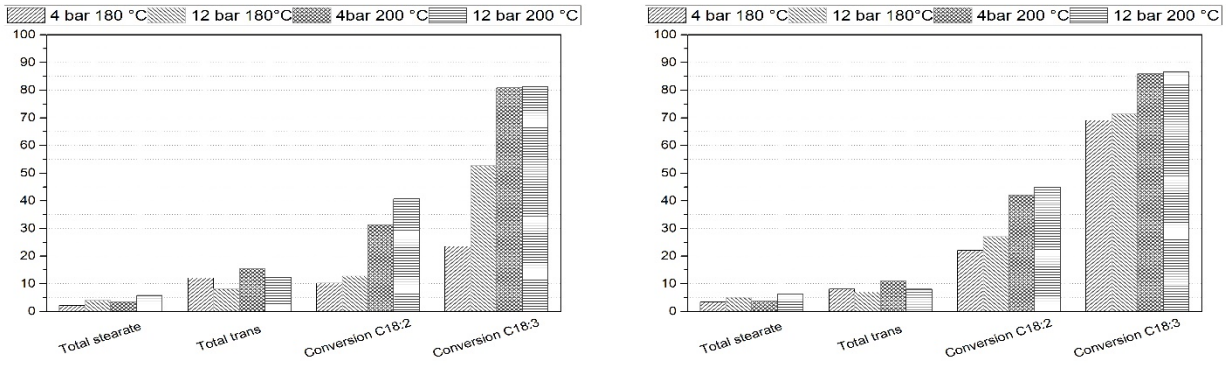

Figure 1 Conversion C18:2, conversion C18:3, isomères trans et acide saturé total de l'hydrogénation de l'huile de Canola sur un catalyseur à base de Cu à 10% (4 mg de catalyseur/mLoil) : dans le coin supérieur gauche Cu5SiO2AE, dans le coin supérieur droit Cu10SiO2AE, dans le coin inférieur gauche Cu5SiO2HP et dans le coin inférieur droit Cu10SiO2HP

Une augmentation de la température augmente légèrement l'activité du catalyseur à base de Cu (10%), tandis qu'une augmentation de la pression entraîne des améliorations plus marquée de la conversion, mais aussi la formation d'isomères géométriques à 4 bars. La comparaison avec des essais à une concentration plus élevée de catalyseur (8 mg de catalyseur/ml) est présentée en Figure 2 et Figure 3.

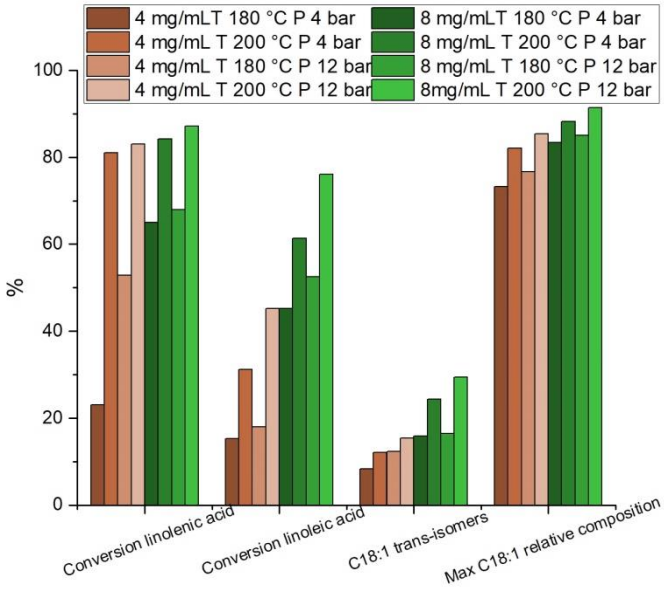

Figure 2 Résultats des tests pour le catalyseur Cu10SiO2AE.

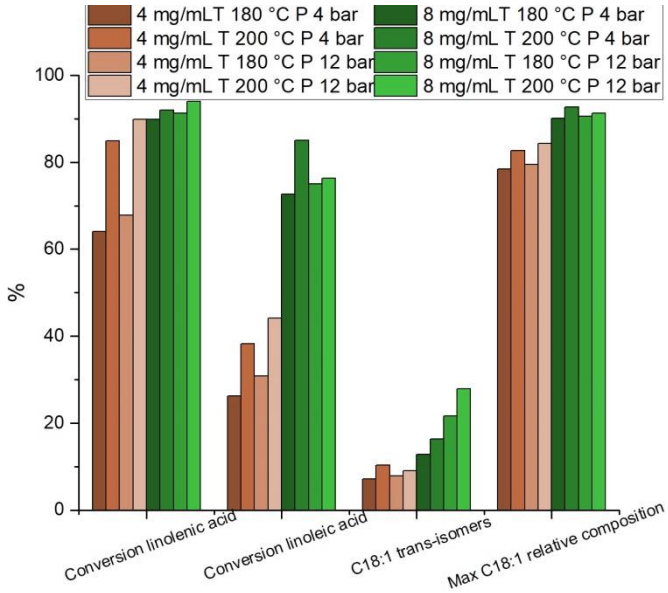

Figure 3 Résultats des tests pour le catalyseur Cu10SiO2HP.

Les résultats des tests suggèrent une meilleure performance globale du catalyseur HP par rapport au catalyseur AE, à une concentration de catalyseur plus élevée. Pour le catalyseur AE, la température et la pression sont toutes deux essentielles pour la conversion des C18:2 et C18:3, tandis que pour le catalyseur HP, l'effet de ces paramètres est moins important lorsque la concentration du catalyseur est augmentée.

La caractérisation DRX indique la formation de silicate de Ni, le cuivre étant sous forme de silicate ou d'hydroxyde et le palladium sous forme d'oxyde de palladium.

Après réduction de l'échantillon, la formation de Ni^0 et de $Cu+/Cu^0$ est observée, la présence des deux éléments et du silicate a également entraîné une augmentation de la température de réduction par rapport à la température de réduction des oxydes de Ni et de Cu (NiO et CuO). Alors qu'en présence de Pd et de Cu, une raie de diffraction a identifié la formation d'un alliage Cu-Pd, il n'y a pas de différence dans la température de réduction des différentes phases.

Des essais avec ces catalyseurs ont été effectués à 180 °C et 4 bars, avec 4 mg de catalyseur/mL d'huile de tournesol. Les principaux résultats sont résumés en Figure 4 et Figure 5.

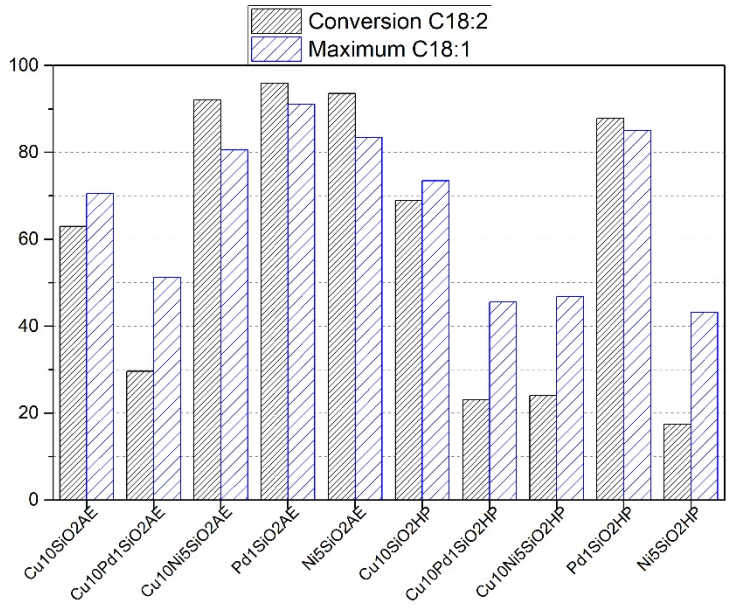

Figure 4 Conversion de C18:2 et pourcentage maximum de C18:1 à 180 °C et 4 bars.

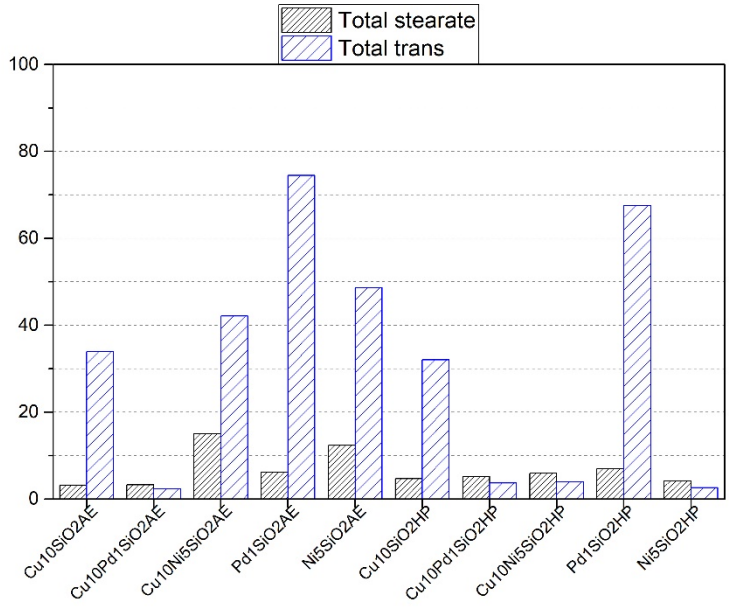

Figure 5 Sélectivité oléique Cis/trans et acide stéarique à 180 °C et 4 bars.

Les résultats des tests effectués sur des échantillons de Cu-Ni montrent que l'activité et la sélectivité des catalyseurs étudiés sont liées à l'activité du Ni. Dans le cas de la synthèse HP, la faible activité du Ni était probablement due à une réduction incomplète de l'échantillon.

Pour le catalyseur Cu-Pd, par rapport au catalyseur Pd monométallique, les résultats indiquent que la phase d'alliage trouvée après réduction n'est pas active vis-à-vis de l'hydrogénation de l'huile végétale à 180°C et 4 bars.

En conclusion, le catalyseur Lindlar commercial et le 1% Pd/HT peuvent hydrogéner des huiles végétales en peu de temps, en maintenant une bonne concentration d'acide oléique avec peu de formation d'isomères trans. Les catalyseurs au cuivre ont des propriétés intéressantes, produisant de petites quantités d'isomères trans et d'acide stéarique. Cependant, pour atteindre une conversion élevée, la concentration de catalyseur dans l'huile doit être augmentée. Dans l'ensemble, la méthode de synthèse HP conduit à des catalyseurs qui présentent de meilleures performances que les catalyseurs issus de la méthode de synthèse AE.

Afin d'augmenter l'activité du Cu, une autre phase active a été ajoutée mais les résultats suggèrent que la seconde phase est trop active (Ni) ou qu'en se combinant avec le Cu, elle ne participe pas à la réaction (Pd).

Tous les résultats sont exploités pour les simulations, la conception industrielle et l'optimisation économique de l'ensemble du processus. Le meilleur catalyseur a ensuite été choisi pour réaliser une conception plus détaillée du processus. Pour ce catalyseur, le $Cu10SiO_2HP$, une installation semi-continue a été conçue pour toutes les opérations : le réacteur fonctionne dans des conditions discontinues alimentant la charge de pétrole et les autres opérations telles que les échangeurs de chaleur, la récupération de chaleur, la filtration des catalyseurs, les séparations gaz-liquide, fonctionnent en continu avec deux réservoirs de retenue où le pétrole est accumulé pendant le temps de réaction (3 h par conception).

V. Application industrielle

Dans la pratique industrielle, la réaction d'hydrogénation est réalisée à la fois dans des réacteurs discontinus et continus. Cependant, la majorité des installations d'hydrogénation, dans le cas de l'hydrogénation complète (IV finale < 0,5) comme dans celui de l'hydrogénation partielle (60 < IV < 85), sont généralement construites en configuration discontinue. Ceci est dû à une série d'avantages opérationnels de l'hydrogénation par batch par rapport à l'hydrogénation en continu.

Le principal avantage de l'hydrogénation discontinue par rapport à l'hydrogénation continue consiste en un plus grand contrôle de la réaction et donc de la composition du produit final ; une meilleure sélectivité est obtenue dans les unités à réacteur discontinu et la flexibilité permettant de changer de matière première ou de produits en fonction de la demande du marché est possible. Souvent, les installations d'hydrogénation discontinue sont constituées d'unités de réacteur plus grandes, où la récupération de chaleur pour un lot pur

n'est pas toujours simple à réaliser, par conséquent, les coûts d'exploitation et d'investissement sont supérieurs à ceux d'un fonctionnement continu.

Il existe une autre possibilité de combiner l'unité de réacteur discontinu, et donc de maintenir la haute sélectivité de ce procédé, avec tous les autres équipements (échangeur de chaleur, séparation gaz-liquide, etc.) fonctionnant en continu, ce qui permet d'avoir le meilleur des deux technologies, en récupérant facilement la chaleur des flux, ce qui réduit les coûts opérationnels de cette application. Cela est possible en utilisant différents récipients de retenue.

L'application industrielle étudiée avec le partenaire industriel du projet, Processi Innovativi Srl, a été développée à partir des résultats obtenus pour le catalyseur $Cu10SiO_2HP$. Elle a notamment été réalisée à 200 °C sous 4 bar de H_2 avec 4 mg de catalyseur/mL et à 200 °C sous 4 bar de H_2 mais avec 8 mg de catalyseur/mL, pendant 180 minutes.

L'installation d'hydrogénation conçue est exploitée par lots pour l'unité de réaction, bien que le procédé semi-continu ait été pris en compte car il permet de récupérer de la chaleur et de réduire les coûts d'exploitation globaux par rapport à l'hydrogénation pure par lots, et donc les autres équipements de l'installation sont exploités en continu. En outre, afin d'améliorer le transfert de masse, le réacteur en boucle a été choisi, pour assurer un mélange élevé entre la phase liquide et la phase gazeuse avec une faible consommation d'énergie.

L'installation industrielle conçue peut traiter aussi bien des huiles végétales que leurs dérivés (évidemment, dans le second cas, les bilans de masse changent). L'huile végétale stockée est introduite dans l'installation dans des conditions de contrôle du débit et est préchauffée jusqu'à 160 °C en récupérant une partie de la chaleur de l'effluent hydrogéné.

La température de réaction finale est atteinte en faisant recirculer le produit dans un dégazeur/réservoir dans un échangeur de chaleur. L'huile échange de la chaleur avec de la vapeur.

La charge est envoyée au réacteur par lots et, en même temps, la quantité requise de catalyseur est mélangée à une quantité préétablie d'huile fraîche, et introduite dans le réacteur, maintenu sous vide. L'hydrogène s'écoule ensuite dans le réacteur, sa masse étant régulée par débitmètre massique. Le réacteur est équipé d'un système spécial de mélange catalyseur/produit hydrogène qui permet un transfert de masse efficace et un contact hydrogène/huile.

La température de la réaction est contrôlée en chauffant/refroidissant le produit dans un échangeur de chaleur. Cette étape est réalisée en faisant circuler de l'eau à partir d'un tambour à vapeur. De cette façon, la chaleur de l'hydrogénation est éliminée, ce qui génère de la vapeur à basse pression.

Une fois le cycle d'hydrogénation terminé, le produit est déchargé dans un réservoir à gouttelettes d'où il est extrait en continu et refroidi dans l'échangeur de récupération de chaleur.

Enfin, le produit hydrogéné est filtré pour éliminer le catalyseur du produit hydrogéné.

La taille de l'installation pour cette application était de 2,4 tonnes d'huile végétale ou d'EMAG ou d'acides gras, ce qui a été choisi sur la base d'une unité d'hydrogénation de taille standard pour l'hydrogénation complète qui est d'environ 20 tonnes par lot avec une production quotidienne de 100-120 tonnes de produits durcis. Comme le produit, dans ce cas, n'a pas de véritable contrepartie sur le marché des graisses hydrogénées, la conception a été faite sur la base d'une usine pilote à petite échelle.

La réaction d'hydrogénation est réalisée, comme mentionné ci-dessus, pendant 3 heures; toutes les procédures secondaires de chargement/déchargement et de nettoyage du réacteur entre une opération d'hydrogénation et la suivante sont supposées prendre près d'une heure. Ainsi, le cycle d'hydrogénation prend près de quatre heures pour être achevé.

Les coûts totaux de l'installation industrielle décrite ci-dessus ont été estimés à partir de la conception et des spécifications de conception des différentes unités présentes (tableau 4). En ce qui concerne les coûts et les recettes par lot de production unique, une estimation a été réalisée sur la base des bilans matière et énergie des différents flux concernés (tableau 5). En utilisant le ROI (retour sur investissement) modifié comme indicateur de la faisabilité d'une installation présentant ces caractéristiques, on a constaté que l'installation est parfaitement réalisable puisque le ROI est non seulement faisable mais est égal à 1,79, ce qui signifie que le retour sur investissement se produit au cours de la deuxième année d'exploitation.

Tableau 4 Répartition des coûts d'investissement totaux selon les règles de Timmerhaus [16]

Coût de l'investissement	**€**	
Coût de l'équipement (CE)	365000 €	
Coût d'installation	36500 €	10% EC
Tuyauterie, instruments et contrôles	73000 €	20% EC
Système électrique	18250 €	5% EC
Total des coûts directs TDC	**495000 €**	

Ingénierie, supervision, chantier	49000	10% TDC
Dépenses de construction	24750	5% TDC
Total des coûts directs + indirects	**570000 €**	
Honoraires du contractant	68500	12% TDC+TIC
Contyngencies	28500	5% TDC+TIC
Fonds de roulement (investissement total)	**667000 €**	

Tableau 5 Calcul du retour sur investissement modifié (ROIm)

Entrées		**m.u.**
Revenus des ventes	4392000	**€**
Coûts	3060000	**€**
R-C	**1332000**	**€**
Amortissement (linéaire sur 5 ans)	133400	**€**
ROI_m= (Revenus Net)/CAPEX	**1,79**	

VI. Conclusions

Parmi tous les catalyseurs, le catalyseur de cuivre sur silice synthétisé par la méthode HP a été identifié comme étant le meilleur candidat pour une application industrielle, ainsi un processus préliminaire et une étude de faisabilité ont été réalisés.

Il a été choisi pour développer un procédé semi-continu afin de bénéficier à la fois des avantages de la sélectivité d'un réacteur discontinu et des coûts d'exploitation plus faibles d'un fonctionnement continu. Le réacteur d'hydrogénation était un réacteur à boucles discontinues qui convertit l'huile de colza ou les acides gras produits à partir de l'huile de colza. L'opération est réalisée dans des conditions isothermes pour maintenir la sélectivité du catalyseur, la chaleur de réaction a été utilisée pour la production de vapeur à basse pression. Comme première hypothèse, le catalyseur est récupéré et réutilisé en 5 cycles (un jour ouvrable).

La faisabilité économique du procédé a été démontrée dans ces conditions.

La thèse permet de mettre en évidence quelques points d'intérêt importants qui doivent être étudiés dans les travaux futurs :

I. La réutilisation du catalyseur est un point clé pour la faisabilité économique de l'ensemble du processus, elle doit être abordée et certains tests avec le catalyseur $Cu10SiO_2HP$ avec récupération seront effectués ;

II. Il est évident que l'augmentation du rendement du catalyseur permet d'augmenter encore les revenus de ce procédé, l'augmentation du rendement du catalyseur au cuivre doit être un point central de la recherche future ;

III. L'étude d'un catalyseur plus actif doit être menée pour améliorer le processus : la synthèse de catalyseurs bimétalliques, bien que ne donnant pas la caractéristique souhaitée, pourrait être modifiée en introduisant peut-être un par un les autres métaux. D'autres métaux devraient être pris en compte, ainsi que le Pd et le Ni utilisés en plus faibles quantités (principalement le nickel) ;

IV. D'autres supports devraient également être pris en compte, en particulier les zéolithes et d'autres matériaux structurés qui pourraient être intéressants pour le catalyseur destiné aux applications industrielles afin de surmonter les problèmes de diffusion intraparticulaire.

Bien qu'il ne soit pas extrêmement actif, le cuivre, par ses caractéristiques intrinsèques semble être la meilleure solution d'un point de vue économique par rapport au Pd.

Les études futures devraient également se concentrer sur la modélisation de la conception cinétique et du transfert de masse du réacteur d'hydrogénation. Un autre point pourrait être la modélisation CFD du réacteur en boucle validant les résultats du modèle avec des tests effectués avec un réacteur en boucle à l'échelle du laboratoire.

VII. Bibliography

[1] Oleic Acid Market, market research reports, market insights, future market insights. Mark Res Rep 2019. https://www.futuremarketinsights.com/reports/oleic-acid-market (accessed January 18, 2019).

[2] Ravasio N, Zaccheria F, Gargano M, Recchia S, Fusi A, Poli N, et al. Environmental friendly lubricants through selective hydrogenation of rapeseed oil over supported copper catalysts. Appl Catal A Gen 2002;233:1–6. doi:10.1016/S0926-860X(02)00128-X.

[3] Zaccheria F, Psaro R, Ravasio N. Selective hydrogenation of alternative oils: a useful tool for the production of biofuels. Green Chem 2009;11:462–5. doi:10.1039/b817625f.

[4] Pérez-Cadenas AF, Zieverink MMP, Kapteijn F, Moulijn JA. Selective hydrogenation of fatty acid methyl esters on palladium catalysts supported on carbon-coated monoliths. Carbon N Y 2006;44:173–6. doi:10.1016/j.carbon.2005.08.014.

[5] Jovanovic D, Radovic R, Mares L, Stankovic M, Markovic B. Nickel hydrogenation catalyst for tallow hydrogenation and for the selective hydrogenation of sunflower seed oil and soybean oil. Catal Today 1998;43:21–8. doi:10.1016/S0920-5861(98)00133-3.

[6] Di Nicola A, Arcadi A, Gallucci K, Mucciante V, Rossi L. Hydrotalcite-supported palladium nanoparticles as catalysts for the hydroarylation of carbon–carbon multiple bonds. New J Chem 2018;42:1952–7. doi:10.1039/C7NJ04046F.

[7] Zhao Y, Li S, Wang Y, Shan B, Zhang J, Wang S, et al. Efficient tuning of surface copper species of Cu/SiO2 catalyst for hydrogenation of dimethyl oxalate to ethylene glycol. Chem Eng J 2017;313:759–68. doi:10.1016/J.CEJ.2016.12.027.

[8] Liang-Feng C, Ping-Jun G, Ming-Hua Q, Shi-Run Y, He-Xing L, Wei S, et al. Cu/SiO2 catalysts prepared by the ammonia-evaporation method: Texture, structure, and catalytic performance in hydrogenation of dimethyl oxalate to ethylene glycol. J Catal 2008;257:172–80. doi:10.1016/J.JCAT.2008.04.021.

[9] IUPAC AOAC. AOAC Official Method 969.33 Fatty Acids in Oils and Fats: Preparation of Methyl Esters Boron Trifluoride Method 2000:2000.

[10] Philippaerts A, Jacobs P, Sels B. Catalytic Hydrogenation of Vegetable Oils. In: Rinaldi R, editor. Catal. Hydrog. Biomass Valorization. 1st ed., Royal Society of Chemistry RSC Energy and Environment Series; n.d., p. 223–41. doi:10.1039/9781782620099-00223.

[11] Lindlar H, Dubuis R. Palladium Catalyst for Partial Reduction of Acetylenes. Org Synth 1966;46:89–89. doi:10.1002/0471264180.os046.27.

[12] Mallát T, Szabó S, Petró J. The role of lead in the selectivity of palladium-lead (lindlar type) catalysts. Appl Catal 1987;29:117–23. doi:10.1016/S0166-9834(00)82611-1.

[13] Tripathi B, Paniwnyk L, Cherkasov N, Ibhadon AO, Lana-Villarreal T, Gómez R. Ultrasound-assisted selective hydrogenation of C-5 acetylene alcohols with Lindlar catalysts. Ultrason Sonochem 2015;26:445–51. doi:10.1016/J.ULTSONCH.2015.03.006.

[14] Rajaram J, Narula APS, Chawla HPS, Dev S. Semihydrogenation of acetylenes : Modified lindlar catalyst. Tetrahedron 1983;39:2315–22. doi:10.1016/S0040-4020(01)91960-X.

[15] Thommes M, Kaneko K, Neimark A V., Olivier JP, Rodriguez-Reinoso F, Rouquerol J, et al. Physisorption of gases, with special reference to the evaluation of surface area and pore size distribution (IUPAC Technical Report). Pure Appl Chem 2015;87:1051–69. doi:10.1515/pac-2014-1117.

[16] Peters MS, Timmerhaus KD. Plant design and economics for chemicals engineers. vol. 2. 4th editio. McGraw Hill International Editions; 1997. doi:10.4324/9780429046377-7.

Università degli Studi dell'Aquila

Dipartimento di Ingegneria Industriale
e dell'Informazione e di Economia

Université de Strasbourg -ICPEES

École decotorale des Sciences
Chimiques

Processi Innovativi S.r.l

THESIS

Presented to obtain the degree of

Dottore di ricerca
dell'università degli studi dell'Aquila
in
Ingegneria Industriale e dell'Informazione e di Economia, XXXII° ciclo

Docteur
de l'Université de Strasbourg
en
Chimie
Specialité :Catalyse hétérogène

Study of selective catalytic hydrogenation of triglycerides and their derivatives

Author

Umberto PASQUAL LAVERDURA

Supervisor

Dr. *Katia* GALLUCCI

Coordinator of the PhD in Industrial and Information engineering and economics

Prof. *Roberto* CIPOLLONE

Supervisor

Dr. *Claire* COURSON

Director of the Doctoral School of chemical sciences (ED-222)

Prof. *Petra* HELLWIG

A.A 2018/2019

PON RICERCA E INNOVAZIONE 2014 - 2020

UNIONE EUROPEA

MINISTERO DELL'ISTRUZIONE DELL'UNIVERSITÀ E DELLA RICERCA

Summary

Index of figures

Index of tables

List of acronyms

C14:0	Myristic acid
C16:0	Palmitic acid
C18:0	Stearic acid
C18:1	Monounsaturated C18 fatty acids
c-C18:1	Oleic acid
t-C18:1	Elaidic acid
iso-C18:2	Isomers of linoleic acid
C18:2	Linoleic acid
C18:3	Linolenic acid
C22:0	Erucic acid
FAME	Fatty Acids Methyl Esters
PUFA	Poly-Unsaturated Fatty Acids
Pd/HT	Palladium 1% hydrotalcite
AE	Ammonia Evaporation method
HP	Hydrolysis Precipitation method
GHGs	Green House Gases
IWI	incipient wetness impregnation
CH	chemisorption-hydrolysis method

PG	precipitation gel method
UHDP	urea hydrolysis deposition-precipitation
TEOS	tetra ethyl ortosilicate
ICP-AES	Ion Coupled Plasma – Atomic Emission Spectroscopy
CCD	charge coupled device, ICP-AES detector
BET	Brunauer-Emmett-Teller
BJH	Barrett-Joyner-Halenda
XRD	x-ray diffraction
PDF	powder diffraction files
ICDD	international centre of diffraction data
JCDPS	joint committee on powder diffraction standards
FWHM	full width at half maximum
FTIR-ATR	fast fourier transform infrared spectroscopy attenuated total reflectance
XPS	x-ray photoelectron spectroscopy
TPR	temperature programmed reduction
TCD	thermal conductivity detector
TPD-N_2O	temperature programmed desorption
SEM	scanning electron microscopy
BSE	back scattering electron
EDS	energy dispersive x-ray spectroscopy
TEM	transmission electron mycroscopy
STEM	scanning transmission electron mycroscopy
FID	flame ionization detector
GC	gas cromatography

GC-MS	gas chromatography coupled with mass spectrometry
SII	specific isomerization index
IV	iodine value

List of symbols

$J_{H_2}a$	hydrogen flux per area
R_{GL}	Gas-Liquid interface resistance
R_{LS}	Liquid-Solid Interface resistance
R_S	Intraparticle resistance
$k_L a$	mass transfer coefficient in liquid phase per area of transfer
$k_s a_s$	mass transfer in the liquid to solid interface for the area
ε_s	solid void degree
ρ_s	catalyst density
p_{H2}	partial pressure of hydrogen
η	effectiveness factor of the reaction
r_{H2}	rate of consumption of H_2
r_{TAG}	rate of reaction for tryglicerides
Φ_{TAG}	Thiele modulus for tryglicerides
d_p	particle size
$D_{TAG,eff}$	effective diffusivity of the oil
S_{BET}	BET surface area
V_{BJH}	volume of the pores
$D_{av,BJH}$	average pore size

P/P_0	equilibrium pressure divided per the saturation pressure at the boiling temperature of N_2
n_m	monolayer adsorbed quantity
C	BET constant
E_m	heat of adsorption for the monolayer
E_L	heat of liquefaction of N_2
R	gas constant
T	absolute temperature
σ_m	molecular cross-sectional area
L	Avogadro number
m	mass sample for BET
γ	surface tension of N_2
V_l	molecular volume of N_2
r_k	Kelvin radius
θ	diffraction angle
λ	wavelength of the incident x-ray wave
K	dimensionless shape factor of the crystallite
β	full width at half maximum
S_{Cu^0}	surface area of copper
V	absorbed volume of N_2O
Vm	molar volume of N_2O
m_{Cu}	Cu mass by ICP-AES
$\chi_{C18:2}$	conversion of linoleic acid
$\chi_{C18:3}$	conversion of linolenic acid
k_3	kinetic constant from linolenic to linoleic

k_2	kinetic constant from linoleic to oleic
k_1	kinetic constant from oleic to stearic
S_{Ln}	linolenic selectivity
S_{Le}	linoleic selectivity
T_{red}	reduction temperature

Abstract of the PhD thesis

In the framework of a funded industrial Ph.D programme (PON FSE FSESR 2014_2020 PhD with Industrial characterization), the proposed research concerns the topics of Green Chemistry, in particular the study of selective catalytic hydrogenation of vegetable oils (soyabean oil and rapeseed oil), in order to maximize the content of oleic acid and expand the range of non-edible uses.

Oleic acid, also known as cis-9-octadecenoic acid, is a monounsaturated carboxylic acid with eighteen carbon atoms, it belongs to omega-9 series. It has the suitable characteristics for use as biodegradable lubricant and is a building block in the production of polymers and plastics from renewable resources, to replace and/or alongside to those obtained from mineral oils. It is considered as a building block of the green polymer chemistry and its use in industry is expected to rise. This stimulates R & D towards the optimization of the production process. In Italy, must be emphasized the commitment of the CNR on the subject [1].

The specific interest towards oleic acid is justified by its stability in the presence of oxygen, not spontaneously polymerizing, and it remains a liquid even at low temperatures. These features facilitate the industrial use in continuous processes of transformation.

The oleic acid production is restricted and only some oils with high oleic acid content can be used (sunflower oil or OGM sunflower oil), limiting the availability of oleic acid on the market. A review of the literature has revealed how to apply selective hydrogenation to all the common oils on the market. Alternately, the triglycerides and methyl esters can be hydrogenated.

The main challenge of this study is represented by the application of heterogeneous catalyst which allows to saturate the double bonds available in C18 fatty acids, such as C18:2 (linoleic acid) and C18:3 (linolenic acid), with low formation of the corresponding saturated acid (stearic acid C18:0) and maximum yield of

C18:1. Currently, the Ni-based catalyst does not allow low percentage of C18:0, they are commonly used in complete hydrogenation in the food industry.

Our research activities concerned the study of a selective catalytic process for the hydrogenation of natural vegetable oils, and validation of the production technology, still at laboratory scale, studying the most updated techniques for both preparation and characterization of catalysts, especially non-noble catalysts copper (Cu) and nickel (Ni) and noble catalysts (Pd, Rh, Ru and Pt), cited in literature about selective hydrogenation.

In addition, during the industrial period of the Ph.D programme, it was expected to perform the development and optimization of the entire innovation process system to be implemented around the reactor, the evolution of the utilities and production costs of oleic acid-enriched oil.

In the framework of a wide literature about vegetable oils hydrogenation, Zaccheria et al. [2] have shown how hydrogenating canola and soybean oils can achieve low levels of saturated acids and trans isomers with a copper-based catalyst prepared by impregnation on an amorphous silica support. Other authors used different kinds of catalysts, both palladium [3] and nickel [4] based, playing on the operative conditions to obtain low content of unwanted reaction products.

In this thesis, both one commercial and 11 synthesised catalysts were tested in a hydrogenation laboratory scale plant to selectively hydrogenate sunflower and canola oil.

The catalysts were characterized by elemental analysis (ICP), X-ray diffraction (XRD), N_2 adsorption (BET), programmed temperature reduction (TPR), Raman spectroscopy, FTIR spectroscopy, X-ray photoelectron spectrometry (XPS), scanning electron microscopy with energy dispersive X-ray spectroscopy (SEM-EDS), and transmission electron microscopy (TEM). Reduced catalysts have also been characterized. Tests were carried out in a laboratory scale plant reactor, the core of this system is a Parr Instrument 4560 (600 mL) reactor unit operated in semi-batch mode, feeding the hydrogen continuously. In order to analyze the composition at different reaction times, samples were taken from the reactor and transesterified with a standardized method [5] and analyzed by GC-FID. The gas chromatograph used was a VARIAN 3400 GC equipped with FID detector, a Split/Splitless injector, and a Supelco SP-2380 capillary column designed for the analysis of Fatty Acids Methyl Esters (FAME); analysis was conducted in isothermal conditions at 180 °C, with detector and injector at 220 °C with nitrogen as carrier gas. The Split/Splitless flow was 25 mL/min.

In order to develop the hydrogenation procedure and the product analysis method, some tests were carried out with a commercial catalyst, **Lindlar catalyst** (reduced Pd supported on calcium carbonate poisoned with lead), normally used for hydrogenation reactions.

The tests were performed combining two levels of temperature 60 °C and 180 °C under two different levels of hydrogen pressure of 4 bar or 12 bar; the amount of catalyst is 4 $mg_{catalyst}/mL_{oil}$, canola oil was used (see Table 1 for starting composition of vegetable oils). A test under middle conditions, 120 °C at 8 bar, was also carried out. Oil samples were taken every 30 minutes for 6 hours.

In successive tests also different concentration of catalyst were tested 2 $mg_{catalyst}/mL_{oil}$ and 1 $mg_{catalyst}/mL_{oil}$.

Table Abs- 1 Composition of canola rapeseed oil and sunflower oil as received samples.

Vegetable oil	C18:0%	C18:1*c*%	C18:1*t* %	C18:2%	C18:2 isom%	C18:3%	Iodine Value
Canola	1.3	67.8	0.0	20.5	0.1	10.3	121
Sunflower	2.8	32.5	0.0	64.5	0.0	0.2	140

These preliminary tests show as the best conversion of polyunsaturated compounds were reached after 1 h at 180 °C and 4 bar: these test's results after 1 h reached relative percentage of C18:1 of 87%, C18:3 and C18:2 conversions are 42% and 69 %, respectively. Increasing the pressure slightly increases the conversions, but more trans isomers were found after the reaction.

The effects of catalyst recycling, catalyst concentration, and vegetable oils type were investigated at the same operative conditions (4 bar of H_2 and 180 °C) over five cycles tests. Cyclic tests show a catalyst loss of activity over hydrogenation runs: 80% of relative percentage of C18:1 with very close conversion of C18:2 and C18:3.

Tests were carried out using less amount of catalyst, 2 $mg_{catalyst}/mL_{oil}$ and 1 $mg_{catalyst}/mL_{oil}$. The results highlight how it is possible to obtain the same conversion of polyunsaturated vegetable oils with slightly higher reaction time (from 1h with 4 $mg_{catalyst}/mL_{oil}$ to 2 h with 1 $mg_{catalyst}/mL_{oil}$).

Another Pd based catalyst, **Pd supported on hydrotalcite** (1% Pd/HT), was synthesized with a method proposed by Di Nicola et al. [6]; in this method the reduction of the Pd is obtained reacting with cyclohexene. Tests were carried out in the same conditions than for Lindlar catalyst with a lower amount of catalyst (from

2 $mg_{catalyst}/mL_{oil}$ to 0.5 $mg_{catalyst}/mL_{oil}$), and recovering the catalyst after the first cycle. Tests show that the activity of the catalyst increases after the first cycle suggesting an activation or modification of the catalyst/support. The results are in line with Lindlar catalyst tests.

Two copper-based catalysts (5% and 10% by weight) on silicon oxide were synthesized by two synthesis methods proposed by Yujun et al. (Hydrolysis-Precipitation noted - HP) [7] and by Liang-Feng et al. (Ammonia-Evaporation noted - AE) [8].

These reduced catalysts were tested at 180 °C and 200 °C under a hydrogen pressure of 4 bar or 12 bar, the quantity of catalyst was 4 $mg_{catalyst}/mL_{oil}$, the used oil was canola oil. The same analysis GC of the oil samples was performed. It appears that the increase in copper content is favourable (180 °C/4 bar), since the conversions of linoleic and linoleic acids fall respectively from 53% to 3% and from 75% to less than 10% and from 60% to 48%, for linoleic acid, by increasing the copper content from 5 to 10% in AE synthesis and in HP synthesis, respectively (Figure 1).

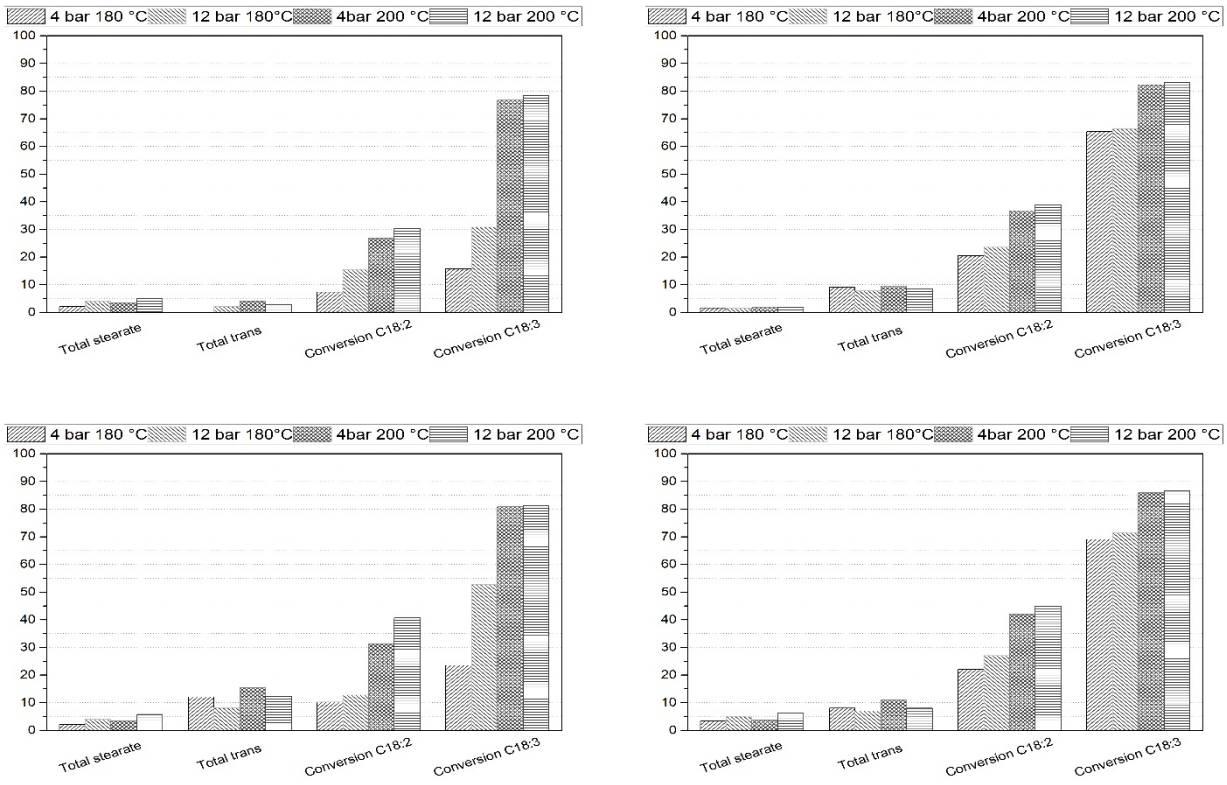

Figure 1 C18:2 conversion, C18:3 conversion, trans isomers, and total saturated acid of canola oil hydrogentation on 10% Cu-based catalyst (4 $mg_{catalyst}/mL_{oil}$): on the left top corner $Cu5SiO_2AE$, on the right top corner $Cu10SiO_2AE$, on the left bottom corner $Cu5SiO_2HP$ and on the right bottom corner $Cu10SiO_2HP$

An increase in temperature slightly increases the activity of the 10% Cu -based catalyst, while an increase in pressure leads to more evident improvements in conversion, but also the formation of geometric isomers at 4 bar. The comparison with tests at higher concentration of catalyst (8 $mg_{catalyst}/mL_{oil}$) is reported in Figure 2 and Figure 3.

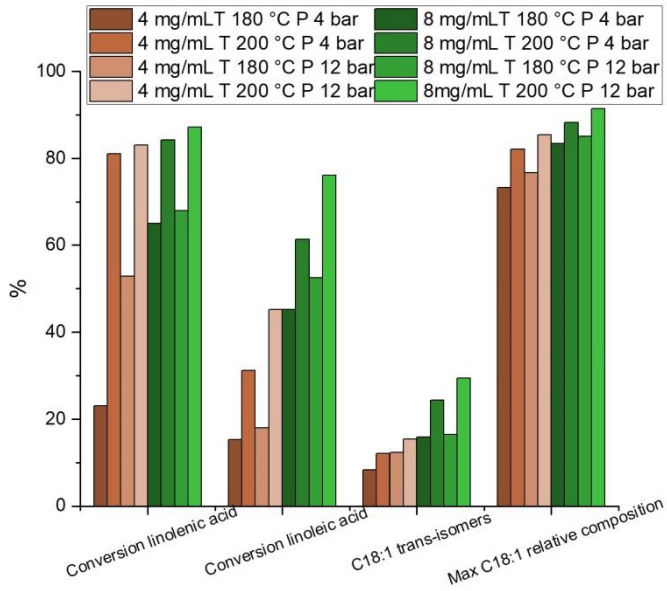

Figure 2 Tests results for Cu10SiO₂AE catalyst.

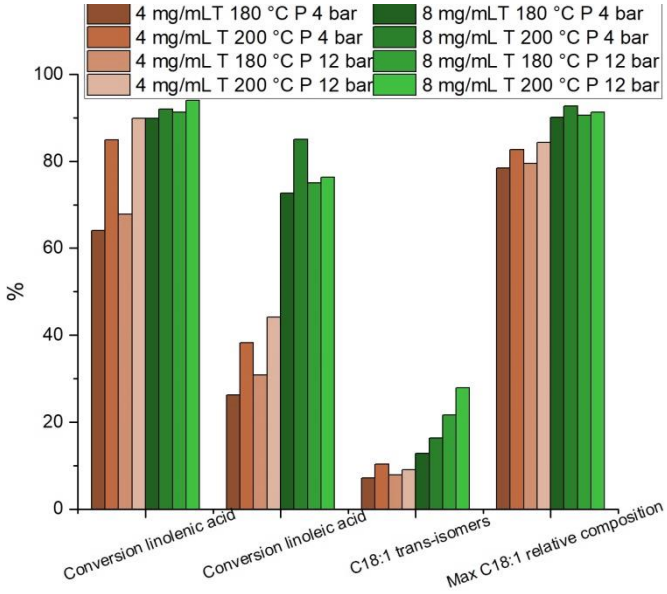

Figure 3 Tests results for Cu10SiO₂HP catalyst.

Tests' results suggest an overall better performance of HP catalyst over the AE catalyst, at higher catalyst concentration. For AE catalyst both temperature and pressure are essential for the conversion of C18:2 and

C18:3, while for HP catalyst the effect of these parameters is less important when the concentration of the catalyst is increased.

In order to improve the activity of the catalysts maintaing the selectivity to oleic acid, copper-nickel or copper-palladium **bimetallic catalysts** have been synthesized. Nickel and palladium are more active phases in fatty acid hydrogenation than copper. The bimetallic samples of copper-palladium and copper-nickel were prepared by the same two methods used for copper samples: Hydrolysis-Precipitation (HP) [7] and Ammonia-Evaporation (AE) [8].

It was also decided to synthesize monometallic samples of palladium and nickel to compare them with bimetallic ones.

XRD characterization indicates the formation of Ni silicate, with copper being in the form of silicate or hydroxide and palladium in the form of palladium oxide.

After sample reduction, the formation of Ni^0 and Cu^+/Cu^0 is observed, the presence of both elements and silicate also led to an increase in the reduction temperature compared to the reduction temperature of Ni and Cu oxides (NiO and CuO). While in the presence of Pd and Cu, a diffraction line has identified the formation of a Cu-Pd alloy, there is no difference in the reduction temperature of the different phases.

Tests with these catalysts were carried out at 180 °C and 4 bar, with 4 $mg_{catalyst}/mL_{oil}$ with sunflower oil. The main results are summarized in Figure 4 and Figure 5.

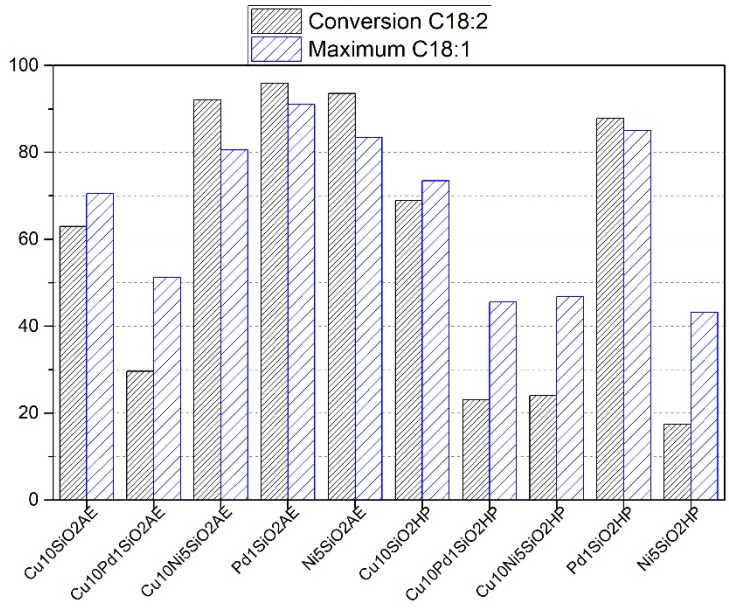

Figure 4 Conversion of C18:2 and maximum percentage of C18:1 at 180 °C and 4 bar.

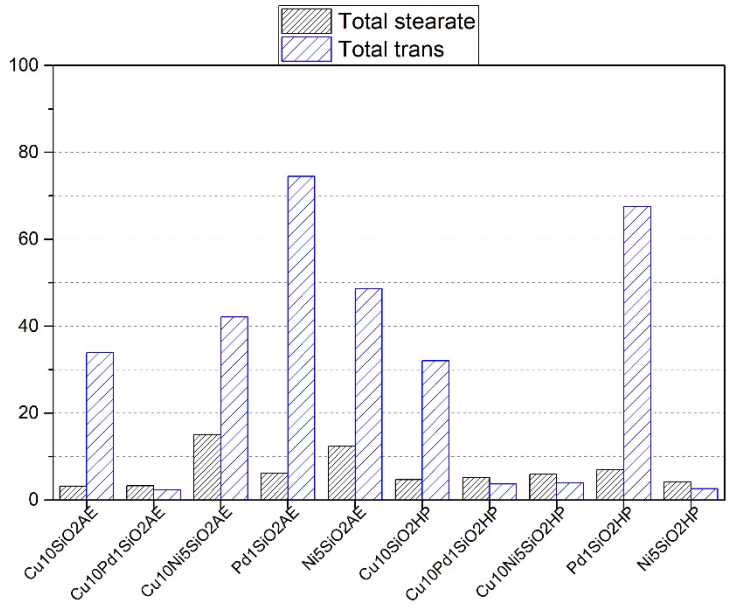

Figure 5 Cis/trans oleic selectivity and stearic acid at 180 °C and 4 bar.

The test results for Cu-Ni samples highlight that the activity and selectivity of the catalysts studied is linked to Ni activity. In the case of HP synthesis, the low activity of Ni was probably due to an incomplete reduction of the sample.

For Cu-Pd, in comparison to monometallic Pd, the results indicate that the alloy phase found after reduction is not active towards the hydrogenation of vegetable oil at 180°C and 4 bar.

In conclusion, the commercial Lindlar catalyst and the 1% Pd/HT can hydrogenate vegetable oils in short time, maintaining a good concentration of oleic acid with little formation of trans isomers.

The copper catalysts have interesting properties producing small amounts of trans isomers and stearic acid. However, in order to reach a high conversion, the concentration of catalyst in the oil must be increased. Overall the HP method shows better performances than AE catalysts.

In order to increase Cu activity, another active phase was coupled with Cu, but the results suggested that the second phase is too active (Ni) or in combination with Cu, it does not participate to the reaction (Pd).

All results are exploited for simulations, industrial design and economical optimization of the whole process, the best catalyst was then chosen to perform a more detailed process design. For this catalyst, $Cu10SiO_2HP$, a semi-continuous plant was designed in all the operations: the reactor is operated in batch conditions feeding the charge of oil and the other operations such as heat exchangers, heat recovery, catalysts filtration, gas-liquid separations, are operated continuously with two hold-up tanks where the oil is accumulated during the reaction time (3 h by design).

Future work on this subject must concentrate on the enhancement of catalysts activity and selectivity which are strongly affecting the industrial performances and the feasibility of a chemical plant for the selective hydrogenation of vegetable oils. One possible solution is the implementation of zeolites as supports. From the active phase point of view for copper the reusability of the catalyst must be confirmed in multiple consecutive hydrogenation tests studying the poisoning effects for this type of catalyst. Poisoning has an important role in the post-treatment of hydrogenated oils.

The introduction of a second transition metal must be exploited more in details, also trying different synthesis methods in which copper and the second metal are deposited in two different steps of the synthesis or on different supports (alumina or zeolite).

Chapter 1

Introduction to the research subject and issues

This chapter gathers information about the subject of this thesis, the selective hydrogenation of vegetable oils and their derivates, providing background and highlighting the significant issues faced in the next chapters.

1.1. Environmental issues of the planet

The impact severity of climate change on health is increasingly clear. Climate change is the greatest challenge of the 21st century, threatening all aspects of the society in which we live [9]. The drivers of climate change – principally fossil fuel combustion – pose a heavy burden of disease, poverty and are a grave menace to life as we know it.

The air pollutants which are causing ill-health, and the greenhouse gases (GHGs) that are causing climate change, are emitted from many of the same sectors, including energy, housing, transport and agriculture. Short-lived climate pollutants (including black carbon, methane and ozone) have important impacts on both climate and health [10].

The Paris Climate Agreement, signed at COP21, is a global safeguard for the planet and human health. It specifies that "Parties should, when taking action to address climate change, respect, promote and consider their respective obligations on the right to health" and recognizes the central role of "mitigation actions and their co-benefits for adaptation, health and sustainable development" in enhanced action before 2020 [11]. At this date, 183 countries have signed the Paris Agreement.

Linked to climate change is also the increasing pollution registered; the products obtained by industrial activities often remain in the environment as wastes and can persist for long periods, one example is obviously plastics. More viciously often these wastes can affect health and the environment aggravating the problem.

The issues of the planet are in a strong way also affected by the continuously growing population, every action on climate or environment "must last and take" into account also how this complex system is linked to the vast increasing numbers of human being [12].

The environmental problem of earth is vast and will impact every aspect of our future as a species and to address the problem a change in paradigm is necessary.

1.1.1. Climate change [13]

Earth climate has changed throughout the long eras of the planet history. During the short period (relatively speaking) our species (*H. Sapiens*) lived on the planet, about 130000 years [14], seven major glaciations in the last 65000 years changed the overall temperature of the planet, the last abruptly ending 11500 years ago (Younger Dryas), leading to the modern climate era and therefore to human civilization [15].

Nevertheless, the global warming trend measured since the second half of 20th century is of noteworthy relevance, as it shows an unprecedented rate over decades to millennia and is extremely likely the result of contribution from anthropogenic activities to the greenhouse-effect [15–22].

The causality relationship between human activities and climate-warming trend over the past century is acknowledged by the 97% per cent of climate scientists, and most leading organizations worldwide have endorsed this position [16–21,23], and also a large part of the population starts to accept the scientific community view [24–26].

The greenhouse-effect (Figure 1-1) consists in the trapping of light radiation in the 4-100 μm longwave field emitted by the Earth's surface, mainly brought about by water vapor, with a substantial contribution from

CO_2 and smaller contributions by other gases, e.g. CH_4, N_2O, O_3 [27]. The presence in Earth's atmosphere of these gases, also known as greenhouse gases (GHG), has made the planet habitable by life as we know it, since they raised the average global temperature by roughly 30 °C, as opposed to the estimated -15 °C without an atmosphere [27].

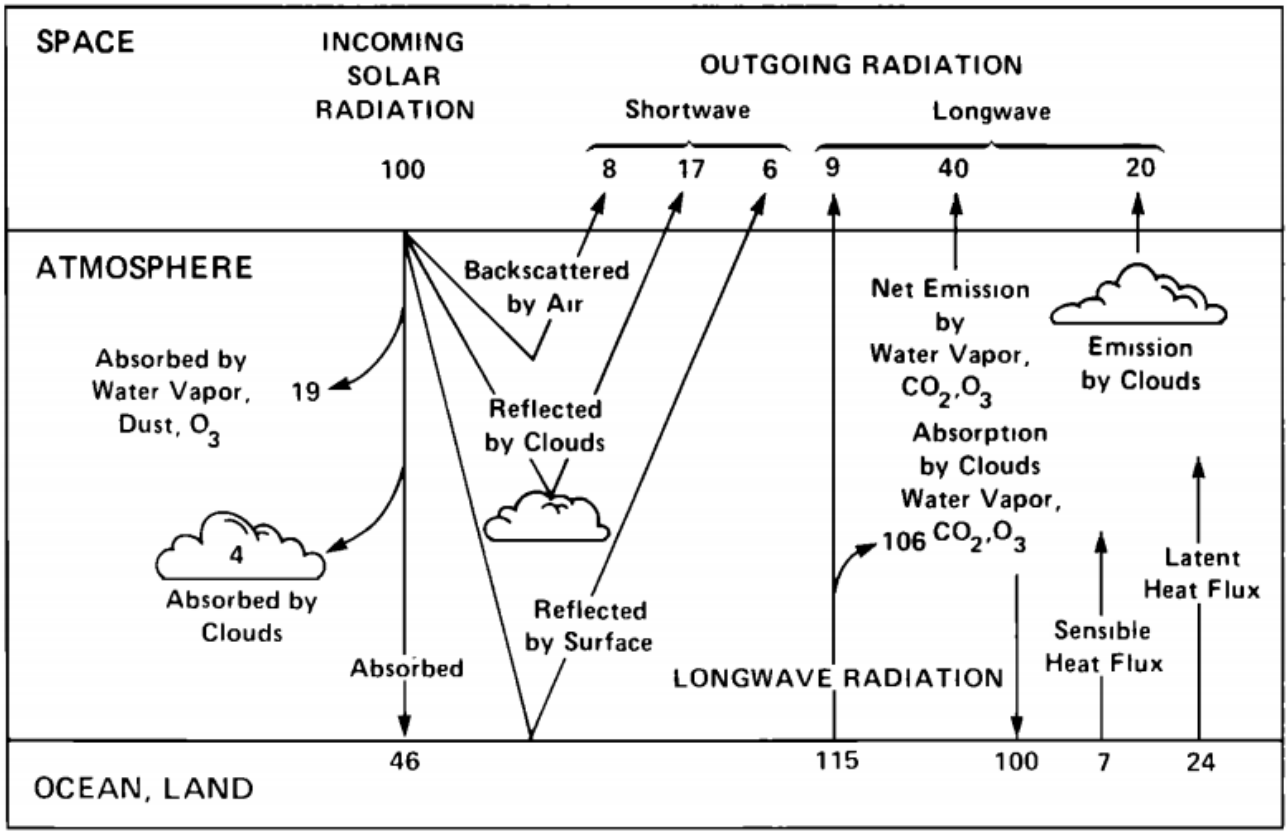

Figure 1-1 Schematic representation of the atmospheric heat balance (unit are per cent of the incoming solar radiation): the solar fluxes are shown on the left-hand side, and the thermal infrared fluxes (long-wave) are on the right-hand side [27].

The problem here is the anthropogenic contribution to the GHG concentration, which is the primary cause of the current climate change [17–21,27]. This contribution consists of the augmentation of CO_2, CH_4, N_2O concentration in the atmosphere, together to the emission of synthetic GHG as chlorofluorocarbons (CFC) and fluorinated gases (F-gases) [27]. In Figure 1-2 are presented the concentration trend for three of the primary GHG produced by human industrial activity in the period between 0 AC to the 2014 AC, for the last few years data from 2014 to 2019 are taken from [28].

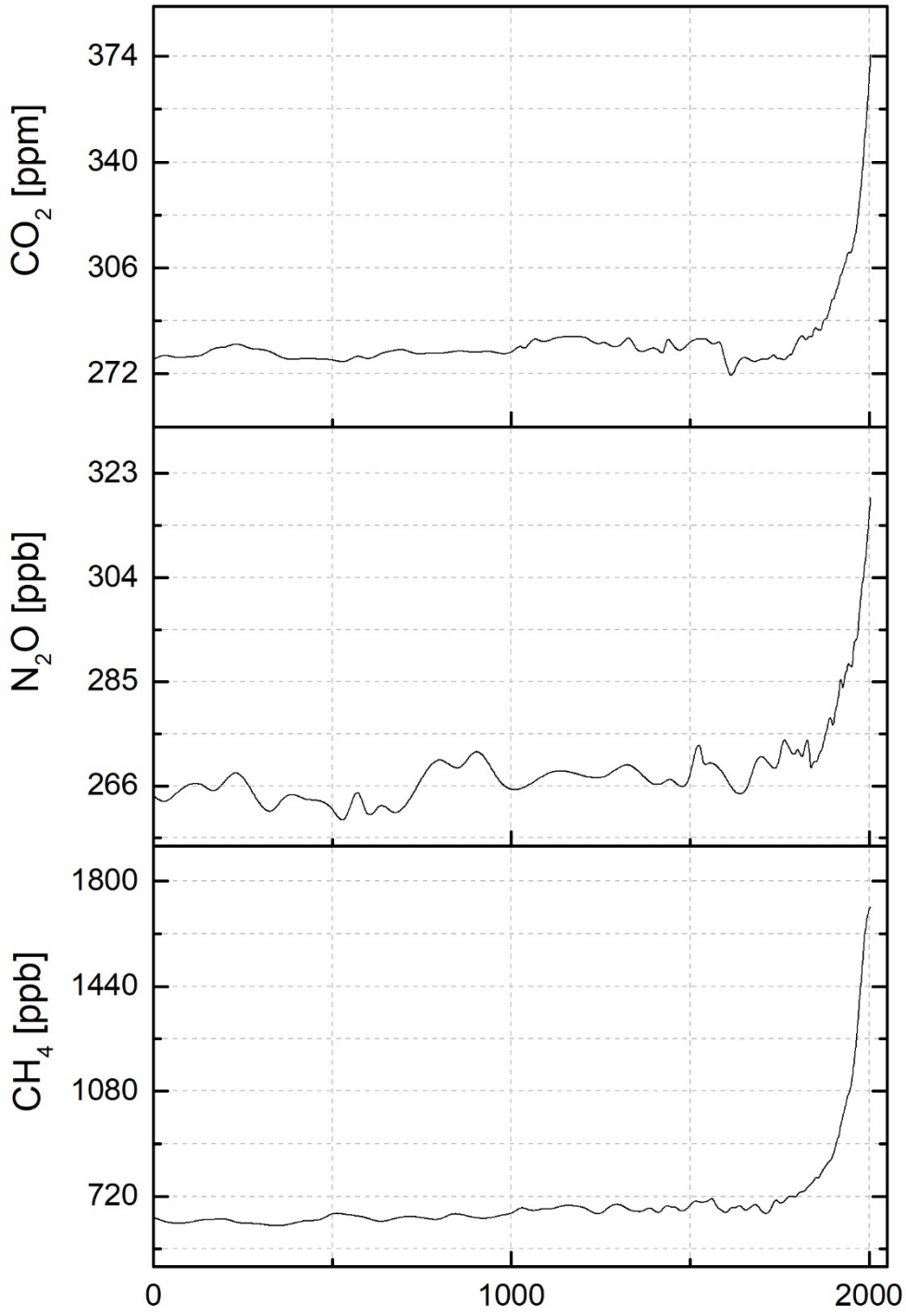

Figure 1-2 CO_2, CH_4 and N_2O concentration series from Law Dome ice records data from CIDAC database [29]

GHG have increased since the preindustrial era due to large population and economic growth, and they are now higher than ever, this atmospheric concentration is at least unprecedented in the last hundred thousand years [30].

Tangible phenomena related to climate change, currently occurring on Earth, are:

- Global temperature rise: planet's average surface temperature has increased by 1.1 °C since the lat 19th century, the most in the last decades [27], and the temperature increase, depending on the different reaction scenario, is previewed to increase more and it will arrive up to 4.8 °C in 2100 in the worst scenario described by UN at the last COP24 [31];
- Warming oceans: the oceans stores most of the heat surplus due to greenhouse-effect, because of their heat capacity (90% of the energy stored by the climate system between 1971 and 2010 [32]), which directly contribute to their temperature increase and indirectly to their level;
- Oceans acidification: because of carbon dioxide emission in the atmosphere, oceanic uptake of CO_2 has increased resulting in the acidification of oceans, with a series of problems bonded to the ecosystem and oceans food production [33–35];
- Shrinking of ice sheets: Greenland and Antartica ice sheets have been losing mass in the last few decades [36–38];
- Declining Arctic sea-ice: its annual mean extent has decreased over the period 1979 to 2012 accompanied by a thickness lowering [39];
- Glacial retreat [40–42] and decreased snow cover [43];
- Sea level rise: it is primarily due to the added water from the melting of ice sheets and glaciers [44];
- Extreme weathers or climate events: weather or climate events considered rare events, at particular places and time of the year, have increased their frequency and/or intensity [45,46].

1.1.2. Pollution and the sustainability problem

Nowadays, the chemical industry produces billions of tons per year of up to 70000 commercial substances that are used for diverse technical and economic purposes [47]. Many of these chemicals and the by-products produced during their life cycle are stable and/or oil-soluble, causing them to persist in the environment and accumulate in food webs [48]. Long-lived pollutants are distributed long distances on currents of wind and water and have accumulated on a truly global basis [49].

The pollution caused by chemicals production not only polluted the air with by-products as such as CO_2 and N_2O, but also the waste produced at the end of chemicals life cycle persists in the ecosystems sometimes longer than their life use.

Globally the production of waste in the year 2016 was estimated to be near 2.01 billion tonnes, with increment respect of 2012 of +45% (1.3 billion tonnes in 2012). Rich and developed countries and the new great economies as China and South East Asia account for more than 60% of the global waste generated. Obviously, correlation exists between waste and the urbanization of these areas, generally more a country is urbanized and rich and more wastes are produced. North America with the USA have the primacy of wastes generated per capita. With the growing population, the wastes are going to increase inexorably and by 2030 it will arrive at 2.59 billion tonnes produced [50].

Almost 12% of solid wastes are composed by plastics which are the first contaminants present in the oceans (if CO_2 captured by the sea are not consider), 44% of wastes are of organic origins.

The collection of these wastes is not complete, especially in poorer area of the world, and when collected almost 33% of them are stored in open dumps, 25% in landfills, and 2% in controlled landfills. It sums up to more than 60% globally untreated. The numbers are less tragic for rich countries, but in the cited report [50] neither the wastes fluxes from rich countries are considered nor where and how they are treated.

1.2. Green chemistry and renewable feedstocks

In the framework of the last COP24 Katowice United Nation Climate Change Conference [51–54], the green chemistry role on the circular economy, on the mitigation of greenhouse gas emission becomes strategic, on the reduction of waste production and management.

In order to more fully appreciate how much Green Chemistry pervaded thus far the chemistry production towards the future potential of global sustainability, it is necessary to review how Green Chemistry is distinct from other approaches currently in use.

The definition of Green Chemistry: " Green chemistry is the utilisation of a set of principles that reduces or eliminates the use or generation of hazardous substances in the design, manufacture and application of chemical products" [55], the principles at the base of Green Chemistry are twelve.

The most relevant (for this thesis purposes in particular) between these principles are:

- **Prevention** preventing waste formation is better than treating;
- **Design for energy efficiency** energy requirements should be minimized whenever possible and reaction condition lower than in standard processes (low P and low T);

- **Use of renewable feedstock** renewable feedstock or raw materials are better than non-renewable ones;
- **Catalysis** catalytic reagents are better than stoichiometric reagents, furthermore catalysis is a very crucial point for green chemistry since new synthesis path must be developed since the raw materials are changing (more robust catalysts, different reactions, etc.)
- **Designed for degradation** chemicals should not pollute the environment, when their life end they will transform in harmless compounds.

Green Chemistry aims at designing the next generation of materials pursuing the minimization of adverse consequences for human health and the environment [55].

One of the aspects of most interest in Green Chemistry is the change of the origins of feedstocks and starting materials through all manufacturing. The use of biomass to produce energy, chemicals and materials is one of the key issues of sustainable development. Indeed, bio-based resources are renewable and CO_2 neutral (in the best-operating conditions) in contrast with fossil fuels.

An advantage of renewable feedstock is the more stable cost of some platform molecules derived from carbohydrates or vegetable oils compared to the fossil fuels and their price tends even to decrease steadily with time.

As far as bioproducts are concerned, there are additional benefits to using renewable feedstocks. In fact, the molecules extracted from bio-based resources are already functionalised so that the synthesis of chemicals may require a lower number of steps than from hydrocarbons, thereby using more efficiently the starting biomass. Also, bio-based products may have unique properties compared to hydrocarbon-derived products, for instance biodegradability and biocompatibility depending on the final molecules composition. Catalytic processes implemented on biomass feedstocks minimise by-products and fulfil at the same time multiple Green Chemistry principles [56].

There is competition to produce food/feed, bio-products (chemical and polymers) and transportation biofuels (bioethanol and biodiesel) from agricultural crops, for technical applications only a small part is used although also this small amount is often perceived by the stakeholders. Conventional crops based on cereals and seed oils could only be a partial answer to the fuel issue, because of the huge needs at stake. To meet biofuels and chemicals demands in a more substantial way, it is recommended that also agricultural wastes are processed, new crops are grown on marginal land (as for example vegetable oils plants such as sunflower or

rapeseed), and fast-growing vegetative biomass (grass, wood, stems, leaves, etc.) consisting of cellulose and lignocellulose (cereals and vegetable oils) [57].

In this thesis the valorization of vegetable oils was considered and their products represents a sustainable alternative to petrochemicals and a renewable building block in industrial applications.

1.3. Vegetable oils

Vegetable oils are the product obtained from the cold pressing or the chemical extraction of a liquid or solid substance from the seed or less commonly from other parts of the fruit of some particular oleaginous plants as sunflower, rapeseed, soybean, olive, etc. They are primarily composed by triglycerides, i.e. esters of glycerine, with different chains of fatty acids with many carbon atoms whose number is usually comprised between 14 and 22 [58].

Since XIXth century, vegetable oils found widespread application in chemical industry and transports, then quite completely substituted by oil drilling exploitation; nevertheless, the recent renewed interest is largely addressed in diesel transport and as raw material for the production of fine chemicals [59]. Currently, 95 % of biodiesel is produced from edible oils via transesterification on different homogeneous and heterogeneous catalysts [60,61], even if some attention is exhibited in implementation of most productive vegetable oil as Sapium tree oil [62] or non-edible oils [63] or in other kinds of biofuels processes, such as deoxygenation and decarboxylation of oils [64].

Given advances in plant genetics and oil processing, there is considerable interest in developing plant oils for the manufacture of polymers such as polyurethanes, polyamides and epoxy resins [65,66]. The versatility of vegetable oils has been demonstrated as precursors of thermosetting materials, with the development of synthesis strategies leading to innovative and highly biodegradable polymeric materials [67].

In Table 1-1, the most common industrial uses of vegetable oils are reported.

Table 1-1 Industrial applications of vegetable oils and derivatives [68]

Food Application	**Oleo-chemicals**	**Energy, Biomass & Others**
Cooking oil	Surfactants	Biodiesel
Industrial frying fats	Personal care	Charcoal
Margarine	Cosmetics	Pulp and paper
Vegetable Ghee	Agrochemical	Animal feeds
Confectionary fats	Lubricant/grease	Bio-composite
Ice cream	Soap	Fertilizer
Non-dairy cream	Industrial cleaning	
Salad dressing	Printing ink	

Cheese analogues	Polyols
Supplements/vitamins	Polyurethanes
	Polyesters
	Polyacids

Among the fatty acids, a specific interest existing for oleic acid is justified by its stability in the presence of oxygen, which avoids spontaneous polymerization, and by the lower melting point in respect of saturated fatty acids (and corresponding trans fatty acids). These characteristics facilitate industrial use in continuous processes of transformation [69].

For this reason, the oleic acid market availability is not sufficient for all potential applications, nowadays also in cosmetics and personal care, pharmaceutical, and food, growing in the developed countries (North America and Europe), where governments' regulations promote bio-based compounds during the manufacturing of products [70]. Commercialized bifunctional building blocks for bio-based plastics include sebacic acid and 11-aminoundecanoic acid, both from castor oil, and azelaic and pelargonic acids derived from oleic acid. Currently, the oleochemical industry is a major producer of bio-based products, such as unsaturated oils (soybean, sunflower, and linseed oil, include alkyd resins, linoleum, and epoxidized oils), sources for bio-lubricants, which low viscosity combined with high oxidative and thermal stability [71]. Furthermore, the researches of different groups reveal a growing interest in the reactivity of their double bonds towards the olefinic metathesis reaction which allows the direct synthesis of a wide variety of monomers [72–75]. The great potential of fatty acids for the polymerization via olefin metathesis is also a reality of our days. On the other hand, the production of monomers and polymers by "thiol-ene coupling" (alkene hydrothiolation) reactions with fatty acid derivatives is a rapidly growing area and will continue to be in the near future due to the considerable, and in part still unexplored, potentiality of thiol-ene / fatty acid combination [67]. However, all this new application remain for the time being at laboratory scale since very often the oils found on the market do not allow large-scale applications due to their chemical composition and their chemical-physical properties.

The raw materials have an intrinsically variable composition (Figure 1-3), but the components usually observed in triglycerides are: oleic acid (C18:1), linoleic acid (C18:2) and linolenic acid (C18:3), stearic acid (C18:0) [76]; other compounds could be arachidonic acid (C14:0), palmitic acid (C16:0), and in non-canola rapeseed oil also erucic acid (C22:0 and C22:1).

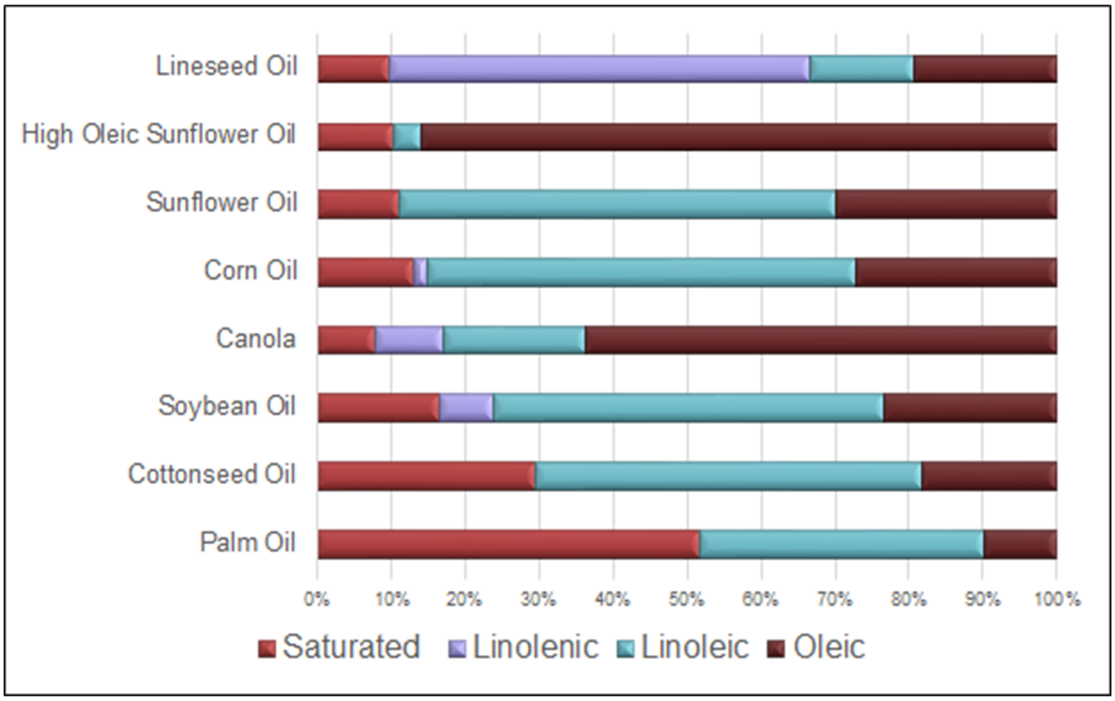

Figure 1-3 C18 fatty acids composition of common plant oils [76]

Mixtures derived from a natural vegetable oil containing at least 72% by weight of oleic acid were found to be suitable for the synthesis of polyol esters to be used in lubricating oils composition [77], while the quality of polyol esters for casting and coating is very much improved when very high oleic, and low stearic vegetable oils are used as a starting materials. The preferred range composition was 85–95% oleic acid, 2–8% linoleic, 0.5–2.5 stearic, and 2–5% palmitic (as whole fatty acids composition) [78]. The presence of poly-unsaturated fatty acids determines the low viscosity and the high thermal instability, important properties for bio-lubricants and biofuels (low pour point) [79], decreasing their content reduces their perishability and improves the oxidation instability [80,81]. The relative oxidation rates of (C18:1):(C18:2).(C18:3) are 1:40:100, respectively [82], and at the same time the fluidity depends on the amount of saturated compounds and the extent of isomerization, higher amount of these compounds are linked to increasing viscosity of the oil and in the worst scenarios they comport the formation of solid phases. In fact, the difference in melting point between cis and trans isomers is at least 15 °C [83].

To reduce the poly-unsaturated fatty acids towards the monoenes production, the selective heterogeneous catalytic hydrogenation of highly unsaturated oils is a key process addressed to a wide range of biocompatible products (green chemicals, bio-lubricants, poly-oils, etc.) [1,84–87]. Nowadays, the industrial processes for their production are limited to high oleic vegetable oils, due to technical constraints such as not adequate

selectivity of only one of the two double bonds of linoleic acid (C18:2) to yield the cis- and trans-C18:1 fatty acids [88] or difficulties in solid catalysts recovery [89]. On the other hand, the heterogeneous catalyst is a fruitful solution, to easily recover catalysts from the oil and reutilize them in further batch.

1.4. Vegetable oils hydrogenation

The origins of the modern process of catalytic hydrogenation are found in the early 1800s. However, the hydrogenation process did not begin before 1897 to be recognized as one of the main new chemical techniques. This was due to the studies of two French chemists, Sabatier and Senderens, who are credited as the founders of the hydrogenation process. They did their studies mainly on organic vapours or vaporizable substances. The low volatilization of liquid fatty acids and the practical impossibility of vaporizing the triglycerides themselves prevented them from converting liquid oils into solid fats by the addition of hydrogen in the presence of a catalyst. Sabatier's main interest was to find a new way to harden liquid oils for use in soaps and he received the Nobel Prize for his work on catalysis in 1912 [90].

The first actual catalytic hydrogenation of liquid oil to make solid fats, based on the preceding work of Sabatier and Senderens, was accomplished in 1902 by Wilhelm Normann who patented the process one year later [91].

Eventually, the process has been firstly commercialized in England and then in America by Procter & Gamble for the food industry, and it radically changed the eating habitudes of at least three human generation. Only after 1960 the scientists became aware of the cardiovascular issues produced by the consumption of large amount of hydrogenated products. However, the health discussion on hydrogenated fats (trans isomers in particular) continued until 2000, when many developed countries start to ban the use of trans fatty acids, commonly found in partially hydrogenated vegetable oils, in food products (causing the equally questionable increase in the use of palm oil); the FDA (U.S. Food and Drug Administration) starts to ban the trans content in food products only in 2013 [92].

Although banned or restricted in food products, as it was reported above, partially hydrogenated oils found uses in oleochemical processes and could be the base for a large number of bio-based compounds (polymers, soaps, lubricants, polyalcohols, etc.), with high potential of exploitation in many industrial fields.

1.4.1. Reaction mechanism

It is now commonly accepted that the nickel-catalysed hydrogenation of unsaturated fatty acids follows the Horiuti-Polanyi mechanism [93]. According to this mechanism, the molecular hydrogen is firstly adsorbed on the catalyst surface and rapidly dissociated in two hydrogen atoms (see Figure 1-4). Contemporary fatty acids, or the fatty acid chains in triglycerides counterparts, could be adsorbed on the catalyst surface by their double bonds, and in a first step one atom of hydrogen is added to the adsorbed C=C, and they form a half-hydrogenated compound. If the second atom of hydrogen is consequently attached to the double bond, this latter becomes saturated, and by the release of the heat of reaction (very high heat of reaction equal to 105 kJ/mol) it is moved away from the active site; the saturation of the double bond at the standard temperature reaction conditions (110-200 °C) is irreversible. However, the addition of the first hydrogen is a reversible step, so the half-hydrogenated intermediate can also dissociate [90].

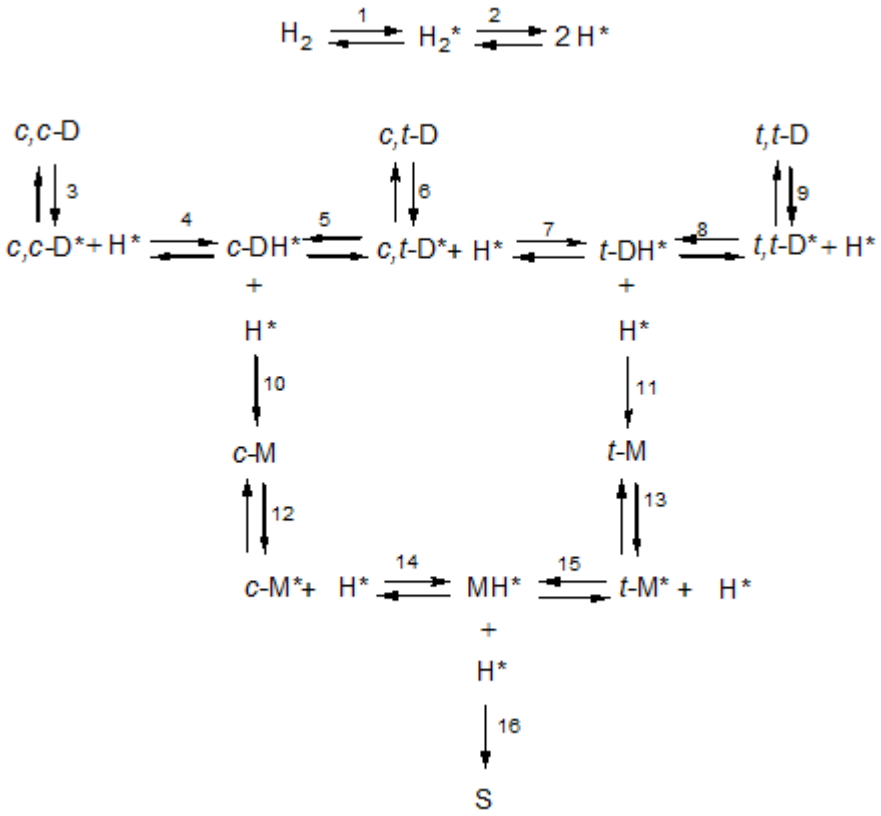

Figure 1-4 Hydrogenation reaction mechanism as described by Dijkstra [90] *where *= adsorbed intermediates, c= cis isomers, t-=trans isomers, M=monoene and D = diene, respectively.*

The above mechanism well explained some of the observations made by the previous scientists on the hydrogenation of vegetable oils or their derivatives. It is worth noting that the proposed scheme does not consider the triglycerides, but the single chain; in the presence of triglycerides the reaction rates could be modified by the steric effect. However, how the steric hindrance affects the reaction mechanism and the kinetics is not known, as stated by Dijkstra [90].

In equilibrium conditions, it was observed that the trans/cis-ratio is of 1 moles of cis isomer for every 3 moles of trans isomer. This ratio stems from the heat of isomerisation, which equals 4.1 kJ/mol [94]. Accordingly, Dijkstra has suggested that the activation energy of step 4 (hydrogen addition to c,c-diene) is lower than the activation energy of step 5 (hydrogen addition to c,t-diene). This would cause the cis-isomer to reacts about three times faster than the trans-isomer and eventually to lead to the cis, trans-equilibrium.

For nickel catalysts, observation on industrial results, accordingly to Applewhite [95], suggests that the main route follows the steps 3, 4, and 10 and steps 5 to 9 are less important. The main consequence is that the main mechanism for elaidic acid produced during the reaction is not from the dienes (c,t-D, t,c-D or t,t-D), but the monoenes (steps 14 and 15).

The last reaction is the stearic acid formation; for Ni catalysts, Dijkstra [96] suggests that the extent of this reaction depends on the concentration of atomic hydrogen on the catalyst surface. When this latter is low, the isomerization prevails and when it is high the saturation reaction prevails. He also observed that the catalyst poisoning by sulphur results in lower [H*] concentration and therefore in higher isomerization and lower saturation. This mechanism can explain how the reaction parameters as temperature, pressure, rate of agitation, amount of catalyst and catalyst activity affect the hydrogen concentration and then the isomerization index or trans selectivity [90]. As an example, increasing the pressure, the solubility of the hydrogen dissolved in the oil increases and thus its concentration on the catalyst. This promotes the saturation reaction at the expense of the isomerization reaction. However, in the initial transient regime of a hydrogenation run, the concentration of hydrogen is so low that these factors are substantially not so important; when the catalyst reactivity partially decreases, their effects become noticeable.

The above mechanism also explains why linoleic acid selectivity depends on external factors. The selectivity definition as the ratio of two rate constants (see §Chapter 2) implies that it should be constant itself which is not the case. The same external factors that affect the trans-selectivity also affect the linoleic acid

selectivity in a similar manner. Process conditions that favour a high-trans-selectivity also favour a high-linoleic acid selectivity. In addition, catalyst properties are known to affect the linoleic acid selectivity.

So far this reasoning is essentially for hydrogenation of free fatty acids and fatty acids methyl esters (FAME); for the raw oil, it was observed that unsaturated fatty acids attached to the same triglyceride affect each other's reactivity, and so, for example, the reaction rates for triglycerides containing oleic acid molecules does not follow the same kinetics of oleic acid content alone [95].

Generally speaking, authors agree with Dijkstra to accept for Pd and other noble metals, the reaction mechanism proposed for Ni [97–99].

The above description must be integrated with two additional information:

- The above mechanism does not consider another side-reaction that occurs during the hydrogenation of both triglycerides, or the corresponding fatty acids, i.e. the double bond migration reaction in which the double bond shift position on the fatty acid moieties chain;
- Not all the catalysts follow entirely this mechanism, but with some extent, some modification occurs. Particularly copper shows different behaviour with respect to Ni.

The first point is not addressed by Dijkstra or other scientists because double bonds position seems to have a random pattern and cannot be estimated *a priori* from the catalysts behaviour [100–105]. In the current state of the art, the positional selectivity is not achieved by any catalyst, and the results of each batch of reaction could be different [90]. Nonetheless, the composition of positional isomers can be evaluated by GC-FID or GC-MS.

For the second point, copper has a different reaction pathway than Ni or the other noble metals; it is crucial to highlight that the noble metals share the same reaction mechanism, but with different reactivity.

With respect to the mechanism of the hydrogenation reaction using copper catalysts, it was proposed quite early [106] that the actual species being hydrogenated could be a conjugated polyene and that conjugation should precede hydrogenation. This assumption was based on the observation of conjugated dienes and trienes formation during the reaction, and the reluctance of copper-based catalyst to hydrogenate methylene interrupted fatty acids. Always in the same work, it was observed that both the conjugated 9-11-13 and the non-conjugated 9-12-15 linolenic fatty acid are hydrogenated at the same rate when hydrogenated separately,

but the first one reacts more than 200 times faster than the second when both are hydrogenated at the same time. Koritala et al. concluded that the "conjugated triene completely dominates the surface of the catalyst".

A first mechanism for the conjugation was suggested by Vigneron et al. [107]: he supposed the addition of hydrogen atom to the double bond following a mechanism equal to the Horiuti-Polanyi mechanism. However, a similar mechanism has some difficulty to explain the effect of pressure on the hydrogenation of conjugated dienes of different fatty acids as well highlighted by Dijkstra [108]. Therefore this latter suggested a different mechanism in which the first step of the conjugation is not hydrogen addition, but hydrogen abstraction, followed by the hydrogenation of the double bonds. This assumption is effectively in accordance with many works on copper catalyst, in particular it explains why the pressure increase does not lead to a proportional increase of hydrogenation rates, but to a maximum value followed by a decrease [109,110]. The abstraction/addition mechanism proposed by Dijkstra is considered the most probable between the two.

Since methylene interrupted fatty acids are not easily saturated, it follows one of the most interesting properties of Cu in catalysed vegetable oils hydrogenation, namely the almost complete impossibility at low pressure for this kind of catalysts to convert oleic acid into stearic acid. Furthermore, this phenomenon was supported by many results [109,111–115].

1.4.2. Mass transfer effect in vegetable oils hydrogenation

Hydrogenation **of** edible oils or fatty acid methyl esters (FAMEs) is a three-phases process in which several transport steps can be distinguished. In the standard hydrogenation process, the H_2 gas is used as reducing agent of the double bonds. The situation is schematized in Figure 1-5. The hydrogen flux (J_{H_2}) can be written as a function of different resistances: the resistance from the bulk of the gas to the gas-liquid interface R_{GL}, the resistance from the liquid to the solid-liuid interface R_{LS} and the resistance inside the catalyst due to diffusion mechanism R_S (Equation 1-1 to Equation 1-4) [116].

$$J_{H_2}a = \frac{He(p_{H_2})}{R_{GL} + R_{LS} + R_S} \qquad \text{Equation 1-1}$$

$$R_{GL} = \frac{1}{k_L a} \qquad \text{Equation 1-2}$$

$$R_{LS} = \frac{1}{\varepsilon_s k_s a_s} \qquad \text{Equation 1-3}$$

$$R_S = \frac{He(p_{H_2})}{\varepsilon_s \rho_s \eta |r_{H_2}|}$$ Equation 1-4

where $k_L a$ is the mass transfer coefficient in liquid phase per area of transfer, $k_s a_s$ is the mass transfer in the liquid to solid interface for the area and ε_s is the void degree, ρ_s is the density of the solid catalyst, $He(P_{H2})$ is a function of the partial hydrogen pressure, η is the effectiveness factor which depends from the reaction kinetic and r_{H2} is the rates of consumption of hydrogen.

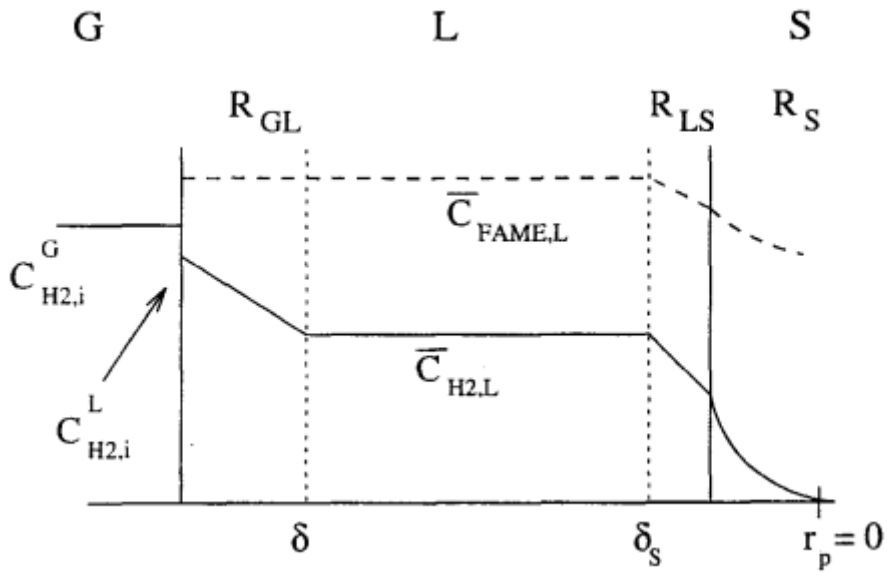

Figure 1-5 Concentrations profiles for hydrogen and fats in the agitated batch stirred reactor [116]

Mass transfer limitations have a strong influence on the linoleic selectivity [95,117,118] and on the double bond migration [119].

Mass transfer of hydrogen from the gas into the liquid is often the rate-controlling step [90,103]. The volumetric mass transfer coefficient $k_L a$ can be obtained by two methods:

- In a slurry reactor, directly from gas adsorption rate in absence of reaction;
- From flux measurements, at sufficiently high catalyst concentration ($R_{GL} >> R_{LS}+R_S$), and the data obtained with this method are more precise [120].

Many correlations were proposed for the estimation of $k_L a$ by many authors [121–124]. Available experimental data on the external catalyst mass-transfer resistance support the assumption that external catalyst transfer limitations can be neglected in comparison to mass transfer limitation from the gas phase to the liquid phase [125].

At last the transport limitation inside the catalyst are also important, because it generates intraparticle gradient inside of the pores of the catalyst. As a result, the available catalyst activity is not fully utilized. In order to demonstrate that the intraparticle resistance is negligible, it is possible to evaluate the Thiele modulus Φ. If the kinetic law is not known, a priori the application of the Weisz-Prater [126,127] modulus can be used (Equation 1-5):

$$\Phi_{TAG} = \frac{d_p^2 \rho_s r_{TAG,H_2}}{D_{TAG,eff} c_A^i} < 1 \qquad \text{Equation 1-5}$$

where d_p is the particle size, ρ_s is the density of the solid catalyst, r_{TAG} and r_{H2} are the rates of reaction of TAG and H_2 respectively, $D_{TAG,eff}$ is the effective diffusivity of the oil (TAG) inside the pore or of H_2, and c_a^i is the concentration of the component TAG or H_2.

It is usually considered that for catalysts with average pore diameter larger than 10 nm, ten times the diameter size of the TAG molecules which it is estimated has a length of 10 Å, intraparticles mass transfer limitations are negligible [125].

Although the mass transfer is of great importance, the core of the process remains the catalyst on which the reaction products depend.

1.4.3. Hydrogenation catalysts

As already mentioned, the catalyst is a fundamental parameter for catalytic hydrogenation of vegetable oils. It is worth mentioning that the different reaction pathways are also reflected by the different results both in correlation to activity and selectivity. Although an absolute agreement was not achieved in the classification of the most active or selective toward isomers active phase, Veldinsk et al. [103] proposed an attempt of classification of the principal catalytic active phase, by combining the observations of many scientists. The results are reported in Table 1-2.

Table 1-2 Ranking of the active phases

Characteristic	
Activity	Pd>Rh>Pt>>Ir>Ru=Ni>>Cu
Selectivity	Cu>Pd>Rh>Pt>>Ir>Ru=Ni
Cis/trans selectivity	Cu≈Pd>Rh>Ru=Ni>>Ir>Pt

Also, Numwong et al. [128] found a similar trend some years later among Pd, Pt and Ni: for activity Pd>Pt>>Ni and for trans selectivity Pd>>Ni>Pt, placing the Pd as the best alternative for both activity and selectivity. As it is expected, there are many articles that contradict this statement, finding condition in which Ni is also considered selective.

1.4.3.1. Homogeneous catalysis

It is worth noting that also homogeneous solutions were studied over the time for the selective hydrogenation of vegetable oils to increase the selectivity by means of metal carbonyls, platinum-tin systems or catalysts of Ziegler-type (Fe, Co and Ni salts activated by tri-ethyl aluminum). Also neutral precious metal-phosphine complexes such as Wilkinson catalysts ($RhCl(PPh_3)_3$, or cationic complexes ($[Rh(cod)(PPh_3)_2]BPh_4$) were tested, but only with moderate success [88]. Promising results were achieved using Pd nanoparticles, produced from palladium dichloride [129,130]. In the attempt to lower the trans fatty acids, the combination of both heterogeneous, industrial Ni catalyst, and homogenous catalysis, complexes of Ru or methyl-benzoate $Cr(CO)_3$ was tested [131,132] with mixed success, identifying a region of work in which the activity and selectivity of the Ni are improved compared with Ni alone. These studies although interesting from the research point of view, never have found industrial interest because of the cost of the homogenous catalysts used and the inherent difficulty in the separation of the catalysts and the products.

1.4.3.2. Heterogeneous catalysis: Ni catalysts

Several industrial catalysts for hydrogenation process use transition metals as supported active phase. For hydrogenation of vegetable oils mainly ***nickel*** on silica, on silicate, on alumina, on kieselguhr or on zirconia support, loaded with 18-25 $\%_{w/w}$ of Ni were studied. Raney nickel, a nickel catalyst produced from the decomposition of Ni-Al alloys with sodium hydroxide attack, was also used [92]. The principal obstacle when Ni is used is the achievement of a high concentration of trans-isomers, with selectivity isomers index (SII) for selective reaction conditions between 1.51 and 1.88 for canola oil, and the formation of saturated fatty acid (C18:0 stearic acid). The selectivity isomers index is

defined as the ratio between the trans isomers formed during the reaction and the drop in Iodine Value, it is a measure to evaluate how much trans isomers are obtained per double bond reacted (§Chapter 2).

However, several tests were made with Ni trying to find selective conditions in which operates industrial available catalysts. Ni catalysts operating at 160–230 °C and 2– 5 bar H_2 are by far the most commonly used in margarine production [125]. Different 22-23% Ni-based catalysts, commonly used in the percentage of 0.02% Ni content by weight of oil, at 180 °C and 50-200 kPa yields very low saturated compounds, but very high trans levels. Vice versa low temperature (120 °C) at 3.5 MPa results in lower trans, but higher saturation [133]. At higher pressure the hydrogenation rate was also higher as reported by other authors, maintaining high selectivity towards oleic acid cis-isomers in accordance with Food and Drugs American (FDA) legislation [134,135] with SII ranging from 0.30 to 0.62. Ni catalysts, well known from the reactivity point of view, are used in many cases in modelling of the process as standard template [92,102,136–138].

In order to reduce the content of unwanted by-products as trans-isomers and also stearic acid, research in this field proceeds following two different paths: the use of noble metal catalysts, mainly Pd and Pt for the properties reported in Table 1-2.

, or the use of Cu, that is less noble and cheaper, but with a lower activity towards complete saturation [92], or eventually by addition of solvents (critical – near-critical) or additives [96].

1.4.3.3. Heterogeneous catalysis: Pt catalysts

Platinum commercial catalysts, with Pt loadings from 1 $\%_{w/w}$ to 5 $\%_{w/w}$, tested at 80-130 °C and 1 atm, show low reaction rate for the linoleic reaction to form monoenes unlike the reaction to complete saturation that is generally faster depleting the reaction media from oleic acid [139]. However, in other conditions, Pt shows good activity, in correlation with more reactive catalysts (Pd, Ru, Rh) with a low formation of trans fatty acids [140,141], despite the lower interaction energy between H_2 and the active site of the catalyst. Some Pt catalysts showed excellent selectivity and in

different conditions [142] can have an isomerization selectivity index (SII) of 0.31 at 100 °C and 0.46 at 170 °C under 3 bar of hydrogen against 0.46 at 100 °C and 0.57 at 130 °C achieved with a Pd catalyst supported on the same support (alumina) and with comparable loading (nominally 2%$_{w/w}$). These values are interesting for the selective hydrogenation point of view, as reported by Veldinsk [125].

Bi-metallic Pt-Ni were also tested; McArdle et al. [143] proposed an innovative approach to synthesize Pt–Ni catalysts supported on mesoporous silica using the surface redox reaction (Srr) technique which resulted in better activity and lower selectivity towards trans-isomer than the traditional successive impregnations and co-impregnation techniques. The Pt-Ni catalysts (Pt 2%$_{w/w}$ and Ni 1%$_{w/w}$) was prepared with these techniques, but also with consecutive impregnations and co-impregnations. They concluded that the introduction of Ni into the palladium catalysts have a beneficial effect on the hydrogenation selectivity, SII index changing from 0.6 with Pt to 0.34 with Srr catalyst, the other Pt-Ni catalysts are between these two values. Furthermore, the Srr technique led to more active catalyst than the other more classic synthesis methods, where Ni would block the Pt catalytic sites. It is worth noting that the content of stearic acid is high (17%$_{w/w}$-25%$_{w/w}$).

1.4.3.4. Heterogeneous catalysis: Pd catalysts

Pd-based catalysts have often been proposed due to their activity at lower temperature (120–140 ◦C) and their lower cis/trans isomerization activity SII (0.18-26), compared to Mo (0.33), Ni (0.375), Co (0.69), Ru (0.45), and Sr (0.6) estimated from data reported by Belkacemi et al. [144][104]. The Pd catalysts showed in many cases an higher selectivity towards the oleic acid formation (monoene) compared with Ni industrial catalysts. However, both Ni and Pd catalysts show a rather low diene/monoene selectivity, in comparison to copper catalysts, thus giving early formation of saturated compounds if the reaction conditions are not well controlled. In this field of selectivity towards oleic acid in the cis configuration, the use of more metals, as additives, is a recurring strategy. More complex catalysts Pd-based enhanced with Mo, Ni, Co, Ru, and Sr were considered [144]; the introduction of Co, Sr, and Ru enhances the activity of the catalysts and, in particular, Ru has some promoting effect on the cis/trans ratio, with a SII value of 0.45 at the same conversion for sunflower oil.

The deep interest on Pd-based catalysts is justified by its reusability, stability and high catalytic activity with appreciable monoenes selectivity ([128,143–148]). Several supporting materials have been investigated SiO_2 [143,146,148], Al_2O_3 [128,146], TiO_2 [143], carbon [148], etc. To enhance catalyst recovery after reaction, magnetic supports were also implemented [149]. Mesoporous silica exhibiting high surface area, uniform pore size-tunable, and surface functional groups [150,151] was studied and it was indicated that the support is not fundamental and does not increase significantly the activity compared to Pd/SiO_2 [145].

Numwong et al. [152] studied palladium catalysts supported on silica concentrating their work on catalyst pore size for hydrogenation of rapeseed oil derived FAME; it was found that these catalysts have a good partial hydrogenation activity, resulting in an improvement of oxidative stability. Moreover, the pore size of SiO_2 support had a significant effect on the catalyst activity. Hydrogenation activity shows that Pd/SiO_2 with ∼45 nm pore size exhibits the highest hydrogenation activity. Furthermore, the cis–trans selectivity probability depends on the contact between reactant and catalyst then on the steric hindrance. The selectivity toward cis-monounsaturated FAME was found to be high for Pd/SiO_2 with ∼2 nm and ∼68 nm pore sizes, the authors claiming that to the reason is the low contact probability between FAME molecules and active sites in very small and large pores. They suggested two possible ways to reduce selectivity toward trans-isomers:

- use of nonporous materials as support;
- use of a large pore size support in order to reduce the contact probability between the reactant and catalyst surface.

As already done for Pt, Pd was also tested in combination with Ni trying to improve the cis/trans selectivity of the Pd. However, Albright et al. [153] demonstrated extensively that the introduction of Ni in small (100 ppm) or large amount (1000 ppm) in the oil does not give substantial modification of the Pd activity and that the slight improvements achieved were related to the Ni that acts as a sponge for poisons present in the oil, diminishing the Pd poisoning.

Finally, the introduction of Pb in the Pd catalysts formulation increases the selectivity towards monoenes, lowering the hydrogenation activity [145,154]: Pb enhanced Pd/SiO_2 catalysts, prepared with catalytic reduction were tested at 40 °C, using ethanol as a solvent medium [145]. Another Pd-Pb supported on γ-Al_2O_3 has been synthesized starting from tetra-butyl-lead with a supported Pd/γ-Al_2O_3, and, in this case, the reaction has been carried out at 100 °C and 0.41 MPa [154]. In these studies, selectivity towards monoenes and cis/trans isomerization increases, SII change from 0.75-0.85 with palladium to 0.70-0.76 when lead is added, but the overall rate of reaction decreases. In the first study the sintering of the Pd particles after reduction with Pb was observed [145], in the latter, a changing in the interatomic spacing occurred [154].

1.4.3.5. Heterogeneous catalysis: Cu catalysts

Cu-based catalysts were also tested because, as shown in the previous section, they provide peculiar reaction results in terms of monoenes formation [108]. The first copper catalyst tested was copper chromate, this catalyst was extensively studied by Koritala and his collaborators [100,109,110,113,155–160], they tested the effect of different reaction parameters (pressure, temperature, agitation, catalysts concentration, etc.), proved the reusability of the catalyst after multiple tests and also the poisoning effect. The copper-based catalysts proved to work at higher temperature than the nickel one and with lower activity; selectivity, on the other hand, was proved to be dependent on the reaction pressure, regarding the cis/trans selectivity with SII values ranging from 0.2 to 1.5 depending on hydrogen pressure. However, copper never found a spread use as nickel probably due to being less robust than nickel, and the hydrogenated products obtained with similar characteristics were more expensive for the food industry.

In the last two decades, it was observed a resurgence of Cu catalyst for vegetable oils hydrogenation, with the particular interest towards the production of lubricants or other products with application beyond the food industry. The products obtained [84] are liquid down to -15 °C, and so

they can be used as lubricant oils for most of the standard conditions, but other applications in the production of new chemicals could be relevant at industrial level.

Cu supported on SiO_2 and Cu-Zn-Al oxides showed activity and selectivity linked to copper dispersion and to porous structure of the support. Poorly dispersed Cu catalyst presents inactivity towards soybean oil hydrogenation; at the same time narrower pores also imply more difficult mass transport and so lower activity [84]. Among all the supported catalysts reported in the literature, Cu on silica showed the best catalytic performances in the hydrogenation of both high linolenic and linoleic oils [161,162].

Since copper catalysts have such interesting properties related to activity and selectivity in this thesis we focused on this kind of catalysts. In fact, they present the wanted properties for the final hydrogenated products because the reaction is stopped before the production of stearic acid, and a high cis/trans selectivity and linoleic selectivity are obtained. Additionally the copper silica showed the best performance comparing to other classic supports as alumina, titania, Zn-Al oxides, and so on.

1.4.4. Copper supported on silica synthesis in literature

Many different techniques exist for the preparation of copper supported on silica, some of these are: incipient wetness impregnation (IWI) [163], chemisorption-hydrolysis method (CH) [164], ammonia-evaporation (AE) [165–168], precipitation gel method (PG) [169], hydrolysis precipitation method (HP) [7], urea hydrolysis deposition-precipitation (UHDP) [170]. In Table 1-3 the synthesis parameters are reported.

All these synthesis methods try to produce Cu/SiO_2 with high copper surface and high dispersion of the copper active phase on the support. Some of these techniques use silica precursor in solid form (IWI, CH, PG), some silica in colloidal phase (AE, UHDP) and one uses tetraethyl orto-silicate (TEOS) as precursor (HP). The surface area of the obtained catalysts is high for all the synthesis methods and depend on the precursor: colloidal and TEOS tend to produce silica with surface area

between 250-400 m^2/g (BET surface) while for solid precursor, the silica surface area depends on the surface area of the precursor itself, varying from 100 m^2/g to 500 m^2/g or more.

One characteristic obtained for most of the catalysts produced with liquid precursor (TEOS or colloidal silica) is a particular form of copper phyllosilicate called chrysocolla. The chrysocolla is not well found by the most used characterization techniques since it is well dispersed in the silica matrix. However, many authors suggested an interpretation of XRD, FTIR and Raman spectra, combining the results with TEM images and XPS spectra in order to highlight the presence of this phase [165–168,170–180]. The copper phyllosilicate ensures a good dispersion of copper onto the support after reduction since it is dispersed in the silica matrix.

Although all the cited articles claimed a high copper dispersion the metallic copper area obtained from N_2O titration and TEM images indicate the best results with ammonia-evaporation (AE) [165–168] (45 m^2/g_{Cu} and crystallite size lower than 7 nm), and hydrolysis precipitation (HP) techniques [7] (72 m^2/g_{Cu} and crystallite size lower than 10 nm). They were then chosen as synthesis methods to prepare Cu/SiO_2 catalysts for hydrogenation of vegetable oils in this thesis work. It is worth highlighting that AE technique changes from author to author, sometimes suggesting introducing a hydrotreatment step. In this work, the techniques used do not reckon such synthesis step.

Table 1-3 Synthesis conditions of copper silica

Copper loading (%)	**Catalyst precursor**	**Support precursor**	**Synthesis conditions**	**Ref.**
10%, 20% and 30%	$Cu(NO_3)_2$	SiO_2 Hisil 110 m^2/g	120 °C evaporation 400 °C, 10°C/min, 4 h calcination	[163]
8%	Copper ammonium nitrate	Grace Davidson	110 °C evaporation	[164]

	$Cu(NO_3)_2$ in NH_4OH solution	400 m^2/g	350 °C, 10°C/min, 4 h calcination	
5% - 30%	$Cu(NO_3)_2$ ammonia aqueous solution 25%	Silica sol Quindao Chem (25%)	120 °C evaporation 450 °C, 10°C/min, 4 h calcination	[165]
10, 15% and 30%	$Cu(NO_3)_2$ NaOH solution	Silica Degussa A200 200 m^2/g	120 °C evaporation 450 °C, 10°C/min, 4 h calcination	[169]
10%, 20%, 30%, 40% and 50%	$Cu(NO_3)_2$	TEOS/EtOH/water	120 °C evaporation 400 °C, 10°C/min, 4 h calcination	[7]
15% and 30%	$Cu(NO_3)_2$	Silica sol Quindao Chem JA-30 (30%)	120 °C evaporation 400 °C, 10°C/min, 4 h calcination	[170]

1.5. Thesis outline

This thesis was carried out in the framework of the PON 2014-2020 “PhD with industrial characterization” with financial contributions by the Italian Ministry of Education, University and Research (MIUR) and the Processi Innovativi Srl. Company. The project saw the collaboration of three entities: two Universities of two different countries and one Italian company in the development of the research theme:

- University of Strasbourg with the ICPEES laboratories commitment where the catalysts were synthetized and characterized. Also the ICPMS laboratory of the University of

Strasbourg was involved for the TEM characterization. Most of the characterizations were carried out in Strasbourg: ICP-AES, BET, XRD, XPS, TEM,TPR, TPD-N_2O, Raman spectroscopy;

- University of L'Aquila in the laboratories of DIIIE, where the reactions system was assembled and the tests performed and analyzed with the help of the gas chromatography experts of DSFC (Chemistry department). Also some characterization of the catalysts were performed with the help of laboratories technicans: FTIR in the DIIIE laboratories and SEM Microscopy at the Microscopy Center in L'Aquila;
- Processi Innovativi Srl which dealt with the design of the industrial process and which provided useful information for the development of the tests, given its long experience in the project and construction of vegetable oils hydrogenation plants.

Research issues are tackled in the next chapters of this manuscript, organized as follows:

- Chapter 2 "Materials and methods", describing materials synthesis procedures, employed characterization techniques, as well as the hydrogenation test procedure with equipment description and data elaboration for the laboratory batch reactor;
- Chapter 3 "Catalysts characterization" summarizing all the results collected from characterization of fresh commercial Lindlar catalyst, and as synthetized for Pd supported hydrotalcite, Cu silica catalysts and bimetallic catalysts as well;
- Chapter 4 "Reactivity tests", presenting all experimental results collected by hydrogenation test in a semi-batch reactor;
- Chapter 5 "Industrial application", where between the different applications proposed for industrial hydrogenation process, one is taken into account and feasibility study is carried out;
- General conclusions, containing a general sum up about main achieved results, points needing more efforts and suggestions for future work.

Chapter 2

Materials and methods

This chapter reports the methodology of the experimental work, with regards to the following major areas:

- *Catalysts and synthesis methods;*
- *Catalysts characterization techniques;*
- *Catalytic tests procedure, sample analysis and data analysis.*

2.1. Catalysts studied

During the development of this doctoral thesis several catalysts were tested for the selective hydrogenation of vegetable oils. The attention was focused on the following different classes of catalysts:

- Lindlar catalysts, a Pd-based commercial catalyst, used as reference catalyst;
- Palladium supported on Mg-Al hydrotalcite;
- Copper catalysts supported on silica;
- Monometallic Ni and Pd catalysts supported on silica;
- Bi-metallic copper catalysts, Cu-Ni and Cu-Pd supported on silica.

2.1.1. Lindlar catalyst

Lindlar catalyst is a common commercial heterogeneous catalyst, mostly employed in selective hydrogenation of alkynes to cis-alkenes [181–183] but also in other reactions [182,184,185]. Lindlar is a

palladium-based catalyst supported on calcium carbonate, associated to lead oxide in order to increase the catalyst selectivity. Lindlar catalysts bought from Sigma Aldrich® have a nominal Pd content around 5%$_{w/w}$.

The common synthesis starts from a slurry of $PdCl_2$ and calcium carbonate ($CaCO_3$), and by the addition of lead acetate ($Pb(OCOCH_3)_2$) or lead oxide (PbO_2). It could be also further associated with ammines or sulphur to reduce the formation of alkanes in the alkynes hydrogenation reaction. However, the manufacturer does not give any clues about this step neither in the security sheet of the sample nor in the technical data.

This catalyst was used as reference catalyst, in a preliminary series of tests carried out in a laboratory scale reaction system.

2.1.2. Palladium supported on hydrotalcite

Palladium catalyst, Pd nominal loading 1%$_{w/w}$, supported on magnesium-aluminium hydrotalcite used in reaction as hydroarylation [6], was tested in this thesis for the hydrogenation of vegetable oils.

This catalyst was produced in a three-step synthesis: 1) synthesis of hydrotalcite (HT) prepared by low oversaturation precipitation with a Mg/Al molar ratio equal to 2:1, 2) Pd impregnation of HT with DMF, 3) palladium reduction from Pd (II) to Pd (0) at low temperature with cyclohexene. All the reactants were purchased from Sigma Aldrich®.

More precisely, a solution containing $Mg(NO_3)_2 \cdot 6H_2O$ and $Al(NO_3)_3 \cdot 9H_2O$ in 125 mL of de-ionized water was prepared. This solution was slowly dropped over 250 mL of a Na_2CO_3 solution, pH 10 at 60 °C under vigorous stirring. The pH was kept constant by adding appropriate volumes of a NaOH (1M) solution during precipitation. The suspension thus obtained was kept at 80 °C for 24 h, after which the solid was filtered and washed with 1 L of de-ionized water.

The solid was dried in a stove at 110 °C overnight. The solid was re-suspended in a solution containing Na_2CO_3 in 200 mL of de-ionized water at 100 °C for 2 h then vacuum filtered, washed with 200 mL of de-ionized water and dried at 110 °C.

Part of the obtained HT was then treated with N,N-dimethylformamide and $Pd(NO_3)_2 \cdot H_2O$ for a final Pd content of 1%$_{w/w}$. The suspension was then stirred at room temperature for 24 h, the solvent was evaporated and the residual powder dried in a stove at 110 °C overnight. The resulting solid, Pd (II)-Pd(0)/HT, was treated with cyclohexene at 83 °C under reflux for 1 h (Figure 2-1). The mixture was then cooled, and the catalyst (Pd^0-Pd/HT) was filtered and washed with cyclohexene and methanol.

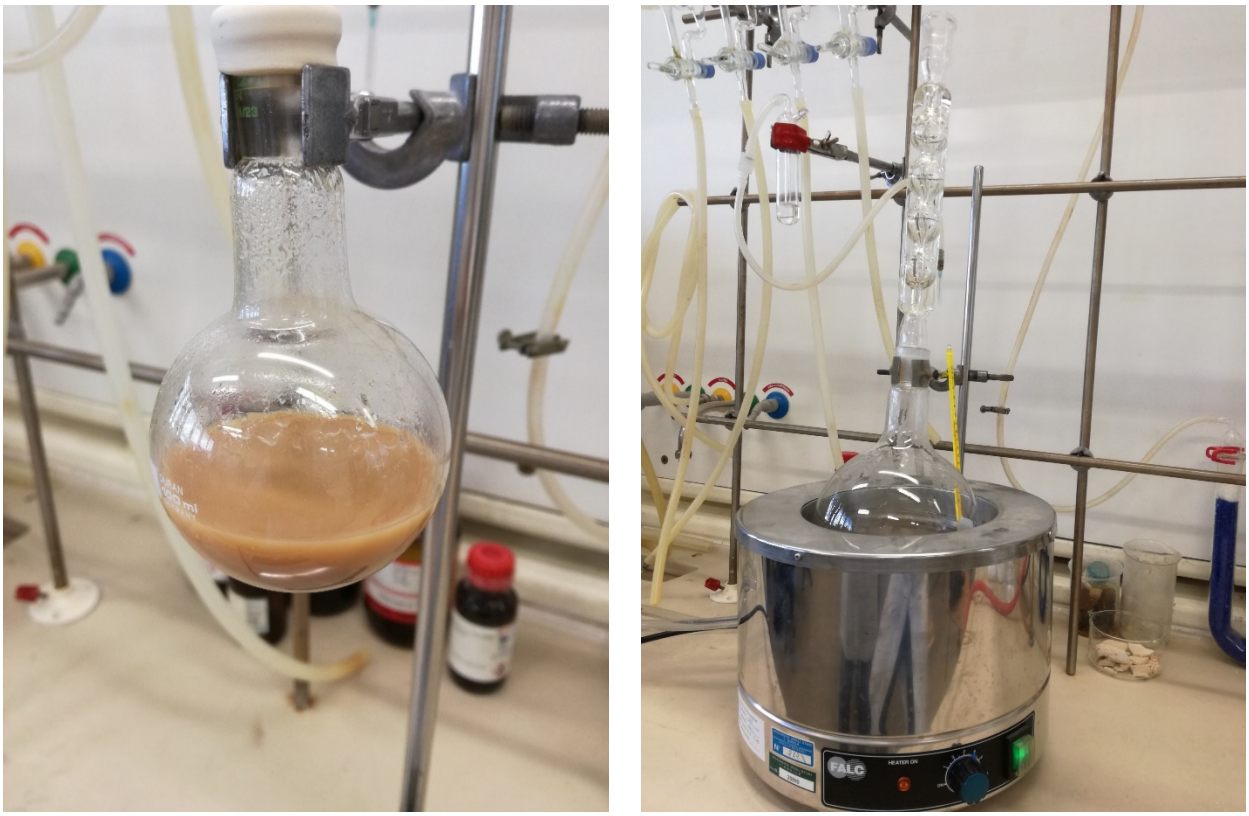

Figure 2-1 Pd(II)-Pd/HT after impregnation with Pd(II) (on the left-handside) and reduction with cyclohexene (on right hand-side).

2.1.3. Copper on silicon oxide

As reported in literature, copper and, more specifically, copper supported on silica shown good performances towards hydrogenation of FAME and vegetable oils [1,84,90,96,108,111,162,186,187].

Among all synthesis methods reported in §Chapter 1, in this work, hydrolysis precipitation [7] and ammonia evaporation, as reported by Li-Feng et al. [166], were chosen. These two methods produce high dispersion of copper species on the support surfaces with a small dimension of the active phase, and so they are considered particularly suitable for the hydrogenation of oils.

Both methods start from the “liquid” silicon oxide precursor, the silica is formed during the precipitation of the copper species. As reported by Li-Feng et al. [166], copper and silica can form some copper phyllosilicates that increase copper dispersion in the silica matrix (Figure 2-2). The support and the active phase are both precipitated at the same time during the synthesis.

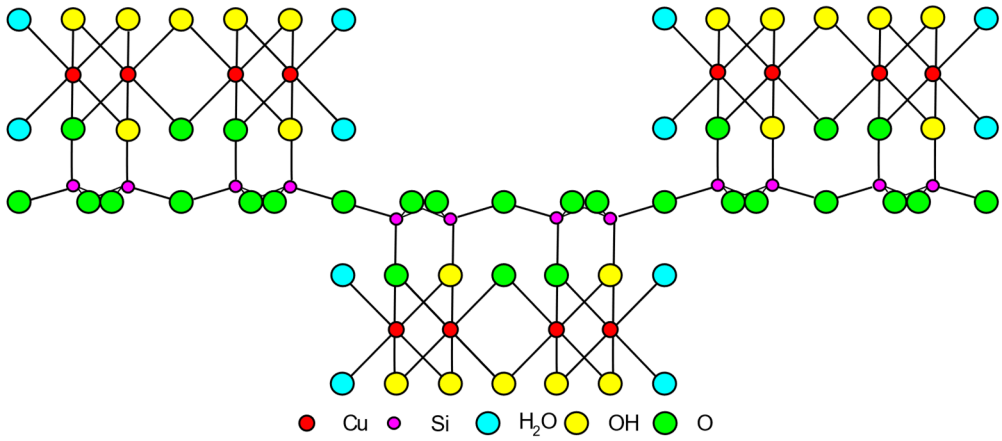

Figure 2-2 Structure of copper phyllosilicate (chrysocolla) as reported by Li-Feng et al. [166] *structure adapted from* [165]

Catalysts with two different copper contents (5% and 10% by weight) were prepared using the two synthesis methods (Hydrolysis precipitation (HP) and ammonia evaporation (AE).

2.1.3.1. Hydrolysis precipitation method (HP)

The employed precursor salts were $Cu(NO_3)_2 \cdot 3H_2O$ (Sigma Aldrich® purity 99% degree of hydratation determined by TGA measures) for copper, and tetra-ethyl-orthosilicate (TEOS Sigma Aldrich® purity 98%) for silica, and ethanol (purity 99.9%), and deionized water were used as solvents.

HP synthesis steps are the following:

- Preparation of A mixture: a required amount of $Cu(NO_3)_2 \cdot 3H_2O$ is dissolved in deionized water, the solution is then added to a solution of TEOS. The amount of TEOS:EtOH:H_2O must respect the proportion 1:1:1 by weight. The mixture is then stirred for 1.5 h at 400 rpm until a single phase is obtained;
- Preparation of $(NH_4)_2CO_3$ solution: a solution of ammonium carbonate in water (0.25M) is prepared. Since $(NH_4)_2CO_3$ is not stable and can start to decompose, the pH of the solution has to be checked before the following step near 9.5;
- Mixture A and the $(NH_4)_2CO_3$ solution are simultaneously added dropwise to deionized water, with vigorously stirring, 500 rpm, at 80 °C, and the pH is maintained between 7 and 7.5;
- After precipitation, the resulting suspension is stirred at 80 °C, with an oil bath, for 18 h;
- The precipitate is separated by filtration and washed with deionized water checking the conductivity of the permeate;

- The recovered solid is dried for 24 h at 105 °C and then calcined at 550 °C under static air, with a heating rate of 5°C/min, and 6 h of dwell.

2.1.3.2. Ammonia evaporation method (AE)

Copper precursor salt was $Cu(NO_3)_2 \cdot 3H_2O$ (Sigma Aldrich® purity 99% degree of hydratation determined by TGA measures), silica precursor was LUDOS AS-40 (Sigma Aldrich® silica concentration 30%$_{w/w}$), and ammonia solution in water concentration was 28%$_{w/w}$ (Sigma Aldrich®).

AE synthesis follows these steps:

- $Cu(NO_3)_2 \cdot 3H_2O$ is dissolved in distilled water adding ammonia solution; the resulting solution presents a pH between 11 and 12. The solution is stirred at room temperature for 30 minutes, in this step the tri-ammonium copper nitrate is formed;
- After stirring, the correct amount of silica precursor is added to the copper ammonia complex solution and stirred for 4 h at room temperature;
- The suspension was then heated in an oil bath at 90 °C to evaporate the ammonia and the process is terminated when the pH reaches a value between 6 and 7;
- The precipitate is separated by filtration and washed with deionized water checking the conductivity of the permeate;
- The recovered solid is dried for 24 h at 105 °C and then calcined at 550 °C under static air, with a heating rate of 5°C/min, and 6 h of dwell.

2.1.4. Bi-metallic (Cu-Ni and Cu-Pd) and monometallic (Ni and Pd) catalysts

In order to increase the activity of copper catalysts, Ni or Pd were added to the copper catalysts (Ni 5%$_{w/w}$ or Pd 1%$_{w/w}$). The same two synthesis methods, HP and AE, were used for the synthesis of bimetallic catalysts Cu-Ni and Cu-Pd. Employed precursor salts were $Cu(NO_3)_2 \cdot 3H_2O$ (Sigma Aldrich® purity 99% degree of hydratation determined by TGA measures) for Cu, $Ni(NO_3)_2 \cdot 6H_2O$ for Ni, and $Pd(NO_3)_2 \cdot 2H_2O$ for Pd (Sigma Aldrich® purity 99% for last two).

The synthesis was changed accordingly to the new salts used. The following changes were implemented:

- In both syntheses, the two salts were added simultaneously during the solution preparation;

- In HP method, the pH precipitation was changed in agreement with literature [188–192] between 7 and 8 for Cu-Ni nitrates solution and between 6 and 6.5 for Cu-Pd nitrates solution.

To compare performances, both activity and selectivity, of Cu catalysts and bimetallic ones, mono-metallic Ni and Pd catalysts were also prepared with both HP and AE methods. The syntheses conditions were the same as for the bi-metallic catalysts with a single modification in HP method. To start the hydrolysis of TEOS, the pH of starting solutions was adjusted to bimetallic case values previously indicated, with few drops of diluted HNO_3 (1:200 Sigma Aldrich® concentrated nitric acid solution 65%$_{w/w}$ and deionized water).

2.1.5. Nomenclature and list of materials

Table 2-1 lists all materials synthesized or used (Lindlar and Pd/HT), with their nominal composition. From here on, the following nomenclature applies for their identification:

- Lindlar and Pd/HT maintain their names in the following discussion;
- Copper catalysts are named *CuxSiO_2XX*, where *x* is the nominal weight percentage of Cu present in the sample, and *XX* is the name of the synthesis (e.g. *Cu5SiO_2AE* nominally contains 5%$_{w/w}$ of copper supported on silica prepared by AE method);
- Nickel and palladium catalysts respect the same nomenclature (e.g. *Ni5SiO_2AE* nominally contains 5%$_{w/w}$ of nickel supported on silica prepared by AE method);
- Bi-metallic catalysts are named *CuxMeySiO_2XX*, where *Me* can be Ni or Pd, *x* is the nominal weight percentage of Cu nominally present in the sample, *y* is the nominal weight percentage of Ni or Pd, *XX* is the name of the synthesis (e.g. *Cu10Pd1SiO_2AE* nominally contains 10%$_{w/w}$ of copper and 1%$_{w/w}$ of Pd supported on silica prepared by AE method).

Table 2-1 Lists of studied materials

Name	**Nominal phase**	**Nominal Cu loading [$\%_{w/w}$]**	**Nominal Ni loading [$\%_{w/w}$]**	**Nominal Pd loading [$\%_{w/w}$]**
Lindlar	Pd-calcium carbonate	0	0	5
Pd/HT	Pd-hydrotalcite	0	0	1
Cu5SiO_2HP	Cu-silica	5	0	0
Cu10SiO_2HP	Cu-silica	10	0	0
Cu5SiO_2AE	Cu-silica	5	0	0
Cu10SiO_2AE	Cu-silica	10	0	0
Cu10Ni5SiO_2HP	Cu/Ni-silica	10	5	0
Cu10Pd1SiO_2HP	Cu/Pd-silica	10	0	1
Cu10Ni5SiO_2AE	Cu/Ni-silica	10	5	0
Cu10Pd1SiO_2AE	Cu/Pd-silica	10	0	1
Ni5SiO_2HP	Ni-silica	0	5	0
Pd1SiO_2HP	Pd-silica	0	0	1
Ni5SiO_2AE	Ni-silica	0	5	0
Pd1SiO_2AE	Pd-silica	0	0	1

2.2. Characterization methods

Characterization techniques used for the studied catalysts are:

- ICP-AES (Inductively Coupled Plasma – Atomic Emission Spectroscopy) for the quantification of:
    - Pd, Ca, and Pb in Lindlar cataysts;
    - Pd, Al, and Mg in Pd/HT;
    - Cu, Pd, and Ni in mono-metallic and bi-metallic systems supported on silica;

- N_2 physisorption associated to BET (Brunauer-Emmett-Teller) multipoint method for surface area quantification [193], and BJH (Barrett-Joyner-Halenda) estimation of pore distribution and pore volume for mesoporous materials [194];
- XRD (X-ray Diffraction) for crystalline phase identification;
- Raman spectroscopy and FTIR-ATR (Fourier-Transform Infrared spectroscopy) for Si-O-H highlight in silica supported catalysts;
- TPR (Temperature Programmed Reduction) to study samples reducibility and reduction temperature of silica supported catalysts;
- TPD- N_2O chemisorption of N_2O for copper surface determination of copper on silica and bi-metallic catalysts;
- XPS (X-ray Photoelectron Spectroscopy) for both superficial elemental composition and electronic state for silica-supported catalysts;
- SEM (Scanning Electron Microscopy) and TEM (Transmission Electron Microscopy) both combined with EDS (Energy Dispersive X-ray Spectrometry) for morphological, textural, and chemical surface analysis.

2.2.1. Ion Coupled Plasma – Atomic Emission Spectroscopy

Mass concentration of elements are measured by a VARIAN 720-ES ICP-AES. Solid samples are dissolved with a concentrated strong acid solution, then diluted in deionized water. A peristaltic pump delivers the diluted solution into a nebulizer and it is introduced inside the plasma flame. Collisions with plasma electrons and charged ions break the molecules to the respective atoms. Atoms repeatedly lose electrons and recombine, giving off the radiation at the specific wavelength of the elements involved. These wavelengths are then collected by the atomic emission spectrometer. The instrument is equipped with a custom designed Charge Coupled Device (CCD) detector, a highly sensitive photon detector. An estimation of detection limits for the quantified metals are: Cu 5 μg/L, Ni 5 μg/L, Pd 50 μg/L, Pb 50 μg/L, Ca 5 μg/L, Mg 5 μg/L, Al 20 μg/L [195].

2.2.2. Surface area and porosity analysis

A MICROMERITICS ASAP 2420 surface area and porosity analyser records N_2 adsorption and desorption isotherms at N_2 boiling point -196°C, and performs calculations by BET and BJH methods with ASAP 2420 software v2.09.

Samples consist of 50-100 mg of powder (average size of the powder between 100 μm and 125 μm). Degassing of the powder is performed before the analysis under a high vacuum, with 10 °C min^{-1} heating ramp until 250 °C and dwell overnight (at least 8 h).

Considered measures are BET surface area (S_{BET}), BJH cumulative pore volumes (V_{BJH}), BJH pore volume distributions with respect to pore sizes, and BJH averaged cylindrical pore diameter ($D_{av,BJH}$). BET isotherms assumes that:

- the heat adsorbed by the first layer is constant;
- the interaction between adsorbed molecules in the same layer can be neglected;
- the adsorbed molecule can form a new absorbing surface making the process continuous;
- the heat of adsorption for all other layers, after the first, is equal to the heat of liquefaction.

For the determination of S_{BET} the BET isotherm in linear form (Equation 2-1) is commonly used:

$$\frac{P/P_0}{n(1-P/P_0)} = \frac{1}{n_m C} + \frac{C-1}{n_m C}(P/P_0) \qquad \textit{Equation 2-1}$$

where: P and P_0 are the equilibrium and the saturation pressure of nitrogen at the temperature of adsorption, n is the quantity adsorbed, n_m is the monolayer adsorbed gas quantity, and C is the BET constant of the material (Equation 2-2):

$$C = \exp\left(\frac{E_m - E_L}{RT}\right) \qquad \textit{Equation 2-2}$$

where E_m is the heat of adsorption for the monolayer, E_L is the heat for the second and higher layers and is equal to the heat of liquefaction or heat of vaporisation. Equation 2-2 is an adsorption isotherm that can be plotted in linear fashion for a restricted portion of the 'BET plot' ($0.05<P/P_0<0.3$) (Figure 2-3):

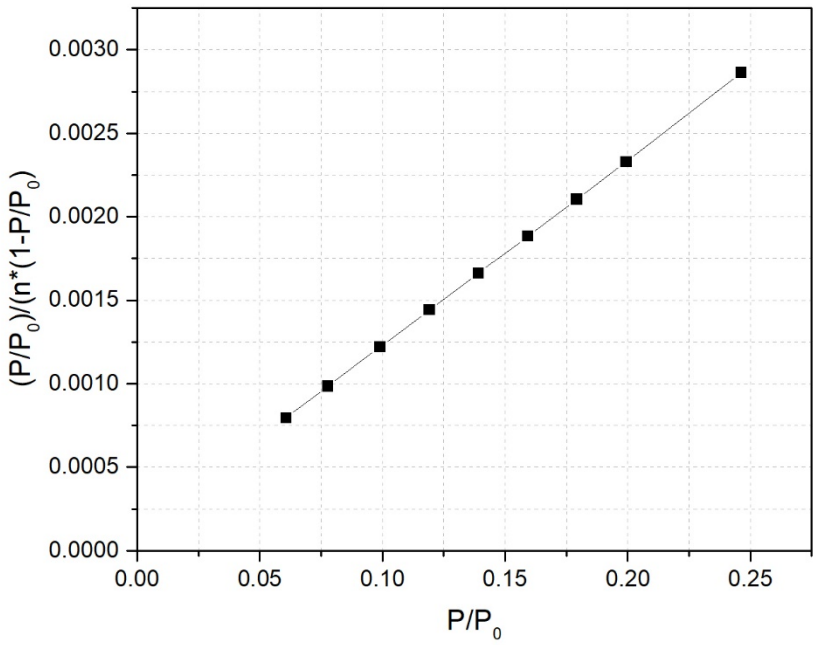

Figure 2-3 'BET plot' for the catalyst Cu10SiO2HP

Finding the intercept and the slope values of the linear 'BET plot', it is possible to calculate the monolayer n_m quantity adsorbed and the BET constant. BET surface is then obtained from the monolayer quantity adsorbed, with the knowledge of the average area occupied by the adsorbate molecules in the complete monolayer σ_m (also called *molecular cross-sectional area*), by using Equation 2-3:

$$S_{BET} = \frac{n_m L \sigma_m}{m} \qquad \textit{Equation 2-3}$$

where: σ_m is the molecular cross-sectional area (0.162 nm^2 for N_2), L is the Avogadro number, and m is the mass of the sample.

N_2 desorption data are recommended for BJH meso-porosity assessment (V_{BJH} and $D_{av,BJH}$), as they are representative of a reversible liquid-vapor transition in the case of capillary condensed molecules typical of mesopores [196–199]. BJH method is an iterative method, it is possible to obtain pore diameter distribution starting from Kelvin equation. This equation links the pore radius with the relative pressure responsible to the nitrogen adsorption or desorption in the pores (**Errore. L'origine riferimento non è stata trovata.**):

$$\ln\frac{P}{P_0} = -\frac{2\gamma V_l}{r_k R T} \qquad \textit{Equation 2-4}$$

where γ is the surface tension, V_l is the molar volume, R is the universal gas constant, T is the temperature of

the adsorption/desorption measure, r_k is the Kelvin radius.

This model is based on two assumptions: (i) all the pores have cylindrical shape, (ii) there are no interconnected pores. Varying the P/P_0, the relative adsorbate volume is recorded, obtaining the adsorption isotherm. By the Kelvin equation and BJH method an integral (i.e. cumulative) V=f(d) results. This curve is then differentiated so to get the correspondent diameter distribution curve. All these calculations are performed by the software routine.

2.2.3. X-ray diffraction

XRD spectra are acquired by an X-ray diffractometer BRUKNER AXS D8 ADVANCED. It uses the CuKα_1 radiation to detect crystalline phases, with a Bragg-Brentano geometry (Figure 2-4 Bragg's Law Reflection) following the Bragg Law (Equation 2-5).

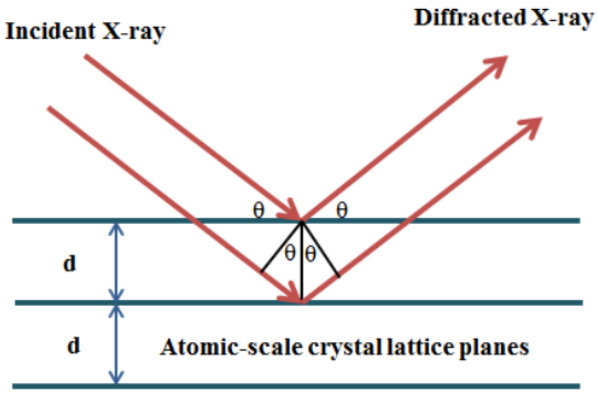

Figure 2-4 Bragg's Law Reflection

This happen when radiations, with a wavelength comparable to atomic spacings, are scattered in a specular fashion by the atoms of a crystalline system, and undergoes constructive interference:

$$2d \sin\theta = n\lambda \qquad \textit{Equation 2-5}$$

Where d is the distance in between different atomic planes, θ is the scattering angle, λ is the wavelength of the incident wave, and n is a positive integer. Powdery samples (average particle dimensions < 70 μm) are distributed on the central zone of a quartz disc sample-holder then are dispersed using pure ethanol (EtOH 99.9%) to form a thin layer.

XRD spectra are recorded in a Bragg angle range from 20° and 90° for all samples at 0.0158° scanning step and a sampling time of 1s per step. Some particular analysis is also performed for these other samples:

- For Pd/HT, since Mg-Al hydrotalcites possesses the most intense ray at 12° the spectra are recorded between 5° and 90°;
- For samples with copper and silica, since amorphous phases are present, in order to improve the resolution of spectra, they are reacquired in the range between 20° and 50° at 0.0158° scanning step and a sampling time of 3 s per step. In this range, it is possible to observe the main rays for the phases previously detected on standard spectra.

Phase identification is performed with the proprietary software environment EVA, by comparison with PDF (Powder Diffraction Files) from the database of the ICDD (International Centre of Diffraction Data), formerly known as JCDPS (Joint Committee on Powder Diffraction Standards).

Acquired spectra are also used, when the main rays could be separated, for the estimation of average crystallite sizes (L) of the main detected phases, by Scherrer equation (Equation 2-6)[200,201]:

$$L = \frac{K\lambda}{\beta \cos(2\theta/2)} \qquad \textit{Equation 2-6}$$

Constants K (dimensionless shape factor of the crystallite) and λ (wavelength of CuKα1 radiation) are set equal to 0.9 and 1.5406 nm, respectively, β (FWHM Full Width at Half Maximum, in radian), and 2θ (Bragg angle in radian) of the main less overlapped crystalline rays. Estimation of these quantities was performed manually using the tools of the EVA software.

2.2.4. Raman and FTIR-ATR Spectroscopy

The Raman spectroscopy is based on the principle of the inelastic scattering of the light in a process. The sample is exposed to a laser. Raman spectra are acquired by an HORIBA JOBIN YVON LabRam ARAMIS equipped with two lasers at 532 nm (green) and 785 nm (red), 6 Raman filters of different types used to prevent undesired light from reaching the spectrometer and drowning out the relatively weak Raman signal, and four different gratings 600, 1200, 1800, and 2400 grid mm^{-1}. Raman spectrometer is coupled with an optical confocal microscope for non-destructive characterization of the molecular composition and the structure of a material. Moreover, by focusing the laser beam via an optical microscope, it can be sound the properties of the material superficially by mapping and in a volume of some μm^3.

The coupled confocal microscope has six different lenses: x10, x50, x50 LWD, x100, x100 LWD, x10 for oil immersion and is motorised in XYZ stage.

The sample, around 20 mg, is deposited on a glass slide and flattened with ethanol. The glass slide is then positioned on the motorised stage and the desired lens is chosen (manually done), the stage is adjusted mechanically and then regulated and the lenses focused with a joystick.

For copper silica catalysts, both calcined and reduced catalysts are analysed with the apparatus described above. In particular, due to instability of the Cu^{+}/Cu^{0} superficial layer that is oxidized by the laser and the air in the chamber, only the low energy laser (532 nm) is used for both samples. Accumulation time of signal is set equal to:

- Calcined samples: 1 minute, 2 minutes and 3 minutes;
- Reduced samples: 1 minutes (same instability detected over longer time acquisition).

Signals are acquired from 200 cm^{-1} to 1850 cm^{-1}.

The spectra acquired are compared to literature results for copper [202] and copper silica catalysts [165,168,176,178,179] and with online databases collected by RRUFF Project [203], the WURM Project for theoretical calculations on Raman spectra [204], and the database of University of Parma [205].

Fast Fourier Transform Infrared Spectroscopy Attenuated Total Reflectance (FTIR-ATR) measures are performed on prepared catalysts to integrate the information obtained by Raman Spectroscopy, in particular trying to better understand the presence of bonds between Si-OH, Si-O-Si, and Cu-OH.

The instrument used is a FT-IR NEXUS 870 THERMONICOLET. The IR sources were: a white incandescence tungsten Globar lamp. FT-IR measures were obtained in the medium infrared field, range 400 cm^{-1} up to 4000 cm^{-1}, utilizing the ATR sampling technique which enables to analyse the samples directly without further preparation. The ATR crystal is a diamond.

2.2.5. X-ray Photoelectron Spectroscopy

The measures are performed in a THERMO VG MULTILAB 2000. An aluminium anode is used as a radiation source. The principle is based on the measurement of kinetic energy emitted from the powder sample under the impact of a photon beam energy of X-ray (hν). Any core or valence electron having a binding energy less than hν may be ejected from the sample and acquired as signal. The binding energy is characteristic of the atomic energy levels of different elements. The analysis depth is lower than 10 nm, and detection limit for the instrument is $0.1\%_{atom}$. The instrument can be operated with powder under ultra-high vacuum.

Both X-ray photoelectron spectroscopy and Auger electron, in particular of the LMM typology, are interesting in the Cu^{+}/Cu^{0} ratio determination, Cu chemical state as reported in literature, but also in the interaction of copper with Ni and Pd [175,180,206–212].

2.2.6. Temperature programmed reduction

Temperature Programmed Reduction (TPR) is carried out on a MICROMERITICS AUTOCHEM II 2920 chemisorption analyser. The sample of 100 mg catalyst, with particles size between 100 μm and 125 μm, loaded in a Flow-Thru "U" shaped fused quartz tube (9 mm ID), placed between two quartz wool flocks to form a packed bed. This reaction cell is placed inside a furnace controlled by internal thermocouple.

Before TPR, a TPD (Temperature Programmed Desorption) is operated to eliminate all the possible absorbed gases on the catalyst surface, with a ramp of 20 °C min^{-1} up to 450 °C, a dwell at 450 °C for 30 minutes, and cooling down to room temperature, all under Ar stream of 50 Nml min^{-1}. After this, actual TPR starts with a 10 °C min^{-1} ramp heating up to 450 °C, a dwell of 2h at 450 °C, under 50 Nml min^{-1} flow of reducing gas ($10\%_{vol}$ H_2 in Ar).

Downstream the reaction cell, a cold trap retains the produced steam then a TCD (Thermal Conductivity Detector) measures H_2 consumption, and then recorded together versus temperature and time. The data are saved by AUTOCHEM II software v4.02.

The reduction degree (R in Equation 2-7) of the samples is evaluated by reducibility of the single active phase present in the catalyst, which is calculated from H_2 consumption measured divided by theoretical H_2 consumption needed for the reduction of the metals oxides, obtained by ICP-AES measures.

$$R = \frac{H_2 consumption\ from\ TPR}{theoretical\ H_2 consumption} \cdot 100 \qquad \textit{Equation 2-7}$$

2.2.7. Temperature programmed desorption with N_2O

The metallic copper surface is characterized by N_2O Temperature Programmed Desorption. The MICROMERITICS AUTOCHEM II 2920 chemisorption analyser is also used for these experiments in continuous flow conditions [213,214]. The N_2 and H_2 signals are measured by TCD.

Firstly 400 mg of sample is charged in the Flow-Thru "U" shaped fused quartz tube (9 mm ID), then the catalyst is reduced under $10\%_{vol}$ H_2 in Ar (50 Nml min^{-1} flow rate) at 300 °C overnight with 3 °C min^{-1}

rate. Before the N_2O TPD, a flow rate of 2% N_2O in Ar (50 Nml min^{-1}) is sent to the TCD detector; TCD signal is acquired until a stable signal is reached. The loop was therefore purged with Ar and then it is oxidized by the same flowrate of 2% N_2O in Ar (50 Nml min^{-1}) for 1 hour at 50 °C. The reaction which takes place is the following (Reaction 2-1):

$$2Cu + N_2O \rightarrow Cu_2O + N_2$$

Reaction 2-1

In Figure 2-5, a curve of N_2O-TPD produced with the AUTOCHEM II 2920 apparatus, is reported for a copper catalyst:

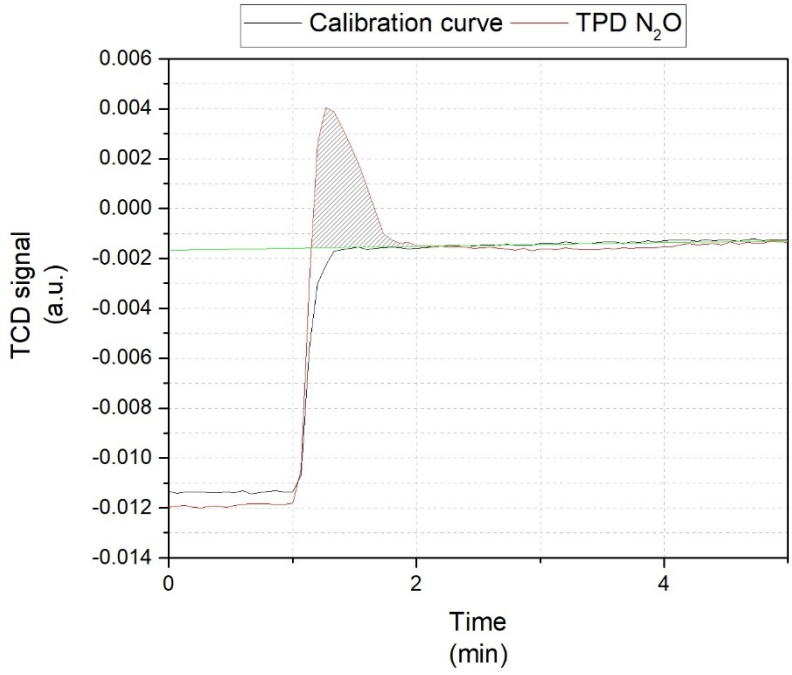

Figure 2-5 TCD signal overtime for the N_2O-TPD of a copper catalyst with MICROMERITICS AUTOCHEM II 2920

After calculating the area under the curve (in Figure 2-5), it is possible to calculate the moles of N_2 formed during the reaction and then to deduct moles of N_2O consumed. With the assumption that the area per copper surface atom in the Cu planes (100), (110), and (111) are 0.065, 0.092, and 0.0563 nm^2, respectively. An equal abundance of these three planes gives an average 0.0711 nm^2, equivalent to $1.46 \cdot 10^{19}$ Cu atoms per square meter. By assuming a spherical shape of the copper metal particles, it is possible to express the surface of Cu as in Equation 2-8:

$$S_{Cu^0}(m^2 g_{Cu}{}^{-1}) = 2\frac{V}{V_m} \cdot \frac{6.022 \cdot 10^{23}}{1.46 \cdot 10^{19} \cdot m_{Cu}}$$

Equation 2-8

where: 2 is the stoichiometric factor for Cu (Reaction 2-1) , *V* is the adsorbed volume of N_2O, *Vm* is the molar volume, $6.022 \cdot 10^{23}$ is the Avogadro number, $1.46 \cdot 10^{19}$ are the number of Cu atoms per square meters, and m_{Cu} is the mass of Cu in the sample measures by ICP-AES.

2.2.8. Scanning electron microscopy

SEM images are recorded by a ZEISS GEMINI SEM 500 device for synthetized catalysts. Operative conditions are: high tension 15 kV, detector BSE (Back Scattering Electron) Z-contrast mode, and vacuum in control-pressure mode.

Samples in powder form are observed on their external surface. At first samples were not metallized with a thin layer of gold on the surface in order to eliminate Au signal from elemental analyses.

Elemental analyses are performed by in-situ EDS, the ZEISS GEMINI SEM 500 is equipped with an OXFORD ENERGY 250 INCAx-act detector. EDS spectra are acquired both on spots or zones of external surfaces. Also, some topography analysis is made with the instrument on the surfaces of the samples; these kinds of maps give qualitative information about the distribution of copper.

2.2.9. Transmission electron microscopy

TEM images are acquired by JEOL 2100 LaB_6 (lanthanum hexaboride filament), operating a 200 kV, with punctual resolution equal to 0.2 nm in parallel mode and 2-3 nm in STEM (Scanning Transmission Electron Microscopy) mode, equipped with a SDD detector (30 mm^2) for elemental analyses by in-situ EDS.

About 5 mg of powder is dispersed in pure ethanol and sonicated for 5 minutes, so to obtain a suspension. 2 or 3 drops of this catalyst suspension is deposited on the sample-holder, a polymeric membrane sustained by copper grid. After ethanol evaporation the particles of powder are dispersed on the membrane.

Because of the sample-holder contains both C and Cu, these two elements easily appear on STEM-EDS elemental analyses as contaminant agents. However, also in some catalysts Cu is present as active phase so when possible, the elemental analyses are performed in an isolated location in a membrane void hole.

2.3. Reaction tests

2.3.1. Oil tested

Two different kinds of commercial vegetable oils were used during the development of this thesis: Canola rapeseed oil (*B. napus*) and sunflower oil (*H. annuus*). The oils used have been previously de-odorized and bleached.

Canola rapeseed oil was chosen because it is more exploitable at the industrial level. On the other hand, sunflower oil allows obtaining higher C18:1 increment during the reaction starting from a relatively low initial percentage of C18:1 and higher content of polyunsaturated compounds (mainly C18:2).

2.3.2. Catalysts reduction

Before each hydrogenation test, the catalytic sample must be reduced as reported in literature [4,92,111,139,143,186,215–218]. Except Lindlar catalyst already bought in reduced form and HT-Pd catalyst reduced by means of reaction of PdO with cyclohexene during the last step of the synthesis, all other catalysts were reduced by ex-situ dry reduction, following indications about copper catalysts reduction in literature [109,111,160,162] and the results of TPR experiments of this work. The core of the reduction apparatus is AISI 316L stainless steel fixed bed reactor in vertical configuration, ½" nominal outside diameter. About 6 g of granular sample, particle size between 70 μm and 100 μm, constitute the bed to be reduced. The reactor is located inside a CARBOLITE MTF cylindrical furnace.

Available inlet gases are H_2 and N_2, their flowrates are regulated by BRONKHORST EL-Prestige mass flow controllers controlled by PC proprietary software Flow-DDE2 and Flow-VIEW. A flow of 200 NmL.min^{-1} (30%$_{v/v}$ of H_2) is fed into the reactor.

Downstream the reactor, a GC-filter charged with zeolite spheres captures water. Overall dried gas flowrate passes through a BRONKHORST mass flow meter, and then access an ABB online system equipped with ADVANCE OPTIMA CALDOS 17 module, measuring H_2 volumetric concentration by TCD. Since ABB system requires a minimum inlet flowrate of about 500 Nml min^{-1} for optimal measures, an additional N_2 dilution stream is needed.

An automated control/acquire system, developed and customized by DigiPower S.r.l., records volumetric concentrations and overall dried gas flowrates, samples were stored under nitrogen atmosphere to avoid reoxidation.

2.3.3. Reactivity tests

In Figure 2-6 the laboratory-scale test apparatus for vegetable oils hydrogenation tests is schematized and in Figure 2-7 a photo of the setup is shown.

The core of the system is a Parr Instruments batch reactor model 4560 with a volume of 600 mL. Reactor heating is provided by the electric furnace managed by the proprietary Parr Instrument 4840 automatic control, associated with a thermocouple (type L) plunged in the reaction volume. The reactor is stirred employing Parr magnetic drive; it uses completely enclosed magnetic couplings. The magnetic agitator is composed of an external drive and an inner drive (driven); they have a neodymium-iron magnets epoxy bonded to iron cores. These components cannot reach 130 °C, temperature which would destroy the bonding of the magnet assemblies resulting in leakage of the system and incorrect functioning of the stirring. In order to prevent this possibility the magnetic drive is cooled by a continuous flow of water; a peristaltic membrane pump STEMPDOS FEM03 provides the flow rate of distilled water (for tests with a temperature higher than 80 °C).

Two feeding lines provide continuously the gases for all operative steps: N_2 flow for pressuring and purging the reactor, and in cooling operation; H_2 flow used during reactivity tests. Flowrates are regulated by already mentioned BRONKHORST EL-Prestige mass flow controllers controlled by PC proprietary software Flow-DDE2 and Flow-VIEW. During all steps, gas flowrate is set to 200 $NmL.min^{-1}$.

Pressure inside the reactor is controlled with a BRONKHORST Back Pressure Regulator (250 $NmL.min^{-1}$ maximum flowrate), that acts also as precision manometer.

The reactor is loaded with 200 mL of oil and the reduced catalyst in the chosen amount (see operating conditions in Table 2-2). Type of oil and amount of catalyst depend on the specific test carried out. Then the reactor is closed and purged for 30 minutes with continuous nitrogen flow. When the operative conditions are reached and stable, the inlet flow is switched from N_2 to pure H_2: this is the starting time of hydrogenation.

During tests, sampling frequency is usually 30 minutes but higher sampling frequency is adopted in some tests. During sampling, the flow in the reactor is interrupted closing the inlet valve and opening the sampling

valve. One millilitre of oil is taken from the reactor, both the oil and the catalyst are sampled. The sample is then centrifuged to remove the catalyst and collected in vial in order to perform the successive analysis steps.

Table 2-2 Reactivity test conditions: catalyst concentration in oil, temperature, pressure, test length, sampling frequency, and number of cycles

Test number	Catalyst	Oil	Catalyst concentration (mg/ml)	Temperature (°C)	Pressure (bar)	Test length (min)	Sampling frequency (min^{-1})	Cycle number
Test 01	Lindlar	Canola	4	60	4	360	30	-
Test 02			4	60	12	360	30	-
Test 03			4	120	8	360	30	-
Test 04			4	180	4	360	10/30	-
Test 05			4	180	12	360	10/30	-
Test 06			2	180	4	120	15	-
Test 07			1	180	4	120	15	-
Test 08			4	180	4	60	15	I
Test 09			4	180	4	60	15	II
Test 10			4	180	4	60	15	III
Test 11			4	180	4	60	15	IV
Test 12			4	180	4	60	15	V
Test 13		Sunflower	4	180	4	360	30	-

Table 2-2 Reactivity test conditions: catalyst concentration in oil, temperature, pressure, test length, sampling frequency, and number of cycles (continue)

Test number	Catalyst	Oil	Catalyst concentration (mg/ml)	Temperature (°C)	Pressure (bar)	Test length (min)	Sampling frequency (min^{-1})	Cycle number
Test 14	Pd/HT	Sunflower	0.5	90	8	120	15	I
Test 15			1	180	4	360	30	I
Test 16			1	180	4	120	30	II
Test 17			1	180	4	120	30	III
Test 18			1	180	4	120	30	IV
Test 19			1	120	4	240	30	I
Test 20			1	120	4	240	30	II
Test 21			1	120	4	120	30	III
Test 22			0.5	120	4	240	30	I
Test 23			0.5	120	4	120	30	II
Test 24			0.5	120	12	240	30	I
Test 25			0.5	120	12	120	30	II
Test 26			2	120	4	240	30	I
Test 27			2	120	4	120	30	II

Table 2-2 Reactivity test conditions: catalyst concentration in oil, temperature, pressure, test length, sampling frequency, and number of cycles (continue)

Test number	Catalyst	Oil	Catalyst concentration (mg/ml)	Temperature (°C)	Pressure (bar)	Test length (min)	Sampling frequency (min^{-1})	Cycle number
Test 28	$Cu5SiO_2AE$	Canola	4	180	4	240	30	-
Test 29			4	180	12	240	30	-
Test 30			4	200	4	240	30	-
Test 31			4	200	12	240	30	-
Test 32	$Cu5SiO_2HP$	Canola	4	180	4	240	30	-
Test 33			4	180	12	240	30	-
Test 34			4	200	4	240	30	-
Test 35			4	200	12	240	30	-
Test 36	$Cu10SiO_2AE$	Canola	4	180	4	240	30	-
Test 37			4	180	12	240	30	-
Test 38			4	200	4	240	30	-
Test 39			4	200	12	240	30	-
Test 40			8	180	4	240	30	-
Test 41			8	180	12	240	30	-
Test 42			8	200	4	240	30	-

Table 2-2 Reactivity test conditions: catalyst concentration in oil, temperature, pressure, test length, sampling frequency, and number of cycles (continue)

Test number	Catalyst	Oil	Catalyst concentration (mg/ml)	Temperature (°C)	Pressure (bar)	Test length (min)	Sampling frequency (min^{-1})	Cycle number
Test 43	$Cu10SiO_2AE$	Canola	8	200	12	240	30	
Test 44			2	180	4	240	30	-
Test 45			2	180	12	240	30	-
Test 46			2	200	4	240	30	-
Test 47		Sunflower	4	180	4	360	30	-
Test 48			4	180	12	360	30	-
Test 49			4	200	4	360	30	-
Test 50	$Cu10SiO_2HP$	Canola	4	180	4	240	30	-
Test 51			4	180	12	240	30	-
Test 52			4	200	4	240	30	-
Test 53			4	200	12	240	30	-
Test 54			8	180	4	240	30	-
Test 55			8	180	12	240	30	-
Test 56			8	200	4	240	30	-
Test 57			8	200	12	240	30	-

Table 2-2 Reactivity test conditions: catalyst concentration in oil, temperature, pressure, test length, sampling frequency, and number of cycles (continue)

Test number	Catalyst	Oil	Catalyst concentration (mg/ml)	Temperature (°C)	Pressure (bar)	Test length (min)	Sampling frequency (min^{-1})	Cycle number
Test 58	$Cu10SiO_2HP$	Canola	2	180	4	240	30	-
Test 59			2	180	12	240	30	-
Test 60			2	200	4	240	30	-
Test 61		Sunflower	4	180	4	360	30	-
Test 62			4	180	12	360	30	-
Test 63			4	200	4	360	30	-
Test 64	$Cu10Ni5SiO_2HP$	Sunflower	4	180	4	360	30	-
Test 65	$Cu10Pd1SiO_2HP$	Sunflower	4	180	4	360	30	-
Test 66	$Cu10Ni5SiO_2AE$	Sunflower	4	180	4	360	30	-
Test 67	$Cu10Pd1SiO_2AE$	Sunflower	4	180	4	360	30	-
Test 68	$Ni5SiO_2HP$	Sunflower	4	180	4	360	30	-
Test 69	$Pd1SiO_2HP$	Sunflower	4	180	4	360	30	-
Test 70	$Ni5SiO_2AE$	Sunflower	4	180	4	360	30	-
Test 71	$Pd1SiO_2AE$	Sunflower	4	180	4	360	30	-
Test 72	$Cu10Pd1SiO_2AE$	Sunflower	4	120	4	360	60	-

Table 2-2 Reactivity test conditions: catalyst concentration in oil, temperature, pressure, test length, sampling frequency, and number of cycles (continue)

Test number	Catalyst	Oil	Catalyst concentration (mg/ml)	Temperature (°C)	Pressure (bar)	Test length (min)	Sampling frequency (min^{-1})	Cycle number
Test 73	$Cu10Pd1SiO_2AE$	Sunflower	4	120	12	360	60	-
Test 74			4	120	20	360	60	-
Test 75			4	180	4	360	60	-
Test 76			4	180	20	360	60	-
Test 77			4	240	4	360	60	-
Test 78			4	240	20	360	60	-
Test 79			4	200	12	360	60	-

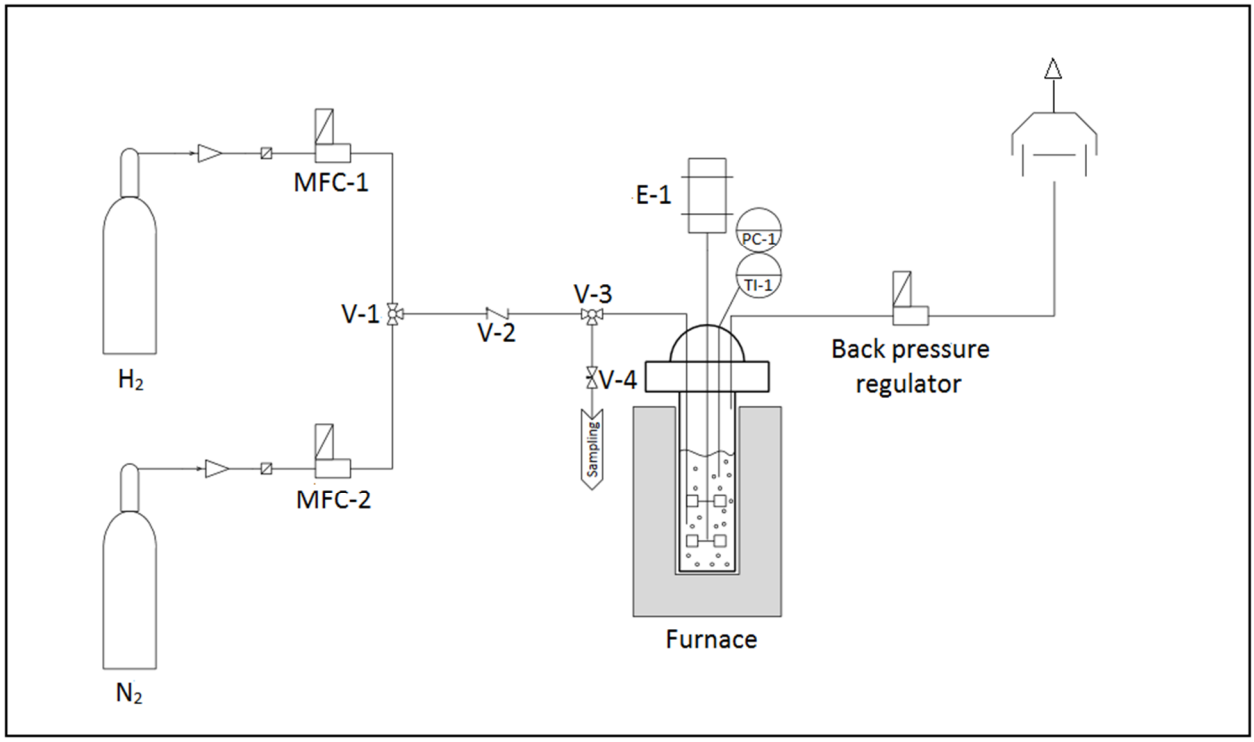

Figure 2-6 Schematic view of semi-batch hydrogenation apparatus for hydrogenation reactivity tests.

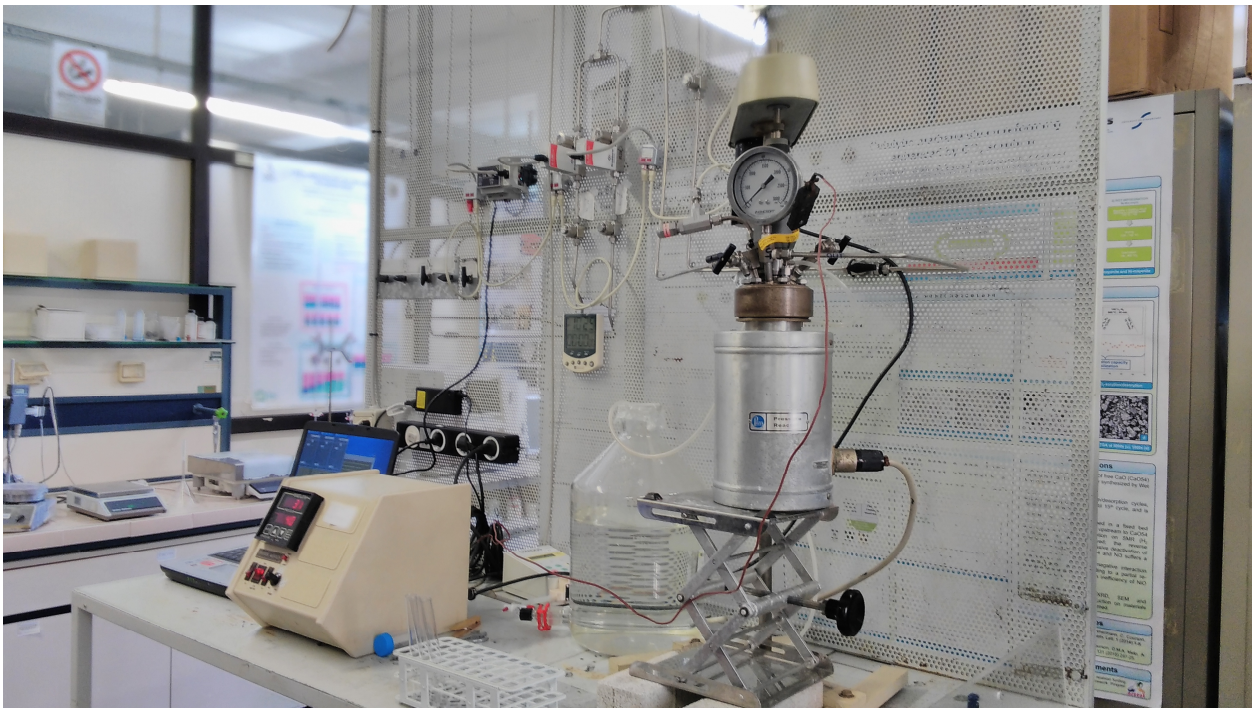

Figure 2-7 Photo of the laboratory scale setup.

2.3.4. Transesterification and GC-analysis

All oil collected samples during the hydrogenation reactivity tests are transesterified by a standardized transesterification method, AOAC 969.33 [5] specifically developed for the preparation of samples of fatty acids methyl esters to be used in GC analysis. The method uses as reagents: collected samples of oils, methanolic solution of BF_3 14%$_{v/v}$ (Sigma Aldrich® ≈14%$_{v/v}$), NaOH solution 0.5 M in methanol (NaOH ACROSS ORGANICS® 99.9%, Methanol Dry Sigma Aldrich® 99.9%), n-Hexane (n-Hexane Sigma Aldrich® GC-grade 99.5%), NaCl saturated solution (Sigma Aldrich® 99%), and Na_2SO_4 for drying (Carlo Erba 98% pure).

350 mg of sample is loaded in a 50 mL flask with 6 mL of NaOH methanolic solution, then a condenser is connected to the flask and the mixture is boiled under reflux since fat globules disappear. For the most of the samples, 10 minutes are needed for this step. After that, 7 mL of BF_3 solution is added from the top of the condenser and the solution is boiled for 2 other minutes. Then, 5 mL of hexane are added through the condenser and boiled 1 minute longer. The heating and the condenser are removed, a saturated solution of NaCl is then added under vigorous agitation to separate the organic phase by decantation into the neck of the flask. About 1 mL of the upper hexane solution is transferred in a 2 mL vial and dried with a small amount of anhydrous Na_2SO_4.

Trans-esterified samples are analysed by GC-FID with a Varian 3400 GC equipped with Flame-Ionization Detector (FID) and with a Supelco® SP-2380 GC capillary column (30 m x 25 µm) composed of stabilized 90% bis-cianopropyl/10%cyanopropylphenyl siloxane. Injection are made with a 10 µL manual syringe HAMILTON®.

Gas chromatography runs were conducted in isothermal conditions at 180 °C during 25 minutes with N_2 carrier (injector at 220 °C; detector at 220 °C). Samples were analysed in split mod analysis with a split flowrate of 25 mL/min. Identification of FAME peaks are achieved by comparison with commercially available standards reported in Table 2-3, bought from Sigma Aldrich® and Supelco®. Data acquisition of the chromatographic peaks is automatically performed by the acquisition software VARIAN Star v6.02; the peaks areas were calculated with the Software VARIAN Star GC-MS v6.02. An analysis with the standards is periodically performed for external calibration. Each sample is analysed at least two times in the same conditions.

Table 2-3 List of samples used in the identification of different peaks

Standards
Canola Oil
Sunflower Oil
F.A.M.E. Mix C14-C22
Linolenic Acid Methyl Esters Mix
Linoleic Acid Methyl Esters Mix
Supelco 37 F.A.M.E. Mix

The retention time for the different components of interest are listed in Table 2-4. As found among the retention times, the peaks of trans oleic acid methyl ester (elaidic acid methyl ester) and the peak of cis oleic methyl acid are very close and when the concentration is high (large peak at the bottom) this could determine the overlapping of the two peaks. In order to solve this problem and give an evaluation of elaidic acid the deconvolution instruments of the software Star Chromatography Workstation Version 6 (previously VARIAN now Agilent) is used. Since the deconvolution is affected by error in §Chapter 5 the elaidic and oleic acid are given as C18:1 together. To calculate the specific isomers index (SII see §2.3.5 for the definition) the evaluation of elaidic acid are reported in Appendix A.

Table 2-4 Retention time for the most interesting FAME individuated by gas chromatography

Component	**Retention Time**
Myristic FAME	4.12
Palmitic FAME	5.23
Stearic FAME	6.81
Elaidic FAME	7.33
Oleic FAME	7.62
t,t Linoleic FAME	8.23
c,t Linoleic FAME	8.58

t,c Linoleic FAME	8.70
c,c Linoleic FAME	9.12
Behenic FAME	9.65
Linolenic FAME	10.81
Erucic FAME	15.22

As an example it is reported one gas chromatogram where the overlapping is visible (Figure 2-8).

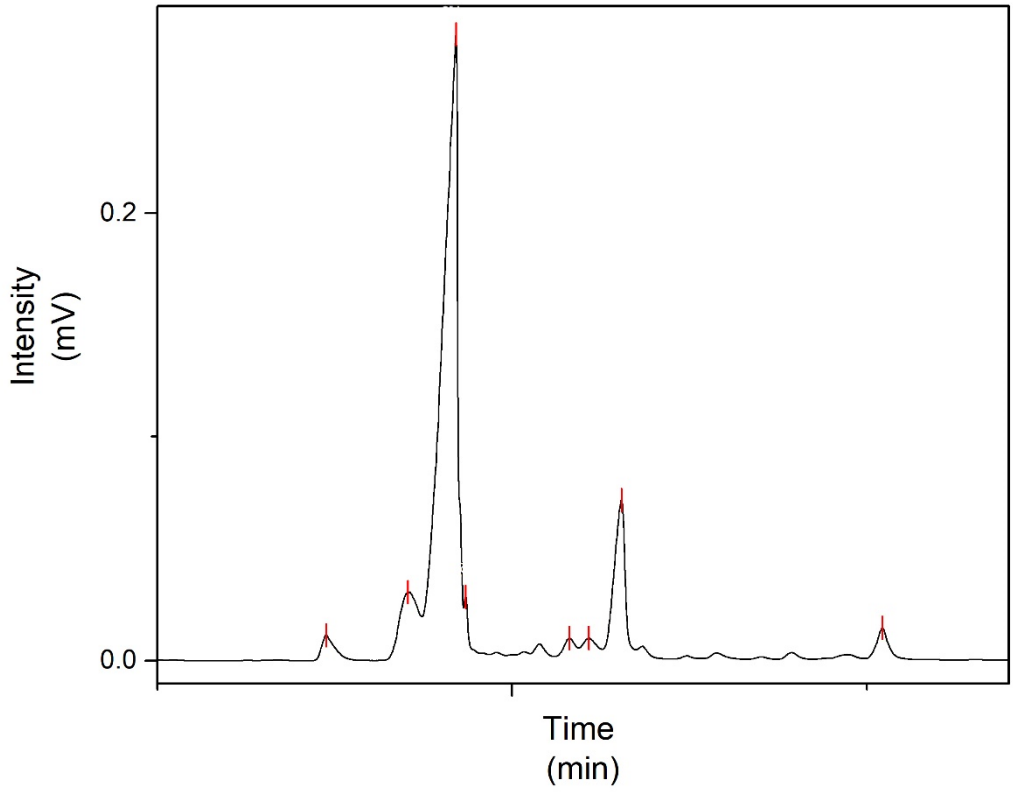

Figure 2-8 Gas Chromatogram of test 07 at 180 °C and 4 bar with 1 $mg_{catalyst}/mL_{oil}$, the specific chromatogram obtained for the sample at 90 minutes, the C18 zone highlighted, from left to right: stearic FAME (C18:0), elaidic FAME (t-C18:1), oleic FAME (c-C18:1), isomers of linoleic FAME (iso -C18:2), linolenic FAME (C18:3)

2.3.5. Reactivity and Selectivity

Reactivity performances were evaluated in terms of linolenic acid conversion (Equation 2-9, when applicable), linoleic acid conversion (Equation 2-10), and Iodine Value variation.

$$\chi_{C18:3} = \frac{(C18:3)_0 - (C18:3)_t}{(C18:3)_0} * 100$$ Equation 2-9

where $(C18:3)_0$ and $(C18:3)_t$ are the relative percentage of linolenic acid at initial time (t = 0) and at given time t.

$$\chi_{C18:2} = \frac{\sum_j (C18:2)_0 - \sum_j (C18:2)_t}{\sum_j (C18:2)_0} * 100$$ Equation 2-10

where $\sum_j (C18:2)_0$ and $\sum_j (C18:2)_t$ are the relative percentage of linoleic acid and its isomers at initial time (t = 0) and at given time t.

Iodine Value (IV) is defined as the mass of iodine in grams that is consumed by 100 grams of a chemical substance, it is used to determine the amount of unsaturations in fatty acids. The higher the IV value, the more double bonds are present in the oils. IV can be calculated using the indication in the international standard ISO 3961:2018 from GC composition [219] (Equation 2-11**Errore. L'origine riferimento non è stata trovata.**):

$$\text{IV} = (x_{C16:1} \cdot 0.950) + (x_{C18:1} \cdot 0.860) + (x_{C18:2} \cdot 1.732) + (x_{C18:3} \cdot 2.616) + (x_{C20:1} \cdot 0.785) + (x_{C22:1} \cdot 0.723)$$ Equation 2-11

where $w_{Cx:y}$ are the percentages of the different unsaturated compounds normally found in vegetable oils.

In order to evaluate the selectivity towards various acids a simple pseudo-first order scheme of series reactions, omitting isomerization of double bonds, was taken into account [116] (Equation 2-12):

$$(C18:3) \overset{k_3}{\rightarrow} (C18:2) \overset{k_2}{\rightarrow} (C18:1) \overset{k_1}{\rightarrow} (C18:0)$$ Equation 2-12

The scheme reported can be used because tests were conducted under mild pressure and temperature conditions. When higher pressures were imposed, direct hydrogenation of C18:2 to C18:0 and C18:3 to C18:1 should be taken into account as reported in literature [220–222].

This system can be described by a series of first order differential equations:

$$\frac{d(C18:3)}{dt} = -k_3 \cdot (C18:3)$$ Equation 2-13

$$\frac{d(C18:2)}{dt} = k_3 \cdot (C18:3) - k_2 \cdot (C18:2)$$ Equation 2-14

$$\frac{d(C18:1)}{dt} = k_2 \cdot (C18:2) - k_1 \cdot (C18:1)$$ Equation 2-15

This set of differential equations was analytically solved by Bailey et al. in [222]; in this manuscript, it was employed the software MAPLE18® for the integration of the differential equation system (see Appendix A).

Instantaneous selectivity is the production rate of one component per production rate of another component. Overall selectivity is defined as the number of moles of desired product per the number of moles of undesired product (Definition 1). However, the definitions of the total amount of reactant to form a product per total amount of reactant consumed is used (Definition 2) as well as the total amount of desired product formed per total amount of limiting reactant consumed (Definition 3)[223].

According to literature [116,222], selectivity of linolenic acid (S_{Ln}) (Equation 2-16) and of linoleic acid (S_{Le}) (Equation 2-17) and selectivity towards geometric isomers of C18:1 expressed by the specific isomers index (SII) (Equation 2-18) were defined as:

$$S_{Ln} = k_3/k_2 \qquad \text{Equation 2-16}$$

$$S_{Le} = \mathrm{k}_2/k_1 \qquad \text{Equation 2-17}$$

$$SII = \frac{(trans)_t - (trans)_0}{IV_0 - IV_t} \qquad \text{Equation 2-18}$$

where IV_0 and IV_t are the iodine value at initial time (t = 0) and at given time t.

Chapter 3

Catalysts characterisation

This chapter reports the characterisation results for each catalyst used or synthesised during the thesis. These characterizations were performed to evaluate the elementary composition (ICP-AES), the textural properties (BET/BHJ from adsorption isotherm), the presence of crystalline phases and their crystallites size (XRD), the morphology and topography (SEM/EDX and/or TEM), the silicium environment (FTIR and Raman), the reducibility of metal oxides (TPR), the phases present after reduction and their crystallites size (XRD), the metallic surface (chemisorption), and the oxidation state of metals (XPS).

Each paragraph contains the results for each one of them in the following order:

- *Lindlar catalyst characterisation;*
- *Pd/HT characterisation;*
- *Silica supported catalysts characterisation.*

3.1. Lindlar catalyst characterisation

In the following, all information on Lindlar catalyst are reported. Since the catalyst is of commercial origin, just the essential characterisations were performed.

3.1.1. Lindlar elemental analysis

Lindlar catalyst ICP-AES elementary results are reported in Table 3-1. The actual Pd load is less than the nominal Pd content (Pd ≤ 5%).

Poisoning with lead is confirmed. Lead content is in accordance with previously reported literature data on synthesised or bought samples of Lindlar, or Lindlar-like catalysts [181–184].

Calcium content is in line with the assumption of calcium carbonate support.

Table 3-1Elementary composition of Lindlar catalyst.

Sample	**Pd (%)**	**Ca (%)**	**Pb (mg/kg)**
Lindlar	2.03±0.07	40±1	0.37±0.03

3.1.2. Lindlar textural properties: BET-BJH results and shape of adsorption isotherms

N_2 adsorption curves (Figure 3-1) permitted to identify mesoporous material (isotherm type IV) and to evaluate low surface area, pore volume and pore size (S_{BET} 4.12±0.09 m^2/g, V_{BJH} 7.81±0.05 mm^3/g and average pore size 7.21±0.87 nm) by BET-BJH methods. The available surface area is in line with the results previously obtained [224]. Probably the specific surface is equal to the surface area of the low porosity calcium carbonate substrate.

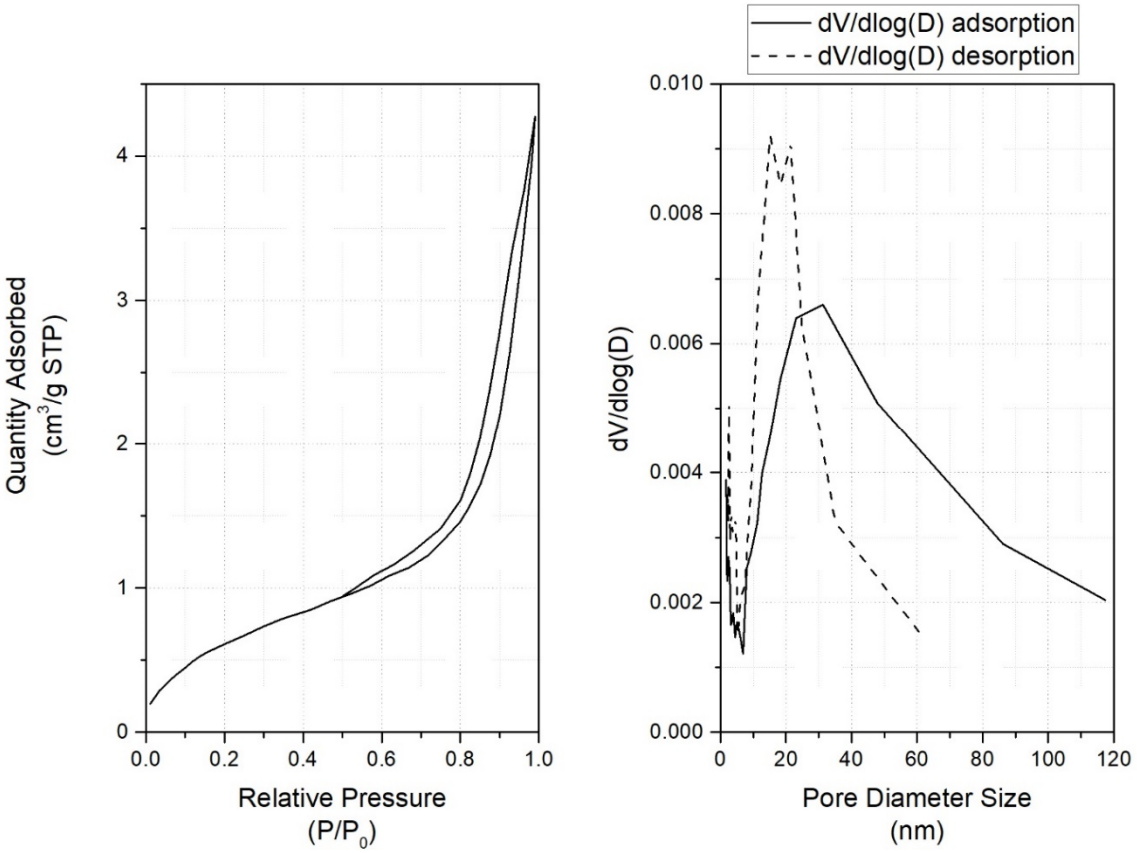

Figure 3-1 BET Isotherms (left) and BJH adsorption and desorption pore size distribution (right).

Analysing the cumulative pores volume and the pores volume distribution (Figure 3-2), it appears that the catalyst presents very few micro-porosities; this could be beneficial in order to avoid diffusion mass-transfer limitation during the reaction. Overall the catalyst presents porosities that well represent mesoporous materials, since the majority of the pores are in the mesopores range with few smaller (below 2 nm) and very few larger pores in the macro-pores area.

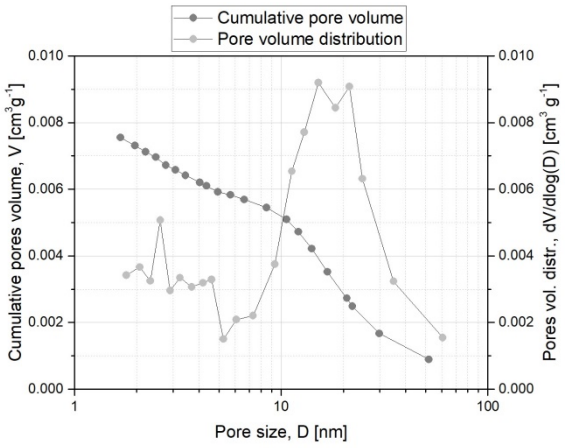

Figure 3-2 Desorption BJH porosity assessment of Lindlar catalyst.

3.1.3. Lindlar crystalline phases analysis

XRD spectra of Lindlar catalyst (Figure 3-3) shows predominance of calcium carbonate in crystalline form (crystallite size around 9 nm calculated from the more intense ray at 29.4°) associated to metallic palladium. In particular, two rays of calcium carbonate cover the most intense ray of Pd^0 at 39.8°, and Pd ray may be the cause for the deformation of the $CaCO_3$ ray at 40°. The secondary rays of Pd^0 are partially covered or are not found. Moreover, XRD spectra did not permit to detect any trace of PdO since the principal rays of this phase (at 34°, 54.9°, and 71.2°) are not present, and cannot overlap with the much more intense rays of calcium carbonate support.

Since a minimal amount of lead is found by ICP-AES, it is also impossible to individuate any ray correlated with lead crystalline phases (Figure 3-3).

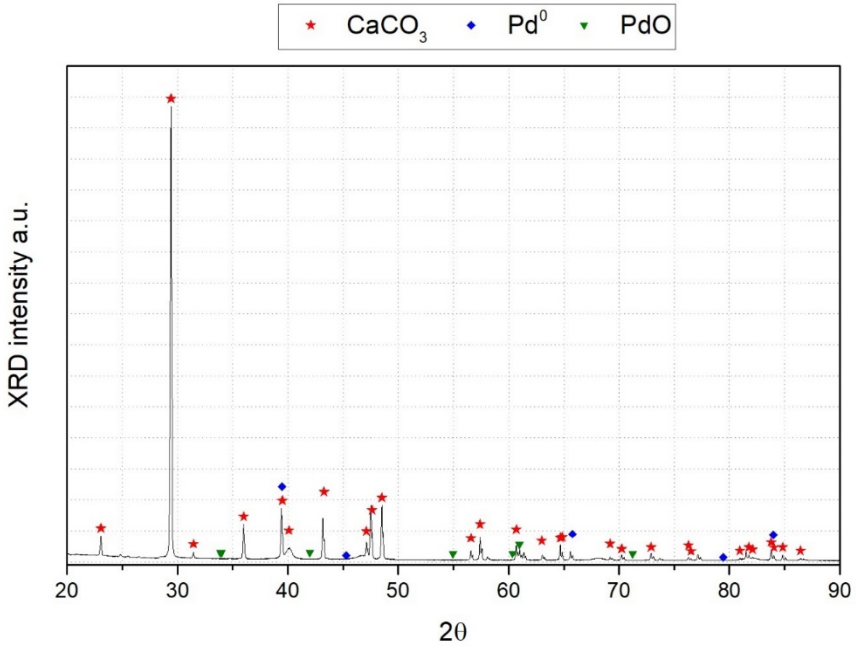

Figure 3-3 XRD spectra of Lindlar catalyst with $CaCO_3$, Pd^0, and PdO principal rays reported.

3.2. Pd/HT catalyst characterisation

In the following section all the information acquired for the Pd/HT catalyst about its elementary composition, textural properties, crystalline phase, and morphology are collected.

3.2.1. Pd/HT elemental analysis

As a starting point for the evaluation of the overall synthesis of Pd/HT, it is important to quantify the content of Pd, Al, and Mg by ICP-AES. Since ICP-AES measures are performed on as-synthesized materials, the nominal content of Pd is referred to metallic palladium. In fact, the last step in the Pd/HT preparation is the reduction by cyclohexene as previously reported in §2.2.2. The nominal value of the Mg/Al molar ratio is equal to 2:1.

ICP-AES elementary results, for Pd/HT, are reported in Table 3-2. Pd load has a slightly higher value than the expected one. That could be ascribed to experimental variability in the synthesis.

Table 3-2 Elementary composition of Pd/HT catalyst.

Sample	**Pd (%)**	**Al (%)**	**Mg (%)**	**Mg/Al**
Pd/HT	1.18±0.06	14.4±0.4	24.7±0.6	1.9

3.2.2. Pd/HT textural properties: BET-BJH results and shape of adsorption isotherms

N_2 adsorption curves (Figure 3-4) permit to identify mesoporous material (isotherm type IV). From the form of the hysteresis loop it is possible to establish, following the indication of IUPAC [199,225], an hysteresis loop of H3 type with the two common characteristics: (i) the adsorption branch resembles a Type II isotherm (ii) the lower limit of the desorption branch is typically located at the cavitation-induced P/P_0. This kind of isotherms are usually associated with plate-like particle aggregates, e.g., certain clays, but also in the case of pore network which consists of some macro-pores, not filled with condensate. In the specific case, hydrotalcites are composed of planar laminar structures.

Since the N_2 adsorption curves in the P/P0=1 is not flat but more similar to isotherms of type II, this hinders the reliability of the pore volume calculation, and therefore the $D_{av,BJH}$ calculations indicate an average pore diameter value.

The structures of the pores network could be oversimplified as larger macro-pores with a broad inlet pore distribution and connected slit-shaped pores of decreasing diameter [225].

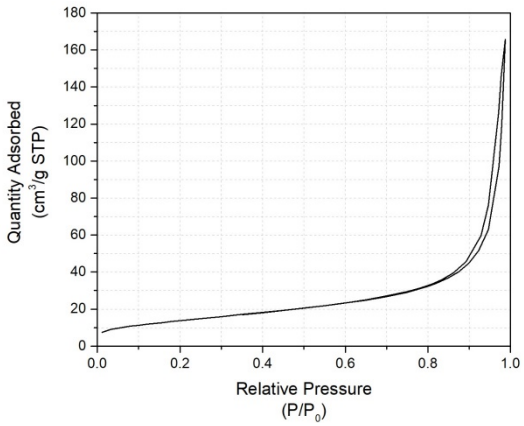

Figure 3-4 BET adsorption curves for the Pd/HT catalyst.

Figure 3-4 curves permit to evaluate an S_{BET} 50.7±0.5 m^2/g, V_{BJH} 0.25±0.02 cm^3/g, and an average pore size 19.92±0.32 nm. The available surface area is in line with the results previously obtained [6,226] and is in line with normal surface area obtained for other 2:1 Mg-hydrotalcites [227–229].

Studying the BJH diagram (Figure 3-5), the type H3 hysteresis is confirmed, the catalyst shows pores in the mesoporous zone but also some macro-pores (between 50 nm and 100 nm). Albeit some micro-porosities are present, they are not significant in the pores volume.

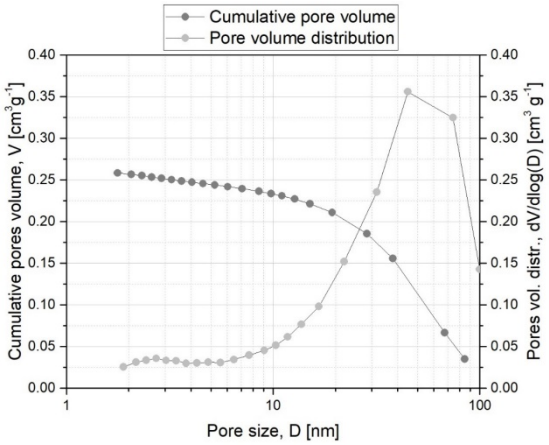

Figure 3-5 Desorption BJH assessment of Pd/HT catalyst.

3.2.3. Pd/HT crystalline phases evaluation

The following Figure 3-6 reports the X-ray diffraction spectrum for Pd/HT. The spectrum analysis allows highlighting the presence of a substantially monophase characterized by the presence of both Al and

Mg in a molar ratio 2:1. This crystalline phase is identified as hydrotalcite with some carbonates groups present inside the structure. The presence of metallic palladium in a little amount could be determined by the enlargement and shift of the two rays of the hydrotalcite at 40° and 46°.

If analysed, these two rays are the only isolated rays of hydrotalcite that have an enlargement of the FHWM. This could be related to the presence of different phenomena: (i) presence of multiple rays of hydrotalcite crystalline phase at this angle (multiple planes with similar plane distance, ray at 40° have a less intense ray at 39.6°) , (ii) orientation of crystalline phase, (iii) presence of the main rays of Pd^0 in the same 2θ position of the hydrotalcite. Moreover, the calculation of Scherrer equation, for all the isolated rays (11.6°, 23.4°, 60.7°, and 62.1°), gives an average value of crystallite size between 18 nm and 25 nm, only at 40° and 46° this value drops below 6 nm.

Reasonably the deformation of this ray should be correlated with the overlap of the rays of more crystalline planes of the hydrotalcite phase.

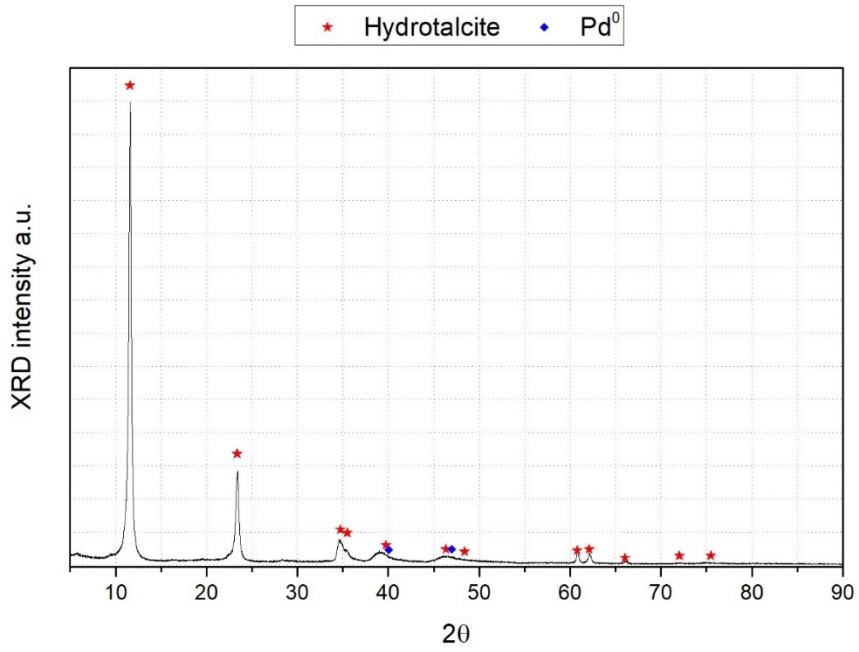

Figure 3-6 XRD spectra of Pd/HT catalyst with hydrotalcite phase ($C_{0.167}Al_{0.333}Mg_{0.667}O_{3.001}$) and Pd^0 rays highlighted.

3.2.4. Pd/HT morphology and topography

SEM micrograph, coupled with the EDS spectra, allows comprehending the morphology and elementary topography of the synthesized Pd hydrotalcite.

Figure 3-7 reports an image of a hydrotalcite particle. The sample is heterogeneous and is formed of some particles attached to bigger, smoother, and more homogenous particles. Moreover, since the image was produced with BSE electron, some surfaces are brighter than others highlighting a higher amount of heavier elements. However, both surfaces contain the same elements (Mg and Al), in similar relative amounts, probably indicating that different colors are linked to sharper surfaces of the sample. Overall the Pd seems well dispersed on the surface because the same amount of Pd is detected in different points on the surface of the catalyst (point 35 and area 36, for example).

Traces of Cl were also detected and are linked to the scotch tape used during the analysis to fix the powdery sample onto the sample holder.

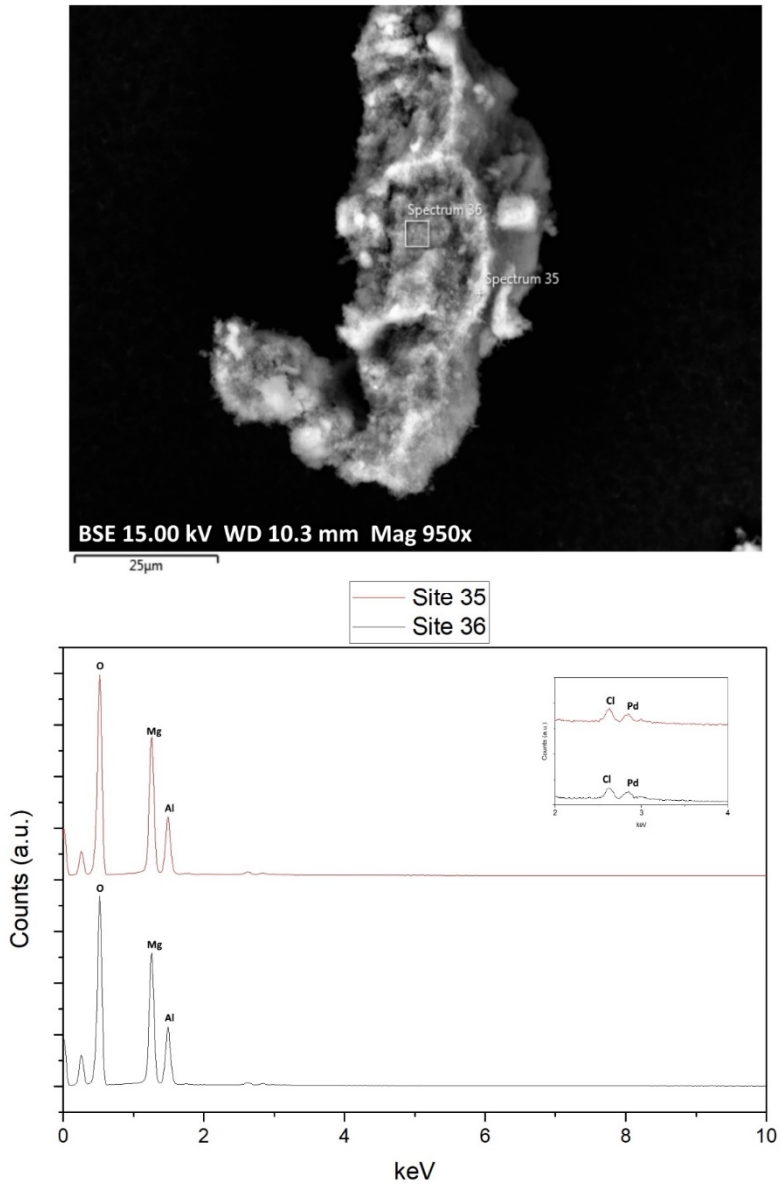

Figure 3-7 SEM image (on top) and relative EDS analysis (on bottom). Site 35 point analysis and Site 36 area analysis.

3.3. Silica supported catalysts characterisation

In the following section are reported the characterization results for the silica-supported catalysts produced with the two synthesis methods, hydrolysis-precipitation (HP) and ammonia-evaporation (AE). Both bimetallic and corresponding monometallic catalysts are reported to compare results of these various syntheses.

3.3.1. Catalysts elementary analysis

As a starting point, in order to evaluate the synthesis results, it is possible to compare the ICP-AES metal content measures with the theoretical loadings introduced during the synthesis. Using ICP-AES it was possible to quantify the content of Cu, Ni, and Pd. In Table 3-3 the nominal contents of metals are referred to the metal contents inside the samples.

Table 3-2 reports the elementary analysis for silica-supported catalysts.

As it is possible to see:

I. The amount of copper is often higher than the nominal loading introduced during the synthesis. In AE synthesis method, the measured copper loading is slightly higher than for the HP method. It is probably due to the synthesis procedure; as a hypothesis, not all silica could have been wholly precipitated after the synthesis while a part is washed away during the filtering;

II. The Cu loading in bi-metallic catalysts is generally lower than expected. However, this can be explained considering that pH during the syntheses were different (5.5 for HP and 5 for AE - §2.2.3.1). The new value is not optimum precipitation pH for both metals, but it is a compromise value;

III. In correlation of the previous point also, the measured values for Pd and Ni bi-metallic catalysts are slightly lower than the nominal contents probably for the same reasons;

IV. The content of Pd and Ni for HP mono-metallic catalysts are, as expected, in line with the value of bimetallic catalyst contents.

V. In the case of AE bi-metallic variations can be ascribed to the experimental error but are in line with the values of $Ni5SiO_2AE$ and $Pd1SiO_2AE$.

Table 3-3 Elemental compositions of silica-supported catalysts.

Sample	**Nominal loadings**			**ICP-AES measures**		
	Cu [%]	**Ni [%]**	**Pd [%]**	**Cu [%]**	**Ni [%]**	**Pd [%]**
Cu5SiO_2HP	5	0	0	5.8±0.2	0	0
Cu10SiO_2HP	10	0	0	10.8±0.3	0	0
Cu5SiO_2AE	5	0	0	6.5±0.1	0	0
Cu10SiO_2AE	10	0	0	11.7±0.2	0	0
Cu10Ni5SiO_2HP	10	5	0	8.3±0.2	4.4±0.1	0
Cu10Pd1SiO_2HP	10	0	1	8.5±0.2	0	0.79±0.05
Cu10Ni5SiO_2AE	10	5	0	8.9±0.2	4.6±0.1	0
Cu10Pd1SiO_2AE	10	0	1	8.7±0.2	0	0.59±0.04
Ni5SiO_2HP	0	5	0	0	3.9±0.1	0
Pd1SiO_2HP	0	0	1	0	0	0.66±0.04
Ni5SiO_2AE	0	5	0	0	4.7±0.1	0
Pd1SiO_2AE	0	0	1	0	0	0.58±0.02

3.3.2. SiO_2-supported catalysts textural properties: BET-BJH results and shape of adsorption isotherm

As already performed for Lindlar and Pd-HT catalysts, the adsorption and desorption N_2 isotherms are reported in the form of adsorbed N_2 per unit of degassed solid mass (mass of the samples after heat treatment at 200 °C for one night under vacuum), as a function of equilibrium relative pressure (P/P_0). Isotherms shape with possible hysteresis loops are observed.

Experimental N_2 adsorption and desorption have the same shape for all the materials synthesised (Table 2-2): a case between Type II and Type IV(a) from IUPAC classification of physisorption isotherms [199], of which the features are reported in §Chapter 2.

All the materials synthesized in this work have a hysteresis loop, corroborating the hypothesis of mesoporosity presence. The hysteresis loop that has characteristics of both hysteresis type H2(a) and type

H2(b) according to IUPAC classification, is associated to complex structures in which there is a network effect between the pores. For this specific form of loops due to a pore-blocking effect or cavitation-induced evaporation, the difference between H2(a) and H2(b) is linked to the neck size of the pores; for the second one the neck distribution is much larger. This kind of hysteresis loops H2(a) are for instance observed for many silica gels, porous glasses, as well as SBA-16 and KIT-5 silica, while H2(b) is observed for mesocellular silica foams and some ordered silica after hydrothermal treatment [199].

At high P/P_0 values, a difference appears between monometallic (Figure 3-8 and Figure 3-9) and bi-metallic catalyst (Figure 3-10 and Figure 3-11):

- monometallic catalysts, independently to the active supported metal, presents the flat line characteristic to mesoporous materials;
- instead, at P/P_0 close to 1, bi-metallic catalysts do not end up with a flat line; the adsorption curves have a nearly vertical segment reveling the presence of some macroporosity. This reduces, as for Pd-HT catalyst, the significance of average pore size calculations.

Pores volumes distribution with respect to pore size confirms deductions collected just above for both monometallic and bimetallic catalysts: for the monometallic ones, the majority of the pores is in the mesopores range, for bimetallic ones, the majority is in mesoporous zone with a tail crossing of 50 nm, the meso/macro border value.

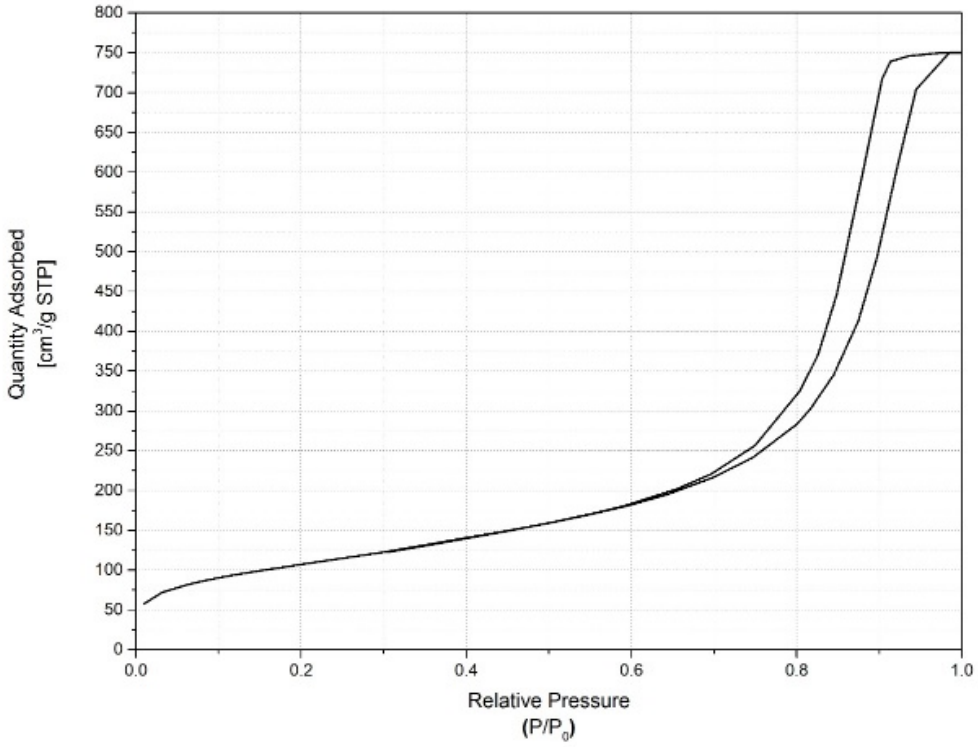

Figure 3-8 BET adsorption/desorption isotherms of Cu10SiO₂HP.

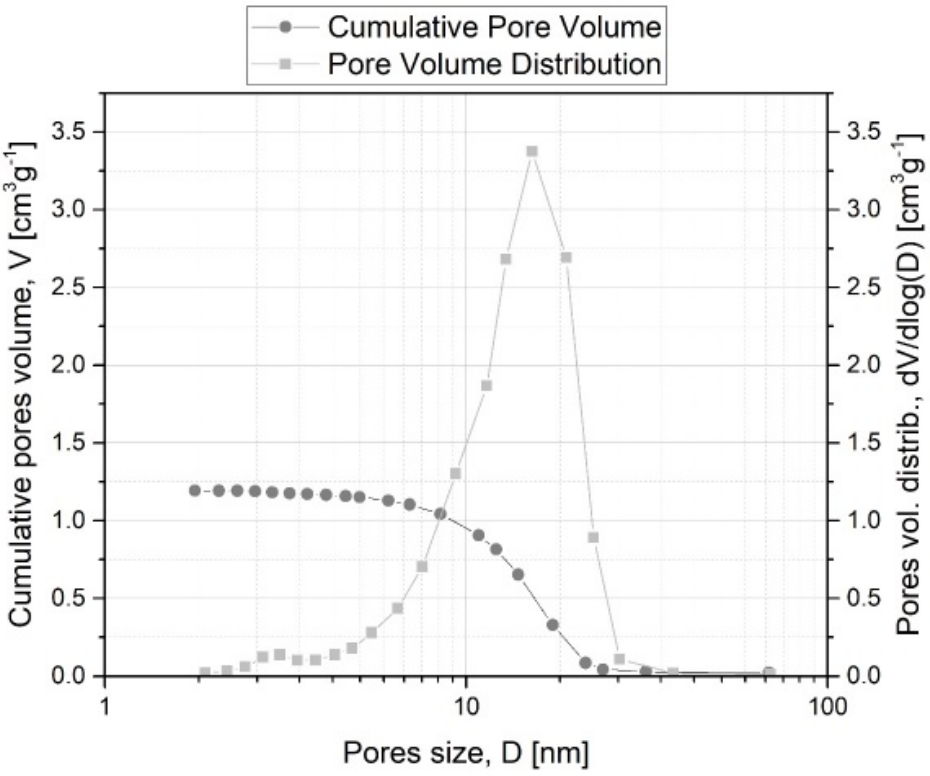

Figure 3-9 Desorption BJH assessment of Cu10SiO₂HP.

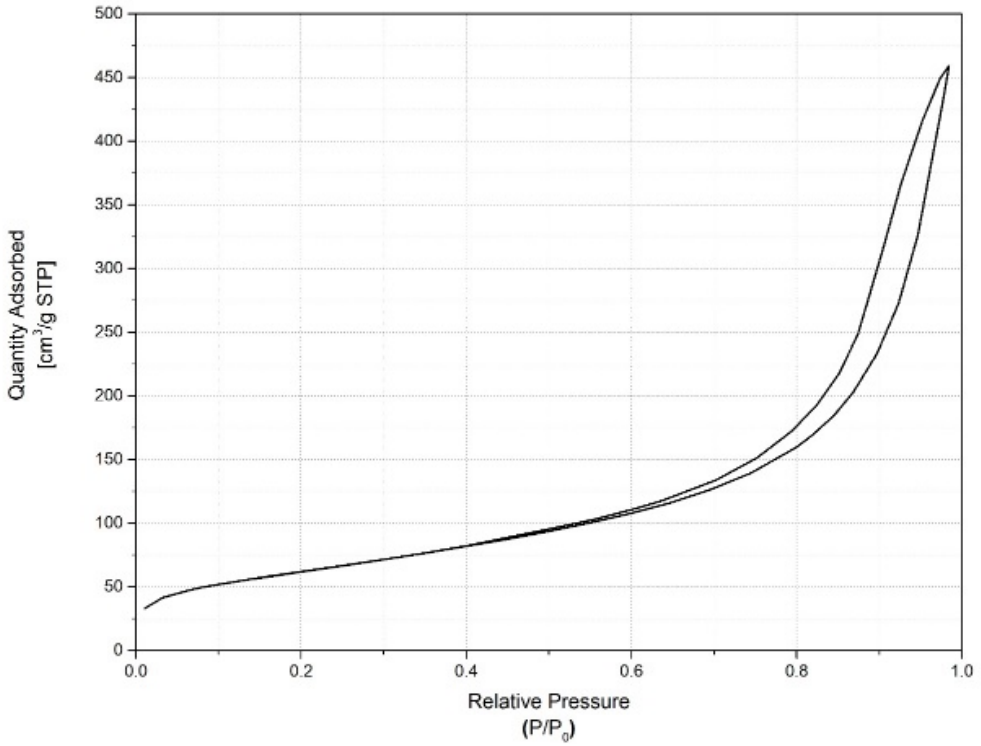

Figure 3-10 BET adsorption/desorption isotherms of Cu10SiO₂AE.

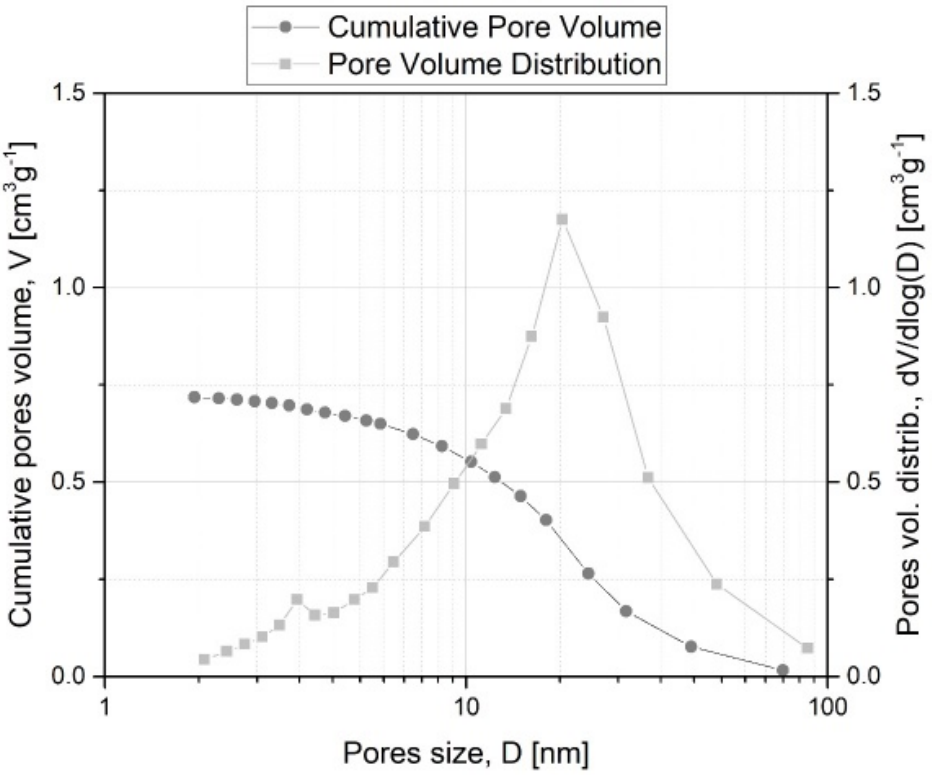

Figure 3-11 Desorption BJH assessment of Cu10SiO₂AE.

Table 3-4 reports experimental measures of BET surface (S_{BET}), BJH cumulated pores volume calculated for the desorption branch ($V_{BJH,des}$), and the estimation of pore diameter ($D_{av,BJH}$). Consequently, to the previous considerations, BET surface values are reliable, while BJH ones could be affected by macroporosity and network effects.

Table 3-4 Measured BET surface area (S_{BET}), BJH cumulative volume ($V_{BJH,des}$) and average pore diameters (Dav,BJH) for as synthesized materials.

Materials	S_{BET} [m^2g^{-1}]	$V_{BJH,des}$ [cm^3g^{-1}]	$D_{av,BJH}$ [nm]
$Cu5SiO_2HP$	342	1.58	18.7
$Cu10SiO_2HP$	359	1.71	20.3
$Cu5SiO_2AE$	208	0.55	10.6
$Cu10SiO_2AE$	256	0.69	10.8
$Cu10Ni5SiO_2HP$	277	0.59	10.0
$Cu10Pd1SiO_2HP$	225	0.81	14.9
$Cu10Ni5SiO_2AE$	263	0.53	6.41
$Cu10Pd1SiO_2AE$	194	0.61	12.3

Ni5SiO_2HP	332	0.69	14.2
Pd1SiO_2HP	321	0.95	10.8
Ni5SiO_2AE	311	0.69	8.9
Pd1SiO_2AE	274	0.55	8.0

An increase in the copper load seems to have a beneficial role in the surface area of the catalysts.

Being the nominal metals fraction equal, HP products show higher BET surface area than the corresponding AE ones and also, the volume of the pores and then the average diameter.

The different pore sizes can have an essential role in the diffusion into the pores during the reaction. So, the AE catalysts could have lower activity since the reagents, and the reaction products could take much time to diffuse inside and outside the pores of the catalyst, representing a further barrier to the reaction. The lower area in the case of AE can be explained by the lower temperature maintained during the SiO_2 formation, in AE the silica formation happens during the precipitation and growth at room temperature, against 110 °C for HP, and also the different pH during the formation of the copper-silica structure could have an effect. Moreover, the different structures observed with XRD and FTIR, and also by Raman spectroscopy for monometallic copper catalysts could influence the BET surface area. However, the materials obtained have surface area values in line with the literature values [7,166,168].

The lower surface area for bimetallic catalysts could be explained by the lower pH at which the formation of silica and the precipitation of copper occurred; the same trend was found by Dong et al. [230] and evaluating different synthesis techniques for copper supported on silica [231].

3.3.3. As-synthesized materials

3.3.3.1. Crystalline phases (XRD results)

X-ray diffractograms (Figure 3-12, Figure 3-13, and Figure 3-14) show crystalline phases detected in as-synthesized materials: all the materials show a contribution of an amorphous phase. It happens because the support on which the active phases are deposed is mainly composed of amorphous silica, SiO_2, both synthesis methods give similar diffractograms.

As far as monometallic copper catalysts are concerned (Figure 3-12), the calcination of the samples should more probably produce phases as copper oxide relatively to the calcination temperature (550 °C) as reported in the literature about calcination of copper catalysts [232–236]. In Figure 3-12, the rays relative to this phase are covered by the shoulder of amorphous silica (between 20° and 30°), the other peaks are not detected, this could happen when Cu and silicon oxides are involved. As previously stated in this thesis §2.1.3 [166], the phase that could appear during the preparation of copper catalysts, starting from silicon oxide reagents in liquid or colloidal form, can be a copper phyllosilicate, in which the copper is very well dispersed inside the silica matrix, forming chemical bonds between Si and Cu.

Whereas sometimes oxides and hydroxides are developed during the thermal treatment, the high dispersion of Cu in the phyllosilicate promotes the formation of tiny crystallites of Cu phases (< 3 nm) not easily detected by XRD. In particular, from the spectra of the catalysts prepared with HP method (Figure 3-12) at around 32° and 37°, two changes can be found. Toupance et al. and Dong et al. related similar behavior in their catalysts to the presence of a particular copper phyllosilicate called chrysocolla [174,237]. It is crucial to indicate that contingent chrysocolla and copper hydroxide, sharing the same orthorhombic crystal system, can be ascribed to the calcination of the sample. In literature, both structures are found together since the synthesis of pure chrysocolla is a difficult task, and sometimes the copper hydroxide could be reformed by the decomposition of the copper phyllosilicate [173,174,176,177].

FTIR and Raman techniques are used to confirm the presence of copper phyllosilicates, and better try to characterize the bulk of the amorphous phase (see **Errore. L'origine riferimento non è stata trovata.** and Figure 3-18 explained in the following section).

For monometallic Ni catalysts, the synthesis method affects the structure after calcination. In particular, HP method produces NiO (bunsenite form in Figure 3-13) whereas by AE synthesis, a nickel hydroxisilicate (pimelite = a synthetic form of willemseite where Mg is not present) is formed. One can hypothesize that the calcination temperature is not high enough to completely expel the OH^- groups from this structure, as also reported in literature [238].

The pimelite structure is also observed in copper-nickel bi-metallic catalysts Figure 3-13, presumably in combination with chrysocolla or copper oxide suggested by the position of the broad peak at 35°. The

simultaneous presence of both copper and nickel in a single structure cannot be excluded from the spectra Figure 3-12 and Figure 3-13.

Finally, in the case of monometallic Pd catalysts, the principal ray detected is that of PdO phase (at 34.6°). In bimetallic Cu/Pd catalysts, this ray is shifted at 34.9°. Christensen and Langell [208] in their work on CuO and PdO solid solution reported that Cu^{2+} randomly substitutes Pd^{2+} in the lattice of PdO, this also affects the XRD with shifting to higher 2θ. More Cu^{2+} is in the structure of PdO higher is the ray shifting.

Table 3-5 reports the average crystalline sizes estimated by the Scherrer equation (Equation 2-2). Since an amorphous phase constitutes the support of these catalysts and not isolated rays are found, Scherrer equation acquires a merely indicative value.

Table 3-5 Average crystalline sizes (L) estimation by Scherrer equation (Equation 2-2) for calcined materials phases.

Material	**CuO**	**$Cu(OH)_2$**	**Chrysocolla**	**Pimelite**	**NiO**	**PdO**
$Cu5SiO_2HP$	n.d.*	n.d.*	n.d.*			
$Cu10SiO_2HP$	n.d.*	n.d.*	n.d.*			
$Cu5SiO_2AE$	n.d.*	n.d.*	n.d.*			
$Cu10SiO_2AE$	n.d.*	n.d.*	n.d.*			
$Cu10Ni5SiO_2HP$	n.d.*	n.d.*	n.d.*	2.6 nm	-	
$Cu10Pd1SiO_2HP$	n.d.*	n.d.*	n.d.*			5.2 nm
$Cu10Ni5SiO_2AE$	n.d.*	n.d.*	n.d.*	2.5 nm	-	
$Cu10Pd1SiO_2AE$	n.d.*	n.d.*	n.d.*			4.3 nm
$Ni5SiO_2HP$				-	7.9 nm	
$Pd1SiO_2HP$						5.2 nm
$Ni5SiO_2AE$				3.1 nm	-	
$Pd1SiO_2HP$						5.0 nm

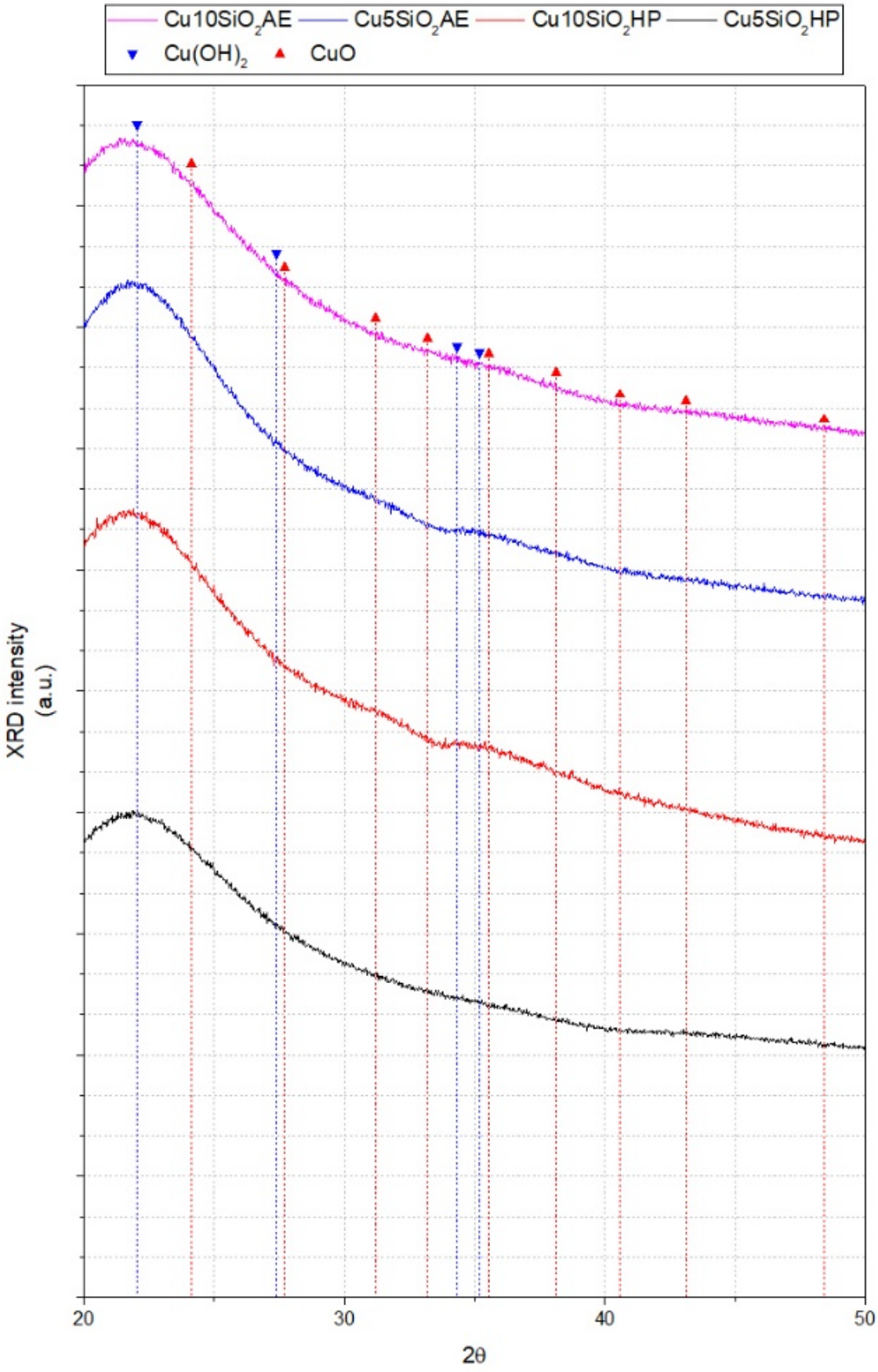

Figure 3-12 X-ray diffractograms of Cu/SiO_2 supported catalysts.

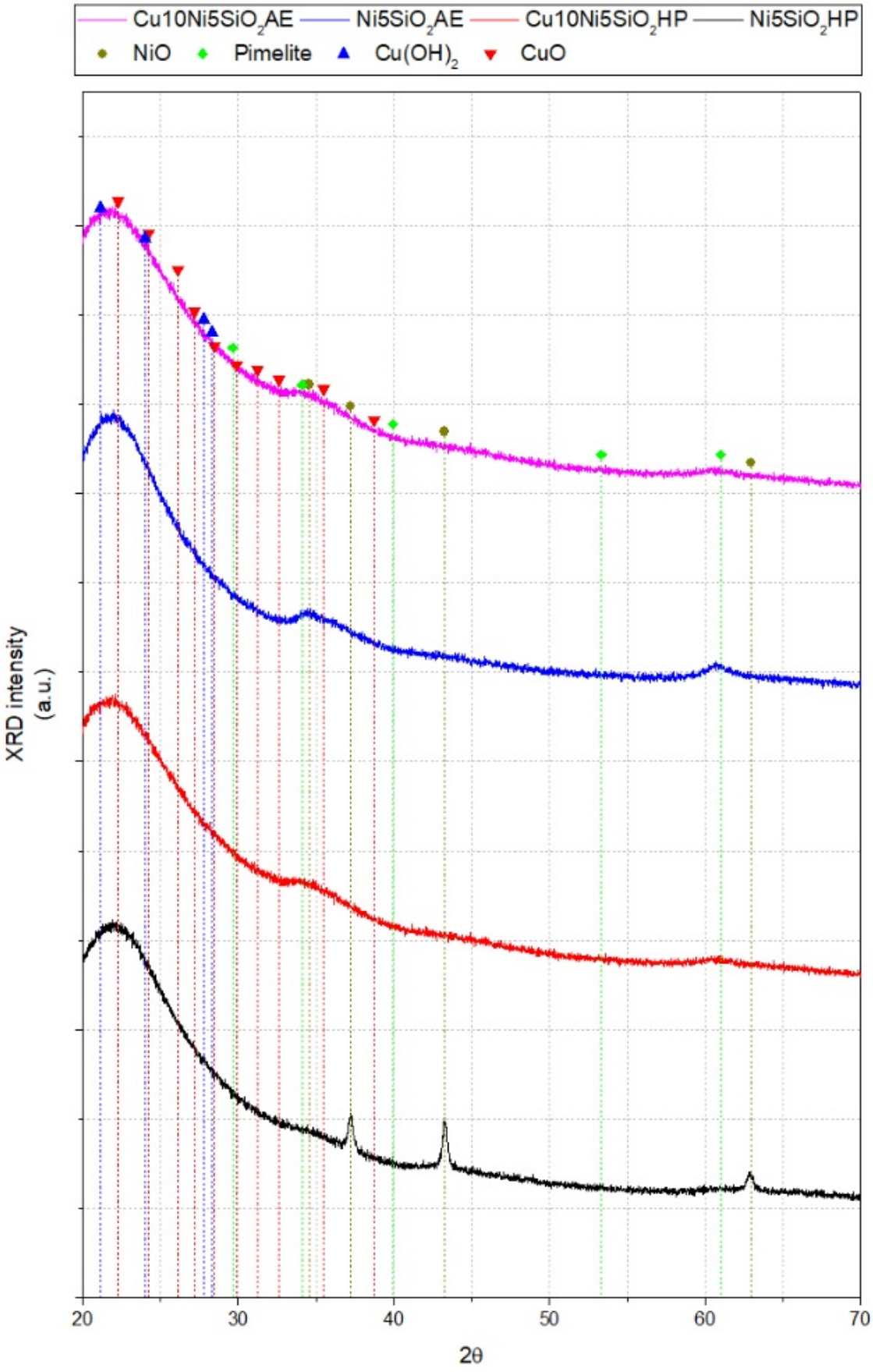

Figure 3-13 X-ray diffractograms of Cu-Ni/SiO_2 catalysts.

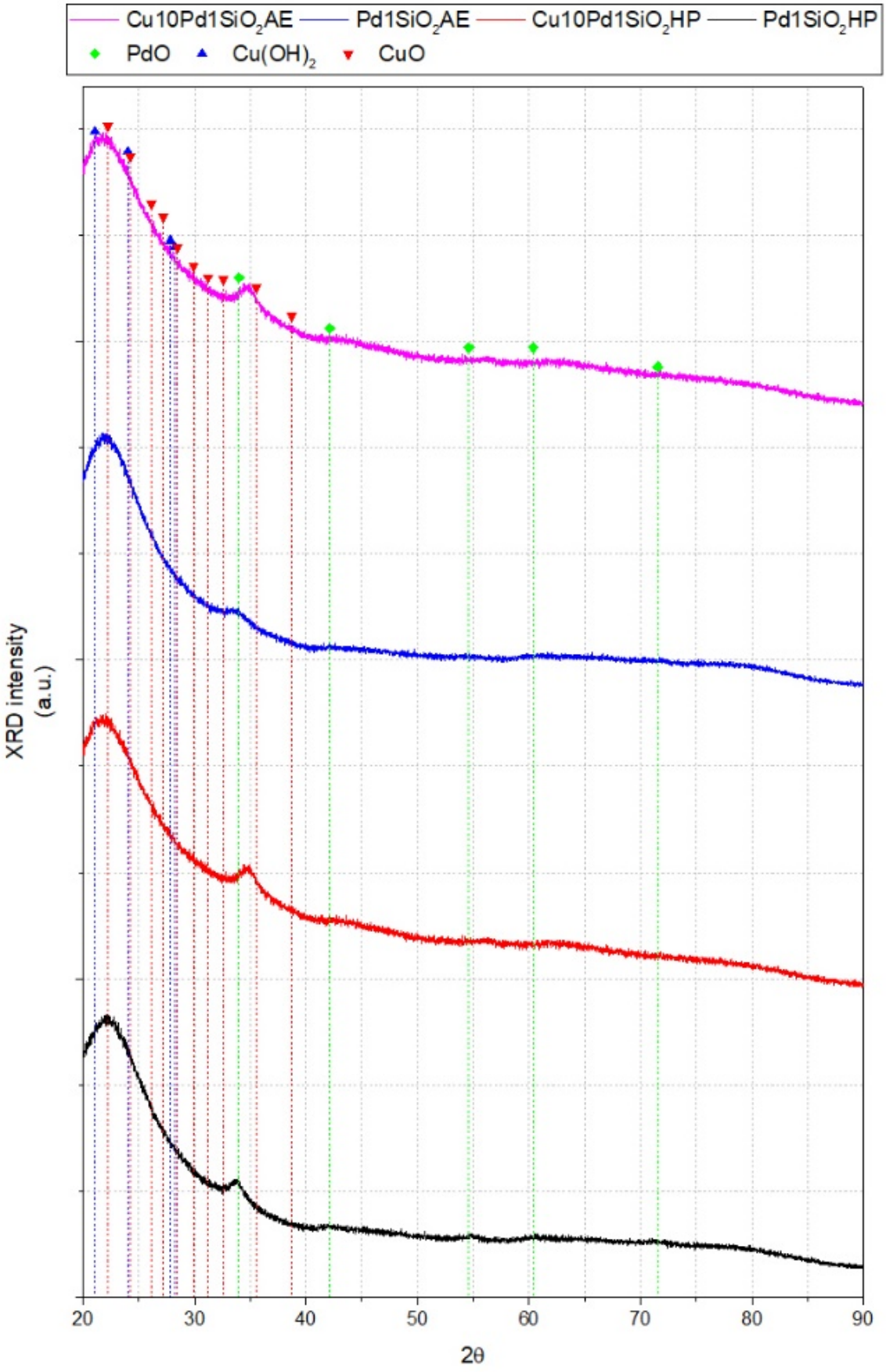

Figure 3-14 X-ray diffractograms of Cu-Pd/SiO_2 catalysts.

3.3.3.2. FTIR results for as-synthesized samples

The infrared spectra recorded between 4000 cm^{-1} and 400 cm^{-1} (**Errore. L'origine riferimento non è stata trovata.**) for each as-synthesized sample are very similar to each other, the only characteristic peaks detected in all samples is associated to silica. However, the presence of Cu, Ni, and Pd alters the wavelength of these bands of silica.

These bands were assigned in literature [239–241] in this way:

- at 450 cm^{-1} and 800 cm^{-1} is the symmetric stretching of siloxane groups (Si-O-Si);
- at 1060 cm^{-1} there are the asymmetric stretching of the same siloxane groups;
- the shoulder at 960 cm^{-1} is related to the angular deformation of the Si-OH silanol group; some samples lack this shoulder.

In the spectra presented there is no other band relative to organics phases, this is of particular importance for HP produced catalysts because it highlights that during the synthesis all the TEOS is converted in SiO_2.

With modified silica, the most significant variation to the spectra described above should appear in the region between 400 cm^{-1} and 2000 cm^{-1}. Both copper [166,176,242] and nickel silicates [243], in a similar way, change the spectra lowering the 1112 cm^{-1} band to 1080 for nickel and 1060 for copper. Moreover, in the presence of copper phyllosilicate and other structure bonded to silica, as for examples, Ni silicates, another band at 1630 cm^{-1} appears as illustrated in Figure 3-17 [166]. Its intensity is linked to the amount of active phase bonded to the support of the silica.

With only copper catalysts, curves (a) and (b) in **Errore. L'origine riferimento non è stata trovata.**, the infrared bands characteristic of CuO at 575 cm^{-1}, 500 cm^{-1} and 460 cm^{-1} are overlapped with the intensive band at 450-460 cm^{-1} of Si-O-Si stretching and is only recognizable by a shoulder at 580 cm^{-1}; one can hypothesize that, in as-synthesized samples, since the calcination temperature was also of 550 °C, the copper phyllosilicate and CuO co-existed. Furthermore, analyzing the spectra, it is not possible to individuate the bands at 938 cm^{-1} and 694 cm^{-1}, typically correlated to $Cu(OH)_2$. Li et al. [166] suggest that this indicates the absence of copper hydroxide. However, the absolute absence of copper hydroxide is not entirely sure using FTIR-ATR characterization.

If a confrontation between the HP catalysts and the AE catalysts is carried out, one can see that in the latter, the shifting of the 1112 cm^{-1} band is more evident and the band is shifted to 1060 cm^{-1}; this can be related to a lower amount of CuO produced by calcination of these AE catalysts. Higher content of CuO should be formed after calcination with HP synthesis procedure.

As far as Pd monometallic catalysts are concerned, curves (g) and (h), no particular change is detectable. Comparing these results with other Pd supported on silica, analyzed by FTIR or FTIR-ATR techniques, the band at 2236 cm^{-1}, found by Cheng et al. [244] with lower content of Pd ($0.1\%_{w/w}$)is not detected. For these materials, the spectrum is identical to SiO_2 one, and any difference is found.

FTIR-ATR spectra of $Cu5SiO_2HP$ and $Cu5SiO_2AE$ show spectra similar to silica with minor modifications due to the lower amount of active phase present, they are not illustrated in this paragraph.

Figure 3-15 FTIR-ATR spectra of : Cu10SiO₂HP, Cu10SiO₂AE, Cu10Pd1SiO₂HP, Cu10Pd1SiO₂AE, Cu10Ni5SiO₂HP,Cu10Ni5SiO₂AE, Pd1SiO₂HP, Pd1SiO₂AE, Ni5SiO₂HP, Ni5SiO₂AE.

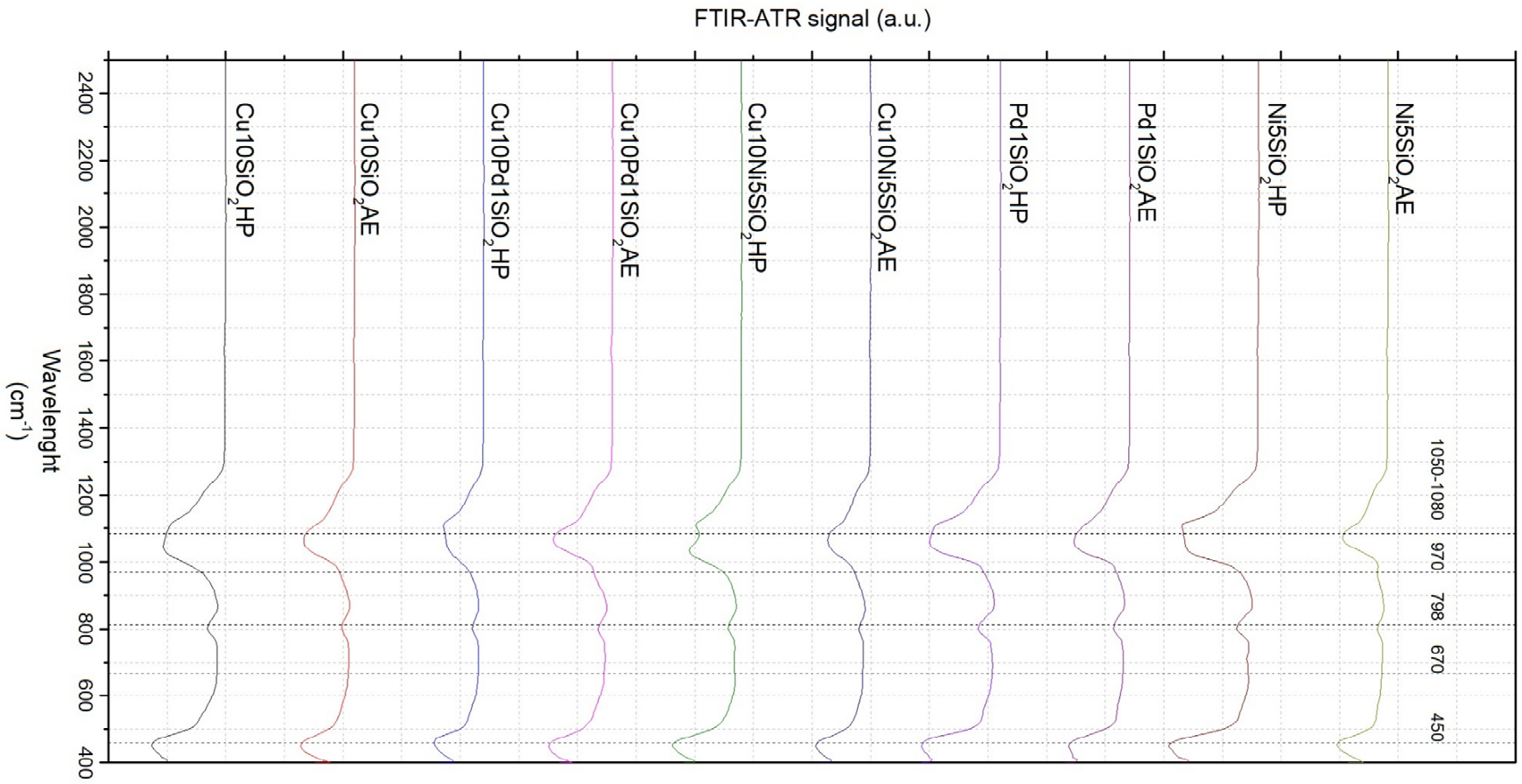

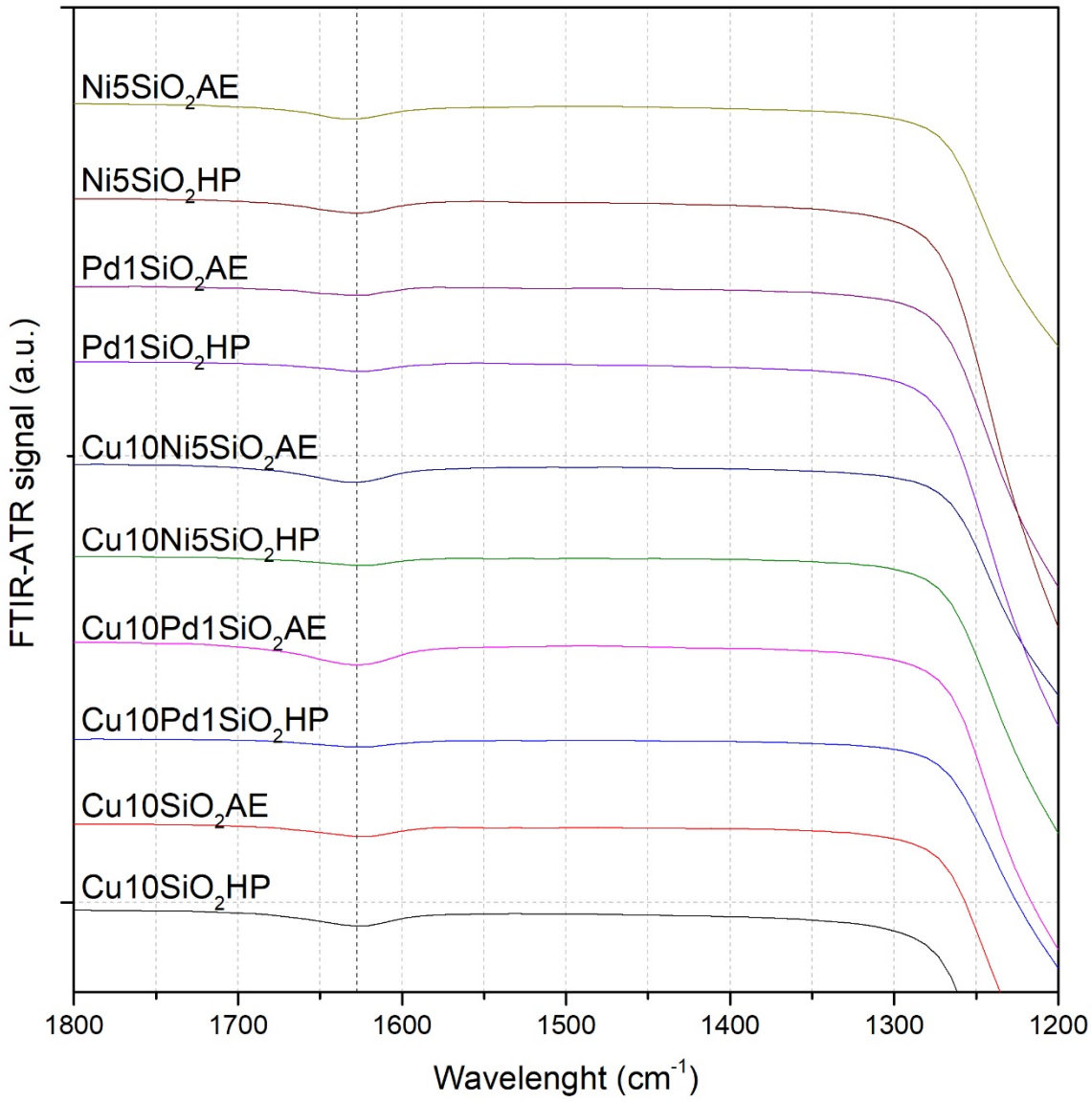

Figure 3-17 FTIR-ATR spectra details at 1630 cm^{-1}.

3.3.4. Raman Spectroscopy results for monometallic samples

In order to complete the analysis of the amorphous phase of as-synthesized catalysts the characterization with Raman techniques was also carried out. Raman spectroscopy is sometimes combined with FTIR analysis to integrate the information between the two technics for copper-based catalysts.

In Figure 3-18, the Raman bands relatives to different phases are highlighted. In as-synthesized samples, the presence of copper phyllosilicate is confirmed, the presented Raman bands are those of natural chrysocolla (copper phyllosilicate).

In reduced samples, the bands of chrysocolla are less intense and bands relative to Cu^{+} oxide appear, as illustrated in literature [1,7,166], formed from the reduction of chrysocolla or phyllosilicates like phases. In Figure 3-18 the bands colors are referred to the values as indicated in Table 3-6, the bands value are found from the reported literature.

Table 3-6 Raman bands position for Cu and Si phases, the band positions are taken from the literature references

Phase	Bands position	References
SiO_2 hydrate	263, 424, 603, 1060, 1189 (orange)	[202,203]
Copper phyllosilicate	240, 670, 778 (green)	[166,202,203]
Cu_2O	330, 342, 628 (violet)	[202,203]
$Cu(OH)_2$	292, 488 (blue)	[202,203]

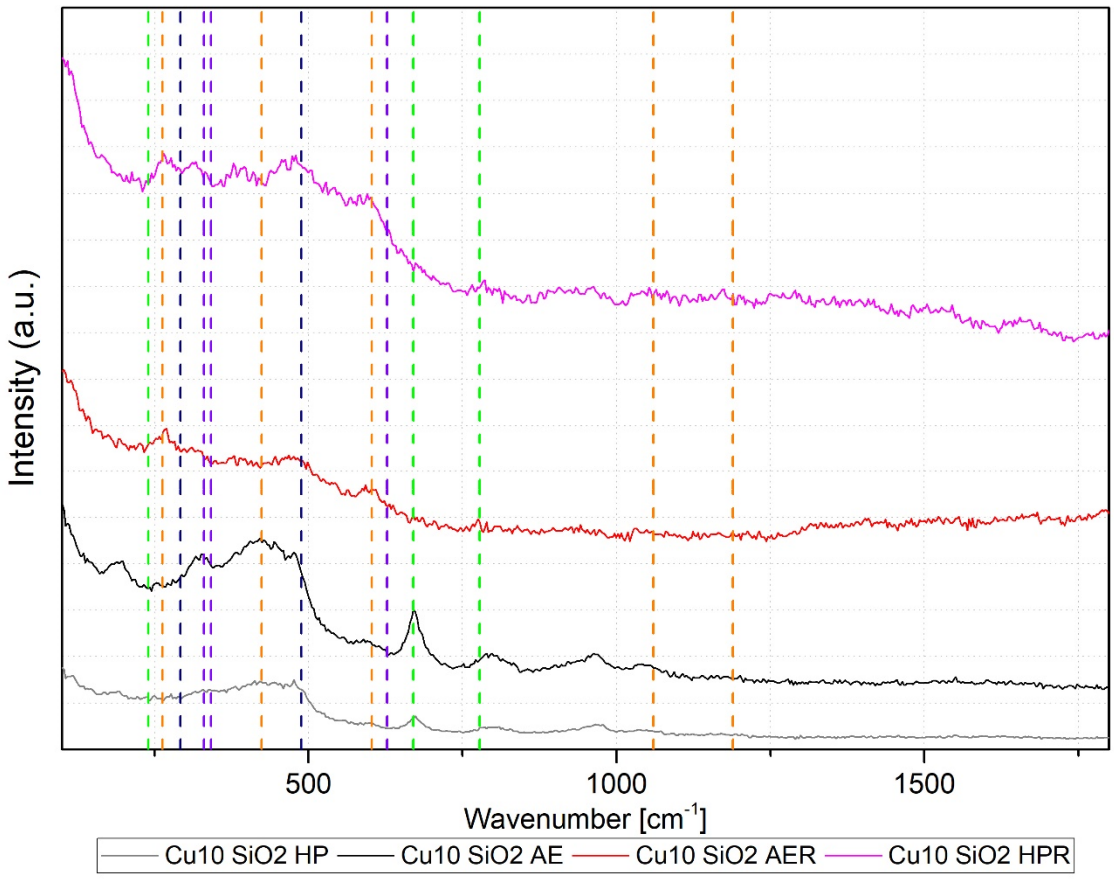

Figure 3-18 Raman spectra for Cu based catalysts with highlighted bands SiO_2 (orange), Copper phyllosilicate (green), Cu_2O (violet), and $Cu(OH)_2$ (blue).

On the other hand, by reduction of copper oxide CuO, the preeminent phases formed is metallic Cu and Cu_2O as it will be shown in the next section.

3.3.5. Reducibility properties

3.3.5.1. TPR and chemisorption results

TPR data interpretation follows the principle that peaks of hydrogen consumption depict a chart of the interactions energies between the active phase (or phases) and the surroundings, the support. The stronger the interactions, the higher the reduction temperatures measured. The nature of the support, its affinity with reducible species and the synthesis methods have a remarkable effect on the reducibility of samples.

In Table 3-7 is gathered all the results of TPR reduction temperature for the as-synthesized samples. The temperatures in the table are the reduction temperature peaks when more than one value is reported linked to the fact that in bi-metallic catalysts both phases are reduced at different temperatures.

Temperature Programmed Reduction with H_2 indicates that the active copper phase is not strongly bonded to the silica substrate because no increase in the reduction temperature (232-242 °C) is observed compares compared to CuO bulk reduction temperature (between 220-250 °C) reported by different authors [166,214,245,246]. The presence of chrysocolla does not affect the reduction temperature of the samples [7,166,176] and only a single reduction peak with no shoulders was observed. HP samples exhibit slightly higher reduction temperatures linked to higher copper dispersion due to the use effect of the different SiO_2 precursors.

Ni catalysts prepared by HP and AE methods exhibit different reduction temperatures as one can also expected from the XRD results. The samples where NiO is observed, i.e. in the monometallic Ni HP sample, show a lower reduction temperature (383-411 °C) showing that in this case, free NiO is present on the support surfaces (temperature reduction of free NiO is normally below 400 °C). For AE samples, the peaks are individuated in the region between 400-450 °C (443 °C) where moderate interactions with the support, as for Pimelite or other Ni silicates, are found [247].

However, the simultaneous presence of both Cu and Ni decreases the reduction temperature of Ni species (from 383-411 °C to 356°C for HP samples and from 443 °C to 362 °C for AE samples) and increase the reduction temperature of Cu species (from 239 °C to 260 °C for HP samples and from 235 °C to 265 °C for AE samples) [248–250]. It is worth to stress that the reduction temperature is very similar in both HP and

AE samples. The reduction of NiO at lower temperature than in bulk form can be attributed to the previous reduction of copper oxide.

As far as Cu10Pd1SiO$_2$HP catalyst is concerned, it keeps the reduction temperature of the monometallic catalysts prepared with the same techniques, both monometallic Cu (245 °C compared to 242 °C) and Pd (87 °C compared to 88 °C), the slightly higher value can be related to the alloy formation. Similar considerations stand for the AE catalyst (244 °C compared to 235 °C) and Pd (89 °C compared to 90 °C).

The copper surface area of bimetallic Cu-Pd does not change comparing it with the copper monometallic materials synthesised. Pd does not have a significant impact on the copper surface, probably also because of the amount of Pd, in respect of the Ni effect. The copper surface area is lower, suggesting that the presence of Ni alter the surface properties of the supported copper.

Table 3-7 Reduction temperatures for the reducible Cu, Ni and Pd species, and metallic copper surface area.

Material	**Cu T_{red} (°C)**	**Ni T_{red} (°C)**	**Pd T_{red} (°C)**	**Cu surface* (m^2_{Cu}/g_{Cu})**
Cu5SiO$_2$HP	242	-	-	-
Cu10SiO$_2$HP	239	-	-	55
Cu5SiO$_2$AE	232	-	-	-
Cu10SiO$_2$AE	235	-	-	41
Cu10Ni5SiO$_2$HP	260	356	-	31
Cu10Pd1SiO$_2$HP	245	-	87	51
Cu10Ni5SiO$_2$AE	265	362	-	28
Cu10Pd1SiO$_2$AE	244	-	89	38
Ni5SiO$_2$HP	-	383, 411	-	-
Pd1SiO$_2$HP	-	-	88	-
Ni5SiO$_2$AE	-	443	-	-
Pd1SiO$_2$AE	-	-	90	-

*reduction at 300 °C, ramp 1°C/min, 4 hours

The copper surface area of bimetallic Cu-Pd (51 m^2_{Cu}/g_{Cu} for HP and 38 m^2_{Cu}/g_{Cu} for AE) does not change compared to the copper monometallic materials (55 m^2_{Cu}/g_{Cu} for HP and 41 m^2_{Cu}/g_{Cu} for AE). Pd does not have a significant impact on the copper surface, probably because of its low loading.

The copper surface area of bimetallic Cu-Ni (31 m^2_{Cu}/g_{Cu} for HP and 28 m^2_{Cu}/g_{Cu} for AE) is lower than the copper monometallic materials, suggesting that the presence of Ni alters the surface properties of the supported copper.

3.3.5.2. Crystalline phases after TPR

XRD analysis on silica-supported catalysts after TPR confirms the reduction of all the reducible species (see Figure 3-19, Figure 3-20, and Figure 3-21). In Cu supported on silica catalysts, both HP and AE present metallic copper Cu and Cu_2O. As indicated by Hope et al. [176] and by Yunjun et al. [7], the formation of metallic copper is related to the reduction of CuO, and of Cu_2O to the reduction of copper phyllosilicates. The observed rays, as in the case of as-synthesized samples, are not well separated from the background and are broad, this highlights that the crystallites size is very small for both phases. Moreover, only the most intense peak of Cu_2O at 36° is differentiable from the spectra, and of Cu at 42.3°. In fact, the principal ray for Cu^0 is covered by the SiO_2 shoulder at 22°. It is barely distinguishable for samples with 10%$_{w/w}$ then almost impossible to find for 5%$_{w/w}$ catalysts Figure 3-19.

In Cu-silica AE samples, the ray relative to Cu_2O is more intense than the ray of Cu^0. Comparing these results to as-synthesized catalysts, one can hypothesize that the materials synthesized by AE contain a more significant amount of chrysocolla phase than the HP ones, the reduction of the sample giving place to more copper oxide. Instead, more metallic copper is formed reducing HP samples.

Bi-metallic Cu-Ni catalysts also present both Cu and Cu_2O, but in this case, the principal rays of metallic Ni are also present due to the reduction of Pimelite or NiO. The peaks of metallic Ni are less intense and defined than for monometallic Ni catalysts; it is related to the overlapping of Ni phase rays by the rays of Cu and Cu_2O (Figure 3-20).

In monometallic Pd catalysts, metallic Pd are formed during TPR. It is interesting to focus attention on what happens for bi-metallic catalysts (Figure 3-21). As already said in section §3.3.3.1, Pd is introduced in the structure of CuO when reduction happens, forming a combined CuPd phase. As indicated by Norhona et al. [251] and by Spee et al. [210], the potential formation of CuPd alloys with different Cu/Pd ratios happens

when CuO and PdO phases are involved. For 9:1 Cu/Pd molar ratio and below, these phases are highly crystalline and so easily detected with x-ray diffraction technique. A detail, easily found in $Cu10Pd1SiO_2HP$, is the duplication of the peak relative to CuPd alloy, as also reported for reduced samples in literature [210].

Table 3.5 summarizes the average crystalline sizes estimated by Scherrer equation, whenever possible, for samples after TPR. The overall broad peaks do not permit an accurate estimation of the crystallite size. However, more than for as-synthesized samples, the crystalline phases are better described by this technique. For Cu_2O or Cu^0 the peaks are too large, and the values are such that the predicted value is smaller than 3 nm which is the limit of accuracy of Scherrer equation. For this phases, a better evaluation of average crystallites size could be obtained by TEM observation, as reported below in section §3.3.7.2.

Table 3-8 Average crystallite size for samples after reduction by H_2.

Material	**CuPd [nm]**	**Pd [nm]**	**Ni [nm]**
$Cu5SiO_2HP$	n.d.*	-	-
$Cu10SiO_2HP$	n.d.*	-	-
$Cu5SiO_2AE$	n.d.*	-	-
$Cu10SiO_2AE$	n.d.*	-	-
$Cu10Ni5SiO_2HP$	n.d.*	-	--
$Cu10Pd1SiO_2HP$	3.5	7	-
$Cu10Ni5SiO_2AE$	n.d.*	-	-
$Cu10Pd1SiO_2AE$	4.1	5	-
$Ni5SiO_2HP$	-	-	10
$Pd1SiO_2HP$	-	5	-
$Ni5SiO_2AE$	-	-	11
$Pd1SiO_2HP$	-	4	-

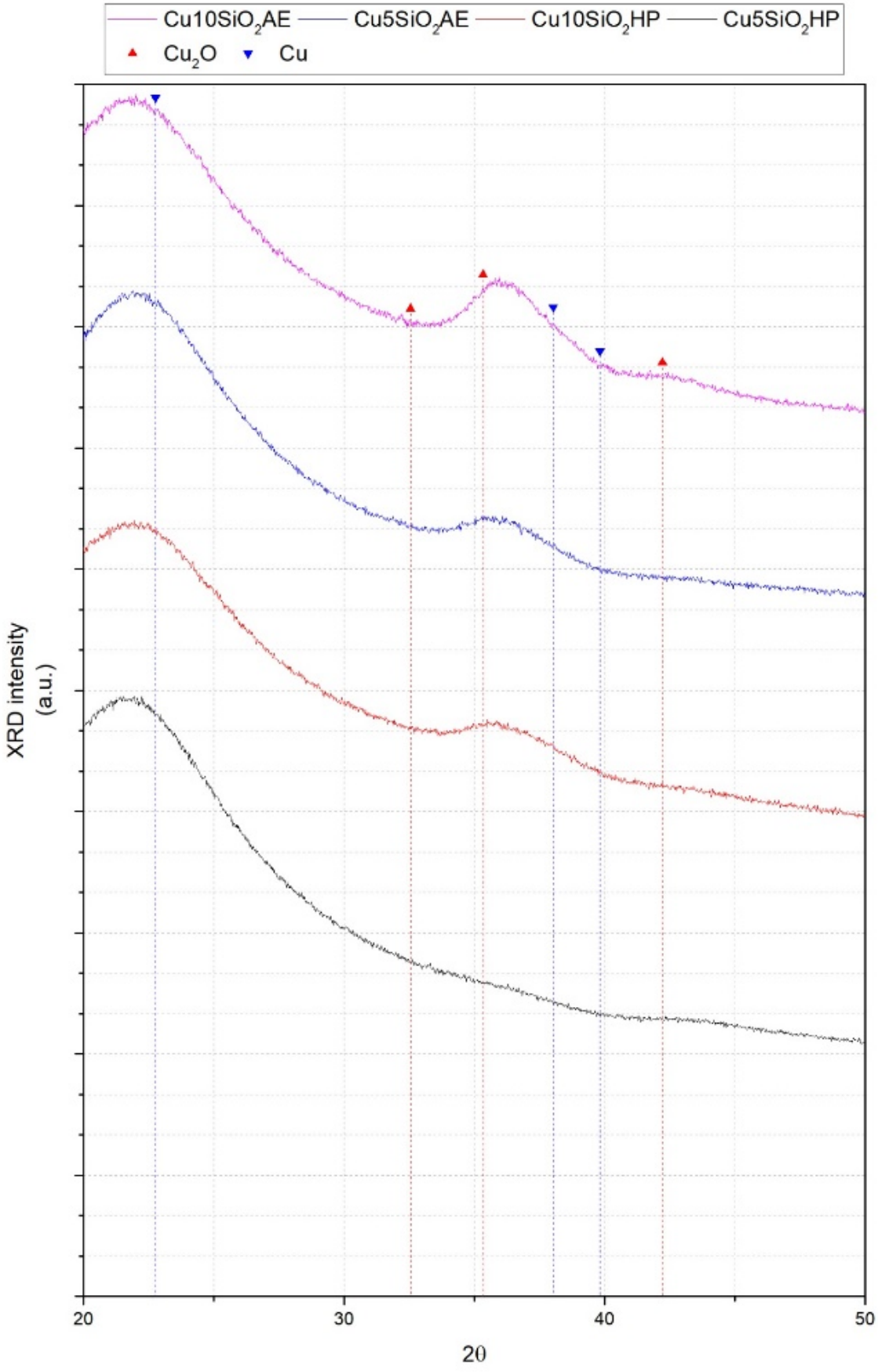

Figure 3-19 X-ray diffractograms of Cu/SiO_2 catalysts after TPR.

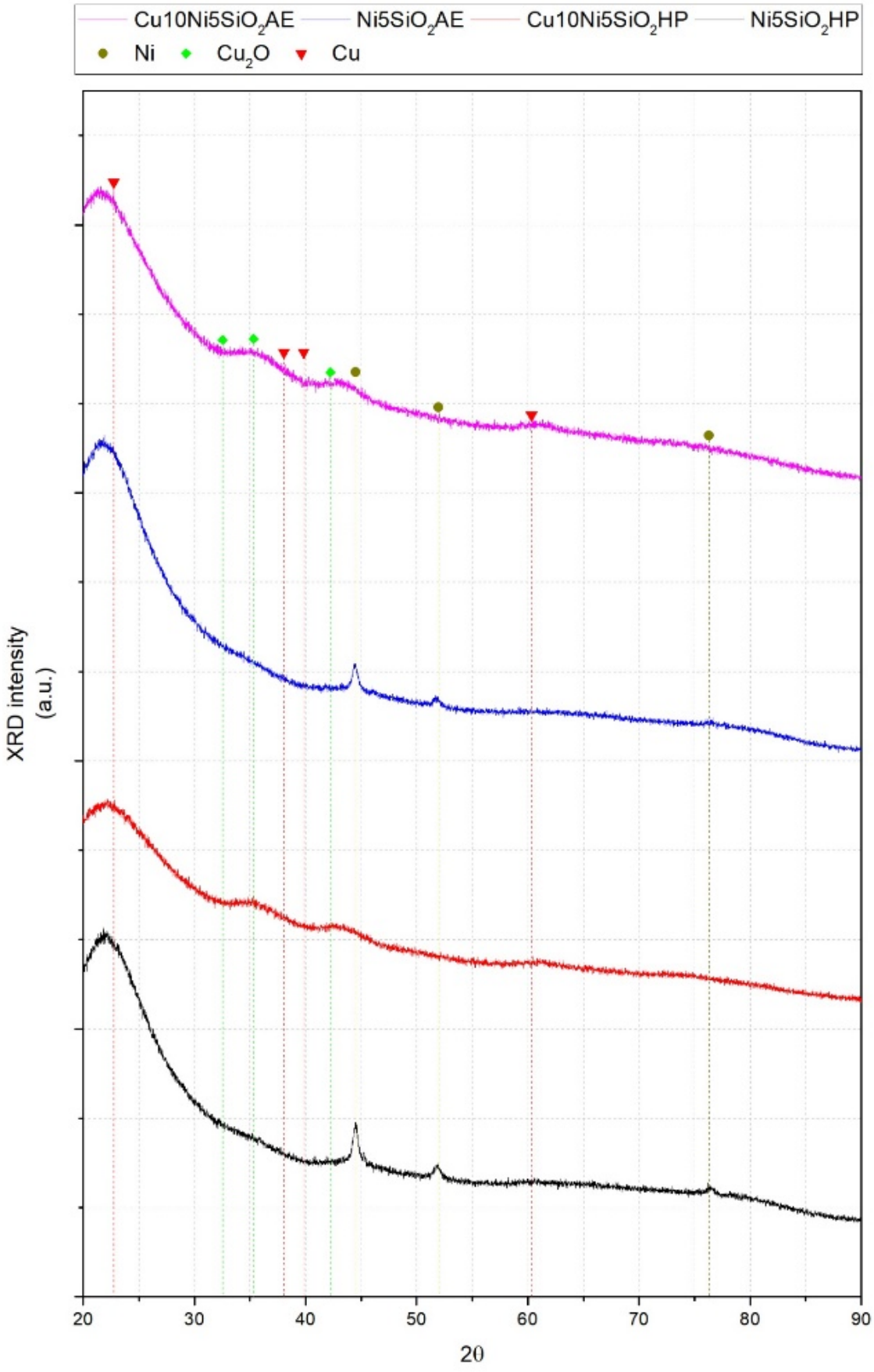

Figure 3-20 X-ray diffractograms of Cu-Ni/SiO_2 catalysts after TPR.

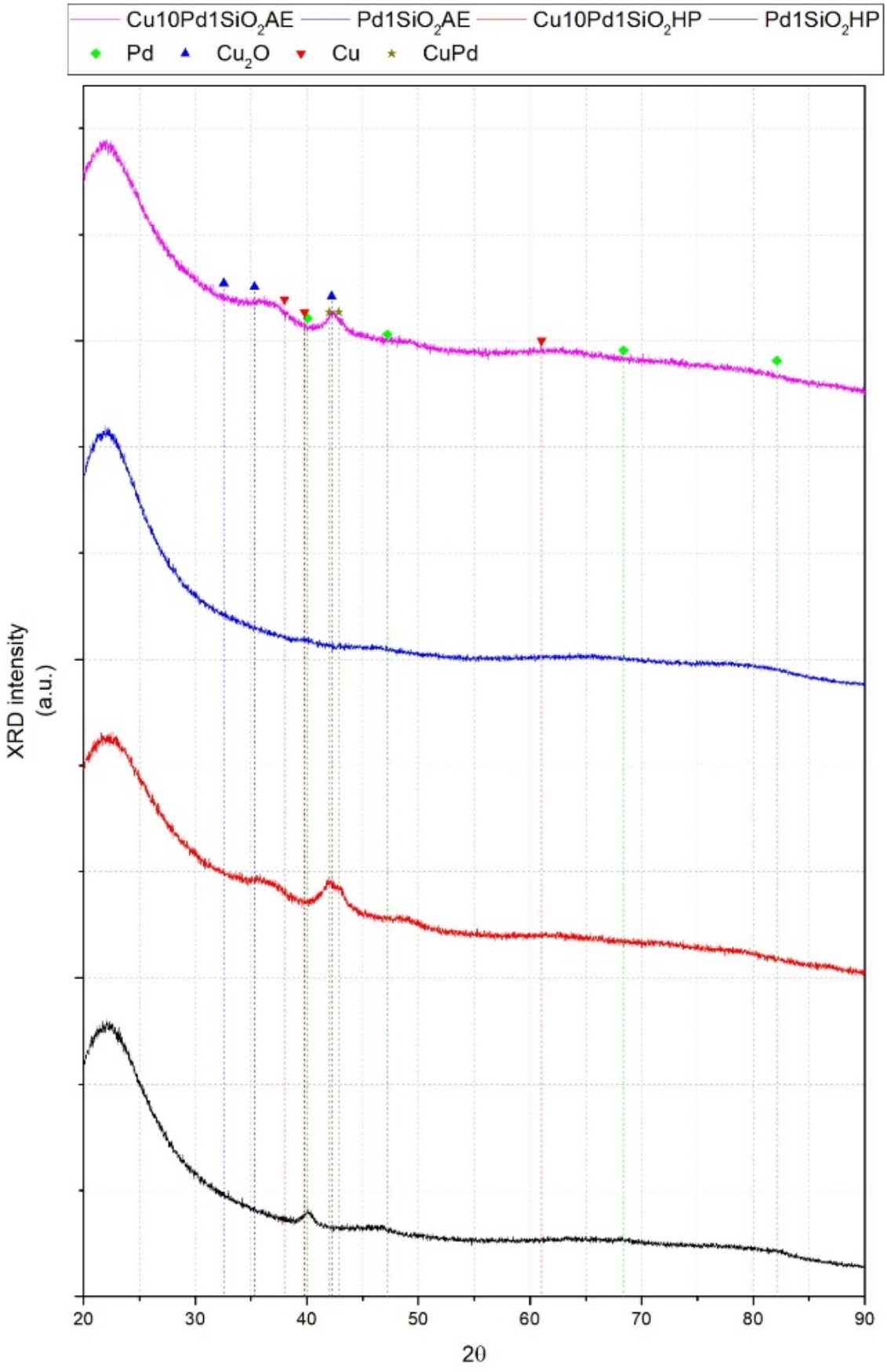

Figure 3-21 X-ray diffractograms Cu-Pd/SiO_2 catalysts after TPR.

3.3.6. Surface oxidation state

The surface chemical states of the reduced copper catalysts were detected by XPS and X-ray induced Auger spectra (XAES) measurements (Figure 3-22 to Figure 3-27). Figure 3-22 and Figure 3-24 present the XPS spectra relative to as-synthesized Cu10SiO_2AE and Cu10SiO_2HP samples, respectively. For these catalysts, the peaks at 942.5 eV and 962.4 eV are identifiable as CuO peaks, and the Cu^{2+} strong satellites are also present and probably linked to phyllosilicate.

After reduction (Figure 3-22 and Figure 3-24 for Cu10SiO_2AE and Cu10SiO_2HP samples, respectively), the intensity of the Cu^{2+} satellites decreases, and the main peaks are observed at 938.6 eV and 960.1 eV for HP and 938.1 eV and 959.5 eV for AE. For Cu10SiO_2AE catalyst, weak satellites are also observed after reduction, and this happens when Cu_2O is formed in large quantities on the support. For Cu10SiO_2AE catalyst, the satellites are less intense after reduction then it was assumed that the Cu_2O is less concentrated at the surface of this catalyst, and so more Cu^0 is exposed. However, it is crucial to point out that the possibility of Cu_2O in HP is not excluded, as also reported in the literature about the two synthesis methods [7,166].

In order to quantify the two low valence phases (Cu^+ and Cu^0), one cannot only rely on the XPS spectra, because of the similar Binding Energy between Cu^+ and Cu^0 species. LMM peak produced by the Auger effect must be studied.

As shown in Figure 3-26 and Figure 3-27, the two LMM spectra present an asymmetrical and broad peak, suggesting the coexistence of both Cu^+ and Cu^0 as stable species. The two symmetrical peaks obtained by deconvolution with the software CasaXPS were attributed to Cu^0 species for the higher peak, and to Cu^+ species for the other one. In Table 3-9, the ratio between $Cu^+/(Cu^+ + Cu^0)$ species is reported to identify which catalysts present the strongest interactions between silica support and copper species. It is evident that AE catalyst presents more Cu_2O than HP catalyst after reduction by H_2. As previously observed by XRD, this difference can be linked to the reduction of copper phyllosilicate. Although, in HP there are freer CuO on the surface and then, after reduction, more metallic copper is formed onto the surface.

Table 3-9 Cu^{+} and Cu^{0} distribution obtained by deconvolution with software CasaXPS.

Material	$(Cu^{+}/Cu^{0}+Cu^{+})*100$
$Cu10SiO_2HP$	45.4 ± 0.2%
$Cu10SiO_2AE$	62.0 ± 0.2%

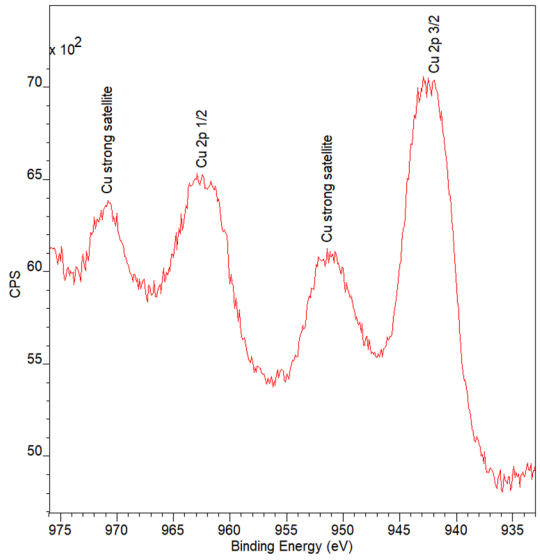

Figure 3-22 XPS of $Cu10SiO_2AE$ Cu 2p region.

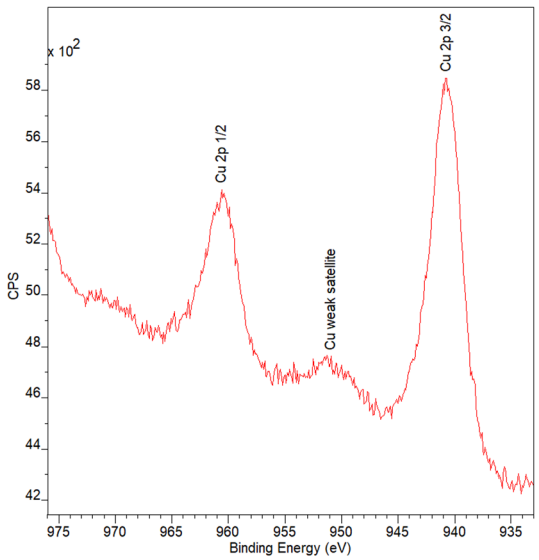

Figure 3-23 XPS of reduced $Cu10SiO_2AE$ Cu 2p region.

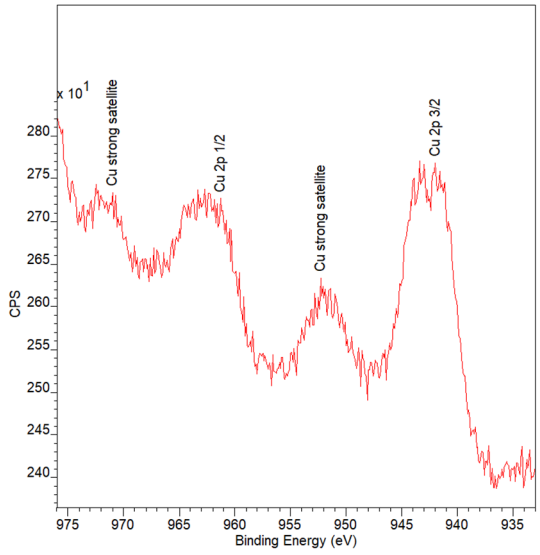

Figure 3-24 XPS of $Cu10SiO_2HP$ Cu 2p region.

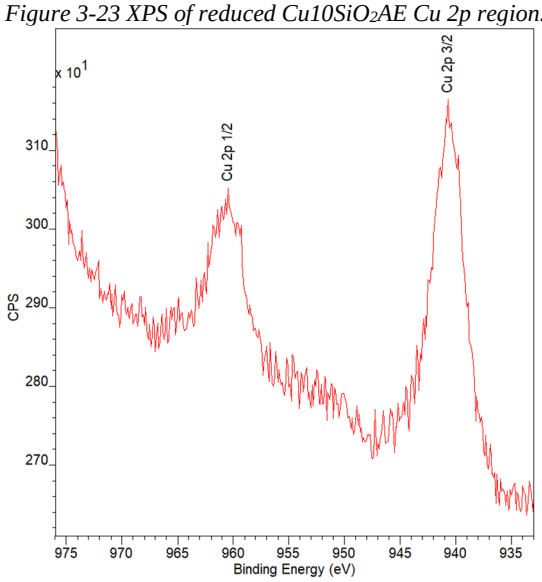

Figure 3-25 XPS of reduced $Cu10SiO_2HP$ Cu 2p region.

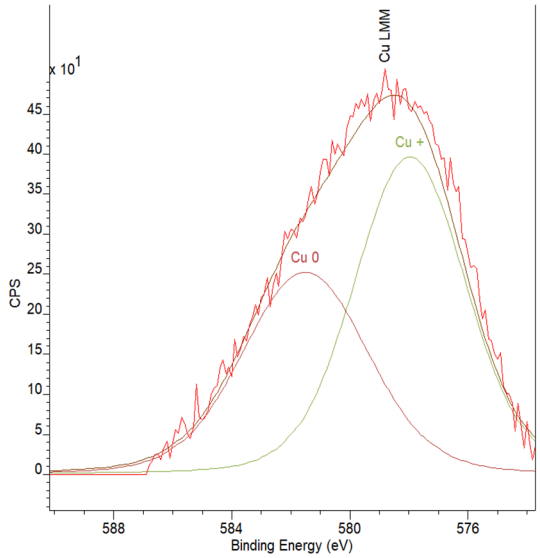

Figure 3-26 XPS of Cu10SiO₂AE reduced Cu LMM.

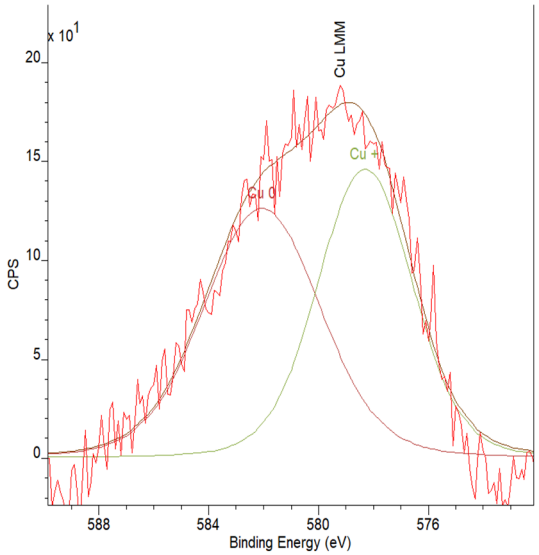

Figure 3-27 XPS of Cu10SiO₂HP reduced Cu LMM.

Monometallic and bimetallic nickel XPS spectra are quite difficult to read since multiple peaks are present for both metallic Ni and Ni bonded to other elements in the 2p region for this element. To simplify the analysis, and since reduced nickel samples were used for reactivity tests, the XPS analysis was performed on reduced samples. As shown in Figure 3-28 and Figure 3-29, the peak at 864.5 eV associated to the 2p 3/2 is a single peak and not a doublet composed by two very close peaks as individuated in the literature for NiO species [252–254]. This characteristic suggests the complete reduction of Ni species. In HP catalyst, the peaks are less intense, it is related to the content of Ni that is of 3.9%$_{w/w}$ for HP material against 4.7%$_{w/w}$ of the AE material (see elementary analysis Table 3-3).

Ni 2p region for the bimetallic catalysts is equivalent to the monometallic one, the same single peak of Ni 2p 3/2 is individuated (Figure 3-30 and Figure 3-31) and can be related to the absence of NiO species or other species containing Ni, O, and Si.

Studying the behavior of Cu 2p in bimetallic Cu/Ni catalysts, the XPS measurements show similar results than those obtained for monometallic copper, showing little interactions between copper and nickel, at least on the catalyst surface.

At last, the measurements performed on the monometallic palladium catalyst could not give crucial result on the Pd oxidation state. For palladium, the most used Binding Energy value of Pd3d(5/2) core level is the most widely used region to compare different systems [255,256], but here the peaks are confused with the measure error, probably due to the low content of Pd and to the metal dispersion onto the catalyst surface.

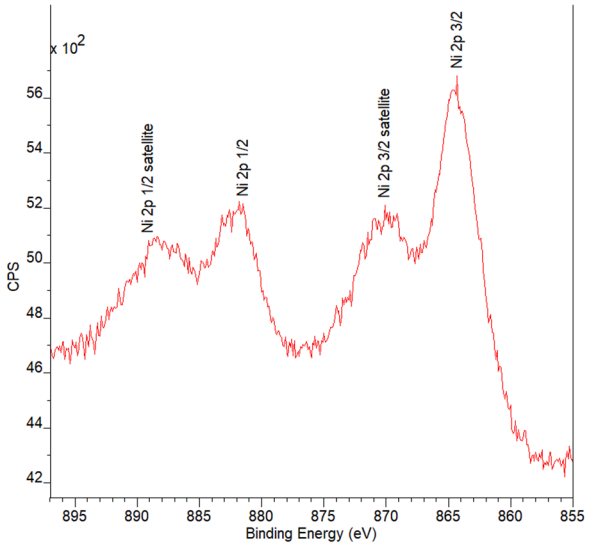

Figure 3-28 XPS Ni5SiO$_2$AE reduced 2p region.

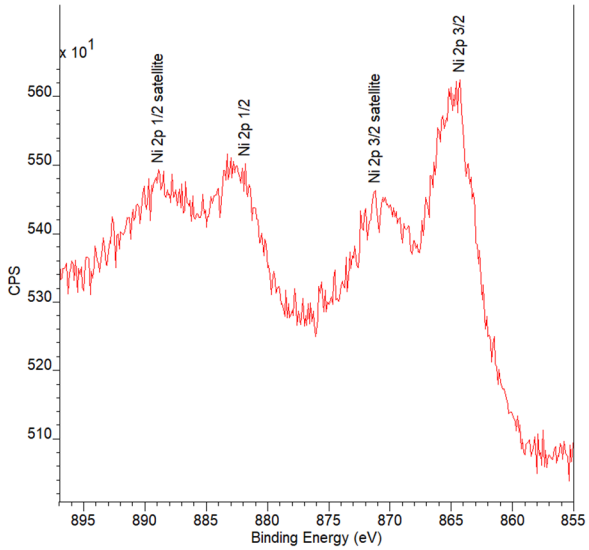

Figure 3-29 XPS Ni5SiO$_2$HP reduced 2p region.

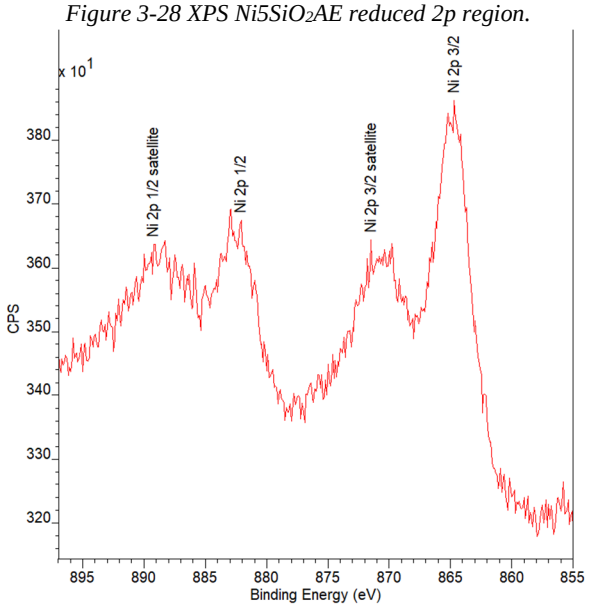

Figure 3-30 XPS Cu10Ni5SiO$_2$AE reduced 2p region.

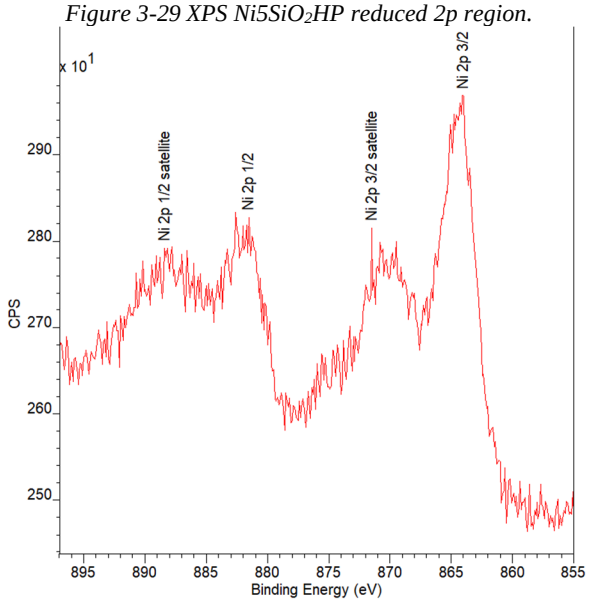

Figure 3-31 XPS Cu10Ni5SiO$_2$AE reduced 2p region.

As for bi-metallic Cu-Ni, Cu-Pd materials also have the same trend for Cu 2p peaks and that confirms the coexistence of Cu^+ and Cu^0 species. In Table 3-8, the results of Auger x-ray electron study are presented.

Table 3-10 Copper Cu^+ and Cu^0 distribution obtained by deconvolution with software CasaXPS.

Material	**$(Cu^+/Cu^0+Cu^+)*100$**
Cu10Ni5SiO$_2$HP	41.2±0.3%
Cu10Ni5SiO$_2$AE	40.5±0.2%
Cu10Pd1SiO$_2$HP	20.9±0.2%
Cu10Pd1SiO$_2$AE	68.4±0.4%

Bi-metallic samples containing Cu and Ni show almost the same amount of Cu in Cu^+ form after reduction, although there is a significant difference between the Cu^+ species in Cu-Pd catalysts. As XRD reveals the formation of CuPd combined species, HP catalysts contain these species showed by the typical overlapped peaks (Figure 3-21). For the AE samples, the peaks of Cu_2O are more significant, see in Figure 3-32 and Figure 3-33, as already mentioned and probably due to higher interactions with the support producing more chrysocolla or phyllosilicate.

As observed by XRD, it is possible to conclude that a larger quantity of copper is in Cu^0 state when more CuO is free in the as-synthesized sample and more interaction CuPd are formed after calcination/reduction.

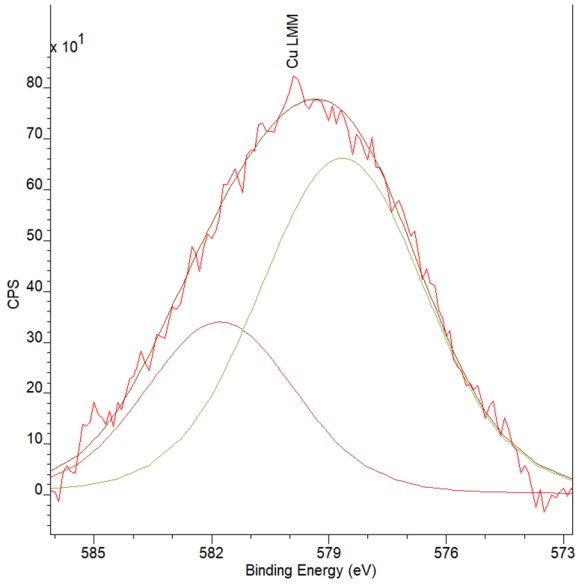

Figure 3-32 XPS Cu10Pd1SiO$_2$AE reduced Cu LMM.

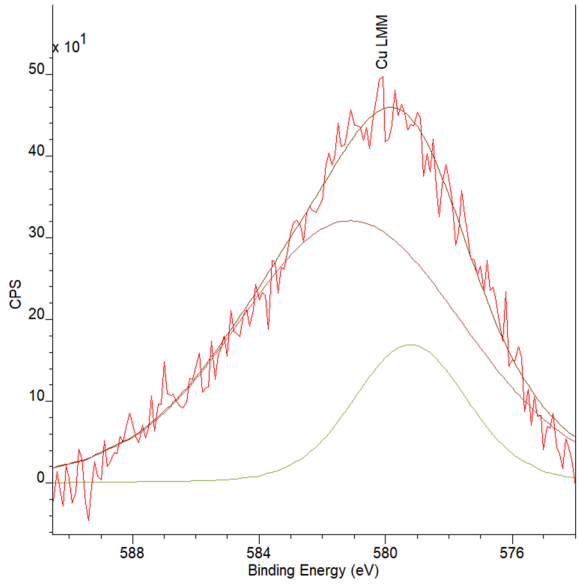

Figure 3-33 XPS Cu10Pd1SiO$_2$HP reduced Cu LMM.

3.3.7. Morphology and topography

In the following, morphologic and topographic evidences observed by SEM and TEM are reported.

3.3.7.1. SEM

SEM coupled with EDS elementary analyses, allow a better understanding of the morphology and elementary distribution of synthesized materials.

Figure 3-34 and Figure 3-35 show the external porous textures of Cu10SiO$_2$HP and Cu10SiO$_2$AE, respectively. The Cu10SiO$_2$AE material (Figure 3-35) has a much smoother surface with the presence of some

aggregates, however these aggregates have similar elemental composition than the bulk of the homogeneous support (see analyses spectra 14 to 16).

EDS on the same samples (Figure 3-34 and Figure 3-35) detects elemental Cu and Si with similar peak intensity in different spots over the surface. In accordance with all the previous discussions, this fact can be related to the good distribution of copper over the surface of the catalyst.

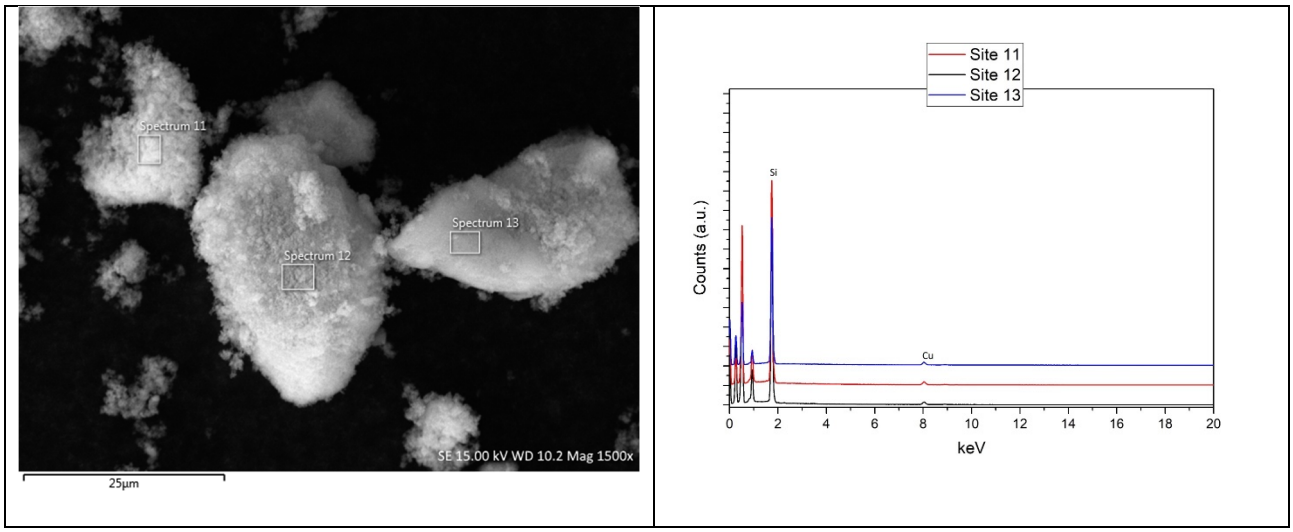

Figure 3-34 Cu10SiO$_2$HP secondary electron images with EDS analysis.

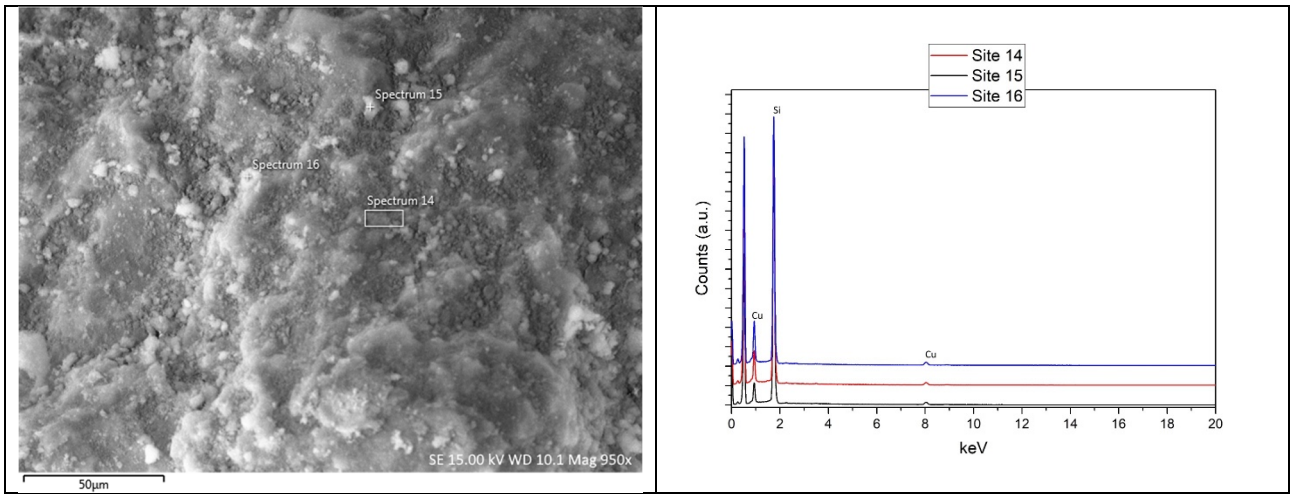

Figure 3-35 Cu10SiO$_2$AE secondary electron images with EDS analysis.

Figure 3-36 reports EDS maps over the surface of Cu10SiO$_2$HP and confirms the excellent distribution of copper over the silica support after calcination. Similar results were obtained for AE catalyst.

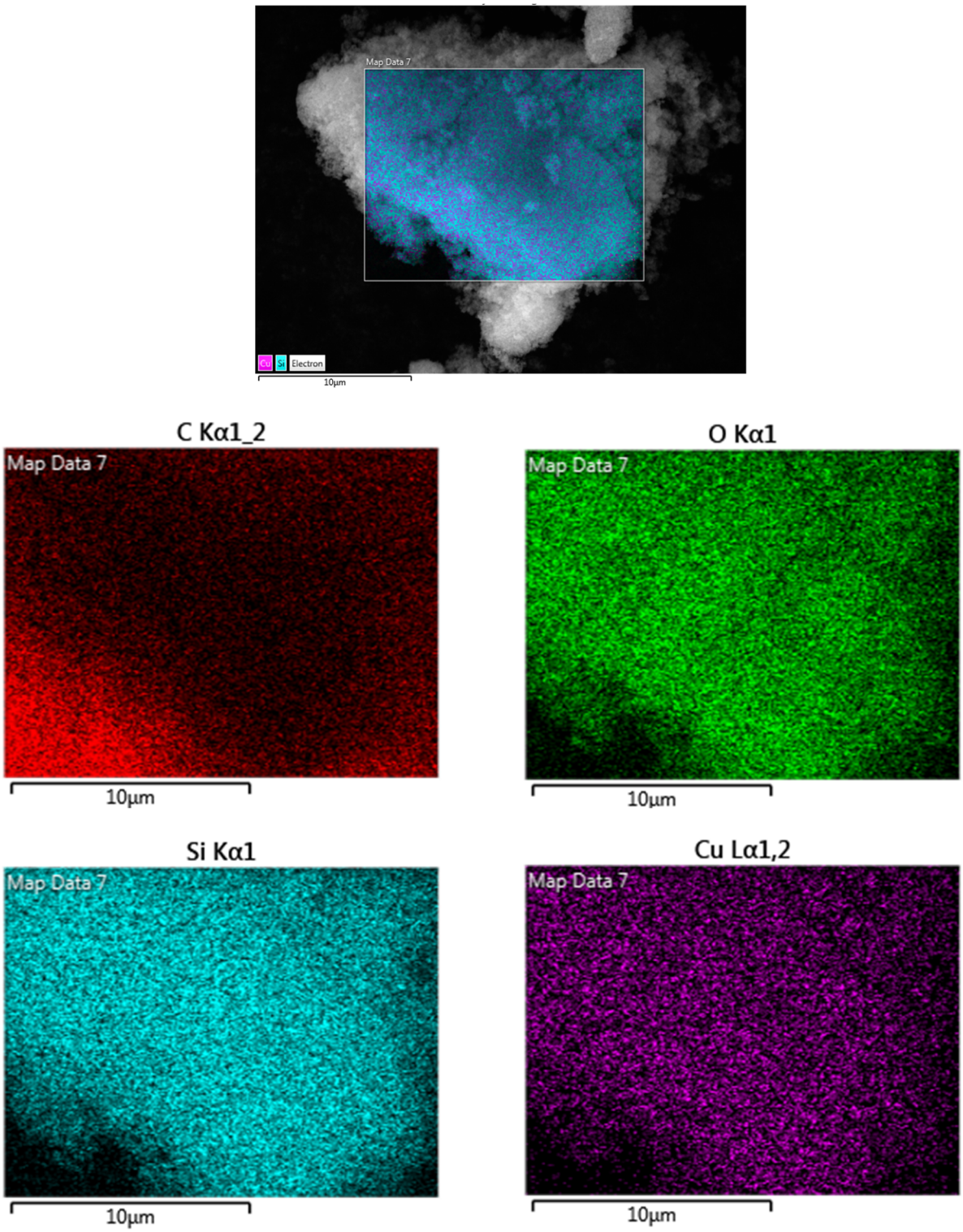

Figure 3-36 Cu10SiO$_2$HP EDS elementary distribution maps.

Moving the attention to bimetallic catalysts, the images for Cu10Pd1SiO$_2$AE is reported as an example (Figure 3-40). This material presents similar morphology than the monometallic copper, exposing some granular particles attached to a very homogenous support. The EDS results (Figure 3-37) do not show

difference with the monometallic material (Figure 3-35), and only traces of palladium can be found (Figure 3-38) due to its small load (less than 1%$_{w/w}$ measured by ICP-AES).

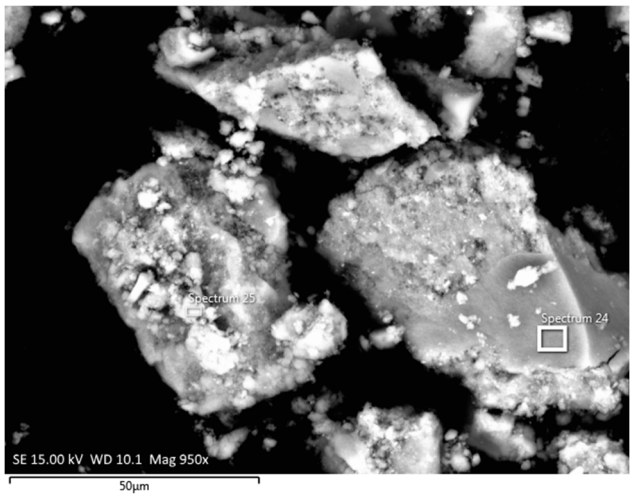

Figure 3-37 Cu10SiO$_2$AE secondary electron image.

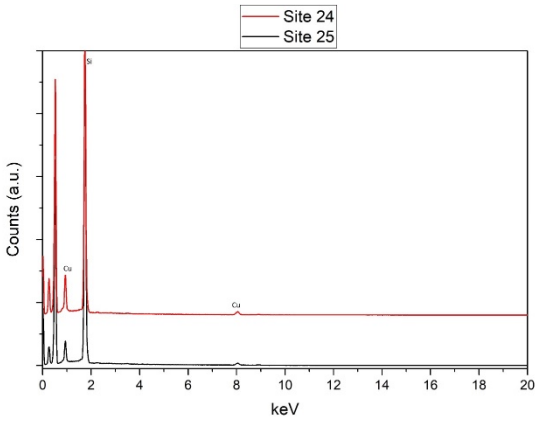

Figure 3-38 Cu10SiO$_2$AE EDS scan punctual and area.

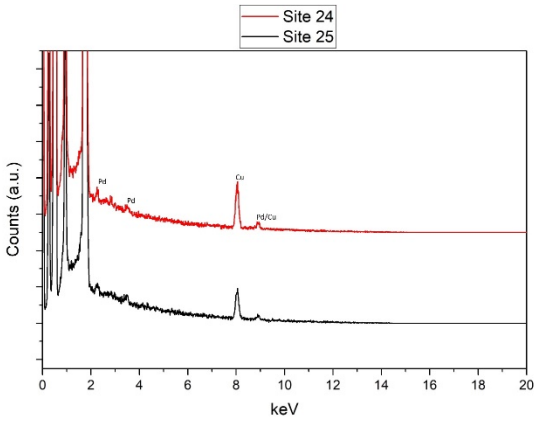

Figure 3-39 Cu10SiO$_2$AE EDS scan punctual and area focused on Pd identification.

The catalyst was also observed in its reduced form in order to see any differences after reduction with H_2. The introduction of second metal salt during the synthesis does not cause a significant alteration in the structure of the catalyst (Figure 3-39), in comparison with Cu10SiO$_2$AE.

As shown by EDS, Pd was only found at the trace level and well dispersed on the support corroborating the hypothesis of a good dispersion of the metallic species.

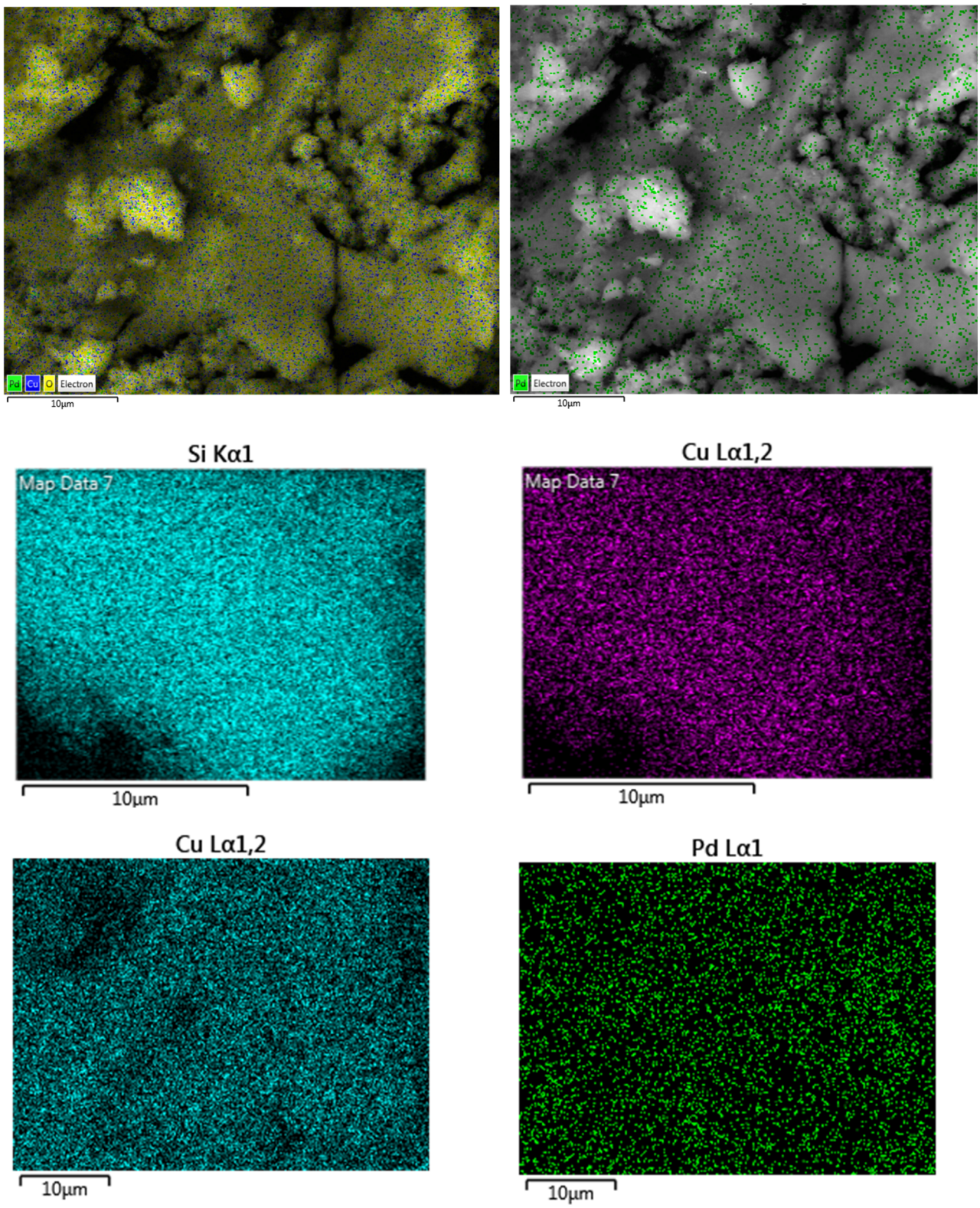

Figure 3-40 Cu10Pd1SiO$_2$AE reduced EDS maps.

3.3.7.2. TEM

TEM micrographs of monometallic copper catalysts in both as-synthesized and reduced forms are presented in Figure 3-41.

As-synthesized sample of $Cu10SiO_2AE$ presents a lamellar structure were any crystalline structure is observed (Figure 3-41a and Figure 3-41b), suggesting that copper is integrated inside the matrix. Moreover a difference between HP and AE materials stands out, indeed for the HP material (Figure 3-41c and Figure 3-41d) some crystals were observed, in particular on the border of the materials, this crystalline structures could be associated with CuO crystals because of their small size (3-5 nm), observed by XRD.

Another difference between the two syntheses is present in the arrangement of the silica matrix. For HP sample, the surface seems much smoother than for the AE catalyst, which is composed of small lamellar structures.

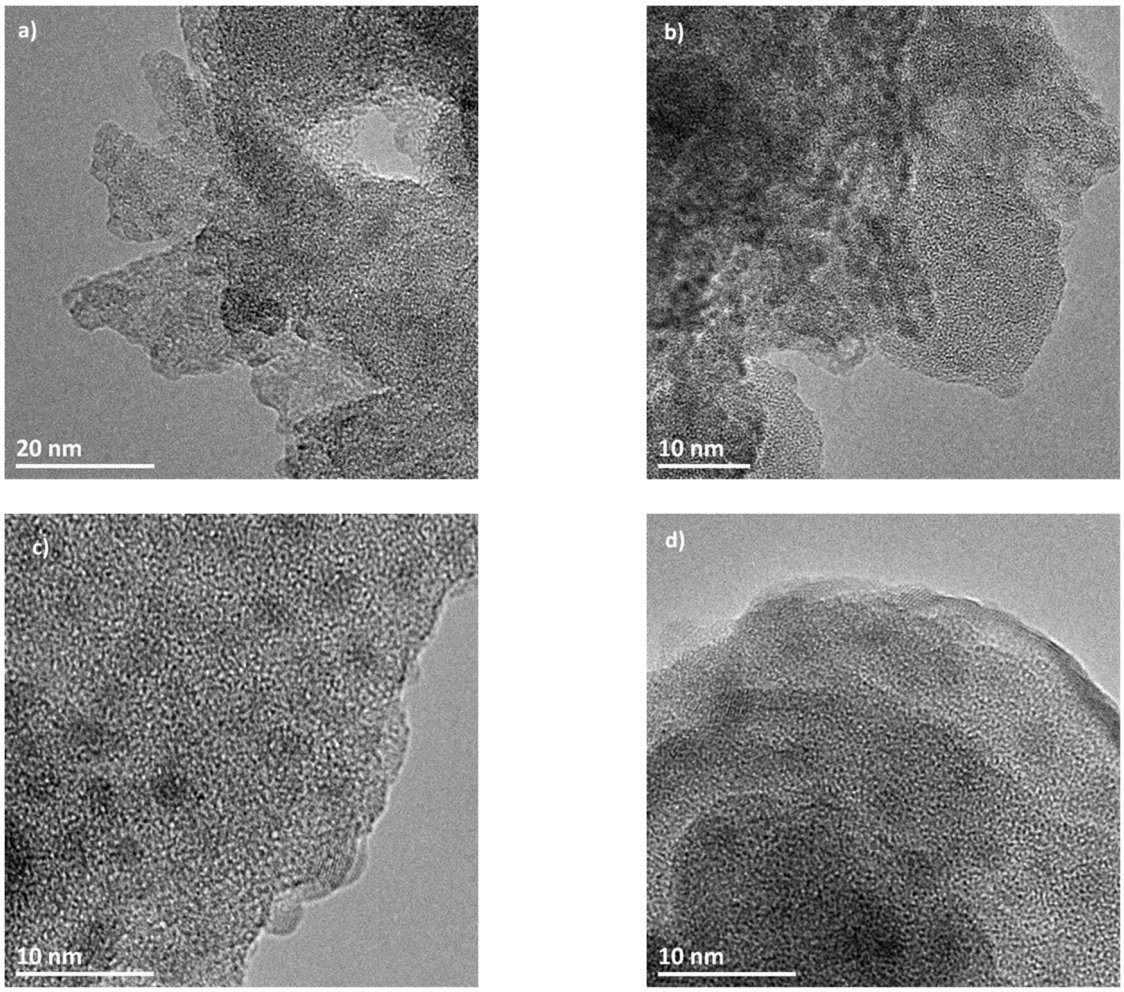

Figure 3-41 TEM micrographs of as-synthesized $Cu10SiO_2AE$ (a) and b)), and $Cu10SiO_2HP$ (c) and d)).

The reduced samples micrographs (Figure 3-42) reveal more evident crystalline structures. This was also evident by XRD with some Cu_2O and Cu^0 detectable peaks. The EDS analysis suggests that the small particles observed (for both HP and AE samples) (smaller than 7 nm) are composed of metallic copper or Cu_2O, also confirming XPS results.

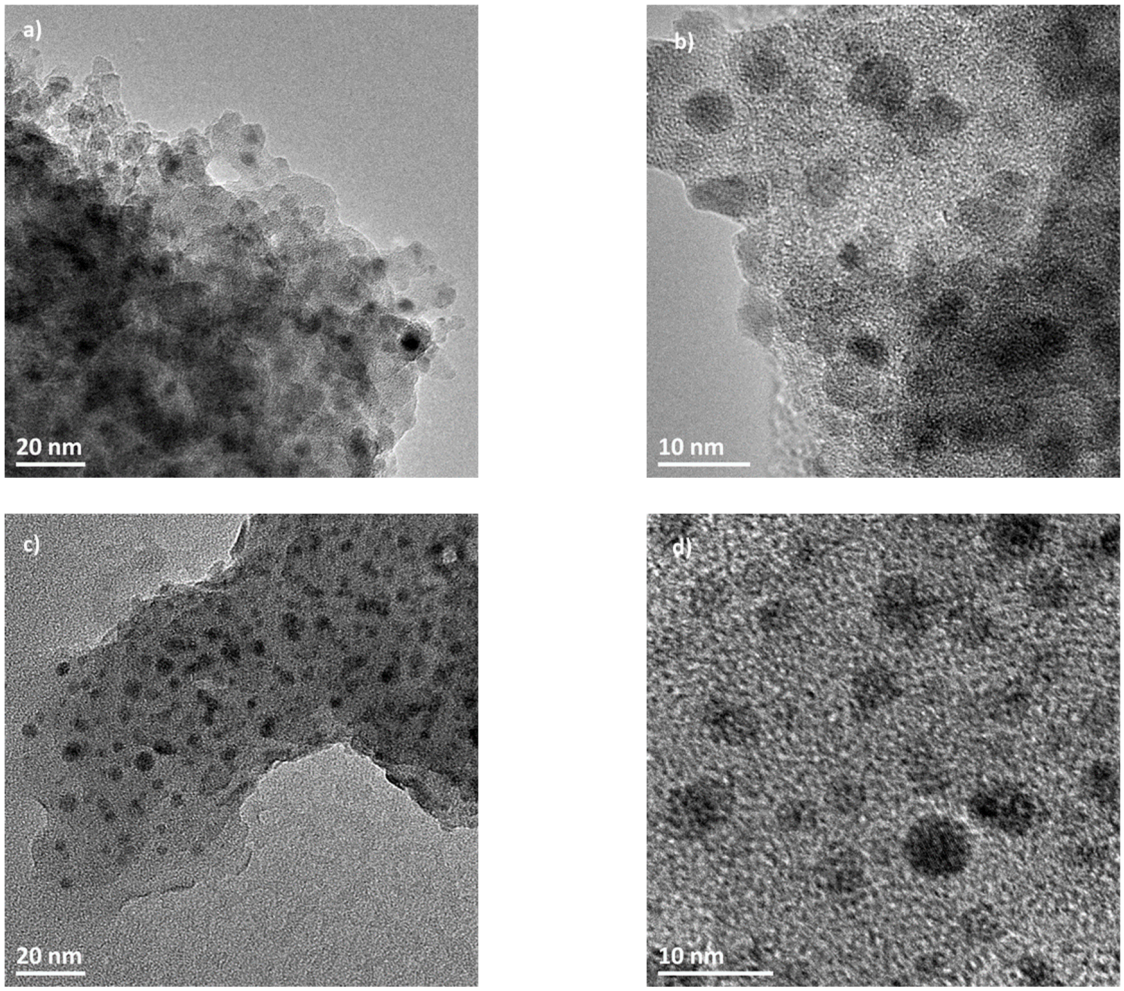

Figure 3-42 TEM micrographs of reduced Cu10SiO$_2$AE (a) and b)), and Cu10SiO$_2$HP (c) and d)).

At last, since reduced samples shown better images, it is possible to identify some crystalline phases in the silica matrix of the reduced bimetallic Cu-Ni materials observed by TEM. As an example, the images for Cu10Ni5SiO$_2$HP sample and for its relative monometallic Ni5SiO$_2$HP are presented (Figure 3-43). The two materials share characteristics with the monometallic copper HP catalyst: in the monometallic Ni catalyst the metallic Ni small size particles (3-5 nm) are well dispersed, in the bimetallic catalyst on the other hand, it was impossible to discriminate copper and nickel particles, since their sizes are very close and EDS analysis showed both elements.

The other bimetallic materials showed similar characteristics.

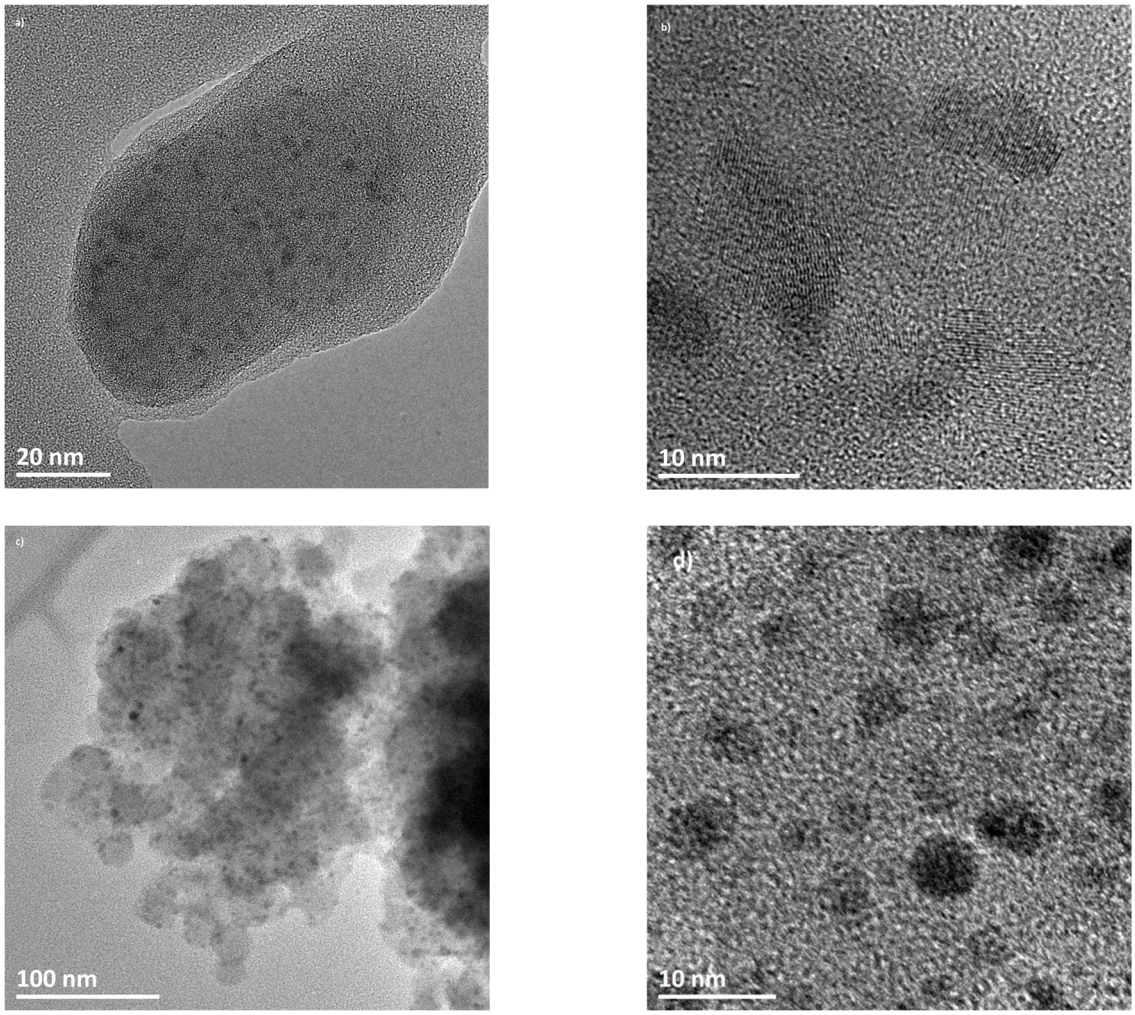

Figure 3-43 TEM micrographs of reduced Cu10Ni5SiO$_2$HP (a) and b)), and Ni5SiO$_2$HP (c) and d)).

3.3.8. Conclusions

Different materials were characterized before the reactivity tests as shown in this chapter. The major results obtained for Lindlar and Pd/HT, the materials characterized with less techniques, are the following:

I. For Lindlar catalysts, a small surface area related to the low pore area of the support calcium carbonate is observed. Calcium carbonate by XRD is the only phase that it is possible to establish the presence;

II. The Pd/HT catalyst method proves to be reliable in the synthesis of palladium supported hydrotalcites with the wanted content of Pd (ICP-AES); the materials have the BET surface area, and the shape of isotherms characteristic of this kind of materials. As in the case of Lindlar, for Pd/HT it is not possible to identify the Pd phases by XRD, due to the low Pd content.

HP and AE synthesis methods are generally capable to produce Cu-silica catalysts, and with less extent it is also proved that Ni and Pd catalysts are possibly synthesized by the same methods as shown by the following results:

I. With the exclusion of some singularities with Ni and Pd, ICP-AES (§3.3.1), results acceptably match the desired amount of metal content for all the materials;

II. Texture (§3.3.2) is a common characteristic among monometallic catalysts prepared with HP and AE methods, all the materials present features that are ascribable to mesoporous materials with large surface area. Although the surface area of materials produced by HP method are higher than those produced by AE, this is also reflected by pores volume and averaged diameters which are lower for the AE catalysts;

III. XRD (§3.3.3.1) detects with difficulty phases which are formed by the combination of Cu and Si, this is eventually resolved by the study of FTIR and Raman spectra (§3.3.3.2) identifying chrysocolla (Cu phyllosilicates). The same trend is also observed for Ni monometallic catalysts: after the heat treatment, a particular form of Ni silicate (Pimelite) for AE is found; Pd monometallic catalysts present the Pd in its oxide form;

IV. From a morphological point of view the two synthesis methods give two different external structures, in particular AE seems to be formed by smooth lamellae-like structures while HP is much more porous as also observed by SEM (§3.3.7.1). TEM images on the other hand show that in HP synthesis some crystals with average size lower than 5 nm are identifiable, AE materials is more uniform and less structure is found. An essential information was given on the metals distribution which appears to be well spread on the support.

The catalysts samples were analysed after reduction and lead to the following results:

I. TPR (§3.3.5.1) results show that the materials present a single H_2 consumption peak for all the samples, independently of the synthesis method. This peak is in the range reported in the literature for the reduction of the metal oxide precursors. The Cu area was studied by chemisorption of N_2O and highlighted higher area, and so higher dispersion, for HP samples than for AE samples;

II. XRD after reduction of copper catalysts, show the contemporary presence of both metallic copper and Cu_2O, with different respective proportions depending from the synthesis method, in particular AE method materials contain higher amount of metallic Cu. Monometallic palladium and nickel samples show, after reduction, metallic Pd and Ni,respectively;

III. The same conclusions obtained from XRD is also found by XPS on reduced materials (§3.3.6): different ratios are observed between metallic Cu and Cu_2O on the catalysts surface;

IV. After reduction morphology highlights small crystals of active phase which are well distributed and have average dimensions lower than 7 nm for both syntheses.

Bimetallic catalysts are also studied and give interesting and unique features:

I. ICP-AES results for bimetallic materials indicates that the Cu content is lower than expected. This is associated with the different conditions used during synthesis of monometallic Cu samples and bimetallic ones, in particular the pH is chosen as a compromise between the best pH value for the two metals;

II. XRD of as-synthesized materials are similar to the monometallic ones, with a contingent difference for Cu-Pd:the XRD ray are shifted by the effect of PdO introduction in the CuO structure. Similar effect was observed for the reduced samples with the formation of CuPd structure, it must be specified that for HP method this CuPd is more evident;

III. Reduction temperatures of the bimetallic materials are higher for Cu than the corresponding monometallic Cu, indicating higher interaction with the support. However, the copper surface areas are in line with the values obtained with monometallic Cu catalysts;

IV. Bimetallic catalysts share the same XPS features with Pd and Ni monometallic ones; for Cu-Pd, the content of Cu^0 over Cu^+ is more evident probably due to the CuPd structures;

V. At last, the morphological characteristics of these materials do not deviate too much from the features found in monometallic materials; it is important to say that it is practically impossible to differentiate Cu and Ni or Cu and Pd with in-situ EDS analysis or by some morphological feature.

Chapter 4

Reactivity tests

This chapter reports the activity test results for the tests performed as indicated in Table 2.5; test results follow the same order of Chapter 3:

- *Lindlar catalyst reactivity tests;*
- *HT-Pd reactivity tests;*
- *Silica-supported catalysts reactivity tests.*

4.1. Lindlar catalyst reactivity tests

Before the hydrogenation reaction campaign, blank tests without catalyst were carried out under the corresponding conditions for six hours, in order to evaluate some possible homogeneous phase reactions. In all these preliminary cases, the oil was analyzed at the end of the test, indicating no homogenous phase reactions occur, and detected composition's changes are within the range of the experimental error of the gas chromatography analysis.

All the results of catalytic activity tests performed with canola rapeseed oil were reported in this section. Selectivities and conversions were detected depending on different reaction conditions, and the evolution of the composition of fatty acids during the reaction time was evaluated. The most significative tests' results are reported in Table 4-1 and Table 4-2.

Table 4-1 Test results, isomer index SII index and conversions calculated when the highest amount of oleic acid was observed

Entry	Oil	T* (min)	S_{Ln} (%)	S_{Le} (%)	SII	$\chi_{C18:3}$ (%)	$\chi_{C18:2}$ (%)	(C18:1)**(%)
Test 03	Canola	120	1.3	23.9	0.7	84.6	60.8	82.6
Test 04	Canola	90	1.4	33.6	1.4	90.1	84.6	88.4
Test 05	Canola	60	1.3	20.2	1.2	92.7	84.3	86.0
Test 06	Canola	120	1.7	35.8	1.5	92.1	51.4	83.2
Test 07	Canola	120	2.2	37.3	1.8	90.6	51.0	84.4
Test 08	Sunflower	240	-	13.9	2.3	-	98.7	83.0

*Time corresponding to the maximum relative percentage of C18:1

**Maximum C18:1 relative percentage obtained during the test

The linolenic acid selectivity S_{Ln} results are in line with literature values [92,257] between 1 and 3%, but for the linoleic selectivity S_{Le} values are higher (at 180 °C for Test 04 at 4 bar and Test 05 at 12 bar) or comparable (120 °C for Test 03) to the threshold indicated for selective reaction conditions as reported by Simakova [104]. The S_{Le} values suggest that the reaction rates of linolenic and linoleic fatty acids are higher than the formation rate of stearic acid (consumption of oleic acid) and so the reaction is halted before the complete saturation of double bonds. The reaction proceeds after the hydrogenation of polyunsaturated fatty acids with the conversion of C18:1 in stearic acid, it is possible to conclude that the scheme of three reaction in series proposed in §2.3.5 explains what happens and the direct hydrogenation to form stearic acid from polyunsaturated compounds occur only in very small amount. However, not only stearic acid is formed during the conversion of oleic acid but also his geometric isomer is rapidly formed when the more unsaturated compounds start to disappear from the reaction medium.

Table 4-2 Test results, SII and IV at 50% conversion of linolenic and at 50% conversion of linoleic

	Linolenic $\chi_{C18:3}$ 50%				**Linoleic $\chi_{C18:2}$ 50%**			
Entry	**t (min)**	**IV**	**SII**	**(C18:1) (%)**	**t (min)**	**IV**	**SII**	**(C18:1) (%)**
Test 03	40	109.7	0.32	73.1	90	86.28	0.43	78.3
Test 04	40	102.52	0.44	81.3	50	89.79	0.50	83.8
Test 05	15	111.8	0.40	73.2	30	88.43	0.42	81.8
Test 06	30	111.22	0.64	72.4	100	87.08	1.77	83.2
Test 07	35	108.5	0.68	71.1	110	83.27	1.73	82.5
Test 08	-	-	-	-	75	115.1	0.80	62.1

From hydrogenation runs conducted at 60 °C under 4 bar and 12 bar (Tests 01 and 02 in Table 2-2) even after 6 hours of reaction, a negligible conversion of both linoleic and linolenic acids was observed and so they are not reported in Table 4-1.

At higher temperatures, conversions of linoleic and linolenic fatty acids increase, until nearly complete saturation of double bonds. At 120 °C and under 8 bar (Test 03), the polyunsaturated compounds are almost entirely converted in C18:1 and C18:0 compounds, after four hours of test (Figure 4). Besides, we observe the rapid isomerization of oleic acid in elaidic acid (about 67.0 %) of the global monoene concentration (58.6 % at the end of the test). This value is below the equilibrium value reported in the literature [96,258]. At 120 minutes the maximum concentration of C18:1 was reached (82.6 %), with a corresponding stearic acid composition is 7.8 %. At this reaction time, 8.1 % of C18:2 and 1.6 % C18:3 remain unreacted (Figure 4-1).

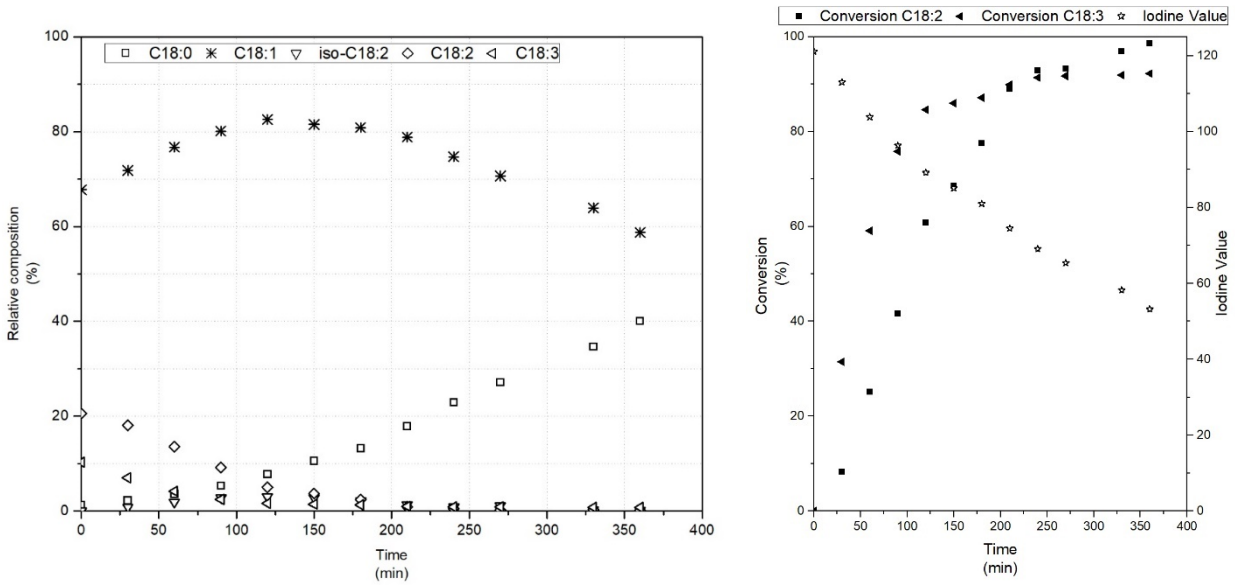

Figure 4-1 Test 03 Hydrogenation results at 120 °C and 8 bar: on the right-hand side relative percentage of C18 compounds vs time, on the left-hand side the conversions of linolenic and linoleic acid and iodine alue vs time

Similar behavior was observed for the Test 04 at 180 °C and 4 bar (Figure 4-2): after 120 min, polyunsaturated compounds are less than 3%. At 60 minutes, the composition is 85.1% and 4.5 % of C18:1 and of stearic acid, respectively, with a small amount of elaidic acid (estimated below 15%, see Appendix A for elaidic acid, t-C18:1, estimation during the tests), and with better results comparing SII, 0.59 in this conditions, with experimental data obtained in other works for palladium catalysts where the SII is actually in the range 0.8 and 0.85 for Pd alone and in between 0.7 and 0.75 for Pd combined with lead [145,259]. Between 60 minutes and 90 minutes, C18:1 faster reacts by hydrogenating and isomerizing simultaneously: SII increased up to 1.4 when maximum C18:1 concentration is reached. In this case, we observe 88.4% of C18:1 after 90 min of reaction, compared to the 82.6% of the previous test obtained after 120 min. When the maximum was achieved the relative percentage of elaidic acid increases.

It is interesting to compare the results in Table 4-4 when C18:3 and C18:2 are half reacted. In these conditions, 81.3% (50% conversion of C18:3) and 83.8 (50% of conversion of C18:2) of C18:1 are reached, respectively, and a high amount of linolenic and linoleic acids is still available to react.

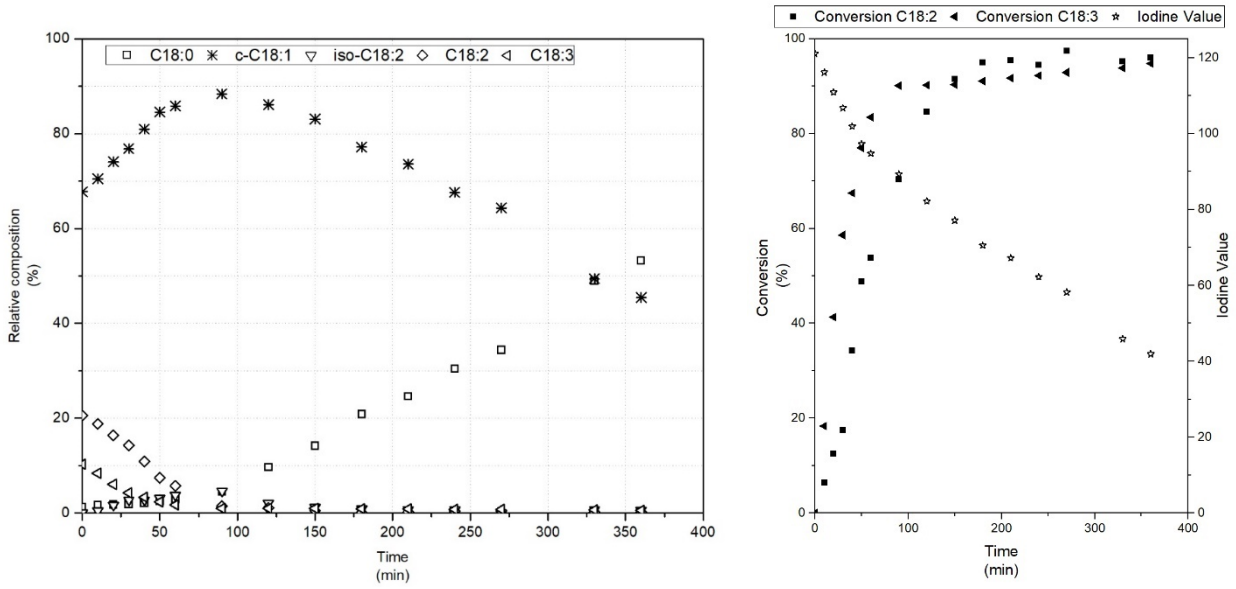

Figure 4-2 Test 04 Hydrogenation results at 180 °C and 4 bar: on the right-hand side relative percentage of C18 compounds vs time, on the left-hand side the conversions of linolenic and linoleic acid and iodine value vs time

An higher pressure of H_2 (12 bar) involves a higher concentration of molecular H_2 solubilized in the oil. Thus, the reaction rate increases and the complete conversion of C18:2 and C18:3 is achieved after only 90 minutes (Figure 4-3). However, at this reaction time, the competitive hydrogenation of C18:1 to C18:0 and the isomerization of the monoene also increase the amounts of undesired products: trans isomers less than 50% and C18:0 is 11.1% when C18:1 reaches the maximum relative percentage. Since a high concentration of monoene is desired, preferably in the cis configuration, while keeping a low concentration of stearic acid and trans isomer, it is necessary to stop the reaction before the complete conversion of the polyenes. In order to identify the best reactions conditions and rates, reference was made to the greatest conversion of polyunsaturated fatty acids, the highest concentration of C18:1 fatty acid, the lowest concentration of C18:1*t*. By evaluating these parameters, the hydrogenation results observed at 180 °C (Test 04 and Test 05) are better than that obtained at 120°C (Test 03, Table 4-1), since the same degree of conversion is obtained with shorter reaction times and higher amounts of C18:1.

It is worth mentioning that, when results at the same conversion are evaluated with higher pressure, lower amount of trans isomers is found, this affects the lower SII index as reported in Table 4-2. This effect is in line with similar behavior for other palladium catalysts as reported by Hsu et al. [64].

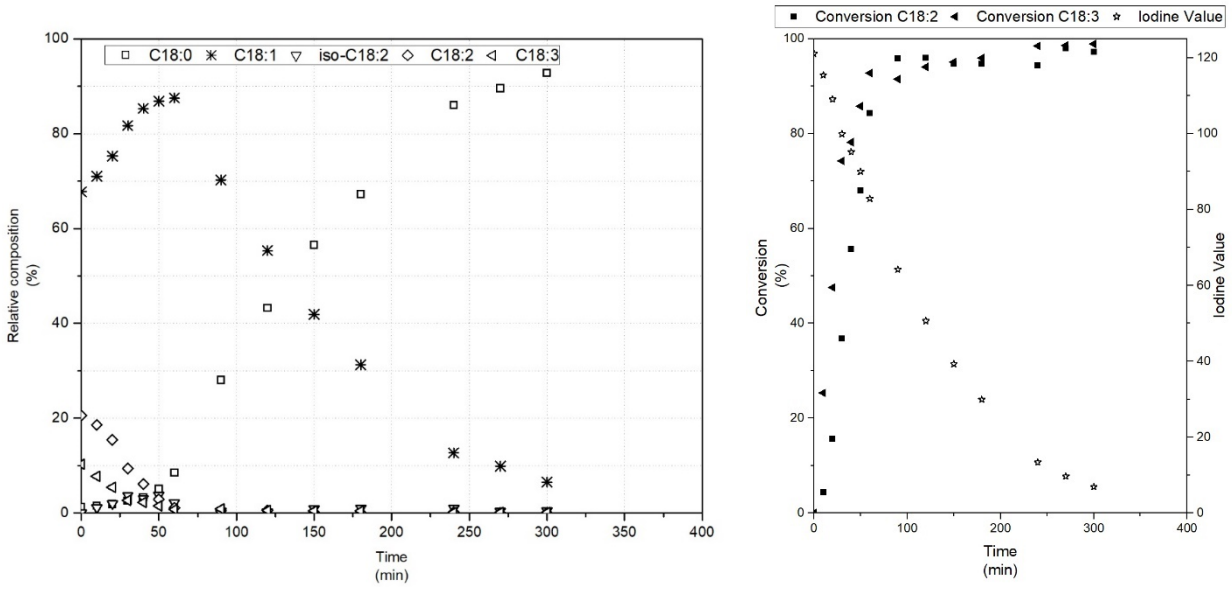

Figure 4-3 Test 05 Hydrogenation results at 180 °C and 12 bar: on the right-hand side relative percentage of C18 compounds vs time, on the left-hand side the conversions of linolenic and linoleic acid and iodine value vs time

The lower pressure test seems to be slightly better (Test 04 Figure 4-2 at 90 minutes *vs* Test 05 Figure 4-3 at 60 minutes) from the point of view of the maximum amount of C18:1 (88.4 % *vs* 86.0 %) and less efficient from the point of view of the corresponding C18:2 and C18:3 conversions (84.6 % *vs* 84.3 % and 90.1 % *vs* 92.7 %, respectively). From the point of view of relative percentages of elaidic acid and stearic acid, better results in the maximum C18:1 concentration were achieved at lower pressure.

The effect of catalyst' recycling, catalyst concentration, and vegetable oils type was investigated at the best operative conditions of 4 bar of pure hydrogen and 180 °C. Repeated tests of 1h were conducted to evaluate the efficiency of the catalyst after several cycles. The conversions and the selectivities over 5 cyclic tests were calculated with the Eq.2-13/18 and are reported in Table 4-3 and Table 4-4. Tests results for the composition after 1 h are reported in Figure 4-4, while C18:3 and C18:2 conversions are reported in Figure 4-4.

Table 4-3 Test results for the cyclic test at 180 °C under 4 bar pressure. SII, conversions and selectivities calculated at 1 h.

Entry	Oil	S_{Ln}	S_{Le}	SII	$\chi_{C18:2}$ (%)	$\chi_{C18:3}$ (%)	(C18:1) (%)*
Test 09	Canola	1.21	47.8	0.40	42.8	65.8	86.6
Test 10	Canola	1.24	40.8	0.76	55.2	80.8	86.2
Test 11	Canola	1.05	39.3	0.93	54.2	75.1	83.8
Test 12	Canola	1.01	26.0	0.94	49.2	67.7	81.4
Test 13	Canola	1.11	20.5	0.75	42.8	65.8	80.7

*Maximum C18:1 relative percentage obtained at 60 minutes

Table 4-4 Test results for the cyclic test at 180 °C under 4 bar pressure, SII and IV at 50% conversion of linolenic and at 50% conversion of linoleic.

	Linolenic $\chi_{C18:3}$ 50%				Linolenic $\chi_{C18:2}$ 50%			
Entry	t (min)	IV	SII	(C18:1) (%)	t (min)	IV	SII	(C18:1) (%)
Test 09	23	110.0	0.41	73.4	47	99.99	0.40	83.5
Test 10	25	108.5	0.42	73.5	53	97.01	0.66	85.3
Test 11	30	106.9	0.37	77.1	53	97.51	0.69	83.4
Test 12	36	103.2	0.64	74.2	62	93.46	0.86	81.2
Test 13	39	106.4	0.67	73.2	73	96.08	0.82	81.0

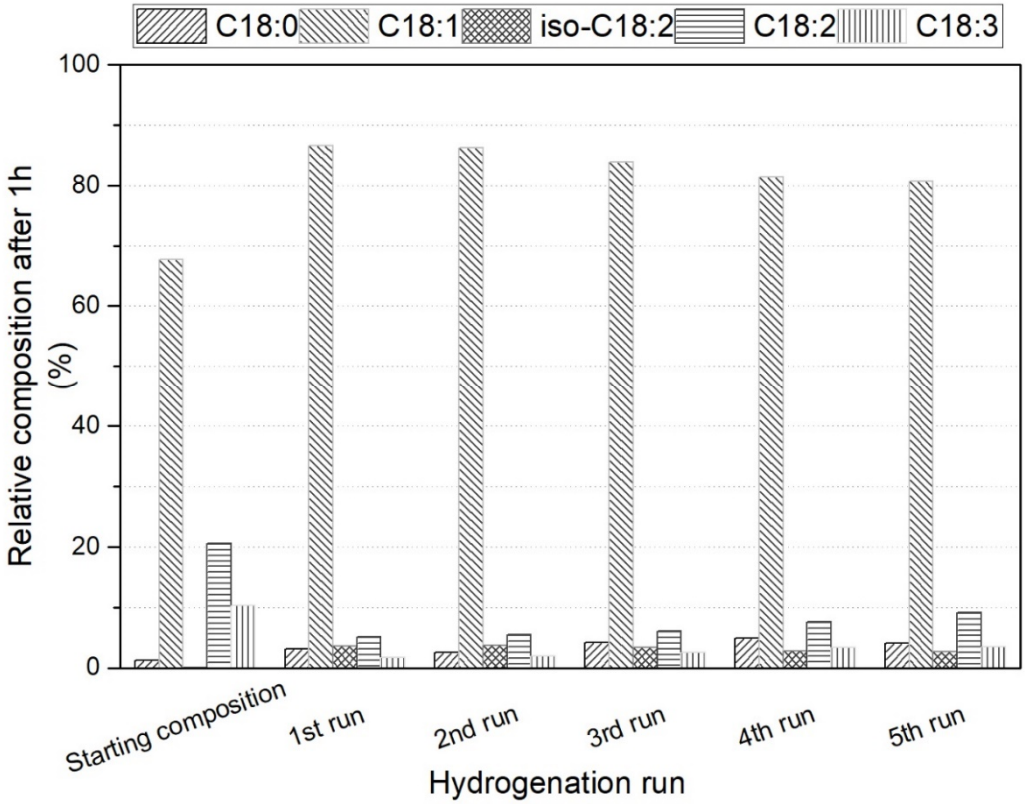

Figure 4-4 Hydrogenated oil composition at 1h over five cyclic tests at 180°C under 4 bar pressure (test 09-13)

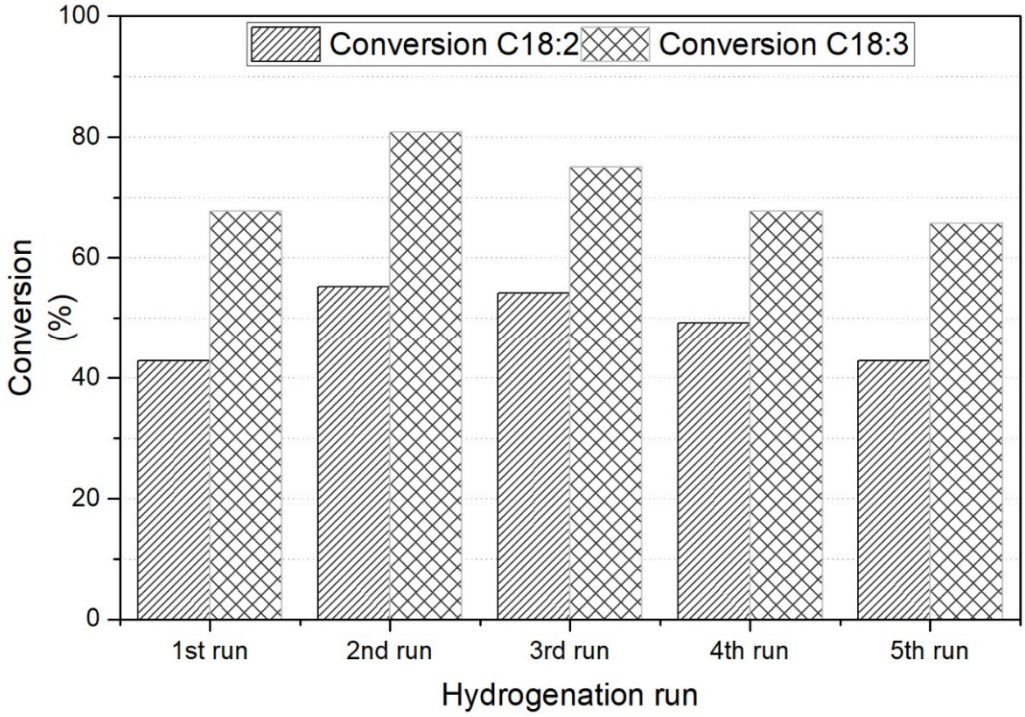

Figure 4-5 C18:1 and C18:2 conversions at 1h over five cyclic tests at 180°C under 4 bar pressure (test 09-13)

Cyclic tests show a slightly progressive loss of catalytic activity over hydrogenation runs and the possible explanations are:

– the poisons present in the oil (sulfur and phosphorous compounds or heavy metals traces) could affect the catalytic properties, lowering conversions and changing selectivities [156,260,261];

– some complex molecules naturally present in vegetable oils, such as chlorophyll, also if they not directly poison the Pd, can occlude the pores of the catalyst, preventing the access for reactants;

– some Pd leaching may occur [262]: however, post-test ICP-AES analysis on recovered catalyst washed with acetone, and n-hexane shows a loss of Pd less than 10 $_{\%w/w}$;

– deactivation of the catalyst due to the formation of coke or carbon monoxide: this effect is reported in literature and it could occur in continuous operation or for long-time reaction[263].

The catalyst deactivation could be solved by making-up the appropriate amount of fresh catalyst.

In order to test the efficiency of the fresh catalyst, tests were carried out using less amount of catalyst (2 $mg_{catalyst}/mL_{oil}$, and 1 $mg_{catalyst}/ mL_{oil}$).

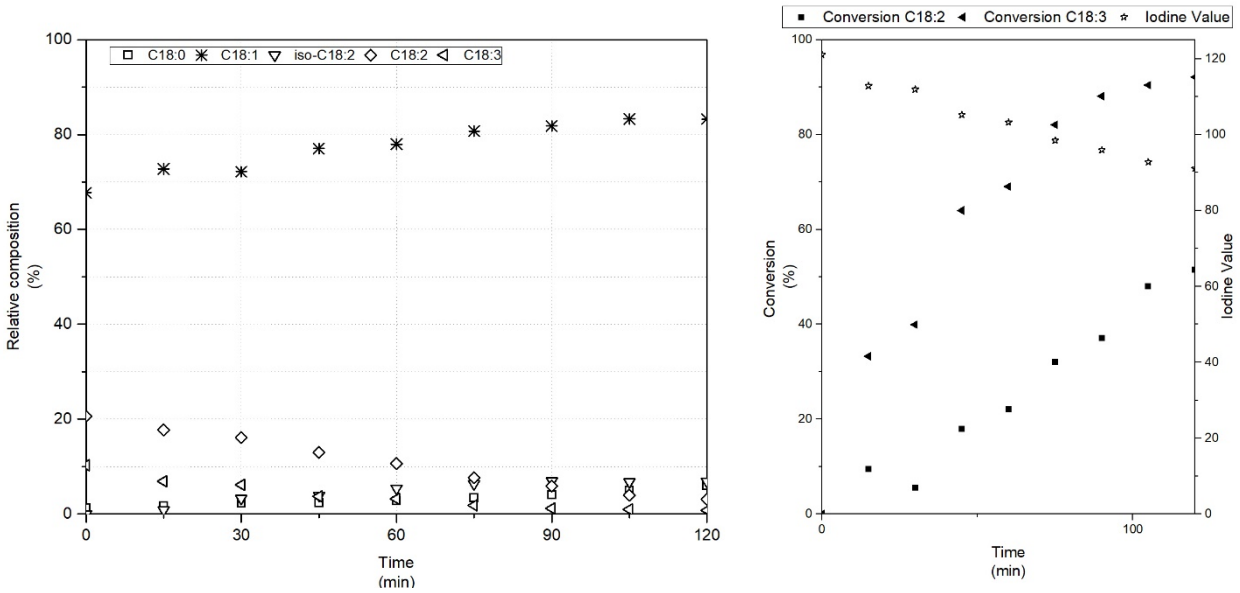

Figure 4-6 Test 06. Hydrogenation results at 180 °C and 4 bar with 2 $mg_{catalyst}/mL_{oil}$ of Lindlar catalyst: on the right-hand side relative percentage of C18 compounds vs time, on the left-hand side the conversions of linolenic and linoleic acid and iodine value vs time

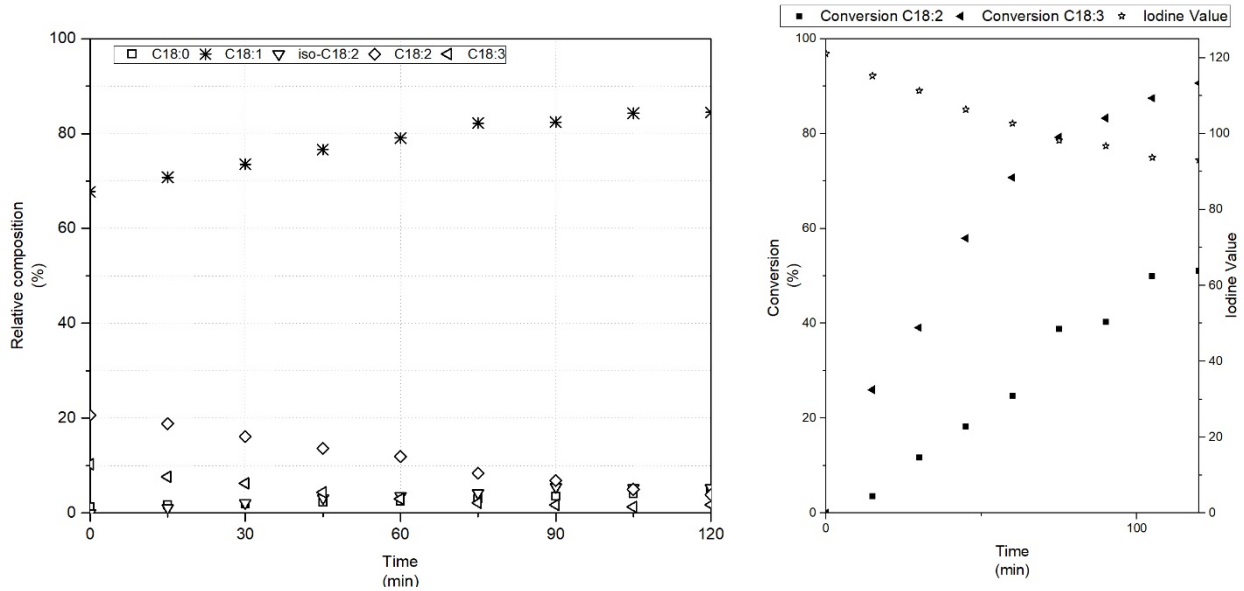

Figure 4-7 Test 07. Hydrogenation results at 180 °C and 4 bar with 1 $mg_{catalyst}/mL_{oil}$ of Lindlar: on the right-hand side relative percentage of C18 compounds vs time, on the left-hand side the conversions of linolenic and linoleic acid and iodine value vs time

The tests with different catalyst concentrations (Figure 4-6 and Figure 4-7) show only a slight decrease in the hydrogenation rate. Comparing the 1 $mg_{catalyst}/mL_{oil}$ test with 2 $mg_{catalyst}/mL_{oil}$ one after 2 h of reaction, almost the same conversions for linolenic (92.1±0.4 % *vs* 90.6±0.5 %) and linoleic (51.4±0.5 % *vs* 51.0±0.3 %) acid were observed in both tests. So, we can obtain comparable results using a quarter of the amount of the initial catalyst (1 $mg_{catalyst}/mL_{oil}$ *vs* 4 $mg_{catalyst}/mL_{oil}$), but with longer reaction time than the case with 4 $mg_{catalyst}/mL_{oil}$ (Test 04 Table 4-3 and Figure 4-2).

Although for SII, it was observed almost the same results, with lower amount of catalyst less stearic acid was formed comparing with the results achieved during Test 04 (4.5 % in Test 04 and 6 % in Test 06 and Test 07, see Figure 4-2, Figure 4-6, and Figure 4-7, respectively) but also less C18:1 (results in Table 4-3). However, comparing SII index with higher concentration of catalyst (Test 04), it is possible to highlight that for a longer time of reaction higher SII are reached, and so higher amount of trans formed from the double bond hydrogenated (see Table 4-3 and Table 4-4).

Considering all the tests carried out, the best conditions are 180 °C under 4 bar of pure hydrogen with 4 mg of Lindlar catalyst of 1 mL_{oil}. Besides, comparable results were obtained with less amount of catalyst, but at longer reaction time.To prove the versatility of the catalyst, a test was carried out at 180 °C and 4 bar (Test 08 Figure 4-8) using commercial sunflower oil, with lower initial contents of C18:1 and C18:3, and higher content of C18:2.

Hydrogenation results for Test 08 are shown in Figure 4-8. The conversion of C18:2 is almost quantitative after 4 hours. At the same time, we observe a maximum in the production of C18:1 (83 %). Low amount of C18:0 (12 %) were also detected. Nevertheless, high contents of C18:1*t* (about 51 % after 4 h) is presently showing a low selectivity towards the cis isomer, especially if compared to hydrogenation of canola oil in the same reaction conditions (about 5 % of C18:1*t*). So, the comparison with canola rapeseed oil indicates that in an oil having significant content of C18:3, the hydrogenation of polyenes is favoured over both the isomerization and hydrogenation of monoene.

This is probably due to the different reactivity of fatty acids. It is reported that polyenes react more easily in correlation with the number of double bonds present on the fatty acids chain: generally C18:3 and C18:2 react with similar rates, but the reaction rate for C18:1 is of one order of magnitude lower than the other two, as reported in the following scheme [31] (Equation 4-1):

$$C18{:}3 \geq C18{:}2 > C18{:}1 \qquad \text{Equation 4-1}$$

In the case of sunflower oil, it was observed that the C18:2 hydrogenation and C18:1 isomerization/hydrogenation happen simultaneously. However, when canola rapeseed oil is considered, the combined presence of C18:3 and C18:2 with more unsaturations react more easily because more double bonds are available in the chain that can be adsorbed on the catalyst surface. C18:1 would react in a second time when the C18:2 and C18:3 are consumed and so it is observed less C18:1*t* and C18:0 formation.

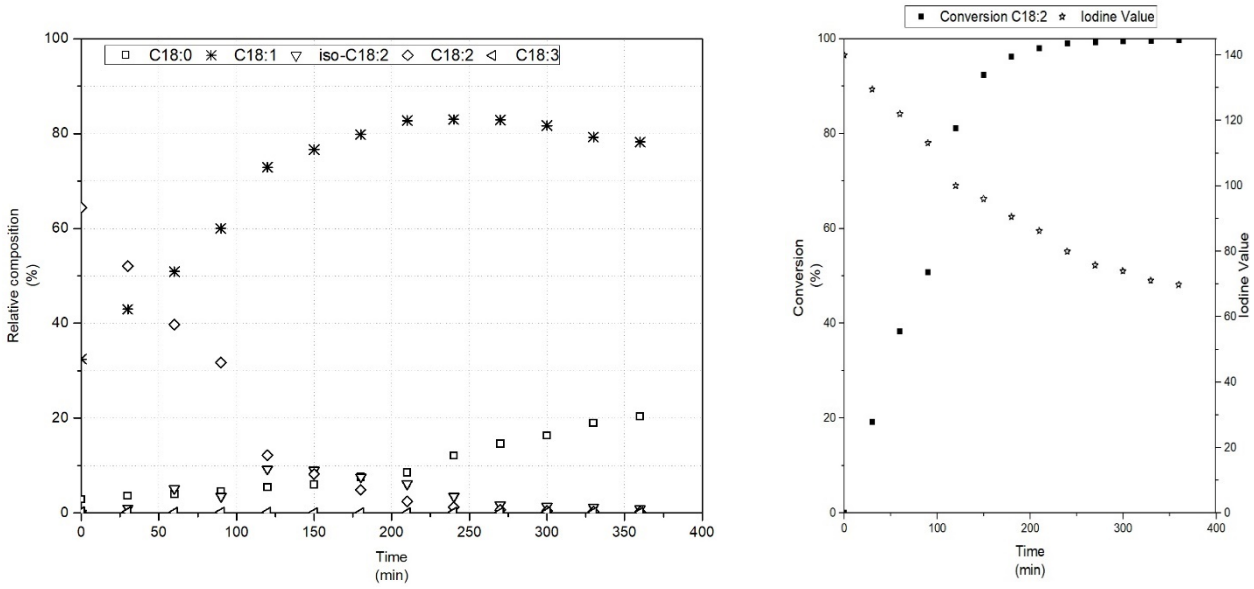

Figure 4-8 Test 08 Hydrogenation test at 180 °C and 4 bar with 4 $mg_{catalyst}/mL_{oil}$ with sunflower oil : on the right-hand side relative percentage of C18 compounds vs time, on the left-hand side the conversions of linolenic and linoleic acid and iodine value vs time

In the case of canola rapeseed oil, the proposed model, §Chapter 3, fits well (see Figure 4-9) the composition data for C18:2 and C18:3, for C18:1 this model gives a discrepancy between the measured value and the predicted one. For sunflower oil hydrogenation, the first reaction (from C18:3 to C18:2) was neglected, because the initial concentration of linolenic acid (0.2 % percentage of C18:3), and so, the relative variation were low. The model predicts the compositions of C18:1 and C18:2 with an error less than 3 %. Two examples of the fitting data, for the best tests' conditions, are shown in Figure 4-9, on the right the fitting model for Test 04 with canola rapeseed oil (stopped at 120 min reaction) and the second one on the left for sunflower oil, Test 13. The discrepancies, mainly observed for C18:1 composition trend for canola oil, between the experimental data and the calculated results from the model, albeit acceptable, could be correlated to both a possibly different order of reaction and a more complex reaction mechanism.

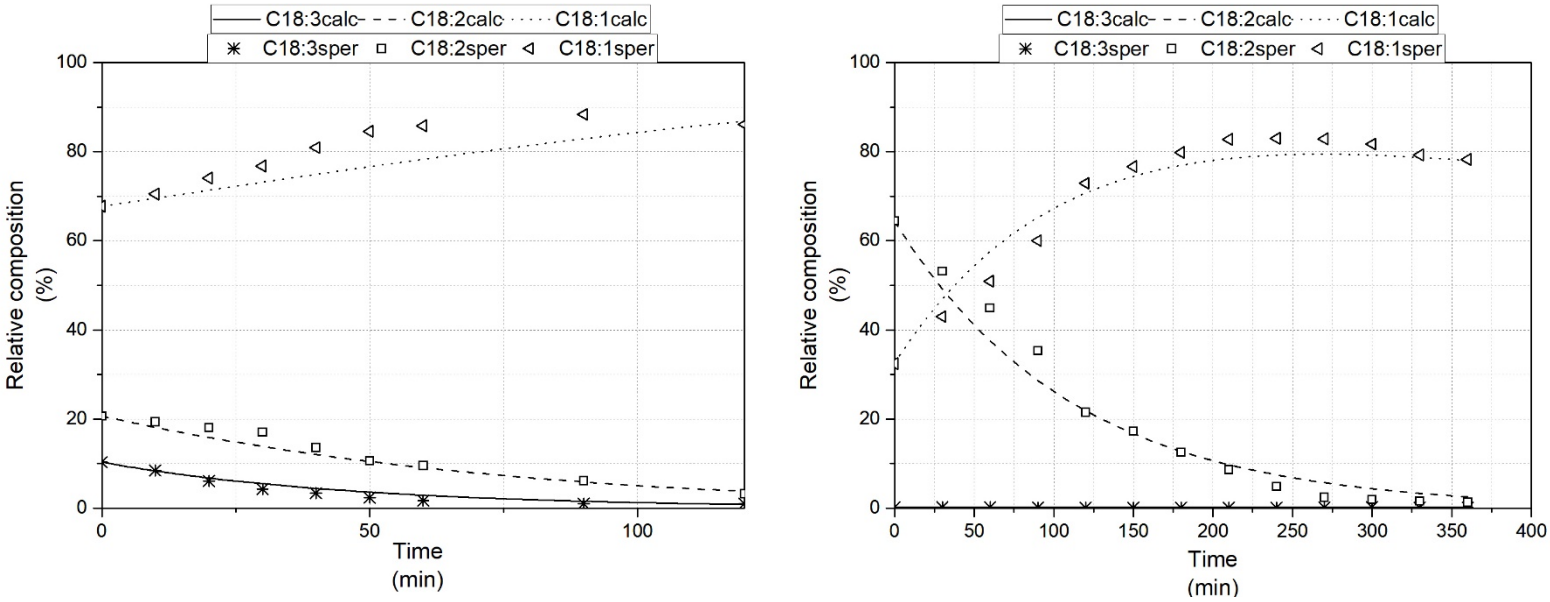

Figure 4-9 Experimental and calculated compositions for test 04-canola rapeseed oil (left) and test 08-sunflower oil (right).

4.2. Pd/HT catalyst reactivity tests

4.2.1. Pressure, temperature and concentration effect

Since few data were found in the literature describing the behavior of hydrotalcites-supported catalyst in the hydrogenation of vegetable oils, a preliminary test (Test 14) was performed for this catalyst at 90 °C under 4 bar of H_2 and with 0.5 $mg_{catalyst}/mL_{oil}$, operating conditions milder than for the Lindar catalyst. It is important to remember that Pd/HT is not doped with Pb as in the case of Lindlar.

The conditions of this preliminary test were chosen following the indications of Fernández et al. [146], who individuate low temperature and pressure to operate with Pd on γ-Al_2O_3 when using sunflower oil. In Figure 4-10 the results for Test 14 are reported; the test indicated that in these conditions the linoleic conversion reaches just 31%, an interesting result in the activity of the catalyst at low temperature. After that, it was decided to increase the temperature and catalysts concentration in order to compare different catalysts performance under the same operating conditions, to perform tests reaching higher conversion and to recovery and reuse the catalyst after test at the best operating conditions, as already done for Lindlar catalyst.

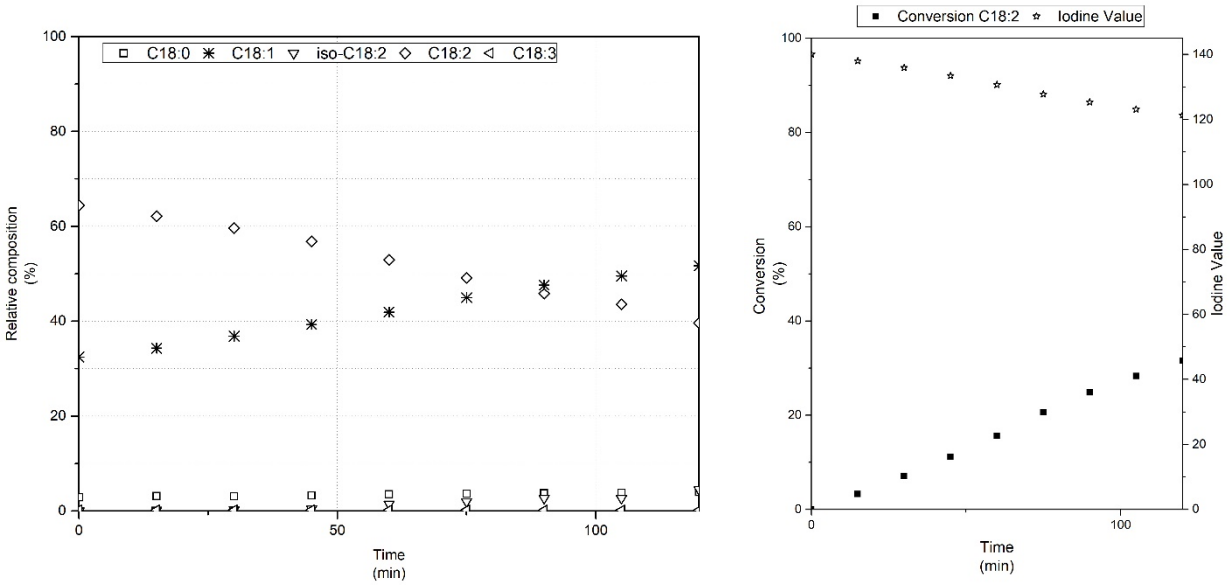

Figure 4-10 Test 14. Hydrogenation results at 90°C and 8 bar with 0.5 $mg_{catalyst}/mL_{oil}$ of Pd/HT

The results of the tests at different temperatures and pressures are summarized in Table 4-5:

Table 4-5 Test results, SII index and conversions calculated when the highest amount of oleic acid was observed

Entry	Cat.conc. (mg/ml)	T (°C)	P (bar)	T (min)	S_{Le}	SII	$\chi_{C18:2}$ (%)	(C18:1) (%)
Test 26	2	120	4	210	32.3	0.98	96.0	89.3
Test 15	1	180	4	270	31.2	0.44	89.1	85.8
Test 19	1	120	4	240	27.5	0.22	29.0	51.2
Test 22	0.5	120	4	240	36.75	0.23	13.6	40.9
Test 24	0.5	120	12	240	18.8	0.53	31.6	51.2

Only at the highest temperature (Test 15, see Table 2-2) and for high concentration at 120 °C (Test 26), the relative percentage of C18:1 reached a value higher than 85% and C18:2 conversions higher than 90%.

As it is expected, comparing Test 15 at 180 °C (Figure 4-11) and Test 19 at 120 °C (Figure 4-12), it is evident that increased activity and higher conversion of linoleic acid are reached, as it also happened for Lindlar catalyst. From the selectivity point of view, the $S_{Le,}$ and so the SII, increased with temperature, showing a decreased selectivity towards trans isomers when the catalyst was more active. The values of S_{Le} are higher than the data found in the literature at 160 °C for alumina supported catalysts and ZSM-5 catalysts [146], evaluated between 7 and 15 depending on the catalyst support, and palladium supported on diatomite [264], where the calculated S_{Le} is at around 17 (the comparison was made at the same conversion level. However, it is worth noting that these catalysts work better than the Pd/HT at lower temperature (below 120°), reaching high linoleic conversion after 3 h reaction with reasonable values of linoleic selectivity S_{Le}, between 30 and 35 (comparable with Pd/HT values), but the SII selectivity is above 0.6-0.8. In the end, the Pd/HT shown better performance than the Lindlar, since comparable results are obtained with less amount of catalyst.

Similar results are obtained with the data in the conditions carried out by McArdle et al. [265] at 100 °C and 170 °C under 3 bar of pure H_2 maintained continuously during the reaction, with catalyst concentration of 1.5 $mg_{catalyst}/mL_{oil}$. In the work of McArdle, a Pd (1%$_{w/w}$) supported on Al_2O_3 reaches high conversion (>85%), with calculated S_{Le} of 25 and a value of SII equal to 0.65 [265], higher than Pd/HT, (SII= 0.44 in Test 15), showing lower selectivity than Pd/HT synthetized in our laboratories.

The reaction time at the same conversion of 25% of C18:2 is reported in Table 4-6: as already observed, the slowest reaction is also the most selective one. Almost the same relative percentage of C18:1 is obtained, but with lower content of elaidic acid (2% vs 4%) and, regarding trans isomers in general, 7.6% vs 23% (combined elaidic and trans isomers of linoleic acid) are detected value. This fact suggests that at higher temperature also the reaction isomerization of linoleic acid happens more frequently.

Table 4-6 Test results, SII and IV at 25% conversion of linoleic at different temperature 180 °C test 15 and 120 °C test 19

	Linoleic $\chi_{C18:2}$ 25%			
Entry	**t (min)**	**IV**	**SII**	**(C18:1) (%)**
Test 15	110	123.4	0.25	50.2
Test 19	325	124.7	0.22	49.3

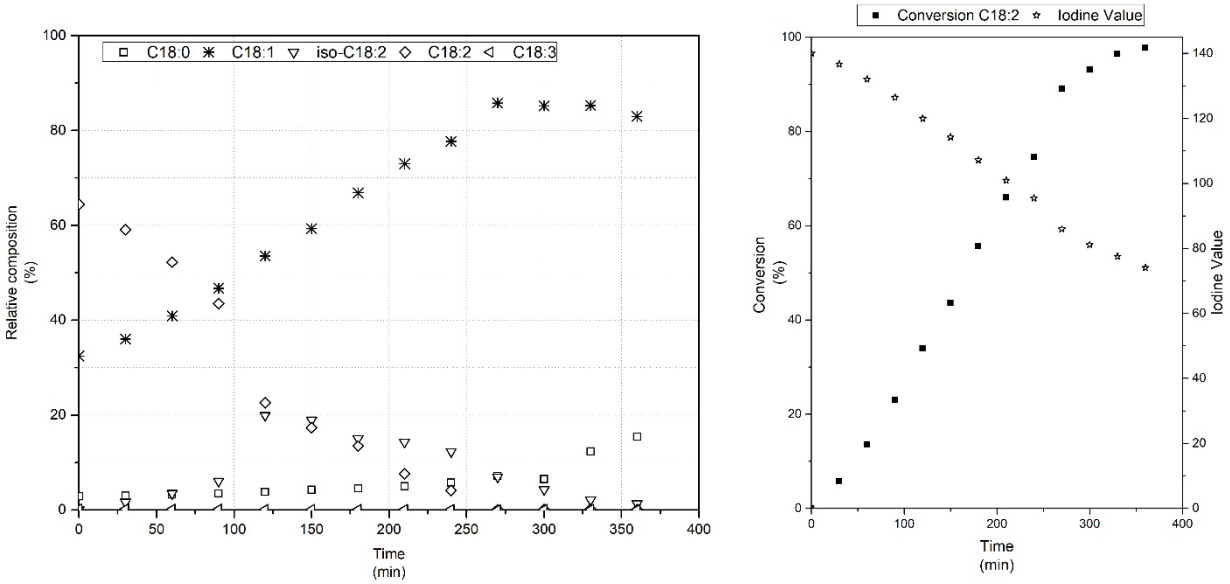

Figure 4-11 Test 15. Hydrogenation results at 180 °C and 4 bar with 1 $mg_{catalyst}/mL_{oil}$ of Pd/HT bar: on the right-hand side relative percentage of C18 compounds vs time, on the left-hand side the conversions of linolenic and linoleic acid and iodine value vs time

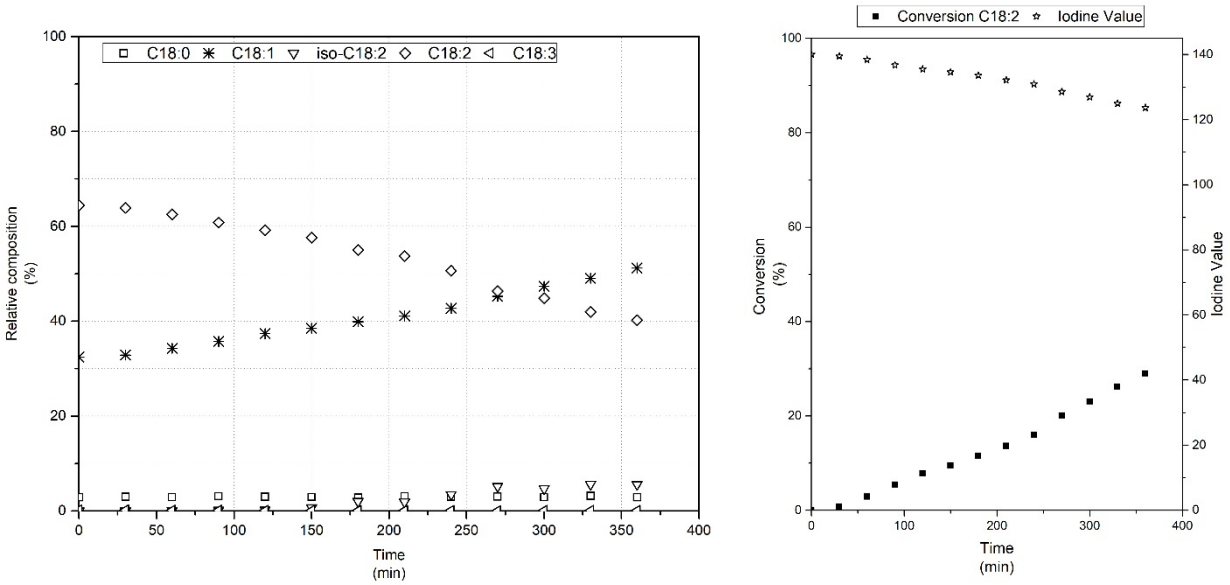

Figure 4-12 Test 19. Hydrogenation results at 120 °C and 4 bar with 1 $mg_{catalyst}/mL_{oil}$ of Pd/HT bar: on the right-hand side relative percentage of C18 compounds vs time, on the left-hand side the conversions of linolenic and linoleic acid and iodine value vs time

Pressure effect was studied at 120 °C. Changing the pressure from 4 bar to 12 bar, the conversion of linoleic acid significantly increased, although the formation of trans isomers is affected: after 4 hours of reaction, relative percentage of elaidic acid was about 2% at 4 bars and 10% at 12 bars, respectively.

The results at 25% of linoleic acid conversion and at different pressures are reported in Table 4-7. These comparison gives an important overview on the selectivity of the catalysts; at 25% of conversion, it is possible to say that the increase of pressure has a positive effect on the global trans isomers, lowering their content, although this comports the formation of a higher content of stearic acid. It is worth noting that the relative percentage of elaidic acid is practically unaffected by the change of pressure, the higher amount of trans isomers it is related to the isomers of linoleic acid (12.7% at 12 bar *vs* 2.4% at 4 bar), as shown in Figure 4-13.

Table 4-7 Test results, SII and IV at 25% conversion of linoleic at different pressures

	Linoleic $\chi_{C18:2}$ 25%			
Entry	**t (min)**	**IV**	**SII**	**(C18:1) (%)**
Test 22	345	132.08	0.37	47.3
Test 24	325	122.7	0.25	48.5

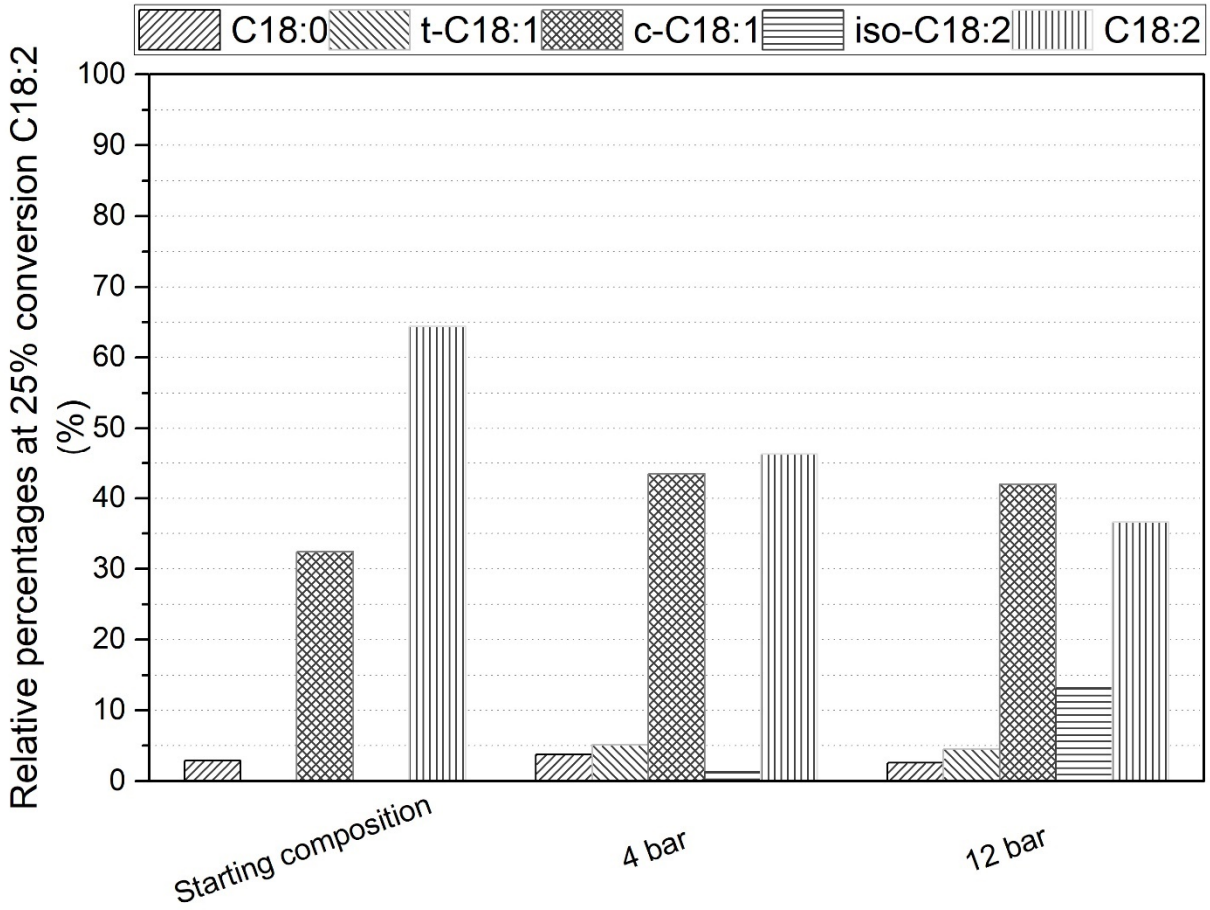

Figure 4-13 Hydrogenation results at 120 °C and 0.5 $mg_{catalyst}/mL_{oil}$ and different pressures (4 and 12 bar) linolenic percentage is omitted since lower than 0.5% (Test 22 and Test 24 respectively)

The effect of pressure on the trans isomers selectivity (SII) is in line with the results described by Veldinsk et al. [94] for different Pd catalysts. Veldinsk et al. correlated the effect of pressure on trans selectivity to how strongly the polyunsaturated semihydrogenated intermediates formed during the reaction are attached to the active phase. In particular at lower pressure, since the H_2 coverage on Pd is also lower, the effect is that the C18:2 interact more with Pd and monopolize the surface of the catalyst, substantially decreasing the monoene on the catalyst. This is reflected by the higher S_{Le}, as shown in Table 4-5, but it also involves longer time in which the C18:2 is attached on the catalytic surface and so possible secondary reactions.

In the end, the effect of catalysts concentration was studied. The decrease in the catalyst's concentration has a drastic effect on both activity and selectivity. Tests 19, 23 and 25 are compared together in Figure 4-14 and Table 4-8, showing how a decrease of the quantity of catalyst changes the catalyst reactivity that converts a lower amount of linoleic acid; this happens with an improving of the selectivity.

At 25% conversion of linoleic acid, the results follow the same trend as reported in Table 4-8. The effect of concentration is of extreme importance for activity, probably it is also due to the mixing of the three phases during the hydrogenation, with higher dispersion of the catalyst when the concentration is higher.

In these conditions, it was obtained a slightly more significant amount of both elaidic and trans isomers of C18:2 as the results in Figure 4-14 indicate. At the same conversions the catalyst is still selective in all three tests, the differences of SII must be ascribed to the content of linolenic acid isomers (Figure 4-14) ranging from 2.5 (Test 22) to 5 % (Test 19), and the content of elaidic acid for Test 26 (46.8% vs 44%). Obviously, as the linoleic conversion increases and the reaction proceeds, also the formation of trans isomers increase and the trans isomers selectivity decrease considerably (increase in SII in Table 4-5 test 26). It seems that any appreciable differences were found when different concentrations of catalyst are tested, but as Table 4-8 highlights the results are obtained at different times.

Table 4-8 Test results, SII and IV at 25% conversion of linoleic at a different catalyst concentrations

	Linoleic $\chi_{C18:2}$ 25%			
Entry	**t (min)**	**IV**	**SII**	**(C18:1) (%)**
Test 19	325	124.7	0.32	49.3
Test 22	345	132.08	0.37	47.3
Test 26	50	108.2	0.46	52.7

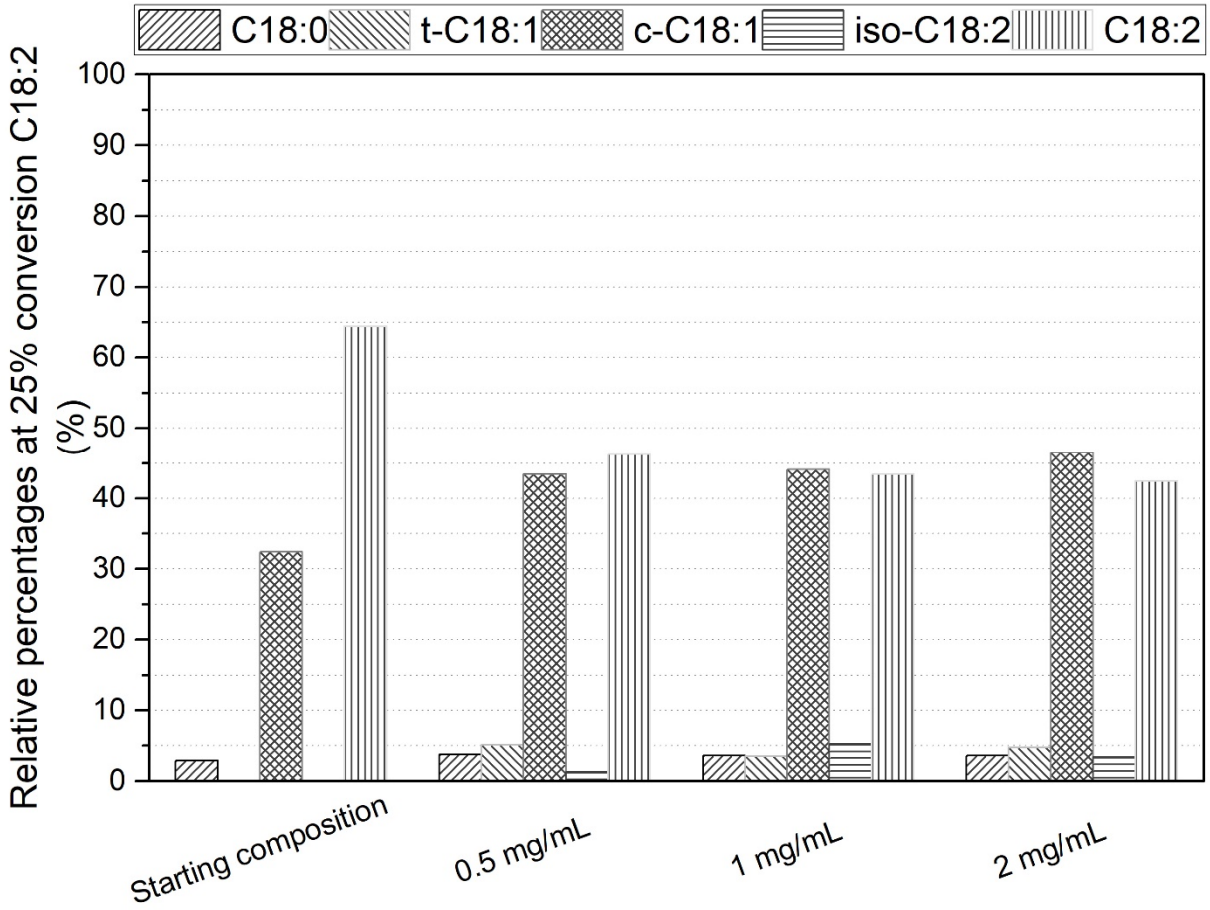

Figure 4-14 Hydrogenation results at 120 °C and 4 bar with different catalyst concentrations(0.5, 1 and 2 $mg_{catalyst}/mL_{oil}$); linolenic percentage is omitted since lower than 0.5% (test 22, test 19 and test 26 respectively)

4.2.2. Cyclic tests

As reported in Table 2-2, the catalyst was recovered from the reaction medium and reutilized in consecutive runs. Relating to the quantity of the catalyst and the amount recovered, one or more tests were carried out at the same conditions: the repeated tests are: test 15 (4 cycles), test 19 (3 cycles), test 22 (2 cycles), test 24 (2 cycles) and test 26 (2 cycles).

In consecutive cycles after the second one, the activity of the catalyst first increases in the second cycle and then start to decrease from the third cycle onward, probably for some activation mechanism already discussed in the case of Lindlar catalyst in §4.1: poisoning with components of the oil, formation of coke on the palladium catalyst, recovery not complete and loss in catalyst mass. The post characterization of the samples was not possible since the reacted hydrogenated oil remains inside the catalyst also after a washing protocol with different solvents (toluene, exane, acetone, and chloroform) for three times.

Table 4-9 Test results for the cyclic test at 180 °C. SII, conversions and selectivities calculated at 2 h.

Entry	S_{Le}	SII	$\chi_{C18:2}$ (%)	(C18:1) (%)
Test 15	31.2	0.44	34.02	53.5
Test 16	35.3	0.41	82.8	82.8
Test 17	39.5	0.32	68.5	74.1
Test 18	20.7	0.2	56.8	67.1

Table 4-10 Test results for the cyclic test at 180 °C, SII and IV at 50% conversion of linoleic

	Linolenic $\chi_{C18:2}$ 50% *			
Entry	t (min)	IV	SII	(C18:1) (%)
Test 15	160	110.3	0.33	63.4
Test 16	70	109.1	0.28	62.9
Test 17	85	110.5	0.31	63.5
Test 18	110	110.8	0.32	63.2

*Data obtained from the fitting model §2.3.5

Results in Table 4-10Figure 4-14 suggests that the selectivity to cis/trans isomers of the Pd/HT remains more or less the same at 50% conversion of linoleic acid. On the contrary, the activation after the first cycle is evident; the catalyst converts the 50% of linoleic acid after only 70 minutes in the second cycle compared to the 160 minutes required to reach the same values in the first one.

In comparison to this test with catalyst recovery, the results for the repeated test at 120 °C, 4 bar and 1 $mg_{catalyst}/mL_{oil}$ are reported in Table 4-11 and Table 4-12.

The activation is observed also in this case after the first cycle, but the successive cycle the activity continues to increase slightly; it was hypothesized that at 120 °C the phenomena, who contribute to the activation, have a less impact on the catalyst reactivity.

Table 4-11 Test results for the cyclic test at 120 °C. SII, conversions and selectivities calculated at 2 h.

Entry	S_{Le}	SII	$\chi_{C18:2}$ (%)	(C18:1) (%)
1st test	27.5	0.22	29.0	51.2
2nd test	29.6	0.37	33.2	52.8
3rd test	30.5	0.42	37.5	55.7

Table 4-12 Test results for the cyclic test at 120 °C, SII and IV at 50% conversion of linoleic

	Linolenic $\chi_{C18:2}$ 25%			
Entry	t (min)	IV	SII	(C18:1) (%)
1st test	325	125.1	0.13	49.7
2nd test	80	125.1	0.34	48.2
3rd test	65	123.4	0.37	49.0

All these tests share one characteristic, activation phenomena after the first reaction cycle. The most representative of this activation mechanism is test 15 at 180 °C.

It is possible to hypothesize two different mechanisms:

- The hydrogen present in the reaction medium alters the oxidation state of the superficial layer of Pd ;
- The combined effect of high temperature and pressure alters the hydrotalcites, also changing the characteristics of the catalyst, as XRD results highlight.

The two mechanisms can also work together to improve the activity of the Pd/HT catalyst. In both cases, it is difficult to remove the oil from the catalysts in order to characterize better the catalyst after the hydrogenation, for example, performing XPS. XRD spectrum and BET results of washed catalyst shown no apparent differences from the reduced material.

4.3. Silica-supported catalysts reactivity tests

4.3.1. Content of copper load

The first investigated parameter is the copper load on the silica-supported catalysts. Both AE and HP catalysts were tested at the same conditions in order to understand how the synthesis affects the activity and selectivity of the catalysts. In order to understand which catalysts convert more C18:2 and C18:3, the results at 3 hours reaction for the four copper catalysts are analyzed: $Cu5SiO_2AE$ (Figure 4-15) $Cu10SiO_2AE$ (Figure 4-16), $Cu5SiO_2HP$ (Figure 4-17), $Cu10SiO_2HP$ (Figure 4-18), tests studied were made with canola oil and 4 $mg_{catalyst}/mL_{oil}$. The relative percentages of C18 components, conversions of C18:2 and C18:3, Iodine Values trend, fitting model results and kinetic constants, and elaidic acid evaluation are presented in a more complete form in §Appendix A, all tests are reported by test name as in Table 2-2.

It is decided to shows the results at 3 hours because they are somehow representative of the behavior of the "catalyst" as a group. The results after 3 h of reaction give essential information: overall, for both synthesis methods, the increasing on copper load have a beneficial effect on the activity of the catalysts which results larger amounts of linoleic and linolenic acid converted, obviously at the expense of selectivities (see Table 4-13 and

Table 4-14).

As already highlighted for Lindlar and Pd/HT, also in this case, copper silica catalysts are more active at higher temperatures, the kinetic constant following an Arrhenius type law. The effect of temperature is already visible with a little increase in temperature from 180 °C to 200 °C. 200 °C is the maximum temperature carried out because of the decomposition temperature of Canola oil is around 210-220 °C [266].

The effect of the temperature is always relevant, for both syntheses at all pressures (all four catalysts share this trend). On the contrary, the pressure has only a stronger effect on conversions at 180 °C than at 200 °C, for $5\%_{w/w}$ copper load catalysts for AE. For $10\%_{w/w}$ HP, $Cu10SiO_2HP$, catalyst have a slightly worse activity than the corresponding $Cu10SiO_2AE$, but this last exhibits a better selectivity after 3 hours reaction. Furthermore, the pressure effect is more evident on the conversion of linoleic acid than linolenic acid; this happens because the linolenic acid is more reactive than the linoleic acid (see §1.4 about mechanism of reaction for Cu catalyst), since is more simple to form the conjugated diene as reaction intermediate.

Concerning the selectivity, it is more difficult to compare results, since fewer data are presented in the literature, mainly produced by Koritala et al. [113], Ravasio et al. [22] and Zaccheria et al. [23]. Although the catalyst Cu/SiO_2 produced by Ravasio et al. [22] shown almost complete conversion after 3 hours reaction

with similar conditions (Test 36 and Test 50 at 180 °C and 4 bar *vs* 180 °C and 6 bar of Ravasio et al. [22]) their catalyst concentration in the reaction medium is five times higher 20 $mg_{catalyst}/mL_{oil}$, high enough to be near mass transfer limited conditions, although the copper load is similar $8\%_{w/w}$ *vs* $10\%_{w/w}$.

The Cu/SiO_2 synthesized by Ravasio et al. has a drop of IV of 45 (ΔIV) and obtained almost 20% of trans isomers, by using rapeseed oil with a composition similar to the Canola used in this work; the calculated SII of 0.44 is compatible with the values obtained for both $Cu10SiO_2HP$ and $Cu10SiO_2AE$ (Table 4-13 and Table 4-14) catalysts.

By comparing the results obtained for Lindlar catalyst, it is possible to see how in this case the S_{Ln} is higher and this parameter can be correlated with the different mechanisms of the reaction as described by Dijkstra et al. [90,108], since the preliminary reaction could be the formation of conjugated diene inside the polyunsaturated acid chain, and so the faster reaction of linolenic acid. The selectivity S_{Ln} values are in line with the results found by Koritala et al. [109]. The synthetized copper catalysts are less active than the Lindlar catalyst, although, their linoleic selectivity is higher (see Table 4-13 and Table 4-14) and comparing it with the values presented in section §4.1 (Table 4-1 and Table 4-3).

When the HP catalysts are used (both 5% and 10% load see Figure 4-15 and Figure 4-16) under more severe reaction conditions of 12 bars and 200 °C, another significant result is the small amount of stearic acid formed during the reaction, up to a maximum 5% relative percentage; on the other hand, in the work of Ravasio et al. [22] a lower amount of stearic acid was formed or none at all as presented by Koritala [112,113].

The kinetic constant k_1 of Equation 2-12 of oleic acid found by Koritala et al. [113] was zero, giving very high S_{Le} and any increase in stearic acid, throughout the reaction, was reported by Koritala [113] and Ravasio found only small increase less than +0.7% (starting from 3.0 % up to 3.7 %) [22]. In the present work, the kinetic constant k_1 of oleic acid consumption is three order of magnitude higher than k_2 of Equation 2-12 , value not equals to zero but very near (comprises between 0.0000101-0.0000289 see Appendix A for all the constants values), furthermore there is a formation of stearic acid which reaches 7% for test 43 with $Cu10SiO_2AE$ at 200 °C and 12 bars which it is the highest increase observed, but in all other cases the increase of stearic acid raging from +62 % (from 1.28 % to 2.08 % at the end of the reaction) up to +421% (from 1.28 to 6.74%.

Table 4-13 Test results, SII index and conversions calculated after 3 h test for $Cu5SiO_2AE$ (tests from test 28 to test 31) and for $Cu10SiO_2AE$ (tests from test 36 to test 39), both catalysts at 4 $mg_{catalyst}/mL_{oil}$ concentration with Canola oil

Entry	S_{Ln}	S_{Le}	SII	$\chi_{C18:3}$ (%)	$\chi_{C18:2}$ (%)	(C18:1) (%)
Test 28	6.7	-	0.18	15.8	7.3	70.1
Test 29	6.1	-	0.13	30.8	15.5	71.4
Test 30	6.9	-	0.26	76.7	26.8	79.1
Test 31	6.8	-	0.17	78.5	30.4	78.5
Test 36	6.9	-	0.32	23.4	10.2	66.9
Test 37	6.0	-	0.39	52.7	12.7	68.2
Test 38	6.3	-	0.35	80.2	31.2	78.3
Test 39	6.7	-	0.42	81.3	40.7	78.6

Table 4-14 Test results, SII index and conversions calculated after 3 h test for $Cu5SiO_2HP$ (tests from test 32 to test 35) and for $Cu10SiO_2HP$ (tests from test 50 to test 53), both catalysts at 4 $mg_{catalyst}/mL_{oil}$ concentration with Canola oil

Entry	S_{Ln}	S_{Le}	SII	$\chi_{C18:3}$ (%)	$\chi_{C18:2}$ (%)	(C18:1) (%)
Test 32	6.1	-	0.32	65.3	20.5	68.3
Test 33	6.5	-	0.35	66.3	23.5	69.7
Test 34	6.1	-	0.31	82.3	36.7	79.1
Test 35	6.5	-	0.35	83.1	38.9	80.2
Test 50	6.3	-	0.41	69.0	22.0	74.5
Test 51	6.8	-	0.48	71.5	27.3	76.2
Test 52	6.6	-	0.5	86.1	42.5	81.5
Test 53	6.5	-	0.55	86.5	45.4	83.1

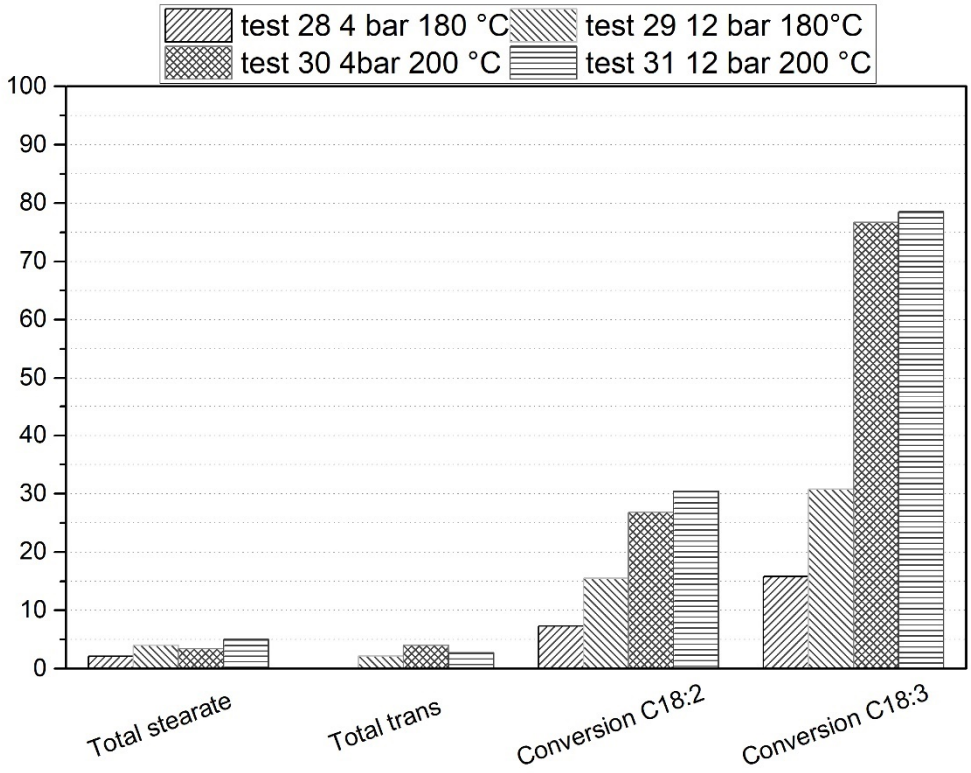

Figure 4-15 Tests from test 28 to test 31: total stearate, total trans, C18:2 and C18:3 conversion, after 3h with Cu5SiO$_2$AE, 4 mg$_{catalyst}$/mL$_{oil}$ using canola oil

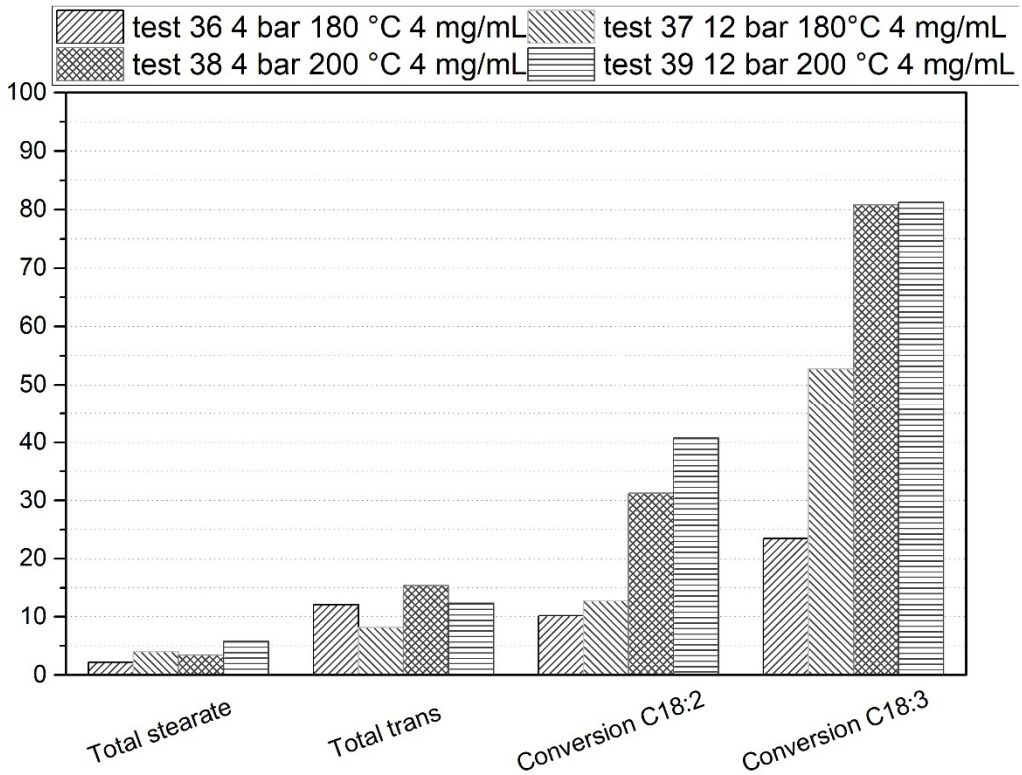

Figure 4-16 Tests from test 36to test 39: total stearate, total trans, C18:2 and C18:3 conversion, after 3h with Cu10SiO$_2$AE , 4 mg$_{catalyst}$/mL$_{oil}$ using canola oil

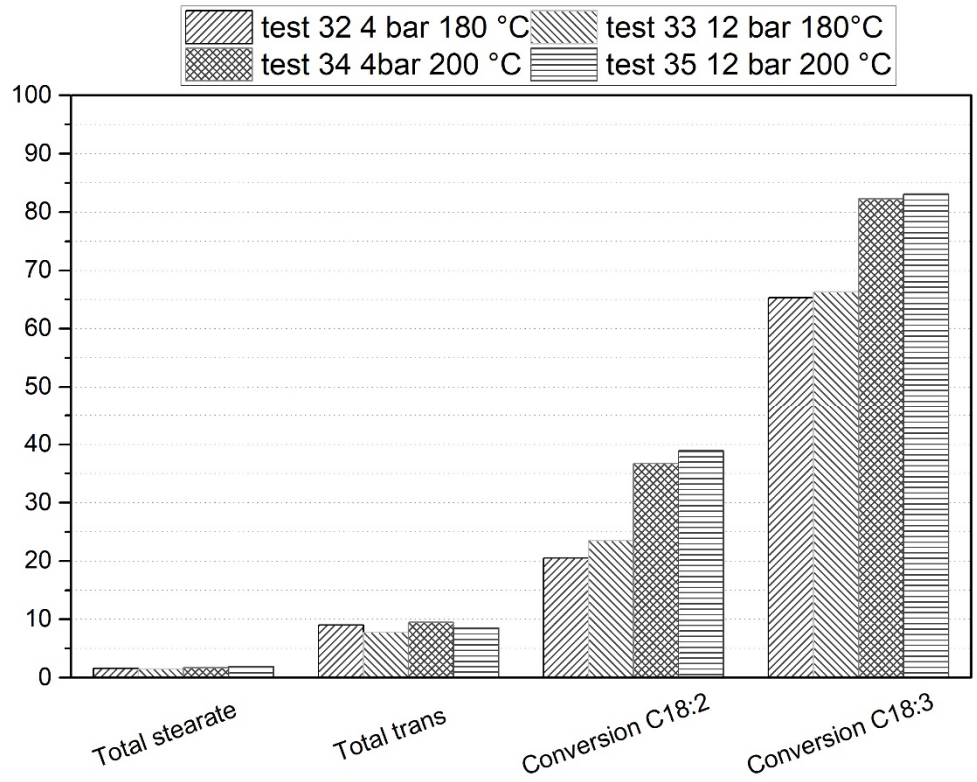

Figure 4-17 Tests from test 32 to test 35: total stearate, total trans, C18:2, and C18:3 conversion, after 3h with Cu5SiO$_2$HP, 4 mg$_{catalyst}$/mL$_{oil}$ using canola oil

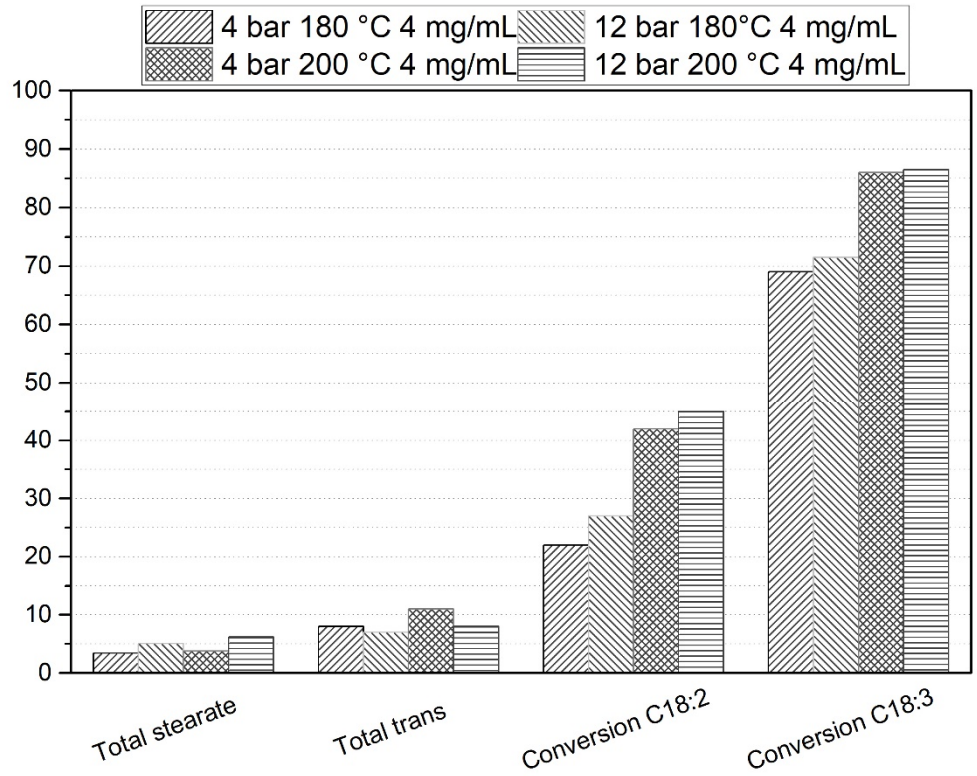

Figure 4-18 Tests from test 50 to test 53: total stearate, total trans, C18:2 and C18:3 conversion, after 3h with Cu10SiO$_2$HP, 4 mg$_{catalyst}$/mL$_{oil}$ using canola oil

On the basis of the data presented in Figure 4-15 (from test 28 to test 31), Figure 4-16 (from test 36 to test 39), Figure 4-17 (from test 32 to test 35), Figure 4-18 (from test 50 to 53), it was decided to stop the tests on catalysts with 5 $\%_{w/w}$ of copper and concentrate the work on $Cu10SiO_2AE$ and $Cu10SiO_2HP$. With these two catalysts it is possible to achieve the reduction of C18:2 and C18:3 fatty acids in the oil produced after hydrogenation, with high conversion of both dienes and trienes.

4.3.2. Effect of catalyst concentration parameter

Tests with higher concentration were only carried out with 10%w/w catalysts; to complete the information acquired also tests with a lower concentration of catalysts were carried out.

Starting from the tests at lower concentration, at 180 °C practically any evident activity is found for both $Cu10SiO_2AE$ (test 44 at 4 bar and test 45 at 12 bar) and $Cu10SiO_2HP$ (test 58 at 4 bar and test 59 at 12 bar), the C18 components graph are presented in Appendix A.

At higher temperature of 200 °C the conversion of C18:3 start to rise, after 4 h it reaches 53.20 % for $Cu10SiO_2AE$ (test 46) and 37.48 % for $Cu10SiO_2HP$ (test 59), in test 59 also the conversion of C18:3 is more significative and 26.24 % of linolenic acid is converted. In these conditions, small amount of trans isomers are formed hence the small SII calculated (Table 4-15 and Table 4-16).

As expected, the increase in catalyst concentration has an essential role in the conversion of more linoleic acid and almost complete conversion of C18:3 for tests with 8 $mg_{catalyst}/mL_{oil}$ with $Cu10SiO_2AE$ reaching 1.22 % of linolenic acid (test 42 and test 43) and with $Cu10SiO_2HP$ 0.75 %, at 200 °C (test 56 and test 57). Although this second catalyst converted more C18:2 in every test carried out (see Table 4-15 and Table 4-16, and Figure 4-19 and Figure 4-20).

As an example, in the Table 4-15 and Table 4-16, the results of selectivity and activity at 180 °C and 200 °C at the same pressure 4 bar (for $Cu10SiO_2AE$: test 36, test 38, test 40, test 42 and test 46, and for $Cu10SiO_2HP$ test 50, test 52, test 54, test 56, test 60 at the three different levels of concentration) are summarized, for $Cu10SiO_2AE$ ***Table 4-15****, and $Cu10SiO_2HP$ catalyst respectively.*

Table 4-16

Table 4-15 Test results, SII index and conversions calculated after 3 h test for AE catalysts at 2 $mg_{catalyst}/mL_{oil}$ (Test 44 and 46) 4 $mg_{catalyst}/mL_{oil}$ concentration (Test 36 and 38) and at 8 $mg_{catalyst}/mL_{oil}$ (Test 40 and 42).

Entry	S_{Ln}	S_{Le}	SII	$\chi_{C18:3}$ (%)	$\chi_{C18:2}$ (%)	$(C18:1)_{max}$(%)
Test 36	6.9	-	0.32	23.4	10.2	66.9
Test 38	6.3	-	0.35	80.2	31.2	78.3
Test 40	7.0	-	0.56	66.2	40.7	76.3
Test 42	6.8	-	0.58	65.4	51.6	77.4
Test 46	7.5	-	0.15	52.3	12.1	68.2

Table 4-16 Test results, SII index and conversions calculated after 3 h test for AE catalysts at 2 $mg_{catalyst}/mL_{oil}$ (Test 44 and 46) 4 $mg_{catalyst}/mL_{oil}$ concentration (Test 36 and 38) and at 8 $mg_{catalyst}/mL_{oil}$ (Test 40 and 42).

Entry	S_{Ln}	S_{Le}	SII	$\chi_{C18:3}$ (%)	$\chi_{C18:2}$ (%)	$(C18:1)_{max}$(%)
Test 50	5.3	-	0.41	69.0	22.0	74.5
Test 52	5.6	-	0.50	86.1	42.5	81.5
Test 54	5.8	-	0.75	89.1	73.6	88.5
Test 56	5.5	-	0.82	91.6	76	89.7
Test 60	6.0	-	0.20	37.2	26.2	72.3

The increase of the temperature has a positive effect on the conversions of polyunsaturated compounds (see also §4.3.1), at 8 $mg_{catalyst}/mL_{oil}$ and 200 °C for $Cu10SiO_2HP$ it was reached the highest conversions of C18:3 and C18:2 (see Table 4-16 and Figure 4-20). However, for $Cu10SiO_2AE$ one test is in contrast with this observation (Figure 4-19): test 38 at 180 °C and 4 bar, at 4 $mg_{catalyst}/mL_{oil}$ shows the best performances for conversion of linolenic acid, 81.26 % conversion of C18:3, higher than the values obtained at higher concentration (8 $mg_{catalyst}/mL_{oil}$).

At higher concentration of both catalysts, the operative parameters less affect the results. The increase in C18:2 conversion was by far more evident at lower concentration than at higher ones and at 8 $mg_{catalyst}/mL_{oil,}$ linolenic acid conversion has almost the same values for all the operative conditions for $Cu10SiO_2HP$ (Figure 4-20); although for $Cu10SiO_2AE$, the pressure has an essential impact on the conversions also at higher concentrations (Figure 4-19), at 8 $mg_{catalyst}/mL_{oil}$ C18:3 conversions changes from 66.2 % up to 80.2 and C18:2 40.7 to 51.6 at 200 °C.

On the other hand, selectivities after 3 hours for 8 $mg_{catalyst}/m$ follow the trend already observed at 4 $mg_{catalyst}/mL_{oil}$, and only linolenic selectivity S_{Ln} changes when the catalyst concentration is lowered, since the final concentration of stearic acid is always lower than 3% in the three conditions tested (tests 38, test 42 and test 46 of Table 4-15 And test 52, test 56 and test 60Table 4-16).

At the highest temperature 200 °C and pressure 12 bar, the total trans content reaches 23% of relative percentage: this represents the worst case, where near 15% of product is elaidic acid, and the remaining fraction percentage consists of isomers of linoleic acid with $Cu10SiO_2HP$.

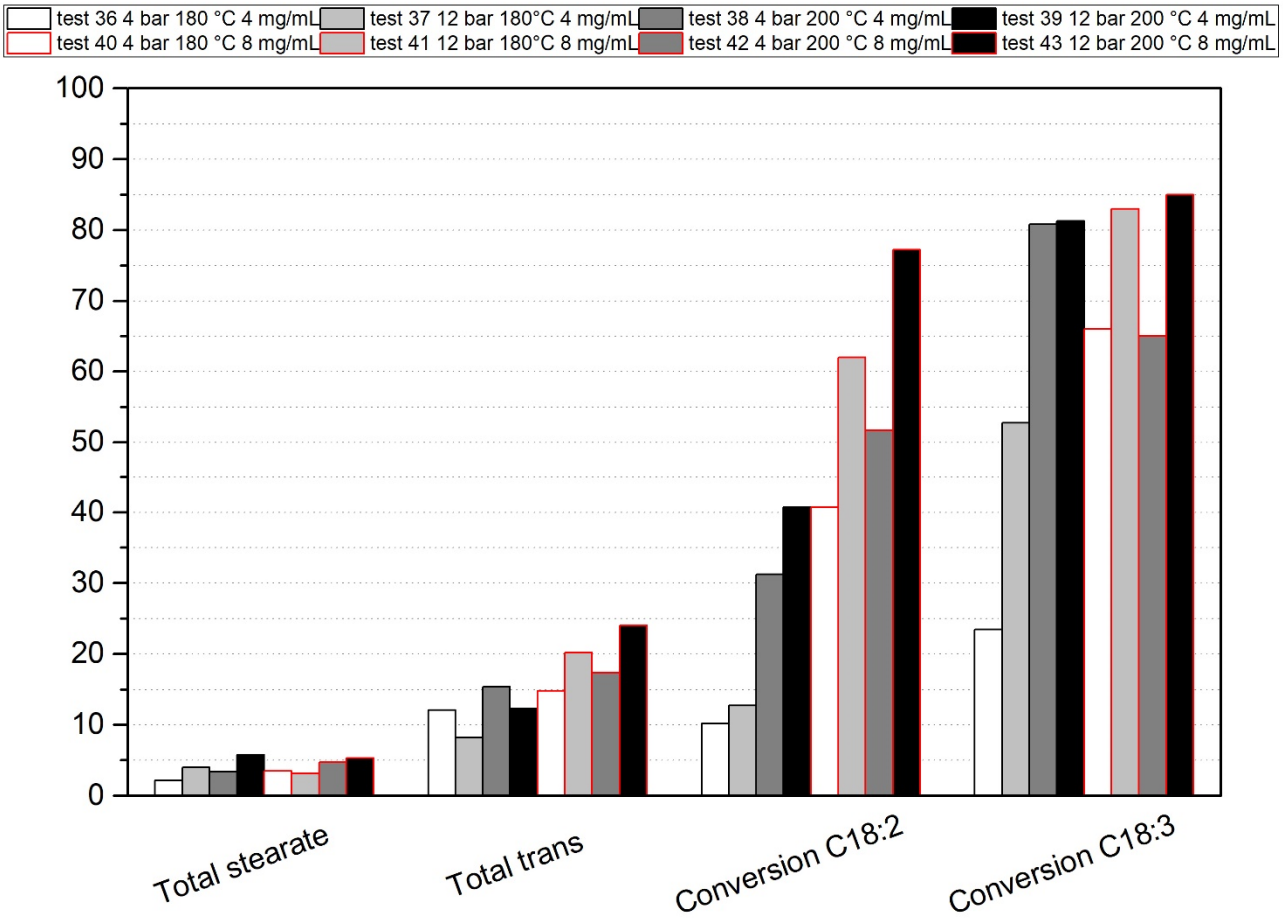

Figure 4-19 Tests result for $Cu10SiO_2AE$ catalyst at two different catalyst concentrations 4 mgcatalyst/mLoil (test 36, test 37, test 38, test 39 with black border), and 8 $mg_{catalyst}/mL_{oil}$ (test 40, test 41, test 42, test 43 with red border), two levels of temperature 180 °C (test 36, test 37, test 40, test 41) and 200 °C (test 38, test 39, test 42 and test 43) and two different levels of pressure 4 bar and 12 bar, test results presented after 3 h of reaction

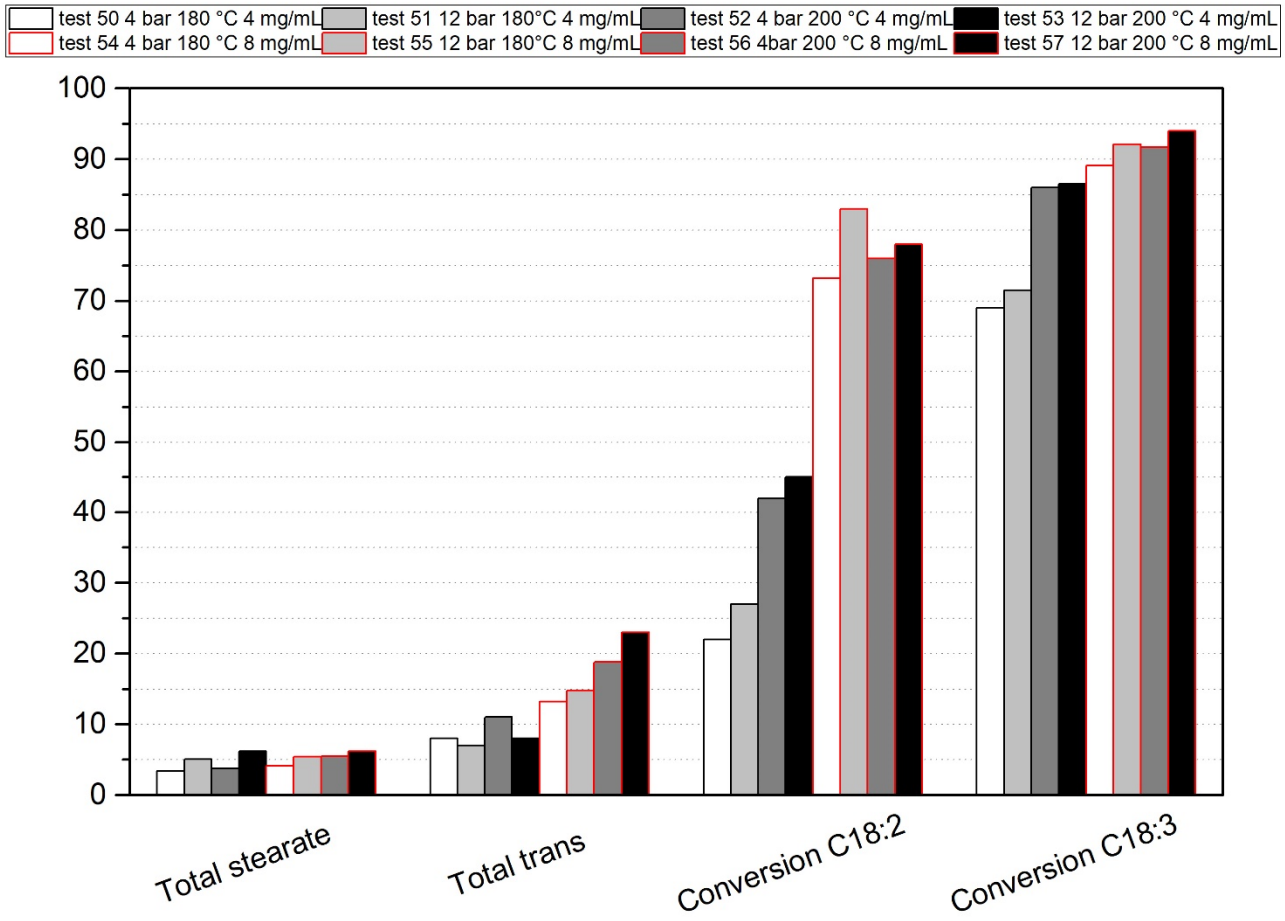

Figure 4-20 Tests result for Cu10SiO₂HP catalyst at two different catalyst concentrations 4 $mg_{catalyst}/mL_{oil}$ (test 50, test 51, test 52, test 53 with black border), and 8 $mg_{catalyst}/mL_{oil}$ (test 54, test 55, test 56, test 57 with red border), two levels of temperature 180 °C (test 50, test 51, test 54, test 55) and 200 °C (test 52, test 53, test 56 and test 57) and two different levels of pressure 4 bar and 12 ba, test results presented after 3h of reaction

The changes in the catalyst's concentration made possible to achieve a linolenic acid conversion higher than 50%. In Table 4-17 and Table 4-18 the results for AE and HP catalysts at 4 $mg_{catalyst}/mL_{oil}$ and 8 $mg_{catalyst}/mL_{oil}$ are summarized and their comparison gave an overview of how the selectivity is affected by the catalyst concentration change during the reaction. Also if the amount of catalyst is doubled, it is not necessary to increase too much the amount of catalyst, in comparison with the amount described by Ravasio et al. [22] 20 $mg_{catalyst}/mL_{oil}$.

Table 4-17 Test results, SII and IV at 50% conversion of linolenic for Cu10SiO2AE at 4 $mg_{catalyst}/mL_{oil}$ and 8 $mg_{catalyst}/mL_{oil}$

	Linolenic $\chi_{C18:3}$ 50%				
Entry	**t (min)**	**IV**	**SII**	**(C18:0) (%)**	**(C18:1) (%)**
Test 36	-	-	-	-	-

Test 37	237	110.2	0.25	1.8	67.5
Test 38	223	109.4	0.26	2.0	68.3
Test 39	175	111.3	0.17	1.8	66.0
Test 40	155	110.5	0.35	2.5	67.4
Test 41	134	110.0	0.27	3.1	67.8
Test 42	122	109.7	0.40	4.3	68.9
Test 43	105	109.4	0.36	3.7	69.1

Table 4-18 Test results, SII and IV at 50% conversion of linolenic and at 50% conversion of linoleic for Cu10SiO$_2$HP at 4 mg$_{catalyst}$/mL$_{oil}$ and 8 mg$_{catalyst}$/mL$_{oil}$

	Linolenic $\chi_{C18:3}$ 50%					**Linoleic $\chi_{C18:2}$ 50%**				
Entry	**t (min)**	**IV**	**SII**	**(C18:0) (%)**	**(C18:1) (%)**	**t (min)**	**IV**	**SII**	**C18:0) (%)**	**(C18:1) (%)**
Test 52	165	109.2	0.26	1.5	69.0	-	-	-	-	-
Test 53	152	108.9	0.17	1.8	69.3	-	-	-	-	-
Test 54	132	109.6	0.31	1.6	68.1	-	-	-	-	-
Test 55	124	108.6	0.24	2.0	67.9	-	-	-	-	-
Test 56	95	109.2	0.45	3.0	69.7	122	87.91	0.50	5.1	77.8
Test 57	96	110.3	0.41	2.8	69.9	114	85.46	0.58	4.7	77.2

For Cu10SiO$_2$AE and Cu10SiO$_2$HP catalysts, the isomerization selectivity during the hydrogenation run increases with temperature (test 37 *vs* test 39, test 38 *vs* test 40 Table 4.17 and test 52 *vs* test 54, test 53 *vs* test 55 Table 4-18) and decreases with pressure (test 37 *vs* test 38, test 39 *vs* test 40, test 41 *vs* test 42 Table 4-17 and test 52 *vs* test 53, test 54 *vs* test 55, test 56 *vs* test 57 Table 4-18), but at the cost of a higher amount of stearic acid produced. It is also highlighted that the reactivity of the catalysts increases changing the operative parameters since the reaction time needed to reach 50 % of conversion of C18:3 (and 50 % C18:2 for Cu10SiO$_2$HP at 8 mg$_{catalyst}$/mL$_{oil}$) augments accordingly to the parameters' decrease for both temperature and pressure.

The SII calculated values at the same conversion of linolenic acid show clearly that the HP synthesis produced a more active catalyst with similar selectivity. However, since the HP catalyst is more active, it produce for the same reaction time higher amount of trans isomers and stearic acid due to conversions of C18:2 and C18:3 bringing to lower final selectivity.

4.3.3. Sunflower oil tests

In addition, $Cu10SiO_2AE$ (see Table 2-2 test 47-49) and $Cu10SiO_2HP$ (see Table 2-2 test 61-63) are tested with sunflower oil.

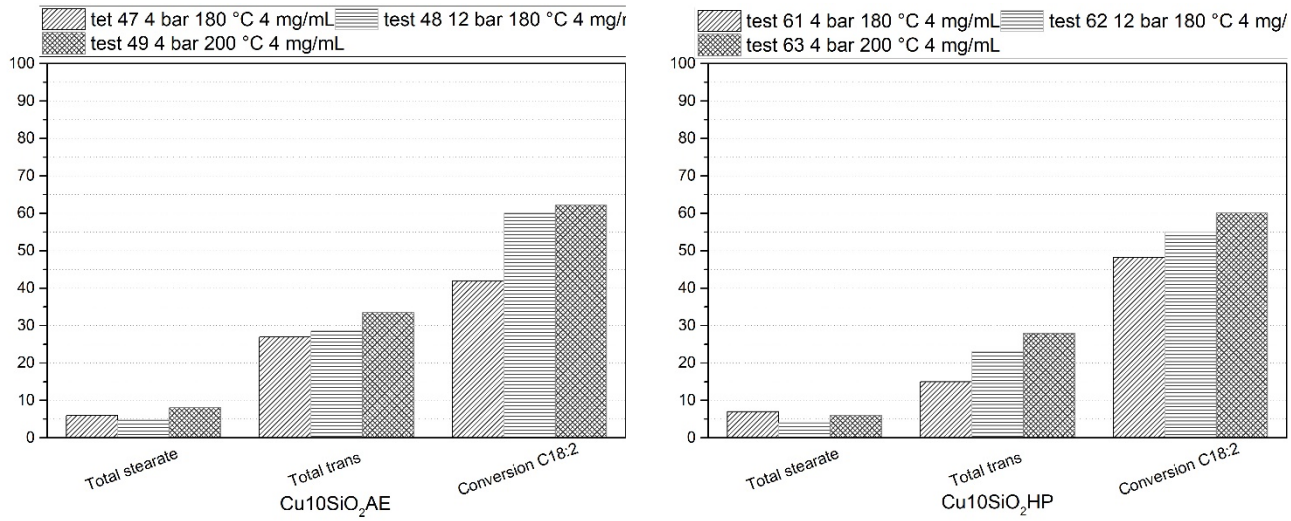

Figure 4-21 Total stearate, total trans, C18:2 and C18:3 conversion, after 6h with Cu10SiO2AE (left) and Cu10SiO2AE (right) at 4 $mg_{catalyst}/mL_{oil}$: in order test on the right-hand side test 47, test 48, and test 49, and on the left-hand side test 61, test 62 and test 63 respectively

In Figure 4-21, the attained results are in line with sunflower data obtained with the Lindlar catalyst (§4.1) and with the results obtained with copper catalysts when the amount of linolenic acid reaches 0 % (in reality the behaviour of the catalyst when only linoleic acid is present is already visible when C18:3 is below 1%) in section §4.3.2. In details:

- The $Cu10SiO_2HP$ HP exhibits a slightly higher linoleic conversion than the $Cu10SiO_2AE$ at a comparable degree of hydrogenation (i.e. 43.3% of linoleic conversion on $Cu10SiO_2AE$ versus 50.2% on $Cu10SiO_2HP$ at 6 h of reaction time, 180 °C and 4 bar), the selectivity towards the trans isomers is higher for $Cu10SiO_2HP$.
- The SII selectivity is higher for $Cu10SiO_2HP$, the elaidic acid content is not so different, as reported in Figure 4-21 for 180 °C and 4 bar, but higher content of C18:2 isomers are produced for $Cu10SiO_2AE$ catalyst. This could be related to the formation of conjugated diene as reported for the mechanism of

reaction [108], on reduced copper catalysts where the hydrogenation of polyunsaturated oils proceeds through conjugation of the methylene interrupted double bonds, in turn caused by hydrogen abstraction and sequent hydrogen addiction (Horiuti Polanij mechanism [108]). Therefore, the hydrogenation observed for oils with high linolenic content like sunflower oil is much faster [111]. Furthermore, Dijkstra [96] suggested that the higher content of trans isomers observed are linked not to the isomerization of cis-monoenes but to the conjugation reaction. Taking into account the literature interpretation of hydrogenation data, Cu10SiO_2HP catalyst is more active towards the reduction of conjugated double bonds, at least when a low amount of linolenic acid is present. The higher activity could be related to the different oxidation on the catalyst surface, but in the literature there are not further data which support this hypothesis and evaluating the post reaction oxidation surface status is almost impossible since the solvent used during washing steps of the catalyst (in order to remove oil before characterization) becomes trapped inside the catalyst and the application of vacuum (BET, XPS or TEM-SEM low or high vacuum) release the solvent risking to ruin the apparatus.

- S_{Le} results for all sunflowers tests are higher than the rapeseed case, reaching S_{Le} values higher than 1000, closer to the hypothetical infinite selectivity found by Koritala [155,157] than the selectivities values of the two catalysts when the reaction medium was rapeseed oil.

4.3.4. Bimetallic catalysts

The bimetallic catalysts were tested at 180 °C under 4 bar and 4 $mg_{catalyst}/mL_{oil}$ with sunflower oil and the duration of each test was set at 6 hours.

In Figure 4-22 the conversion of linoleic acid and the maximum concentration of C18:1 are presented and in Figure 4-23 total stearic acid and trans isomers formed during the reaction are provided. The results are provided for bimetallic catalysts and monometallic ones.

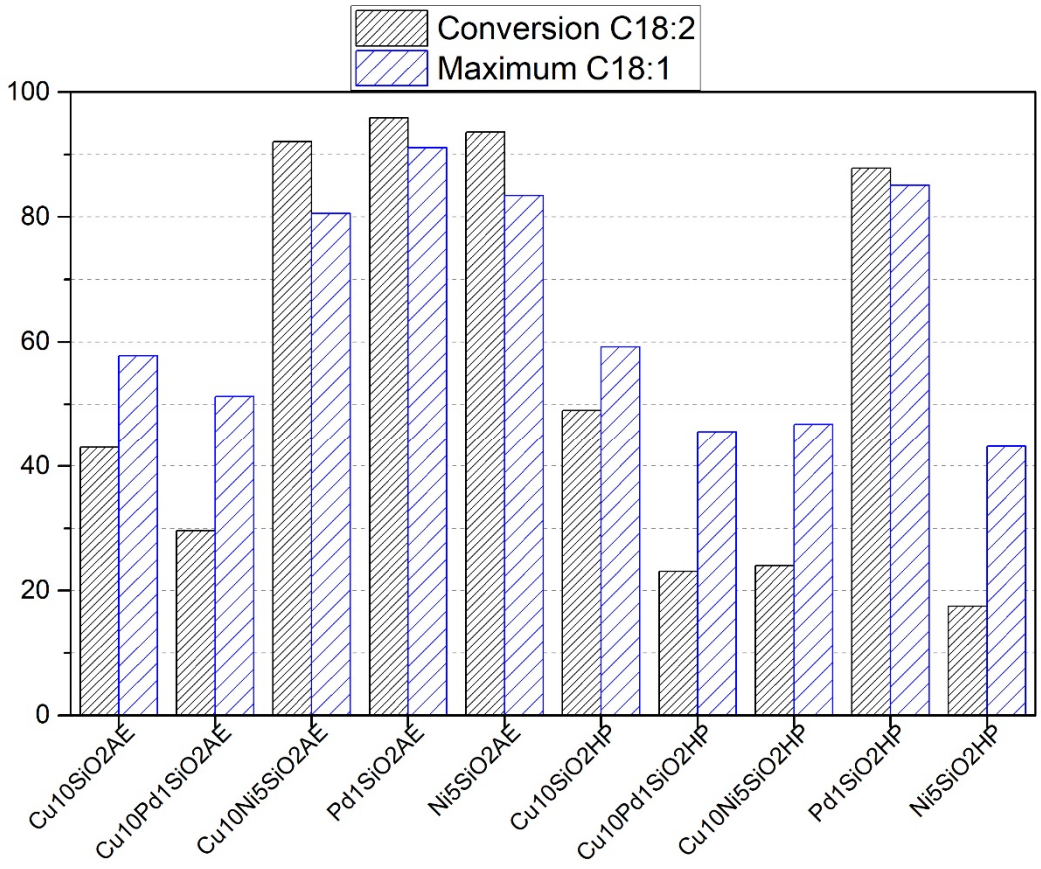

Figure 4-22 C18:2 conversion and maximum C18:1 relative percentage achieved during hydrogenations runs at 180 °C and 4 bar pressure with sunflower oil and 4 $mg_{catalyst}/mL_{oil}$ catalyst concentration, data are reported at when the maximum C18:1 is reached for mono- and bimetallic catalysts (see Table2-2)

The conversion data give an overview of the activity of the catalysts. Figure 4-22 indicates that:

- Catalysts containing 1% Pd, $Pd1SiO_2AE$ and $Pd1SiO_2HP$, are largely more active than the other catalysts;
- Copper-palladium catalysts show an interesting activity, although lower to both monometallic copper and palladium catalysts; probably this worst behaviour is related to to the CuPd phases formed during the synthesis in the reduction step;
- $Cu10Ni5SiO_2AE$ reaches C18:2 conversions of 92.5%. The activity of this catalyst is practically comparable (see Figure 4-22), to the results obtained with $Ni5SiO_2AE$, 93.4% conversion of C18:2 , and it is superior to that achieved with $Cu10SiO_2AE$ of 42.7%, therefore the improving on the activity should be ascribed to Ni active phase (see Figure 4-22). It is interesting to noticed that the selectivity of $Cu10Ni5SiO_2AE$, represented in Figure 4-23, are better than the monometallic $Ni5SiO_2AE$ since lower relative percentages of trans isomers and stearate are produced;

- As far as it is concerned bimetallic Cu10Ni5SiO_2HP catalyst (test 64), the result underlines lower conversion and this also happens for the corresponding Ni monometallic catalyst, Ni5SiO_2HP (test 68). As already shown in §3.3.5.1, the Ni catalysts prepared with the HP methods present the reduction temperature at 450 °C, so probably the Ni HP catalyst is not completely reduced because the reduction is carried out in a fixed bed in which the temperature is controlled externally by the furnace thermocouple. In this case possibly the temperature reached by the furnace (485 °C on the furnace wall, checked with external thermocouple on the ½" tube reaction wall 475 °C in the bed zone) is not high enough to allow the complete Ni reduction, although the reduction temperature of this Ni catalyst was already near 450 °C in the u-shaped bed reactor used for TPR measures;
- By comparing the bimetallic catalysts regarding two investigated synthesis methods, on the contrary of the monometallic copper where HP method presented the best performances, when a second metal is introduced AE synthesis seems to produce more active catalysts. For Ni catalyst it is probably linked to the higher temperature reduction of HP as above described. On the other hand, for palladium catalysts it is more complicated to understand why this happens, in fact, it was observed that the ICP-AES content of AE is lower than HP, and the same reduced CuPd are formed as shown in XRD spectra of these materials, §3.3. However, XPS spectra of reduced catalysts pointed out that the ratio between Cu^+ and Cu^0 is different for the two syntheses, probably HP synthesis producing more interactions between Cu and Pd as shown previously in Chapter 3 (see §3.3.1 for ICP-AES results and §3.3.6 for XPS results).

It was not possible to conclude all the tests since with Pd1SiO_2AE, Pd1SiO_2HP and Ni5SiO_2AE monometallic catalysts, it happens that the sampling valve was clogged before the end of tests because an almost solid product was obtained from the hydrogenation (high content of stearic and trans isomers).

In Figure 4-23 the results for the selectivities towards stearic acid formation, indicated as total stearate formed, and the total content of trans isomers are reported. These data are important to make a comparison of the obtained results at the same degree of conversion. It is chosen 25% conversion of C18:2, in analogy to Pd/HT results and because this conversion is almost reached by all the catalysts studied (except for Ni5SiO_2HP see Figure 4-23).

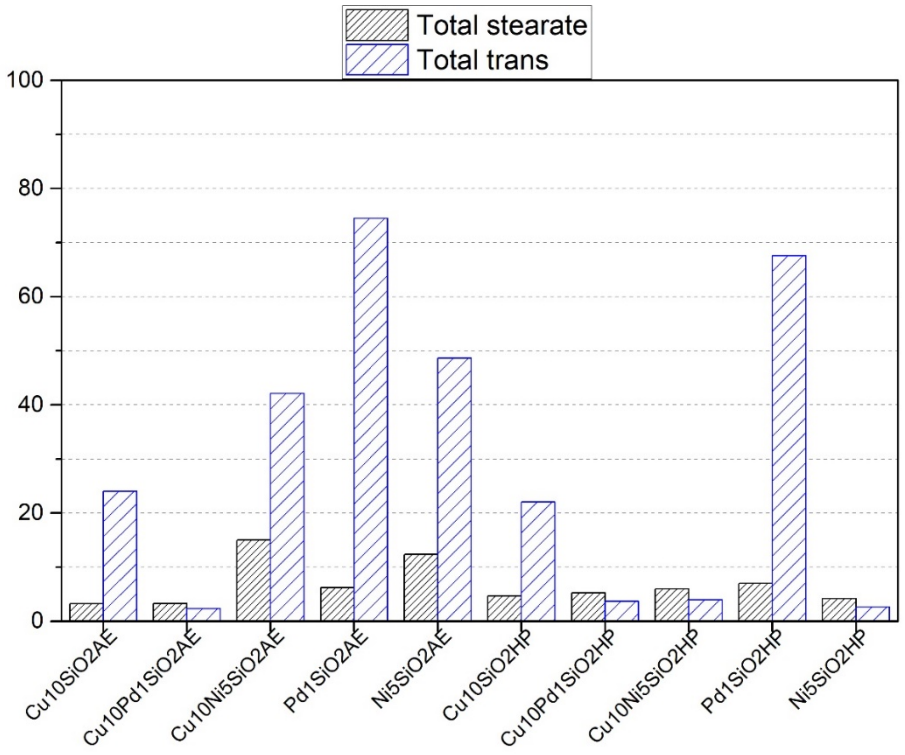

Figure 4-23 Total stearate and total trans produced at the maximum C18:1 for mono and bimetallic catalysts (test 36, test 50 and tests from 64 to 71 of Table 2-2)

Table 4-19 Selectivities at 25% conversion linoleic acid, C18:0 and C18:1 content for test 36, test 50 and tests form test 64 to test 71, data for Ni5SiO₂HP are omitted since the conversion is below 15%

			Linoleic $\chi_{C18:2}$ 25% *			
Entry	**S_{Le}**	**t (min)**	**(C18:0) (%)**	**IV**	**SII**	**(C18:1) (%)**
Cu10SiO₂AE	>100	137	2.50	127.1	0.85	47.00
Cu10Pd1SiO₂AE	37.35	335	3.0	125.1	0.1	45.67
Cu10Ni5SiO₂AE	13.1	37	3.18	124.2	0.31	46.04
Pd1SiO₂AE	4.5	52	4.0	124.8	1.75	45.62
Ni5SiO₂AE	6.9	21	4.81	124.7	0.25	43.64
Cu10SiO₂HP	>100	126	2.85	127.3	0.68	45.94
Cu10Pd1SiO₂HP	36.5	376	5.20	125.7	0.26	45.60
Cu10Ni5SiO₂HP	28.6	369	6.01	125.2	0.26	46.80
Pd1SiO₂HP	3.9	15	3.05	126.4	2	45.18

* Data are obtained from model results §2.3.5

An interesting point for the monometallic palladium catalysts is that the catalysts are very active, more active than the Pd/HT or the Lindlar catalyst which have higher Pd ($2\%_{w/w}$ from ICP-AES) content as measured by ICP-AES. Between the two catalysts, $Pd1SiO_2HP$ shows the highest activity, reaching 25% conversion after only 15 minutes of reaction, associated a poor S_{Le} and SII. The obtained values for the linoleic selectivity suggests a rapid growth of the oleic acid content, then converted in stearic acid. The trans selectivity indicates that the catalyst promotes not only the conversion to stearic acid of the oleic acid but also the secondary reactions of isomerization. The trans isomers are divided equally in elaidic acid and trans isomers of linolenic for both $Pd1SiO_2AE$ and $Pd1SiO_2HP$. This activity is probably linked to the good dispersion of Pd active phase on both catalysts.

$Ni5SiO_2AE$ and the bimetallic $Cu10Ni5SiO_2AE$ have analogous behaviours if confronted in the explored conditions (180 °C and 4 bar with 4 $mg_{catalyst}/mL_{oil}$), the different reactivity, highlighted by the longer time required to reach the 25% linoleic conversion, 21 minutest *vs* 37 minutes, is probably due to the copper which lowers the activity of the nickel and modify the selectivity towards the stearic acid formation, but it does not change significantly the trans selectivity (Table 4-19).

At last, the reactivity of the $Cu10Pd1SiO_2AE$ and of $Cu10Pd1SiO_2HP$ seems to be interesting. The catalysts present utterly different behaviours to the corresponding monometallic ones. As already said these catalysts are less active, although the $Cu10Pd1SiO_2AE$ E is more active, reaching the target conversion in 335 minutes of reaction and the HP in slightly more than 360 minutes. Comparing the results, it seems that the catalysts behave rather like copper catalyst than palladium (longer reaction time, similar conversions and better trans selectivities to Cu monometallic catalysts). Although the catalysts presented worst S_{Le} with respect to monometallic copper ones, they give the best results among the bimetallic materials synthesized. Between the Cu/Pd catalysts, $Cu10Pd1SiO_2AE$ also has the best selectivity towards trans isomers, which relative percentage of elaidic acid is near zero and so all the trans isomers are due to the isomerization of the diene.

As already mentioned, the operative parameters can have a strong influence over the reactivity of the catalyst during hydrogenation, and so it was decided to test the most promising bimetallic catalyst under different reaction conditions. Since $Cu10Pd1SiO_2AE$ shown the best selectivity it was the catalyst chosen for the last campaign of tests. Table 2-2 reports the conditions of the tests from test 72 to test 79. In particular, it was established to test the catalyst at high temperature over 200 °C (240 °C, temperature compatible with the

limit decomposition temperature of the sunflower oil 255 °C as the producer labelled on the product) since the catalyst seems to have activity related to copper, which (as already described in the section §4.3.3 dedicated to sunflower hydrogenation with Cu) is less active towards the hydrogenation of dienes.

First, three tests at 120 °C were carried out and no conversion of C18:2 linoleic acid was found after 6 hours of reaction. These tests have been taken as reference for the next ones at 180 °C, 240 °C, and an intermediate temperature of 200 °C; the pressure of the tests was varied between 4 and 20 bar.

At 180°C,the pressure growth from 4 to 20 bar does not have a significant effect on conversion which essentially remains the same; The selectivities S_{Le} and SII also are constant, at 37.5 (37.4 at 20 bar *vs* 37.5 at 4 bar) and 0.11 (calculated at 25% conversion of C18:2), respectively. The intermediate point at 200 °C under 12 bar of H_2 does not point out different behaviour than the 180 °C tests (test 75 and test 76), the selectivities are analogues with a linoleic selectivity of 35.4 and SII of 0.19 (always at 25% conversion of C18:2).

The temperature increase gives a crucial boost to the conversion of the Cu10Pd1SiO$_2$AE which after 3 hours reaches almost complete hydrogenation of all the dienes (see Figure 4-24 and Figure 4-25), and also the effect of pressure becomes visible. As for the pressure by ranging its value from 4 bar to 20 bar, the formation of trans isomers after 2 hours is almost reduced to zero and consequently the stearic content is increased.

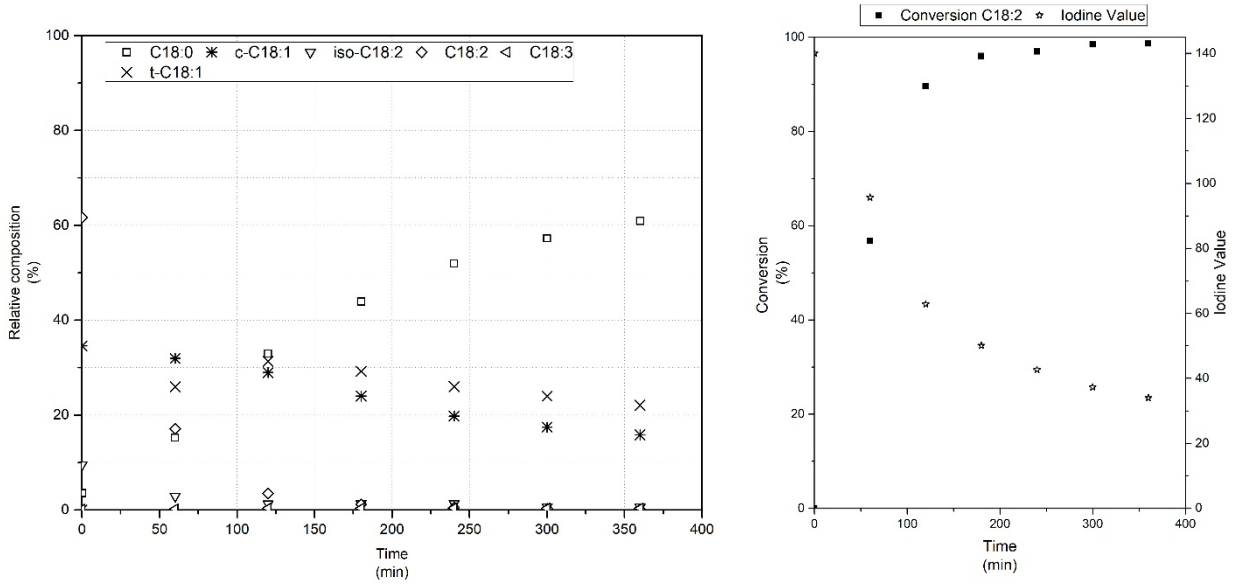

Figure 4-24 Hydrogenation results at 240 °C and 20 bar with 4 $mg_{catalyst}/mL_{oil}$ of Cu10SiO$_2$AE (test 78)

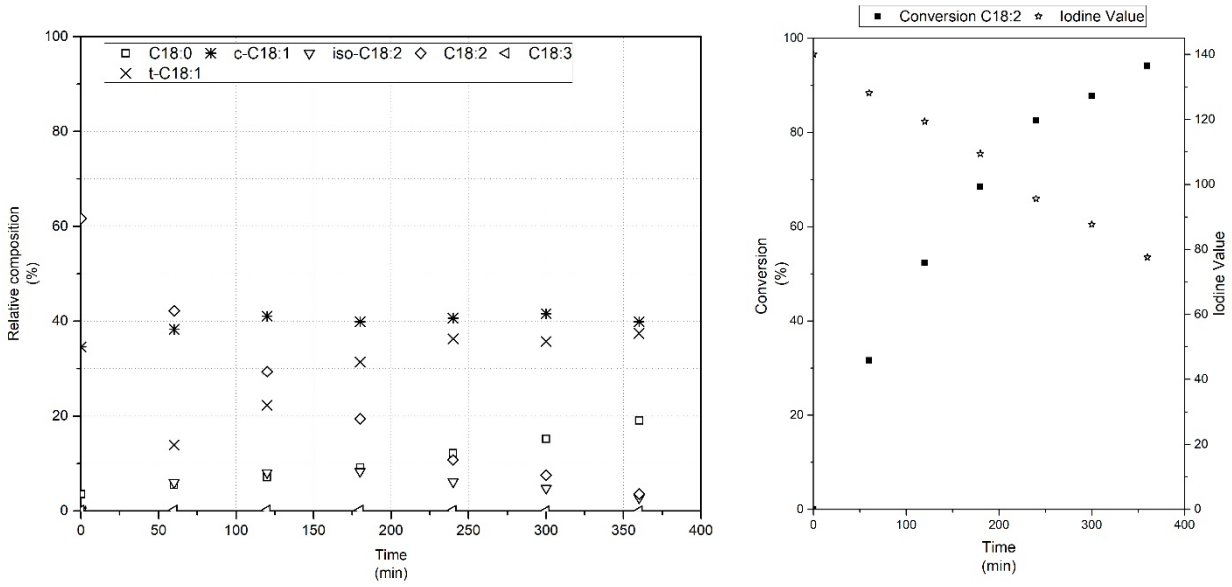

Figure 4-25 Hydrogenation results at 240 °C and 4 bar with 4 $mg_{catalyst}/mL_{oil}$ of Cu10SiO2AE (test 77)

During the reaction a noteworthy thing happens, the content of oleic acid remains the same during the reaction or varies slightly at higher pressure, and the elaidic acid also follows well the trend of oleic acid when formed. On the contrary, the stearic acid is formed constantly during the hydrogenation and not only when the oleic acid start to react. Therefore, from these trends the catalyst follows a pathway slightly different which allows us to formulate the hypothesis is the direct hydrogenation of linoleic acid to stearic acid, in addition to the standard way described in chapter §1.7 and §2.3.5. It is probably due to the temperature at which the reaction is carried out; in fact, at this temperature, it seems evident that the CuPd, or the Pd inside it, becomes active. There is probably a synergic effect between the Cu and the Pd at 240 °C, multiple double bonds can react at the same time on the catalyst surface.

The selectivities are quite different from the test at 180 °C and 4 bar (test 72) (Table 4-19), with S_{Le} equals of 9.2 at 4 bar and 2.2 at 20 bar and SII ranging between 2.9-3.0: this means the catalyst is no more selective in the conditions of test 75 and test 76.

The comparison between the tests at 180 °C and 200 °C with the tests at 240 °C suggests that an intermediate condition in which the conversion of C18:2 are quite high during the 6 hours tests can be found, but probably the catalyst would begin to lose selectivity in a narrow range of temperature.

4.4. Conclusions

As far as Lindlar catalyst is concerned, the main features are:

I. It is active at 180 °C with high formation of C18:1 (both elaidic and oleic) and low formation of stearic acid (less than 10% at the maximum C18:1 relative percentage);

II. The catalyst loses its selectivity at high pressure (12 bar) and high temperature (180 °C).

III. Compared to other palladium catalysts in the literature, the Lindlar catalyst is more selective towards the formation of trans isomers and stearic acid, at least in the tested conditions;

IV. The activity of the catalyst was tested in cyclic tests, and although it decreases by every cycle, with a catalyst make-up it is probably reusable over multiple cycles. The mechanism of deactivation of the catalyst must be ascribed to a poisoning linked to the natural poisons found in vegetable oils or due to a loss of catalyst between one cycle and the successive;

V. The versatility of the application was tested with sunflower oil, and although the Lindlar showed good activity in 6 hours of the tests, it had quite worse selectivity; it can be related to the different reaction velocity of linolenic and linoleic acid reaction rates

A synthetized Pd/HT catalyst was tested under conditions similar of the Lindlar catalyst test campaign and the Pd/HT shown different features:

I. Pd/HT had lower activity than Lindlar catalyst, longer reaction times were required to obtain the same degree of hydrogenation (IV or conversion of C18:2) at high temperature;

II. At 120 °C the catalyst presents a good combination of both activity and cis/trans selectivity;

III. For this catalyst cyclical tests were also investigated and, unlike Lindlar, during the first repeated tests, the catalyst underwent an activation mechanism probably related to a change in the structure of the hydrotalcites as also found by XRD characterization, induced by the combined effect of temperature and pressure, or to an activation of the palladium surface. Post-test characterization does not provide a definitive statement about the real mechanism. After the first test, the catalyst is deactivated more quickly than the Lindlar;

Another family of catalyst-containing Cu on SiO_2 support was studied, and two different materials' syntheses were investigated: the AE (Ammonia Evaporation) and the HP (Hydrolysis Precipitation) methods. Between the two syntheses, the HP synthesis gave the best results both in activity and in selectivity under all tested operating conditions, due to more metallic Cu present. Main features of these materials are:

I. Compared to Lindlar catalyst, in all tested conditions, an overall lower conversion, better cis/trans selectivity and higher linoleic selectivity were obtained, due to different reaction mechanisms;

II. The effect of temperature was important in both synthesized families, and a slightly higher temperature than 180 °C was required to increase the catalyst activity. However, the pressure effect was not extremely relevant, at least for HP catalyst. This makes possible to work at lower pressure (4 bar) and still obtain conversion of linoleic higher than 75%;

III. The conversion reached high values (up to 90% for C18:3 and 80% for C18:2) when the amount of catalyst was increased, the required reaction time to carry out the tests were compatible with hydrogenation time of industries processes [260];

IV. The maximum observed amount of t-C18:1 was at 200 °C under 12 bar of pure H_2 and it was about 23% of relative percentage.

At last, the bimetallic and the corresponding monometallic catalysts were tested, but the desired increase in activity was not obtained. The main results can be summarised as:

I. Both Pd1SiO_2AE and Pd1SiO_2HP were largely more active than Pd/HT and Lindlar catalyst, at the cost of worse selectivities. Hydrogenation rates of linoleic and oleic acid were very close, giving rise to large amount of both elaidic and stearic acid;

II. Ni5SiO_2AE was subject to the same problems of Pd1SiO_2AEhowever after the reaction lesser amount of trans isomers was found, but greater amount of stearic acid. The bi-metallic Cu-Ni had characteristics similar to the monometallic ones;

III. Ni and Cu-Ni catalysts, synthesized via HP method were not active, probably due to not complete reduction in the fixed bed reactor;

IV. Eventually, Cu-/Pd catalysts produced conversions lower than the Pd and Cu ones; nevertheless, Cu10Pd1SiO_2AE had a good selectivity to cis/trans isomers and it was tested in a wider experimental campaign. The results of the campaign highlighted that the catalyst had similar characteristics at 180 °C and 200 °C, but the increase in temperature up to 240 °C led to a change in the catalyst mechanism, producing large amount of stearic acid and elaidic acid in a short time reaction, losing the selectivity recorded at 180 °C and 4 bar.

Two catalysts shown the best performances for the catalytic hydrogenation of vegetable oils: Lindlar catalyst and $Cu10SiO_2HP$. The best operative conditions for Lindlar catalyst in terms of selectivity are 180 °C under 4 bar with 4 $mg_{catalyst}/mL_{oil}$ the reaction carried out for 1h or the reaction or 2 h with 1 $mg_{catalyst}/mL_{oil}$; for $Cu10SiO_2HP$ the operative conditions individuated are 200 °C and 4 bar with 8 $mg_{catalyst}/mL_{oil}$ the hydrogenation run length of 3 h.

It was chosen the $Cu10SiO_2HP$ to study an industrial solution since the palladium is more expensive and is price is growing for the effect of commodities speculation that the market of this metals has been affected as shown in Figure 4-26. Also if it is a "bubble" (due to speculation) as some experts suggest in the short and long term this metals (and also all the products obtained) experienced a high price volatility.

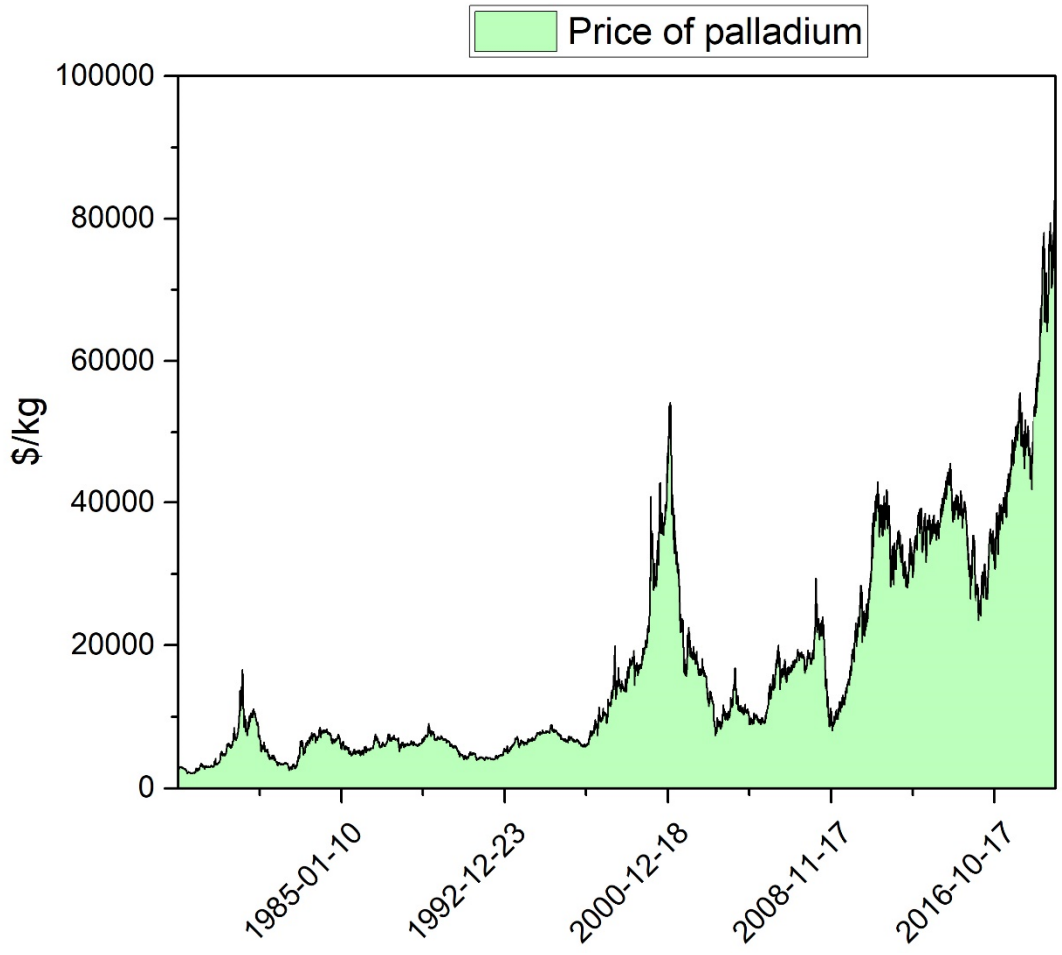

Figure 4-26 Price of palladium $/kg in the last 30 years (from 1977 to 2019) [285]

Chapter 5

Industrial application

This chapter reports a short introduction on the most common implemented technology of hydrogenation of fatty acids and fats, the methodology of the industrial work carried out at NextChem (ex Processi Innovativi S.r.l.), the design of a semicontinuos plant, and the economics of the case studied. This version of the thesis part of the work is omitted since copyright ownership of NextChem.

5.1. Overview of industrial hydrogenation reactors

The core of a hydrogenation plant is the hydrogenation reactor. In section §5.1.1.“Batch vs continuous”, it will be discussed the different kinds of reactors used to carry out this reaction discussing the advantages and the constrains of batch or continuously operated reactor.

5.1.1. Batch vs continuous

As already reported in §Chapter 1, hydrogenation of vegetable oils is a long-time exploited reaction. Since 1911 when Procter & Gamble started exploiting the patented process by Normann [91]. Although, vegetable

oils hydrogenation has a very long history, not so many changes to the basic process were achieved in industrial applications.

In the industrial practice, this reaction is carried out both in batch and continuous reactors. However, the majority of the hydrogenation plants, as in case of complete hydrogenation (final IV < 0.5) as for partial hydrogenation plants (60 < IV < 85), are commonly built in batch configuration. This is due to a series of operative advantages of batch hydrogenation over continuous one. In Table 5-2 and in Table 5-2 pros and cons of both technologies are indicated.

Table 5-1 Pros and cons of batch vegetable oil hydrogenation technology [92]

Batch hydrogenation process	
Pros	**Cons**
+Greater control in the final composition +Higher selectivity because more parameters controlled +Flexibility of the feedstock used in the same plant +Flexibility in the production	-Big reactors -No easy recovery of heat -Difficult mixing -Smaller production scale

Table 5-2 Pros and cons of continuous technologies [92]

Continuous hydrogenation process	
Pros	**Cons**
+Stable production with standardized product +Smaller reactor units	-Back mixing problems resulting in low selectivity -Problems in the controls or changing the products specifications may result in a large amount of off-grade products

+Heat of reaction recovered for the heating of the feed +More interesting for products where selectivity and isomerization are less important	-The time to reach a stable product could be large -Off-grade products must be blended with fresh oil (not always easy to do) -Poor mixing (or contacting) between the oil and the hydrogen throughout all the reactor

The main advantage of batch hydrogenation over continuous hydrogenation consists in a greater control over the reaction and so on the final product composition; better selectivity is achieved in batch reactor units and the flexibility switching the feedstock or the products following the market demand is possible. Many times batch hydrogenation plants consist of bigger reactor unit, where heat recovery for a pure batch is not always simple to achieve, consequently, the operative and capital costs are greater than continuous operation.

For continuous hydrogenation, two considerations are involved: the possibility to readily obtain the reaction conditions required for an optimal technical specification of the product, i.e. the selectivity of the catalyst permits to obtain little formation of unwanted products when the production is changed for a period of time. Secondly, there is the point of view of the production program of a particular product that must be sufficiently constant to afford economical uninterrupted operations from a reasonably consistent feedstock. In continuous operated hydrogenation plants changeover from a product to another should not give rise to a large amount of intermediate, and this is not often the case with vegetable oil hydrogenation.

If these two highlighted conditions can be met, then several advantages in operative cost reduction, space reduction (reactor smaller than the batch counterpart), and labour cost can be achieved [92]. Having said this, nevertheless the vast majority of vegetable oils hydrogenation is carried out in batch reactors both for triglycerides and their derivatives, and little indication is shown that this situation is about to change [92,267–269]; this is mainly due to the greater flexibility of this kind of industrial plants, whereas the continuous hydrogenation, where selectivity is less critical, is quite popular.

It exists another possibility to combine the batch reactor unit, and so maintaining the high selectivity of this process, with all the other equipment (heat exchanger, gas-liquid separation, etc.) operated continuously,

this allows having the best of the two technologies, easily recovering the heat from the streams, lowering the operative costs of such application. This is possible utilizing different holdup vessels.

5.1.2. Industrial hydrogenation processes

On the batch kind of reactors three main reactor typologies find common use in batch hydrogenation:

- **Dead end reactor with mechanical mixing:** a batch reactor with mechanical agitation which is charged with oil, catalyst and which is fed with hydrogen following the reaction trend [92];
- **EKATO blade mixing reactor:** similar to the previous typology of reactors it has a special impeller blade; this kind of blades have many shapes and share the feature of a cave throughout the hydrogen is distributed [270]. This highly improves the gas/liquid mixing. Desmet-Ballestra sells a hydrogenation process under the name of Hydrotherm®[270];
- **Loop reactor:** a particular family of reactors vessel in which the agitation is made up of a high-performance gas/liquid ejector to achieve high mass transfer rates; between the three kinds of reactors, this one has the best mass transfer per power unit consumed with low energy consumption and not special sealings are required concerning mechanical agitation.

Over the years many continuous applications were developed, but in many cases, they are just utilized to produce low selective products as shortenings (Lurgi Process). In this case, the reactors are of column types with multiple hydrogen ingress points at different levels in the column to assure the good mixing of the slurry and high contact of the three phases. Also Procter & Gamble developed one of this application but the use was limited to one product [260].

5.2. Case of study

The industrial application studied with the industrial partner of the project, Processi Innovativi Srl, was developed from the results for the $Cu10SiO_2HP$ catalyst. In particular, the tests 52 and 56 which give the best results in terms of activity of the catalyst and selectivity (see §Appendix A) were considered. Test 52 was carried out at 200 °C under 4 bar of H_2 with 4 $mg_{catalyst}/mL_{oil}$ and test 56 at 200 °C under 4 bar of H_2 but with 8 $mg_{catalyst}/mL_{oil}$. In the end, it was chosen the test 56 because almost complete conversion of both linolenic and linoleic acid was achieved after 180 minutes, tests results are presented in Figure 5-1.

At 180 minutes and 240 minutes, the relative composition of C18 compounds (for trans elaidic composition see §Appendix A) is reported in Table 5-3. Since the differences between the reaction at 180 minutes and at 240 minutes are negligible and the reduction of reaction time comports an increase in the productivity, it was decided to perform the hydrogenation plant design on the basis of three hours of hydrogenation reaction.

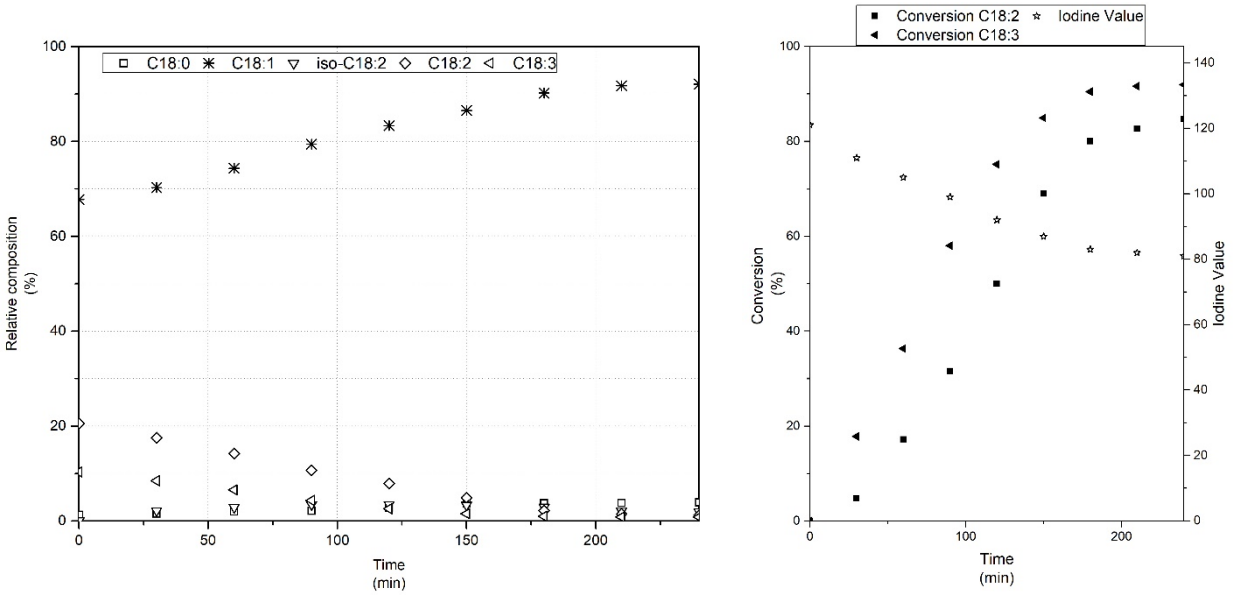

Figure 5-1 Hydrogenation results at 200 °C and 4 bar with 8 $mg_{catalyst}/mL_{oil}$ of $Cu10SiO_2HP$: on the right-hand side relative percentage of C18 compounds vs time, on the left-hand side the conversions of linolenic and linoleic acid and iodine value vs time

Table 5-3 Relative composition for C18:0 components at the hydrogenation start of the reaction and after 180 and 240 minutes

Time (min)	C18:0	t-C18:1	C18:1	iso-C18:2	C18:2	C18:3
0	1.3	0.00	67.8	0.1	20.6	10.3
180	3.7	13.5	90.2	2.9	2.2	0.9
240	3.9	17.1	92.1	2.0	1.2	0.8

The above information (Table 5-3 and Figure 5-1), combined with the analysis of the saturated components not involved in the reaction (C14:0, C16:0, C20:0 and C22:0), forms the basis of the material balances developed for the industrial application under consideration. In particular, the tests' results are used to determine the mass composition of the vegetable oil and the vegetable oil mass flow after reaction condition.

The hydrogenation plant designed is operated batchwise for the reaction unit, although as described in §5.1.1 the semi-continuous process was taken into account since it allows to recover heat and to reduce the overall operative costs compared to pure batch hydrogenation, and so the remaining equipment of the plant is

operated continuously. Furthermore, in order to improve mass transfer, the loop reactor was chosen, to assure elevated mixing between the liquid and the gas phase (§5.1.2) with low power consumption.

The hydrogenation process description of each unit follows in §5.2.1; the layout of the process is not reported in this text (copyrighted by NextChem) but it is based on a common hydrogenation process, in this case, it was adapted to the selective hydrogenation of Canola oil with copper on silica catalyst.

5.2.1. Process description

It can process both vegetable oils or their derivatives (obviously in the second case the mass balances changes). The vegetable oil from storage is fed to the plant under flow control conditions and is preheated up to 160 °C recovering part of the heat from the effluent hydrogenated product .

The final reaction temperature is reached recirculating the product inside a degasifier/tank in a heat exchanger. The oil exchanges heat with steam.

The charge is sent to the reactor batchwise and at the same time, the required quantity of catalyst is mixed with a prefixed amount of fresh oil, and fed into the reactor, kept under vacuum. The hydrogen then flows into the reactor unit, its mass regulated by a mass flow controller. The reactor is equipped with a special catalyst/product hydrogen mixing system that allows efficient mass transfer and hydrogen/oil contact.

The reaction temperature is controlled by heating/cooling the product in an heat exchanger. This step is realized by circulating water from a steam drum . In this way, the heat of hydrogenation is removed generating low-pressure steam.

After the hydrogenation cycle is completed the product is discharged into a drop tank from which it is continuously extracted and cooled in the heat recovery exchanger.

Finally, the hydrogenated product is filtered through filters to remove the catalyst from the hydrogenated product.

5.2.2. Plant size choice & Mass balances

The plant size for this application was of 2.4 tonnes of vegetable oil or FAME or fatty acids, this was chosen on the basis of a standard-size hydrogenation unit for complete hydrogenation which is of around 20 tonnes for batch with a daily production of 100-120 tonnes of hardened products. Since the product, in this

case, does not have a real counterpart among the hydrogenated fats market, the design was made based on a pilot-short scale plant.

The hydrogenation reaction is carried out, as mentioned above, for 3 hours of reaction; all the secondary procedures of reaction charge/discharge and reactor cleaning between one hydrogenation run and the successive is hypothesized to take almost one hour. So, the hydrogenation cycle takes almost four hours to be completed.

The catalyst filtered could be recovered, using the data obtained by Ravasio et al. [1] and by Koritala et al. [156], and reused for almost 10 cycles without losing activity.

In one 24 hours day, 6 hydrogenation runs can be completed and the production in a working day is of 14.4 tonnes of hydrogenated product. Also, a venting of the system must be considered in order to remove possible unwanted gases accumulated inside vessels.

The mass balances expressed in kg/batch are reported in Table 5-4, the mass flowrates for gases are reported in Nm^3. The oil/FAME physical properties were taken from Sahasrabudhe et al. [271]. In this document not all the mass flows are reported but only: vegetable oil inlet in the system, vegetable oil hydrogenated outlet from the reactor, and final product. All the other streams are omitted as well as the name of the streams for copyright reasons.

Table 5-4 Mass balances for process stream

Stream n°	In		Out		Product
Temp (°C)	50.0		200.0		50.0
Press. (barg)	3.0		3.0		3.0
Total FAME (kg/batch)	2000.0		2005.2		2002.6
Total (kg/batch)	2452.6		2460.3		2442.4
Flow rates kg/batch					
C14:0	1.0		1.0		1.0
C16:0	80.0		80.0		79.9
C18:0	24.2		70.3		70.2
C18:1	1284.2		1714.9		1712.6
C18:2	391.4		96.9		96.7
C18:3	195.6		18.5		18.5
C20:0	14.0		14.0		14.0
C22:0	6.0		6.0		6.0
other	3.6		3.6		3.6
Glycerol	440.4		440.4		439.8
Water	12.2		0.0		0.0
Air	0.2 Nm^3		0.0		0.0
H_2	0.0		0.0		0.0
Catalyst	0.0		14.7		0.0

5.2.3. Units designs

In the following sections (from §5.2.3.1 to §5.3.2.3.8) the design or the specification for each unit are reported.

For the materials used in the construction of these units Austenitic Stainless Steel of 316 grade was hypothesized, in calculations for vessel and heat exchangers as well as pumps and other equipment. The choice of these alloys essentially eliminates the possibility of iron and other metal contaminations which may either degrade the product or catalyze undesirable oxidation and other side reactions. With certain exceptions, it has been found that Type 304 stainless steel may be used in fatty chemical processing at temperatures up to 150 °C and Type 316 stainless steel for tanks and vessels designed for use above that temperature [273].

5.2.3.1. Hydrogenation reactor

The loop reactor was designed following the indication of PED directive of EU [274] and the ASME rules for pressure vessel and boilers design [275,276]. The reactor is substantially a cylindrical vessel with ellipsoidal 2:1 heads, the Height/Diameter (H/D) ratio is related to the value of a similarly shaped reactor designed for the complete hydrogenation of vegetable oils.

The thickness values t for the cylindrical mantle and for the elliptical heads are given in

$$t = \frac{P * ID}{2 * z * f + P} \qquad \text{Equation 5-1}$$

$$t = \frac{P * ID}{2 * z * f - 0.5P} \qquad \text{Equation 5-2}$$

Where z is the weld joint efficiency, f is maximum allowable stress, ID the internal diameter, and P the design pressure. Also, the corrosion allowance was considered for the wall thickness, and it was chosen equal to 1 mm. In first approximation, the same value for cylindrical wall thickness and for the heads thickness was used. In order to be in conservative conditions for safety reasons the temperature is taken above the reaction temperature and the pressure is taken 10 bar.

In Table 5-5 the data for the reactor unit are listed:

Table 5-5 R-1 designed characteristics

Name	Height (mm)	Diameter (mm)	[redacted]	t (mm)	P design (bar)	T design (°C)	Volume (m^3)	Weight (kg)	Volume liquid (m^3)	H liquid (mm)
Reactor	5252	955		7	10	250	4.02	1107.22	3.02	4026

For the jet-mixer inside the reactor some specifications are given to the producer who will design the final object. These specifications are reported in Table 5-6 (design pressure and temperature are equal to the reactor unit R-1):

Table 5-6 J-1 specification for the jet mixer producer

Name	Specific Weight (kg/m^3)	Viscosity (cP)	Catalyst concentration ($g_{catalyst}/mL_{oil}$)	Operating P (bar)	Operating T (°C)
Jet mixer	806 [271]	10-12 [271]	8	4	200

At last for the recirculating pump (P-1) specification of flowrate, pump power required and NPSH available are shown in Table 5-7:

Table 5-7 Pump specification

Name	Flowrate (m^3/h)	Pump power (kW)	NPSH available (m)
P-1	15	3.5	100

5.2.3.2. Catalyst charge vessel

A vessel is used to prepare the catalyst charge before its introduction in the reactor. In standard complete hydrogenation, the catalyst is mixed with hydrogenated product and then sent to the reactor; the choice for this chemical plant is different and the catalyst is mixed with fresh oil, the mixer has the purpose of suspend the catalyst in the oil and facilitating the pumping in the reactor.

The vessel is maintained under vacuum in order to prevent air contact with the oil and the catalyst. The design of this vessel followed the indication for vessel subjected to external pressure found in the PED rules [275].

Table 5-8 Catalyst charge preparation vessel

Name	Height (mm)	Diameter (mm)	H/D ratio	t (mm)	T design (°C)	Volume (m^3)	Weight (kg)	Liquid volume (m^3)	Liquid height (mm)
	950	475	2	4	100	0.19	58.66	0.012	515

For this application, to perform the agitation a standardised mechanical stirrer, pitched-blade, has been considered [277]. The power required to mix catalyst and the oil was evaluated with the definition of power number (*P*) Equation 5-3:

$$P = k * \rho * n^3 D^5 \qquad \text{Equation 5-3}$$

where k is the constant relative to the specific impeller (1.37 for the pitched-blade), ρ is the density of the fluid, *n* is the rotation velocity of the impeller in rpm, and *D* is the diameter of the impeller in this case was taken 0.5 ID of the vessel. The required calculated power was 0.12 kW, assuming 80% efficiency of the motor, the required power is 0.15 kW.

It is essential to highlight that for all the vessels under vacuum the thickness was in first attempt calculated without considering the introduction of the so-called stiffening ring. The stiffening rings are almost all the times used in vacuum operation happens because with the use of stiffening rings with different geometries (welded completely or not on the mantle of a vessel) are possible to reduce the thickness of the wall and so reduce the cost of the unit. Although, at this point in the design of the hydrogenation process it is unnecessary to enter in a so advanced design, and the evaluations made are conservative for a point of view of the cost of the vessel.

5.2.3.3. Hold-up vessel

The hold up vessel/degasifier purpose is to eliminate moisture and air trapped inside the oil; the unit is operated under a vacuum.

The amount of water inside the oil is taken equal to 0.5% of the mass of oil from literature data: on bleached oils, oxygen content from [58] is 200 mg_{oxygen}/kg_{oil}. The amount of gas to separate from the oil is

equal to 4.03 kg/h of mixed oxygen and water, but the air re-entered from the sealing must also be considered using the empirical equation commonly [278]:

$$F = k * V^{2/3} \quad \text{Equation 5-4}$$

where F is the flow of re-entered air inside the vessel in kilogrammes per hour, k is a constant equal to 0.8 (value come from the sealing used for the vacuum pressure 100 mbar), and V is the volume of the unit. Equation 5-4 comes from practical experience of industrial designer, and the results are just a conservative estimation of the real quantity. The re-entered air inside the vessel is estimated to be 2.33kg/h. The total flow from the oil is 6.36 kg/h at 200 °C and 100 mbar.

Vapor Liquid separators are one of the most common types of process equipment. Vapor liquid separation occurs in three stages:

- The first stage: primary separation uses an inlet diverter so that momentum of the liquid entrained in the vapor/gas causes the largest droplets to impinge on the diverter and then drop by gravity;
- The next phase: secondary separation is gravity separation of smaller droplets as the vapor flows through the disengagement area;
- The final stage is mist elimination, where the smallest droplets are formed which will separate by gravity.

For maximum allowable gas/vapor velocity (v) ,it was used the Sounders-Brown equation[279]:

$$v = K * \sqrt{\frac{\rho_L - \rho_V}{\rho_V}} \quad \text{Equation 5-5}$$

where ρ_V and ρ_L are the density of the vapor and of the liquid, respectively and K at pressure of 0 bar is 0.107 m/s, and so the vapor velocity in the studied condition is 8.74 m/s.

From the velocity the minimum internal diameter is calculated, the vessel is also the holdup vessel before the reactor. The vessel thickness was calculated following the rules for the design of pressure subjected to external pressure (pressure inside 100 mbar), i.e. PED rules [275].

Table 5-9 Design of separator/hold-up vessel

Name	Height (mm)	Diameter (mm)	H/D ratio	t (mm)	T design (°C)	Volume (m^3)	Weight (kg)
Hold up vessel	950	475	3	9	250	5.62	1371.11

The different levels inside the degasifier were determined following information reported by the Gas Processors Suppliers Association (GPSA) in the Engineering Data Book [280], see Figure 5-2 and Table 5-10:

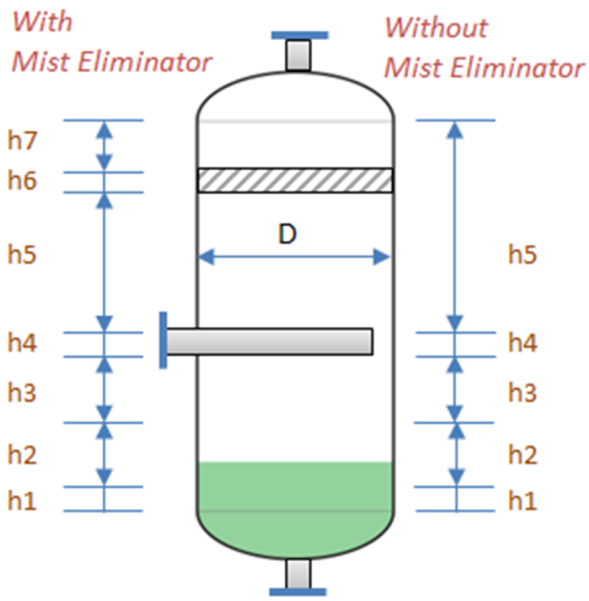

Figure 5-2 Gas-Liquid separator height with demister eliminator and without demister

Table 5-10 Liquid separator with levels: $H_1(H_{LLL})$ low-level liquid, $H_2(H_H)$ hold up, H3(HS) surge gas, $H_4(H_{IN})$inlet height, $H_5(H_{DIS})$ disengage height, $H_6(H_{MIST})$ demister height, $H_7(H_{Top})$ from demister to top.

H_{tot} (mm)	$H_1=H_{LLL}$ (mm)	$H_2=H_H$ (mm)	$H_3=H_S$ (mm)	$H_4=H_{IN}$ (mm)	$H_5=H_{DIS}$ (mm)	$H_6=H_{MIST}$ (mm)	$H_7=H_{Top}$ (mm)
3900	150	2000	200	600	500	150	300

5.2.3.4. Filters

The F-1 unit, represented in **Errore. L'origine riferimento non è stata trovata.**, consists of two so-called Cricketfilter® [279], filters commonly used in filtration of vegetable oils, since the common small size of the catalyst commonly used. This kind of filters required a short time of regeneration under N_2 atmosphere, and have higher filtration areas per volume of the filtration equipment due to the shape of the filter.

This unit is bought from the manufacturer, the catalyst cake is removed by pulsing nitrogen backward (1-2 pulses). Some specifications for the manufacturer are:

Table 5-11 Cricket filters specifications

Name	**Design Pressure (bar)**	**Feed**	**Max oil content in catalyst**	**Nitrogen pressure**
F-1	9	Oil+8$mg_{catalyst}/mL_{oil}$	20%$_{w/w}$	6 barg

Nitrogen is also used for the cleaning and drying of the filter in between each filtration. Buffer tank of nitrogen and the nitrogen heater are also bought from the apparatus manufacturer.

5.2.3.5. Vacuum system

The vacuum system maintains all the necessary unit at 100 mbar, in order to remove gas and vapors. iIt was decided to use a vacuum pump of liquid ring pump type. The fluid that should be evacuated are summarized in Table 5-12:

Table 5-12 Gas flowrate to be evacuated in PV-1

Fluid	**Flowrate (kg/h)**
Oxygen	0.48
Water	3.15
Unreacted Hydrogen	Negligible
Air inlets	2.47
Total	6.10

The specifications for the manufacturer of the pump are found in Table 5-14, the specifications comes from the plant parameters:

Table 5-13 Flowrate description of vacuum system

Name	Normal Flowrate (kg/h)	Design Flowrate (kg/h)	Suction Pressure (mbar)	Discharge Pressure (mbar)	Suction Temperature (°C)
	6.10	8.35	60	200	100

5.2.3.6. Heat exchangers

The heat exchangers in **Errore. L'origine riferimento non è stata trovata.** were designed and rated using the package utility CC-Therm of the software ChemCAD in combination with the standards of the tubular exchanger manufacturers Association [281]. The four heat exchangers are all of tubes and shell typology (T&S):Bonnet one pas shell with fixed tubesheets (BEM) configuration (see Figure 5-3) for accessibility of the heat exchanger in case of fouling.

Heat Exchanger reoval of reaction heat

This heat exchanger is designed to maintain throughout the reaction the reactor at 200 °C; to evaluate the heat duty to eliminate, it was used the iodine values trend. It was used the empiric correlation found in List et al. [92] and of common use in the hydrogenation of vegetable oils: for a drop of IV equal to 1 the increase in temperature is equal to 1.5 °C. From this data using Figure 5-1 results for IV the heat produced during the reaction was calculated to 30935 kcal/h.

The steam produced is at low-pressure 4 bar at 145 °C (superheated steam).

The heat exchanger was then designed on these values, the results for the heat exchanger are in Table 5-14:

Table 5-14 Design details for heat exchanger for reaction heat removal

Name	
Q (kW)	35.97
U (W/m^{2}K)	196.38
A (m^2)	15
Over design	25%

Low-pressure steam	10 kg/batch
Exchanger Type	BEM
Exchanger orientation	Vertical
Shell size (mm)	150
Shell in series	1
Number of tubes	19
Tube length (mm)	2000
Number of tubes passing	2
Material	AISI AS240-Gr316

Heat Exchanger maintain reaction temperature

This heat exchanger is designed to bring the oil up to the reaction temperature of 200 °C, and to maintain this temperature at 200 °C when D-3 is filling before a hydrogenation cycle. This operation is made with medium pressure steam at 17 bar (around 205 °C), the heating of the oil is made with the latent heat of evaporation of the steam.

Table 5-15 Design details fo heat exchanger

Name	
Q (kW)	108.46
U (W/m^{2}K)	414.23
A (m^2)	7.29
Over design	25%
Medium pressure steam used	50 kg/h
Exchanger Type	BEM
Exchanger orientation	Vertical
Shell size (mm)	150
Shell in series	3
Baffles	7
Number of tubes	15
Tube length (mm)	2500
Number of tubes passing	4
Material	AISI AS240-Gr316

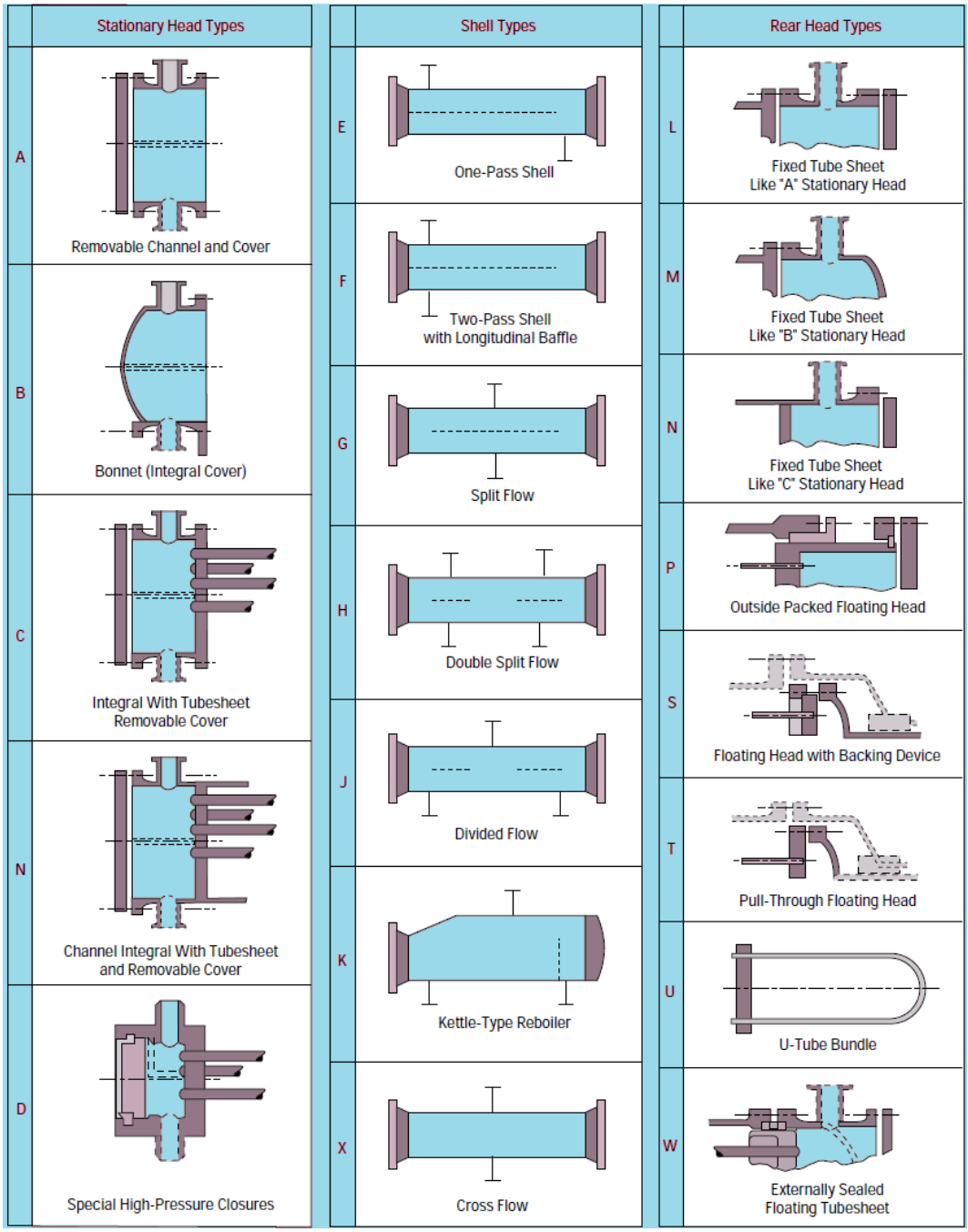

Figure 5-3 TEMA representation as in TEMA standards [281]

Heat Recovery and cooling

A first heat exchanger is the heat recovery unit, it exchanges heat between the fresh oil alimentation (50 °C) and the hydrogenated product (200 °C), it exchanges in both shell and tubes the sensible heat of the oil as highlighted in the global coefficient of heat transfer U that in comparison to all the other cases is lower (due to the properties of the oil). In order to perform this operation, it was required to design many passages on the tubes side and more than one shell were carefully designed to be in series.

The last heat exchanger is a cooler: the purpose is to bring down the temperature from 95 °C to 50 °C, cooling water was used as service fluid at 30 °C, the design results are indicated in Table 5-16.

Table 5-16 Design details for heat recovery exchanger

Name	
Q (kW)	63.55
U (W/m^{2}K)	109.05
A (m^2)	5.06
Over design	25%
Cooling water	0.5 m^3/h
Exchanger Type	BEM
Exchanger orientation	Vertical
Shell size (mm)	175
Shell in series	2
Number of tubes	18
Tube length (mm)	2500
Number of tubes passing	1
Material	AISI AS240-Gr316

5.2.3.7. Pumps systems

All the pumps can be of centrifugal types, and their prevalence, flowrate and power pump are reported in Table 5-19:

Table 5-17 Liquid pumps specifications

Name	**Flowrate (m^3/h)**	**Pump power (kW)**	**NPSH available (m)**
P-1	15.2	3.54	100
P-2	1.09	0.52	23
P-3A	6.05	1.82	45
P-3B	1.23	1.06	33
P-4	0.89	1.12	28
P-5	15.1	2.87	100
P-6	1.09	1.02	25
P-7	0.12	-	35

5.2.4. Economic evaluation

With the help of NextChem - Processi Innovativi [282] expertise on chemical plant design, estimations of the CAPEX costs, OPEX costs, and COP for the designed plant were realized. The reliability of such evaluation is normally affected by an error of ±30% and it is necessary to study in deep some aspects (such as insulation, thickness, cladding, etc.) in the later development of industrial design.

At this point, in the design a reliable estimation could be carried out.

5.2.4.1. CAPEX evaluation

CAPEX estimation of vessels was made on the basis of the euros per kilogrammes of stainless steel AISI SA-240-Gr.316. The cost of this material is about 16 €/kg [282]. For mechanical agitator cost for D-1 and D-6 the Timmerhaus [283] estimation rules and an internet database were used [284].

The cost of the vessels is then calculated, results are given in Table 5-18:

Table 5-18 Reactor and vessels cost

Name	**Weight (kg)**	**Cost (€)**
Reactor	1107.22	25000

Cat. mixer	58.66	10000
Buffer vessel	-	10000
Hold-up vessel	1371.11	22000
Drop tank	-	15000
Other vessel	328.63	12000
Other vessel	1076.6	20000
Total		**114000 €**

The cost of S&T heat exchangers is related to the cost per square metres of exchange surface; following Table 5-19 provided by the industrial partner it is possible to calculate the cost for heat exchangers(Table 5-201)[282]:

Table 5-19 Cost per exchange surface area for S&T heat exchanger

Exchanger area	Exchanger area cost
5-20 m^2	2500 €/m^2
20-25 m^2	1800 €/m^2
25-50 m^2	1000 €/m^2

Table 5-20 Heat Exchangers cost

Name	Exchange Area (m^2)	Cost (€)
Reactor	15	37500
Other	7.9	20000
Cooler	5	12500
Heat recovery	31.4	32000
Tot		**102000 €**

*cost of the impeller estimated with Timmerhaus correlations [283]

The cost of the filters, the jet mixer, the vacuum system and for the pumps is reported in Table 5-23; the cost of the recirculation pump is much higher than the other pumps because this pump requires a special anti-explosion double sealing since hydrogen is fed in the system through this pump.

Table 5-21 Other equipment costs

Name	Cost (€)
Filters	55000

Jet mixer	15000
Vacuum	20000
P-1	20000
P-2	5000
P-3A	7000
P-3B	5000
P-4	5000
P-5	7000
P-6	5000
P-7	5000
Tot	**149000 €**

The total direct costs for the equipment is 365000 €, the cost of the investment is evaluated with the methods present in Timmerhaus et al. [283]. In particular, all the other indirect costs are expressed as a percentage of the equipment cost (Table 5-24).

Table 5-22 Total investment costs distribution following Timmerhaus rules [283]

Investment cost	**€**	
Equipment cost (EC)	365000 €	
Installation cost	36500 €	10% EC
Piping, Instruments and controls	73000 €	20% EC
Electric system	18250 €	5% EC
Total direct costs TDC	**495000 €**	
Engineering, supervision, site	49000	10% TDC
Construction expenses	24750	5% TDC
Total costs direct + indirect	**570000 €**	
Contractor's fee	68500	12% TDC+TIC
Contyngencies	28500	5% TDC+TIC
Working Capital (Total Investment)	**667000 €**	

5.2.4.2. OPEX estimation

In order to estimate the operative costs due to the consummation of utilities some data are reported:

Table 5-23 Costs of utilities

Utility	**Cost**	**m.u.**
Electricity	0.054	€/kWh
Vapor	0.02	€/kg
Hydrogen trough electrolysis	4	€/kg
Catalyst	50	€/kg
Cooling water	0.03	€/m^3

To calculate labor cost the number of operators required was estimated considering 2 operators for every work shift of 8 hours, for 245 shifts/operator/year and a 300 working days/year, 3 shifts/day. Estimating that each operator will receive a salary of 2200 €/month for 12 months/year, the cost of labour is evaluated in Table 5-24:

Table 5-24 Labor cost in one year

Labor Cost	**Cost**	**m.u.**
Labor	200000	€/year
Labor costs per ton produced	55	€/ton

On the same yearly basis the cost of raw materials was estimated [282] and equal to:

Table 5-25 Raw materials costs

Raw material	**Cost**	**m.u.**
Canola oil	650	€/ton

The costs of utilities per ton of hydrogenated oil produced are:

Table 5-26 Product costs

Product costs	**Cost**	**m.u.**
Electricity	1.62	€/$ton_{product}$
Vapor	2	€/$ton_{product}$
Hydrogen trough electrolysis	30	€/$ton_{product}$
Catalyst	100	€/$ton_{product}$
Cooling water	0.09	€/$ton_{product}$
Total	**150**	**€/$ton_{product}$**

It is worth noticing that the production costs in Table 5-26 are conservative values, and the total product cost is 850 €/$ton_{product}$.

For the hydrogenated oil, it was taken as reference the price per ton of high oleic sunflower oil with similar oleic content of fatty acid that is the only product that shares the same market role. The cost of this commodity is actually 1400 €/ton[285], it was decided to use 1200 €/ton as the selling price of the product.

The total revenues produced by the plant and the total costs in one-year activity are listed in Table 5-29:

Table 5-27 Calculation of the modified return on the investment (ROI_m)

Entry		**m.u.**
Sell revenues	4392000	**€**
Costs	3060000	**€**
R-C	**1332000**	**€**
Depreciation (linear 5 years)	133400	**€**
ROI_m= (Net Revenues)/CAPEX	**1.79**	

The modified return on the investment of 1.79 or 179% in a year of plant working, this means that in less than one year the revenues of the hydrogenation plant cover the capital costs (CAPEX) of the plant. This values are in line with other hydrogenation processes.

5.3. Conclusions

In this chapter, it was presented the results of the design and of the economical evaluation analysis for the production of an oleic acid-enriched oil produced from commercial canola oil. The design developed produces yearly 3600 tonnes of enriched vegetable oil and from the economic evaluation results, it was guaranteed the profitability of this process.

The oil produced contains a blend of fatty acids which can be used in the production of azelaic acid of high purity or in the production of fatty acids methyl esters for coatings or surfactants. Although not pure oleic is produced, the oil have a technical grade of C18:1 fatty acid considering fatty acids mixture ($\geq 85\%_{w/w}$ concentration of oleic acid).

From the economic evaluation, apart from the cost of the raw materials which depends on the market selling price (about 50% of the final cost), the main costs are related to the used catalysts, i.e. the high concentration of catalyst/oil. To improve the profitability of the hydrogenation plant, the main road is to reduce

the cost of the catalyst: this can be done by improving the reusability of the catalyst between different batch cycles and the performances of the Cu catalyst.

Chapter 6

General Conclusion

In this PhD thesis, a study on the selective catalytic hydrogenation was carried out; the objective of the work was to develop a catalyst and to design a process for the production of high oleic vegetable oils to be used for many different industrial applications, such as production of lubricants and coatings or the production of azelaic acid, reducing the formation of unwanted by-products.

Many different catalysts, both commercial and synthetized in the laboratory, were characterized and tested in different operating conditions; an overview of the main results for each catalysts is summarized here.

For the commercial Lindlar catalyst it was found that (§3.1 and §4.1):

I. A small surface area related to the low pore area of the support calcium carbonate is observed. Calcium carbonate by XRD is the only phase that it is possible to establish the presence;
II. It is active at 180 °C with high formation of C18:1 (both elaidic and oleic) and low formation of stearic acid (less than 10% at the maximum C18:1 relative percentage); at lower temperature (120 °C), it is less active and more trans C18:1 was formed;
III. The catalyst loses its selectivity at high pressure (12 bar) and high temperature (180 °C).
IV. In one hour of reaction, it is possible to achieve more than 85% of oleic acid relative percentage with content of trans isomers comprised between 10% and15%;
V. The activity of the catalyst was tested in cyclic tests, and although it decreased by every cycle, with a catalyst make-up it is probably reusable over multiple cycles;

VI. The versatility of the application was tested with sunflower oil, and although the Lindlar shows good activity in 6 hours of the tests, it has quite worse selectivity related to the different linolenic and linoleic acid reaction rates.

Laboratory palladium supported on hydrotalcite (Pd/HT) was then produced and characterized (§2.2 and §3.2) and tested (§4.2):

I. The Pd/HT catalyst method proves to be reliable in the synthesis of palladium supported hydrotalcites with the wanted content of Pd (ICP-AES); the materials have the BET surface area, and the shape of isotherms characteristic of hydrotalcites;

II. Pd/HT has lower activity than Lindlar catalyst, longer reaction times are required to obtain the same degree of hydrogenation (IV or conversion of C18:2) at high temperature;

III. At 120 °C the catalyst presents a good combination of both activity and cis/trans selectivity;

IV. Cyclical tests are also investigated and, unlike Lindlar, during the first repeated tests, the catalyst undergoes an activation mechanism probably related to a change in the structure of the hydrotalcites, induced by the combined effect of temperature and pressure, or to an activation of the palladium surface. Post-test characterization does not provide reliable results and a definitive statement about real mechanism is not achieved. After the first test, the catalyst is deactivated more quickly than the Lindlar.

Two different syntheses of silica-supported catalysts were carried out, overall ten different catalysts were produced: hydrolysis-precipitation (HP) and ammonia-evaporation (AE) synthesis methods. These synthesis are generally capable to produce Cu-silica catalysts, and with less extent it is also proved that Ni and Pd catalysts are synthesizable by the same methods as demonstrated:

I. With the exclusion of some singularities with Ni and Pd, ICP-AES (§3.3.1), results acceptably match the desired amount of metal content for all the materials;

II. Texture (§3.3.2) is a common characteristic among monometallic catalysts prepared with HP and AE methods, all the materials present features that are ascribable to mesoporous materials with a large surface area. Although the surface area of materials produced by HP method are higher than those produced by AE one, this is also reflected by pores volume and averaged diameters which are lower for the AE catalysts;

III. XRD (§3.3.3.1) detects with difficulty phases which are formed by the combination of Cu and Si, this is eventually partially resolved by the study of FTIR and Raman spectra (§3.3.3.2) identifying chrysocolla (Cu phyllosilicates). The same trend is also observed for Ni monometallic catalysts: after the heat treatment, a form of Ni silicate (Pimelite) for AE synthesis is found; Pd monometallic catalysts present the Pd in its oxide form;

IV. From a morphological point of view the two synthesis methods give two different external structures, in particular the AE synthesis seems to be formed by smooth lamellae-like structures while the HP one is much more porous as also observed by SEM (§3.3.7.1). TEM images, on the other hand, show that in HP synthesis some crystals with average size lower than 5 nm are identifiable, AE materials is more uniform and less structure is found. Essential information are found on the metals distribution which appears to be well spread on the support.

The catalysts are analysed after reduction and lead to the following results:

I. TPR (§3.3.5.1) results show that monometallic materials present a single H_2 consumption peak for all the samples, independently of the synthesis method. This peak is in the range reported in the literature for the reduction of the metal oxide precursors. The Cu area was studied by chemisorption of N_2O and highlighted higher area, and so higher dispersion, for HP samples than for AE samples;

II. XRD after reduction of copper catalysts, shows the contemporary presence of both metallic copper and Cu_2O, with different respective proportions depending on the synthesis method, in particular AE method materials contain higher amount of metallic Cu. Monometallic palladium and nickel samples show, after reduction, metallic Pd and Ni, respectively;

III. The same conclusions obtained from XRD are also found by XPS on reduced materials (§3.3.6): different ratios are observed between metallic Cu and Cu_2O on the catalysts surface;

IV. After reduction morphology highlights small crystals of active phase which are well distributed and have average dimensions lower than 7 nm for both syntheses.

Bimetallic catalysts are also studied and give interesting and unique features:

I. ICP-AES results for bimetallic materials indicate that the Cu content is lower than expected (§3.3.1). This is associated with the different conditions used during synthesis of monometallic Cu samples and

bimetallic ones, in particular the pH is chosen as a compromise between the best pH value for the two metals;

II. XRD of as-synthesized materials are similar to the monometallic ones, with a contingent difference for Cu-Pd: the XRD rays are shifted by the effect of PdO introduction in the CuO structure. A similar effect was observed for the reduced samples with the formation of CuPd structure, it must be specified that for the HP method, this CuPd is more evident;

III. Reduction temperatures of the bimetallic materials are higher for Cu than the corresponding monometallic Cu, indicating higher interaction with the support. However, the copper surface areas are in line with the values obtained with monometallic Cu catalysts;

IV. Bimetallic catalysts share the same XPS features with Pd and Ni monometallic ones; for Cu-Pd, the content of Cu^0 over Cu^+ is more evident probably due to the CuPd structures;

V. At last, the morphological characteristics of these materials do not deviate too much from the features found in monometallic materials; it is important to say that it is practically impossible to differentiate Cu and Ni or Cu and Pd with in-situ EDS analysis or by some morphological feature.

All these catalysts being tested, and some considerations are extrapolated (§4.3):

I. In all tested conditions copper catalysts shown worse conversion of linolenic and linoleic acid, although better results in terms of selectivity both in oleic acid production (high S_{Le}) and cis/trans isomers obtained (§4.3.1, §4.3.2 and §4.3.3);

II. The effect of temperature is important in both synthesized families, and a slightly higher temperature than 180 °C is required to increase the catalyst activity. However, the pressure effect is not extremely relevant, at least for Cu10SiO_2HP. This makes possible to work at lower pressure (4 bar) and still obtain conversion of linoleic higher than 75% (§4.3.1);

III. The conversion reaches high values (up to 90% for C18:3 and 80% for C18:2) when the amount of catalyst is increased from 4 $mg_{catalyst}/mL_{oil}$ to 8 $mg_{catalyst}/mL_{oil}$, the required reaction time to carry out the tests is of 3 hours (§4.3.2);

IV. The amount of elaidic acid for all the conditions is lower than 23%, and for a lower pressure 4 bar and high temperature 200 °C its maximum is at 13%.

At last, the bimetallic and the corresponding monometallic catalysts were tested, but the desired increase in activity for which they were developed is not obtained. The main results can be summarised as (§4.3.4):

V. Both the 1% palladium on silica synthesized with AE method and HP method, $Pd1SiO_2AE$ and $Pd1SiO_2HP$, are largely more active than Pd/HT and Lindlar catalyst with poor selectivity. Hydrogenation rates of linoleic and oleic acid are very close, giving rise to large amount of both elaidic and stearic acid;

VI. $Ni5SiO_2AE$ is subject to the same problems as $Pd1SiO_2AE$. However, after the reaction lesser amount of trans isomers is found, but greater amount of stearic acid. The bi-metallic Cu-Ni has characteristics similar to the monometallic ones;

VII. Ni and Cu-Ni catalysts, synthesized via HP method are not active, probably due to not complete reduction in the fixed bed reactor;

VIII. Eventually, Cu-/Pd catalysts produce conversions lower than the Pd and Cu ones; nevertheless, $Cu10Pd1SiO_2AE$ has a good selectivity to cis/trans isomers and it is tested in a wider experimental campaign. The results of the campaign highlighted that the catalyst has similar characteristics at 180 °C and 200 °C, but the increase in temperature up to 240 °C leads to a change in the catalyst mechanism, producing large amount of stearic acid and elaidic acid in a short time reaction, losing the selectivity recorded at 180 °C and 4 bar.

Among all catalysts, the copper on silica catalyst synthetized with HP synthesis was individuated to be the best candidate for an industrial application and so a preliminary process and feasibility design was carried out.

It was chosen to develop a semi-continuous process in order to have the advantages of both selectivity of batch reactor and the lower operative costs of continuous operation. The hydrogenation reactor was a batch loop reactor which converts canola oil or fatty acids produced from the canola oil, the operation is carried out in isotherm conditions to maintain the selectivity of the catalyst, the heat of reaction was used for the production of low-pressure steam. As first hypothesis the catalyst is recovered and reused in 5 cycles (a working day).

It was demonstrated the economic feasibility of the process in these conditions.

All the thesis permits to highlight some important points of interest that must be studied in future works:

I. The catalyst reusability is a key point for the economic feasibility of the whole process, it must be addressed and some tests with $Cu10SiO_2HP$ with recovery will be carried out;

II. Obviously increasing the catalyst yield permits to increase further the revenues of this process, augmenting copper catalyst yield must be a focal point of further research;

III. Study of more active catalyst must be carried out to improve the process: the synthesis of bimetallic catalysts although did not give the wanted characteristic could be changed maybe introducing one by one the other metals. Other metals should be taken into account and also Pd and Ni used in lower amounts (mostly nickel);

IV. Also, other supports should be addressed in particular zeolites and other structured materials could be of interest for the catalyst for industrial applications in order to overcome intraparticle diffusion problems.

Although not extremely active for the intrinsic characteristics of copper, it seems the best solution from an economic point of view over Pd.

Future studies should also be focused on the modelling of both the kinetic and the mass transfer design of the hydrogenation reactor. Another point could be the CFD modelling of the loop reactor validating the model results with tests carried out with a laboratory-scale loop reactor.

References

[1] Ravasio N, Zaccheria F, Gargano M, Recchia S, Fusi A, Poli N, et al. Environmental friendly lubricants through selective hydrogenation of rapeseed oil over supported copper catalysts. Appl Catal A Gen 2002;233:1–6. doi:10.1016/S0926-860X(02)00128-X.

[2] Zaccheria F, Psaro R, Ravasio N. Selective hydrogenation of alternative oils: a useful tool for the production of biofuels. Green Chem 2009;11:462. doi:10.1039/b817625f.

[3] Pérez-Cadenas AF, Zieverink MMP, Kapteijn F, Moulijn JA. Selective hydrogenation of fatty acid methyl esters on palladium catalysts supported on carbon-coated monoliths. Carbon N Y 2006;44:173–6. doi:10.1016/j.carbon.2005.08.014.

[4] Jovanovic D, Radovic R, Mares L, Stankovic M, Markovic B. Nickel hydrogenation catalyst for tallow hydrogenation and for the selective hydrogenation of sunflower seed oil and soybean oil. Catal Today 1998;43:21–8. doi:10.1016/S0920-5861(98)00133-3.

[5] IUPAC AOAC. AOAC Official Method 969.33 Fatty Acids in Oils and Fats: Preparation of Methyl Esters Boron Trifluoride Method 2000:2000.

[6] Di Nicola A, Arcadi A, Gallucci K, Mucciante V, Rossi L. Hydrotalcite-supported palladium nanoparticles as catalysts for the hydroarylation of carbon–carbon multiple bonds. New J Chem 2018;42:1952–7. doi:10.1039/C7NJ04046F.

[7] Zhao Y, Li S, Wang Y, Shan B, Zhang J, Wang S, et al. Efficient tuning of surface copper species of Cu/SiO2 catalyst for hydrogenation of dimethyl oxalate to ethylene glycol. Chem Eng J 2017;313:759–68. doi:10.1016/J.CEJ.2016.12.027.

[8] Liang-Feng C, Ping-Jun G, Ming-Hua Q, Shi-Run Y, He-Xing L, Wei S, et al. Cu/SiO2 catalysts prepared by the ammonia-evaporation method: Texture, structure, and catalytic performance in hydrogenation of dimethyl oxalate to ethylene glycol. J Catal 2008;257:172–80. doi:10.1016/J.JCAT.2008.04.021.

[9] Butler CD. Climate Change, Health and Existential Risks to Civilization: A Comprehensive Review (1989–2013). Int J Environ Res Public Health 2018;15. doi:10.3390/IJERPH15102266.

[10] UNFCC. COP24 SPECIAL REPORT - HEALTH & CLIMATE CHANGE. 2018.

[11] Leading Health Organizations Rally Around Call to Action to Protect People's Health from Climate Change - Public Health Institute n.d. https://www.phi.org/news-events/1494/leading-health-organizations-rally-around-call-to-action-to-protect-peoples-health-from-climate-change (accessed July 6, 2019).

[12] Murtaugh PA, Schlax MG. Reproduction and the carbon legacies of individuals. Glob Environ Chang

2009;19:14–20. doi:10.1016/J.GLOENVCHA.2008.10.007.

[13] Di Giuliano A. Synthesis, characterization and industrial applicability of Combined Sorbent.Catalyst Materials for Sorption Enhanced Steam Methane Reforming. Università degli studi dell'Aquila /Université de Strasbourg, 2017.

[14] McDougall I, Brown FH, Fleagle JG. Stratigraphic placement and age of modern humans from Kibish, Ethiopia. Nature 2005;433:733–6. doi:10.1038/nature03258.

[15] Gettelman A, Rood RB. Climate Change and Global Warming, Springer, Berlin, Heidelberg; 2016, p. 23–35. doi:10.1007/978-3-662-48959-8_3.

[16] Zhen-shan Li, Ning-sheng C, Huang Y. Effect of Preparation Temperature on Cyclic CO2 Capture and Multiple Carbonation−Calcination Cycles for a New Ca-Based CO2 Sorbent 2006. doi:10.1021/IE051211L.

[17] Santer BD, Taylor KE, Wigley TML, Johns TC, Jones PD, Karoly DJ, et al. A search for human influences on the thermal structure of the atmosphere. Nature 1996;382:39–46. doi:10.1038/382039a0.

[18] Fuso Nerini F, Sovacool B, Hughes N, Cozzi L, Cosgrave E, Howells M, et al. Connecting climate action with other Sustainable Development Goals. Nat Sustain 2019;2:674–80. doi:10.1038/s41893-019-0334-y.

[19] Beckage B, Gross LJ, Lacasse K, Carr E, Metcalf SS, Winter JM, et al. Linking models of human behaviour and climate alters projected climate change. Nat Clim Chang 2018;8:79–84. doi:10.1038/s41558-017-0031-7.

[20] Fang J, Yu G, Liu L, Hu S, Chapin FS. Climate change, human impacts, and carbon sequestration in China. Proc Natl Acad Sci U S A 2018;115:4015–20. doi:10.1073/pnas.1700304115.

[21] Creutzig F, Roy J, Lamb WF, Azevedo IML, Bruine de Bruin W, Dalkmann H, et al. Towards demand-side solutions for mitigating climate change. Nat Clim Chang 2018;8:260–3. doi:10.1038/s41558-018-0121-1.

[22] Robin L. Environmental humanities and climate change: understanding humans geologically and other life forms ethically. Rev Clim Chang 2018;9:499. doi:10.1002/wcc.499.

[23] Lewandowsky S, Gignac GE, Vaughan S. The pivotal role of perceived scientific consensus in acceptance of science. Nat Clim Chang 2013;3:399–404. doi:10.1038/nclimate1720.

[24] Hartter J, Hamilton LC, Boag AE, Stevens FR, Ducey MJ, Christoffersen ND, et al. Does it matter if people think climate change is human caused? Clim Serv 2018;10:53–62. doi:10.1016/J.CLISER.2017.06.014.

[25] Cramer W, Guiot J, Fader M, Garrabou J, Gattuso J-P, Iglesias A, et al. Climate change and interconnected risks to sustainable development in the Mediterranean. Nat Clim Chang 2018;8:972–80. doi:10.1038/s41558-018-0299-2.

[26] Li J, Chen YD, Gan TY, Lau N-C. Elevated increases in human-perceived temperature under climate warming. Nat Clim Chang 2018;8:43–7. doi:10.1038/s41558-017-0036-2.

[27] Mitchell JFB. The "Greenhouse" effect and climate change. Rev Geophys 1989;27:115. doi:10.1029/RG027i001p00115.

[28] Rubino M, Etheridge DM, Thornton DP, Howden R, Allison CE, Francey RJ, et al. Revised records of atmospheric trace gases over the last 2000 years from Law Dome, Antarctica. Earth Syst Sci Data 2019;11:473–92. doi:10.5194/essd-11-473-2019.

[29] Carbon Dioxide Information Analysis Center (CDIAC) n.d. https://cdiac.ess-dive.lbl.gov/ (accessed

October 4, 2019).

[30] Change IP on C. Technical Summary. In: Intergovernmental Panel on Climate Change, editor. Clim. Chang. 2013 - Phys. Sci. Basis, Cambridge: Cambridge University Press; 2014, p. 31–116. doi:10.1017/CBO9781107415324.005.

[31] COP24 | KATOWICE n.d. http://www.cop24.katowice.eu/ (accessed January 24, 2019).

[32] Edenhofer, O. R, Pichs-Madruga, Y. Sokona, E. Farahani, S. Kadner, K. Seyboth, A. Adler, I. Baum, S. Brunner, P. Eickemeier, B. Kriemann J, Savolainen, S. Schlömer C von S. Climate Change 2014: Mitigation of Climate Change. Contribution of Working Group III to the Fifth Assessment Report of the Intergovernmental Panel on Climate Change. IPCC, 2014. Cambridge University Press; n.d.

[33] Hall-Spencer JM, Rodolfo-Metalpa R, Martin S, Ransome E, Fine M, Turner SM, et al. Volcanic carbon dioxide vents show ecosystem effects of ocean acidification. Nature 2008;454:96–9. doi:10.1038/nature07051.

[34] Orr JC, Fabry VJ, Aumont O, Bopp L, Doney SC, Feely RA, et al. Anthropogenic ocean acidification over the twenty-first century and its impact on calcifying organisms. Nature 2005;437:681–6. doi:10.1038/nature04095.

[35] Guinotte JM, Fabry VJ. Ocean Acidification and Its Potential Effects on Marine Ecosystems. Ann N Y Acad Sci 2008;1134:320–42. doi:10.1196/annals.1439.013.

[36] Trusel LD, Das SB, Osman MB, Evans MJ, Smith BE, Fettweis X, et al. Nonlinear rise in Greenland runoff in response to post-industrial Arctic warming. Nature 2018;564:104–8. doi:10.1038/s41586-018-0752-4.

[37] Tollefson J. Greenland is losing ice at fastest rate in 350 years. Nat 2019 2018.

[38] Rignot E, Mouginot J, Scheuchl B, van den Broeke M, van Wessem MJ, Morlighem M. Four decades of Antarctic Ice Sheet mass balance from 1979-2017. Proc Natl Acad Sci U S A 2019;116:1095–103. doi:10.1073/pnas.1812883116.

[39] Witze A. Dramatic sea-ice melt caps tough Arctic summer. Nature 2019;573:320–1. doi:10.1038/d41586-019-02653-x.

[40] Haeberli W, Hoelzle M, Paul F, Zemp M. Integrated monitoring of mountain glaciers as key indicators of global climate change: the European Alps. Ann Glaciol 2007;46:150–60. doi:10.3189/172756407782871512.

[41] Raina VK. Himalayan glaciers: a state-of-art review of glacial studies, glacial retreat and climate change. Himal Glaciers a State-of-Art Rev Glacial Stud Glacial Retreat Clim Chang 2009.

[42] Oerlemans J. Sensitivity of Glaciers and Small Ice Caps to Greenhouse Warming. Science (80-) 1994;258:115–7. doi:10.1126/science.258.5079.115.

[43] Cohen J. Snow cover and climate. Weather 1994;49:150–6. doi:10.1002/j.1477-8696.1994.tb05997.x.

[44] Gornitz V, Oppenheimer M, Kopp R, Orton P, Buchanan M, Lin N, et al. New York City Panel on Climate Change 2019 Report Chapter 3: Sea Level Rise. Ann N Y Acad Sci 2019;1439:71–94. doi:10.1111/nyas.14006.

[45] Roxburgh N, Guan D, Shin KJ, Rand W, Managi S, Lovelace R, et al. Characterising climate change discourse on social media during extreme weather events. Glob Environ Chang 2019;54:50–60. doi:10.1016/J.GLOENVCHA.2018.11.004.

[46] Maxwell SL, Butt N, Maron M, McAlpine CA, Chapman S, Ullmann A, et al. Conservation implications of ecological responses to extreme weather and climate events. Divers Distrib

2019;25:613–25. doi:10.1111/ddi.12878.

[47] ORGANISATION FOR ECONOMIC CO-OPERATION AND DEVELOPMENT. OECD Environmental Outlook for the Chemicals Industry. 2001.

[48] Lebreton L, Andrady A. Future scenarios of global plastic waste generation and disposal. Palgrave Commun 2019;5:6. doi:10.1057/s41599-018-0212-7.

[49] Lebreton LCM, van der Zwet J, Damsteeg J-W, Slat B, Andrady A, Reisser J. River plastic emissions to the world's oceans. Nat Commun 2017;8:15611. doi:10.1038/ncomms15611.

[50] Kaza S, Yao L, Bhada-Tata P, Van Woerden F. What a Waste 2.0: A Global Snapshot of Solid Waste Management to 2050. The World Bank; 2018. doi:10.1596/978-1-4648-1329-0.

[51] UNFCC. Katowice Climate Change Conference – December 2018 | UNFCCC n.d. https://unfccc.int/katowice (accessed January 24, 2019).

[52] http://www.cop24.katowice.eu/# n.d. http://www.cop24.katowice.eu/# (accessed January 24, 2019).

[53] Search Results - OECD n.d. http://www.oecd.org/general/searchresults/?q=bio-plastic&cx=012432601748511391518:xzeadub0b0a&cof=FORID:11&ie=UTF-8 (accessed January 24, 2019).

[54] OECD Policy Paper no.12. Improving Plastics Management: Trends, policy responses and the role of international co-operation and trade. 2018. doi:10.1126/sciadv.1700782.

[55] Mulvaney D, Gibbs BJ. Green Metrics. vol. 11. WILEY-VCH; 2012. doi:10.4135/9781412975704.n61.

[56] Lieberman D, Doherty from the Center for Resource Solutions S. Commission for Environmental Cooperation Renewable Energy as a Hedge Against Fuel Price Fluctuation How to Capture the Benefits. 2018.

[57] Anastas PT, Warner JC. Green Chemistry: Theory and practice. Oxford: Oxford University Press; 1998.

[58] Gunstone FD, Padley FB. Lipid Technologies and Applications. 1st editio. Marcel Dekker, Inc.; 1997.

[59] Knothe G, Derksen JTP. Recent developments in the synthesis of fatty acid derivatives. AOCS Press; 1999.

[60] Gui MM, Lee KT, Bhatia S, Gui MM, Lee KT, Bhatia S. Feasibility of edible oil vs. non-edible oil vs. waste edible oil as biodiesel feedstock. Energy 2008;33:1646–53.

[61] Leung DYC, Wu X, Leung MKH. A review on biodiesel production using catalyzed transesterification. Appl Energy 2009;87:1083–95. doi:10.1016/j.apenergy.2009.10.006.

[62] Cogollo-Herrera K, Lombana-Carmona S, Bonilla-Correa D, Peralta-Ruiz Y. Evaluation of Biodiesel Production Process from Sapium Tree Oil Sebiferum using Exergy Analysis Methodology. Chem Eng Trans 2015;43:463–8. doi:10.3303/CET1543078.

[63] Ashraful AM, Masjuki HH, Kalam MA, Fattah IMR, Imtenan S, Shahir SA, et al. Production and comparison of fuel properties, engine performance, and emission characteristics of biodiesel from various non-edible vegetable oils: A review 2014. doi:10.1016/j.enconman.2014.01.037.

[64] Romero MJA, Pizzi A, Toscano G, Bosio B, Arato E. Study of an Innovative Process for the Production of Biofuels using Non-edible Vegetable Oils. Chem Eng Trans 2014;37:883–8. doi:10.3303/CET1437148.

[65] Gunstone FD. The chemistry of oils and fats : sources, composition, properties and uses. 2nd ed. Blackwell; 2004.

[66] Taylor DC, Smith MA, Fobert P, Mietkiewska E, Weselake RJ. Metabolic Engineering of Higher Plants to Produce Bio-Industrial Oils. In: Murray M-Y, editor. Compr. Biotechnol. 2nd ed., Academic Press Elsevier; 2011, p. 67–85. doi:10.1016/B978-0-08-088504-9.00256-7.

[67] Montero de Espinosa L, Meier MAR. Plant oils: The perfect renewable resource for polymer science?! Eur Polym J 2011;47:837–52. doi:10.1016/j.eurpolymj.2010.11.020.

[68] IHS Markit. Major Fats and Oils Industry Overview - Chemical Economics Handbook (CEH) | IHS Markit. n.d.

[69] Berenblyum AS, Danyushevsky VY, Kuznetsov PS, Katsman EA, Shamsiev RS. Catalytic methods for the manufacturing of high-production volume chemicals from vegetable oils and fats (review). Pet Chem 2016;56:663–71. doi:10.1134/S0965544116080028.

[70] Oleic Acid Market, market research reports, market insights, future market insights n.d. https://www.futuremarketinsights.com/reports/oleic-acid-market (accessed January 24, 2019).

[71] Home - Task 42 n.d. http://task42.ieabioenergy.com/ (accessed January 24, 2019).

[72] Jean-Louis Hérisson P, Chauvin Y. Catalyse de transformation des oléfines par les complexes du tungstène. II. Télomérisation des oléfines cycliques en présence d'oléfines acycliques. Die Makromol Chemie 1971;141:161–76. doi:10.1002/macp.1971.021410112.

[73] Chatterjee AK, Choi T-L, Sanders DP, Grubbs RH. A General Model for Selectivity in Olefin Cross Metathesis. J Am Chem Soc Artic 2003;125:11360–70. doi:10.1021/ja0214882.

[74] Schrock RR. Multiple Metal–Carbon Bonds for Catalytic Metathesis Reactions (Nobel Lecture). Angew Chemie Int Ed 2006;45:3748–59. doi:10.1002/anie.200600085.

[75] Grubbs RH, Wenzel AG. Handbook of metathesis. Volume 1, Catalyst development and mechanism. n.d.

[76] Lligadas G, Ronda JC, Galià M, Cádiz V. Renewable polymeric materials from vegetable oils: a perspective. Mater Today 2013;16:337–43. doi:10.1016/J.MATTOD.2013.08.016.

[77] Lawate SS, Lal K. US 339821 High oleic polyol esters, compositions and lubricants functional fluids and greases containing the same, 1995.

[78] Heidbreder A, Gruetzmacher R, Nagorny U, Westfechtel A. METHOD OF PREPARING CASTING AND (86) PCT No.: PCT/EP97/06054 COATING COMPOSITIONS USING POLYOLS DERVED FROM HIGH OLEC (30) Foreign Application Priority Data ACID CONTENT FATTY ACID MIXTURES, 1996.

[79] MacKenzie SL, Taylor DC. Seed oils for the future 1992.

[80] Erhan SZ, Sharma BK, Perez JM. Oxidation and low temperature stability of vegetable oil-based lubricants. Ind Crops Prod 2006;24:292–9. doi:10.1016/J.INDCROP.2006.06.008.

[81] Behr A, Westfechtel A, Pérez Gomes J. Catalytic processes for the technical use of natural fats and oils. Chem Eng Technol 2008;31:700–14. doi:10.1002/ceat.200800035.

[82] Frankel EN. Lipid oxidation. 2nd editio. Oily Press; 2005.

[83] Smith LI. Fatty Acids, Their Chemistry and Physical Properties. By K. S. Markley. J Phys Colloid Chem 1947;51:1450–1. doi:10.1021/j150456a020.

[84] Trasarti AF, Segobia DJ, Apesteguía CR, Santoro F, Zaccheria F, Ravasio N. Selective Hydrogenation of Soybean Oil on Copper Catalysts as a Tool Towards Improved Bioproducts. J Am Oil Chem Soc 2012;89:2245–52. doi:10.1007/s11746-012-2119-6.

[85] Knothe G. “Designer” Biodiesel: Optimizing Fatty Ester Composition to Improve Fuel Properties. Energy & Fuels 2008;22:1358–64. doi:10.1021/ef700639e.

[86] Moser BR, Haas MJ, Winkler JK, Jackson MA, Erhan SZ, List GR. Evaluation of partially hydrogenated methyl esters of soybean oil as biodiesel. Eur J Lipid Sci Technol 2007;109:17–24. doi:10.1002/ejlt.200600215.

[87] Bouriazos A, Mouratidis K, Psaroudakis N, Papadogianakis G. Catalytic Conversions in Aqueous Media. Part 2. A Novel and Highly Efficient Biphasic Hydrogenation of Renewable Methyl Esters of Linseed and Sunflower Oils to High Quality Biodiesel Employing Rh/TPPTS Complexes. Catal Letters 2008;121:158–64. doi:10.1007/s10562-007-9314-3.

[88] Behr A, Westfechtel A, Pérrez Gomes J. Catalytic processes for the technical use of natural fats and oils. Chem Eng Technol 2008;31:700–14. doi:10.1002/ceat.200800035.

[89] Liu W, Tian F, Yu J, Bi Y. Magnetic Mesopourous Palladium Catalyzed Selective Hydrogenation of Sunflower Oil. J Oleo Sci 2016;15:1–8. doi:10.5650/jos.ess15169.

[90] Dijkstra AJ. Kinetics and mechanism of the hydrogenation process - the state of the art. Eur J Lipid Sci Technol 2012;114:985–98. doi:10.1002/ejlt.201100405.

[91] Normann Wilhelm. GB190301515 (A) - Process for Converting Unsaturated Fatty Acids or their Glycerides into Saturated Compounds. GB190301515, 1903.

[92] List GR, King JW. Hydrogenation of fats and oils : theory and practice. 2nd editio. Academic Press Elsevier and AOCS Press; 2015.

[93] Horiuti I, Polanyi M. Exchange reactions of hydrogen on metallic catalysts. Trans Faraday Soc 1934;30:1164. doi:10.1039/tf9343001164.

[94] Veldsink JW, Bouma MJ, Schöön NH, Beenackers AACM. Heterogeneous Hydrogenation of Vegetable Oils: A Literature Review. Catal Rev 1997;39:253–318. doi:10.1080/01614949709353778.

[95] Applewhite TH. Nutritional effects of hydrogenated soya oil. J Am Oil Chem Soc 1981;58:260–9. doi:10.1007/BF02582353.

[96] Dijkstra AJ. Revisiting the formation oftrans isomers during partial hydrogenation of triacylglycerol oils. Eur J Lipid Sci Technol 2006;108:249–64. doi:10.1002/ejlt.200500335.

[97] Dietz A, Julcour C, Wilhelm A., Delmas H. Selective hydrogenation in trickle-bed reactor: experimental and modelling including partial wetting. Catal Today 2003;79:293–305. doi:10.1016/S0920-5861(03)00053-1.

[98] Wright AJ, Mihele AL, Diosady LL. Cis selectivity of mixed catalyst systems in canola oil hydrogenation. Food Res Int 2003;36:797–804. doi:10.1016/S0963-9969(03)00074-7.

[99] Bernas A, Myllyoja J, Salmi T, Murzin DY. Kinetics of linoleic acid hydrogenation on Pd/C catalyst. Appl Catal A Gen 2009;353:166–80. doi:10.1016/J.APCATA.2008.10.059.

[100] Koritala S, Selke E, Dutton HJ. Deuteration of Methyl Linoleate with Nickel, Palladium, Platinum and Copper-Chromite Catalysts. JAOCS, J Am Oil Chem Soc 1973;50:310–6.

[101] Nielsen K, Hansen HJM, Nielsen VR. Selectivity in the Hydrogenation of Oleic-Linoleic Acid Oils with Commercial Nickel Catalysts. J Am Chem Soc Artic 1960;37:271–4.

[102] Krstić J, Gabrovska M, Lončarević D, Nikolova D, Radonjić V, Vukelić N, et al. Influence of Ni/SiO2 activity on the reaction pathway in sunflower oil hydrogenation. Chem Eng Res Des 2015;100:72–80. doi:10.1016/j.cherd.2015.05.001.

[103] Veldsink JW, Bouma MJ, Schöön NH, Beenackers AA. Heterogeneous Hydrogenation of Vegetable Oils : A literature Review. Catal Rev Sci Eng 1997;39:253–381. doi:10.1080/01614949709353778.

[104] Simakova IL, Simakova OA, Romanenko A V, Murzin DY. Hydrogenation of Vegetable Oils over Pd on Nanocomposite Carbon Catalysts. Ind Eng Chem 2008;47:7219–25. doi:10.1021/ie800663j.

[105] Irandoust S, Edvardsson J. Poisoning of Nickel-Based Catalysts in Fat Hydrogenation. vol. 70. 1993.

[106] Koritala S, Butterfield RO, Dutton HJ. Selective hydrogenation with copper catalysts: II. Kinetics. J Am Oil Chem Soc 1970;47:266–8. doi:10.1007/BF02609489.

[107] Vigneron PY, Koritala S, Butterfield RO, Dutton HJ. Kinetics of copper-chromite hydrogenation in soybean and linseed oils: Effect of pressure. J Am Oil Chem Soc 1972;49:371–5. doi:10.1007/BF02633392.

[108] Dijkstra AJ. On the mechanism of the copper-catalysed hydro-genation; a reinterpretation of published data. Eur J Lipid Sci Technol 2002;104:29–35. doi:10.1002/1438-9312(200201)104:1<29::AID-EJLT29>3.0.CO;2-O.

[109] Mounts TL, Koritala S, Friedrich JP, Dutton HJ. Selective hydrogenation of soybean oil: IX. Effect of pressure in copper catalysis. J Am Oil Chem Soc 1978;55:402–6. doi:10.1007/BF02911901.

[110] Koritala S, Friedrich JP, Mounts TL. Selective hydrogenation of soybean oil: X. Ultra high pressure and low pressure. J Am Oil Chem Soc 1980;57:1–5. doi:10.1007/BF02675514.

[111] Zaccheria F, Psaro R, Ravasio N. Selective hydrogenation of alternative oils: a useful tool for the production of biofuels. Green Chem 2009;11:462–5. doi:10.1039/b817625f.

[112] Okkerse C, de Jonge A, Coenen JWE, Rozendaal A. Selective hydrogenation of soybean oil in the presence of copper catalysts. J Am Oil Chem Soc 1967;44:152–6. doi:10.1007/BF02558177.

[113] Koritala S, Dutton HJ. Selective hydrogenation of soybean oil. II. Copper-chromium catalysts. J Am Oil Chem Soc 1966;43:556–8. doi:10.1007/BF02679872.

[114] Johansson LE. Copper catalysts in the selective hydrogenation of soybean and rapeseed oils: IV. Copper on silica gel, phase composition and preparation. J Am Oil Chem Soc 1980;57:16–22. doi:10.1007/BF02675518.

[115] Yang R, Su M, Li M, Zhang J, Hao X, Zhang H. One-pot process combining transesterification and selective hydrogenation for biodiesel production from starting material of high degree of unsaturation. Bioresour Technol 2010;101:5903–9. doi:10.1016/j.biortech.2010.02.095.

[116] Philippaerts A, Jacobs P, Sels B. Catalytic Hydrogenation of Vegetable Oils. In: Rinaldi R, editor. Catal. Hydrog. Biomass Valorization. 1st ed., Royal Society of Chemistry RSC Energy and Environment Series; n.d., p. 223–41. doi:10.1039/9781782620099-00223.

[117] Hashimoto K, Teramoto M, Nagata S. Effect of mass transfer on the selectivity in the hydrogenation of fatty oils. J Chem Eng Japan 1971;4:150–5. doi:10.1252/jcej.4.150.

[118] Colen GCM, Van Duijn G, Van Oosten HJ. Effect of pore diffusion on the triacylglycerol distribution of partially hydrogenated trioleoylglycerol. Appl Catal 1988;43:339–50. doi:10.1016/S0166-9834(00)82736-0.

[119] Cordova WA, Harriott P. Mass transfer resistances in the palladium-catalyzed hydrogenation of methyl linoleate. Chem Eng Sci 1975;30:1201–6. doi:10.1016/0009-2509(75)85040-8.

[120] Stenberg O, Schöön N-H. Aspects of the graphical determination of the volumetric mass-transfer coefficient (kLa) in liquid-phase hydrogenation in a slurry reactor. Chem Eng Sci 1985;40:2311–9. doi:10.1016/0009-2509(85)85134-4.

[121] Yagi H, Yoshida F. Gas Absorption by Newtonian and Non-Newtonian Fluids in Sparged Agitated Vessels. Ind Eng Chem Process Des Dev 1975;14:488–93. doi:10.1021/i260056a024.

[122] Susu AA. Kinetics, mass transfer and scale-up in nickel-catalyzed oil hydrogenators. Appl Catal 1982;4:307–20. doi:10.1016/0166-9834(82)80130-9.

[123] Dietrich E, Mathieu C, Delmas H, Jenck J. Raney-nickel catalyzed hydrogenations: Gas-liquid mass transfer in gas-induced stirred slurry reactors. Chem Eng Sci 1992;47:3597–604. doi:10.1016/0009-2509(92)85075-M.

[124] Beenackers AACM, Van Swaaij WPM. Mass transfer in gas—liquid slurry reactors. Chem Eng Sci 1993;48:3109–39. doi:10.1016/0009-2509(93)80199-Z.

[125] Veldsink JW, Bouma MJ, Schöön NH, Beenackers AACM. Heterogeneous Hydrogenation of Vegetable Oils: A Literature Review. Catal Rev 1997;39:253–318. doi:10.1080/01614949709353778.

[126] Bern L, Hell M, Schöön NH. Kinetics of hydrogenation of rapeseed oil: I. Influence of transport steps in kinetic study. J Am Oil Chem Soc 1975;52:182–7. doi:10.1007/BF02672166.

[127] Westerterp KR, Swaaij WPM van., Beenackers AACM, Kramers H. Chemical reactor design and operation. 2nd editio. Wiley; 1984.

[128] Numwong N, Luengnaruemitchai A, Chollacoop N, Yoshimura Y. Effect of Metal Type on Partial Hydrogenation of Rapeseed Oil-Derived FAME. J Am Oil Chem Soc 2013;90:1431–8. doi:10.1007/s11746-013-2276-2.

[129] Behr A, Doering N, Kozik C, Schmidtke H, Durowicz S. Preparation of singly unsaturated fatty acid or derivate by hydrogenating poly-unsaturated fatty acid or derivatives on catalyst containing palladium salt and nitrogenous aprotic solvent as activator 1990.

[130] Behr A, Döring N, Durowicz-Heil S, Ellenberg B, Kozik C, Lohr C, et al. Selektive Härtung mehrfach ungesättigter Fettsäuren in der Flüssigphase. Fett Wiss Technol Sci Technol 1993;95:2–12. doi:10.1002/lipi.19930950103.

[131] Wright AJ, Mihele AL, Diosady LL. Cis selectivity of mixed catalyst systems in canola oil hydrogenation. Food Res Int 2003;36:797–804. doi:10.1016/S0963-9969(03)00074-7.

[132] Rubin LJ, Köseoglu SS, Diosady LL, Graydon WF. Hydrogenation of canola oil in the presence of nickel and the methyl benzoate-chrome carbonyl complex. J Am Oil Chem Soc 1986;63:1551–7. doi:10.1007/BF02553083.

[133] List GR, Neff WE, Holliday RL, King JW, Holser R. Hydrogenation of soybean oil triglycerides: Effect of pressure on selectivity. J Am Oil Chem Soc 2000;77:311–4. doi:10.1007/s11746-000-0050-4.

[134] Eller FJ, List GR, Teel JA, Steidley KR, Adlof RO. Preparation of Spread Oils Meeting U.S. Food and Drug Administration Labeling Requirements for Trans Fatty Acids via Pressure-Controlled Hydrogenation. J Agric Food Chem 2005;53:5982–4. doi:10.1021/JF047849+.

[135] Beers AEWB. Low trans hydrogenation of edible oils. Lipid Technol 2007;19:56–8. doi:10.1002/lite.200600019.

[136] Cabrera MI, Grau RJ. Advanced Concepts for the Kinetic Modeling of Fatty Acid Methyl Esters Hydrogenation. Int J Chem React Eng 2008;6:1–37. doi:10.2202/1542-6580.1718.

[137] Belkacemi K, Hamoudi S. Low Trans and Saturated Vegetable Oil Hydrogenation over Nanostructured Pd/Silica Catalysts: Process Parameters and Mass-Transfer Features Effects. Ind Eng Chem Res 2009;48:1081–9. doi:10.1021/ie800559v.

[138] Boyes AP, Chugtai A, Khan Z, Raymahasay S, Sulidis AT, Winterbottom JM. The cocurrent downflow

contactor (CDC) as a fixed bed and slurry reactor for catalytic hydrogenation. J Chem Technol Biotechnol 1995;64:55–65. doi:10.1002/jctb.280640110.

[139] Cheng HN, Dowd MK, Easson MW, Condon BD. Hydrogenation of cottonseed oil with nickel, palladium and platinum catalysts. JAOCS, J Am Oil Chem Soc 2012;89:1557–66. doi:10.1007/s11746-012-2036-8.

[140] Deliy IV, Simakova IL, Ravasio N, Psaro R. Catalytic behaviour of carbon supported platinum group metals in the hydrogenation and isomerization of methyl oleate. Appl Catal A Gen 2009;357:170–7. doi:10.1016/J.APCATA.2009.01.026.

[141] Philippaerts A, Paulussen S, Breesch A, Turner S, Lebedev OI, Van Tendeloo G, et al. Unprecedented Shape Selectivity in Hydrogenation of Triacylglycerol Molecules with Pt/ZSM-5 Zeolite. Angew Chemie Int Ed 2011;50:3947–9. doi:10.1002/anie.201007513.

[142] Mcardle S, Girish S, Leahy JJ, Curtin T. Selective hydrogenation of sunflower oil over noble metal catalysts. J Mol Catal A Chem 2011;351:179–87. doi:10.1016/j.molcata.2011.10.004.

[143] McArdle S, Leahy JJ, Curtin T, Tanner D. Hydrogenation of sunflower oil over Pt-Ni bimetallic supported catalysts: Preparation, characterization and catalytic activity. Appl Catal A Gen 2014;474:78–86. doi:10.1016/j.apcata.2013.08.033.

[144] Belkacemi K, Kemache N, Hamoudi S, Arul J. Hydrogenation of sunflower oil over bimetallic supported catalysts on mesostructured silica material. Int J Chem React Eng 2007;5:1–25. doi:10.2202/1542-6580.1528.

[145] Nohair B, Especel C, Lafaye G, Marécot P, Hoang LC, Barbier J. Palladium supported catalysts for the selective hydrogenation of sunflower oil. J Mol Catal A Chem 2005;229:117–26. doi:10.1016/J.MOLCATA.2004.11.017.

[146] Fernández MB, Tonetto GM, Crapiste GH, Ferreira ML, Damiani DE. Hydrogenation of edible oil over Pd catalysts: A combined theoretical and experimental study. J Mol Catal A Chem 2005;237:67–79. doi:10.1016/j.molcata.2005.04.047.

[147] Shakun JD, Clark PU, He F, Marcott SA, Mix AC, Liu Z, et al. Global warming preceded by increasing carbon dioxide concentrations during the last deglaciation. Nature 2012;484:49–54. doi:10.1038/nature10915.

[148] Numwong N, Luengnaruemitchai A, Chollacoop N, Yuji Y. Partial hydrogenation of polyunsaturated fatty acid methyl esters over Pd/activated carbon: Effect of type of reactor. Chem Eng J 2012;210:173–81. doi:10.1016/j.cej.2012.08.034.

[149] Liu W, Tian F, Yu J, Bi Y. Magnetic Mesoporous Palladium Catalyzed Selective Hydrogenation of Sunflower Oil. J Oleo Sci 2016;65:451–8. doi:10.5650/jos.ess15169.

[150] Davis ME. Ordered porous materials for emerging applications. Nature 2002;417:813–21. doi:10.1038/nature00785.

[151] Ying W, Zhao D. On the Controllable Soft-Templating Approach to Mesoporous Silicates. Chem Rev 2007;107:2821–60. doi:10.1021/CR068020S.

[152] Numwong N, Luengnaruemitchai A, Chollacoop N, Yoshimura Y. Effect of SiO2 pore size on partial hydrogenation of rapeseed oil-derived FAMEs. Appl Catal A Gen 2012;441:72–8. doi:10.1016/j.apcata.2012.07.020.

[153] Wright A., Wong A, Diosady L. Ni catalyst promotion of a Cis-selective Pd catalyst for canola oil hydrogenation. Food Res Int 2003;36:1069–72. doi:10.1016/J.FOODRES.2003.08.005.

[154] Fernández MB, Piqueras CM, Tonetto GM, Crapiste G, Damiani DE. Hydrogenation of edible oil over

Pd-Me/Al2O3 catalysts (Me=Mo, V and Pb). J Mol Catal A Chem 2005;233:133–9. doi:10.1016/j.molcata.2005.02.012.

[155] Popescu O, Koritala S, Dutton HJ. High oleic oils by selective hydrogenation of soybean oil. J Am Oil Chem Soc 1969;46:97–9. doi:10.1007/BF02541217.

[156] Koritala S. Selective hydrogenation of soybean oil: VII. Poisons and inhibitors for copper catalysts. J Am Oil Chem Soc 1975;52:240–3. doi:10.1007/BF02639150.

[157] Koritala S, Dutton HJ. Selective hydrogenation of soybean oil. II. Copper-chromium catalysts. J Am Oil Chem Soc 1966;43:556–8. doi:10.1007/BF02679872.

[158] Koritala S, Frankel EN. Selective conjugation of soybean esters to increase hydrogenation selectivity. J Am Oil Chem Soc 1981;58:553–6. doi:10.1007/BF02541593.

[159] Koritala S. Selective hydrogenation of soybean oil. VI. Copper-on-silica gel catalysts. J Am Oil Chem Soc 1972;49:83–4. doi:10.1007/BF02545148.

[160] Koritala S. Selective hydrogenation of soybean oil: V. A Novel copper catalyst with excellent re-use properties. J Am Oil Chem Soc 1970;47:106–7. doi:10.1007/BF02612948.

[161] Okkerse C, de Jonge A, Coenen JWE, Rozendaal A. Selective hydrogenation of soybean oil in the presence of copper catalysts.pdf. JAOCS, J Am Oil Chem Soc 1967;44:152–6.

[162] Pecchia P, Galasso I, Mapelli S, Bondioli P, Zaccheria F, Ravasio N. Stabilisation of camelina oil methyl esters through selective hydrogenation. Ind Crops Prod 2013;51:306–9. doi:10.1016/j.indcrop.2013.09.021.

[163] Sitthisa S, Sooknoi T, Ma Y, Balbuena PB, Resasco DE. Kinetics and mechanism of hydrogenation of furfural on Cu/SiO2 catalysts. J Catal 2011;277:1–13. doi:10.1016/J.JCAT.2010.10.005.

[164] Carniti P, Gervasini A, Modica VH, Ravasio N. Catalytic selective reduction of NO with ethylene over a series of copper catalysts on amorphous silicas. Appl Catal B Environ 2000;28:175–85. doi:10.1016/S0926-3373(00)00172-7.

[165] Dong F, Ding G, Zheng H, Xiang X, Chen L, Zhu Y, et al. From chip-in-a-lab to lab-on-a-chip: towards a single handheld electronic system for multiple application-specific lab-on-a-chip (ASLOC). Catal Sci Technol 2014;6:767. doi:10.1039/c5cy00857c.

[166] Li F, Wang L, Han X, He P, Cao Y, Li H, et al. Influence of support on the performance of copper catalysts for the effective hydrogenation of ethylene carbonate to synthesize ethylene glycol and methanol. RSC Adv 2016;6:45894–906. doi:10.1039/C6RA06464G.

[167] Ding T, Tian H, Liu J, Wu W, Zhao B. Effect of promoters on hydrogenation of diethyl malonate to 1,3-propanediol over nano copper-based catalysts. Catal Commun 2016;74:10–5. doi:10.1016/j.catcom.2015.10.031.

[168] Zhu S, Gao X, Zhu Y, Fan W, Wang J, Li Y. A highly efficient and robust Cu/SiO $_2$ catalyst prepared by the ammonia evaporation hydrothermal method for glycerol hydrogenolysis to 1,2-propanediol. Catal Sci Technol 2015;5:1169–80. doi:10.1039/C4CY01148A.

[169] Huang X, Ma M, Miao S, Zheng Y, Chen M, Shen W. Hydrogenation of methyl acetate to ethanol over a highly stable Cu/SiO2 catalyst: Reaction mechanism and structural evolution. Appl Catal A Gen 2017;531:79–88. doi:10.1016/J.APCATA.2016.12.006.

[170] Zhang B, Hui S, Zhang S, Ji Y, Li W, Fang D. Effect of copper loading on texture, structure and catalytic performance of Cu/SiO2 catalyst for hydrogenation of dimethyl oxalate to ethylene glycol. J Nat Gas Chem 2012;21:563–70. doi:10.1016/S1003-9953(11)60405-2.

[171] Dong X, Ma X, Xu H, Ge Q, Sio C/. From chip-in-a-lab to lab-on-a-chip: towards a single handheld electronic system for multiple application-specific lab-on-a-chip (ASLOC). Catal Sci Technol 2014;6:4151. doi:10.1039/c5cy01965f.

[172] Wang X, Ma K, Guo L, Tian Y, Cheng Q, Bai X, et al. Cu/ZnO/SiO2 catalyst synthesized by reduction of ZnO-modified copper phyllosilicate for dimethyl ether steam reforming. Appl Catal A Gen 2017;540:37–46. doi:10.1016/J.APCATA.2017.04.013.

[173] Toupance T, Kermarec M, Louis C. Metal Particle Size in Silica-Supported Copper Catalysts. Influence of the Conditions of Preparation and of Thermal Pretreatments 2000. doi:10.1021/jp993399q.

[174] Toupance T, Kermarec M, Lambert J-F, Louis C. Conditions of Formation of Copper Phyllosilicates in Silica-Supported Copper Catalysts Prepared by Selective Adsorption. J Phys Chem B 2002;106:2277–86. doi:10.1021/JP013153X.

[175] Xu C, Chen G, Zhao Y, Liu P, Duan X, Gu L, et al. Interfacing with silica boosts the catalysis of copper. Nat Commun 2018;9:3367. doi:10.1038/s41467-018-05757-6.

[176] Hope GA, Buckley AN, Parker GK, Numprasanthai A, Woods R, McLean J. The interaction of n-octanohydroxamate with chrysocolla and oxide copper surfaces. Miner Eng 2012;36–38:2–11. doi:10.1016/j.mineng.2012.01.013.

[177] Dong F, Ding G, Zheng H, Xiang X, Chen L, Zhu Y, et al. Highly dispersed Cu nanoparticles as an efficient catalyst for the synthesis of the biofuel 2-methylfuran. Catal Sci Technol 2016;6:767–79. doi:10.1039/C5CY00857C.

[178] Zhu S, Gao X, Zhu Y, Zhu Y, Zheng H, Li Y. Promoting effect of boron oxide on Cu/SiO2 catalyst for glycerol hydrogenolysis to 1,2-propanediol. J Catal 2013;303:70–9. doi:10.1016/j.jcat.2013.03.018.

[179] Zhu Y, Zhu Y, Ding G, Zhu S, Zheng H, Li Y. Highly selective synthesis of ethylene glycol and ethanol via hydrogenation of dimethyl oxalate on Cu catalysts: Influence of support. Appl Catal A Gen 2013;468:296–304. doi:10.1016/j.apcata.2013.09.019.

[180] Ding J, Popa T, Tang J, Gasem KAM, Fan M, Zhong Q. Highly selective and stable Cu/SiO2 catalysts prepared with a green method for hydrogenation of diethyl oxalate into ethylene glycol. Appl Catal B Environ 2017;209:530–42. doi:10.1016/j.apcatb.2017.02.072.

[181] Lindlar H, Dubuis R. Palladium Catalyst for Partial Reduction of Acetylenes. Org Synth 1966;46:89–89. doi:10.1002/0471264180.os046.27.

[182] Mallát T, Szabó S, Petró J. The role of lead in the selectivity of palladium-lead (lindlar type) catalysts. Appl Catal 1987;29:117–23. doi:10.1016/S0166-9834(00)82611-1.

[183] Tripathi B, Paniwnyk L, Cherkasov N, Ibhadon AO, Lana-Villarreal T, Gómez R. Ultrasound-assisted selective hydrogenation of C-5 acetylene alcohols with Lindlar catalysts. Ultrason Sonochem 2015;26:445–51. doi:10.1016/J.ULTSONCH.2015.03.006.

[184] Rajaram J, Narula APS, Chawla HPS, Dev S. Semihydrogenation of acetylenes : Modified lindlar catalyst. Tetrahedron 1983;39:2315–22. doi:10.1016/S0040-4020(01)91960-X.

[185] Righi G, Rossi L. Mild Regioselective Catalytic Hydrogenation of α,β-Unsaturated Carbonyl Compounds with Lindlar Catalyst. Synth Commun 1996;26:1321–7. doi:10.1080/00397919608003491.

[186] Dijkstra AJ. Kinetics and mechanism of the hydrogenation process - the state of the art. Eur J Lipid Sci Technol 2012;114:985–98. doi:10.1002/ejlt.201100405.

[187] Boccuzzi F, Coluccia S, Martra G, Ravasio N. Cu/SiO2 and Cu/SiO2–TiO2 Catalysts: I. TEM, DR UV-Vis-NIR, and FTIR Characterisation. J Catal 1999;184:316–26. doi:10.1006/jcat.1999.2428.

[188] Ramesh TN, Kamath PV. Synthesis of nickel hydroxide: Effect of precipitation conditions on phase selectivity and structural disorder. J Power Sources 2006;156:655–61. doi:10.1016/J.JPOWSOUR.2005.05.050.

[189] Ehlsissen KT, Delahaye-Vidal A, Genin P, Figlarz M, Willmann P. Preparation and characterization of turbostratic Ni/Al layered double hydroxides for nickel hydroxide electrode applications. J Mater Chem 1993;3:883. doi:10.1039/jm9930300883.

[190] Rozaimah S, Rakmi A, Rahman A, Abu B, Mohamad M, Marzuki M, et al. Removal of Mixed Heavy Metals by Hydroxide Precipitation. n.d.

[191] and LH, Edwards* M. Role of Temperature and pH in Cu(OH)2 Solubility 1999. doi:10.1021/ES981121Q.

[192] Toebes ML, van Dillen JA, de Jong KP. Synthesis of supported palladium catalysts. J Mol Catal A Chem 2001;173:75–98. doi:10.1016/S1381-1169(01)00146-7.

[193] Brunauer S, Emmett PH, Teller E. Adsorption of Gases in Multimolecular Layers. J Am Chem Soc 1938;60:309–19. doi:10.1021/ja01269a023.

[194] Barrett EP, Joyner LG, Halenda PP. The Determination of Pore Volume and Area Distributions in Porous Substances. I. Computations from Nitrogen Isotherms. J Am Chem Soc 1951;73:373–80. doi:10.1021/ja01145a126.

[195] Agilent 700 Series ICP Optical Emission Spectrometers User's Guide 2 Agilent 700 Series ICP Optical Emission Spectrometers User's Guide Notices Manual Part Number Instrument Manufacturing. 8510.

[196] Landers J, Gor GY, Neimark A V. Density functional theory methods for characterization of porous materials. Colloids Surfaces A Physicochem Eng Asp 2013;437:3–32. doi:10.1016/j.colsurfa.2013.01.007.

[197] Monson PA. Understanding adsorption/desorption hysteresis for fluids in mesoporous materials using simple molecular models and classical density functional theory. Microporous Mesoporous Mater 2012;160:47–66. doi:10.1016/J.MICROMESO.2012.04.043.

[198] Thommes M, Cychosz KA. Physical adsorption characterization of nanoporous materials: progress and challenges. Adsorption 2014;20:233–50. doi:10.1007/s10450-014-9606-z.

[199] Thommes M, Kaneko K, Neimark A V., Olivier JP, Rodriguez-Reinoso F, Rouquerol J, et al. Physisorption of gases, with special reference to the evaluation of surface area and pore size distribution (IUPAC Technical Report). Pure Appl Chem 2015;87:1051–69. doi:10.1515/pac-2014-1117.

[200] Monshi A, Foroughi MR, Monshi MR, Monshi A, Foroughi MR, Monshi MR. Modified Scherrer Equation to Estimate More Accurately Nano-Crystallite Size Using XRD. World J Nano Sci Eng 2012;02:154–60. doi:10.4236/wjnse.2012.23020.

[201] Langford JI, Wilson AJC, IUCr. Scherrer after sixty years: A survey and some new results in the determination of crystallite size. J Appl Crystallogr 1978;11:102–13. doi:10.1107/S0021889878012844.

[202] Deng Y, Handoko AD, Du Y, Xi S, Yeo BS. *In Situ* Raman Spectroscopy of Copper and Copper Oxide Surfaces during Electrochemical Oxygen Evolution Reaction: Identification of Cu ^{III} Oxides as Catalytically Active Species. ACS Catal 2016;6:2473–81. doi:10.1021/acscatal.6b00205.

[203] Lafuente B, Downs RT, Yang H, Stone N. The power of databases: The RRUFF project. n.d.

[204] Caracas R, Bobocioiu E. The WURM project-a freely available web-based repository of computed physical data for minerals. vol. 96. 2011.

[205] Raman Database - University of Parma n.d. http://www.fis.unipr.it/phevix/ramandb.php (accessed June 7, 2019).

[206] Shimokawabe M, Takezawa N, Kobayashi H. Characterization of copper-silica catalysts prepared by ion exchange. Appl Catal 1982;2:379–87. doi:10.1016/0166-9834(82)80156-5.

[207] A. R. Naghash, T. H. Etsell * and, Xu S. XRD and XPS Study of Cu−Ni Interactions on Reduced Copper−Nickel−Aluminum Oxide Solid Solution Catalysts 2006. doi:10.1021/CM051910O.

[208] Christensen GL, Langell MA. Characterization of Copper Palladium Oxide Solid Solutions by X-ray Diffraction, X-ray Photoelectron Spectroscopy, and Auger Electron Spectroscopy. J Phys Chem C 2013:117–7039. doi:10.1021/jp310344r.

[209] Espinós JP, Morales J, Barranco A, Caballero A, Holgado JP, González-Elipe AR. Interface Effects for Cu, CuO, and Cu 2 O Deposited on SiO 2 and ZrO 2. XPS Determination of the Valence State of Copper in Cu/SiO 2 and Cu/ZrO 2 Catalysts 2002. doi:10.1021/jp014618m.

[210] Spee MPR, Boersma J, Meijer MD, Slagt MQ, Van Koten G, Geus JW. Selective Liquid-Phase Semihydrogenation of Functionalized Acetylenes and Propargylic Alcohols with Silica-Supported Bimetallic Palladium-Copper Catalysts † 2001. doi:10.1021/jo001246p.

[211] Suzana M, Francisco P, Mastelaro VR, Nascente PAP. Activity and Characterization by XPS, HR-TEM, Raman Spectroscopy, and BET Surface Area of CuO/CeO 2-TiO 2 Catalysts 2001. doi:10.1021/jp0109675.

[212] Wang Z, Liu Q, Yu J, Wu T, Wang G. Surface structure and catalytic behavior of silica-supported copper catalysts prepared by impregnation and sol–gel methods. Appl Catal A Gen 2003;239:87–94. doi:10.1016/S0926-860X(02)00421-0.

[213] Hinrichsen O, Genger T, Muhler M. Chemisorption of N2O and H2 for the Surface Determination of Copper Catalysts. Chem Eng Technol 2000;23:956–9. doi:10.1002/1521-4125(200011)23:11<956::AID-CEAT956>3.0.CO;2-L.

[214] Guggilla Vidya Sagar, Pendyala Venkat Ramana Rao, Chakravartula S. Srikanth and, Chary* KVR. Dispersion and Reactivity of Copper Catalysts Supported on Al2O3−ZrO2 2006. doi:10.1021/JP0575153.

[215] Snyder JM, Dutton HJ, Scholfield CR. Laboratory-scale continuous hydrogenation. J Am Oil Chem Soc 1978;55:383–6. doi:10.1007/BF02911896.

[216] Balakos MW, Hernandez EE. Catalyst characteristics and performance in edible oil hydrogenation. Catal Today 1997;35:415–25. doi:10.1016/S0920-5861(96)00212-X.

[217] Jang ES, Jung MY, Min DB. Hydrogenation for Low Trans and High Conjugated Fatty Acids. Compr Rev Food Sci Food Saf 2005;4:22–30. doi:10.1111/j.1541-4337.2005.tb00069.x.

[218] Belkacemi K, Boulmerka A, Arul J, Hamoudi S. Hydrogenation of Vegetable Oils with Minimum trans and Saturated Fatty Acid Formation Over a New Generation of Pd-catalyst. Top Catal 2006;37:113–20. doi:10.1007/s11244-006-0012-y.

[219] ISo/TC 34/SC 11. ISO 3961:2018 - Animal and vegetable fats and oils -- Determination of iodine value 2018.

[220] Albright LF, Wisniak J. Selectivity and isomerization during partial hydrogenation of cottonseed oil and methyl oleate: Effect of operating variables. J Am Oil Chem Soc 1962;39:14–9. doi:10.1007/BF02633340.

[221] Albright LF. Quantitative measure of selectivity of hydrogenation of triglycerides. J Am Oil Chem Soc 1965;42:250–3. doi:10.1007/BF02541141.

[222] Bailey AE. Some additional notes on the kinetics and theory of fatty oil hydrogenation. J Am Oil Chem Soc 1949;26:644–8. doi:10.1007/BF02651503.

[223] Fogler HS. Elements of Chemical Reaction Engineering Fifth Edition. Fifth. Prentice Hall; 2016.

[224] Vilé G, Almora-Barrios N, Mitchell S, López N, Pérez-Ramírez J. From the Lindlar Catalyst to Supported Ligand-Modified Palladium Nanoparticles: Selectivity Patterns and Accessibility Constraints in the Continuous-Flow Three-Phase Hydrogenation of Acetylenic Compounds. Chem - A Eur J 2014;20:5926–37. doi:10.1002/chem.201304795.

[225] Sing KSW. Reporting physisorption data for gas/solid systems with special reference to the determination of surface area and porosity (Recommendations 1984). Pure Appl Chem 1985;57:603–19. doi:10.1351/pac198557040603.

[226] Parabello L, Micheli F, Gallucci K, Rossi L, Foscolo PU. Studio e sperimentazione sulla cattura della CO 2 da miscele gassose tramite sorbenti. Rep Enea 2013.

[227] Cobden PD, van Beurden P, Reijers HTJ, Elzinga GD, Kluiters SCA, Dijkstra JW, et al. Sorption-enhanced hydrogen production for pre-combustion CO2 capture: Thermodynamic analysis and experimental results. Int J Greenh Gas Control 2007;1:170–9. doi:10.1016/S1750-5836(07)00021-7.

[228] Valente JS, Cantú MS, Cortez JGH, Montiel R, Bokhimi X, López-Salinas E. Preparation and Characterization of Sol−Gel MgAl Hydrotalcites with Nanocapsular Morphology. J Phys Chem C 2007;111:642–51. doi:10.1021/jp065283h.

[229] Hibino T, Tsunashima A. Characterization of repeatedly reconstructed Mg-Al hydrotalcite-like compounds: gradual segregation of aluminum from the structure. Chem Mater 1998:4055–61. doi:10.1021/cm980478q.

[230] Dong X, Ma X, Xu H, Ge Q. Comparative study of silica-supported copper catalysts prepared by different methods: formation and transition of copper phyllosilicate. Catal Sci Technol 2016;6:4151–8. doi:10.1039/C5CY01965F.

[231] Guerreiro E., Gorriz O., Larsen G, Arrúa L. Cu/SiO2 catalysts for methanol to methyl formate dehydrogenation. Appl Catal A Gen 2000;204:33–48. doi:10.1016/S0926-860X(00)00507-X.

[232] Kikhtyanin O, Pospelova V, Aubrecht J, Lhotka M, Kubička D, Kikhtyanin O, et al. Effect of Calcination Atmosphere and Temperature on the Hydrogenolysis Activity and Selectivity of Copper-Zinc Catalysts. Catalysts 2018;8:446. doi:10.3390/catal8100446.

[233] Yahiro H, Nakaya K, Yamamoto T, Saiki K, Yamaura H. Effect of calcination temperature on the catalytic activity of copper supported on γ-alumina for the water-gas-shift reaction. Catal Commun 2006;7:228–31. doi:10.1016/J.CATCOM.2005.11.004.

[234] Amadine O, Essamlali Y, Fihri A, Larzek M, Zahouily M. Effect of calcination temperature on the structure and catalytic performance of copper–ceria mixed oxide catalysts in phenol hydroxylation. RSC Adv 2017;7:12586–97. doi:10.1039/C7RA00734E.

[235] Zhu Y, Kong X, Cao D-B, Cui J, Zhu Y, Li Y-W. The Rise of Calcination Temperature Enhances the Performance of Cu Catalysts: Contributions of Support. ACS Catal 2014;4:3675–81. doi:10.1021/cs501155x.

[236] Ding Y, Zhao C, Lia Y, Ma Z, Lv X, Ding Y, et al. Effect of calcination temperature on the structure and catalytic performance pf the Cu-MCM-41 catalysts for the synthesis of dimethyl carbonate. Quim Nova 2018;41:1156–61. doi:10.21577/0100-4042.20170291.

[237] Dong X, Ma X, Xu H, Ge Q. Comparative study of silica-supported copper catalysts prepared by different methods: formation and transition of copper phyllosilicate. Catal Sci Technol 2016;6:4151–8. doi:10.1039/C5CY01965F.

[238] Loaiza-Gil A, Villarroel M, Balbuena JF, Lacruz MA, Gonzalez-Cortés S. Thermal decomposition study of silica-supported nickel catalyst synthesized by the ammonia method. J Mol Catal A Chem 2008;281:207–13. doi:10.1016/j.molcata.2007.11.033.

[239] Boza AF, Kupfer VL, Oliveira AR, Radovanovic E, Rinaldi AW, Meneguin JG, et al. Synthesis of α-aminophosphonates using a mesoporous silica catalyst produced from sugarcane bagasse ash. RSC Adv 2016;6:23981–6. doi:10.1039/C5RA23233C.

[240] Rovani S, Santos JJ, Corio P, Fungaro DA. An Alternative and Simple Method for the Preparation of Bare Silica Nanoparticles Using Sugarcane Waste Ash, an Abundant and Despised Residue in the Brazilian Industry. Artic J Braz Chem Soc 2019;30:1524–33. doi:10.21577/0103-5053.20190049.

[241] Hu S, Hsieh Y-L. Preparation of Activated Carbon and Silica Particles from Rice Straw. ACS Sustain Chem Eng 2014;2:726–34. doi:10.1021/sc5000539.

[242] Yujun Z, Siming L, Yue W, Bin S, Jian Z, Shengping W, et al. Efficient tuning of surface copper species of Cu/SiO2 catalyst for hydrogenation of dimethyl oxalate to ethylene glycol. Chem Eng J 2017;313:759–68. doi:10.1016/J.CEJ.2016.12.027.

[243] Hermida L, Zuhairi Abdullah A, Rahman Mohamed A. FT-IR and TGA of MCF Silica-Supported Nickel Catalyst. vol. 9. 2018.

[244] Cheng T, Chen J, Cai A, Wang J, Liu H, Hu Y, et al. Synthesis of Pd/SiO 2 Catalysts in Various HCl Concentrations for Selective NBR Hydrogenation: Effects of H + and Cl − Concentrations and Electrostatic Interactions 2018. doi:10.1021/acsomega.8b00244.

[245] Liu Y, Murata K, Inaba M, Takahara I. Synthesis of ethanol from methanol and syngas through an indirect route containing methanol dehydrogenation, DME carbonylation, and methyl acetate hydrogenolysis. Fuel Process Technol 2013;110:206–13. doi:10.1016/j.fuproc.2012.12.016.

[246] Komandur V. R. Chary *, Guggilla Vidya Sagar, Chakravarthula S. Srikanth and, Rao VV. Characterization and Catalytic Functionalities of Copper Oxide Catalysts Supported on Zirconia 2006. doi:10.1021/JP063335X.

[247] Afzal M, Theocharis CR, Karim S. Temperature programmed reduction of silica supported nickel catalysts. Colloid Polym Sci 1993;271:1100–5. doi:10.1007/BF00659300.

[248] Louis C, Cheng ZX, Che M. Characterization of nickel/silica catalysts during impregnation and further thermal activation treatment leading to metal particles. J Phys Chem 1993;97:5703–12. doi:10.1021/j100123a040.

[249] Van Stiphout PCM, Stobbe DE, V.D. Scheur FT, Geus JW. Activity and stability of nickel—copper/silica catalysts prepared by deposition-precipitation. Appl Catal 1988;40:219–46. doi:10.1016/S0166-9834(00)80439-X.

[250] Robertson SD, McNicol BD, De Baas JH, Kloet SC, Jenkins JW. Determination of reducibility and identification of alloying in copper-nickel-on-silica catalysts by temperature-programmed reduction. J Catal 1975;37:424–31. doi:10.1016/0021-9517(75)90179-7.

[251] Noronha FB, Schmal M, Primet M, Frety R. Characterization of palladium-copper bimetallic catalysts supported on silica and niobia. Appl Catal 1991;78:125–39. doi:10.1016/0166-9834(91)80093-C.

[252] Biesinger MC, Payne BP, Lau LWM, Gerson A, Smart RSC. X-ray photoelectron spectroscopic chemical state quantification of mixed nickel metal, oxide and hydroxide systems. Surf Interface Anal 2009;41:324–32. doi:10.1002/sia.3026.

[253] Grosvenor AP, Biesinger MC, Smart RSC, McIntyre NS. New interpretations of XPS spectra of nickel metal and oxides. Surf Sci 2006;600:1771–9. doi:10.1016/j.susc.2006.01.041.

[254] Mansour AN. Characterization of NiO by XPS. Surf Sci Spectra 1994;3:231–8. doi:10.1116/1.1247751.

[255] C. D. Wanger, W. M. Riggs, L. E. Davis, J. F. Moulder, G. E.Muilenberg. Handbook of X-ray Photoelectron Spectroscopy. 1st editio. John Wiley & Sons, Ltd; 1981. doi:10.1002/sia.740030412.

[256] Castle JE. Practical surface analysis by Auger and X-ray photoelectron spectroscopy. John Wiley & Sons, Ltd; 1984. doi:10.1002/sia.740060611.

[257] El-Shattory Y, deMan L, deMan JM. Hydrogenation of Canola Oil: Influence of Catalyst Concentration. Can Inst Food Sci Technol J 1981;14:53–8. doi:10.1016/S0315-5463(81)72677-4.

[258] Dijkstra AJ. Selectivities in Partial Hydrogenation. J Am Oil Chem Soc 2010;87:115–7. doi:10.1007/s11746-009-1507-z.

[259] Fernández MB, Piqueras CM, Tonetto GM, Crapiste G, Damiani DE. Hydrogenation of edible oil over Pd-Me/Al2O3 catalysts (Me=Mo, V and Pb). J Mol Catal A Chem 2005;233:133–9. doi:10.1016/j.molcata.2005.02.012.

[260] Edvardsson J, Irandoust S. Reactors for hydrogenation of edible oils. J Am Oil Chem Soc 1994;71:235–42. doi:10.1007/BF02638048.

[261] Balakos MW, Hernandez EE. Catalyst characteristics and performance in edible oil hydrogenation. Catal Today 1997;35:415–25.

[262] Pandarus V, Gingras G, Ois Beíand F, Ciriminna R, Pagliaro M. Selective Hydrogenation of Vegetable Oils over SiliaCat Pd(0) 2012. doi:10.1021/op300115r.

[263] Edvardsson J, Rautanen P, Littorin A, Larsson M. Deactivation and coke formation on palladium and platinum catalysts in vegetable oil hydrogenation. J Am Oil Chem Soc 2001;78:319–27. doi:10.1007/s11746-001-0263-6.

[264] Toshtay K, Auyezov AB, Bizhanov ZA, Yeraliyeva AT, Toktasinov SK, Kudaibergen B, et al. Effect of Catalyst Preparation on the Selective Hydrogenation of Vegetable Oil Over Low Percentage Pd/Diatomite Catalysts. Eurasian Chem J 2014;17:33. doi:10.18321/ectj192.

[265] McArdle S, Girish S, Leahy JJ, Curtin T. Selective hydrogenation of sunflower oil over noble metal catalysts. J Mol Catal A Chem 2011;351:179–87. doi:10.1016/j.molcata.2011.10.004.

[266] Schneider MP. Plant-oil-based lubricants and hydraulic fluids. J Sci Food Agric 2006;86:1769–80. doi:10.1002/jsfa.2559.

[267] Ackman RG, Agustin YT V., Alexandersen KA, Basiron Y. Bailey's Industrial Oil and Fat Products Sixth Edition. vol. 157. 2005. doi:10.1038/157822a0.

[268] Hastert RC. Practical aspects of hydrogenation and soybean salad oil manufacture. J Am Oil Chem Soc 1981;58:169–74. doi:10.1007/BF02582330.

[269] Albright LF. Application of partial hydrogenation theory to the design of commercial reactors for hydrogenating triglyceride oils. J Am Oil Chem Soc 1973;50:255–9. doi:10.1007/BF02641797.

[270] Grothues BGM. Hydrogenation of palm and lauric oils. J Am Oil Chem Soc 1985;62:390–9. doi:10.1007/BF02541410.

[271] Sahasrabudhe SN, Rodriguez-Martinez V, O'Meara M, Farkas BE. Density, viscosity, and surface tension of five vegetable oils at elevated temperatures: Measurement and modeling. Int J Food Prop 2017:1–17. doi:10.1080/10942912.2017.1360905.

[272] Processi Innovativi Srl. Processi Innovativi Srl Property -Hydrogenation Plant. n.d.

[273] Rice EE. Materials of construction in the fatty acid industry. J Am Oil Chem Soc 1979;56. doi:10.1007/BF02667437.

[274] European Parlament. DIRECTIVE 97 / 23 / CE European parlament 1997:8–74.

[275] ASME. ASME Boiler and Pressure Vessel Code Section VIII: Division 1 & 2. Am Soc Mech Eng 2018:888. doi:10.1016/B978-0-323-34126-4.00063-3.

[276] ASME. ASME SECTION II 2018 ASME Boiler and Pressure Vessel Code An International Code 2018.

[277] Paul EL, Atiemo-obeng VA, Kresta SM. Handbook of Industrial Mixing. 2nd editio. Wiley INTERSCIENCE; 2003.

[278] Krüger A/S - Vandbehandling fra A til Z n.d. http://www.kruger.dk/ (accessed October 25, 2019).

[279] Maroño M, Torreiro Y, Montenegro L, Sánchez J. Lab-scale tests of different materials for the selection of suitable sorbents for CO2 capture with H2 production in IGCC processes. Fuel 2014;116:861–70. doi:10.1016/j.fuel.2013.03.067.

[280] GPSA. Engineering Data Book - GPSA Vol. 1&2. 12th editi. 2011. doi:10.1002/9781444341294.

[281] TEMA. TEMA 10th Ed. 8th editio. Tubular Exchangers Manufacturers Association, Inc.; 2017.

[282] KT kinetics - Maire Technimont group. KT kinetics - materials and equipment sheets. 2018.

[283] Peters MS, Timmerhaus KD. Plant design and economics for chemicals engineers. vol. 2. 4th editio. McGraw Hill International Editions; 1997. doi:10.4324/9780429046377-7.

[284] Matches' 275 Equipment Cost Estimates. n.d. https://www.matche.com/equipcost/Default.html (accessed October 25, 2019).

[285] Commodity Prices | Commodity Market | Markets Insider 2019. https://markets.businessinsider.com/commodities (accessed October 25, 2019).

Appendice A

Appendix A: tests results

```
> restart
> with(ExcelTools) :
> Ln0 := Import("Hydrogenation.xlsx", "Test01", "B1", emptycell
      = 0.0) :
> Ln := Import("Hydrogenation.xlsx", "Test01", "B2", emptycell = 0.0)
> Le := Import("Hydrogenation.xlsx", "Test01", "C1", emptycell = 0.0) :
> Le0 := Import("Hydrogenation.xlsx", "Test01", "C2", emptycell
      = 0.0) :
> Ol := Import("Hydrogenation.xlsx", "Test01", "D1", emptycell = 0.0) :
> Ol0 := Import("Hydrogenation.xlsx", "Test01", "D2", emptycell
      = 0.0) :
> t := 30 :
>
> eq1 := Ln - Ln0·exp(-k3·t) = 0
> eq2 := Le - Ln0·(k3/(k2 - k3))·(exp(-k3·t) - exp(-k2·t)) - Le0
      ·exp(-k2·t) = 0
>
> eq3 := Ol - Ln0·(k3/(k2 - k3))·(k2/(k1 - k3))·(exp(-k3·t) - exp(-k1
      ·t)) + Ln0·(k3/(k2 - k3))·(k2/(k1 - k2))·(exp(-k2·t) - exp(-k1
      ·t)) - Le0·(k3/(k2 - k3))·(exp(-k2·t) - exp(-k1·t)) - Ol0·(-k1
      ·t) = 0
>
> solve({eq1, eq2, eq3}, {k1, k2, k3})
```

A.1 Test 01: Lindlar – Canola – 60 °C – 4 bar – 4 $mg_{catalyst}/mL_{oil}$

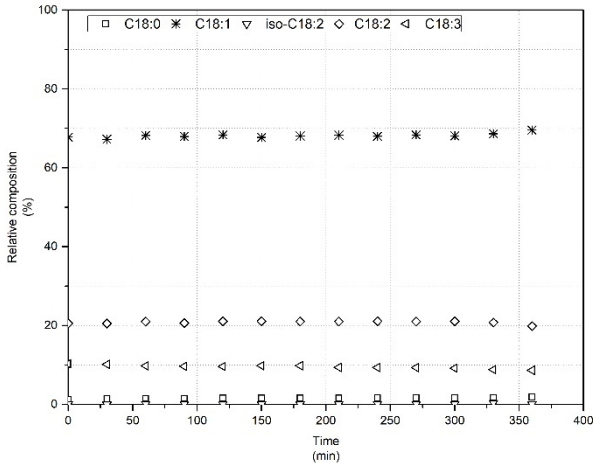

Figure A-1 Test 01 relative percentages of C18:0, C18:1, isomers C18:2, C18:2, C18:3

A.2 Test 02: Lindlar – Canola – 60 °C – 12 bar – 4 $mg_{catalyst}/mL_{oil}$

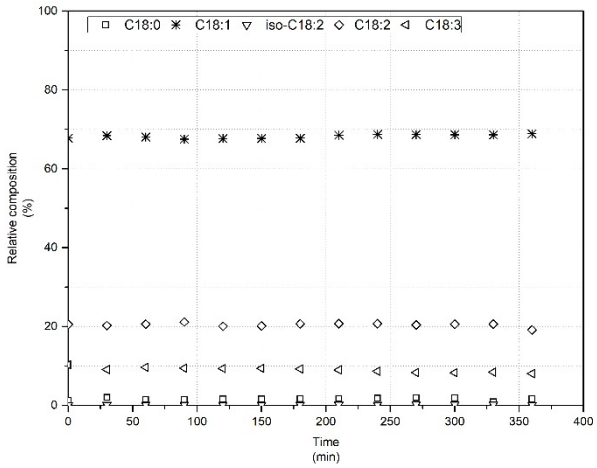

Figure A-2 Test 02 relative percentages of C18:0, C18:1, isomers C18:2, C18:2, C18:3

A.3 Test 03: Lindlar - Canola – 120 °C – 8 bar – 4 $mg_{catalyst}/mL_{oil}$

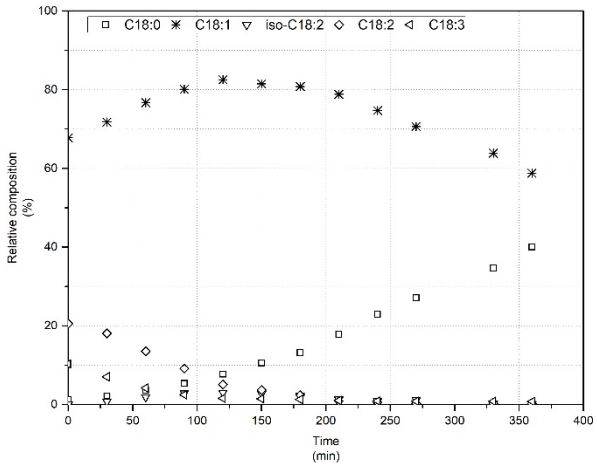

Figure A-3 Test 03 relative percentages of C18:0, C18:1, isomers C18:2, C18:2, C18:3

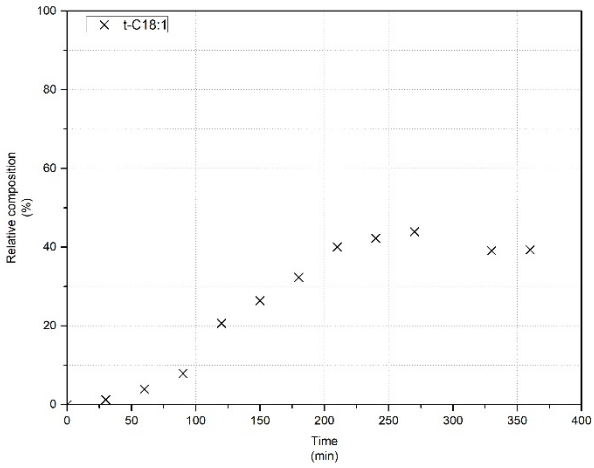

Figure A-4 Test 03 relative percentage of t-C18:1 estimated from the chromatogram

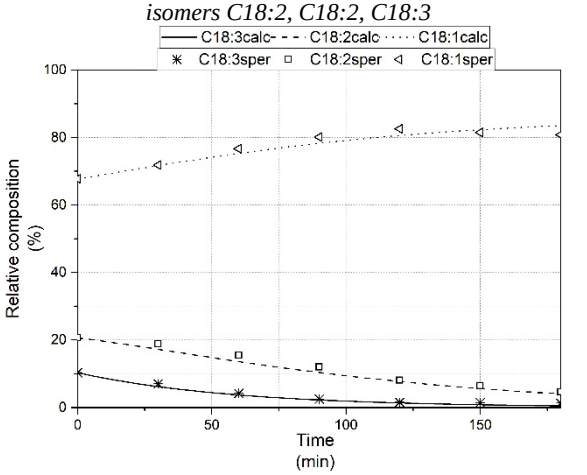

Figure A-5 Test 03 Model fitting for C18:1, C18:2 and C18:3, k1=0.0006, k2=0.0132, k3=0.017

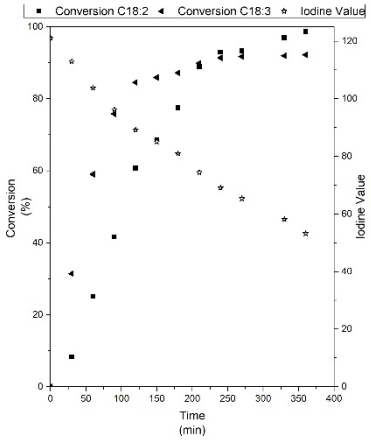

Figure A-6 Test 03 conversions of C18:2 and C18:3, and Iodine Value trend

A.4 Test 04: Lindlar - Canola – 180 °C – 4 bar – 4 $mg_{catalyst}/mL_{oil}$

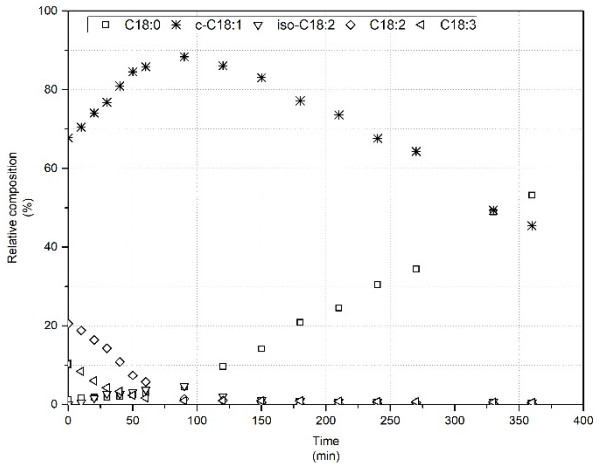

Figure A-7 Test 04 relative percentages of C18:0, C18:1, isomers C18:2, C18:2, C18:3

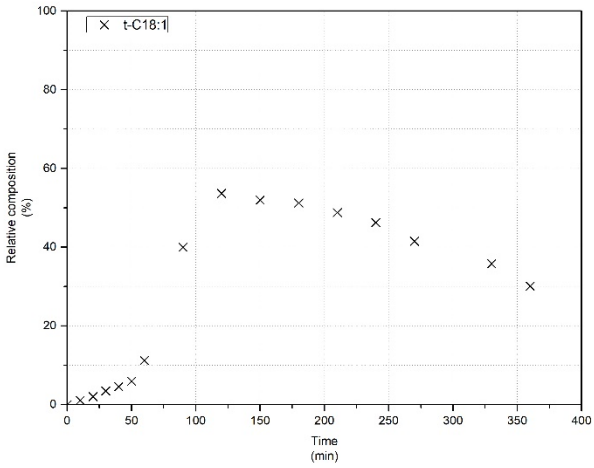

Figure A-8 Test 04 relative percentage of t-C18:1 estimated from the chromatogram

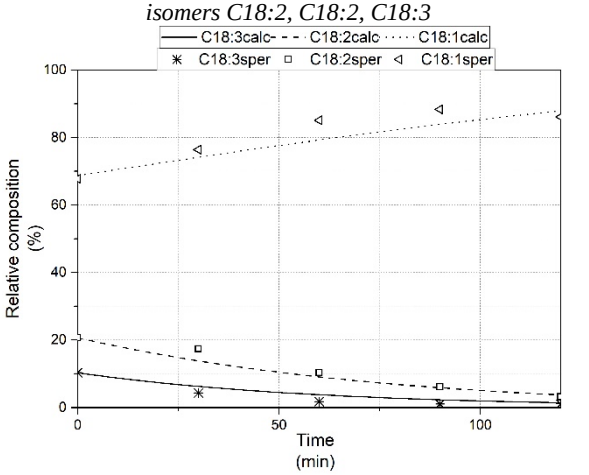

Figure A-9 Test 04 Model fitting for C18:1, C18:2 and C18:3, k1=0.000600, k2=0.0132, k3=0.0170

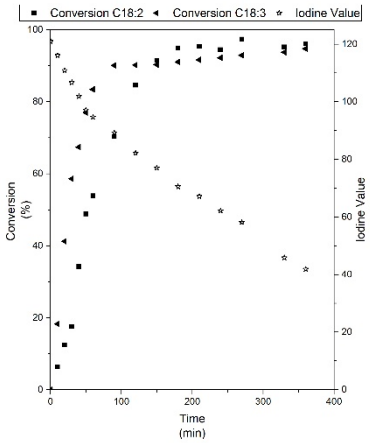

Figure A-10 Test 04 conversions of C18:2 and C18:3, and Iodine Value trend

A.5 Test 05: Lindlar - Canola – 180 °C – 12 bar – 4 $mg_{catalyst}/mL_{oil}$

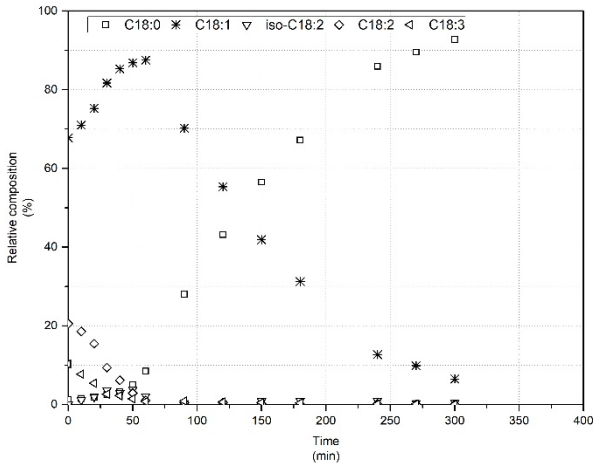

Figure A-511 Test 05 relative percentages of C18:0, C18:1, isomers C18:2, C18:2, C18:3

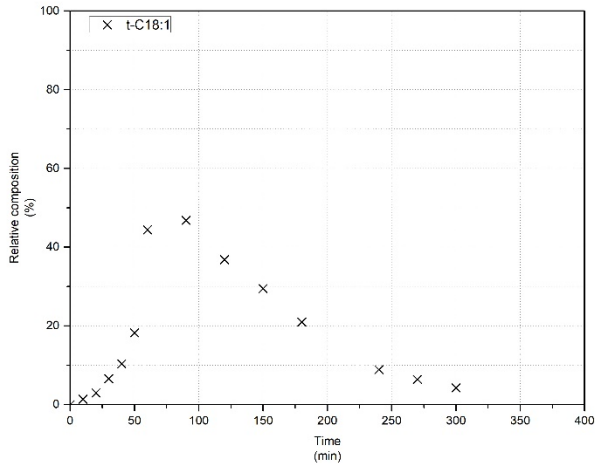

Figure A-12 Test 05 relative percentage of t-C18:1 estimated from the chromatogram

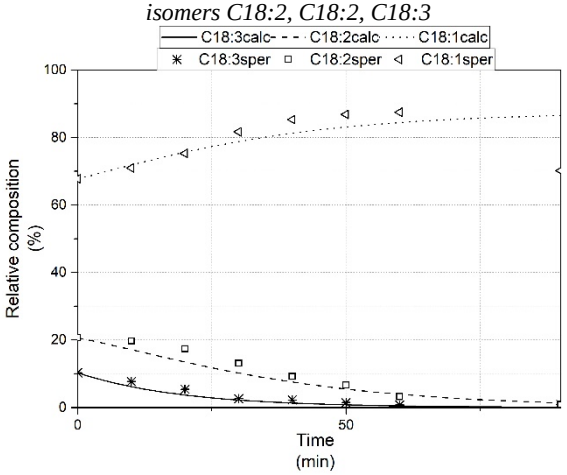

Figure A-13 Test 05 Model fitting for C18:1, C18:2 and C18:3, k1=0.002, k2=0.0402, k3=0.0511

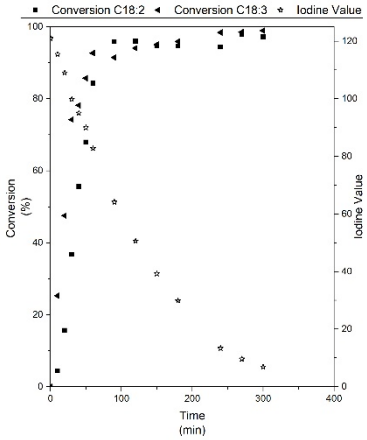

Figure A-14 Test 05 conversions of C18:2 and C18:3, and Iodine Value trend

A.6 Test 06: Lindlar - Canola – 180 °C – 4 bar – 2 $mg_{catalyst}/mL_{oil}$

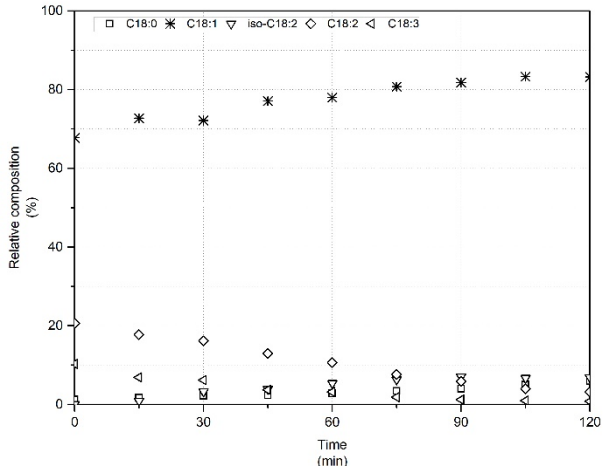

Figure A-15 Test 06 relative percentages of C18:0, C18:1, isomers C18:2, C18:2, C18:3

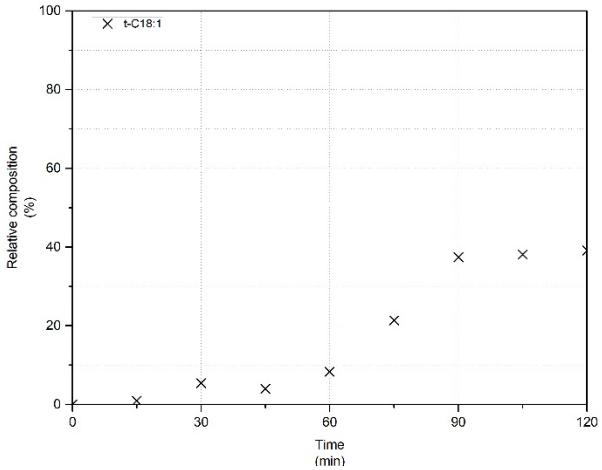

Figure A-16 Test 06 relative percentage of t-C18:1 estimated from the chromatogram

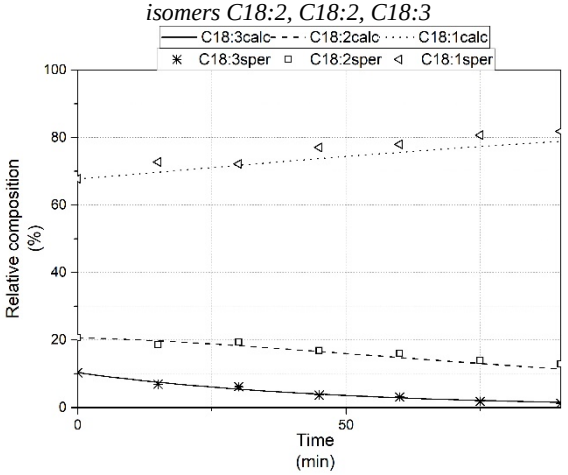

Figure A-17 Test 06 Model fitting for C18:1, C18:2 and C18:3, k1=0.000341, k2=0.0122, k3=0.0212

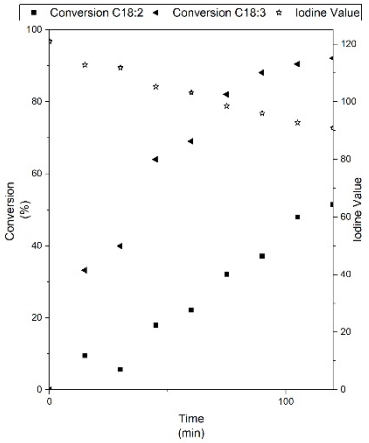

Figure A-18 Test 06 conversions of C18:2 and C18:3, and Iodine Value trend

A.7 Test 07: Lindlar - Canola – 180 °C – 4 bar – 1 $mg_{catalyst}/mL_{oil}$

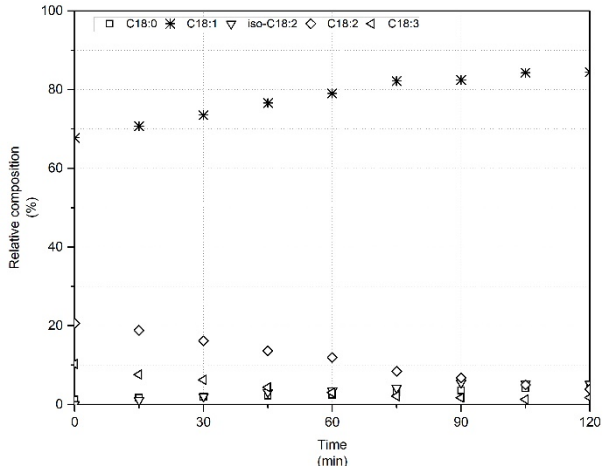

Figure A-19 Test 07 relative percentages of C18:0, C18:1, isomers C18:2, C18:2, C18:3

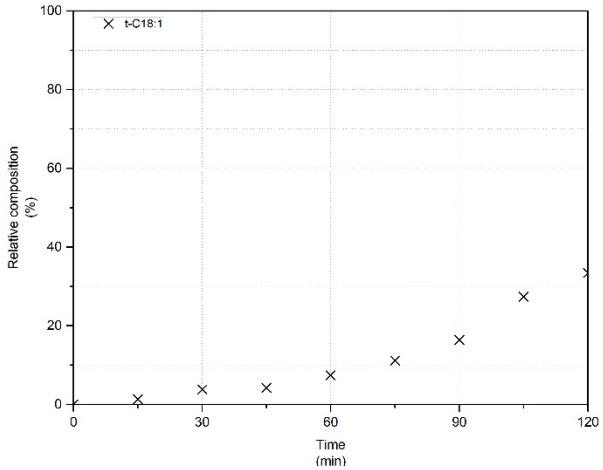

Figure A-20 Test 07 relative percentage of t-C18:1 estimated from the chromatogram

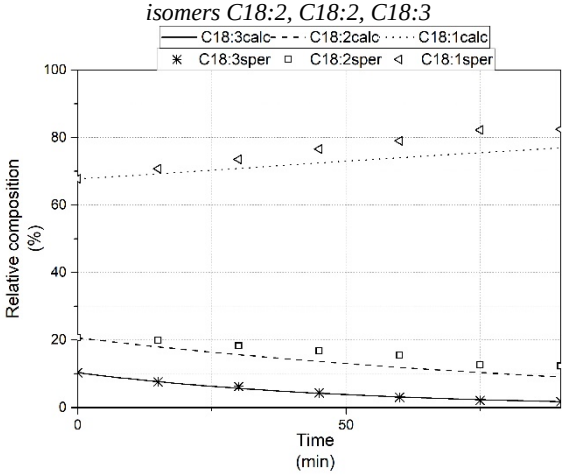

Figure A-21 Test 07 Model fitting for C18:1, C18:2 and C18:3, k1=0.000244, k2=0.0091, k3=0.0198

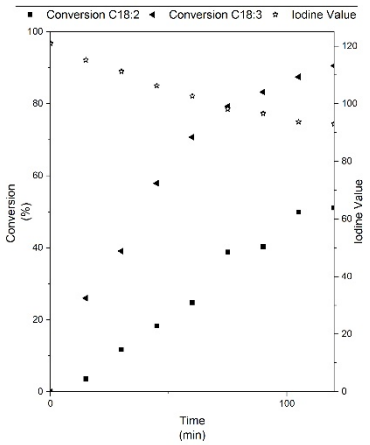

Figure A-22 Test 07 conversions of C18:2 and C18:3, and Iodine Value trend

A.8 Test 08: Lindlar - Canola – 180 °C – 4 bar – 4 $mg_{catalyst}/mL_{oil}$ – 1st cycle

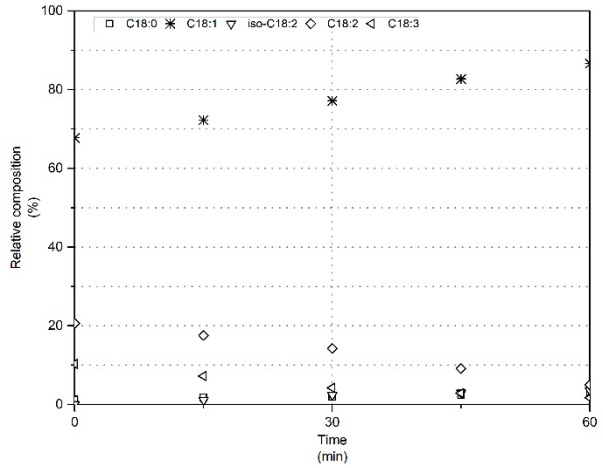

Figure A-23 Test 08 relative percentages of C18:0, C18:1, isomers C18:2, C18:2, C18:3

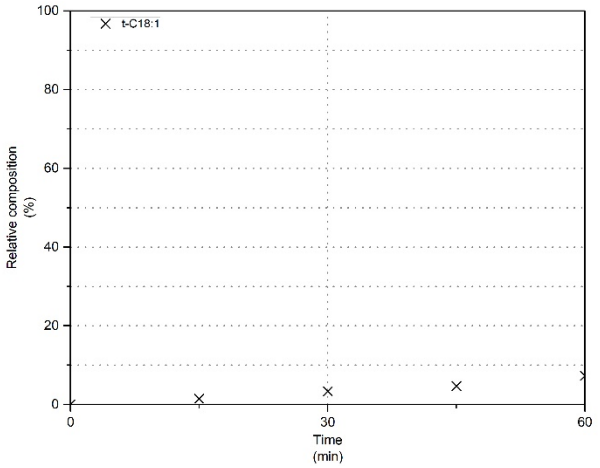

Figure A-24 Test 08 relative percentage of t-C18:1 estimated from the chromatogram

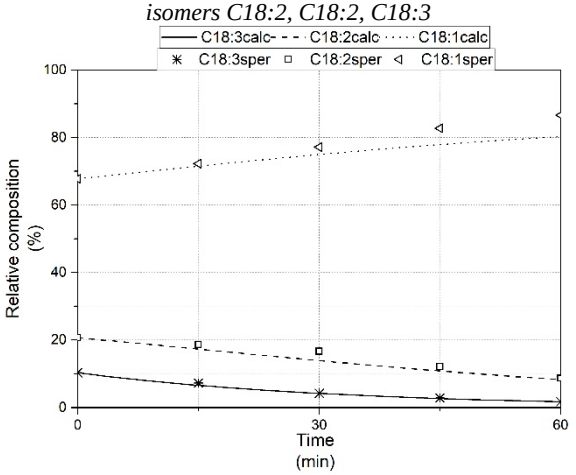

Figure A-25 Test 08 Model fitting for C18:1, C18:2 and C18:3, k1=0.000522, k2=0.0246, k3=0.0300

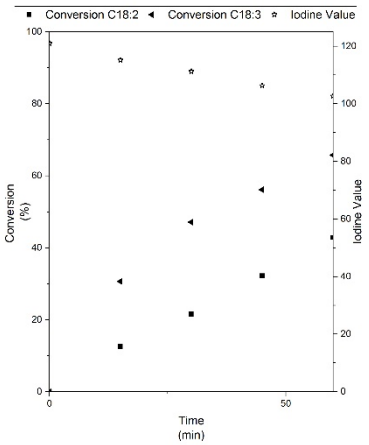

Figure A-26 Test 08 conversions of C18:2 and C18:3, and Iodine Value trend

A.9 Test 09: Lindlar - Canola – 180 °C – 4 bar – 1 $mg_{catalyst}/mL_{oil}$ – 2nd cycle

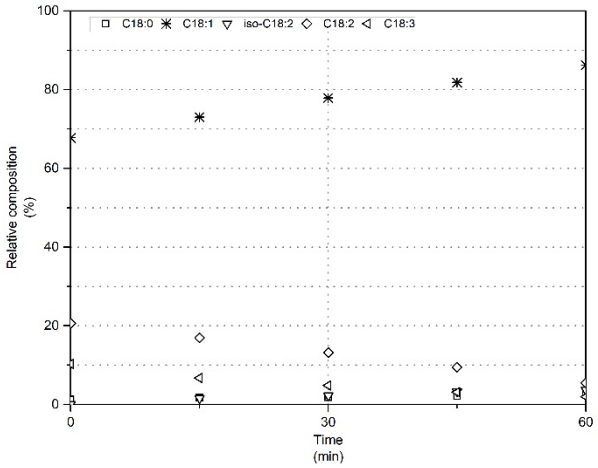

Figure A-27 Test 09 relative percentages of C18:0, C18:1, isomers C18:2, C18:2, C18:3

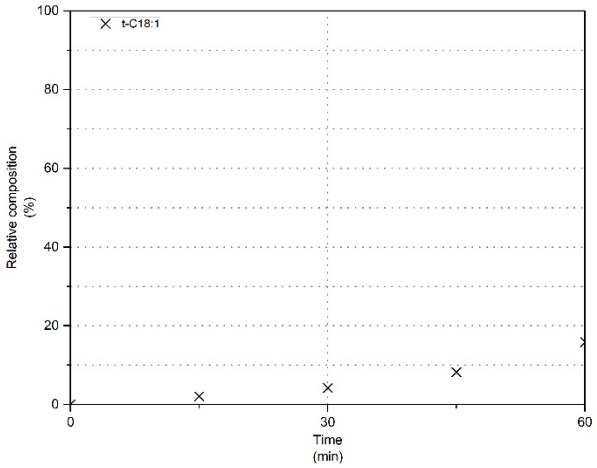

Figure A-28 Test 09 relative percentage of t-C18:1 estimated from the chromatogram

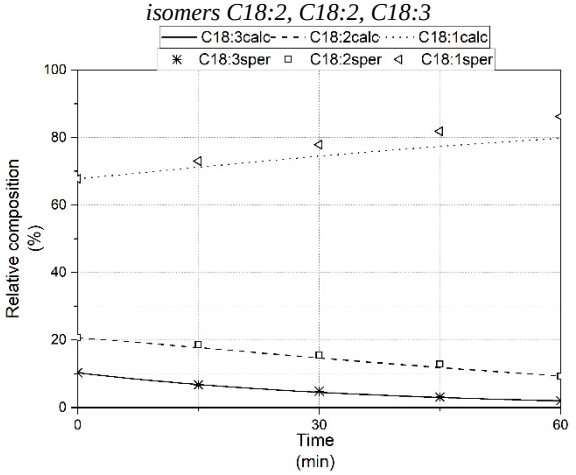

Figure A-29 Test 09 Model fitting for C18:1, C18:2 and C18:3, k1=0.000541, k2=0.0220, k3=0.0275

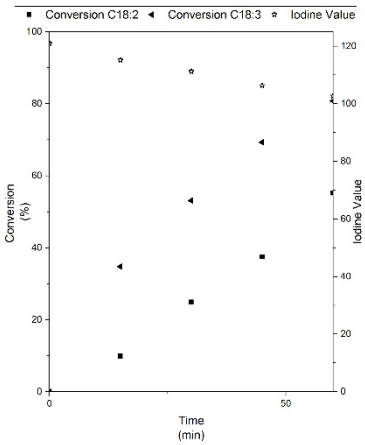

Figure A-30 Test 09 conversions of C18:2 and C18:3, and Iodine Value trend

A.10 Test 10: Lindlar - Canola – 180 °C – 4 bar – 1 $mg_{catalyst}/mL_{oil}$ – 3rd cycle

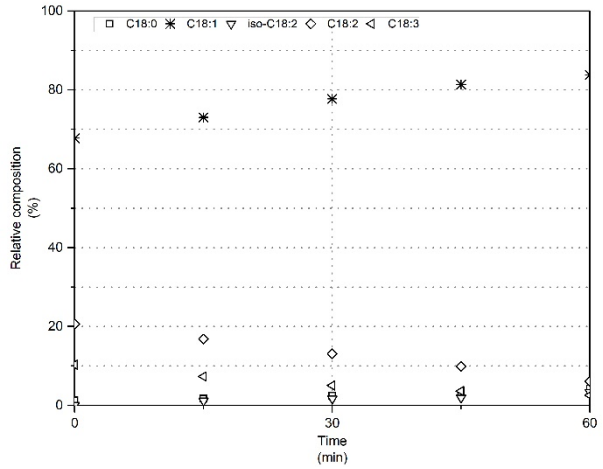

Figure A-31 Test 10 relative percentages of m C18:0, C18:1, isomers C18:2, C18:2, C18:3

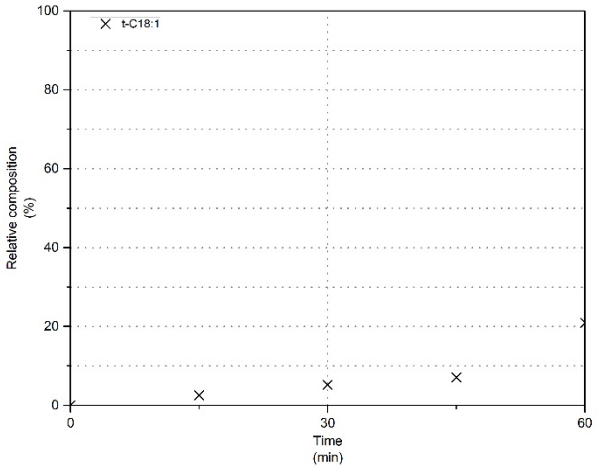

Figure A-32 Test 10 relative percentage of t-C18:1 estimated from the chromatogram

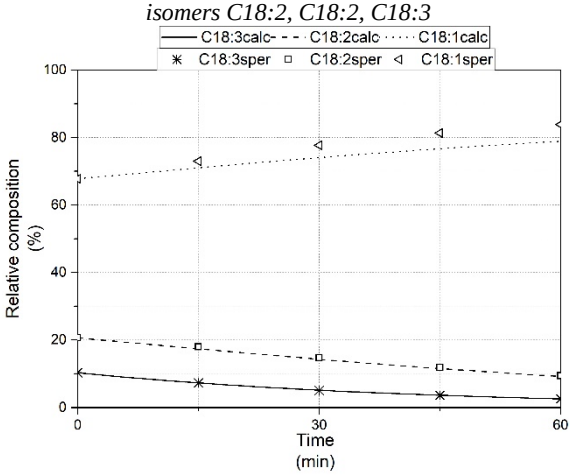

Figure A-33 Test 10 Model fitting for C18:1, C18:2 and C18:3, k1=0.000560, k2=0.0220, k3=0.0232

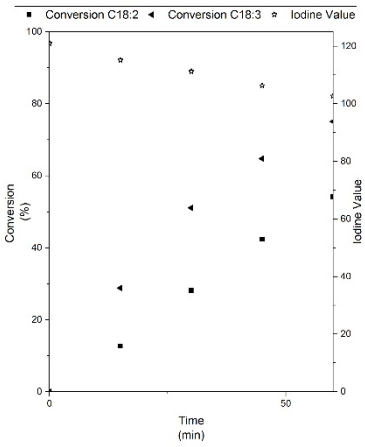

Figure A-34 Test 10 conversions of C18:2 and C18:3, and Iodine Value trend

A.11 Test 11: Lindlar - Canola – 180 °C – 4 bar – 1 $mg_{catalyst}/mL_{oil}$ – 4^{th} cycle

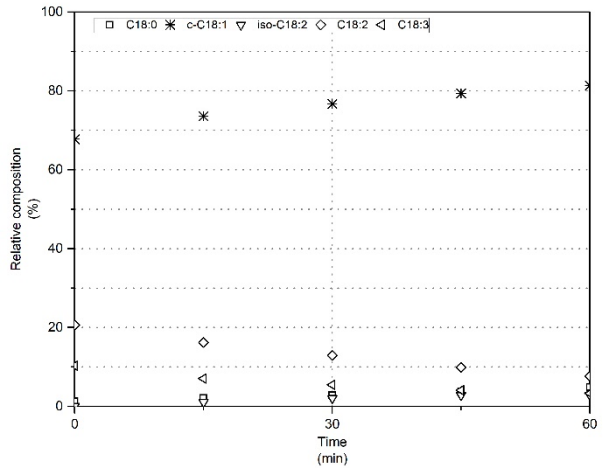

Figure A-35 Test 11 relative percentages of C18:0, C18:1, isomers C18:2, C18:2, C18:3

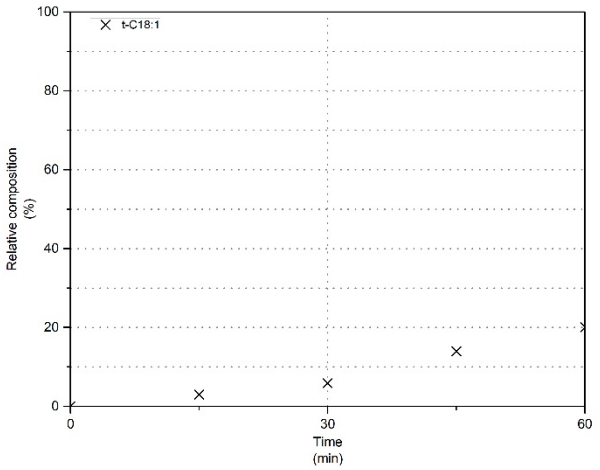

Figure A-36 Test 11 relative percentage of t-C18:1 estimated from the chromatogram

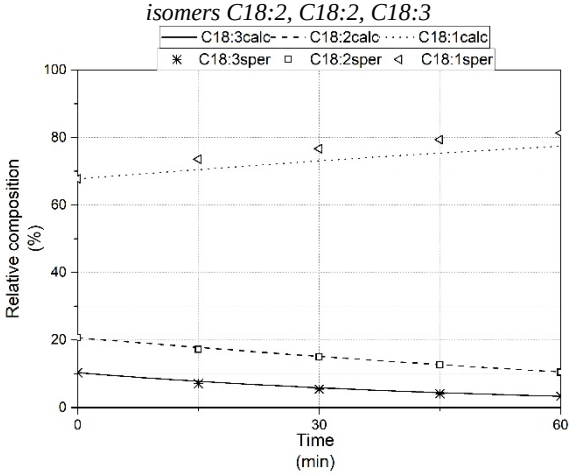

Figure A-37 Test 11 Model fitting for C18:1, C18:2 and C18:3, k1=0.000613, k2=0.00201, k3=0.0196

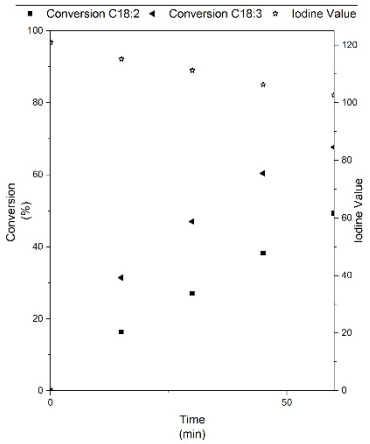

Figure A-38 Test 11 conversions of C18:2 and C18:3, and Iodine Value trend

A.12 Test 12: Lindlar - Canola – 180 °C – 4 bar – 1 $mg_{catalyst}/mL_{oil}$ – 5^{th} cycle

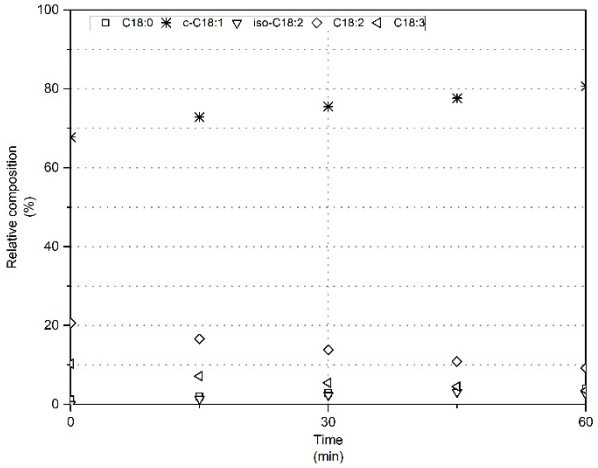

Figure A-39 Test 12relative percentages of C18:0, C18:1, isomers C18:2, C18:2, C18:3

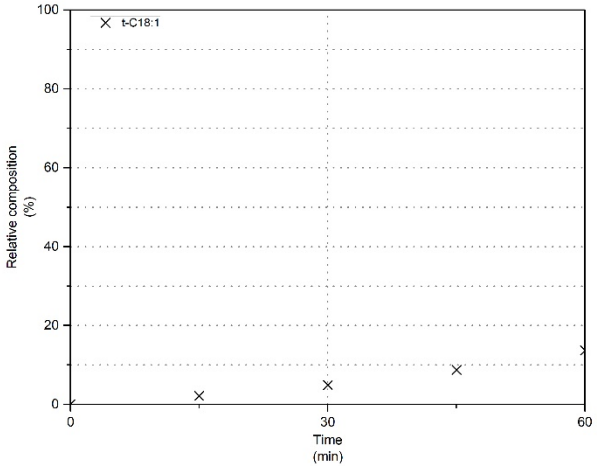

Figure A-40 Test 12 relative percentage of t-C18:1 estimated from the chromatogram

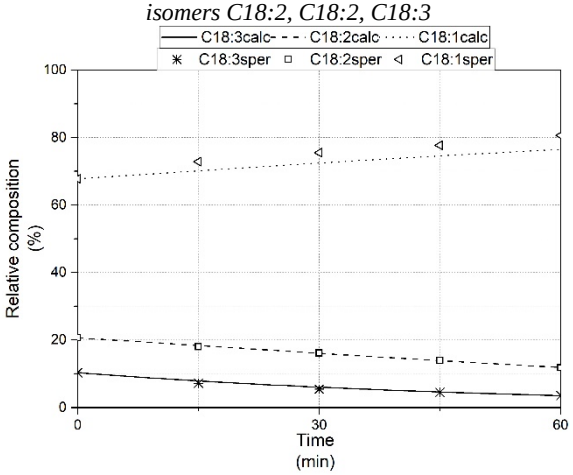

Figure A-41 Test 12 Model fitting for C18:1, C18:2 and C18:3, k1=0.000716, k2=0.00186, k3=0.0189

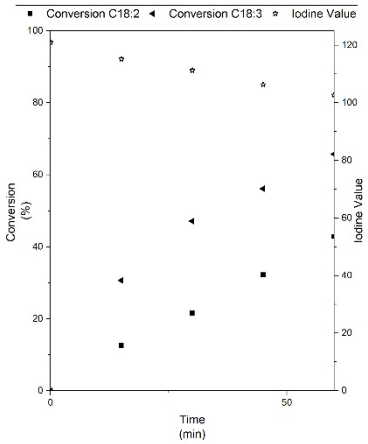

Figure A-42 Test 12 conversions of C18:2 and C18:3, and Iodine Value trend

A.13 Test 13: Lindlar - Sunflower – 180 °C – 4 bar – 4 $mg_{catalyst}/mL_{oil}$

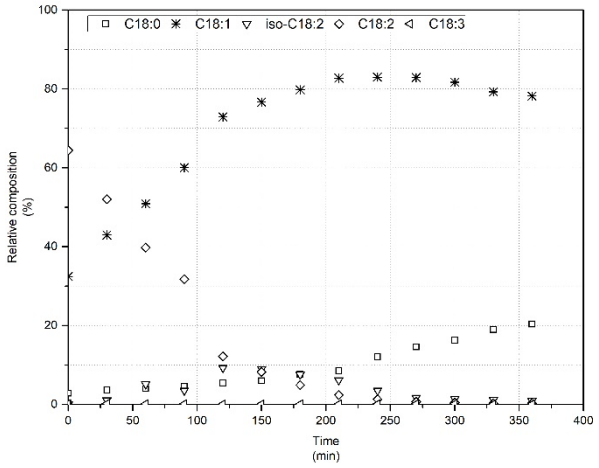

Figure A-43 Test 13 relative percentages of C18:0, C18:1, isomers C18:2, C18:2, C18:3

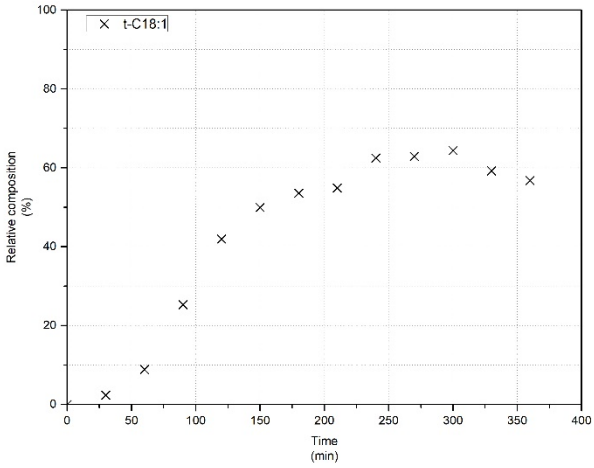

Figure A-44 Test 13 relative percentage of t-C18:1 estimated from the chromatogram

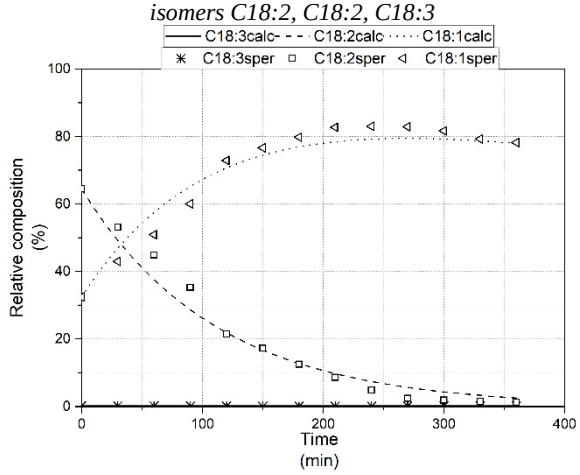

Figure A-45 Test 13 Model fitting for C18:1, C18:2 and C18:3, k1=0.000648, k2=0.00894, k3=0.0000

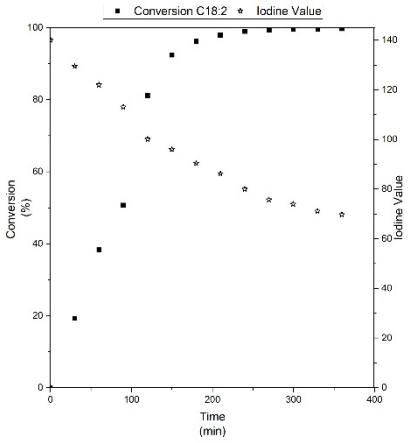

Figure A-46 Test 13 conversions of C18:2, and Iodine Value trend

A.14 Test 14: Pd/HT - Sunflower – 90 °C – 8 bar – 0.5 $mg_{catalyst}/mL_{oil}$

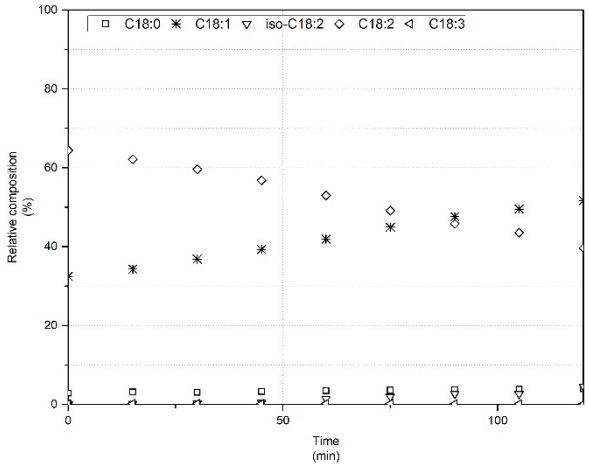

Figure A-47 Test 14 relative percentages of C18:0, C18:1, isomers C18:2, C18:2, C18:3

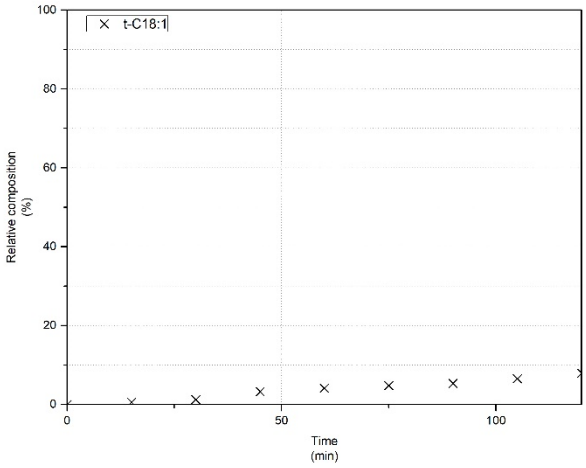

Figure A-48 Test 14 relative percentage of t-C18:1 estimated from the chromatogram

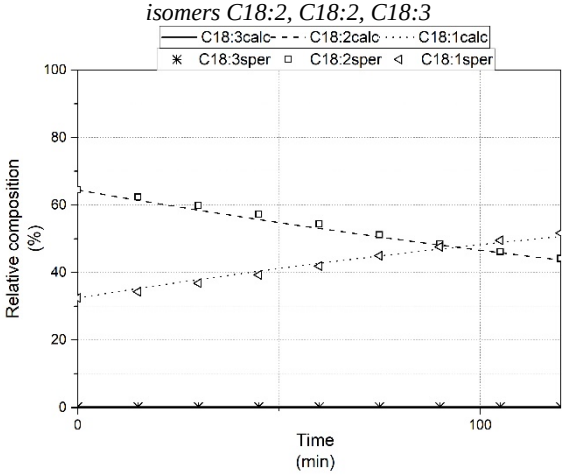

Figure A-49 Test 14 Model fitting for C18:1, C18:2 and C18:3, k1=0.000512, k2=0.00324, k3=0.0000

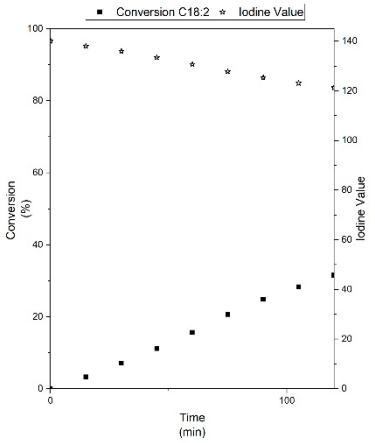

Figure A-50 Test 14 conversions of C18:2, and Iodine Value trend

A.15 Test 15: Pd/HT - Sunflower – 180 °C – 4 bar – 1 $mg_{catalyst}/mL_{oil}$ – 1st cycle

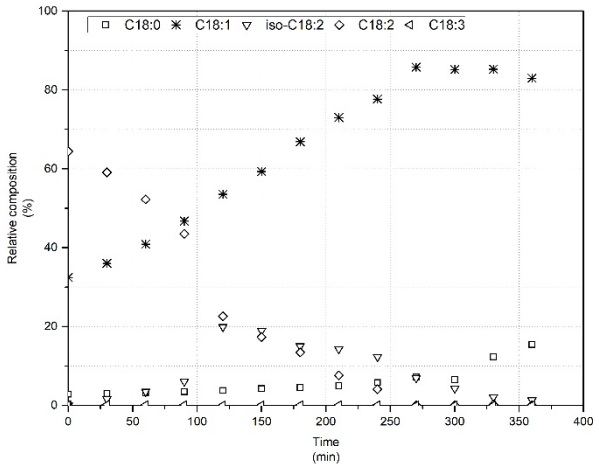

Figure A-51 Test 15 relative percentages of C18:0, C18:1, isomers C18:2, C18:2, C18:3

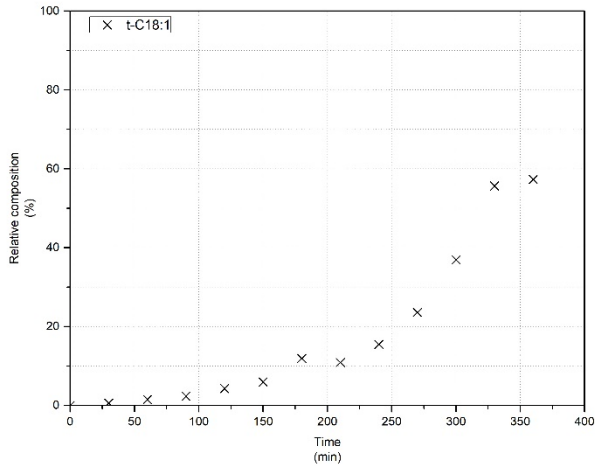

Figure A-52 Test 15 relative percentage of t-C18:1 estimated from the chromatogram

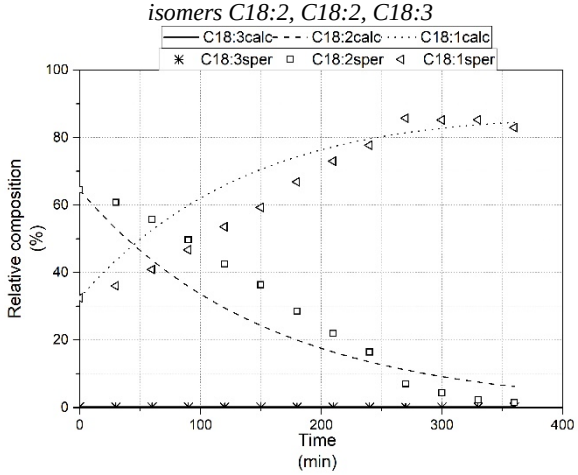

Figure A-53 Test 15 Model fitting for C18:1, C18:2 and C18:3, k1=0.000512, k2=0.00324, k3=0.0000

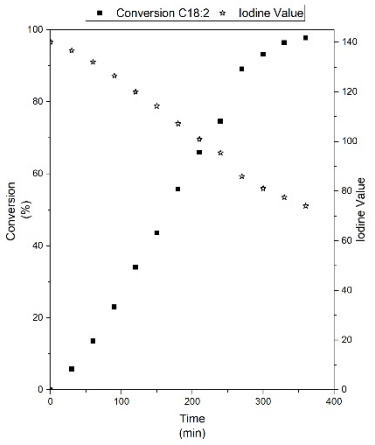

Figure A-54 Test 15 conversions of C18:2, and Iodine Value trend

A.16 Test 16: Pd/HT - Sunflower – 180 °C – 4 bar – 1 $mg_{catalyst}/mL_{oil}$ – 2nd cycle

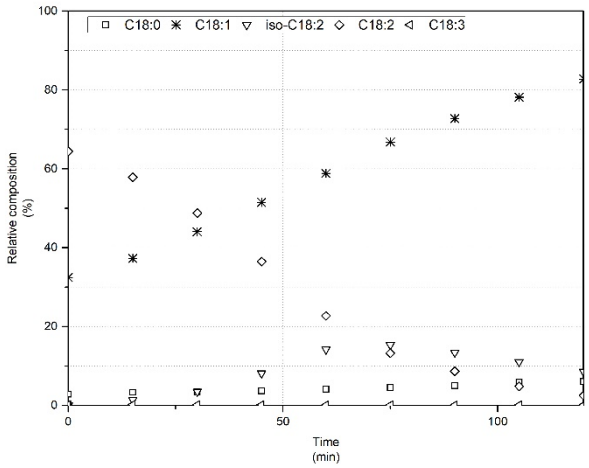

Figure A-55 Test 16 relative percentages of C18:0, C18:1, isomers C18:2, C18:2, C18:3

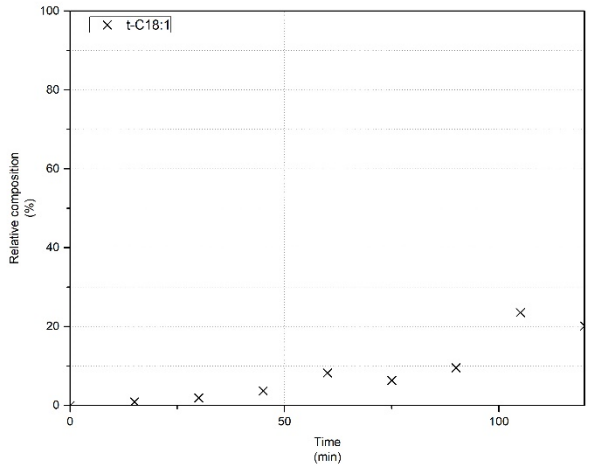

Figure A-56 Test 16 relative percentage of t-C18:1 estimated from the chromatogram

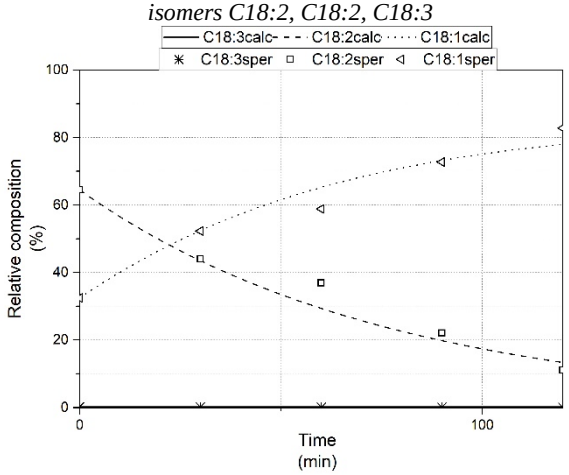

Figure A-57 Test 16 Model fitting for C18:1, C18:2 and C18:3, k1=0.000750, k2=0.00131,, k3=0.0000

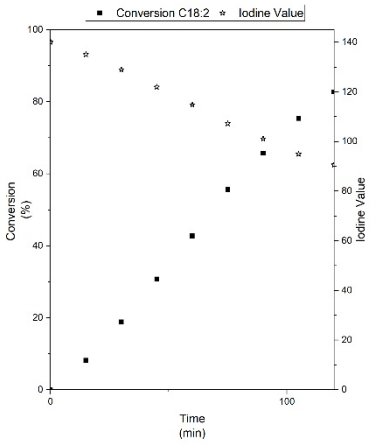

Figure A-58 Test 16 conversions of C18:2, and Iodine Value trend

A.17 Test 17: Pd/HT - Sunflower – 180 °C – 4 bar – 1 $mg_{catalyst}/mL_{oil}$ – 3rd cycle

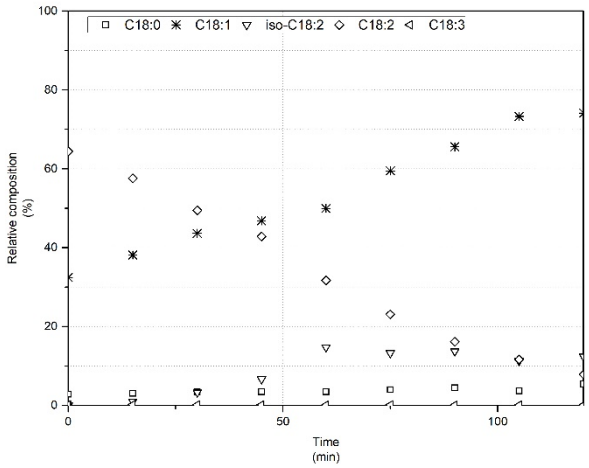

Figure A-59 Test 17 relative percentages of C18:0, C18:1, isomers C18:2, C18:2, C18:3

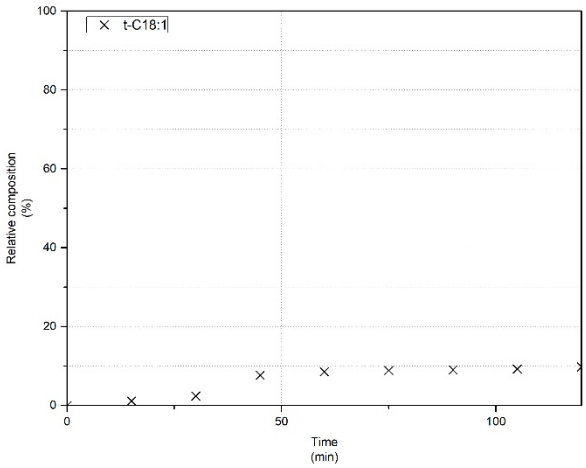

Figure A-60 Test 17 relative percentage of t-C18:1 estimated from the chromatogram

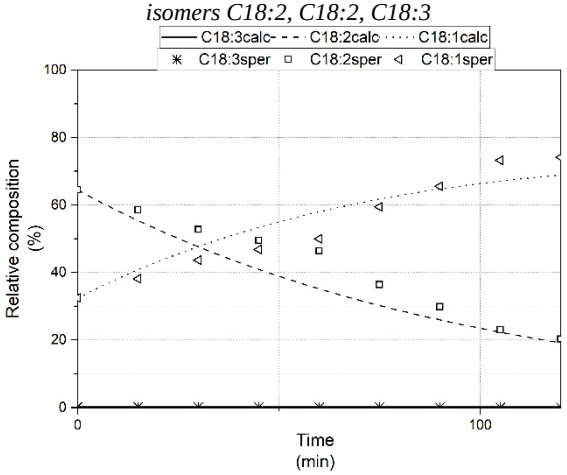

Figure A-61 Test 17 Model fitting for C18:1, C18:2 and C18:3, k1=0.000256, k2=0.00101, k3=0.0000

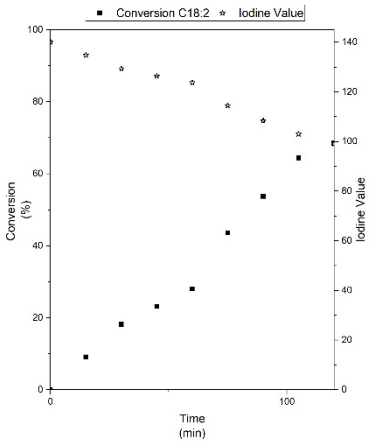

Figure A-62 Test 17 conversions of C18:2, and Iodine Value trend

A.18 Test 18: Pd/HT - Sunflower – 180 °C – 4 bar – 1 $mg_{catalyst}/mL_{oil}$ – 4^{th} cycle

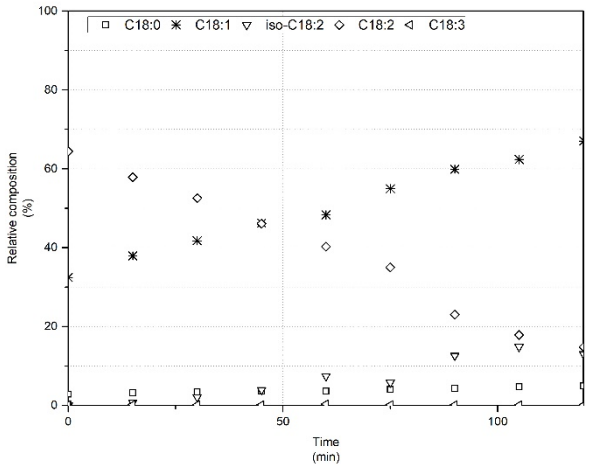

Figure A-63 Test 18 relative percentages of C18:0, C18:1, isomers C18:2, C18:2, C18:3

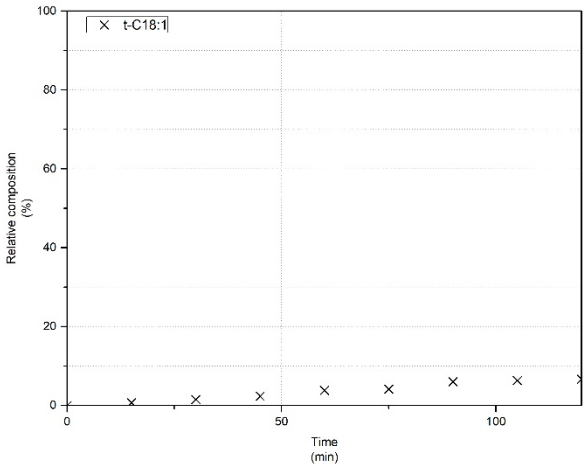

Figure A-64 Test 18 relative percentage of t-C18:1 estimated from the chromatogram

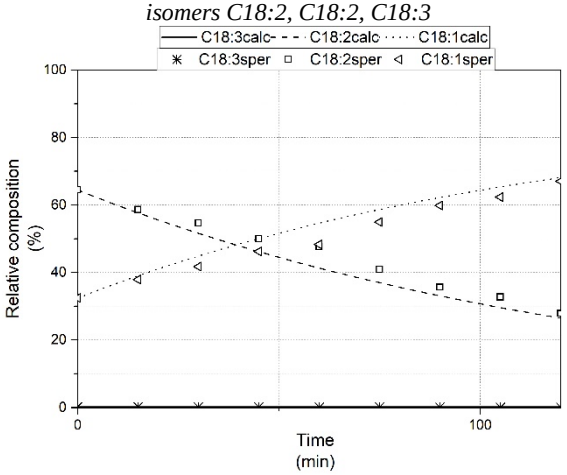

Figure A-65 Test 18 Model fitting for C18:1, C18:2 and C18:3, k1=0.000358, k2=0.00741, k3=0.0000

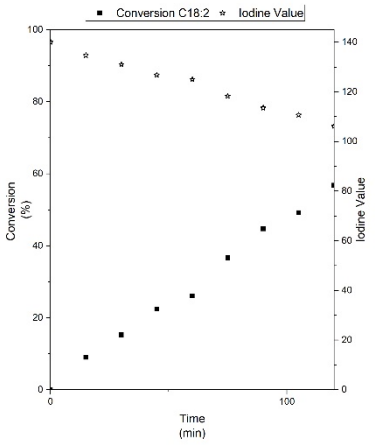

Figure A-66 Test 18 conversions of C18:2, and Iodine Value trend

A.19 Test 19: Pd/HT - Sunflower – 120 °C – 4 bar – 1 $mg_{catalyst}/mL_{oil}$ –1st cycle

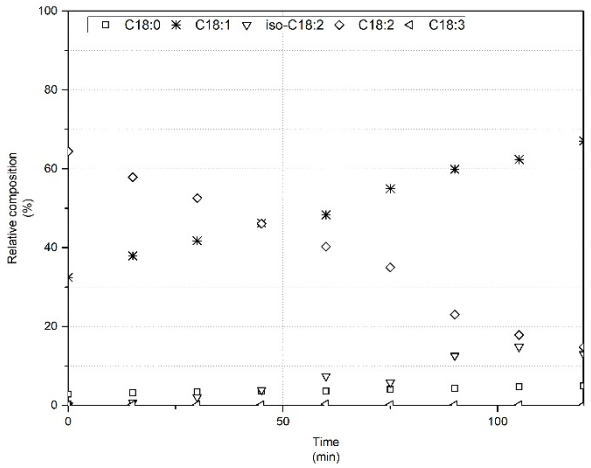

Figure A-67 Test 19 relative percentages of C18:0, C18:1, isomers C18:2, C18:2, C18:3

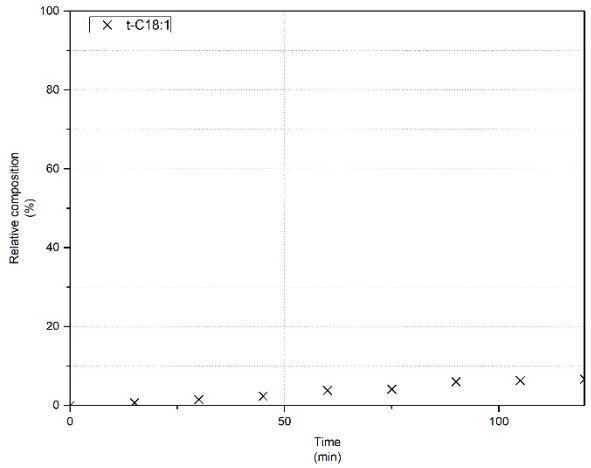

Figure A-68 Test 19 relative percentage of t-C18:1 estimated from the chromatogram

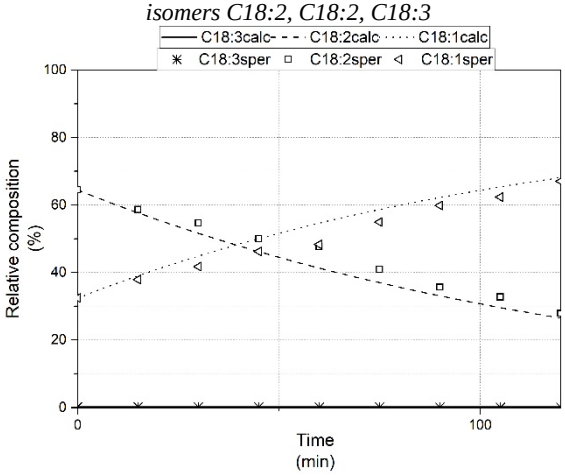

Figure A-69 Test 19 Model fitting for C18:1, C18:2 and C18:3, k1=0.000358, k2=0.00741, k3=0.0000

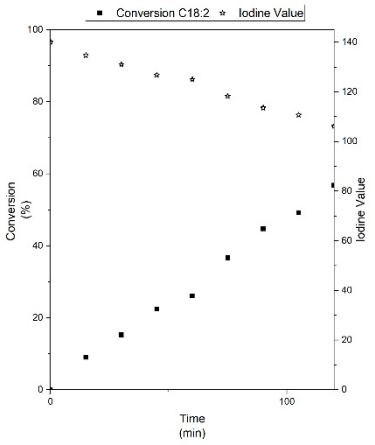

Figure A-70 Test 19 conversions of C18:2, and Iodine Value trend

A.20 Test 20: Pd/HT - Sunflower – 120 °C – 4 bar – 1 $mg_{catalyst}/mL_{oil}$ – 2nd cycle

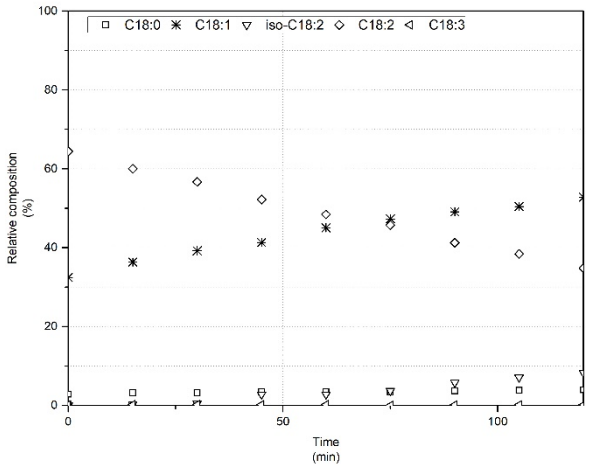

Figure A-71 Test 20 relative percentages of C18:0, C18:1, isomers C18:2, C18:2, C18:3

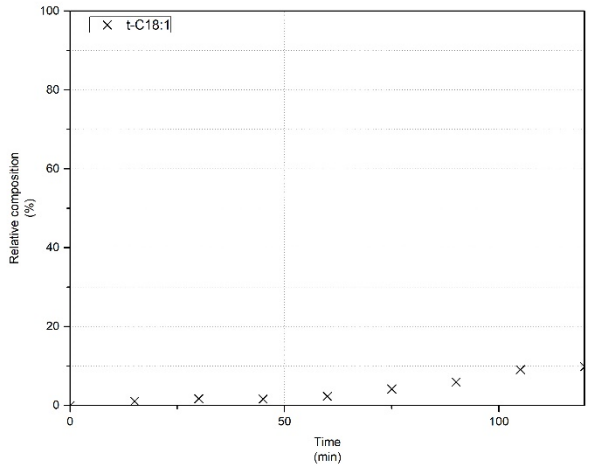

Figure A-72 Test 20 relative percentage of t-C18:1 estimated from the chromatogram

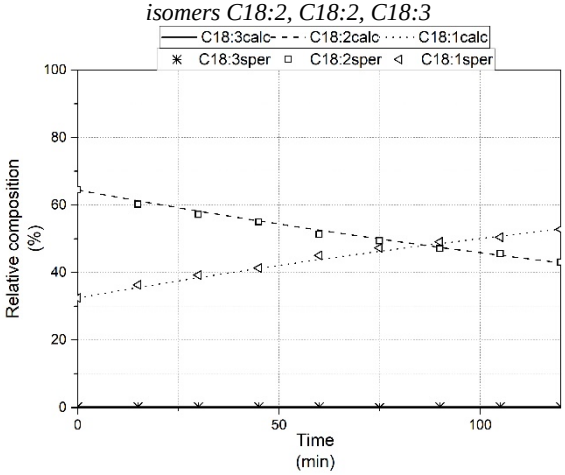

Figure A-73 Test 20 Model fitting for C18:1, C18:2 and C18:3, k1=0.000114, k2=0.0034, k3=0.0000

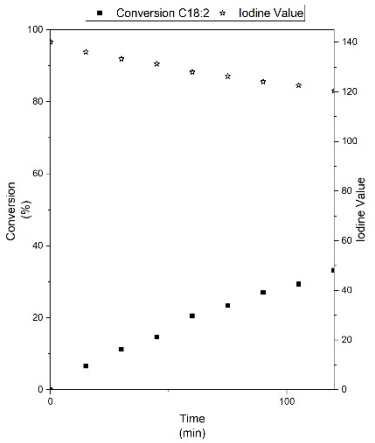

Figure A-74 Test 20 conversions of C18:2, and Iodine Value trend

A.21 Test 21: Pd/HT - Sunflower – 120 °C – 4 bar – 1 $mg_{catalyst}/mL_{oil}$ – 3rd cycle

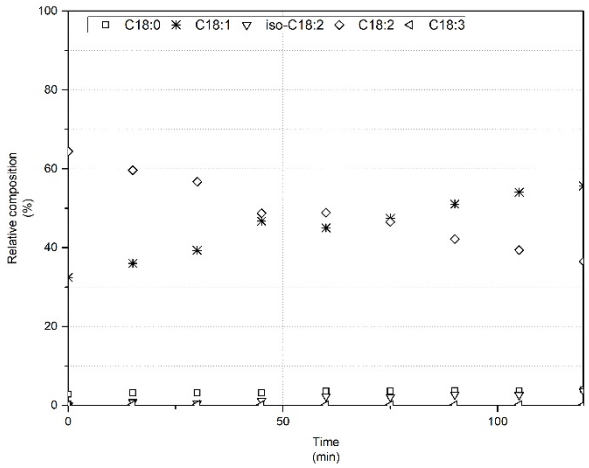

Figure A-75 Test 21 relative percentages of C18:0, C18:1, isomers C18:2, C18:2, C18:3

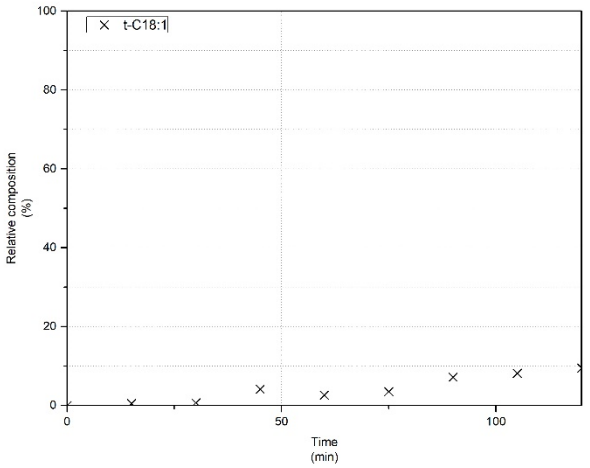

Figure A-76 Test 21 relative percentage of t-C18:1 estimated from the chromatogram

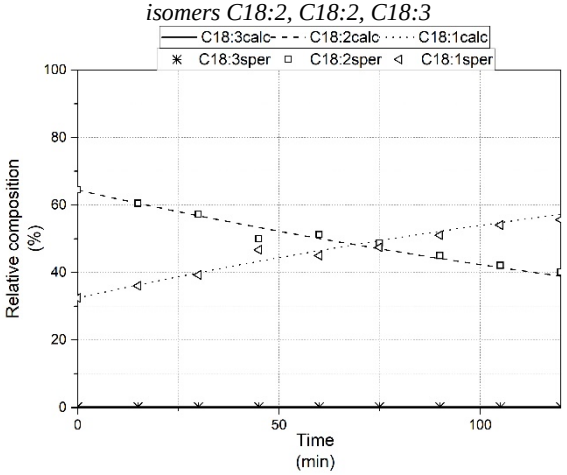

Figure A-77 Test 21 Model fitting for C18:1, C18:2 and C18:3, k1=0.000137, k2=0.0042, k3=0.0000

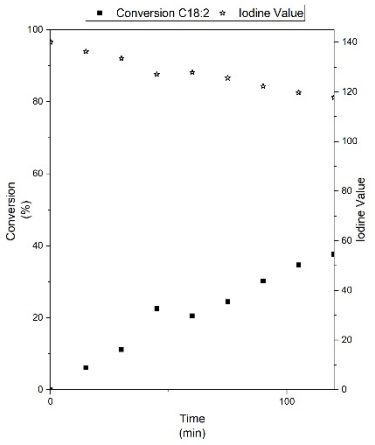

Figure A-78 Test 21 conversions of C18:2, and Iodine Value trend

A.22 Test 22: Pd/HT - Sunflower – 120 °C – 4 bar – 0.5 $mg_{catalyst}/mL_{oil}$ – 1st cycle

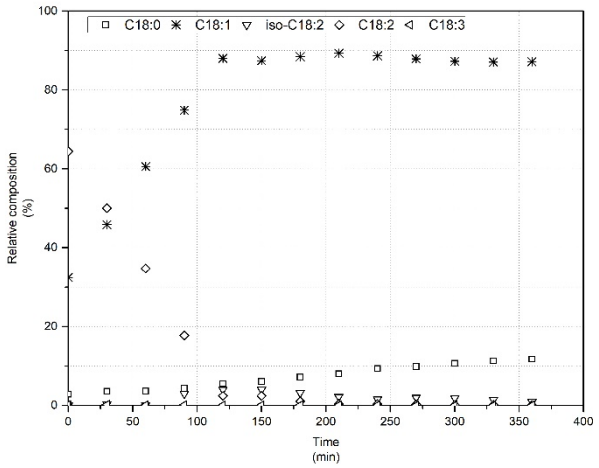

Figure A-79 Test 22 relative percentages of C18:0, C18:1, isomers C18:2, C18:2, C18:3

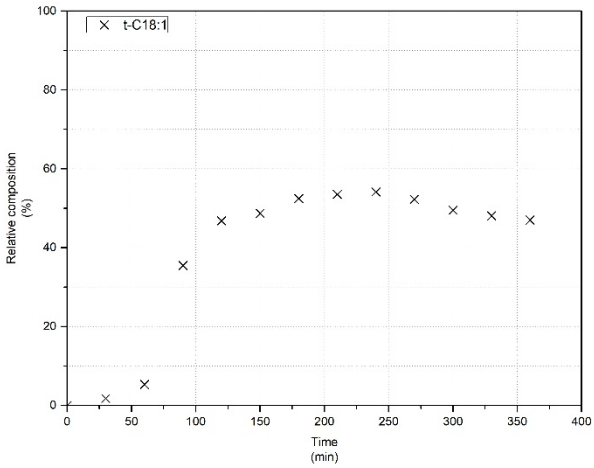

Figure A-80 Test 22 relative percentage of t-C18:1 estimated from the chromatogram

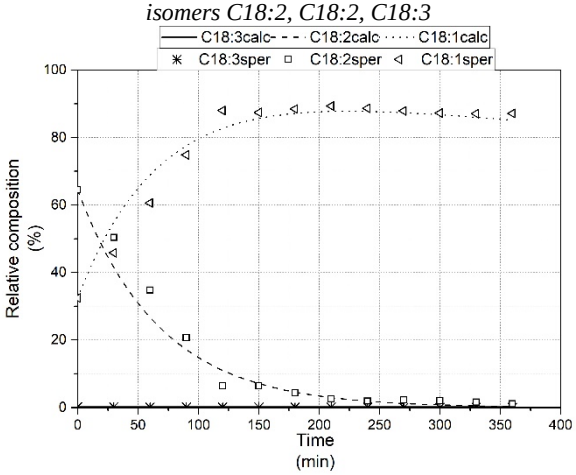

Figure A-81 Test 22 Model fitting for C18:1, C18:2 and C18:3, k1=0.000114, k2=0.0034, k3=0.0000

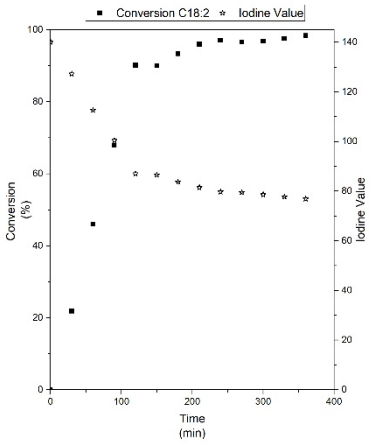

Figure A-82 Test 22 conversions of C18:2, and Iodine Value trend

A.23 Test 23: Pd/HT - Sunflower – 120 °C – 4 bar – 0.5 $mg_{catalyst}/mL_{oil}$ – 2nd cycle

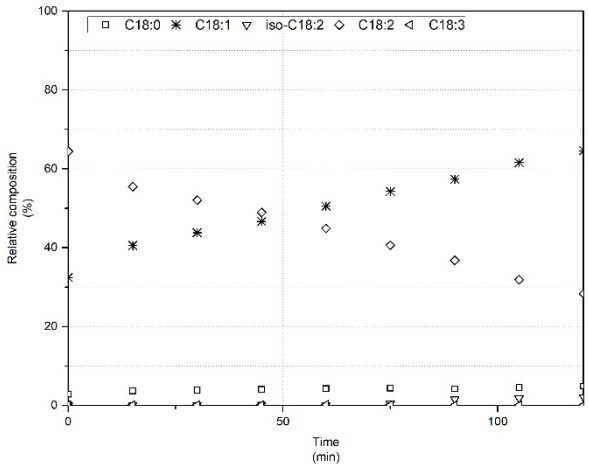

Figure A-83 Test 23 relative percentages of C18:0, C18:1, isomers C18:2, C18:2, C18:3

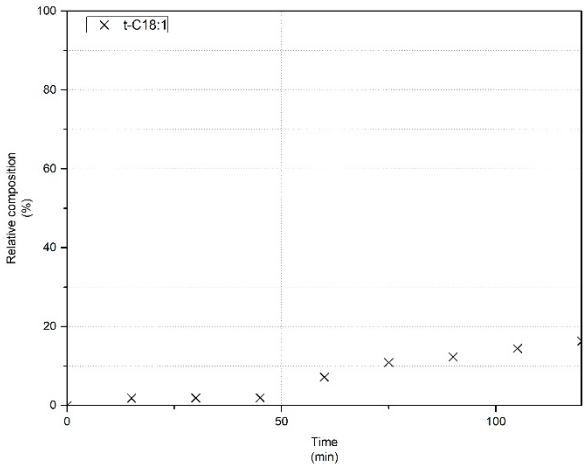

Figure A-84 Test 23 relative percentage of t-C18:1 estimated from the chromatogram

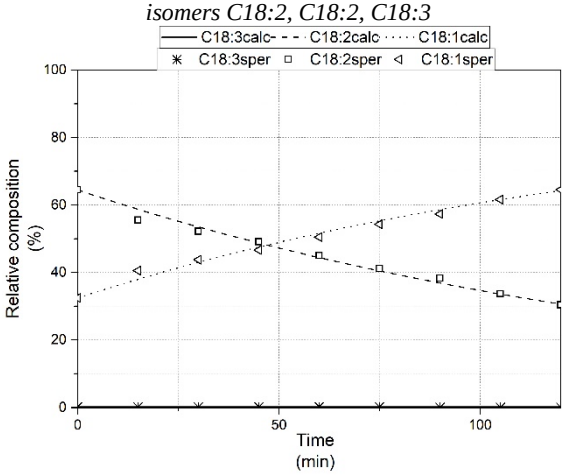

Figure A-85 Test 23 Model fitting for C18:1, C18:2 and C18:3, k1=0.000330, k2=0.0062, k3=0.0000

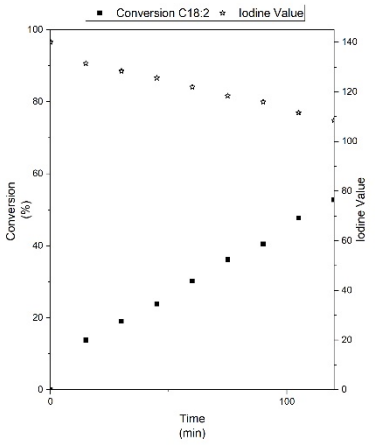

Figure A-86 Test 23 conversions of C18:2, and Iodine Value trend

A.24 Test 24: Pd/HT - Sunflower – 120 °C – 12 bar – 0.5 $mg_{catalyst}/mL_{oil}$ – 1st cycle

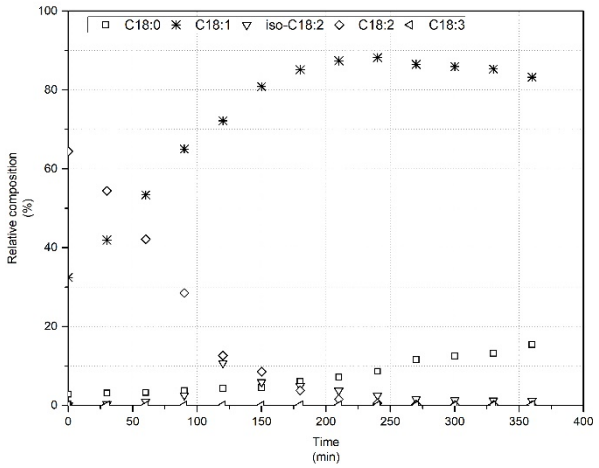

Figure A-87 Test 24 relative percentages of C18:0, C18:1, isomers C18:2, C18:2, C18:3

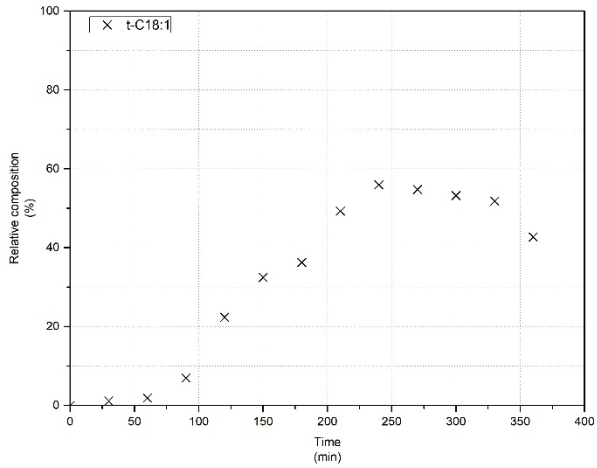

Figure A-88 Test 24 relative percentage of t-C18:1 estimated from the chromatogram

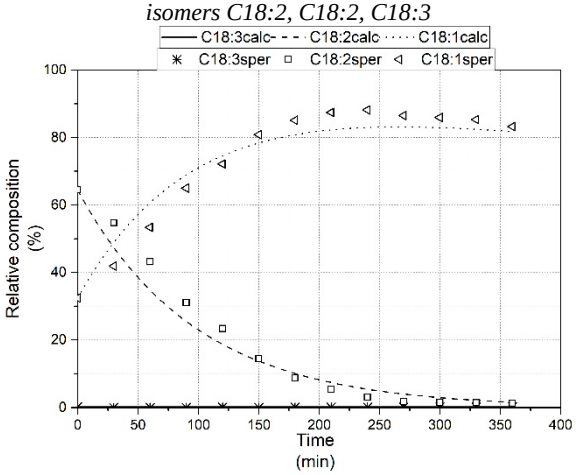

Figure A-89 Test 24 Model fitting for C18:1, C18:2 and C18:3, k1=0.000512, k2=0.0103, k3=0.0000

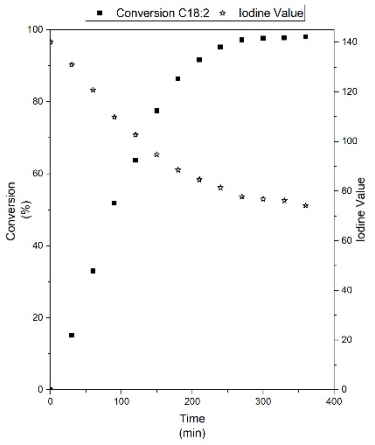

Figure A-90 Test 24 conversions of C18:2, and Iodine Value trend

A.25 Test 25: Pd/HT - Sunflower – 120 °C – 12 bar – 0.5 $mg_{catalyst}/mL_{oil}$ – 2nd cycle

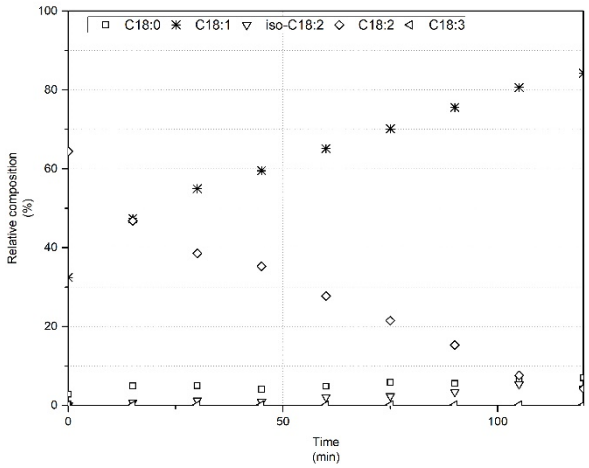

Figure A-91 Test 25 relative percentages of C18:0, C18:1, isomers C18:2, C18:2, C18:3

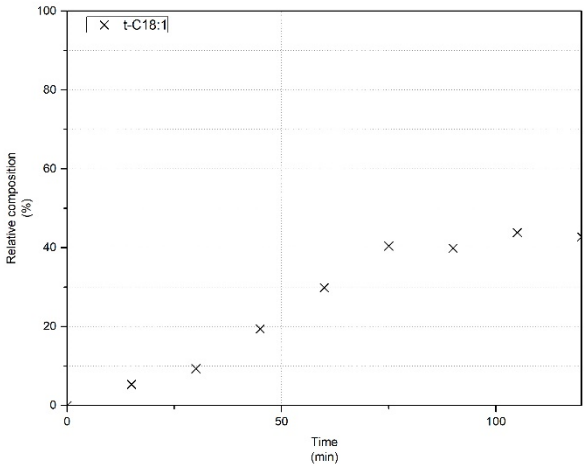

Figure A-92 Test 25 relative percentage of t-C18:1 estimated from the chromatogram

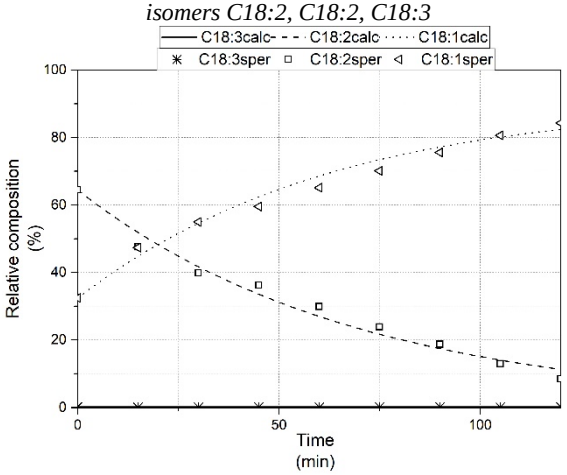

Figure A-93 Test 25 Model fitting for C18:1, C18:2 and C18:3, k1=0.000413, k2=0.0145, k3=0.0000

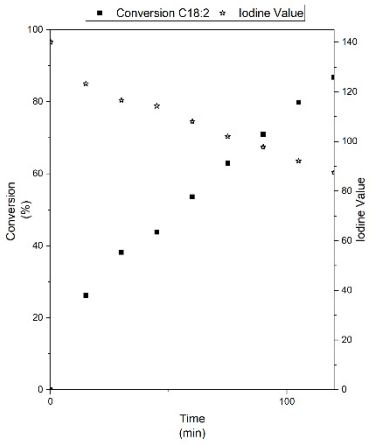

Figure A-94 Test 25 conversions of C18:2, and Iodine Value trend

A.26 Test 26: Pd/HT - Sunflower – 120 °C – 4 bar – 2 $mg_{catalyst}/mL_{oil}$ – 1st cycle

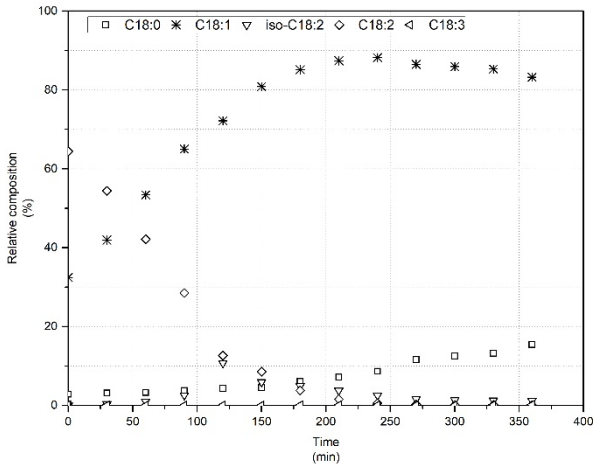

Figure A-95 Test 26 relative percentages of C18:0, C18:1, isomers C18:2, C18:2, C18:3

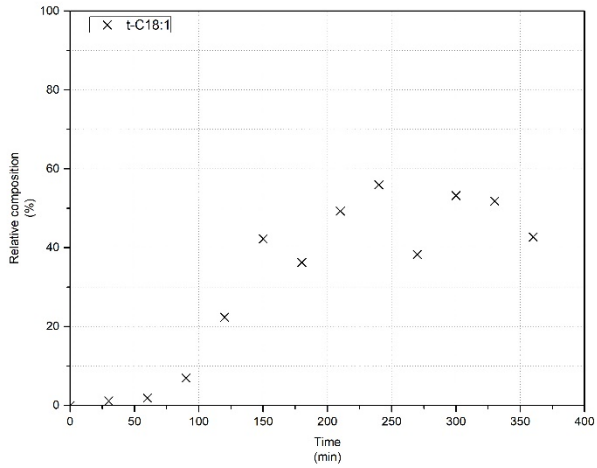

Figure A-96 Test 26 relative percentage of t-C18:1 estimated from the chromatogram

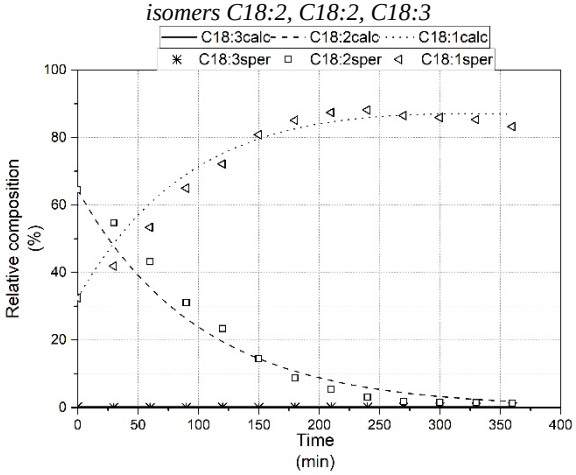

Figure A-97 Test 26 Model fitting for C18:1, C18:2 and C18:3, k1=0.000302, k2=0.0096, k3=0.0000

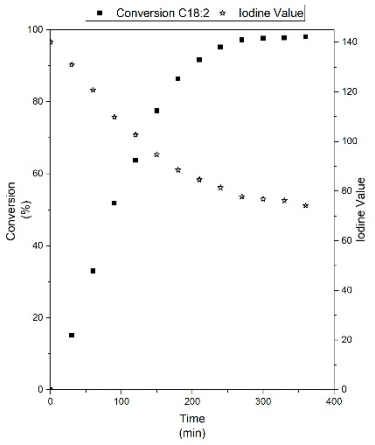

Figure A-98 Test 26 conversions of C18:2, and Iodine Value trend

A.27 Test 27: Pd/HT - Sunflower – 120 °C – 4 bar – 2 $mg_{catalyst}/mL_{oil}$ –2nd cycle

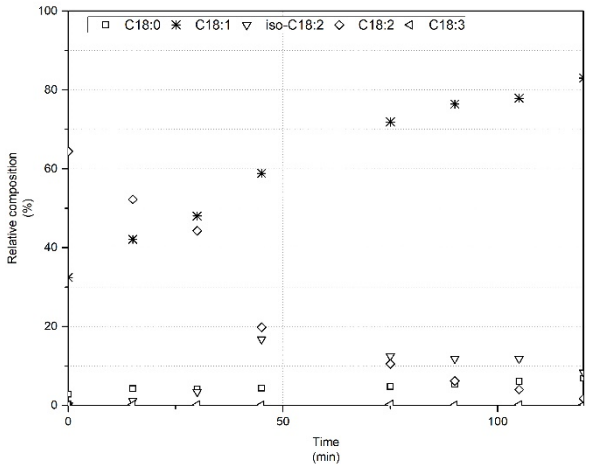

Figure A-99 Test 27 relative percentages of C18:0, C18:1, isomers C18:2, C18:2, C18:3

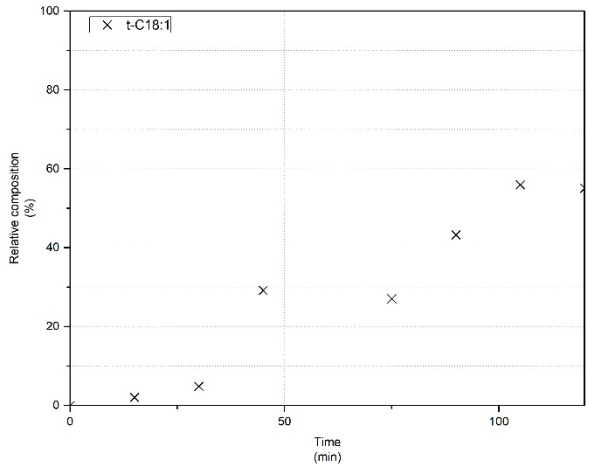

Figure A-100 Test 27 relative percentage of t-C18:1 estimated from the chromatogram

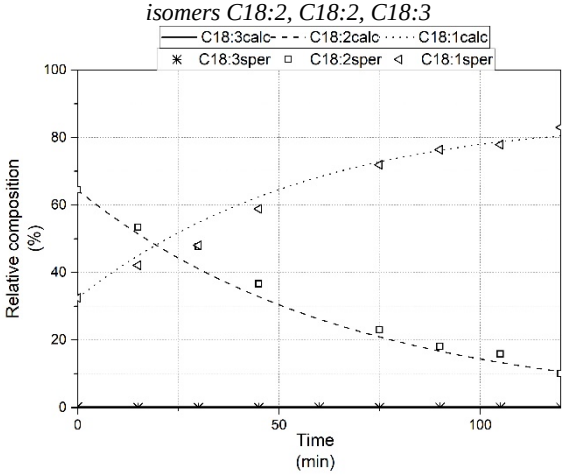

Figure A-101 Test 27 Model fitting for C18:1, C18:2 and C18:3, k1=0.000745, k2=0.015, k3=0.0000

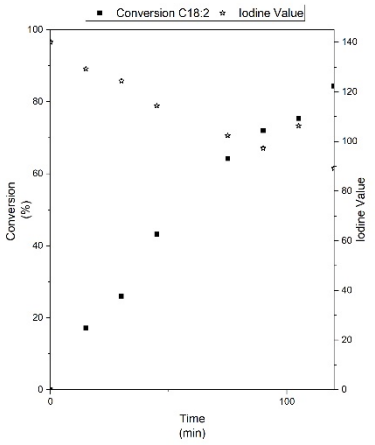

Figure A-102 Test 27 conversions of C18:2, and Iodine Value trend

A.28 Test 28: Cu5SiO$_2$AE - Canola – 180 °C – 4 bar – 4 mg$_{catalyst}$/mL$_{oil}$

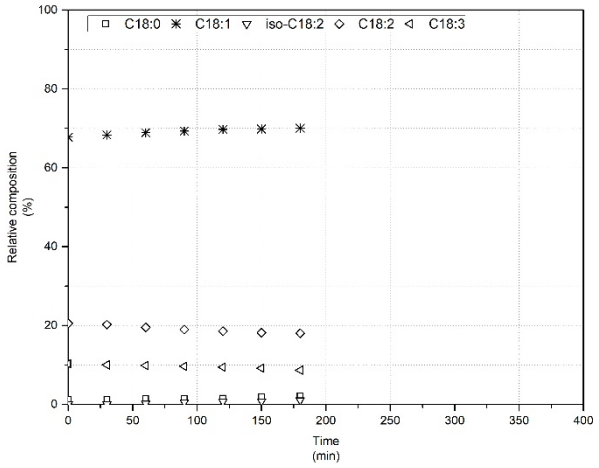

Figure A-103 Test 28 relative percentages of C18:0, C18:1, isomers C18:2, C18:2, C18:3

A.29 Test 29: $Cu5SiO_2AE$ - Canola – 180 °C – 12 bar – 4 $mg_{catalyst}/mL_{oil}$

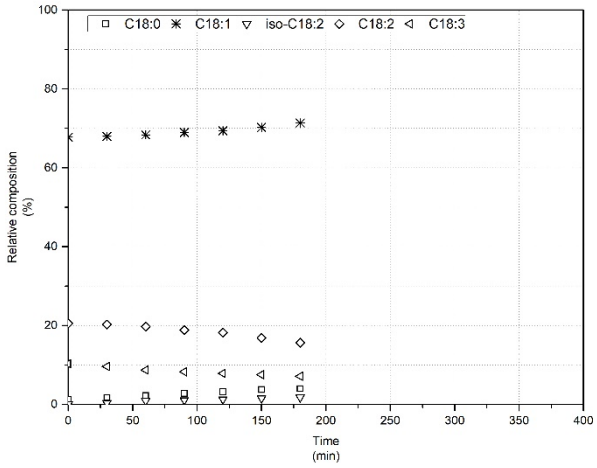

Figure A-104 Test 29 relative percentages of C18:0, C18:1, isomers C18:2, C18:2, C18:3

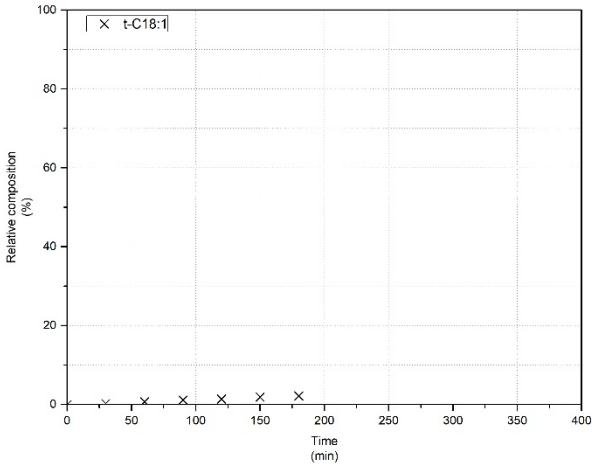

Figure A-105 Test 29 relative percentage of t-C18:1 estimated from the chromatogram

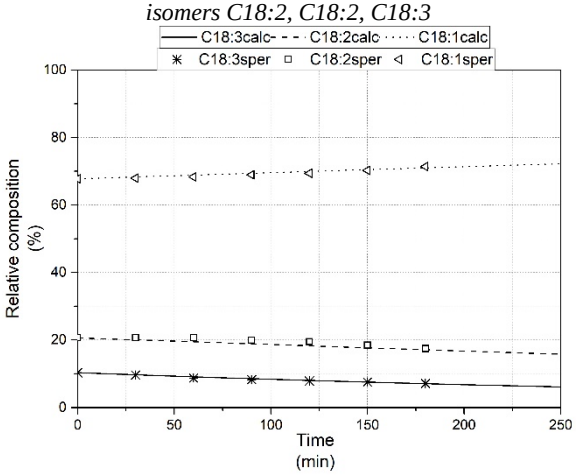

Figure A-106 Test 29 Model fitting for C18:1, C18:2 and C18:3, k1=0.00000302, k2=0.000314, k3=0.00201

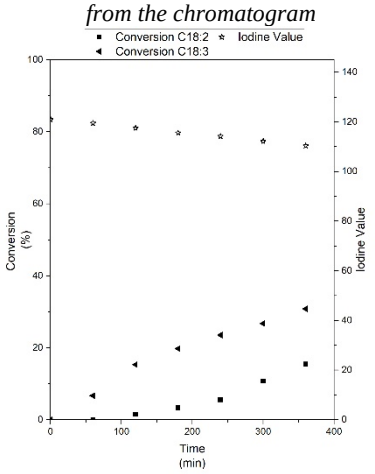

Figure A-107 Test 29 conversions of C18:2 and C18:3, and Iodine Value trend

A.30 Test 30: $Cu5SiO_2AE$ - Canola – 200 °C – 4 bar – 4 $mg_{catalyst}/mL_{oil}$

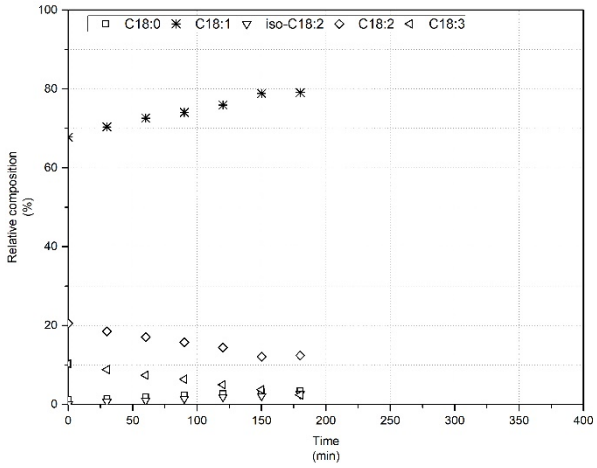

Figure A-108 Test 30 relative percentages of C18:0, C18:1, isomers C18:2, C18:2, C18:3

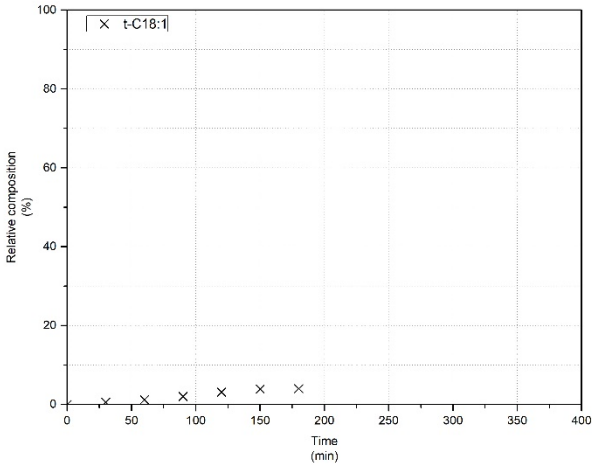

Figure A-109 Test 30 relative percentage of t-C18:1 estimated from the chromatogram

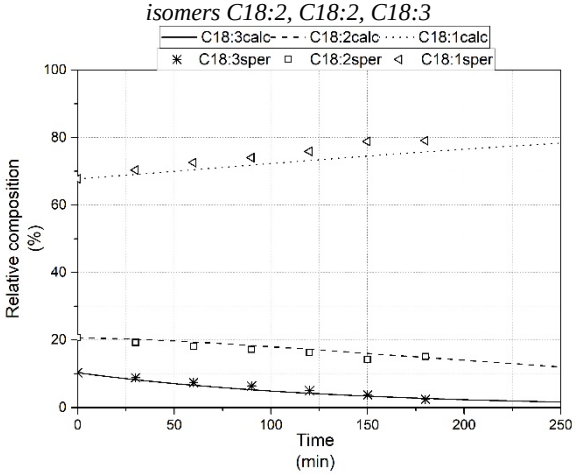

Figure A-110 Test 30 Model fitting for C18:1, C18:2 and C18:3, k1=0.0000649, k2=0.00411, k3=0.00746

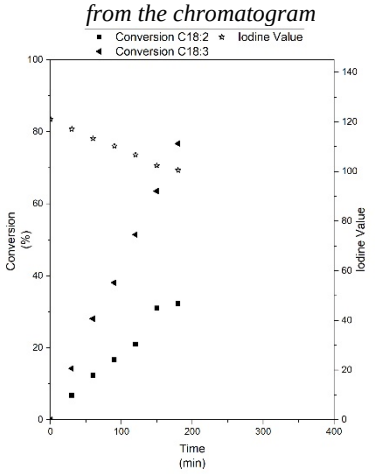

Figure A-111 Test 30 conversions of C18:2 and C18:3, and Iodine Value trend

A.31 Test 31: Cu5SiO$_2$AE - Canola – 200 °C – 12 bar – 4 mg$_{catalyst}$/mL$_{oil}$

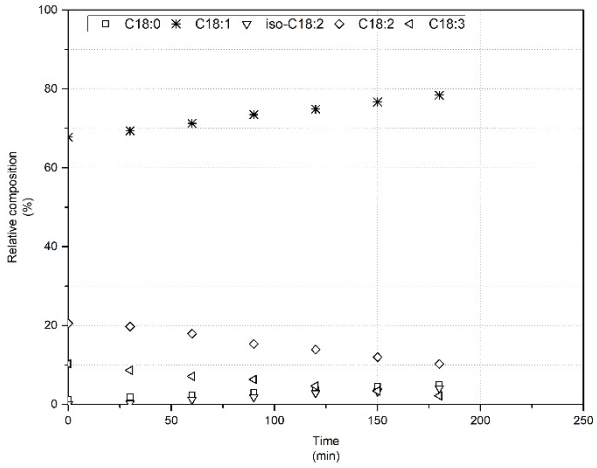

Figure A-112 Test 31 relative percentages of C18:0, C18:1, isomers C18:2, C18:2, C18:3

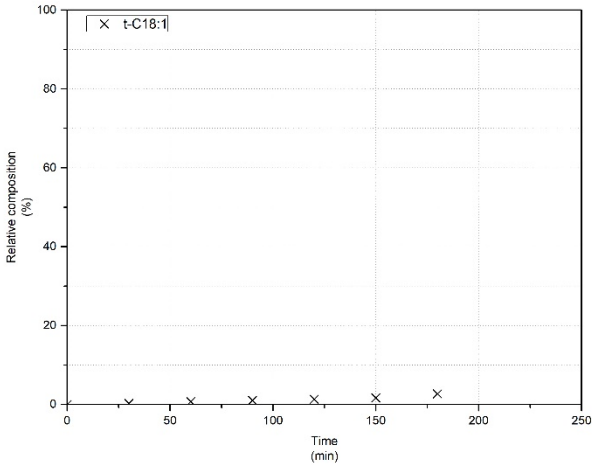

Figure A-113 Test 31 relative percentage of t-C18:1 estimated from the chromatogram

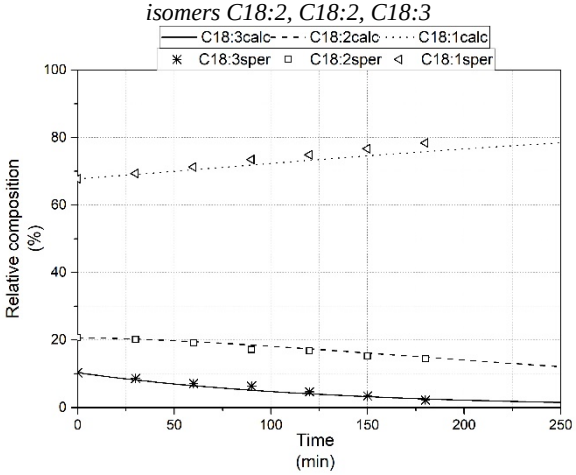

Figure A-114 Test 31 Model fitting for C18:1, C18:2 and C18:3, k1=0.0000619, k2=0.00112, k3=0.000778

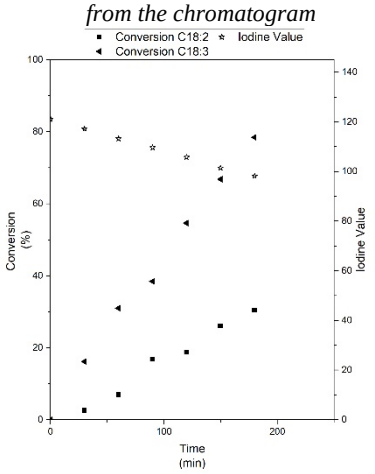

Figure A-115 Test 31 conversions of C18:2 and C18:3, and Iodine Value trend

A.32 Test 32: Cu5SiO$_2$HP - Canola – 180 °C – 4 bar – 4 mg$_{catalyst}$/mL$_{oil}$

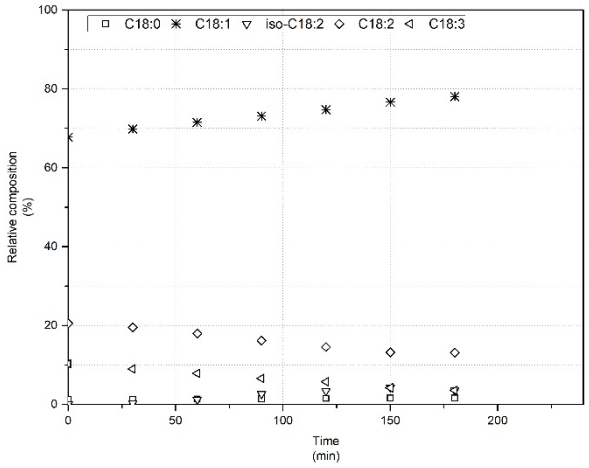

Figure A-116 Test 32 relative percentages of C18:0, C18:1, isomers C18:2, C18:2, C18:3

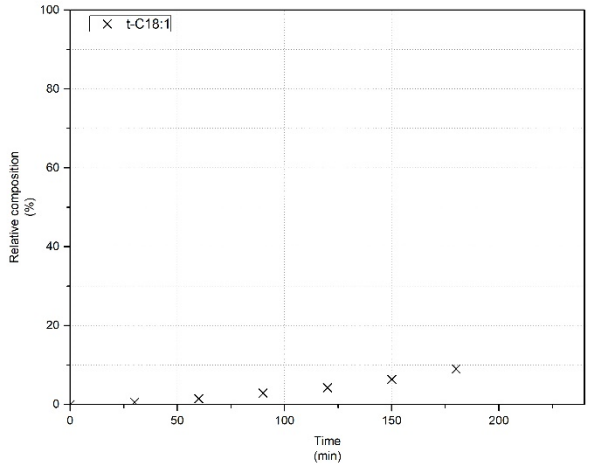

Figure A-117 Test 32 relative percentage of t-C18:1 estimated from the chromatogram

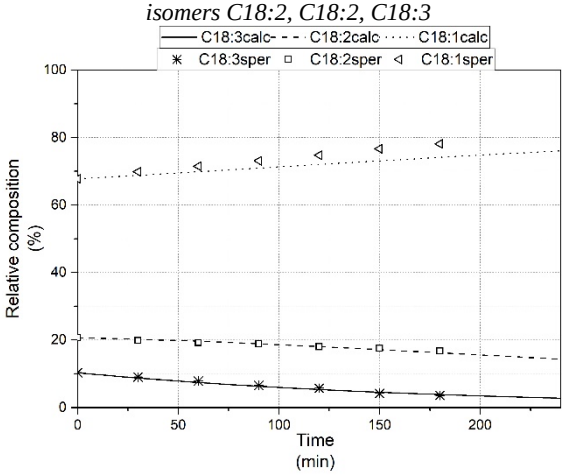

Figure A-118 Test 32 Model fitting for C18:1, C18:2 and C18:3, k1=0.000000126, k2=0.000902, k3=0.00588

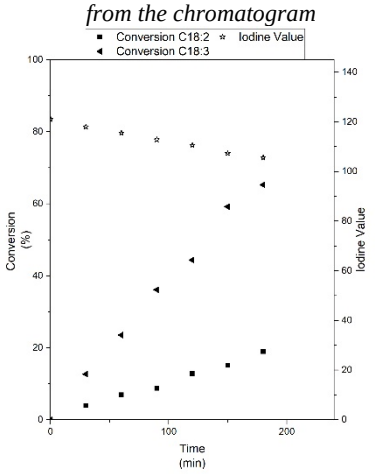

Figure A-119 Test 27 conversions of C18:2 and C18:3, and Iodine Value trend

A.33 Test 33: Cu5SiO$_2$HP - Canola – 180 °C – 12 bar – 4 mg$_{catalyst}$/mL$_{oil}$

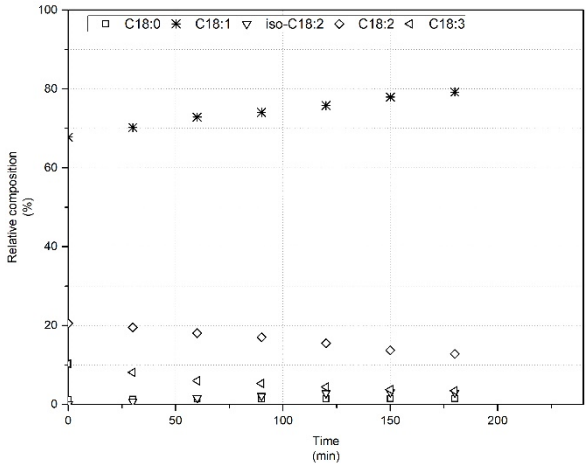

Figure A-120 Test 33 relative percentages of C18:0, C18:1, isomers C18:2, C18:2, C18:3

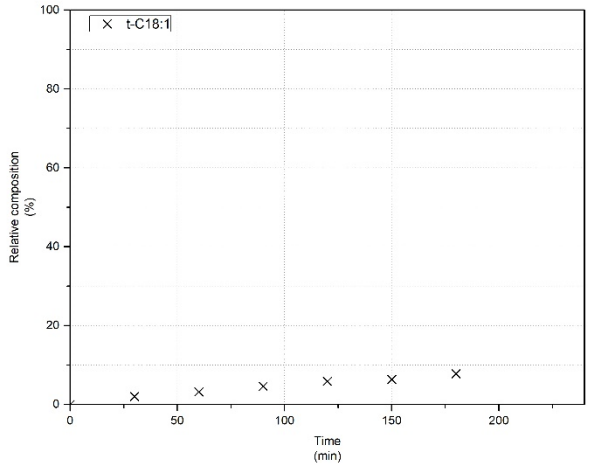

Figure A-121 Test 33 relative percentage of t-C18:1 estimated from the chromatogram

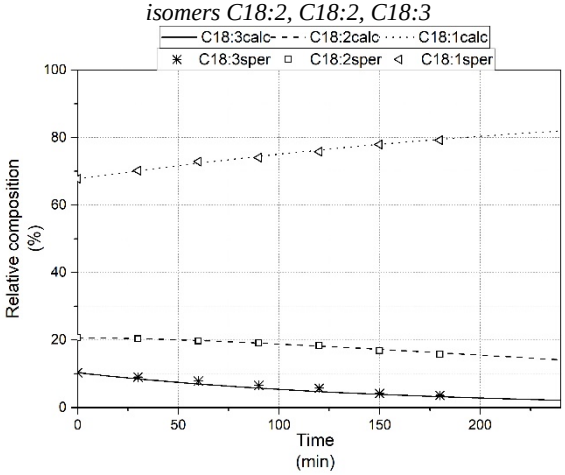

Figure A-122 Test 33 Model fitting for C18:1, C18:2 and C18:3, k1=0.000000349, k2=0.000124, k3=0.00650

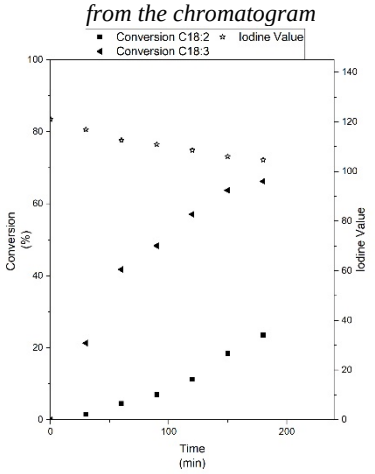

Figure A-123 Test 33 conversions of C18:2 and C18:3, and Iodine Value trend

A.34 Test 34: Cu5SiO$_2$HP - Canola – 200 °C – 4 bar – 4 mg$_{catalyst}$/mL$_{oil}$

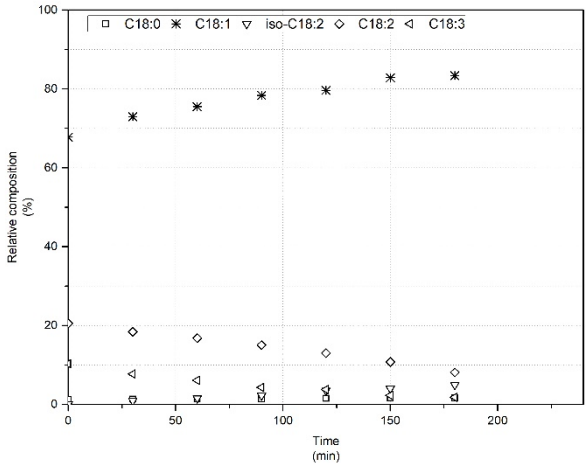

Figure A-124 Test 34 relative percentages of C18:0, C18:1, isomers C18:2, C18:2, C18:3

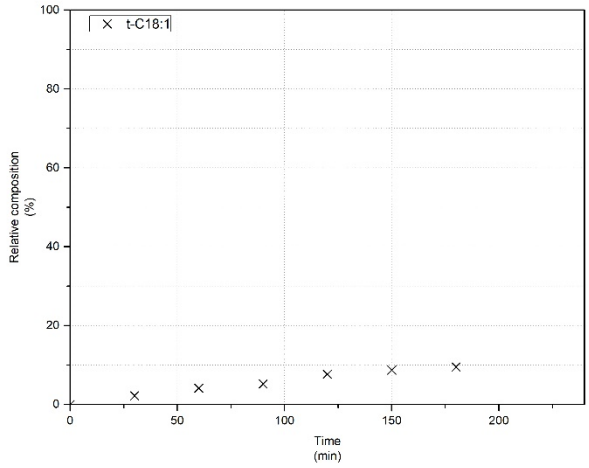

Figure A-125 Test 34 relative percentage of t-C18:1 estimated from the chromatogram

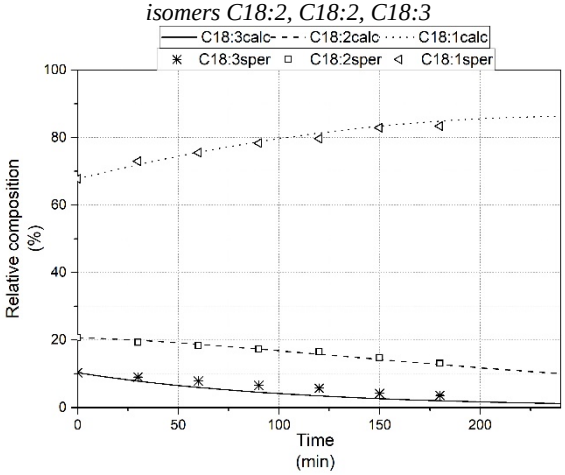

Figure A-126 Test 34 Model fitting for C18:1, C18:2 and C18:3, k1=0.00000526, k2=0.00141, k3=0.00913

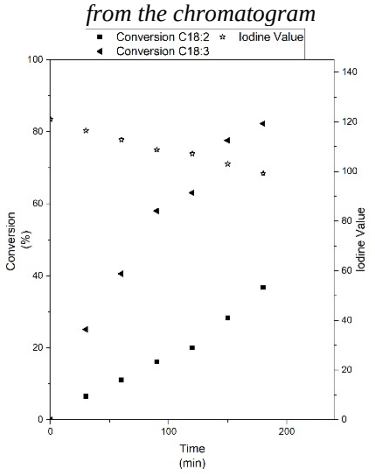

Figure A-127 Test 34 conversions of C18:2 and C18:3, and Iodine Value trend

A.35 Test 35: Cu5SiO$_2$HP - Canola – 200 °C – 12 bar – 4 mg$_{catalyst}$/mL$_{oil}$

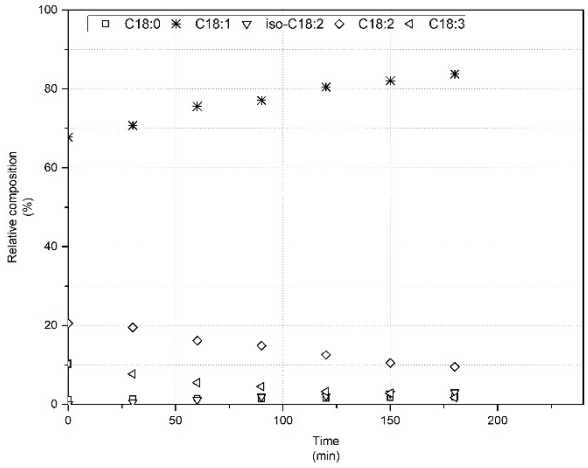

Figure A-128 Test 35 relative percentages of C18:0, C18:1, isomers C18:2, C18:2, C18:3

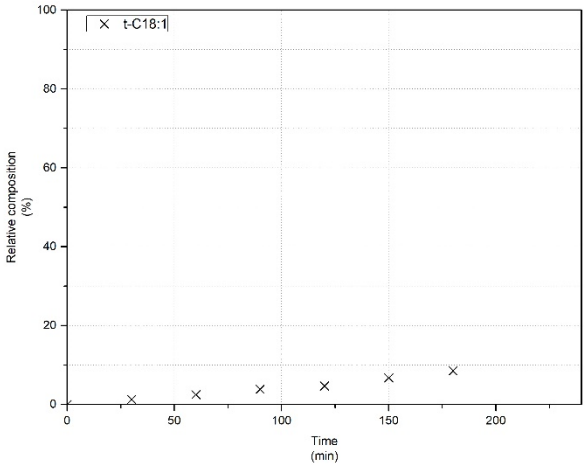

Figure A-129 Test 35 relative percentage of t-C18:1 estimated from the chromatogram

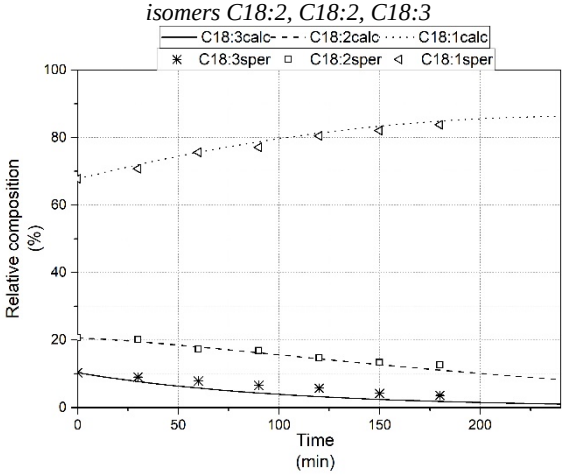

Figure A-130 Test 35 Model fitting for C18:1, C18:2 and C18:3, k1=0.00000674, k2=0.00148, k3=0.00973

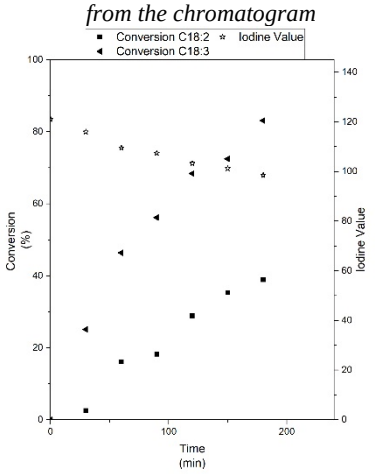

Figure A-131 Test 35 conversions of C18:2 and C18:3, and Iodine Value trend

A.36 Test 36: Cu10SiO$_2$AE - Canola – 180 °C – 4 bar – 4 mg$_{catalyst}$/mL$_{oil}$

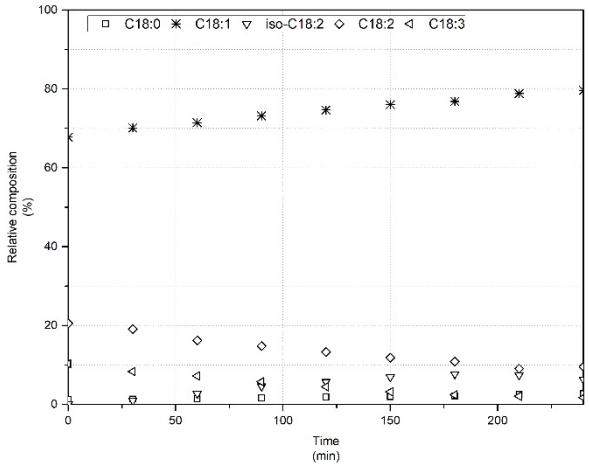

Figure A-132 Test 36 relative percentages of C18:0, C18:1, isomers C18:2, C18:2, C18:3

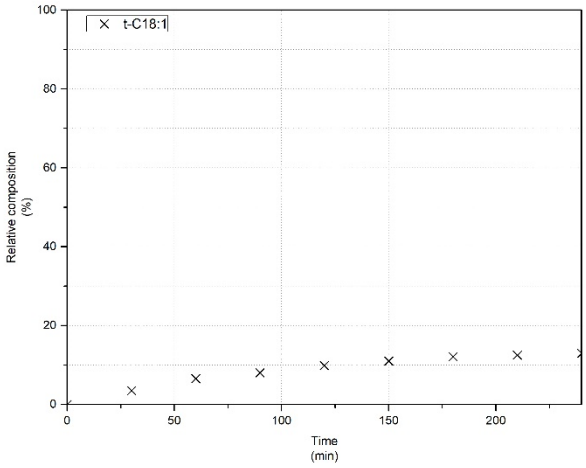

Figure A-133 Test 36 relative percentage of t-C18:1 estimated from the chromatogram

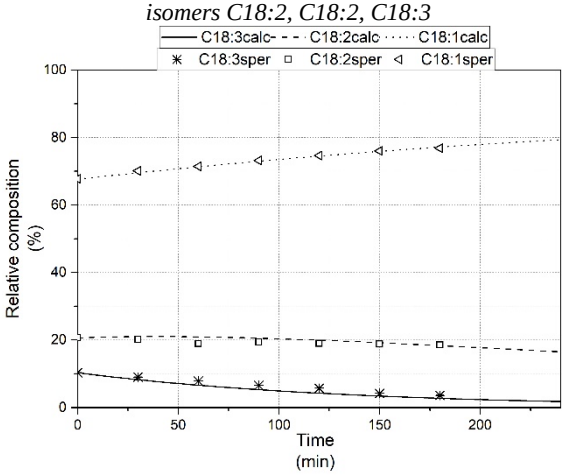

Figure A-134 Test 36 Model fitting for C18:1, C18:2 and C18:3, k1=0.00000125, k2=0.00107, k3=0.00741

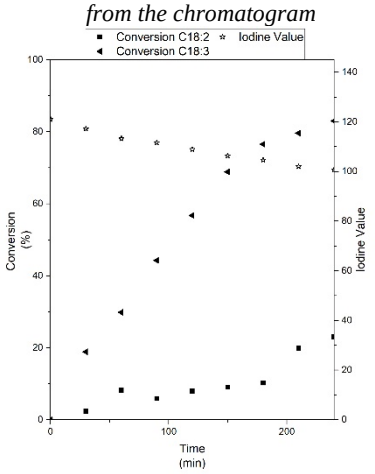

Figure A-135 Test 36 conversions of C18:2 and C18:3, and Iodine Value trend

A.37 Test 37: Cu10SiO$_2$AE - Canola – 180 °C – 12 bar – 4 mg$_{catalyst}$/mL$_{oil}$

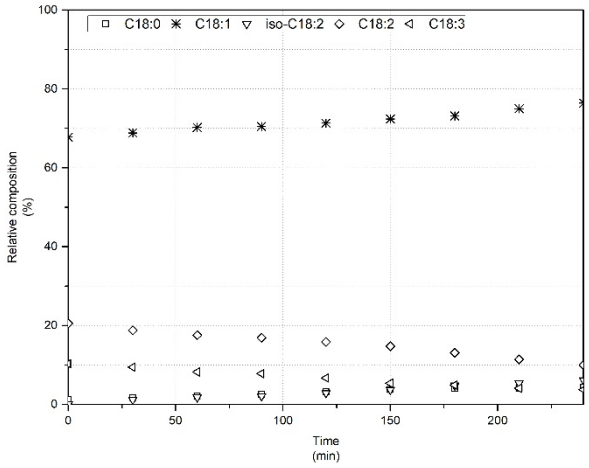

Figure A-136 Test 37 relative percentages of C18:0, C18:1, isomers C18:2, C18:2, C18:3

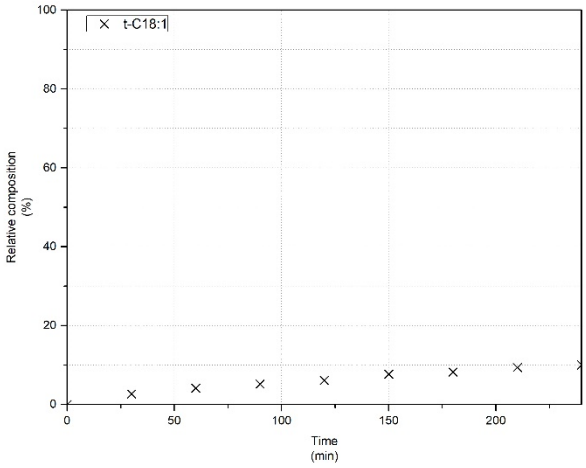

Figure A-137 Test 37 relative percentage of t-C18:1 estimated from the chromatogram

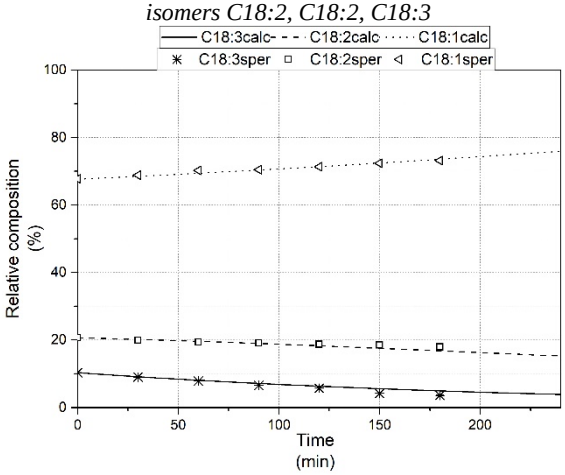

Figure A-138 Test 37 Model fitting for C18:1, C18:2 and C18:3, k1=0.00000234, k2=0.000596, k3=0.00411

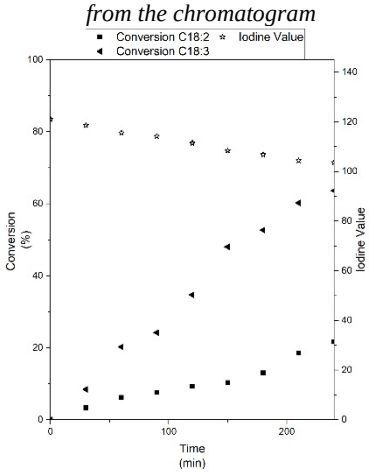

Figure A-139 Test 37 conversions of C18:2 and C18:3, and Iodine Value trend

A.38 Test 38: $Cu10SiO_2AE$ - Canola – 200 °C – 4 bar – 4 $mg_{catalyst}/mL_{oil}$

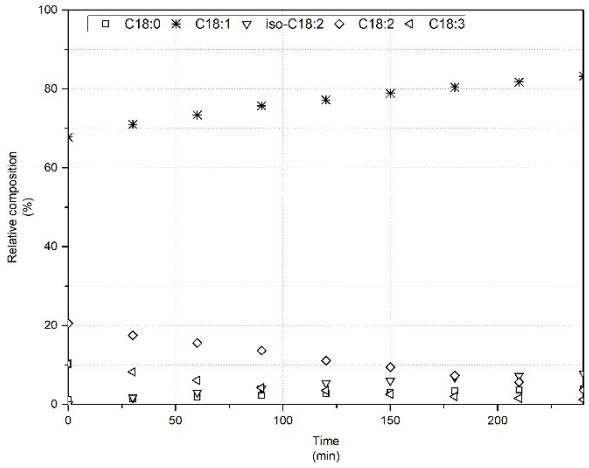

Figure A-140 Test 38 relative percentages of C18:0, C18:1, isomers C18:2, C18:2, C18:3

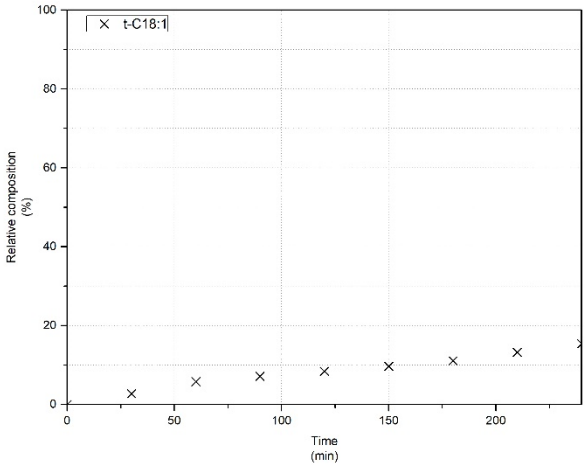

Figure A-141 Test 38 relative percentage of t-C18:1 estimated from the chromatogram

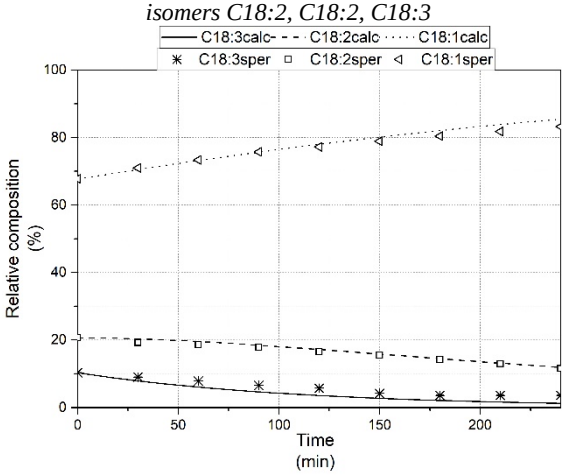

Figure A-142 Test 38 Model fitting for C18:1, C18:2 and C18:3, k1=0.00000302, k2=0.00129, k3=0.00889

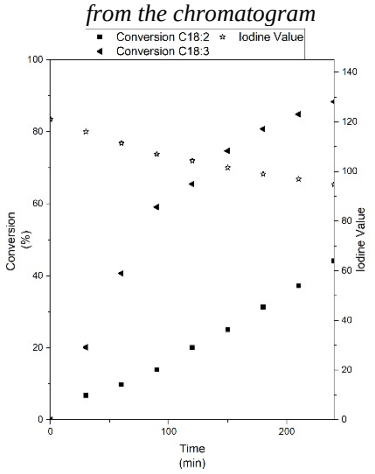

Figure A-143 Test 38 conversions of C18:2 and C18:3, and Iodine Value trend

A.39 Test 39: Cu10SiO$_2$AE - Canola – 200 °C – 12 bar – 4 mg$_{catalyst}$/mL$_{oil}$

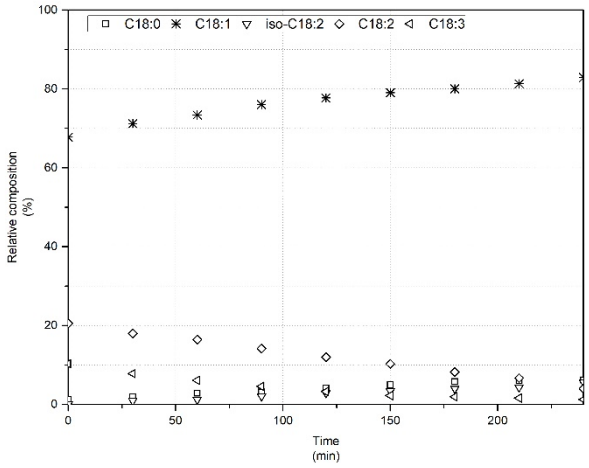

Figure A-144 Test 39 relative percentages of C18:0, C18:1, isomers C18:2, C18:2, C18:3

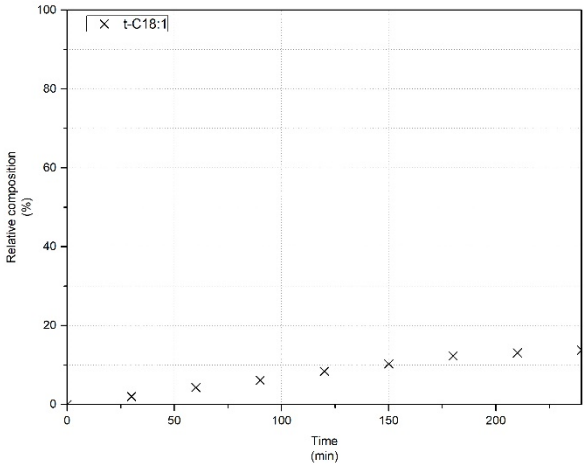

Figure A-145 Test 39 relative percentage of t-C18:1 estimated from the chromatogram

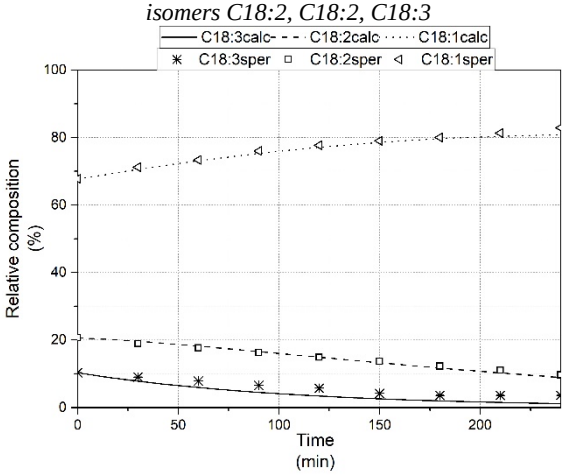

Figure A-146 Test 39 Model fitting for C18:1, C18:2 and C18:3, k1=0.00000469, k2=0.00134, k3=0.00925

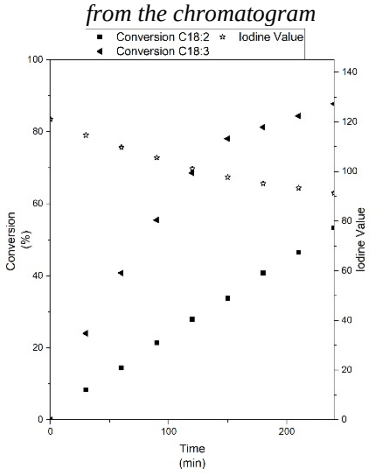

Figure A-147 Test 39 conversions of C18:2 and C18:3, and Iodine Value trend

A.40 Test 40: Cu10SiO$_2$AE - Canola – 180 °C – 4 bar – 8 mg$_{catalyst}$/mL$_{oil}$

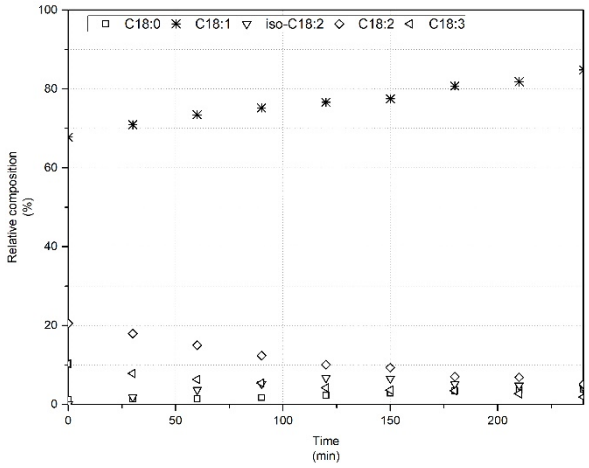

Figure A-148 Test 40 relative percentages of C18:0, C18:1, isomers C18:2, C18:2, C18:3

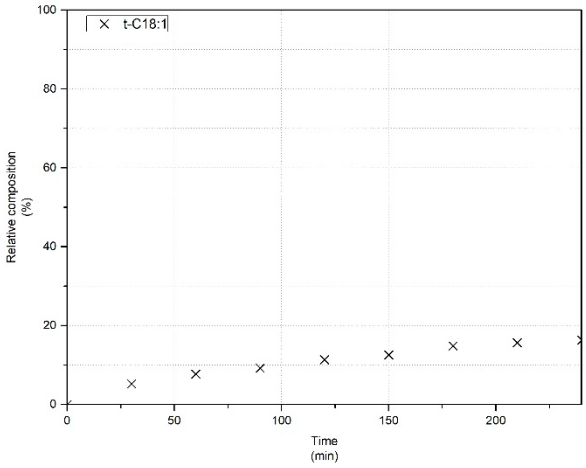

Figure A-149 Test 40 relative percentage of t-C18:1 estimated from the chromatogram

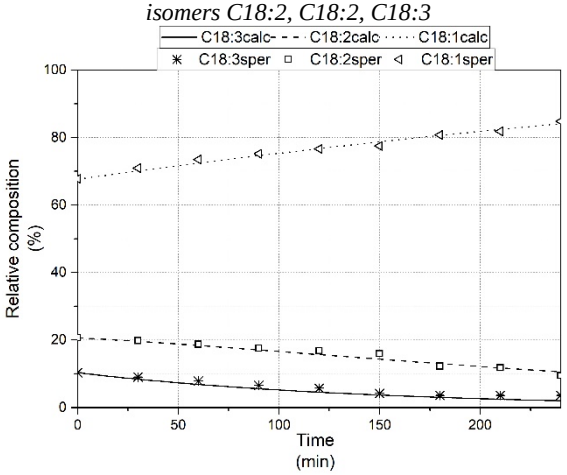

Figure A-150 Test 40 Model fitting for C18:1, C18:2 and C18:3, k1=0.00000871, k2=0.000979, k3=0.00685

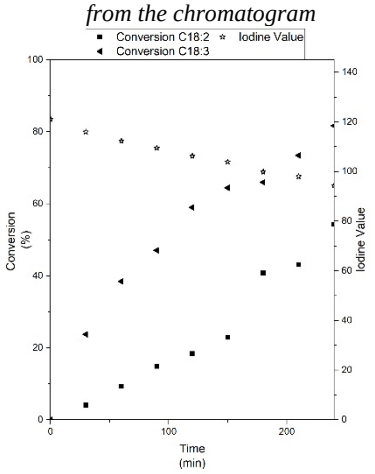

Figure A-151 Test 40 conversions of C18:2 and C18:3, and Iodine Value trend

A.41 Test 41: Cu10SiO$_2$AE - Canola – 180 °C – 12 bar – 8 mg$_{catalyst}$/mL$_{oil}$

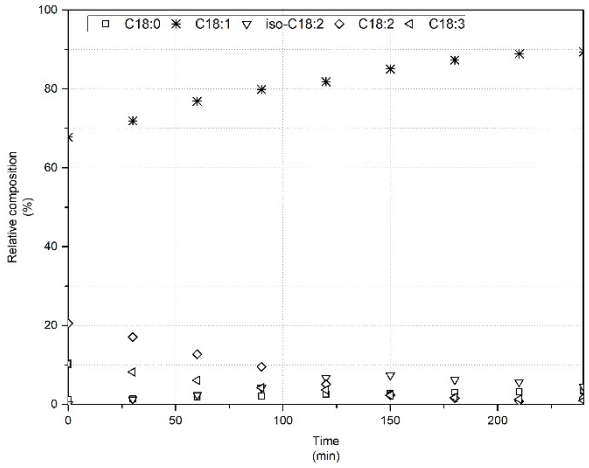

Figure A-152 Test 41 relative percentages of C18:0, C18:1, isomers C18:2, C18:2, C18:3

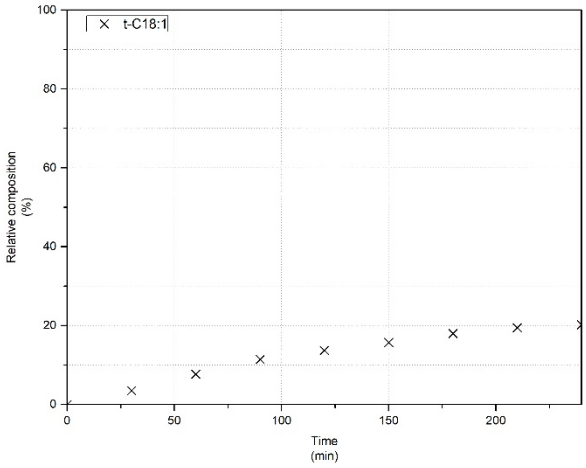

Figure A-153 Test 41 relative percentage of t-C18:1 estimated from the chromatogram

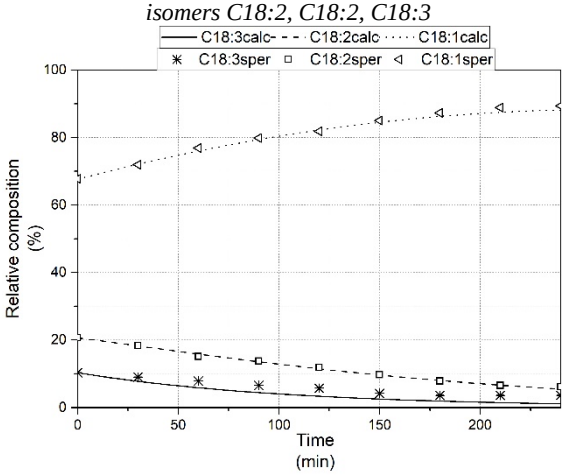

Figure A-154 Test 41 Model fitting for C18:1, C18:2 and C18:3, k1=0.0000138, k2=0.001385, k3=0.00942

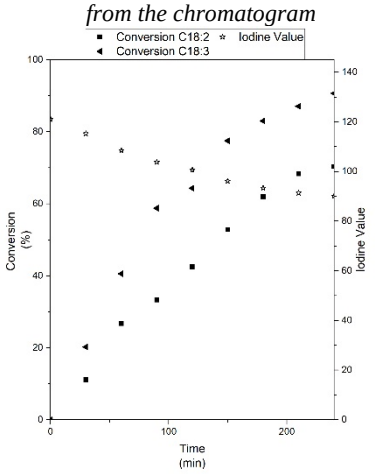

Figure A-155 Test 41 conversions of C18:2 and C18:3, and Iodine Value trend

A.42 Test 42: $Cu10SiO_2AE$ - Canola – 200 °C – 4 bar – 8 $mg_{catalyst}/mL_{oil}$

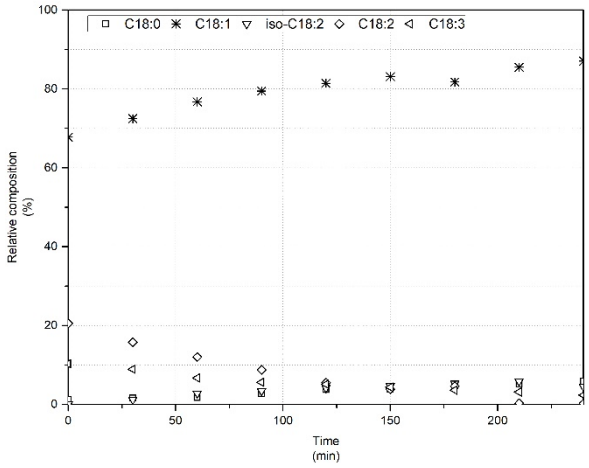

Figure A-156 Test 42 relative percentages of C18:0, C18:1, isomers C18:2, C18:2, C18:3

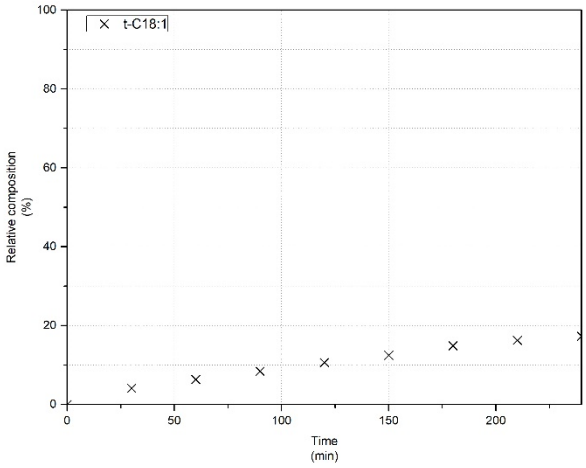

Figure A-157 Test 42 relative percentage of t-C18:1 estimated from the chromatogram

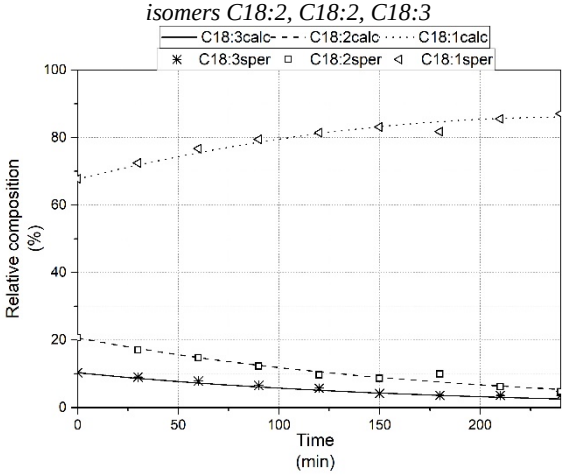

Figure A-158 Test 42 Model fitting for C18:1, C18:2 and C18:3, k1=0.00000263, k2=0.000781, k3=0.00586

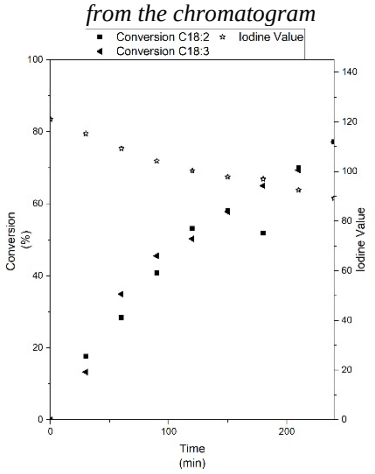

Figure A-159 Test 42 conversions of C18:2 and C18:3, and Iodine Value trend

A.43 Test 43: Cu10SiO$_2$AE - Canola – 200 °C – 12 bar – 8 mg$_{catalyst}$/mL$_{oil}$

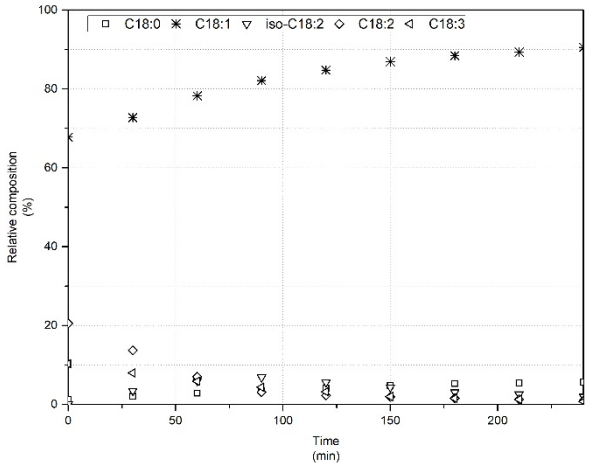

Figure A-160 Test 43 relative percentages of C18:0, C18:1, isomers C18:2, C18:2, C18:3

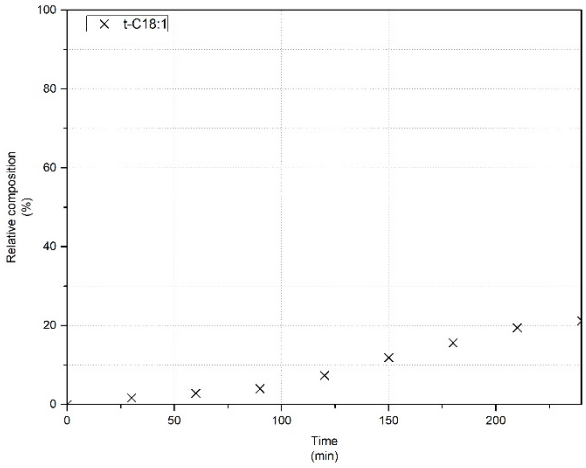

Figure A-161 Test 43 relative percentage of t-C18:1 estimated from the chromatogram

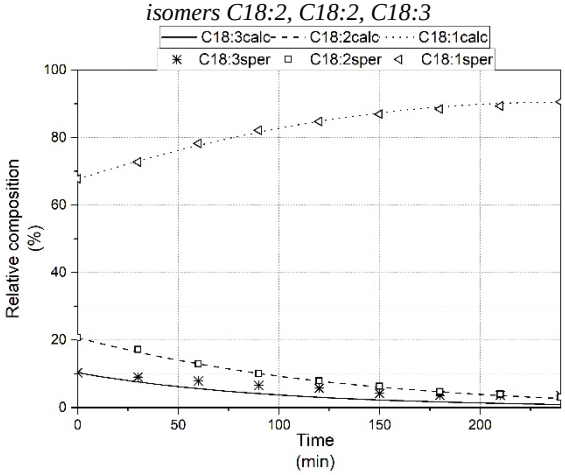

Figure A-162 Test 43 Model fitting for C18:1, C18:2 and C18:3, k1=0.00000598, k2=0.0369, k3=0.0102

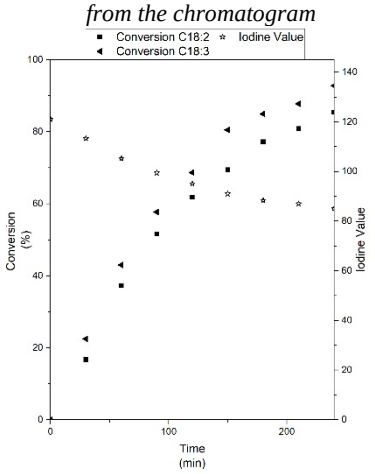

Figure A-163 Test 43 conversions of C18:2 and C18:3, and Iodine Value trend

A.44 Test 44: Cu10SiO$_2$AE - Canola – 180 °C – 4 bar – 2 mg$_{catalyst}$/mL$_{oil}$

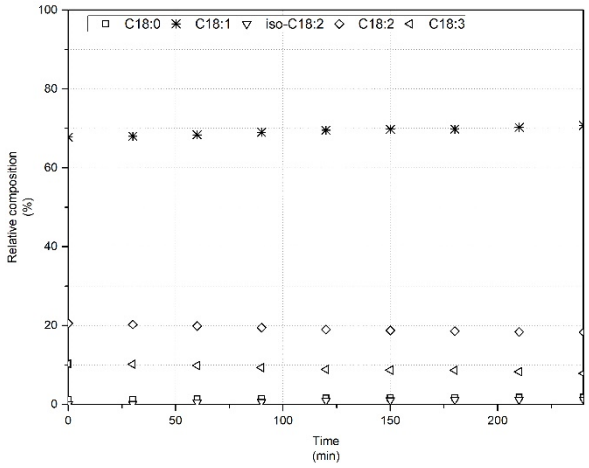

Figure A-164 Test 44 relative percentages of C18:0, C18:1, isomers C18:2, C18:2, C18:3

A.45 Test 45: Cu10SiO$_2$AE - Canola – 180 °C – 12 bar – 2 mg$_{catalyst}$/mL$_{oil}$

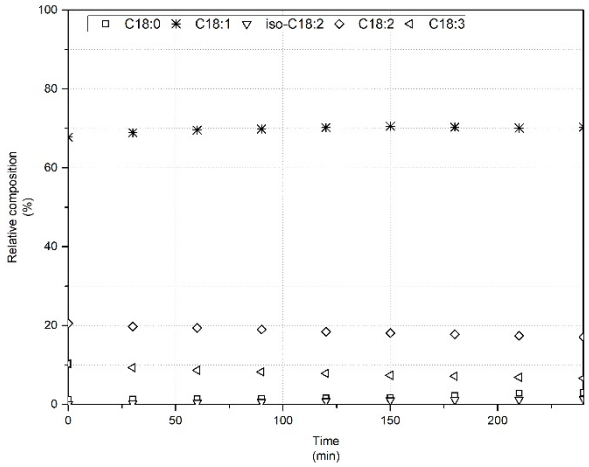

Figure A-165 Test 45 relative percentages of C18:0, C18:1, isomers C18:2, C18:2, C18:3

A.46 Test 46: $Cu10SiO_2AE$ - Canola – 200 °C – 4 bar – 2 $mg_{catalyst}/mL_{oil}$

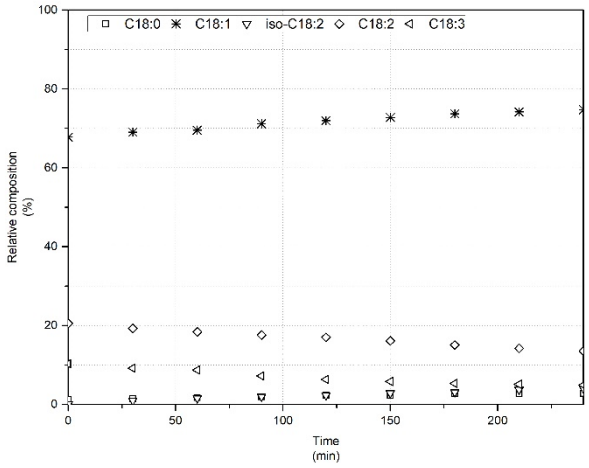

Figure A-166 Test 46 relative percentages of C18:0, C18:1, isomers C18:2, C18:2, C18:3

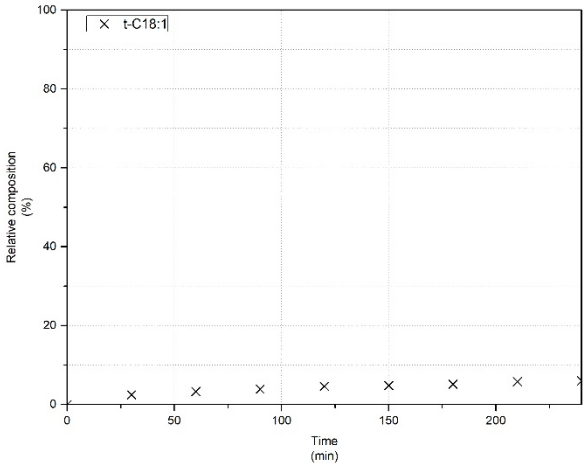

Figure A-167 Test 27 relative percentage of t-C18:1 estimated from the chromatogram

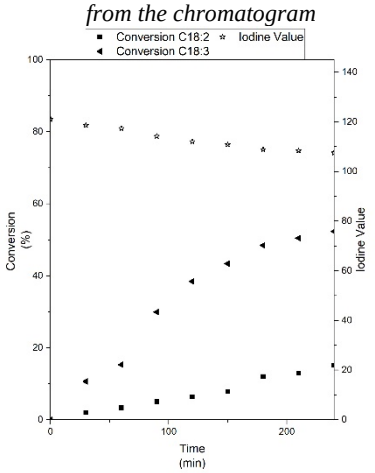

Figure A-168 Test 27 conversions of C18:2 and C18:3, and Iodine Value trend

A.47 Test 47: Cu10SiO$_2$AE - Sunflower – 180 °C – 4 bar – 4 mg$_{catalyst}$/mL$_{oil}$

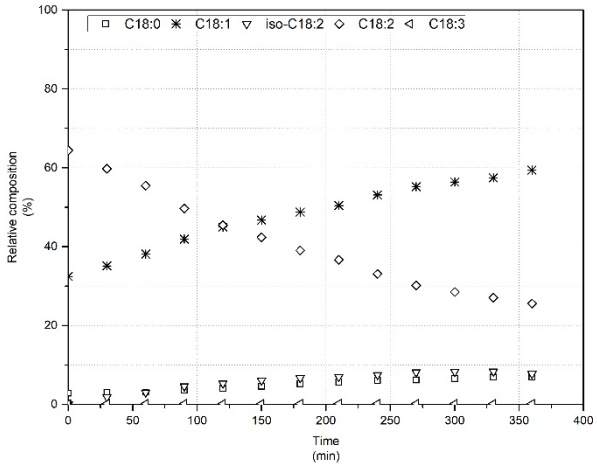

Figure A-169 Test 47 relative percentages of C18:0, C18:1, isomers C18:2, C18:2, C18:3

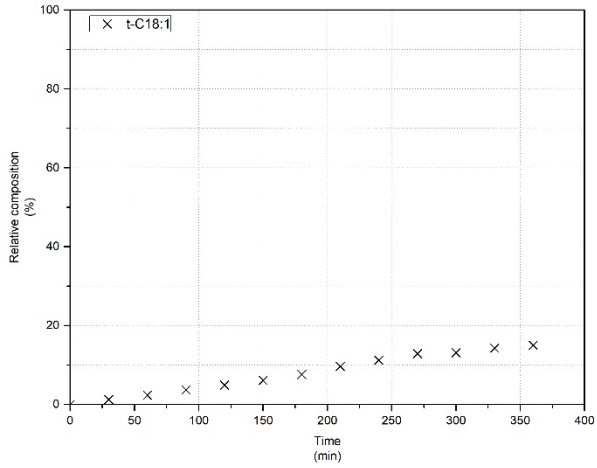

Figure A-170 Test 47 relative percentage of t-C18:1 estimated from the chromatogram

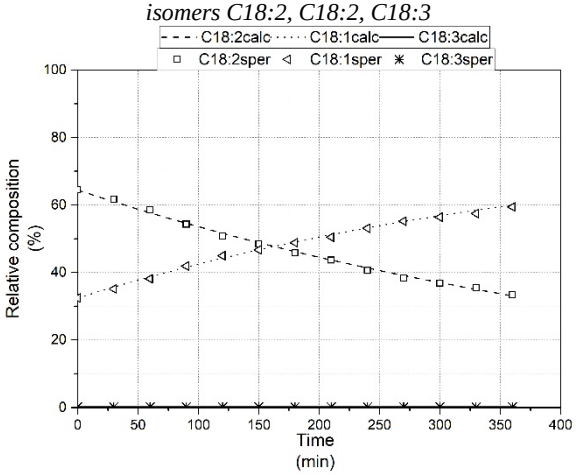

Figure A-171 Test 47 Model fitting for C18:1, C18:2 and C18:3, k1=0.0000122, k2=0.00252, k3=0.0000

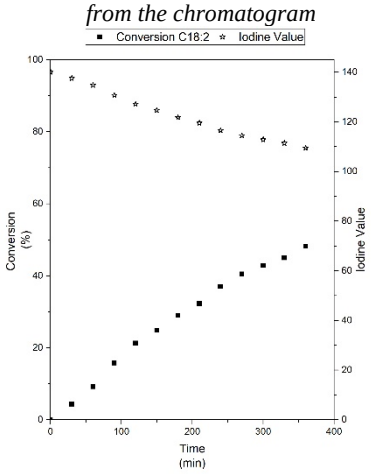

Figure A-172 Test 47 conversions of C18:2, and Iodine Value trend

A.48 Test 48: $Cu10SiO_2AE$ - Sunflower – 180 °C – 12 bar – 4 $mg_{catalyst}/mL_{oil}$

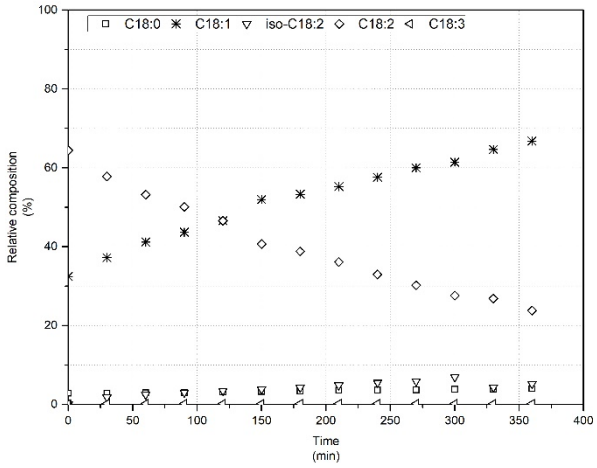

Figure A-173 Test 48 relative percentages of C18:0, C18:1, isomers C18:2, C18:2, C18:3

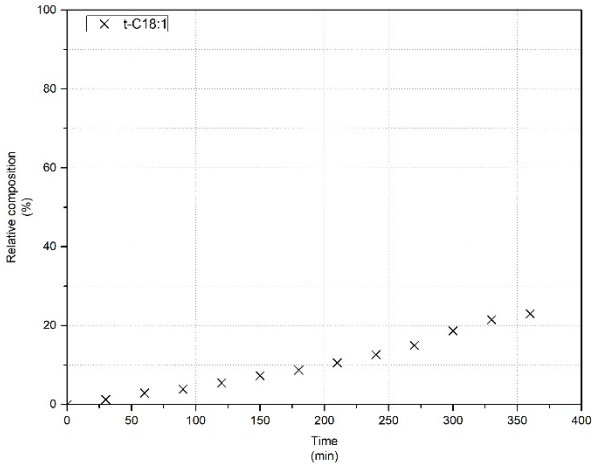

Figure A-174 Test 48 relative percentage of t-C18:1 estimated from the chromatogram

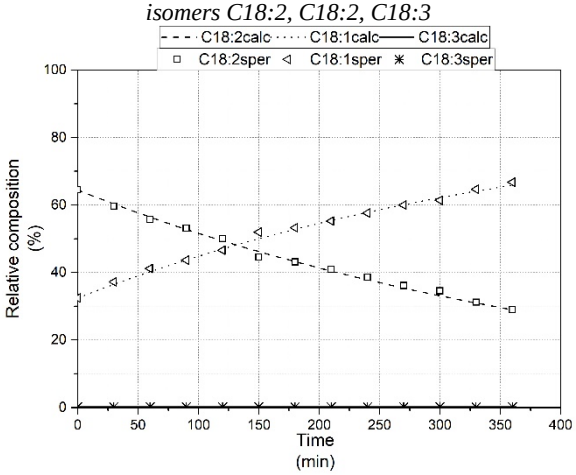

Figure A-175 Test 48 Model fitting for C18:1, C18:2 and C18:3, k1=0.0000137, k2=0.00222, k3=0.0000

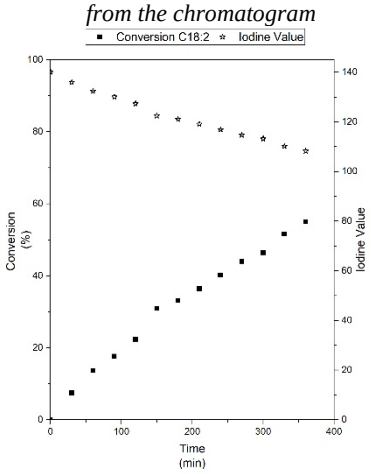

Figure A-176 Test 48 conversions of C18:2, and Iodine Value trend

A.49 Test 49: Cu10SiO$_2$AE - Sunflower – 200 °C – 4 bar – 4 mg$_{catalyst}$/mL$_{oil}$

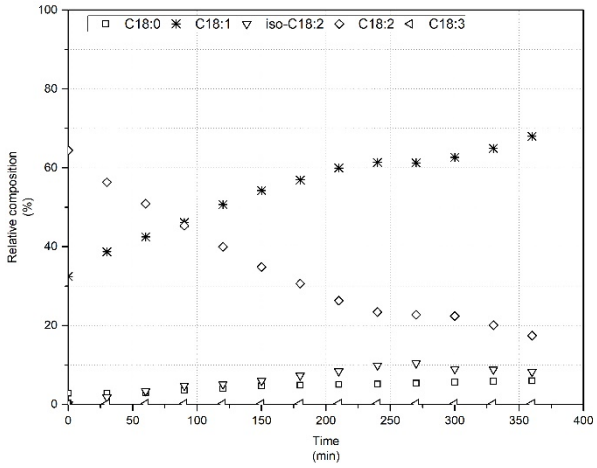

Figure A-177 Test 49 relative percentages of C18:0, C18:1, isomers C18:2, C18:2, C18:3

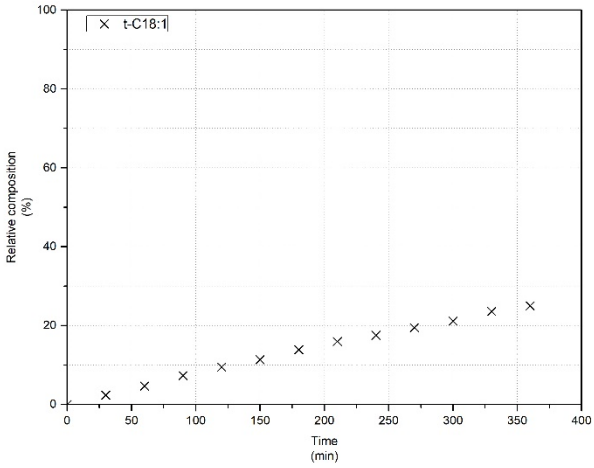

Figure A-178 Test 49 relative percentage of t-C18:1 estimated from the chromatogram

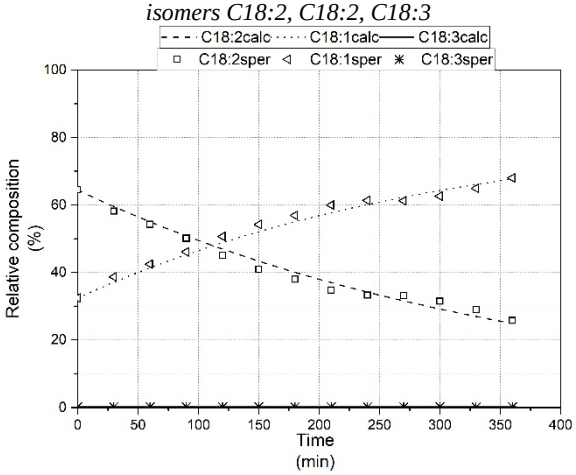

Figure A-179 Test 49 Model fitting for C18:1, C18:2 and C18:3, k1=0.0000148, k2=0.00264, k3=0.0000

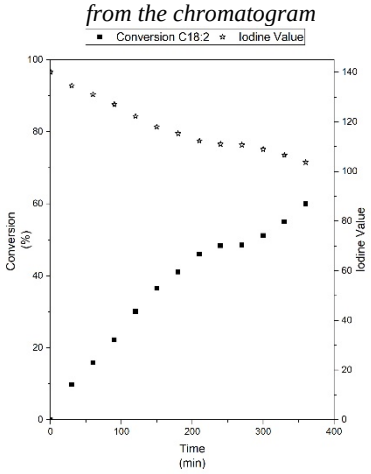

Figure A-180 Test 49 conversions of C18:2, and Iodine Value trend

A.50 Test 50: $Cu10SiO_2HP$ - Canola – 180 °C – 4 bar – 4 $mg_{catalyst}/mL_{oil}$

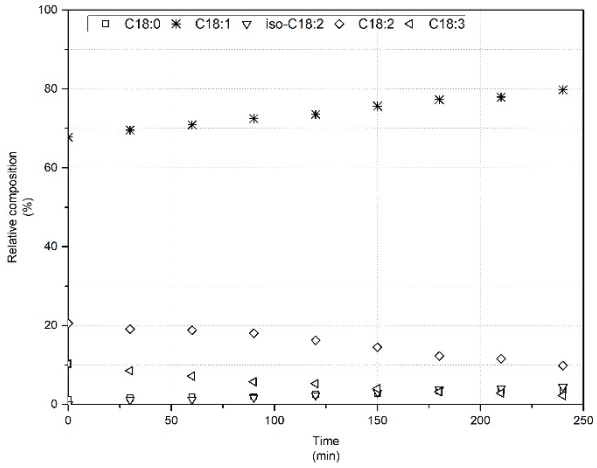

Figure A-181 Test 50 relative percentages of C18:0, C18:1, isomers C18:2, C18:2, C18:3

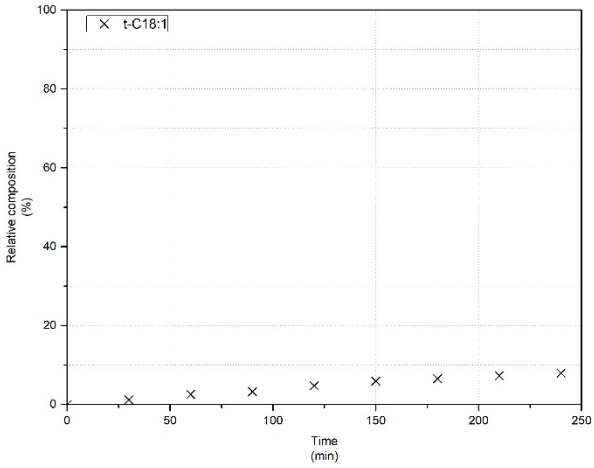

Figure A-182 Test 50 relative percentage of t-C18:1 estimated from the chromatogram

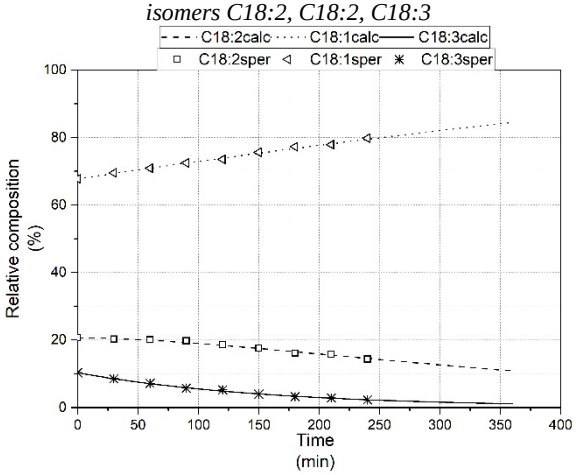

Figure A-183 Test 50 Model fitting for C18:1, C18:2 and C18:3, k1=0.00000223, k2=0.00118, k3=0.00628

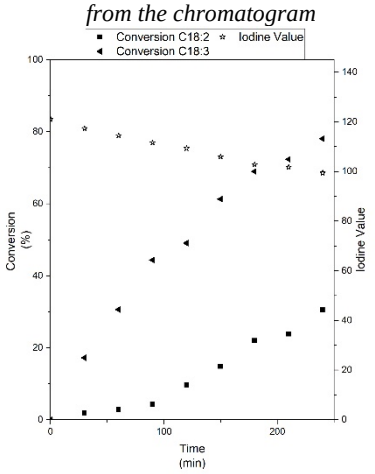

Figure A-184 Test 50 conversions of C18:2, and Iodine Value trend

A.51 Test 51: Cu10SiO$_2$HP - Canola – 180 °C – 12 bar – 4 mg$_{catalyst}$/mL$_{oil}$

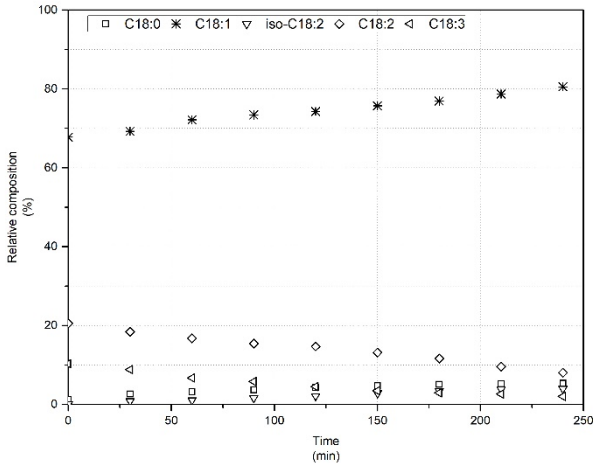

Figure A-185 Test 51 relative percentages of C18:0, C18:1, isomers C18:2, C18:2, C18:3

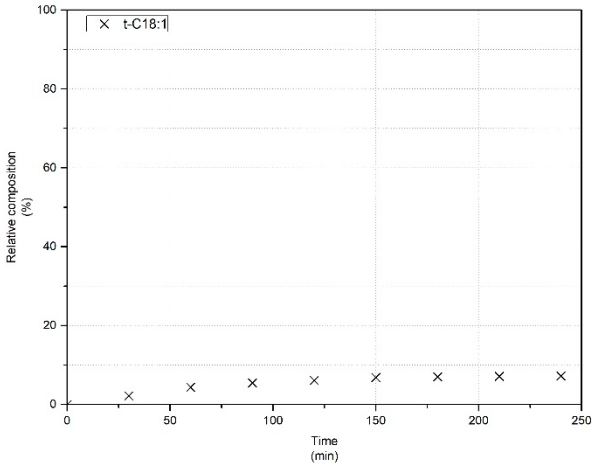

Figure A-186 Test 51 relative percentage of t-C18:1 estimated from the chromatogram

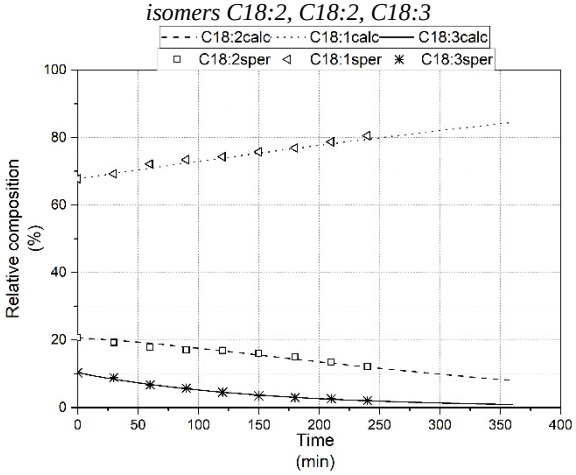

Figure A-187 Test 51 Model fitting for C18:1, C18:2 and C18:3, k1=0.00000281, k2=0.00122, k3=0.00685

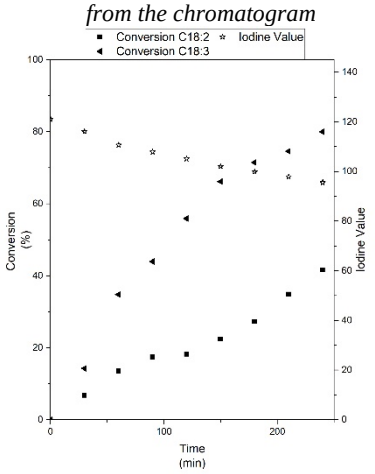

Figure A-188 Test 51 conversions of C18:2 and C18:3, and Iodine Value trend

A.52 Test 52: $Cu10SiO_2HP$ - Canola – 200 °C – 4 bar – 4 $mg_{catalyst}/mL_{oil}$

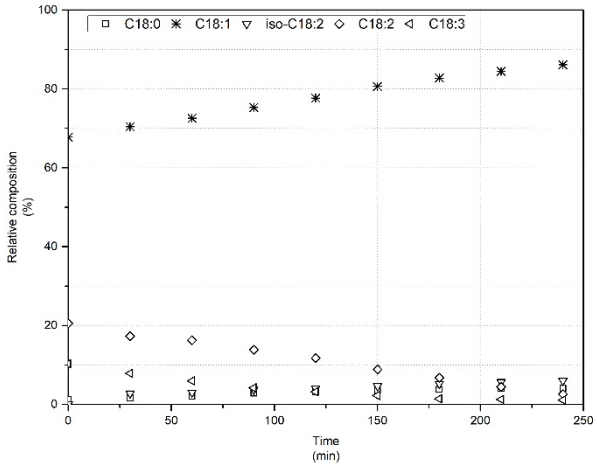

Figure A-189 Test 52 relative percentages of C18:0, C18:1, isomers C18:2, C18:2, C18:3

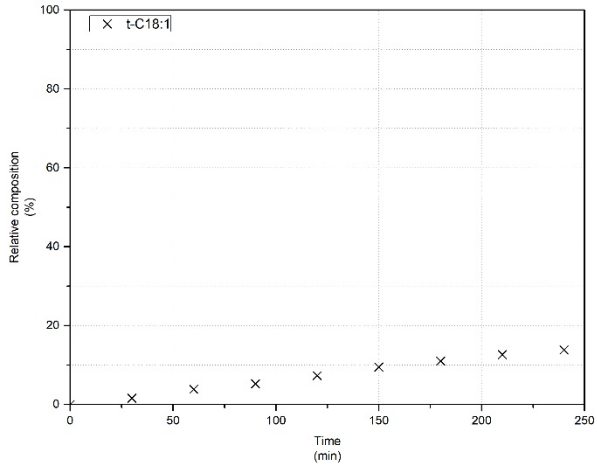

Figure A-190 Test 52 relative percentage of t-C18:1 estimated from the chromatogram

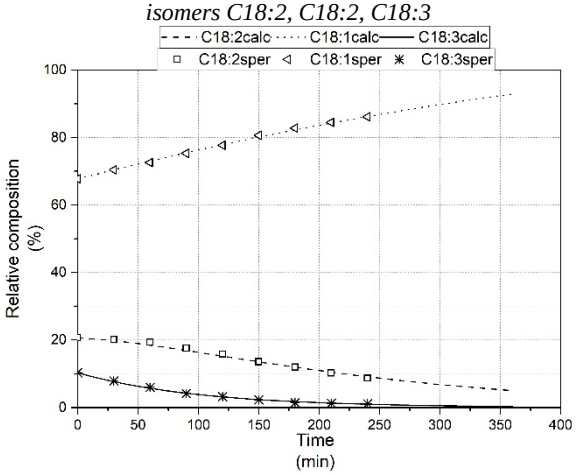

Figure A-191 Test 52 Model fitting for C18:1, C18:2 and C18:3, k1=0.00000456, k2=0.00178, k3=0.00988

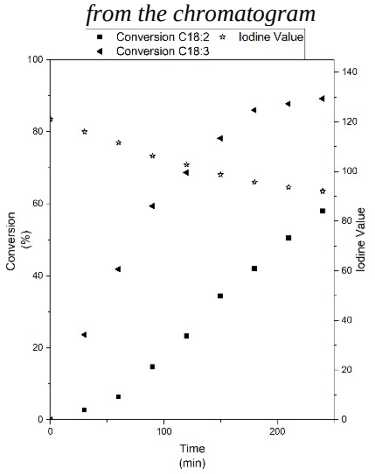

Figure A-192 Test 52 conversions of C18:2 and C18:3, and Iodine Value trend

A.53 Test 53: Cu10SiO$_2$HP - Canola – 200 °C – 12 bar – 4 mg$_{catalyst}$/mL$_{oil}$

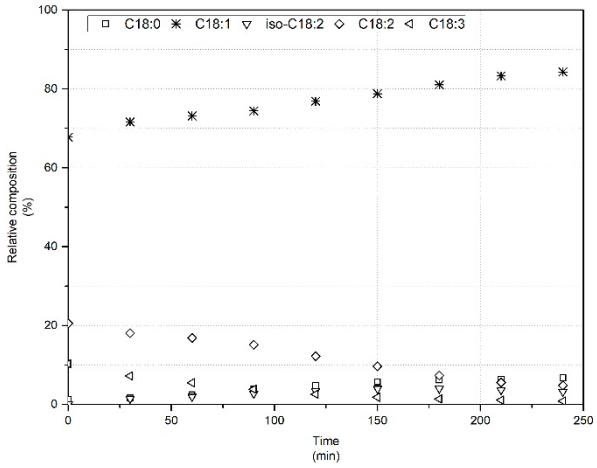

Figure A-193 Test 53 relative percentages of C18:0, C18:1, isomers C18:2, C18:2, C18:3

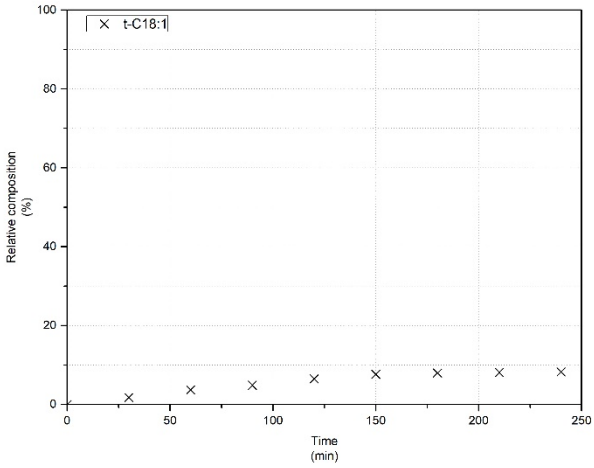

Figure A-194 Test 53 relative percentage of t-C18:1 estimated from the chromatogram

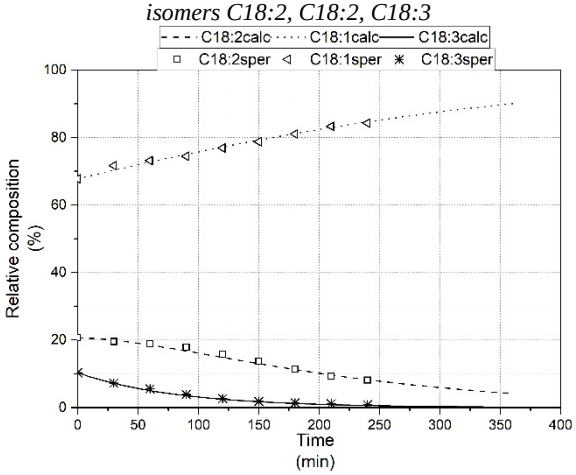

Figure A-195 Test 53 Model fitting for C18:1, C18:2 and C18:3, k1=0.00000566, k2=0.00207, k3=0.012

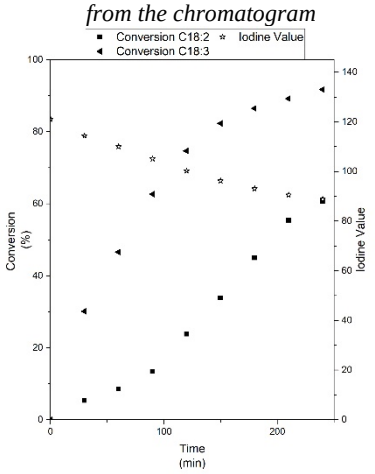

Figure A-196 Test 53 conversions of C18:2, and Iodine Value trend

A.54 Test 54: Cu10SiO$_2$HP - Canola – 180 °C – 4 bar – 8 mg$_{catalyst}$/mL$_{oil}$

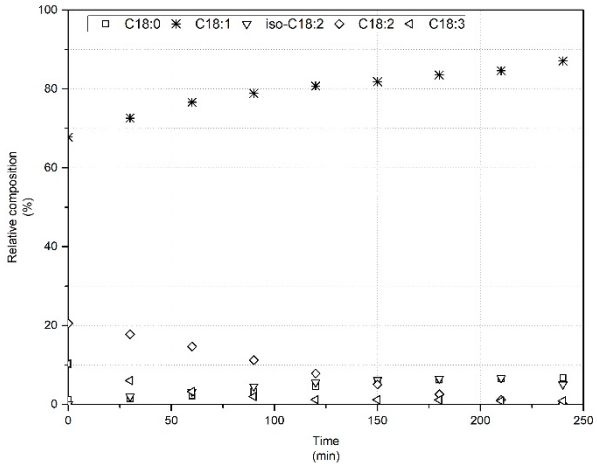

Figure A-197 Test 54 relative percentages of C18:0, C18:1, isomers C18:2, C18:2, C18:3

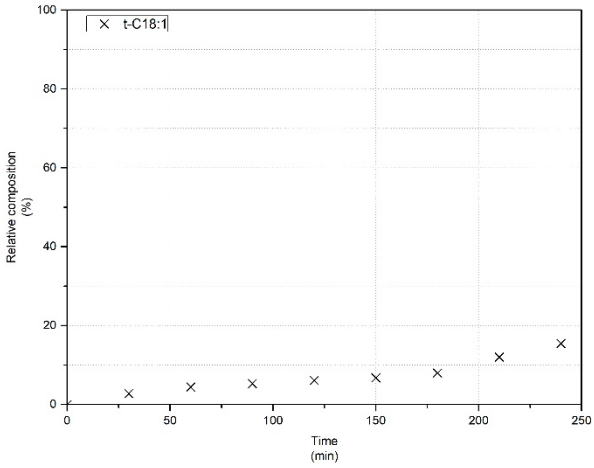

Figure A-198 Test 54 relative percentage of t-C18:1 estimated from the chromatogram

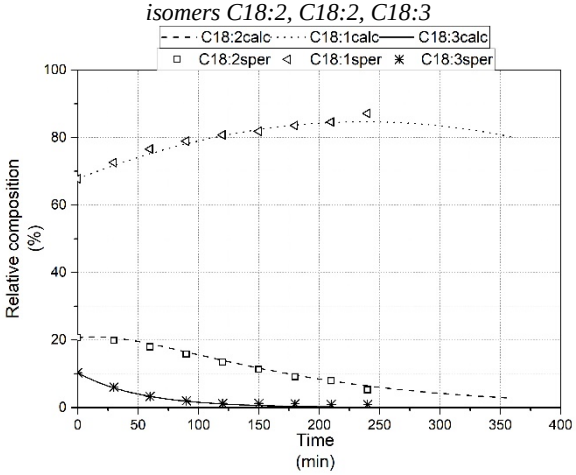

Figure A-199 Test 54 Model fitting for C18:1, C18:2 and C18:3, k1=0.00000114, k2=0.00333, k3=0.019

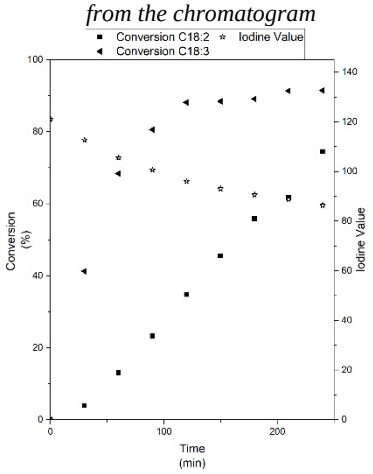

Figure A-200 Test 54 conversions of C18:2, and Iodine Value trend

A.55 Test 55: Cu10SiO$_2$HP - Canola – 180 °C – 12 bar – 8 mg$_{catalyst}$/mL$_{oil}$

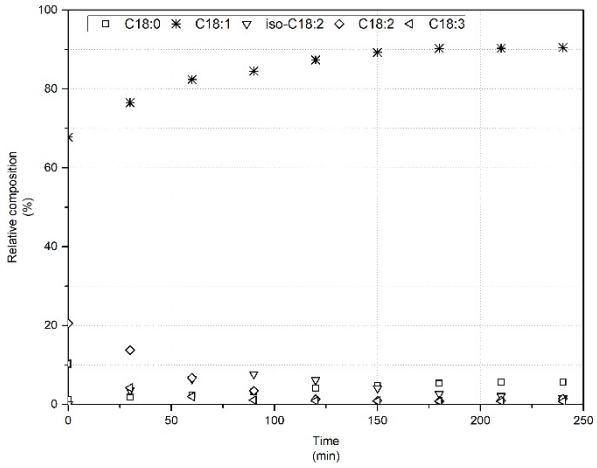

Figure A-201 Test 27 relative percentages of C18:0, C18:1, isomers C18:2, C18:2, C18:3

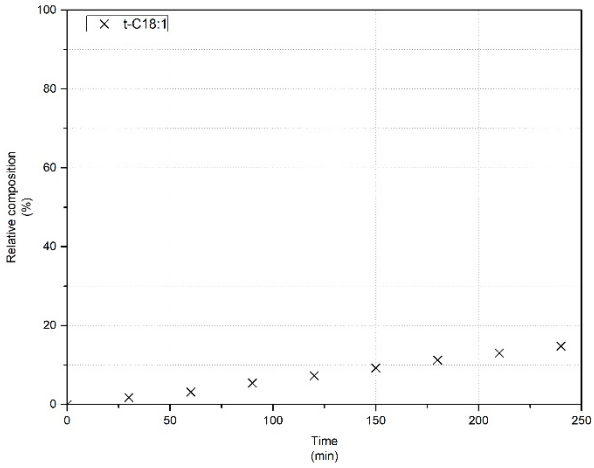

Figure A-202 Test 27 relative percentage of t-C18:1 estimated from the chromatogram

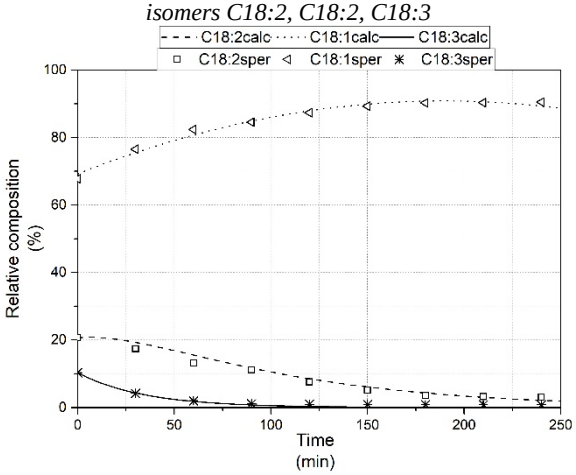

Figure A-203 Test 27 Model fitting for C18:1, C18:2 and C18:3, k1=0.00000196, k2=0.00509, k3=0.029

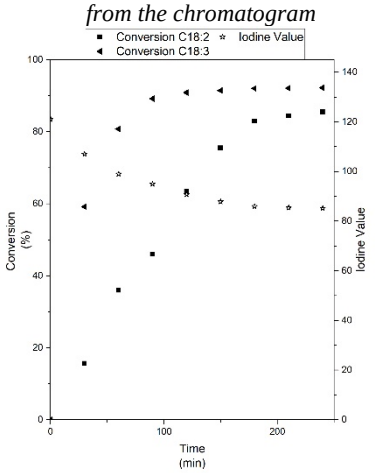

Figure A-204 Test 27 conversions of C18:2, and Iodine Value trend

A.56 Test 56: $Cu10SiO_2HP$ - Canola – 200 °C – 4 bar – 8 $mg_{catalyst}/mL_{oil}$

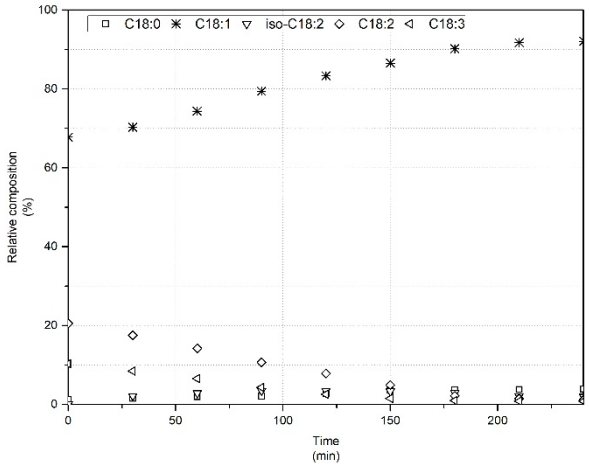

Figure A-205 Test 27 relative percentages of C18:0, C18:1, isomers C18:2, C18:2, C18:3

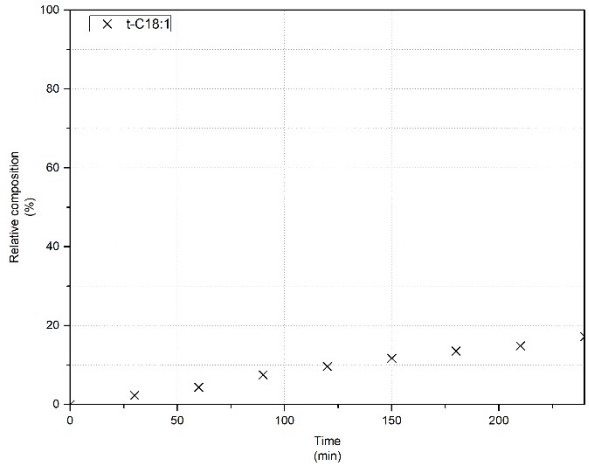

Figure A-206 Test 27 relative percentage of t-C18:1 estimated from the chromatogram

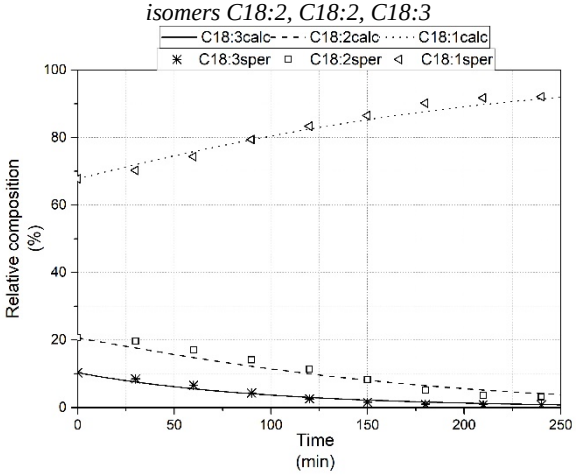

Figure A-207 Test 27 Model fitting for C18:1, C18:2 and C18:3, k1=0.00000254, k2=0.00181, k3=0.0103

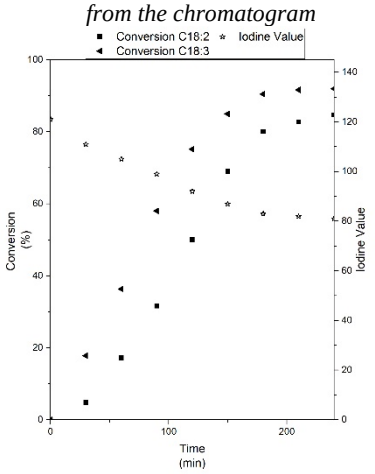

Figure A-208 Test 27 conversions of C18:2, and Iodine Value trend

A.57 Test 57: Cu10SiO$_2$HP - Canola – 200 °C – 12 bar – 8 mg$_{catalyst}$/mL$_{oil}$

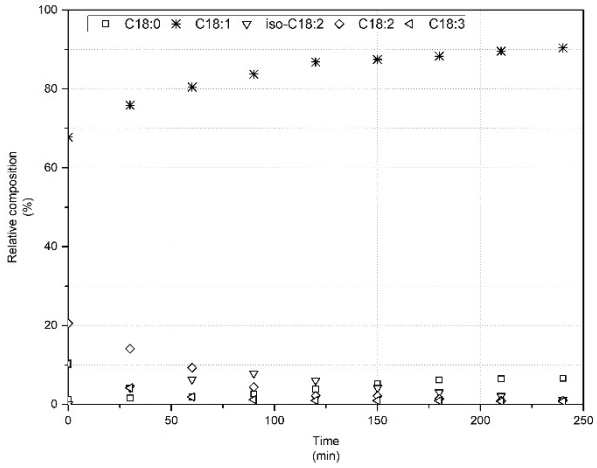

Figure A-209 Test 27 relative percentages of C18:0, C18:1, isomers C18:2, C18:2, C18:3

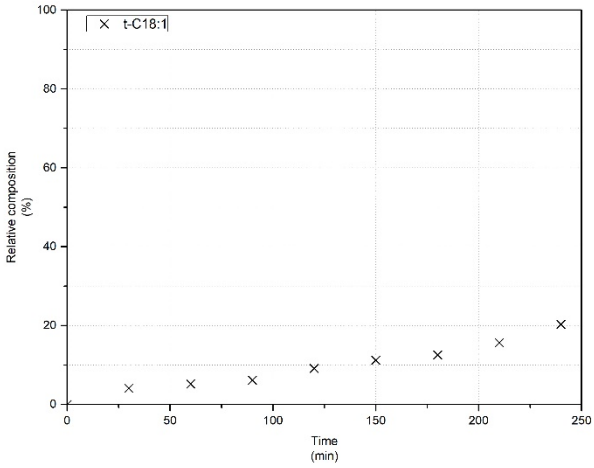

Figure A-210 Test 27 relative percentage of t-C18:1 estimated from the chromatogram

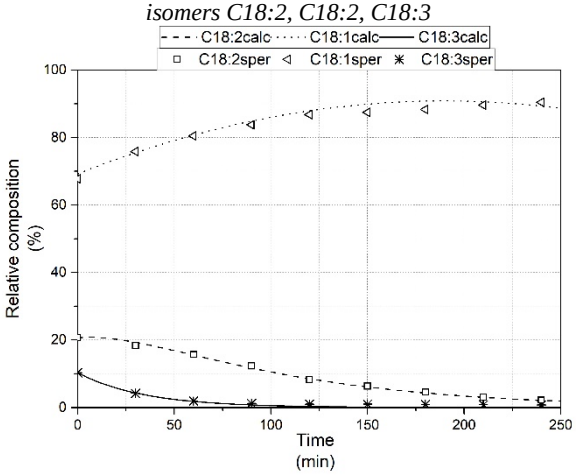

Figure A-211 Test 27 Model fitting for C18:1, C18:2 and C18:3, k1=0.00000233, k2=0.00504, k3=0.029

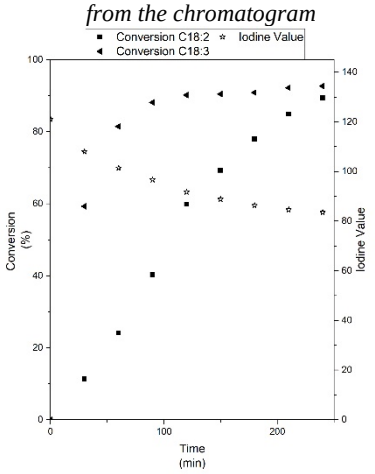

Figure A-212 Test 27 conversions of C18:2, and Iodine Value trend

A.58 Test 58: Cu10SiO$_2$HP - Canola – 180 °C – 4 bar – 2 mg$_{catalyst}$/mL$_{oil}$

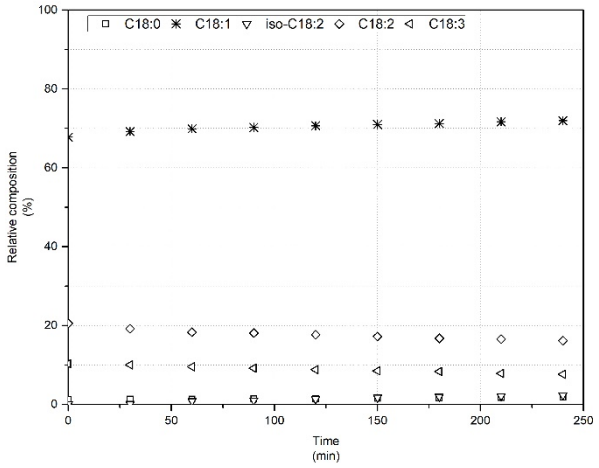

Figure A-213 Test 27 relative percentages of C18:0, C18:1, isomers C18:2, C18:2, C18:3

A.59 Test 59: Cu10SiO$_2$HP - Canola – 180 °C – 12 bar – 2 mg$_{catalyst}$/mL$_{oil}$

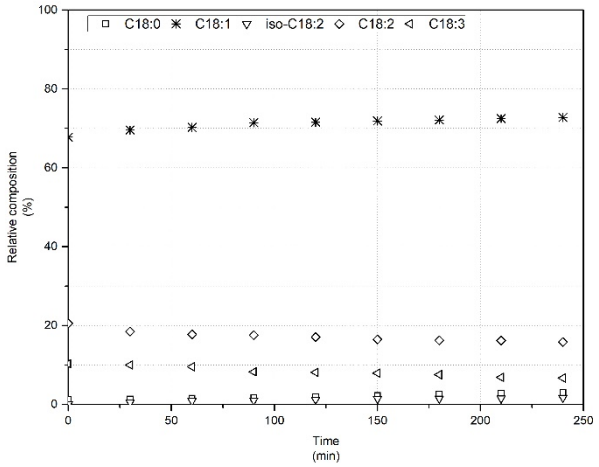

Figure A-214 Test 59 relative percentages of C18:0, C18:1, isomers C18:2, C18:2, C18:3

A.60 Test 60: Cu10SiO$_2$HP - Canola – 200 °C – 4 bar – 2 mg$_{catalyst}$/mL$_{oil}$

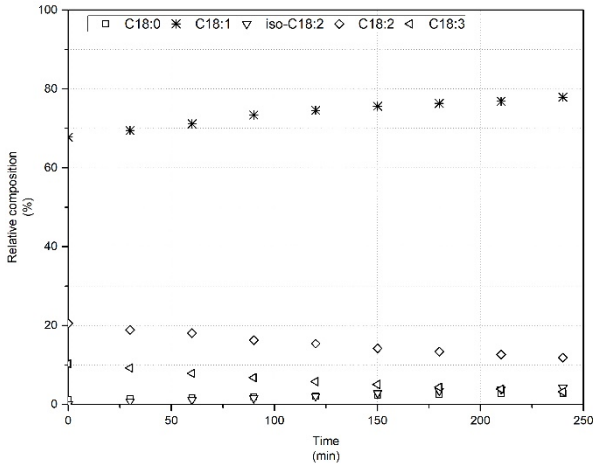

Figure A-215 Test 60 relative percentages of C18:0, C18:1, isomers C18:2, C18:2, C18:3

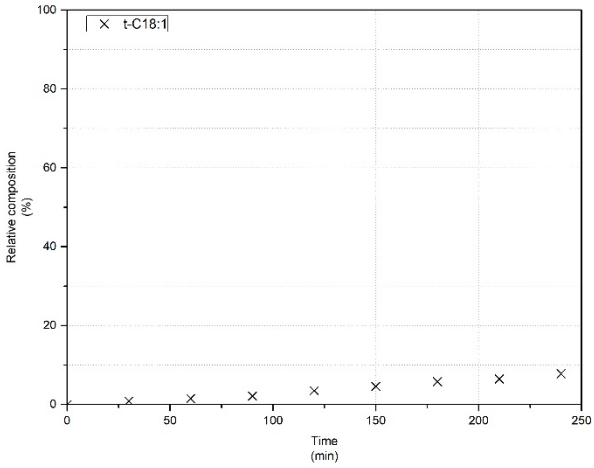

Figure A-216 Test 60 relative percentage of t-C18:1 estimated from the chromatogram

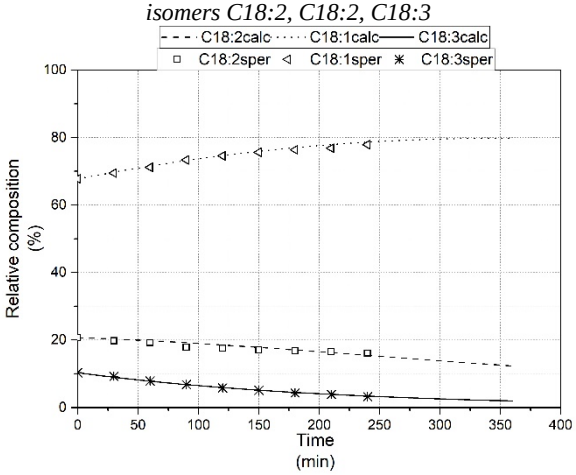

Figure A-217 Test 60 Model fitting for C18:1, C18:2 and C18:3, k1=0.000745, k2=0.015, k3=0.0000

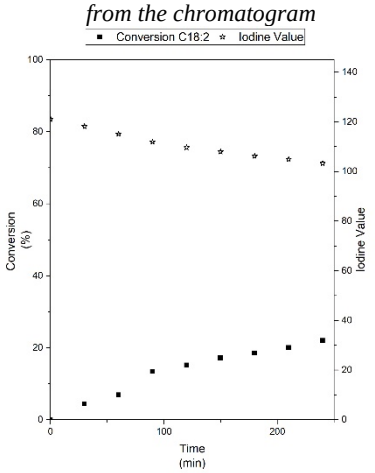

Figure A-218 Test 60 conversions of C18:2 and C18:3, and Iodine Value trend

A.61 Test 61: Cu10SiO$_2$HP - Sunflower – 180 °C – 4 bar – 4 mg$_{catalyst}$/mL$_{oil}$

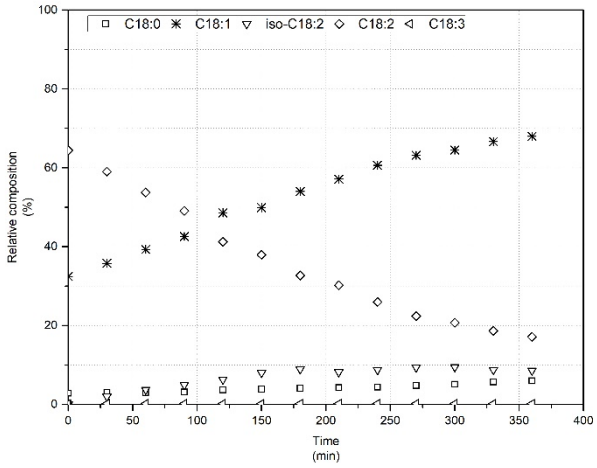

Figure A-219 Test 61 relative percentages of C18:0, C18:1, isomers C18:2, C18:2, C18:3

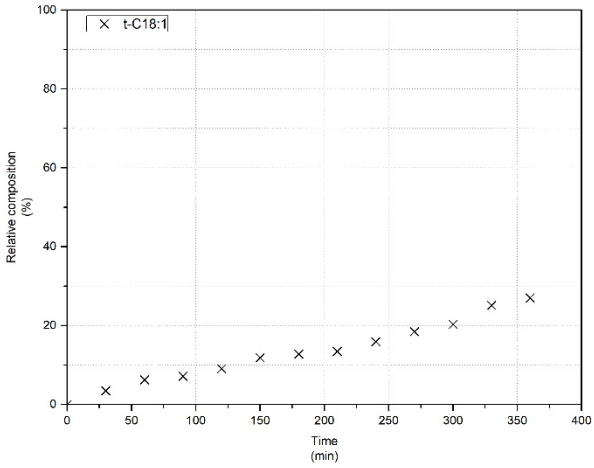

Figure A-220 Test 61 relative percentage of t-C18:1 estimated from the chromatogram

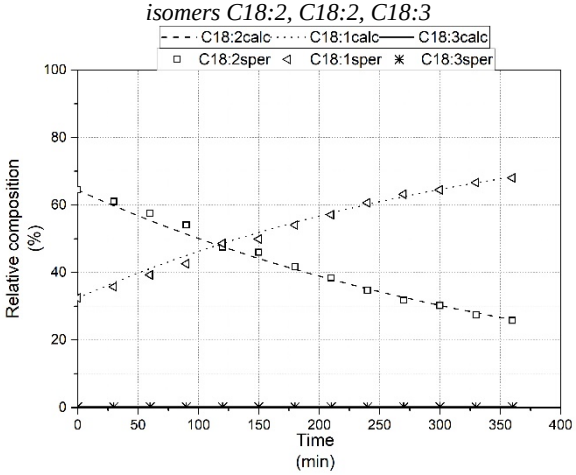

Figure A-221 Test 61 Model fitting for C18:1, C18:2 and C18:3, k1=0.0000132, k2=0.00252, k3=0.0000

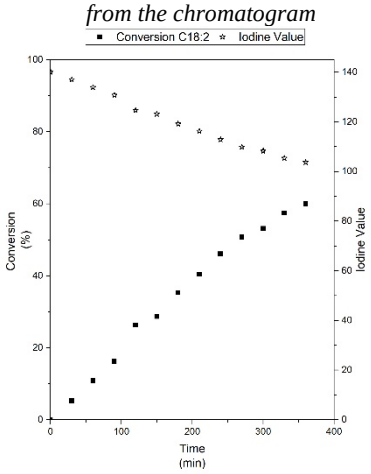

Figure A-222 Test 61 conversions of C18:2, and Iodine Value trend

A.62 Test 62: Cu10SiO$_2$HP - Sunflower – 180 °C – 12 bar – 4 mg$_{catalyst}$/mL$_{oil}$

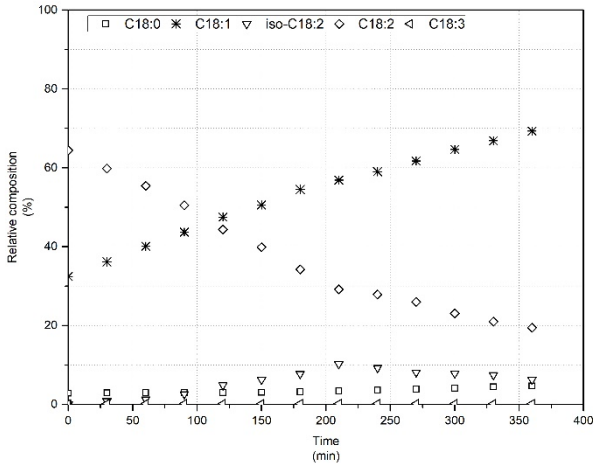

Figure A-223 Test 62 relative percentages of C18:0, C18:1, isomers C18:2, C18:2, C18:3

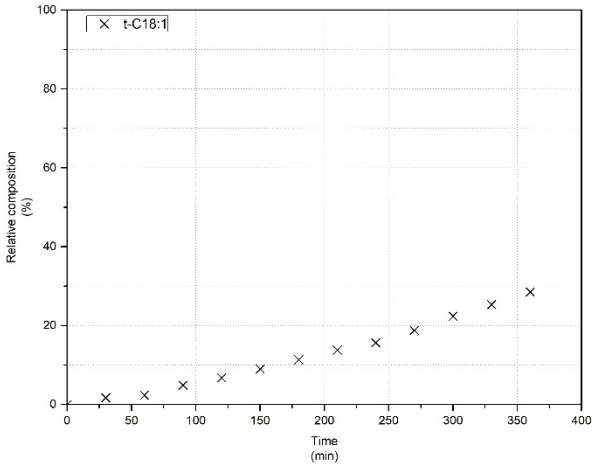

Figure A-224 Test 62 relative percentage of t-C18:1 estimated from the chromatogram

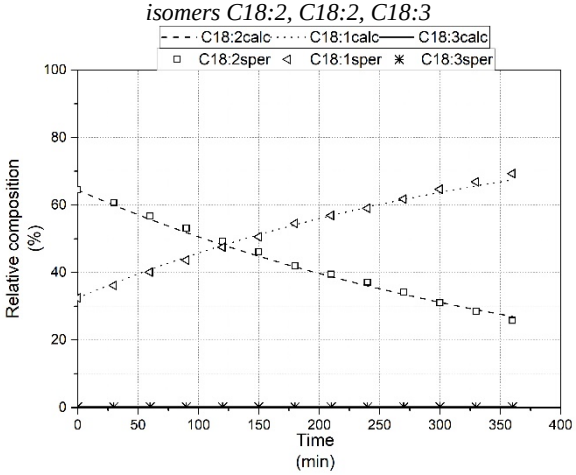

Figure A-225 Test 62Model fitting for C18:1, C18:2 and C18:3, k1=0.00000198, k2=0.00266, k3=0.0000

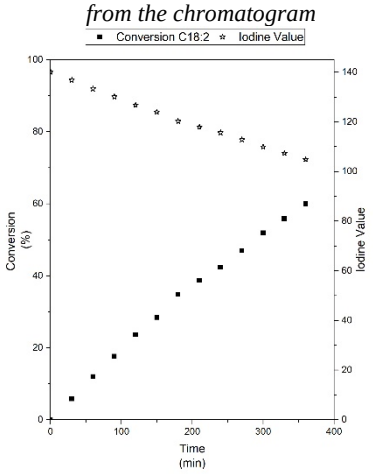

Figure A-226 Test 62 conversions of C18:2, and Iodine Value trend

A.63 Test 63: $Cu10SiO_2HP$ - Sunflower – 200 °C – 4 bar – 4 $mg_{catalyst}/mL_{oil}$

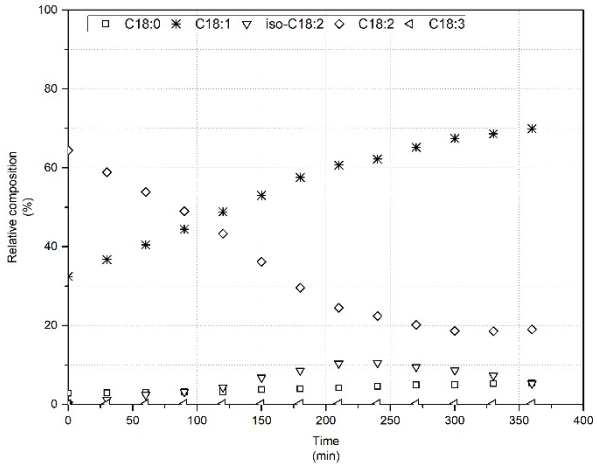

Figure A-227 Test 63 relative percentages of C18:0, C18:1, isomers C18:2, C18:2, C18:3

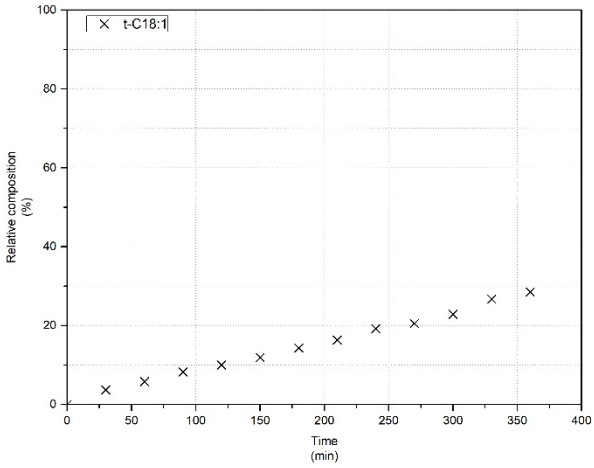

Figure A-228 Test 63 relative percentage of t-C18:1 estimated from the chromatogram

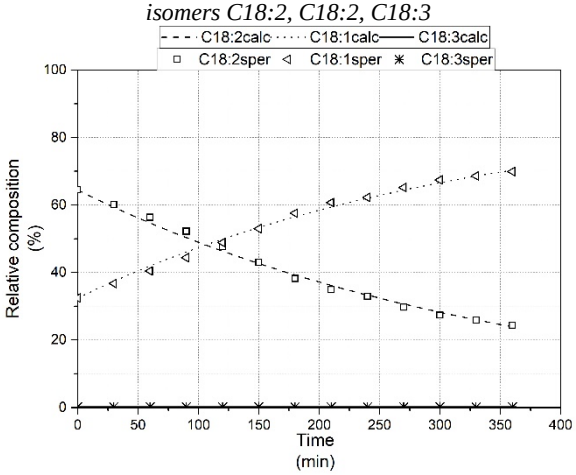

Figure A-229 Test 63 Model fitting for C18:1, C18:2 and C18:3, k1=0.0000175, k2=0.00275, k3=0.0000

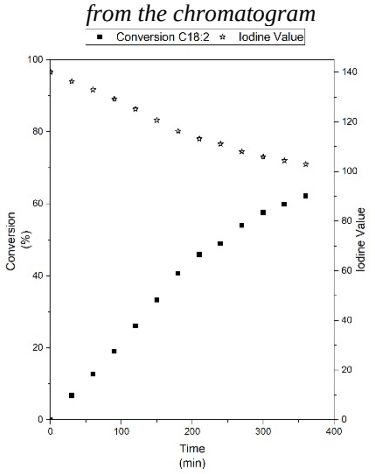

Figure A-230 Test 63 conversions of C18:2, and Iodine Value trend

A.64 Test 64: $Cu10Ni5SiO_2HP$ - Sunflower – 180 °C – 4 bar – 4 $mg_{catalyst}/mL_{oil}$

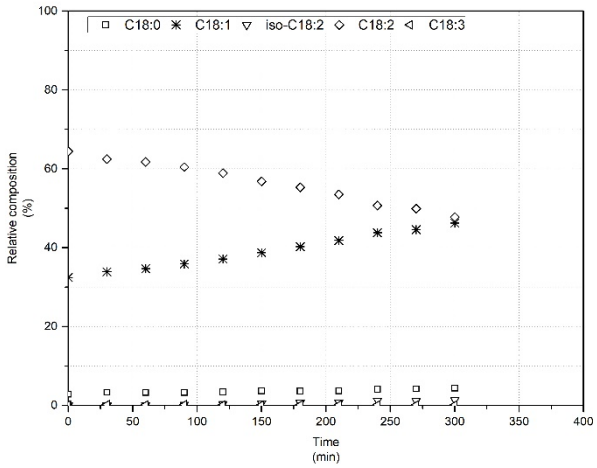

Figure A-231 Test 64 relative percentages of C18:0, C18:1, isomers C18:2, C18:2, C18:3

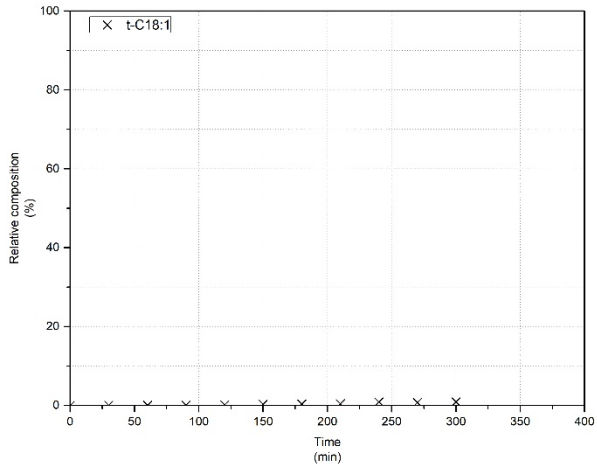

Figure A-232 Test 64 relative percentage of t-C18:1 estimated from the chromatogram

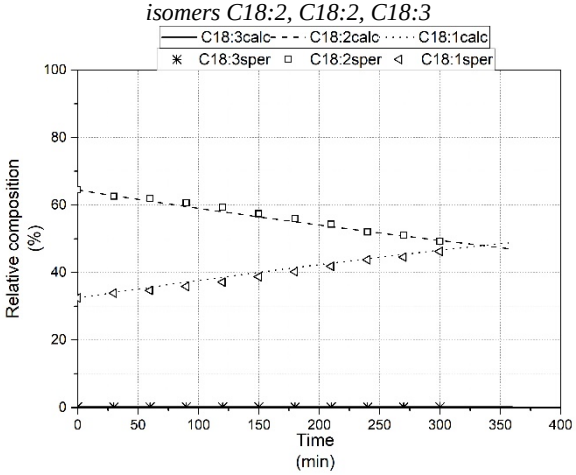

Figure A-233 Test 64 Model fitting for C18:1, C18:2 and C18:3, k1=0.0000210, k2=0.000785, k3=0.0000

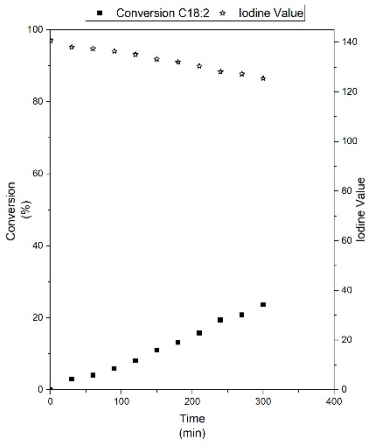

Figure A-234 Test 64 conversions of C18:2, and Iodine Value trend

A.65 Test 65: $Cu10Pd1SiO_2HP$ - Sunflower – 180 °C – 4 bar – 4 $mg_{catalyst}/mL_{oil}$

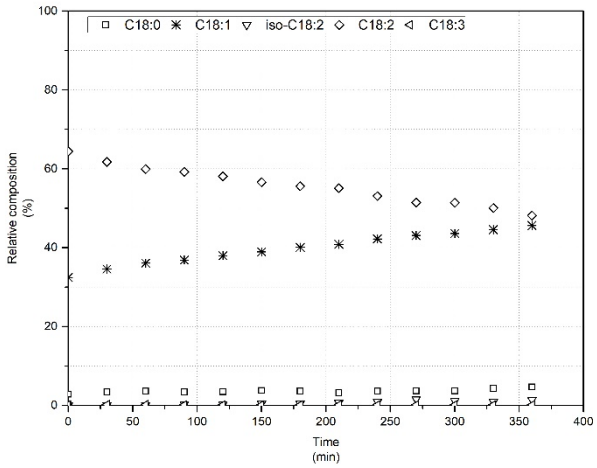

Figure A-235 Test 65 relative percentages of C18:0, C18:1, isomers C18:2, C18:2, C18:3

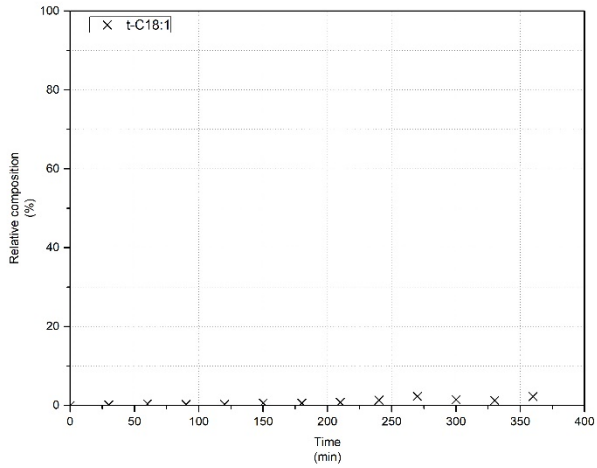

Figure A-236 Test 65 relative percentage of t-C18:1 estimated from the chromatogram

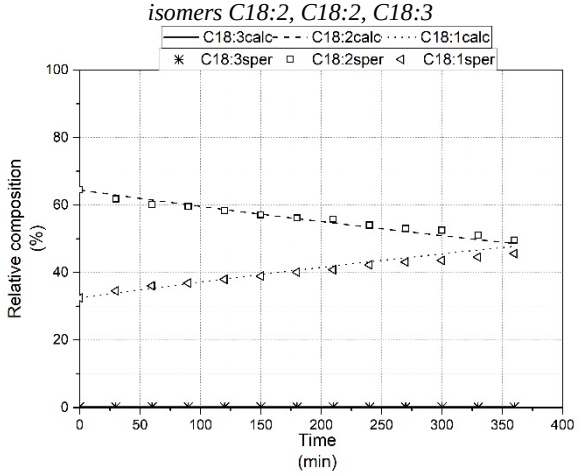

Figure A-237 Test 65 Model fitting for C18:1, C18:2 and C18:3, k1=0.0000210, k2=0.000785, k3=0.0000

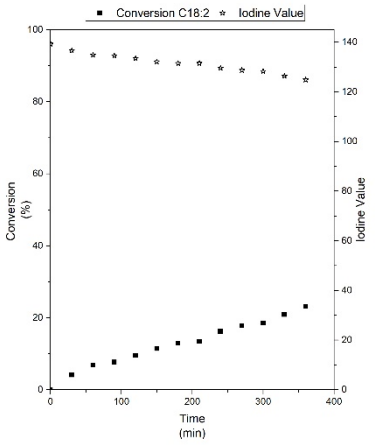

Figure A-238 Test 66 conversions of C18:2, and Iodine Value trend

A.66 Test 66: $Cu10Ni5SiO_2AE$ - Sunflower – 180 °C – 4 bar – 4 $mg_{catalyst}/mL_{oil}$

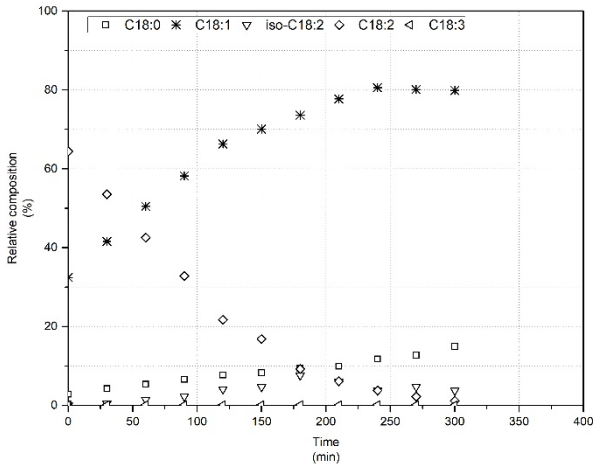

Figure A-239 Test 66 relative percentages of C18:0, C18:1, isomers C18:2, C18:2, C18:3

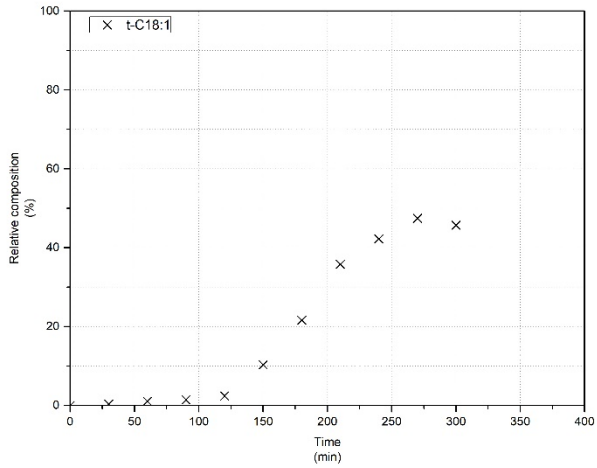

Figure A-240 Test 66 relative percentage of t-C18:1 estimated from the chromatogram

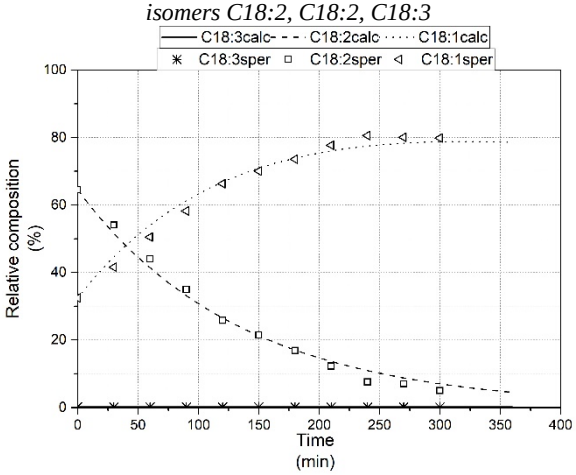

Figure A-241 Test 66 Model fitting for C18:1, C18:2 and C18:3, k1=0.000564, k2=0.00739, k3=0.0000

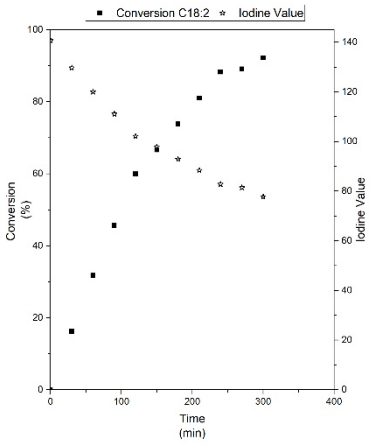

Figure A-242 Test 66 conversions of C18:2, and Iodine Value trend

A.67 Test 67: $Cu10Pd1SiO_2AE$ - Sunflower – 180 °C – 4 bar – 4 $mg_{catalyst}/mL_{oil}$

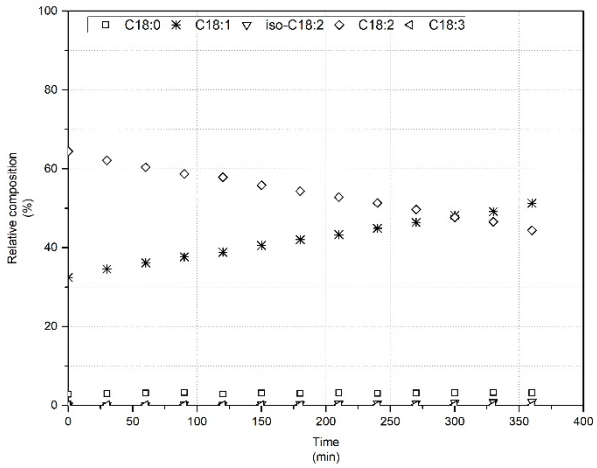

Figure A-243 Test 27 relative percentages of C18:0, C18:1, isomers C18:2, C18:2, C18:3

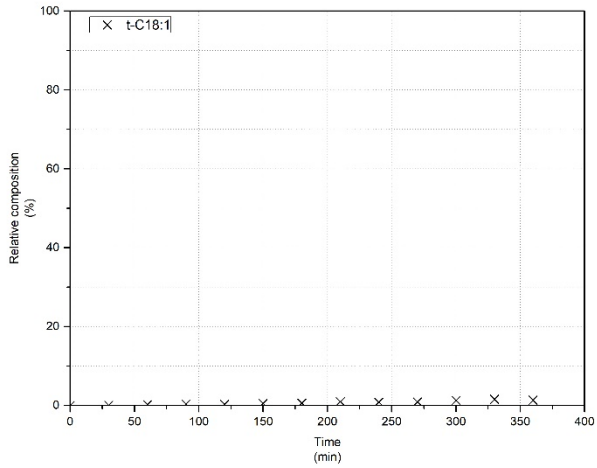

Figure A-244 Test 27 relative percentage of t-C18:1 estimated from the chromatogram

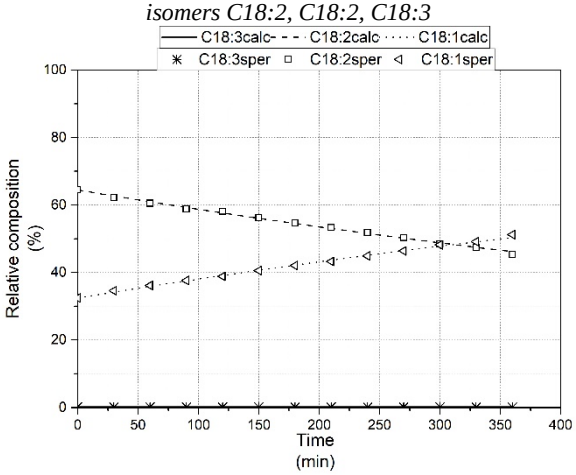

Figure A-245 Test 27 Model fitting for C18:1, C18:2 and C18:3, k1=0.0000248, k2=0.000927, k3=0.0000

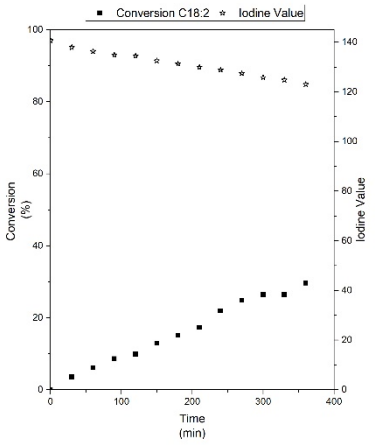

Figure A-246 Test 27 conversions of C18:2, and Iodine Value trend

A.68 Test 68: Ni5SiO$_2$HP - Sunflower – 180 °C – 4 bar – 4 mg$_{catalyst}$/mL$_{oil}$

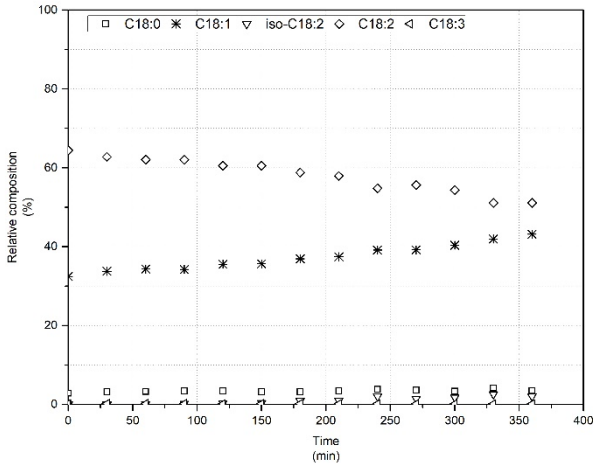

Figure A-247 Test 27 relative percentages of C18:0, C18:1, isomers C18:2, C18:2, C18:3

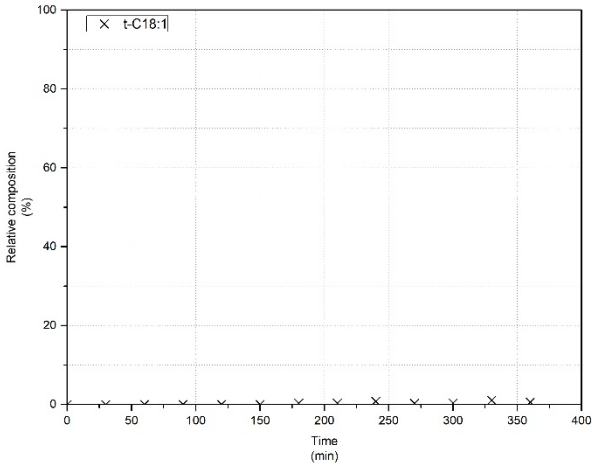

Figure A-248 Test 27 relative percentage of t-C18:1 estimated from the chromatogram

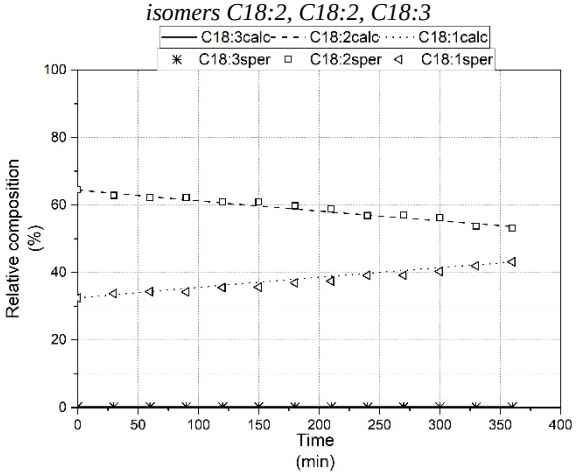

Figure A-249 Test 27 Model fitting for C18:1, C18:2 and C18:3, k1=0.0000154, k2=0.000511, k3=0.0000

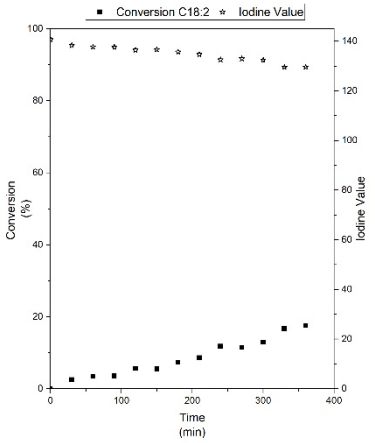

Figure A-250 Test 27 conversions of C18:2, and Iodine Value trend

A.69 Test 69: Pd1SiO$_2$HP - Sunflower – 180 °C – 4 bar – 4 mg$_{catalyst}$/mL$_{oil}$

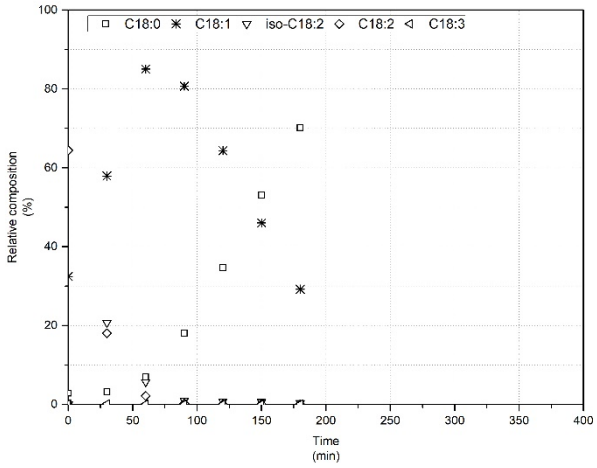

Figure A-251 Test 27 relative percentages of C18:0, C18:1, isomers C18:2, C18:2, C18:3

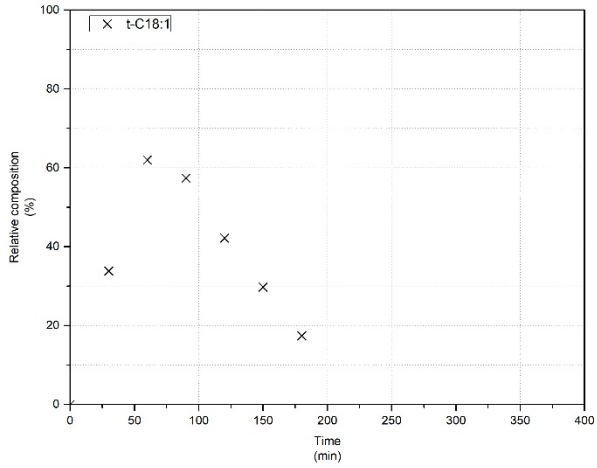

Figure A-252 Test 27 relative percentage of t-C18:1 estimated from the chromatogram

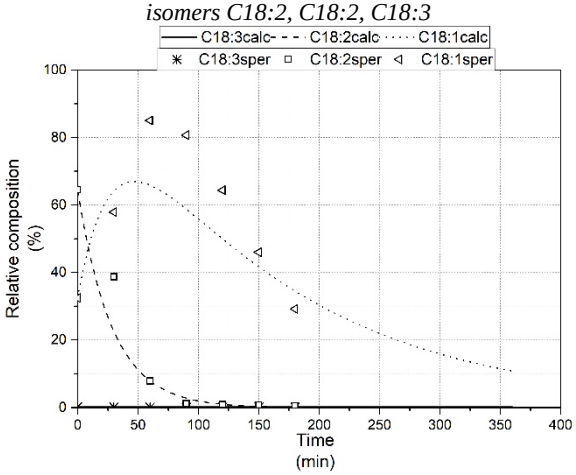

Figure A-253 Test 27 Model fitting for C18:1, C18:2 and C18:3, k1=0.00651, k2=0.035, k3=0.0000

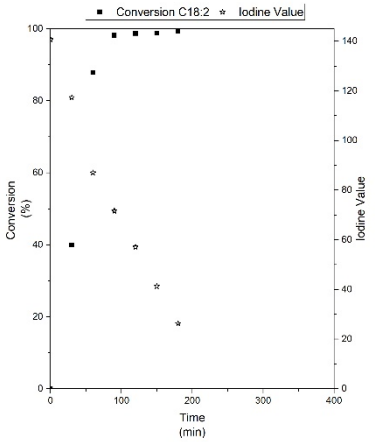

Figure A-254 Test 27 conversions of C18:2, and Iodine Value trend

A.70 Test 70: Ni5SiO$_2$AE - Sunflower – 180 °C – 4 bar – 4 mg$_{catalyst}$/mL$_{oil}$

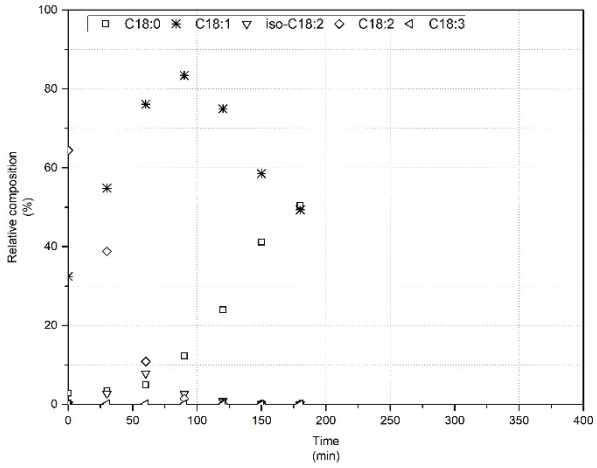

Figure A-255 Test 70 relative percentages of C18:0, C18:1, isomers C18:2, C18:2, C18:3

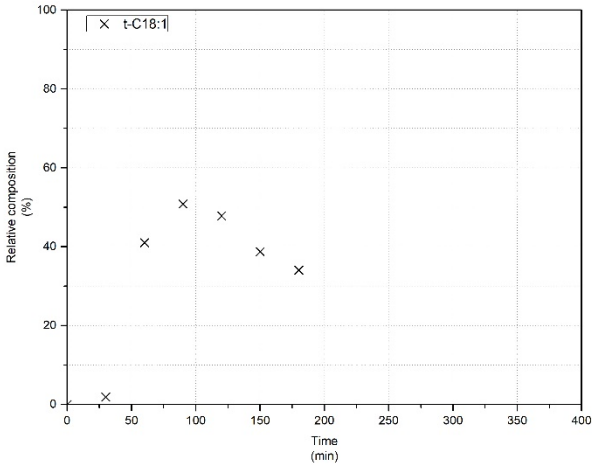

Figure A-256 Test 70 relative percentage of t-C18:1 estimated from the chromatogram

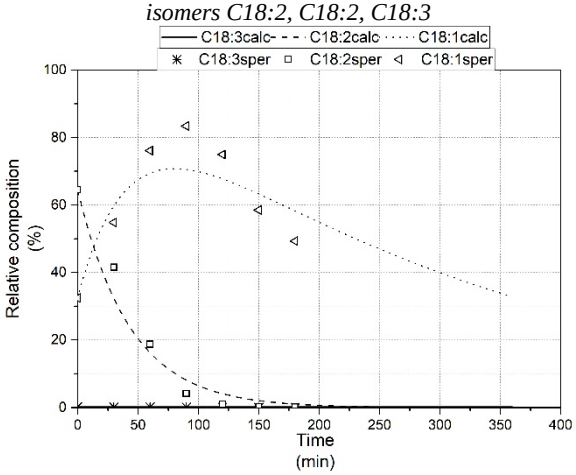

Figure A-257 Test 70 Model fitting for C18:1, C18:2 and C18:3, k1=0.0033, k2=0.023, k3=0.0000

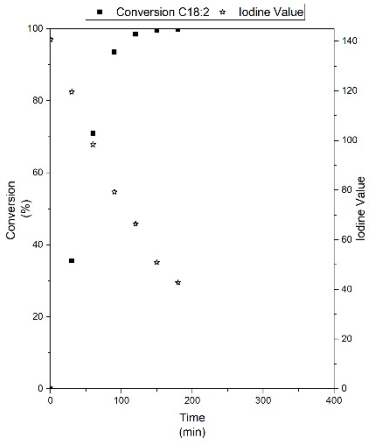

Figure A-258 Test 70 conversions of C18:2, and Iodine Value trend

A.71 Test 71: Pd1SiO$_2$AE - Sunflower – 120 °C – 4 bar – 2 mg$_{catalyst}$/mL$_{oil}$

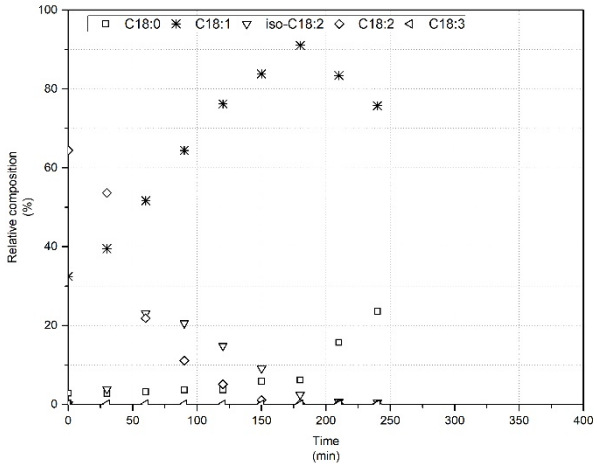

Figure A-259 Test 71 relative percentages of C18:0, C18:1, isomers C18:2, C18:2, C18:3

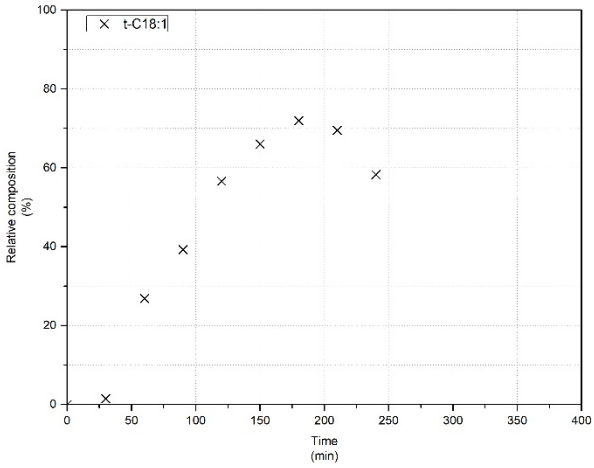

Figure A-260 Test 71 relative percentage of t-C18:1 estimated from the chromatogram

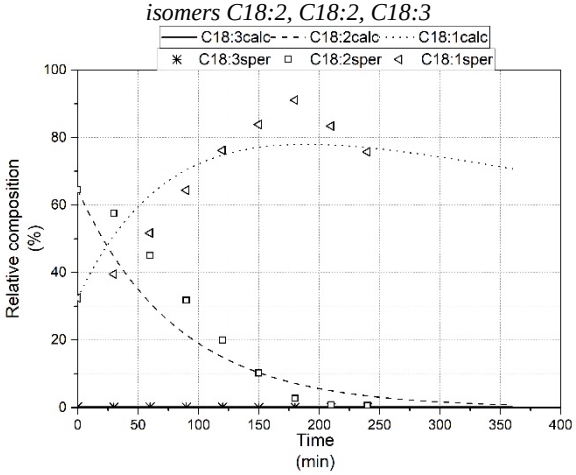

Figure A-261 Test 71 Model fitting for C18:1, C18:2 and C18:3, k1=0.002711, k2=0.0122, k3=0.0000

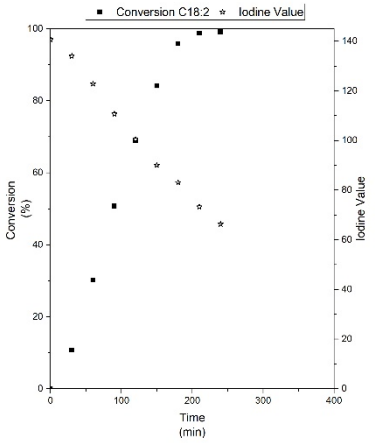

Figure A-262 Test 71 conversions of C18:2, and Iodine Value trend

A.72 Test 72: $Cu10Pd1SiO_2AE$ - Sunflower – 120 °C – 4 bar – 4 $mg_{catalyst}/mL_{oil}$

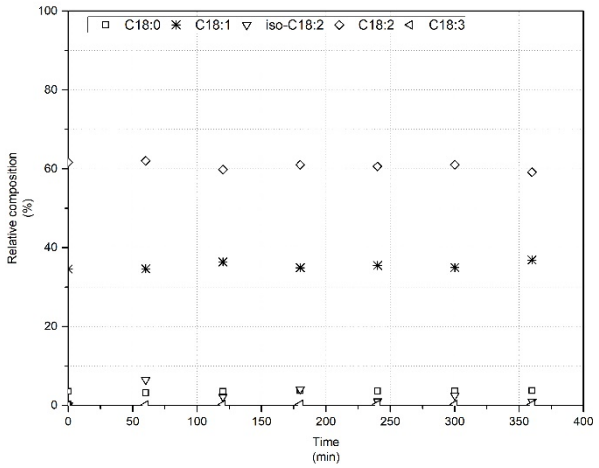

Figure A-263 Test 72 relative percentages of C18:0, C18:1, isomers C18:2, C18:2, C18:3

A.73 Test 73: $Cu10Pd1SiO_2AE$ - Sunflower – 120 °C – 12 bar – 4 $mg_{catalyst}/mL_{oil}$

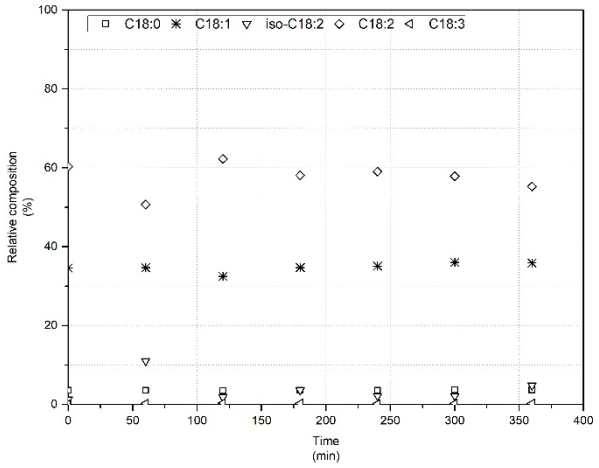

Figure A-264 Test 73 relative percentages of C18:0, C18:1, isomers C18:2, C18:2, C18:3

A.74 Test 74: $Cu10Pd1SiO_2AE$ - Sunflower – 120 °C – 20 bar – 4 $mg_{catalyst}/mL_{oil}$

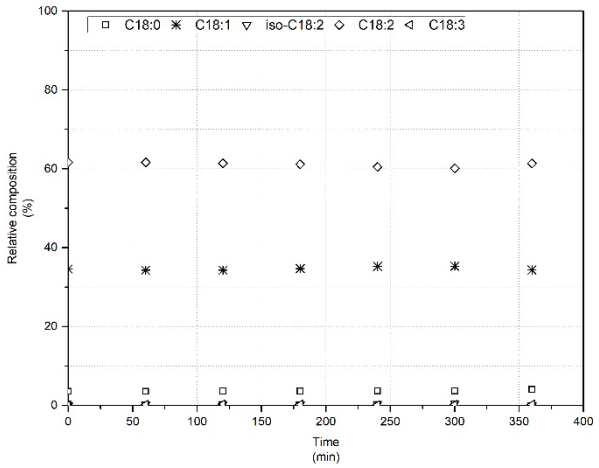

Figure A-265 Test 74 relative percentages of C18:0, C18:1, isomers C18:2, C18:2, C18:3

A.75 Test 75: $Cu10Pd1SiO_2AE$ - Sunflower – 180 °C – 4 bar – 4 $mg_{catalyst}/mL_{oil}$

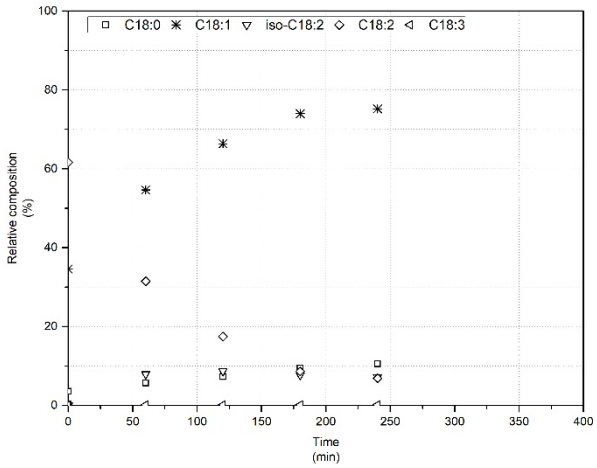

Figure A-266 Test 75 relative percentages of C18:0, C18:1, isomers C18:2, C18:2, C18:3

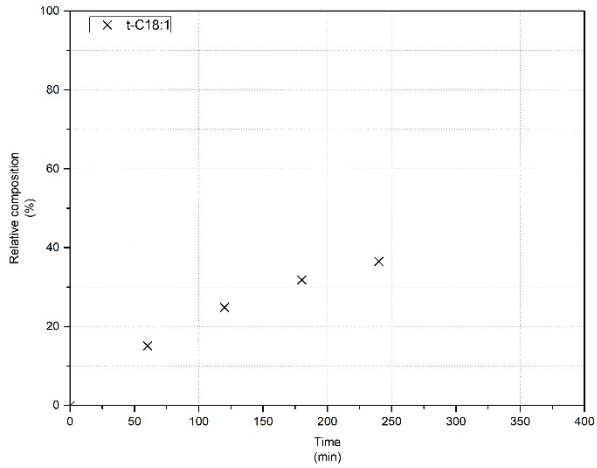

Figure A-267 Test 75 relative percentage of t-C18:1 estimated from the chromatogram

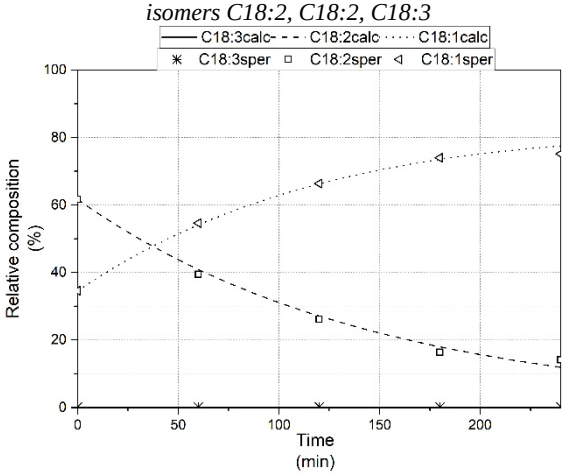

Figure A-268 Test 75 Model fitting for C18:1, C18:2 and C18:3, k1=0.000745, k2=0.00684, k3=0.0000

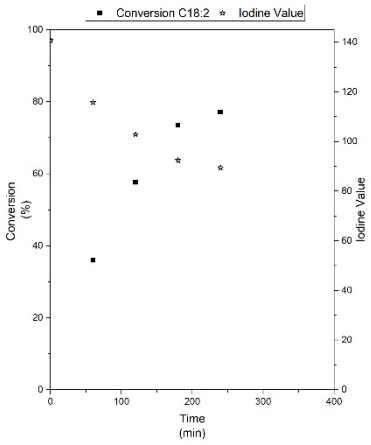

Figure A-269 Test 75 conversions of C18:2, and Iodine Value trend

A.76 Test 76: $Cu10Pd1SiO_2AE$ - Sunflower – 180 °C – 20 bar – 4 $mg_{catalyst}/mL_{oil}$

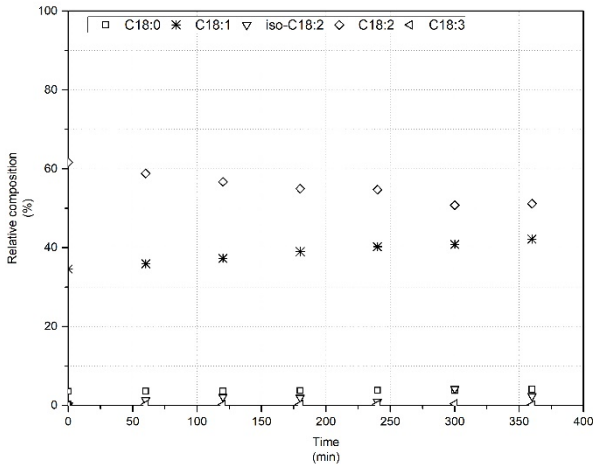

Figure A-270 Test 76 relative percentages of C18:0, C18:1, isomers C18:2, C18:2, C18:3

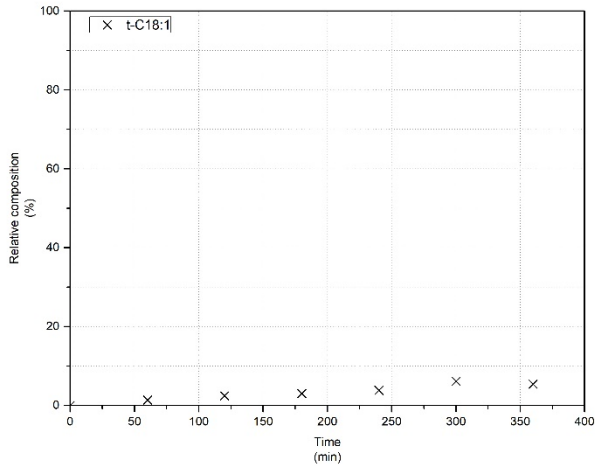

Figure A-271 Test 76 relative percentage of t-C18:1 estimated from the chromatogram

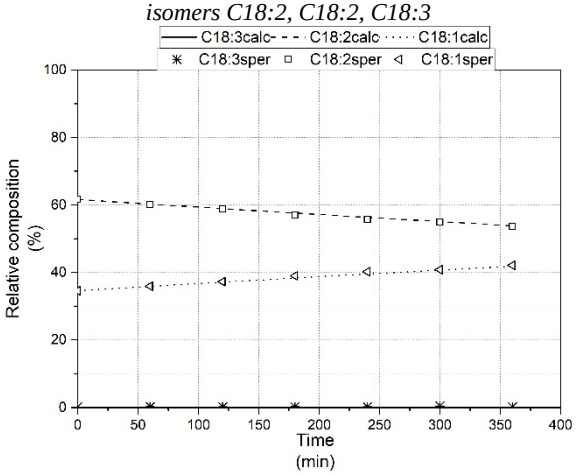

Figure A-272 Test 76 Model fitting for C18:1, C18:2 and C18:3, k1=0.0000102, k2=0.000375, k3=0.0000

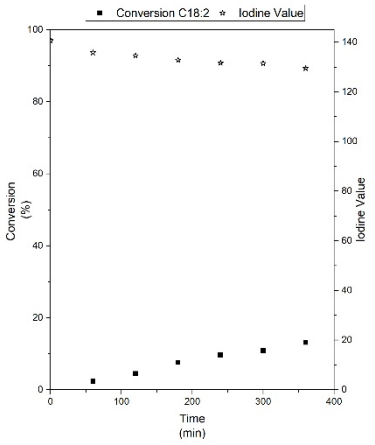

Figure A-273 Test 76 conversions of C18:2, and Iodine Value trend

A.77 Test 77: $Cu10Pd1SiO_2AE$ - Sunflower – 240 °C – 4 bar – 4 $mg_{catalyst}/mL_{oil}$

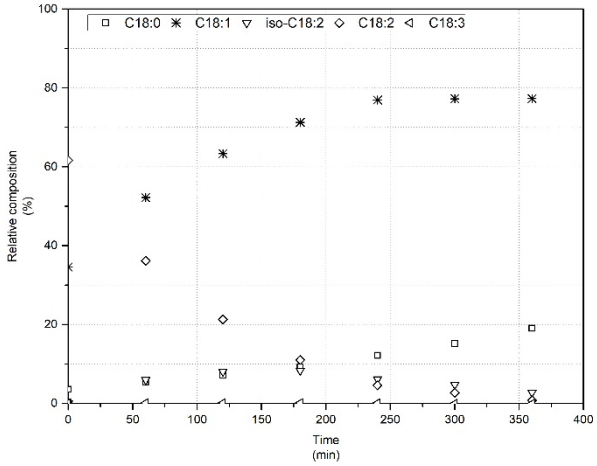

Figure A-274 Test 77 relative percentages of C18:0, C18:1, isomers C18:2, C18:2, C18:3

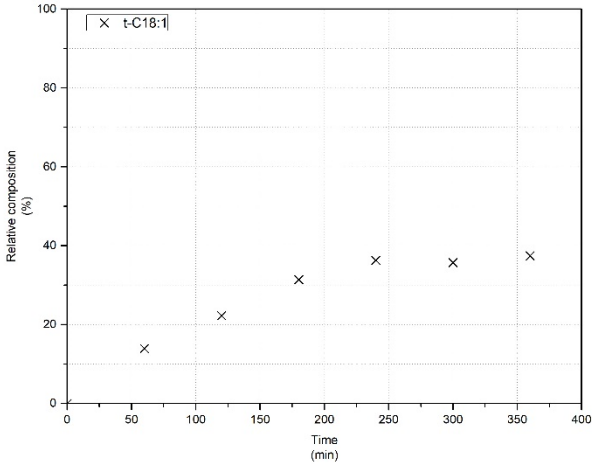

Figure A-275 Test 77 relative percentage of t-C18:1 estimated from the chromatogram

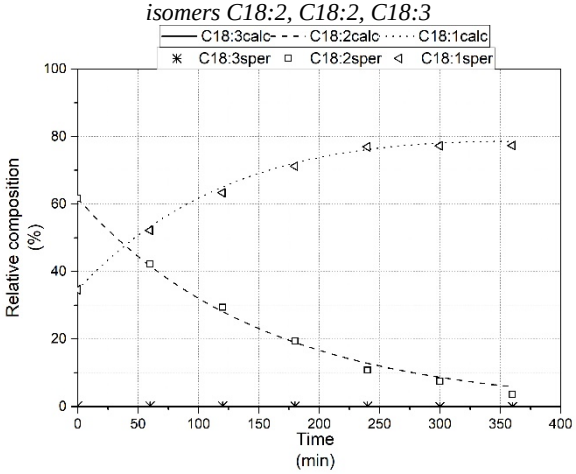

Figure A-276 Test 77 Model fitting for C18:1, C18:2 and C18:3, k1=0.000459, k2=0.00654, k3=0.0000

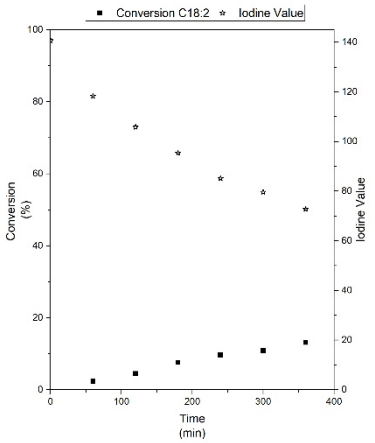

Figure A-277 Test 77 conversions of C18:2, and Iodine Value trend

A.78 Test 78: $Cu10Pd1SiO_2AE$ - Sunflower – 240 °C – 20 bar – 4 $mg_{catalyst}/mL_{oil}$

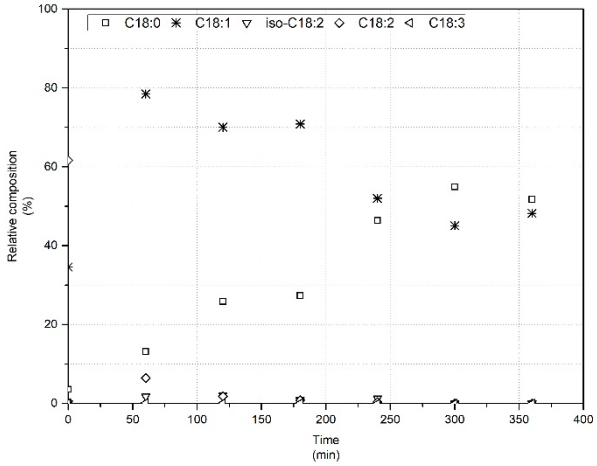

Figure A-278 Test 78 relative percentages of C18:0, C18:1, isomers C18:2, C18:2, C18:3

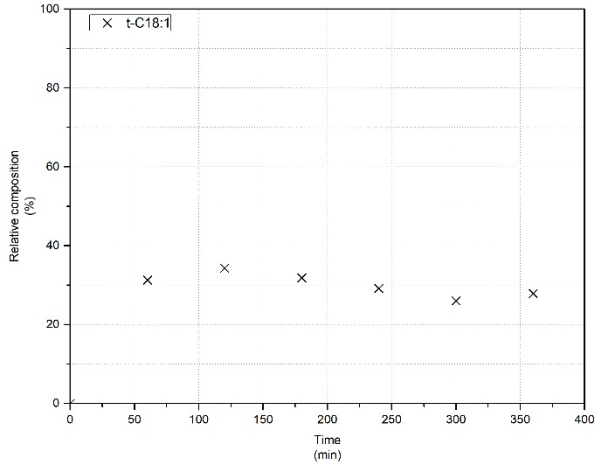

Figure A-279 Test 78 relative percentage of t-C18:1 estimated from the chromatogram

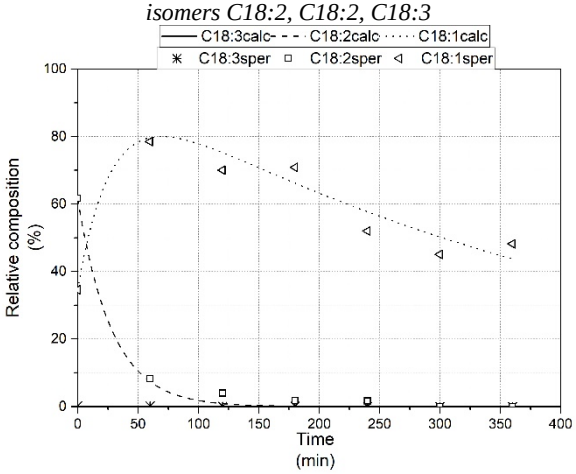

Figure A-280 Test 78 Model fitting for C18:1, C18:2 and C18:3, k1=0.000745, k2=0.015, k3=0.0000

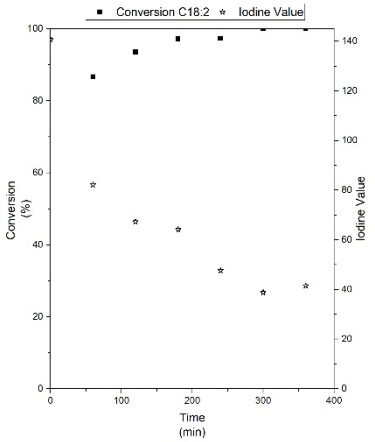

Figure A-281 Test 78 conversions of C18:2, and Iodine Value trend

A.79 Test 79: $Cu10Pd1SiO_2AE$ - Sunflower – 200 °C – 12 bar – 4 $mg_{catalyst}/mL_{oil}$

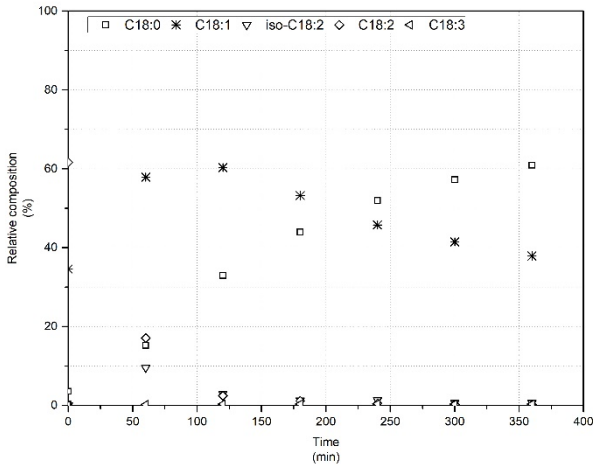

Figure A-282 Test 79 relative percentages of C18:0, C18:1, isomers C18:2, C18:2, C18:3

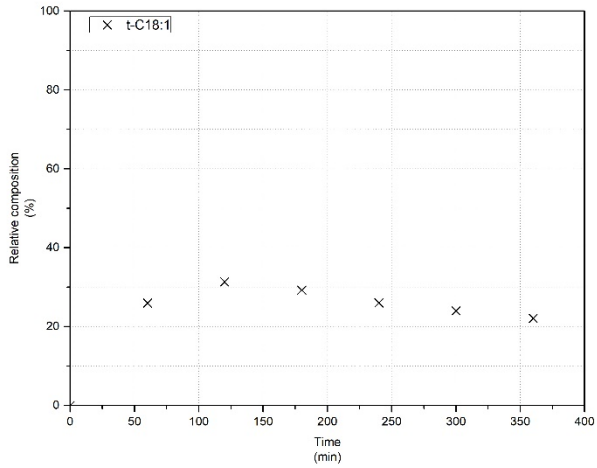

Figure A-283 Test 79 relative percentage of t-C18:1 estimated from the chromatogram

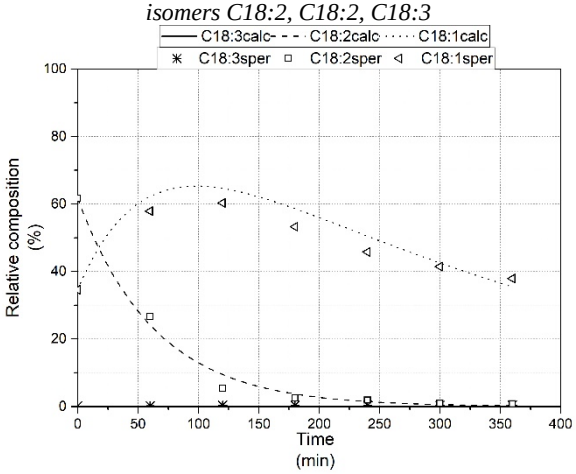

Figure A-284 Test 79 Model fitting for C18:1, C18:2 and C18:3, k1=0.00317, k2=0.0156, k3=0.0000

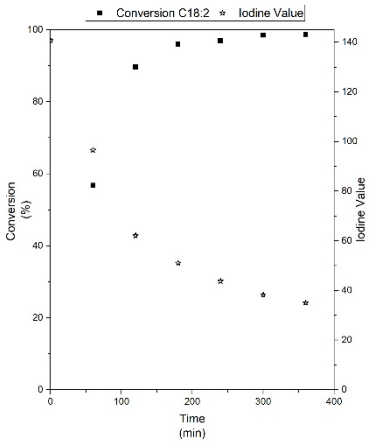

Figure A-285 Test 79 conversions of C18:2, and Iodine Value trend

La borsa di dottorato è stata cofinanziata con risorse del
Programma Operativo Nazionale Ricerca e Innovazione 2014-2020 (CCI 2014IT16M2OP005),
Fondo Sociale Europeo, Azione I.1 "Dottorati Innovativi con caratterizzazione Industriale"

UNIONE EUROPEA
Fondo Sociale Europeo

Ministero dell'Istruzione, dell'Università e della Ricerca

PON RICERCA E INNOVAZIONE 2014 - 2020